DISCOVERY OF NEW REACTION MODES IN ORGANIC SYNTHESIS TRIGGERED BY HFIP

Jiayu Zhang

UNIVERSITAT ROVIRA i VIRGILI

Discovery of new reaction modes in organic synthesis triggered by HFIP

JIAYU ZHANG

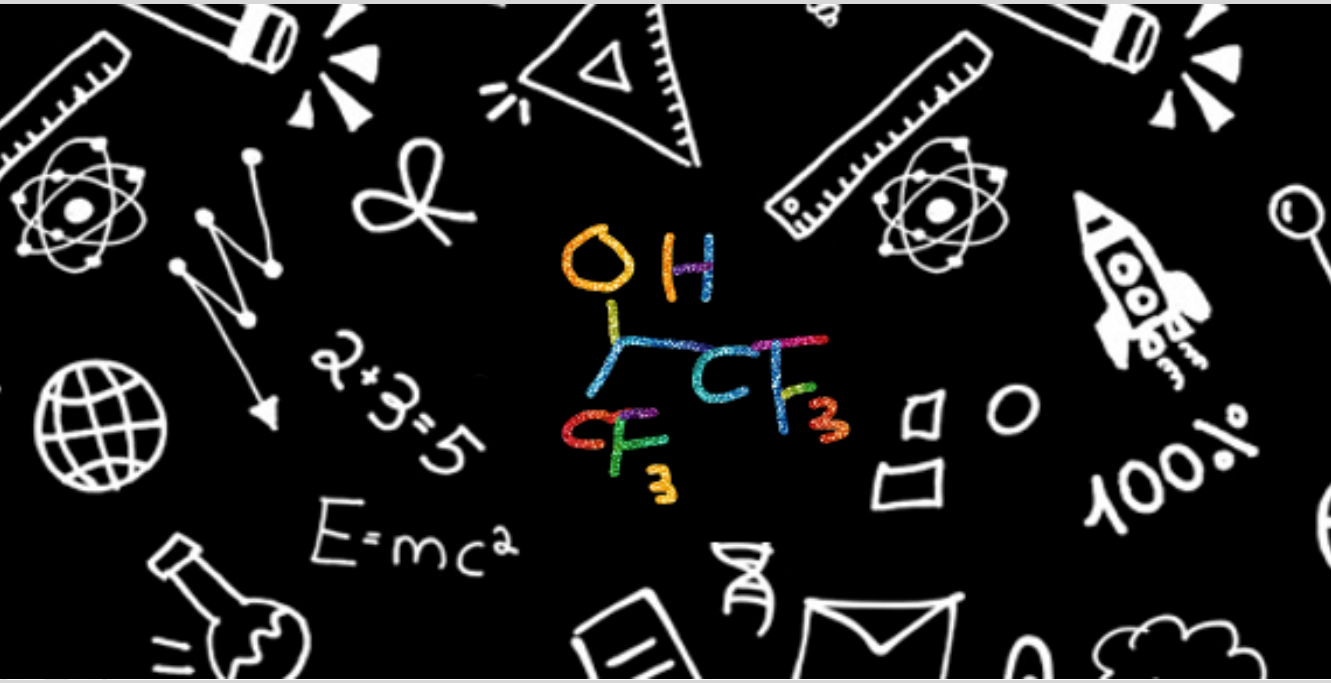

DOCTORAL THESIS
2023

UNIVERSITAT ROVIRA I VIRGILI
DISCOVERY OF NEW REACTION MODES IN ORGANIC SYNTHESIS TRIGGERED BY HFIP
Jiayu Zhang

UNIVERSITAT ROVIRA I VIRGILI
DISCOVERY OF NEW REACTION MODES IN ORGANIC SYNTHESIS TRIGGERED BY HFIP
Jiayu Zhang

UNIVERSITAT ROVIRA I VIRGILI
DISCOVERY OF NEW REACTION MODES IN ORGANIC SYNTHESIS TRIGGERED BY HFIP
Jiayu Zhang

UNIVERSITAT ROVIRA I VIRGILI
DISCOVERY OF NEW REACTION MODES IN ORGANIC SYNTHESIS TRIGGERED BY HFIP
Jiayu Zhang

Jiayu Zhang

Discovery of New Reaction Modes in Organic Synthesis Triggered by HFIP

Doctoral Thesis

Supervised by Prof. Mónica Helvia Pérez-Temprano

Institute of Chemical Research of Catalonia (ICIQ)

Tarragona

2023

UNIVERSITAT ROVIRA I VIRGILI
DISCOVERY OF NEW REACTION MODES IN ORGANIC SYNTHESIS TRIGGERED BY HFIP
Jiayu Zhang

UNIVERSITAT ROVIRA I VIRGILI
DISCOVERY OF NEW REACTION MODES IN ORGANIC SYNTHESIS TRIGGERED BY HFIP
Jiayu Zhang

ICIQ - Institut Català d´Investigació Química

Avgda, Països Catalans 16,

43007 Tarragona (Spian)

Prof. Dr. Mónica H. Pérez-Temprano, Group Leader at the Institute of Chemical Research of Catalonia (ICIQ),

I STATE that the present Doctoral Thesis, entitled “Discovery of new reaction modes in organic synthesis triggered by HFIP” presented by Jiayu Zhang for the award of the degree of Doctor, has been carried out under my supervision at the Institute of Chemical Research of Catalonia (ICIQ).

Tarragona, August 31st, 2023

Doctoral Thesis Supervisor

Prof. Dr. Mónica Helvia Pérez-Temprano

UNIVERSITAT ROVIRA I VIRGILI
DISCOVERY OF NEW REACTION MODES IN ORGANIC SYNTHESIS TRIGGERED BY HFIP
Jiayu Zhang

List of publications

¨Intramolecular C(sp^3)–H Bond Amination Strategies for the Synthesis of Saturated N-containing Heterocycles¨

Zhang, J.; Pérez-Temprano, M. H. *Chimia* **2020**, *74*, 895–903.

¨Transition metal-catalysed directed C–H functionalization with nucleophiles¨

Barranco, S.; Zhang, J.; López-Resano, S.; Casnati, A.; Pérez-Temprano, M. H. *Nat. Synth.* **2022**, *1*, 841–853.

*¨Cp*Co-catalyzed directed hydrogen isotope exchange with substrate-dependent deuterium source¨*

Barranco, S.; Zak, I. L.; Zhang, J.; Milo, A.; Pérez-Temprano, M. H. *ChemRxiv* **2023**, DOI: 10.26434/chemrxiv-2023-bmg14.

UNIVERSITAT ROVIRA I VIRGILI
DISCOVERY OF NEW REACTION MODES IN ORGANIC SYNTHESIS TRIGGERED BY HFIP
Jiayu Zhang

UNIVERSITAT ROVIRA I VIRGILI
DISCOVERY OF NEW REACTION MODES IN ORGANIC SYNTHESIS TRIGGERED BY HFIP
Jiayu Zhang

Table of Contents

Abbreviations and Acronyms

The abbreviations and acronyms used in the following Chapters are those standardized by the "Guidelines for Authors" of the ACS. For ease of reading, the meaning of each abbreviation and acronym has been specified the first time that appears. Additional abbreviations and acronyms are listed below:

AcOH	Acetic acid
Ar	Argon, aryl
BHT	Butylated hydroxytoluene
Bu	Butyl
Boc	Tert-butyloxy carbonyl
cat.	Catalytic
Cp*	Pentamethylcyclopentadienyl
CV	Cyclic voltammetry
CT	Charge transfer
d	Doublet
DCE	1,2-Dichloroethane
DCM	Dichloromethane
DFT	Density functional theory
DG	Directing group
DMSO	Dimethyl sulfoxide
DMF	Dimethylformamide
dr	Diastereomeric ratio
e-	Electron
EPR	Electron paramagnetic resonance
equiv	Enquivalent
ESI	Electrospray ionization
Et	Ethyl
Et_2O	Diethyl ether
Fc	Ferrocene
FG	Functional group
g	Gram(s)
h	Hour(s)
HAT	Hydrogen Atom Transfer
HFIP	1,1,1,3,3,3-Hexafluoroisopropanol
HLF	Hofmann-Löffler-Freytag
Hz	Hertz
HRMS	High-resolution mass spectrometry
HPLC	High performance liquid chromatography
^{i}Pr	Isopropyl
IUPAC	International Union of Pure and Applied Chemistry
ISC	Intersystem crossing
IR	Infrared
J	Coupling constant (in NMR spectrometry)
K	Kelvin(s)
L	Liter(s)
LED	Light emitting diode

LSF	Late-stage functionalization
M	Molar (moles per liter)
m	Multiplet (spectral); milli
*m*CBA	meta Chlorobenzoic acid
mCPBA	meta Chloroperbenzoic acid
m/z	Mass-to-charge ratio
Me	Methyl
min	Minute(s)
mol	Mole(s)
NBS	N-Bromosuccinimide
NCS	N-Chlorosuccinimide
NMR	Nuclear magnetic resonance
Nuc	Nucleophile
Ns	4-Nitrobenzenesulfonyl
OAc	Acetate
^{o}C	Degrees Celsius
OTf	Trifluoromethanesulfonate
OTFA	Trifluoroacetate
OTs	Toluenesulfonate
Ph	Phenyl
PIDA	(Diacetoxyiodo)benzene
PIFA	(Bis(trifluoroacetoxy)iodo)benzene
$PhI(OPiv)_2$	Di-(pivaloyloxy)iodobenzene
PFTB	Perfluoro-*tert*-butanol
ppm	Part(s) per million
q	Quartet
R	Carbon based organic substituent, alkyl or aryl
rt	Room temperature
s	Singlet
SET	Single electron transfer
SES	2-(Trimethylsilyl)ethanesulfonyl
t	Triplet
TEMPO	2,2,6,6-tetramethylpiperidin-1-oxyl
TFA	Trifluoroacetic acid
THF	Tetrahydrofuran
TM	Transition metal
TMS	Trimethylsilyl; tetramethylsilane
TS	Transition state
Ts	4-Methylbenzenesulfonyl
UV	Ultraviolet
Vis	Visible
VTMS	Vinyltrimethylsilane
X	Heteroatom
XRD	X-ray diffraction
δ	Chemical shift (in part per million) downfield form
μ	micro

Abstract

The impact of solvents on chemical reactions holds a paramount role in shaping reaction outcomes and processes. Solvents assume multifaceted roles: they serve as a medium for reactant dissolution, influence reactant interaction and mobility, and exert control over reaction rates, selectivity, and even mechanisms. The solvation environment created by the selected solvent stabilizes intermediates and transition states, leading to shifts in reaction pathways and product distributions. Polarity of solvents significantly affects ionic and polar reactions, whereas nonpolar solvents' hydrophobic interactions can control reaction conformations. Furthermore, the choice of solvent directly influences catalyst solubility, stability, and activity, thereby impacting overall reaction efficiency and selectivity. However, despite these crucial roles, the significance of solvents is often overlooked.

In recent years, the landscape of organic synthesis has been transformed by the emergence of innovative organic solvents, with perfluorinated variants especially 1,1,1,3,3,3-hexafluoroisopropanol (HFIP) leading the charge. These solvents have ushered in remarkable breakthroughs in reaction discovery and synthetic methodologies. The transition of HFIP from an infrequently employed solvent to a prominent choice across various domains of organic synthesis is underpinned by its unique attributes. This shift is primarily driven by empirical observations that consistently demonstrate the superior performance of reactions conducted in HFIP compared to alternative solvents. Consequently, HFIP has garnered increased attention as a solvent of choice. The ongoing exploration of the reactivity interplay between HFIP and organic or organometallic species not only promises to deepen our understanding of reaction mechanisms but also serves as a wellspring of inspiration for the design and development of transformative synthetic pathways.

Within this Doctoral Thesis, our primary objective will be centered around the conception and implementation of novel synthetic protocols, all facilitated by the inclusion of HFIP. The central goal of our endeavor is to broaden the spectrum of functions that this perfluorinated alcohol can undertake in the domains of both metal-free and TM-catalysis. Through a systematic exploration of HFIP's potential, we aim to forge innovative pathways in the realm of catalytic methodologies.

Chapter II, entitled *´HFIP-assisted selective intramolecular synthesis of heterocycles enabled by single electron transfer´* provides a new heterocycles formation protocol involving aliphatic *sp3* C–H functionalization. We reveal that by simply combining bench-stable $PhI(OTFA)_2$ and HFIP we can switch from the well-established HLF mechanism to a new and versatile reaction pathway that enables the selective functionalization of aliphatic C–H bonds. We exploit the facile formation of radical cations via single electron transfer (SET), in the presence or absence of light, to synthesize pyrrolidines and piperidines, including drug-type molecules, along with *O*-heterocycles. Experimental and computational mechanistic studies support two possible mechanistic pathways depending on the electron density of the substrate, where the HFIP plays a multifunctional role.

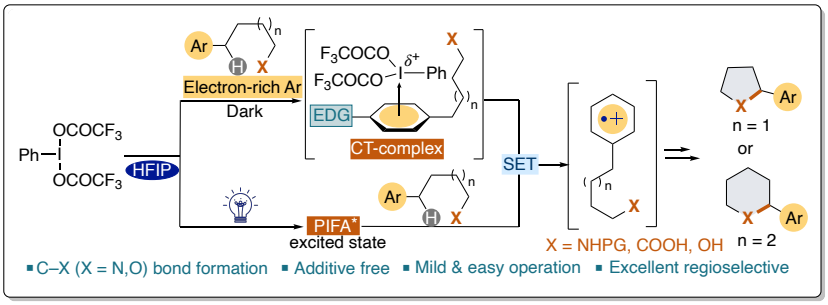

Scheme 1. C(sp^3)–H functionalization triggered by HFIP/PIFA combination

Chapter III, entitled *´HFIP-enabled spin catalysis´* discloses a "non-excited" singlet-triplet intersystem crossing (ISC) via secondary-coordination sphere interactions with HFIP. Despite this perfluorinated solvent has exhibited unique behavior promoting organic and organometallic transformations, its participation in ISC events had not been contemplated. Employing experimental and computational approaches, we investigated this intriguing phenomenon, ultimately harnessing it to develop a versatile site-selective cobalt-catalyzed Mizoroki-Heck protocol, that includes the activation of inexpensive and readily available aryl chlorides, and late-stage functionalization (LSF) strategies.

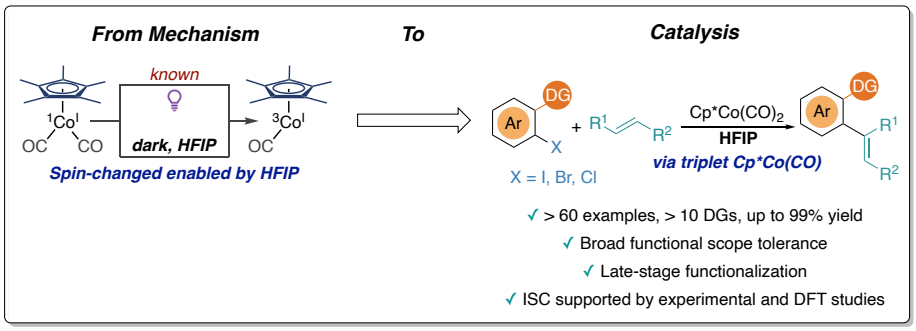

Scheme 2. HFIP-mediated intersystem crossing enables Cp*Co catalysis

Chapter 1. General introduction

1.1. HFIP as solvent in organic chemistry

Solvents play a crucial role in chemical reactions, influencing various aspects such as the reaction rate, product formation, intermediate stereochemistry, and overall product outcome. These effects are controlled by important factors such as acidity, ionic strength, boiling point, H-bonding, and other weak interactions, along with other physical properties. It has come to be appreciated that polar fluorinated alcohols can dramatically influence the outcomes of chemical reactions, becoming widely used solvents in organic synthesis. Among them, 1,1,1,3,3,3-hexafluoroisopropanol (HFIP) particularly stands out for its unique physical and chemical properties, gaining increasing attention within the chemical community compared to direct analogues, such as trifluoroethanol (TFE). As it can be shown in Figure 1.. the number of papers that mention HFIP has tremendously increased over the past years with more than 700 publications having been released in 2022.

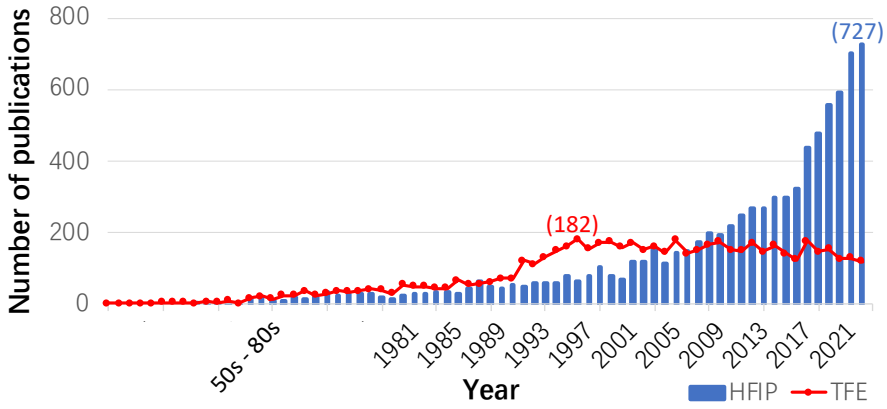

Figure 1.1. Time distribution of the publications that mention HFIP (blue bars) or TFE (red dots and line) between 1950s and 2022. Data for the bar chart were obtained by a SciFinder search in August 2023 using the keywords "hexafluoroisopropanol", "HFIP", "trifluoroethanol," and "TFE."

Table 1. summarizes the most relevant physical and chemical properties of HFIP, along with TFE and their non-fluorinated counterparts. The purpose of this table is to give a general context to facilitate the rationalization of the positive effect that HFIP shows in different synthetic areas.

Table 1.1. Physical and chemical properties of HFIP and comparison to other solvents.

Properties	EtOH	2-propanol	TFE	HFIP
b.p. (ºC)	78	82.5	73.8	58.6
m.p. (ºC)	-114	-89.5	-43.5	-4
density (ρ)	0.789	0.781	1.383	1.605
pK_a	15.9	17.1	12.4	9.3
dielectric constant (ε)	24.5	19.4	26.7	16.7
polarity (E^N_T)	0.654	0.546	0.898	1.068
nucleophilicity ($N_{t\text{–BuCl}}$)	0.09	0.09	-2.78	-3.93
ionizing power ($Y_{t\text{–BuCl}}$)	-2.03	-2.73	1.045	2.46
hydrogen bond donor (α)	0.83	0.76	1.51	1.96
hydrogen bond acceptor (β)	0.77	0.95	0	0

As shown below, HFIP exhibits distinctive properties when compared to common solvents:

Lower boiling point: HFIP (boiling point 58.6 °C) presents lower boiling points and higher melting points in comparison to other alcohols (e.g., bp of 2-propanol is 82.5 °C).[1] These properties allow it to be readily separated from the reaction mixture through distillation. As a result, this characteristic contributes to a decrease in solvent waste and helps offset the initial cost of these solvents in organic synthesis.

Enhanced acidity: Fluorine substituents have a potent negative inductive effect, leading to an enhancement in the acidity of the hydroxyl group. As the number of trifluoromethyl groups in the molecule increases, the corresponding acidity follows the same trend. This is evident in the pK_a values, where HFIP (pK_a 9.3) exhibits higher acidity compared to iPrOH (pK_a 17.1), EtOH (pK_a 15.9), and TFE (pK_a 12.4).[1a]

High hydrogen-bond donating (HBD) ability: HFIP exhibits strong hydrogen bond donor ability, leading to the formation of aggregates, particularly dimers and trimers, which further enhances its hydrogen bond donor capability.[2] Additionally, it is well-established the stabilizing ability that H-bonding of HFIP can play with a wide variety of scaffolds, ranging from organic molecules to organometallic complexes.

Weak nucleophilicity: Despite possessing a hydroxyl group, HFIP differs distinctly from non-fluorinated alcohols and other protic solvents in that it is a poor

1 (a) Eberson, L.; Hartshorn, M. P.; Persson, O. *J. Chem. Soc., Perkin Trans.* 1995, *2,* 1735. (b) Bégué, J.-P.; Bonnet-Delpon, D.; Crousse, B. *Synlett* **2004**, *2004*, 18.

2 Berkessel,A.; Adrio, J. A.; Hüttenhain, D.; Neudörfl, J. M. *J. Am. Chem. Soc*. **2006**, *128*, 8421.

hydrogen-bond acceptor and nucleophile. The solvent nucleophilicity parameter $N_{t\text{-BuCl}}$ represents the nucleophilic strength of solvents based on the solvolysis of *t*-butyl chloride. For HFIP, the value is -3.93, whereas for 2-propanol or EtOH, the value is 0.09 (on a logarithmic scale).[3] Thus, it is important to note that HFIP only exhibits nucleophilic behavior in the presence of highly reactive cationic electrophilic species.[4]

Cation stabilization: The high dielectric constant (ε = 16.7), low nucleophilicity and strong ionizing power ($Y_{t\text{-BuCl}} = 2.46$)[3] of HFIP make it an ideal solvent to generate cations and investigate their reactivity.[5] Indeed, there is an ongoing debate about whether HFIP stabilizes cations through a thermodynamic process or merely allows them to persist long enough to undergo reactions via a kinetic phenomenon.

Owing to its unique properties, it is not surprising that HFIP has become a widespread solvent in synthetic organic chemistry.[6] In the following sections, we will cover its employment in two relevant synthetic areas: hypervalent iodine reagent (HIR)-mediated C–H functionalizations and Cp*Co-catalyzed functionalization reactions. These selected examples show the beneficial effect of this solvent in facilitating and enhancing a wide range of organic reactions and synthetic methodologies. When possible, the role that this perfluorinated alcohol plays in these transformations will also be discussed.

1.2. HFIP in metal-free HIR-mediated C–H functionalization

A hypervalent state is characterized by an atom extending its valence shell beyond the constraints of the Lewis octet rule. Hypervalent compounds are prevalent among elements situated in groups 15 to 18 of the periodic table.[7] For iodine, according to IUPAC, compounds featuring iodine(III) and iodine(V) are termed λ^3- and λ^5-iodanes respectively. $ArIL_2$ represents the most frequently employed λ^3-iodanes species.

3 Schadt, F. L.; Bentley, T. W.; Schleyer, P. v. R. *J. Am. Chem. Soc.* **1976**, *98*, 7667.

4 (a) Colomer, I.; Barcelos, R. C.; Christensen, K. E.; J. Donohoe T. J. *Org. Lett.* **2016**, *18*, 5880. (b) Kelley, B. T.; Walters, J. C.; Wengryniuk, S. E. *Org. Lett.* **2016**, *18*, 1896.

5 Matesich, M. A.; Knoefel, J.; Feldman, H.; Evans, D. F. *J. Phys. Chem.* **1973**, *77*, 366.

6 (a) Bégué, J.-P.; Bonnet-Delpon, D.; Crousse, B.; *Synlett* **2004**, *1*, 18. (b) Shuklov, I. A.; Dubrovina, N. V.; Börner, A. *Synthesis* **2007**, *19*, 2925. (c) Sugiishi, T.; Matsugi, M.; Hamamoto, H.; Amii, H. *RSC Adv.* **2015**, *5*, 17269. (d) Colomer, I.; Chamberlain, A. E. R.; Haughey, M. B.; Donohoe T. J. *Nat. Rev. Chem.* **2017**, *1*, 0088. (e) Motiwala, H. F.; Armaly, A. M.; Cacioppo, J. G.; Coombs, T. C.; Koehn, K. R. K.; Norwood, V. M.; Aubé, J. *Chem. Rev.* **2022**, *122*, 12544.

7 Musher, J. I. *Angew. Chem. Int. Ed.* **1969**, *8*, 54.

Structurally, these reagents adopt a pseudo-trigonal bipyramid T-shaped geometry, where the aryl group and the ligand groups are in perpendicular planes.[8] This arrangement arises from the presence of the less electronegative aryl ring and two lone pairs of electrons occupying equatorial positions, while the electronegative ligands occupy apical positions (Scheme 1.1). The linear hypervalent bond in $ArIL_2$ (L-I-L) takes the form of a 3-center 4-electron (3c-4e) bond. This bond is constructed from the doubly occupied iodine $5p_z$ orbital and one orbital from each of the apical ligands. This fact makes 2 electrons to be placed in the bonding orbital and 2 electrons in the nonbonding orbital (HOMO). Resulting from this overlap between the 5p orbital of the iodine and the orbitals of the ligands.[9]

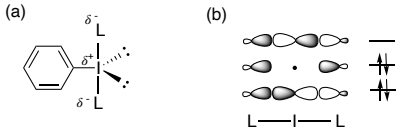

Scheme 1.1. (a) Aryl-λ^3-iodanes (b) electronic configuration of iodanes

In recent decades, the utilization of a wide variety of hypervalent iodine (III) reagents (HIRs) as oxidants has gained a remarkable attention by the chemical community (Scheme 1.2).[10] This surge can be attributed to their attractive properties, such as versatile reactivity, low toxicity, impressive stability. Indeed, research groups worldwide have harnessed them in metal-free transformations.[11]

8 Wirth, T. *Top. Curr. Chem*. **2003**, *224*, 1.

9 (a) Zhdankin, V. V. *Hypervalent Iodine Chemistry: Preparation, Structure and Synthetic Application of Polyvalent Iodine Compounds;* John Wiley & Sons Ltd.: New York, 2014. (b) Kaiho, T., Ed. *Iodine Chemistry and Applications*; John Wiley & Sons, Inc.: New York, 2015.

10 (a) *Hypervalent Iodine Chemistry Modern Developments in Organic Synthesis*. ed. T. Wirth, Springer, Verlag, 2003. (b) *Hypervalent Iodine Chemistry. Topics in Current Chemistry*. ed. T. Wirth, Springer, Cham, 2016, vol. 373 (c) Ishihara, K.; Muñiz, K. in *Iodine Catalysis in Organic Synthesis*, ed. Ishihara, K.; Muñiz, K. John Wiley & Sons, Ltd, Chichester, Ltd, Chichester, 2022.

11 (a) Yusubov; M. S.; Zhdankin, V. V. *Curr. Org. Synth*. **2012**, *9*, 247. (b) Yoshimura, A.; Zhdankin, V. V. *Chem. Rev*. **2016**, *116*, 3328. (c) Flores, A.; Cots, E.; Berges, J.; Muñiz, K. *Adv. Synth. Catal.* **2019**, *361*, 2. (d) Parra, A. *Chem. Rev.* **2019**, *119*, 12033. (e) Singh, F. V.; Shetgaonkar, S. E.; Krishnan, M.; Wirth, T. *Chem. Soc. Rev.* **2022**, *51*, 8102.

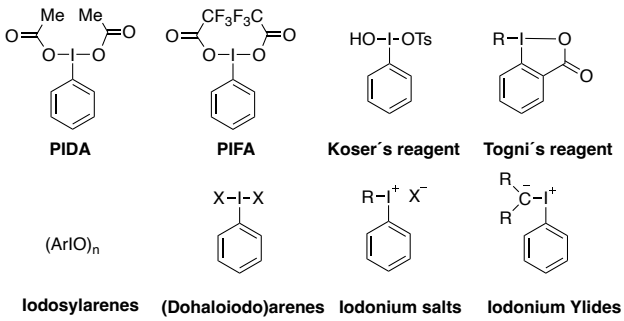

Scheme 1.2. Commonly used HIRs in organic synthesis

When combined with HFIP, the reactivity of HIRs, such as PIFA or PIDA, can be enhanced by increasing their oxidizing capability. Indeed, in 2016, Donohoe and Compton proposed that the formation of a strongly hydrogen-bonded adduct **A**, between the solvent and this type of oxidants and observed by NMR spectroscopy, is key for enabling the synthesis of tetrasubstituted cyclobutanes via styrene dimerization (Scheme 1.3).[12]

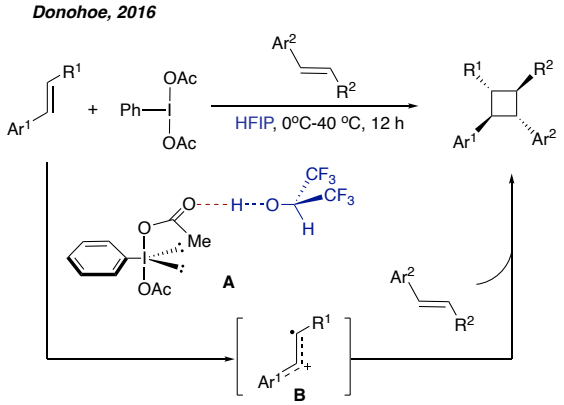

Scheme 1.3. HFIP-promoted the activation of PIDA in dimerization of styrene

The unique behavior of hypervalent iodine(III) reagents in HFIP has also being exploited for engineering oxidative amination reactions. In the following sections, we will focus our attention on relevant examples of HIR-mediated inter- or intramolecular C–N bond-forming reactions here HFIP is key to promote the corresponding reactivity (Scheme 1.4).

12 (a) Colomer, I.; Barcelos, R. C.; Donohoe, T. J. *Angew. Chem. Int. Ed.* **2016**, *55*, 4748. (b) Colomer, I.; Batchelor-McAuley, C.; Odell, B.; Donohoe, T. J.; Compton, R. G. *J. Am. Chem. Soc.* **2016**, *138*, 8855.

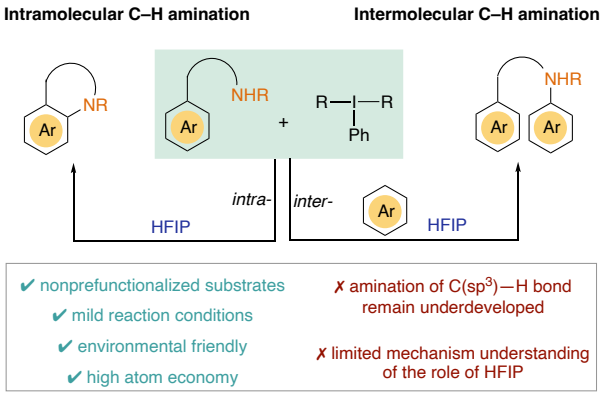

Scheme 1.4. HIR-mediated inter- or intramolecular aminations promoted by HFIP

1.2.1. Intermolecular C–H aminations

In the early 90s, the Kita group pioneered the discovery of HIR-mediated nucleophilic C(sp^2)–H coupling of anisole derivatives **1** with azides using HFIP as solvent (Scheme 1.5).[13]. UV-vis and ESR spectroscopic measurements revealed that the reaction occurred via an aromatic radical cation intermediate $\mathbf{1}^{\bullet+}$, generated through a single-electron transfer (SET) mechanism.[14] The authors uncovered that HFIP plays a multifunctional role in this transformation, enabling the formation of a charge-transfer (CT) complex between the electron-rich arenes and PIFA and subsequently facilitating the formation and stabilization of the radical cation. The importance of the perfluorinated alcohol is supported by the lack of reactivity in common solvents (for example, DCM, MeCN). Although the undesired homo-coupling products cannot be avoided, [15] this discovery led to broader applications in synthesis, providing a route for the direct introduction of a diverse array of nucleophiles into aromatic compounds.[16]

---

13 Kita, Y.; Tohma, H.; Inagaki, M.; Hatanaka, K.; Yakura, T. *Tetrahedron Lett.* **1991**, *32*, 4321.

14 Kita, Y.; Tohma, H.; Hatanaka, K.; Takada, T.; Fujita, S.; Mitoh, S.; Sakurai, H.; Oka, S. *J. Am. Chem. Soc*. **1994**, *116*, 3684.

15 Kita, Y.; Dohi, T. *Chem. Rec.* **2015**, *15*, 886.

16 (a) Kita,Y.; Takada, T.; Tohma, H. *Pure Appl. Chem.* **1996**, *68*, 627. (b) Kita, Y.; Takada, T.; Mihara, S.; Tohma, H. *Synlett* **1995**, 211. (c) Kita, Y.; Takada, T.; Mihara, S.; Whelan, B. A.; Tohma, H. *J. Org. Chem*. **1995**, *60*, 7144. (e) Wang, X.; Donaire, J. G.; Martin, R. *Angew. Chem. Int. Ed.* **2014**, *53*, 11084. (f) Satishkumar, S.; Lakshman, M. K. *Chem. Commun.,* **2017**, *53*, 2226. (g) Satishkumar, S.; Poudapally, S.; Vuram, P. K.; Gurram, V.; Pottabathini, N.; Sebastian, D.; Yang, L.; Pradhan, P.; Lakshman, M. K. *Chem-CatChem.* **2017**, *9*, 4058

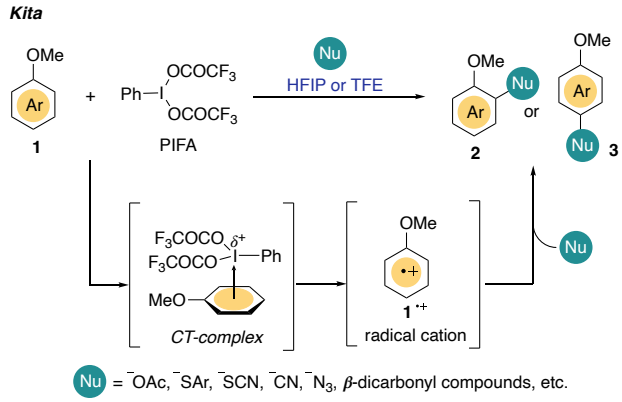

Scheme 1.5. PIFA-induced nucleophilic functionalization of anisole derivatives in HFIP

Since then, HFIP has emerged as a powerful solvent for enhancing the efficiency of HIR-mediated C–N bond-forming reactions[17-18] In comparison to intramolecular C–H amination (see section 1.2.2), the field of intermolecular C–H amination has been barely explored. In 2011, Antonchick and co-workers reported an intermolecular cross-amination involving *N*-acylated aniline derivatives and arenes. This transformation, carried out in the presence of PIDA in HFIP, enabled the creation of *N*-diarylated products **4** (Scheme 1.6a).[17d] The following year, the same group extended this strategy to an oxidative intermolecular diarylation reaction. *para*-Tolyliodonium diacetate was employed as an oxidant, and HFIP was found as the best solvent (Scheme 1.6b).[19] Later in 2015, a PIDA-mediated oxidative C−H amination of electron-rich arenes with amino derivatives was reported by Chupakhin for the synthesis of diaryl amines **6** (Scheme 1.6c).[20] The reaction was conducted in HFIP, a choice attributed to its potential to stabilize the nitrenium ion intermediate generated during the course of the reaction,

17 (a) Liang, D.; He, Y.; Liu, L.; Zhu, Q. A.*Org. Lett*. **2013**, *15*, 3476. (b) Yu, J.; Gao, C.; Song, Z.; Yang, H.; Fu, H. *Eur. J. Org. Chem*. **2015**, *2015*, 5869. (c) Liang, D.; Sersen, D.; Yang, C.; Deschamps, J. R.; Imler, G. H.; Jiang, C.; Xue, F. *Org. Biomol. Chem*. **2017**, *15*, 4390. (d) Antonchick, A. P.; Samanta, R.; Kulikov, K.; Lategahn, J. *Angew. Chem. Int. Ed.* **2011**, *50*, 8605. (e) Zhang, Z.; Zhang, Y.; Huang, G.; Zhang, G. *Org. Chem. Front*. **2017**, *4*, 1372. (f) Zhang, Z.; Gao, X.; Li, Z.; Zhang, G.; Ma, N.; Liu, Q.; Liu, T. *Org. Chem. Front.* **2017**, *4*, 404. (g) Alla, S. K.; Kumar, R. K.; Sadhu P.; Punniyamurthy, T. *Org. Lett*. **2013**, *15*, 1334.

18 (a) Maiti, S.; Achar, T. K.; Mal, P. *Org. Lett*. **2017**, *19*, 2006. (b) Manna, S.; Serebrennikova, P. O.; Utepova, I. A.; Antonchick, A. P.; Chupakhin, O. N. *Org. Lett*. **2015**, 17, 4588. (c) Samanta, R.; Lategahn, J.; Antonchick, A. P. *Chem. Commun*. **2012**, *48*, 3194.

19 Samanta, R.; Lategahn, J.; Antonchick, A. P. *Chem. Commun.* **2012**, *48*, 3194.

20 Manna, S.; Serebrennikova, P. O.; Utepova, I. A.; Antonchick, A. P.; Chupakhin, O. N. *Org. Lett.* **2015**, *17*, 4588.

specifically after the electrophilic aromatic substitution step. In 2017, the Mal research group documented an additional intermolecular C–H amination reaction mediated by HIR (Scheme 1.6d).[21] This process involved dehydrogenative annulation, combining unactivated arenes and anilides in a mixture of 1:1 HFIP and DCM. The outcome was the synthesis of *N*-substituted carbazoles **7** through a tandem formation of C−C and C−N bonds. The reaction exhibited proficiency under both stoichiometric and catalytic conditions, although the catalytic approach generally resulted in lower yields.

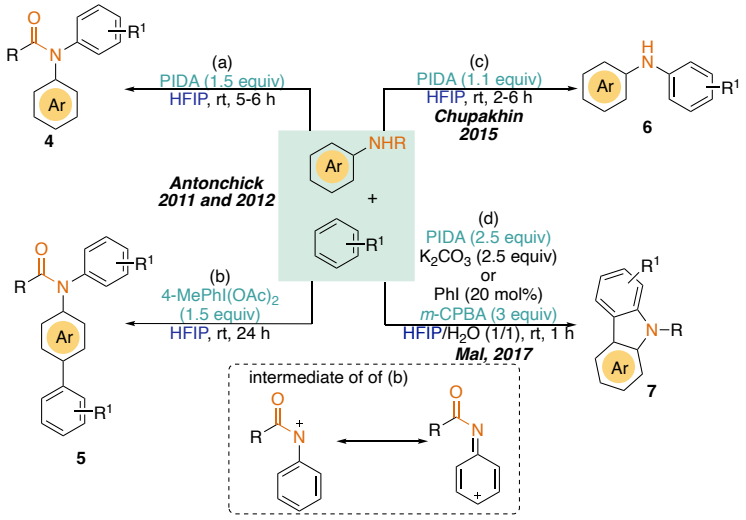

Scheme 1.6. Intermolecular C–H amination

1.2.2. Intramolecular C–H aminations

Structures containing C–N bonds are commonly present in biologically active natural products, pharmaceutical compounds, agrochemicals, and functional materials.[22] For example, approximately more than 60% of the FDA-approved small molecules bear at least one nitrogen heterocycle.[23] Therefore, approaches to development of more convenient and milder intramolecular C–H amination strategies has continuously attracted attention of organic chemists.[24]

21 Maiti, S.; Achar, T. K.; Mal, P. *Org. Lett.* **2017**, *19*, 2006.

22 (a) Goel, R.; Luxami, V.; Paul, K. Curr. *Top. Med. Chem*. **2016**, *16*, 3590. (b) Ricci, A. *Amino Group Chemistry: From Synthesis to the Life Sciences;* Wiley-VCH: Weinheim, 2008.

23 Vitaku, E.; Smith, D. T.; Njardarson, J. T. *J. Med. Chem*. **2014**, *57*, 10257.

24 (a) Park, Y.; Kim, Y.; Sukbok Chang, S. *Chem. Rev*. **2017**, *117*, 9247. (b) Timsina, Y. N.; Gupton, B. F.; Ellis, K. C. *ACS Catal*. **2018**, *8*, 5732.

In the context of HIR-mediated transformations, apart from the SET approach developed by Kita, the prevailing mechanisms for C(sp^2)–N bond-forming reactions are cross-dehydrogenative couplings (CDCs) (Scheme 1.7). Specifically, the reaction initiates with the oxidation of substrate **8** by HIR **9**, leading to the formation of intermediate **A** and the liberation of a singular molecule of RH. Subsequently, the liberation of iodobenzene leads to the formation of nitrenium ion **B**. The nucleophilic arene then attacks the nitrenium ion in **B**, followed by a deprotonation, yielding the desired product **10**.

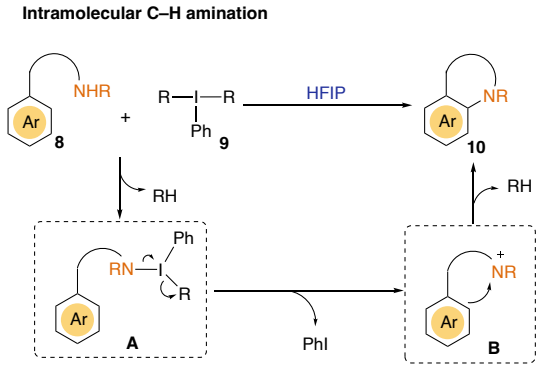

Scheme 1.7. HFIP-promoted CDC aminations mediated by HIRs

Among the different hypervalent iodine(III) reagents, PIDA stands as the prevailing HIR employed for intramolecular C(sp^2)–H aminations. In 2012, Antonchick and co-workers unveiled a PIDA-promoted intramolecular oxidative amination of 2,6-diarylacetanilides in HFIP (Scheme 1.8a).[25] This transformative approach followed a 4π-electron−5-atom electrocyclization process and demonstrates its efficacy in the streamlined synthesis of 1-arylcarbazoles **11**. Subsequently, the Fu research group reported an oxidative C−H amidation strategy mediated by PIDA along with Cs_2CO_3 in HFIP (Scheme 1.8b).[26] This approach enabled the synthesis of diverse benzimidazol-2-one derivatives **12** with great functional group tolerance. Notably, the reaction exhibited its highest yield in HFIP, with TFE also proving effective. In 2016, a series of benzimidazo[1,2-c]quinazoline scaffolds **13** were synthesized via a PIDA-mediated intramolecular oxidative C−H amination reaction of a 4-anilinoquinazolines in HFIP

25 Samanta, R.; Kulikov, K.; Strohmann, C.; Antonchick, A. P. *Synthesis* **2012**, *44*, 2325.
26 Yu, J.; Gao, C.; Song, Z.; Yang, H.; Fu, H. *Eur. J. Org. Chem.* **2015**, *2015*, 5869.

by the Zhang group (Scheme 1.8c).[27] Employing HFIP resulted in a commendable combination of high yield and short reaction time. However, alternative oxidants such as 1,4-benzoquinone (BQ), $K_2S_2O_8$, or CH_3OOOH proved ineffective, failing to yield the desired product. In 2018, the Zhu group introduced a method for synthesizing the spiro[indole-3,2'-pyrrolidine] framework **14** via a PIDA-mediated C–N bond-forming dearomatization process (Scheme 1.8d).[28] Notably, TFE led to a slight decrease in the yield of the desired product compared to HFIP. Other solvents such as DCE, THF and dioxane delivered low yields of the products.

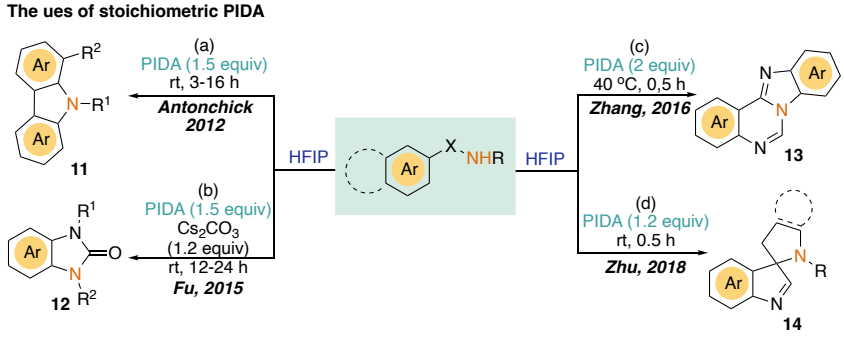

Scheme 1.8. PIDA-mediated intramolecular C(sp^2)–H aminations in HFIP

$PhI(OPiv)_2$ has also demonstrated its efficacy in CDC amination reactions. In 2013, the Zhu research group unveiled a tandem demethylenation/intramolecular C(sp^2)–H amination pathway, facilitated by $PhI(OPiv)_2$ in the presence of HFIP (Scheme 1.9).[29] This procedure was initiated through an *ipso* S_EAr reaction followed by HFIP-assisted C–C and C–N bond cleavage. This tandem amination reaction culminated in the synthesis of pyrido[1,2-a]benzimidazoles derivatives **16**. It is worth noting that despite HFIP's relatively low nucleophilicity, mechanistic studies revealed its involvement in the C–C and C–N bond cleavage processes, affording intermediate **C**, which underscored its crucial role in the overall transformation.

27 Shen, C.; Wang, L.; Wen, M.; Shen, H.; Jin, J.; Zhang, P. *Ind. Eng. Chem. Res.* **2016**, *55*, 3177.
28 Zhou, Y.; Li, D.; Tang, S.; Sun, H.; Huang, J.; Zhu, Q. *Org. Biomol. Chem.* **2018**, *16*, 2039.
29 Liang, D.; He, Y.; Liu, L.; Zhu, Q. A. *Org. Lett.* **2013**, *15*, 3476.

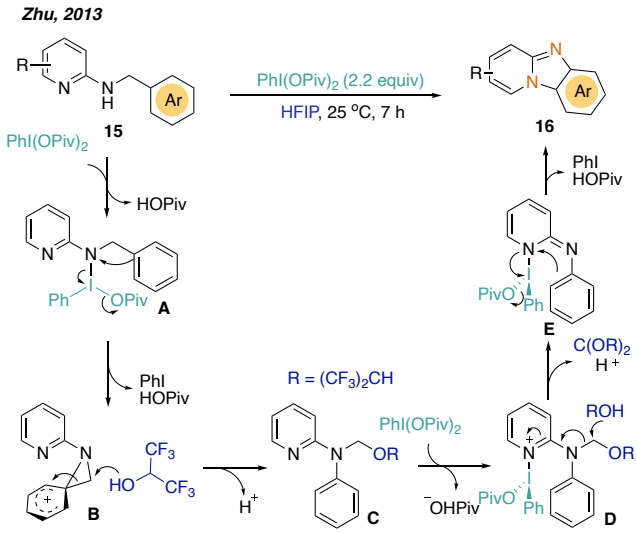

Scheme 1.9. PhI(OPiv)$_2$-mediated tandem demethylenation/intramolecular C(sp^2)−H amination

In 2017, the Zhang group introduced an additional example of PhI(OPiv)$_2$-mediated intramolecular C(sp^2)−H amination (Scheme 1.10a).[30] This method enabled the preparation of a range of cyclopropyl spirooxindoles **17**. Notably, HFIP was identified as the optimal solvent for this process, while alternative solvents like TFE, EtOH, ACN, and DMF did not yield the desired products effectively. The same year, the Zhang group extended their work to encompass two more intramolecular C(sp^2)−H amination approaches. The first involved the synthesis of pyrrolo[3,2-c]quinolinones derivatives **18** (Scheme 1.10b),[31] while the second focused on the creation of 1H-Indazoles derivatives **19** (Scheme 1.10c).[32]

30 Zhang, Z.; Zhang, Y.; Huang, G.; Zhang, G. *Org. Chem. Front.* **2017**, *4*, 1372.
31 Zhang, Z.; Gao, X.; Li, Z.; Zhang, G.; Ma, N.; Liu, Q.; Liu, T.*Org. Chem. Front.* **2017**, *4*, 404−408.
32 Zhang, Z.; Huang, Y.; Huang, G.; Zhang, G.; Liu, Q. *J. Heterocycl. Chem.* **2017**, *54*, 2426−2433.

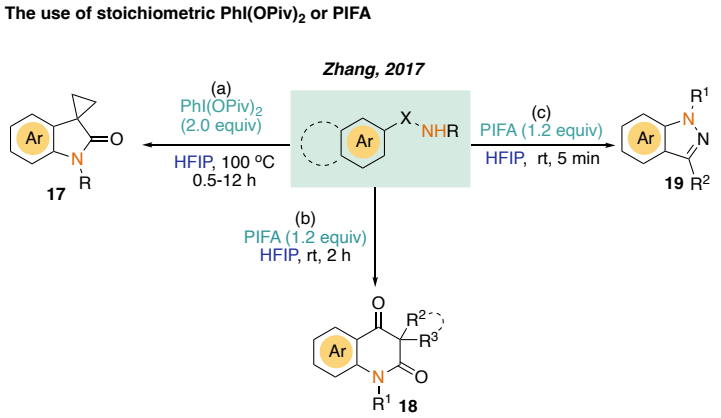

Scheme 1.10. $PhI(OPiv)_2$ and PIFA-mediated intramolecular $C(sp^2)$–H aminations in HFIP

While intramolecular oxidative C–N formation facilitated by HIRs offers an effective route for constructing N-containing compounds as mentioned above, scaling up these reactions can pose challenges due to the high cost associated with the use of HIRs. Nevertheless, a promising avenue to overcome this hurdle involves the in situ generation of catalytic amounts of HIR. This approach entails combining ArI with a stoichiometric, cost-effective oxidant, offering a potential solution to mitigate the limitations arising from the expense of HIRs. (Scheme 1.11).[33] The selection of the oxidant is key for the successful accomplishment of this approach, since the selected oxidant cannot interact with with the substrate, as the starting material should only be oxidized by the HIRs. Sodium periodate ($NaIO_4$),[34] chromium trioxide (CrO_3),[35] or dimethyldioxirane,[36] have been explored for the preparation of hypervalent iodine compounds from iodine-containing precursors, yet they remain unsatisfactory in terms of product yield as well as ease of operation.

33 (a) Richardson R. D.; Wirth, T. *Angew. Chem. Int. Ed*. **2006**, *45*, 4402. (b) Finkbeiner P.; Nachtsheim, B. J. *Synthesis* **2013**, 979. (c) Uyanik, M.; Ishihara, K. *ChemCatChem* **2012**, *4*, 177; (d) Dohi T.; Kita, Y. *Chem. Commun.*, **2009**, 2073.

34 Kazmierczak, P.; Skulski, L.; Kraszkiewicz, L. *Molecules* **2001**, *6*, 881.

35 Kazmierczak, P.; Skulski, L. *Synthesis* **1998**, 1721.

36 Bravo, A.; Fontana, F.; Fronza, G.; Minisci, F.; Serri, A. *Tetrahedron Lett.* **1995**, *36*, 6945.

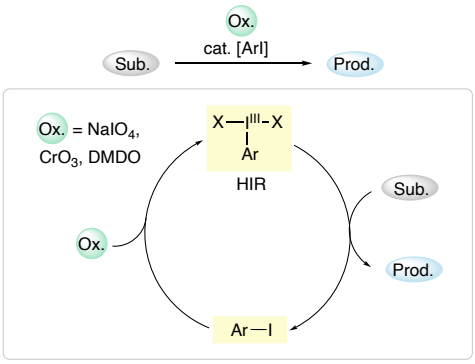

Scheme 1.11. Catalytic cycle with HIR

In this context, the introduction by Kita and co-workers of *m*-chloroperbenzoic acid (*m*-CPBA) for the *in situ* formation of HIRs[37] has sparked a rapid expansion of research in the domain of HIR-catalyzed reactions using HFIP as solvent.[11e] For example, in 2013, the Punniyamurthy group capitalized this strategy for the synthesis of benzimidazoles derivatives **20** in 2013 (Scheme 1.12a).[38] It is important to note that alternative solvents, including DCM, MeOH, DMSO, and DMF, proved ineffective in yielding the desired product conversion, underscoring the unique role of HFIP in this transformation. In 2017, the same procedure was employed for the synthesis of phenanthridinones **21** by the Xue group (Scheme 1.12b).[39] In 2018, the Cai group disclosed an asymmetric protocol for the construction of chiral lactams using a chiral diiodospirobiindane derivative **22** as the catalyst (Scheme 1.12c, in combination with an acid promoter, TFA, for enhancing both yield and enantioselectivity.[40] In 2021, the Li group reported another example of ayrliodine-catalyzed intramolecular C–N bond formation reaction (Scheme 1.12d).[41] This methodology enabled the synthesis of 3,3-disubstituted oxindole derivatives **24** up to 99% yield. The use of fluorinated solvents, including HFIP, TFE, and TFIP (1,1,1-trifluoro-2-propanol), played a crucial role in achieving the obtained high yields, with HFIP emerging as the most effective solvent option.

37 Dohi, T.; Maruyama, A.; Yoshimura, M.; Morimoto, K.; Tohma, H.; Kita, Y. *Angew. Chem. Int. Ed.* **2005**, *44*, 6193.
38 Alla, S. K.; Kumar, R. K.; Sadhu, P.; Punniyamurthy, T. *Org. Lett.* **2013**, *15*, 1334.
39 Liang, D.; Yu, W.; Nguyen, N.; Deschamps, J. R.; Imler, G. H.; Li, Y.; MacKerell, A. D.; Jiang, C.; Xue, F. *J. Org. Chem.* **2017**, *82*, 3589.
40 Ding, Q.; He, H.; Cai, Q. *Org. Lett.* **2018**, *20*, 4554.
41 Wang, Y.; Yang, M.; Sun, Y.-Y.; Wu, Z.-G.; Dai, H.; Li, S. *Org. Lett.* **2021**, *23*, 8750.

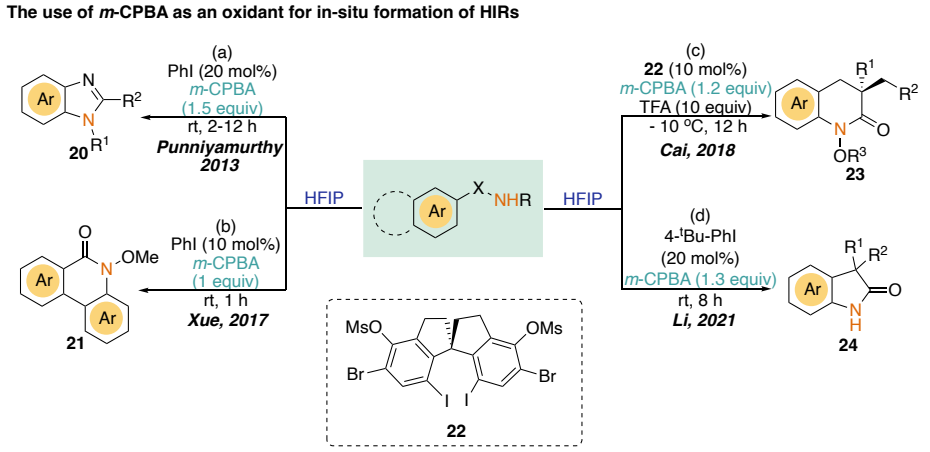

Scheme 1.12. ArI-catalyzed intramolecular C(sp^2)–H aminations using *m*-CPBA as an oxidant

In addition to *m*-CPBA, alternative oxidants, such as AcOOH or selectfluor have also been explored for the intramolecular amination of aromatic C–H bonds. In 2010, the Kita research group introduced an oxidative spirocyclization approach for the C−N bond formation (Scheme 1.13a).[42] The authors utilized AcOOH for the in situ generation of μ-oxo-bridged hypervalent iodine(III) organocatalysts **26** through the oxidation of the bis-(iodoarene) species **25**. Subsequently, the same strategy was employed by the Antonchick and the Zhu groups for the synthesis of carbazoles **28** and pyrido[1,2-a]-benzimidazoles **29**, respectively (Scheme 1.3b and 1.13c).[43,44] Xue *et al.* have also utilized AcOOH as oxidant in the one-pot, sequential synthesis of 2-halophenanthridinones **30** from N-methoxybenzamides (Scheme 1.13d).[45] The authors proposed that the process is initiated by a C−H amidation of arenes, followed by a regioselective halogenation reaction. The introduction of TBAB (tetrabutylammonium bromide) and TBAC (tetrabutylammonium chloride) served as halogen sources. Among the solvents tested, HFIP emerged as the optimal choice, with TFE, DCM, DMF, and DMSO yielding lower product yields.

42 Dohi, T.; Takenaga, N.; Fukushima, K.-i.; Uchiyama, T.; Kato, D.; Motoo, S.; Fujioka, H.; Kita, Y. *Chem. Commun.* **2010**, *46*, 7697.
43 Antonchick, A. P.; Samanta, R.; Kulikov, K.; Lategahn, J. *Angew. Chem., Int. Ed.* **2011**, *50*, 8605.
44 He, Y.; Huang, J.; Liang, D.; Liu, L.; Zhu, Q. *Chem. Commun.* **2013**, *49*, 7352.
45 Liang, D.; Sersen, D.; Yang, C.; Deschamps, J. R.; Imler, G. H.; Jiang, C.; Xue, F. *Org. Biomol. Chem.* **2017**, *15*, 4390.

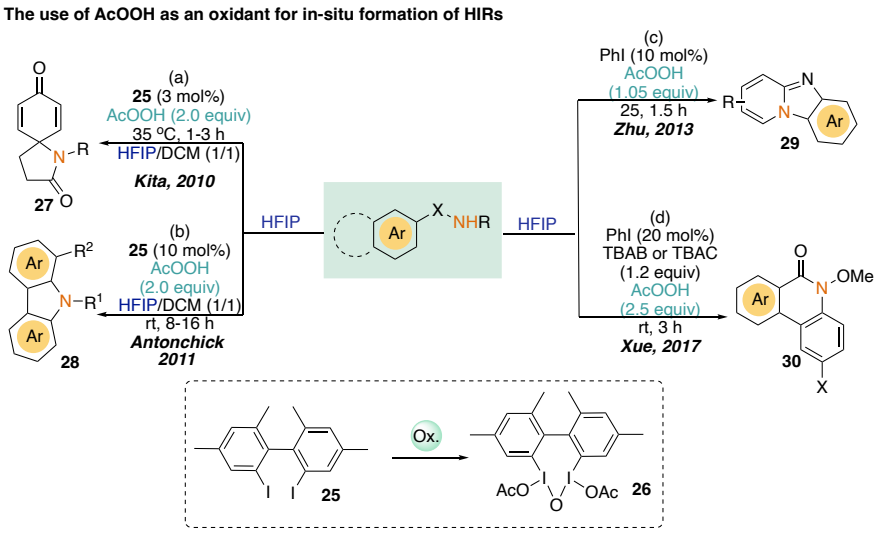

Scheme 1.13. ArI-catalyzed intramolecular C(sp^2)–H aminations using other oxidants

The use of selectfluor as an oxidant for the *in situ* generation of HIR was reported by the Driver group in 2020 (Scheme 1.14).[46] This approach led to the synthesis of a range of spirocyclic 3H-indole derivatives **32**, achieving great yields with low catalyst loading (1 mol% of iodobenzene). Notably, the addition of water as an additive within the HFIP solvent system resulted in enhanced yields compared to using HFIP alone, ultimately leading to nearly quantitative product formation.

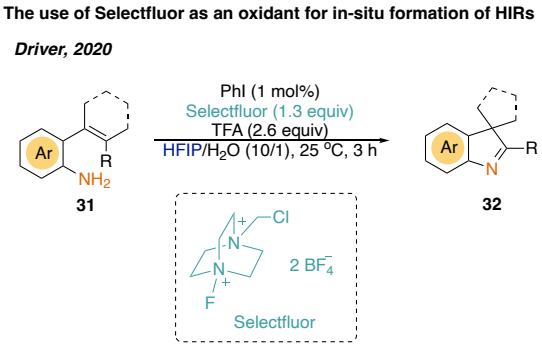

Scheme 1.14. ArI-catalyzed intramolecular C(sp^2)–H aminations using selectfluor as an oxidant

Despite the remarkable importance of saturated aza-heterocycles in medicinal chemistry, the exploration of HFIP-promoted HIR-induced C(sp^3)–H bond cleavage remains extremely limited. Indeed, there is only one example in the literature that

46 Deng, T.; Shi, E.; Thomas, E.; Driver, T. G. *Org. Lett.* **2020**, *22*, 9102.

harnesses this appealing strategy for enabling intramolecular C(sp^3)–N bond-forming reactions (Scheme 1.15). In 2015, the Shi group developed an intramolecular C(sp^3)–H amination protocol that combines catalytic amounts of an iodoarene (**34**) along with *m*-CPBA to functionalize sterically hindered tertiary C–H bonds by generating *in situ* of $ArI(OAc)_2$ reagents.[47] DFT calculations supported a concerted mechanism consisting of the formation of intermediate **A**, resulting from the interaction between benzamide **33** and $ArI(OAc)_2$ through a ligand exchange mechanism with hypervalent iodine. Subsequently, the dissociation of acetate from intermediate **A** led to the creation of an iodonium intermediate **B**. The cation **B** was predicted to be much more reactive toward nucleophilic C(sp^3)–H activation. The hydride transferred from tertiary carbon to nitrogen via an S_N2-like transition state **TS** to form the final product **35**.

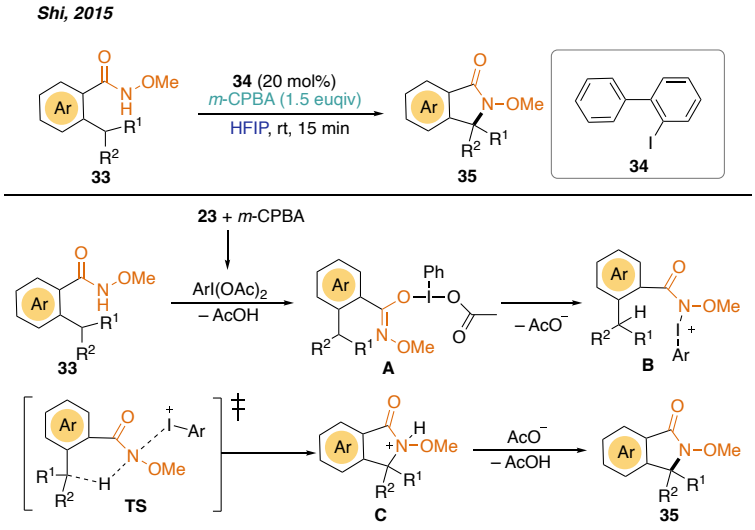

Scheme 1.15. ArI-catalyzed intramolecular C(sp^3)–H aminations using *m*-CPBA as an oxidant

The summarized examples in this section show how merging HIRs with HFIP offers a powerful platform for forging C–N bonds via metal-free C–H functionalization reactions. While inter- and intramolecular strategies have already shown the synthetic potential of this combination with aromatic substrates, aliphatic scaffolds remain barely explored.

47 Zhu, C.; Liang, Y.; Hong, X.; Sun, H.; Sun, W. Y.; Houk, K. N.; Shi, Z. *J. Am. Chem. Soc.* **2015**, *137*, 7564.

1.3. HFIP in Cp*Co catalysis

Now more than ever, organometallic transition metal (TM) catalysis plays an increasingly crucial role for fulfilling humankind necessities and well-being. These reactions have revolutionized how chemists activate and forge chemical bonds by the direct interaction of a TM center with organic fragments. Its importance in our daily lives is undeniable by providing synthetic solutions for constructing highly demanded building blocks for modern life – from improved materials to new drugs. In this context, noble metal-catalyzed cross-coupling and directed C–H functionalization reactions, are stunning testaments to the power of organometallic chemistry to lead to major scientific landmarks in academia and industry (Scheme 1.16). These transformations have opened new venues for the construction of carbon–carbon and carbon–heteroatom bonds in a predictable and regioselective manner. Indeed, in 2010, Suzuki and Negishi, and Heck, received the Nobel Prize in Chemistry for the introduction of Pd-catalyzed cross-couplings into the synthetic toolkit. [48] Moreover, ligand-assisted C–H functionalizations have become a major cornerstone in modern organic synthesis. The continuous improvement of their reaction conditions has pushed both fields towards the development of more efficient and sophisticated transformations.

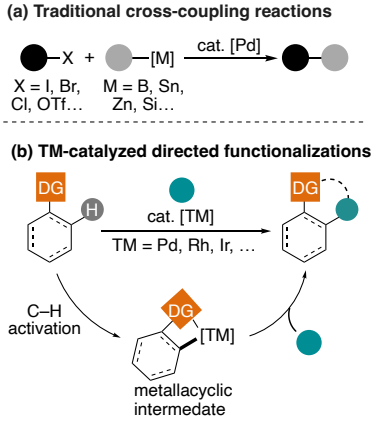

Scheme 1.16. TM-catalyzed cross-coupling reactions and directed C–H functionalizations

While the potential beneficial effect of HFIP in cross-coupling reactions remains completely unprecedented in traditional cross-coupling reactions, this perfluorinated solvent has already demonstrated its remarkable capability to enhance the efficiency of

[48] Johansson Seechurn, C. C. C.; Kitching, M. O.; Colacot, T. J.; Snleckus, V. *Angew. Chem. Int. Ed.* **2012**, *51*, 5062.

directed C–H bond activation reactions. Specifically, in the following sections, we will cover selected examples of directed C–H functionalization reactions catalyzed by Cp^*Co^{III} systems where the employment of HFIP has been found to play a profound influence on reactivity. These transformations are in close relationship, in terms of the elementary steps involved in the corresponding catalytic cycles, with the site-selective Cp*Co-catalyzed cross-couplings promoted by HFIP that will be explored in *Chapter III*.

1.3.1. Cp*Co-catalyzed directed C–H functionalization reactions

Over the past decades, TM-catalyzed directed C–H bond functionalization has emerged as an extremely powerful tool within synthetic organic chemistry for the formation of both C–C and C–heteroatom bonds in an atom-economical manner. These strategies, involving metallacyclic intermediates, exhibit a tremendous potential for *(i)* promoting the coupling with diverse partners, *(ii)* minimizing the by-product formation and *(iii)* controlling the site-selectivity by using substrates containing Lewis basic moieties, commonly named directing groups (DGs). These strongly (e.g., pyridine, pyrimidine, imine) or weakly (e.g., ketone, aldehyde, ester, amide) coordinating moieties bind to the metal center facilitating the reactivity at a proximal site in molecules that contain multitude of C–H bonds. During decades, these catalytic systems required noble TM such as Ru, Rh or Pd for the efficient construction of organic molecules.[49] However, in the decade, catalysts based on more cost-effective first-row metals,[49j] such as cobalt, have emerged as a very attractive alternative to precious metals.[50] Apart from the evident advantages of being earth-abundant and

[49] (a) Lyons, T. W.; Sanford, M. S. *Chem. Rev.* **2010**, *110*, 1147. (b) Engle, K. M.; Mei, T.-S.; Wasa, M.; Yu, J.-Q. *Acc. Chem. Rev*. **2012**, *45*, 788. (c) Rouquet, G.; Chatani, N. *Angew. Chem. Int. Ed*. **2013**, *52*, 11726. (d) Wencel-Delord, J.; Glorius, F. *Nat. Chem.* **2013,** *5*, 369. (e) Arockiam, P. B.; Bruneau, C.; Dixneuf, P. H. *Chem. Rev.* **2015**, *112*, 5879. (f) Daugulis, O.; Roane, J.; Tran, L. D. *Acc. Chem. Res.* **2015**, *48*, 1053. (g) He, J.; Wasa, M.; Chan, K. S. L.; Shao, Q.; Yu, J.-Q. *Chem. Rev.* **2017***, 117*, 8754. (h) Sambiagio, C.; Schönbauer, D.; Blieck, R.; Dao-Huy, T.; Pototschnig, G; Schaaf, P.; Wiesinger, T.; Zia, M. F.; Wencel-Delord, J.; Besset, T.; Maes, B. U. W.; Schnürch, M. *Chem. Soc. Rev.* **2018**, *47*, 6603. (i) Gandeepan, P.; Ackermann, L. *Chem* **2018**, *4*, 199. (j) Gandeepan, G.; Müller, T.; Zell, D.; Cera, G.; Warratz, S.; Ackermann, L. *Chem. Rev.* **2019**, *4*, 2192.

[50] (a) Moselage, M.; Li, J.; Ackermann, L. *ACS Catal.* **2016**, *6*, 498. (b) Wang, S.; Chen, S.-Y.; Yu, X.-Q. *Chem. Commun.* **2017**, *53*, 3165. (c) Chirila, P. G.; Whiteoak, C. J. *Dalton Trans.* **2017**, *46*, 9721. (d) Yoshino, T.; Matsunaga, S. *Adv. Synth. Catal.* **2017**, *359*, 1245. (e) Baccalini, A.; Vergura, S.; Dolui, P.; Zanoni, G.; Maiti, G. *Org. Biomol. Chem.* **2019**, *17*, 10119. (f) Ghorai, J.; Anbarasan, P. *Asian J. Org. Chem.* **2019**, *8*, 430. (g) Mei, R.;

inexpensive ($0.03/g Co vs $132/g Rh),[51] cobalt catalysts offer a rich manifold of reactivity patterns, not only mimicking precious metals but also exhibiting a unique and versatile reactivity due to a facile access to multiple oxidation states through 1- or 2-electron processes. The first example of a chelation-assisted transition-metal catalyzed C–H functionalization was reported by Murahashi in 1950s using a cobalt catalyst.[52] However, the tremendous potential of cobalt for facilitating directed C–H functionalization reactions have remained underexploited for more than 50 year, until its renaissance as a promising tool in organic synthesis.[50a] In particular, over the past years, the employment of Cp*Co^{III} complexes, analogous to active Rh^{III} catalysts for C–H activation[53] and known since the mid-70s,[54] has represented a tremendous advance in cobalt catalysis (Scheme 1.17).[50] Since the pioneering work by Kanai and Matsunaga in 2013,[55] different research groups have demonstrated the potential of Cp*Co^{III} complexes to promote C–C and C–heteroatom bond-forming reactions, specially using electrophilic coupling partners.[50] This distinctive behaviour is attributed to the nature of the Cp*Co^{III}–C bond in the putative cobaltacycle formed via C–H activation.[56] Since cobalt is less electronegative than rhodium, the Cp*Co^{III}–C bond is more polarized than the one present in Cp*Rh^{III}–C species. Thus, the higher nucleophilicity of **A**-type intermediates in Scheme 1.17 allow them to react with less electrophilic moieties.

Dhawa, U.; Samanta, R. C.; Ma, W.; Wencel-Delord, J.; Ackermann, L. *ChemSusChem* **2020**, *13*, 3306.

51 https://www.dailymetalprice.com/ accessed on 23/08/2023.

52 Murahashi, S. *J. Am. Chem. Soc.* **1955**, *77*, 6403.

53 (a) Colby, D. A.; Tsai, A. S.; Bergman, R. G.; Ellman, J. A. *Acc. Chem. Res.* **2012**, *45*, 814. (b) Song, G.; Li, X. *Acc. Chem. Res.* **2015**, *48*, 1020.

54 Roe, D. M.; Maitlis, P. M. *J. Chem. Soc. A* **1971**, 3173.

55 Yoshino, T.; Ikemoto, H.; Matsunaga, S.; Kanai, M. *Angew. Chem. Int. Ed.* **2013**, *52*, 2207.

56 Ikemoto, H.; Yoshino, T.; Sakata, K.; Matsunaga, S.; Kanai, M. *J. Am. Chem. Soc.* **2014**, *136*, 5424.

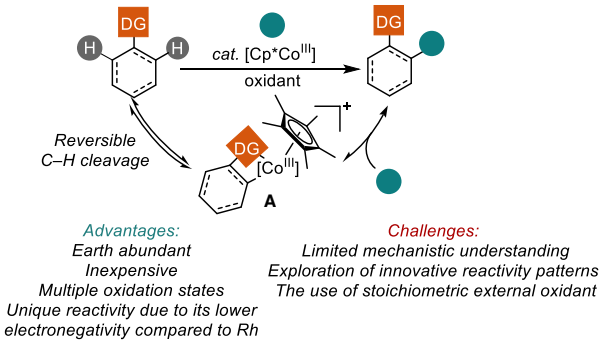

Scheme 1.17. Cp*Co^{III}-catalyzed directed C–H functionalization.

In alignment with synthetic protocols catalyzed by alternative TM-based systems,[57] recent studies have displayed that the efficiency of these cobalt-catalyzed C–H functionalizations can be significantly improved when HFIP is employed as solvent. It has the capability to enhance the electrophilic metallation, interact through hydrogen bonding with the DGs embedded within the starting materials, stabilize the cationic metal species formed along the catalytic cycle or facilitate protodemetalation events. Considering all these factors, it becomes evident that HFIP could significantly influence the reaction pathways of these C–H activation reactions in numerous ways. Yet, the exact role that this perfluorinated alcohol plays remains obscure in most cases. Below, we will summarize relevant examples of the positive effect of HFIP on Cp*Co^{III}-catalyzed C–H functionalization reactions.

1.3.2. Cp*Co^{III}-catalyzed C–H functionalizations enhanced by HFIP

The use as directing groups of strong coordinating functionalities, such as pyridyl, pyrimidinyl or pyrazolyl, has been the primary responsible of the tremendous progress that site-selective TM-catalyzed C–H functionalizations have experienced in the last 15 years (Scheme 1.18).[58] Therefore, it is not a surprise that a significant amount of the disclosed Cp*Co-catalyzed protocols promoted by HFIP involve substrates bearing this type of DGs.

---

57 Motiwala, H. F.; Armaly, A. M.; Cacioppo, J. G.; Coombs, T. C.; Koehn, K. R. K.; Norwood, V. M.; Aubé, J. *Chem. Rev.* **2022**, *122*, 12544.

58 (a) Sambiagio, C.; Schönbauer, D.; Blieck, R.; Dao-Huy, T.; Pototschnig, G.; Schaaf, P.; Wiesinger, T.; Zia, M. F.; Wencel-Delord, J.; Besset, T.; Maes, B. U. W.; Schnürch, M. *Chem. Soc. Rev*. **2018**, *47*, 6603. (b) Shang, R.; Ilies, L.; Nakamura E. *Chem. Rev.* **2017**, *117*, 9086. (c) Liu, W.; Ackermann, L. *ACS Catal*. **2016**, *6*, 3743. (d) Aneeja, T.; Neetha, M.; Afsina, C. M. A.; Anilkumar, G. *RSC Adv*. **2020**, *10*, 34429.

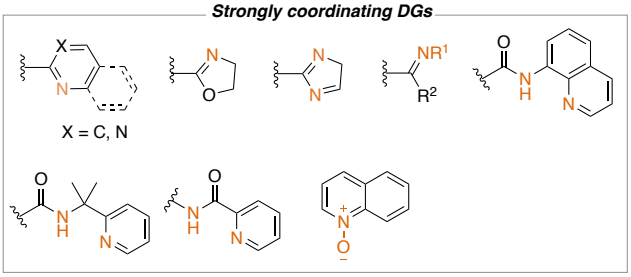

Scheme 1.18. Commonly used strong DGs

For example, in 2018, Matsunaga and co-workers described the coupling of 6-arylpurines and *gem*-difluoroalkenes **36** in HFIP, catalyzed by $[Cp^*Co(CH_3CN)_3](SbF_6)_2$, without requiring any additional additives (Scheme 1.19a).[59] This efficiency of this reaction, that afforded a series of monofluoroalkenes **42**, with a high selectivity for the (Z)-configuration, is diminished when the authors used solvents with lower polarity such as THF, DCE, and toluene. Employing similar reaction conditions, the Niu group developed in 2020 a C−H amidation protocol of *N*-pyrimidyl indolines using dioxazolones as nitrogen sources (Scheme 1.19b).[60] In the next year, the Lei group disclosed the $Cp^*Co(CO)I_2$-catalyzed directed C6 olefination of 2-pyridones with terminal alkynes (**40**and **42**) (Scheme 1.19c).[61] Interestingly when employing diaryl alkynes, a C6 olefination followed by a DG migration process resulted in the formation of tetrasubstituted 6-vinyl-2-pyridones **43**. The success of catalysis depends significantly on the careful selection of both solvent and additives.

59 Murakami, N.; Yoshida, M.; Yoshino, T.; Matsunaga, S. *Chem. Pharm. Bull.* **2018**, *66*, 51.
60 Yan, Q.; Huang, H.; Zhang, H.; Li, M.-H.; Yang, D.; Song, M.-P.; Niu, J.-L. *J. Org. Chem.* **2020**, *85*, 11190.
61 Xu, X.; Zhang, L.; Zhao, H.; Pan, Y.; Li, J.; Luo, Z.; Han, J.; Xu, L.; Lei, M. *Org. Lett.* **2021**, *23*, 4624.

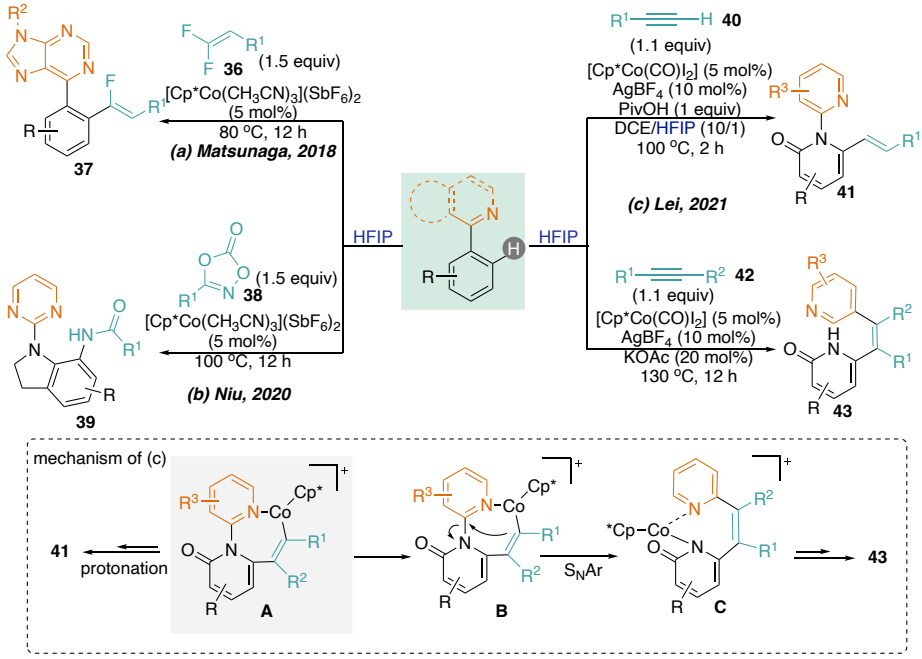

Scheme 1.19. The use N-heterocycles as DGs in Cp*Co^{III}-catalyzed C−H functionalizations

As mentioned above, there is a significant lack of fundamental understanding on how HFIP facilitates C–H functionalization processes. Indeed, one of the few mechanistic study that shows the beneficial effect of this alcohol in multiple elementary steps within a TM catalytic cycles was disclosed by our group in 2018.[62] Our initial studies uncovered a remarkable acceleration in the C–H activation of *N*-(2-pyrimidylindole) **44** by $[Cp^*Co(MeCN)_3](BF_4)_2$ upon the addition of HFIP, reducing the reaction time from 20 hours to just 5 minutes (Scheme 1.20). Driven by this extraordinary boosting effect, we conducted further investigations into the impact of HFIP in catalysis. The reaction between *N*-(2-pyrimidylindole) **44** and diphenylacetylene **47** was selected as the benchmark reaction.[63] Previous literature had described chemodivergent reactivity for these starting materials, leading to different products depending on the reaction conditions: hydroarylation *vs.* oxidative annulation. This diversity in reactivity patterns provided an ideal test case for investigating the role of HFIP, as it could potentially exert opposite effects. In both cases, our findings

62 Sanjosé-Orduna, J.; Sarria Toro, J. M.; Pérez-Temprano, M. H. *Angew. Chem. Int. Ed.* **2018**, *57*, 11369.

63 (a) Hazra, S.; Hirano, K.; Miura, M. *Asian J. Org. Chem.* **2019**, *8*, 1097. (b) Li, S.; Shi, P.; Liu, R.-H.; Hu, X.-H.; Loh, T.-P. *Org. Lett.* **2019**, *21*, 1602.

revealed that the addition of HFIP allowed for the use of milder reaction conditions to achieve the corresponding products in almost quantitative yields, but presumably due to different reasons. In the formation of the annulated product, it seems that its high polarity is crucial for solubilizing the salts present in the reaction mixture. On the other hand, in the hydroarylation reaction, its role as proton source probably facilitates the protodemetalation step of the catalytic cycle.

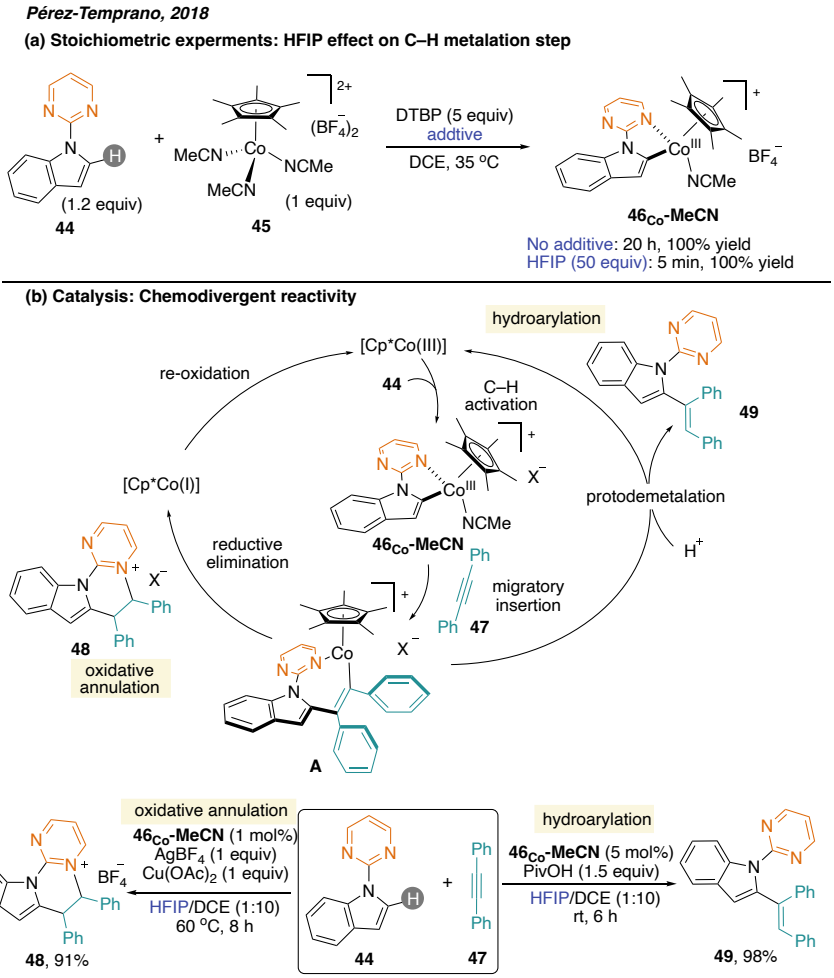

Scheme 1.20. Influence of HFIP on Cp*Co^{III}-catalyzed C−H functionalization

In 2016, Glorius and co-workers disclosed for the first time, how HFIP can favor the catalytic activity of these cobalt-catalyzed transformations. The authors reported a synthetic methodology that enabled the production of indole derivatives **51** using

hydrazines as starting materials (Scheme 1.21a).[64] The reaction pathway proposed for this transformation involved the formation on 7-membered ring cobaltacycle (intermediate **A**) after the C–H activation and alkyne insertion steps. Subsequently, a reductive elimination process yielded intermediate **C**, which was further subjected to an oxidative addition of the N−N bond to cobalt, ultimately leading to the formation of species **D**. As an alternate route, a concerted fragmentation of species **B** was considered as a potential pathway towards intermediate **D**. Protonation of intermediate **D** led to the desired indole product. In 2017, the Ackermann research group disclosed a synthetic approach involving a Cp*Co^{III}-catalyzed domino C−H/N−H allylation of aryl imidates (Scheme 1.21b).[65] This reaction demonstrated the optimal performance in HFIP, as evidenced by the superior yields achieved when compared to DCE, MeOH, or toluene.

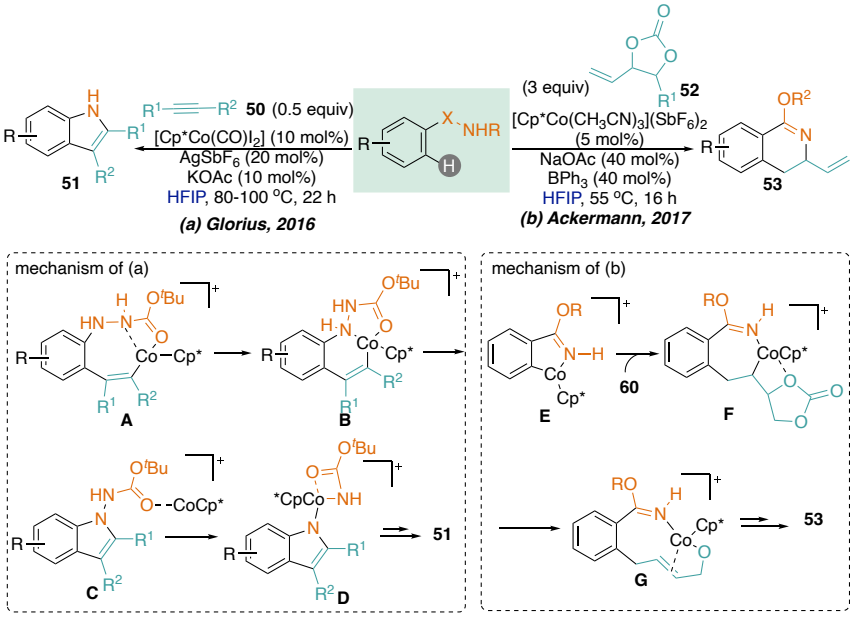

Scheme 1.21. The use of hydrazine and imidate as DGs in Cp*Co^{III}-catalyzed C−H functionalizations

Additionally, the Ackermann group showcased the utility of nitrones as DGs in Cp*Co-catalyzed C–H functionalizations. In 2016, they introduced a method involving the C–H/N–O functionalization of nitrones and alkynes **54** (Scheme 1.22a).[66] This

64 Lerchen, A.; Vasquez-Cespedes, S.; Glorius, F. *Angew. Chem. Int. Ed.* **2016**, *55*, 3208.
65 Wang, H.; Lorion, M. M.; Ackermann, L. *ACS Catal.* **2017**, *7*, 3430.
66 Wang, H.; Moselage, M.; González, M. J. Ackermann, L. *ACS Catal.* **2016**, *6*, 2705.

process was carried out in the presence of either sodium acetate or an amino acid ligand, within HFIP as the solvent. The reaction exhibited remarkable site- and regio-selectivity, particularly notable with unsymmetrical nitrones and alkynes. Moreover, the method displayed exceptional functional group tolerance and proved to be easily scalable. In 2020, Daugulis and co-workers unveiled an annulation reaction under Cp^*Co^{III} catalysis directed by N-iminopyridinium ylides (Scheme 1.22b).[67] Notably, the pyridine component, functioning as an internal oxidant, underwent cleavage during the reaction. HFIP was proved to be the superior choice of solvent, yielding better results compared to TFE. The reaction was found to be amenable to both aromatic and acrylic acid-derived ylides, showcasing its versatility and compatibility. In the same year, a Cp^*Co^{III}-catalyzed C−H amination of quinoline-N-oxides with dioxazolones **58** was reported by the Sharma group (Scheme 1.22c).[68] The reaction proceeded efficiently with excellent functional group compatibility. Optimization revealed that HFIP was the most suitable solvent, with TFE resulting in diminished yields.

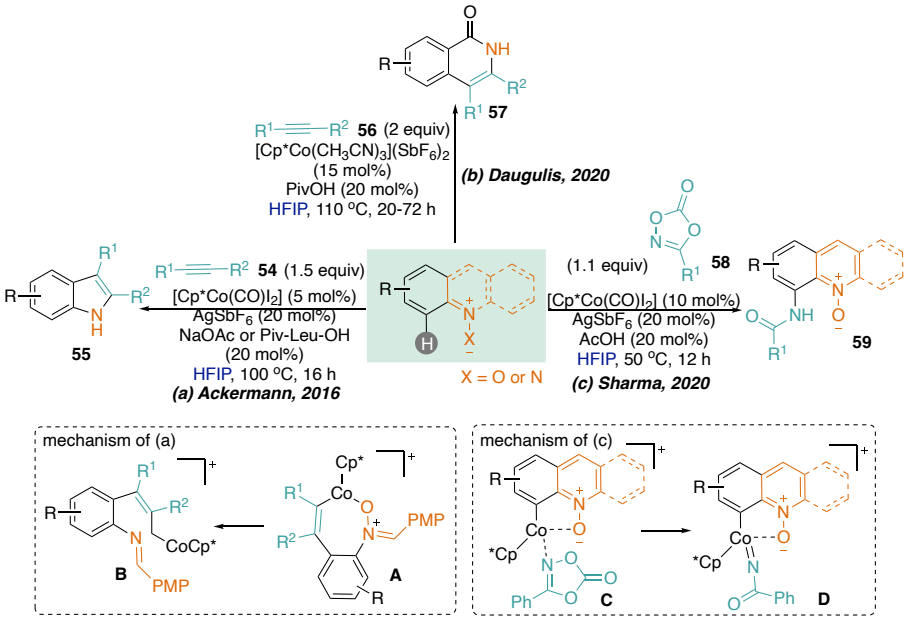

Scheme 1.22. The use of other strong DGs in C−H functionalizations under Cp^*Co^{III} catalysis

[67] Kwak, S. H.; Daugulis, O. *Chem. Commun.* **2020**, *56*, 11070.
[68] Dhiman, A. K.; Thakur, A.; Kumar, I.; Kumar, R.; Sharma, U. *J. Org. Chem.* **2020**, *85*, 9244.

It is worth noting that the the C(sp^3)–H functionalization catalyzed by Cp*Co^{III} could also be accomplished by employing N-heterocycles as DGs in HFIP. For example, the Sun group reported a Cp*Co(CO)I_2-catalyzed 1,4-addition of C(sp^3)–H bond of 8-methylquinolines to maleimides **61** in 2018 (Scheme 1.23).[69] Among the solvents tested, HFIP emerged as the most effective choice. In contrast, DCE and TFE resulted in poor yields of the desired alkylated product, and toluene yielded only trace amounts. The utilization of HFIP was proposed to assist in the protonolysis of the cyclometalated complex, facilitating the regeneration of the active cobalt species and the release of the addition product.

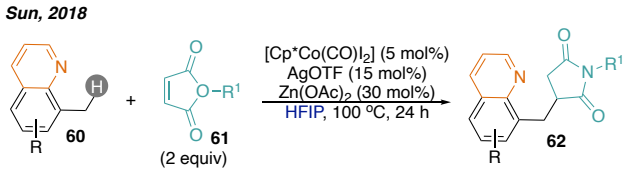

Scheme 1.23. Cp*Co^{III}-catalyzed C(sp^3)–H functionalization promoted by HFIP

Although strong DGs have been fundamental for the development of ligand-assisted C–H functionalizations, their use present multiple shortcomings. Their removal after the accomplishment of the corresponding coupling is often difficult and requires additional steps. Moreover, the substrates containing strongly coordinating DGs usually give metallacyclic intermediates that are thermodynamically too stable, which it might affect their subsequent reactivity with the targeted coupling partners. In addition, many of these DGs are not common functional groups in organic scaffolds, which limits the utility and applicability of the methodologies. In order to address these limitations, the synthetic community has implemented C–H functionalization reactions directe by weakly coordinated functional groups.[70] A key advantage of this approach is that the directing substrates contain common moieties found in synthetically relevant organic compounds (e.g., ketones, aldehydes, amides, or esters), offering a diverse

69 Chen, X.-X.; Ren, J.-T.; Xu, J.-L.; Xie, H.; Sun, W.; Li, Y.-M.; Sun, M. *Synlett* **2018**, *29*, 1601.

70 (a) Sambiagio, C.; Schönbauer, D.; Blieck, R.; Dao-Huy, T.; Pototschnig, G.; Schaaf, P.; Wiesinger, T.; Zia, M. F.; Wencel-Delord, J.; Besset, T.; Maes, B. U. W.; Schnürch M. *Chem. Soc. Rev.* **2018**, *47*, 6603. (b) Murali, K.; Machado, L. A.; Carvalho, R, L.; Pedrosa, L. F.; Mukherjee, R.; Júnior, E. N. D. S.; Maiti, D. *Chem. Eur. J.* **2021**, *27*, 12453. (c) Mandal, R.; Garai, B.; Sundararaju B. *ACS Catal.* **2022**, *12*, 3452.

scope and the potential participation in late-stage functionalization (LSF) strategies (**Scheme 1.24**).

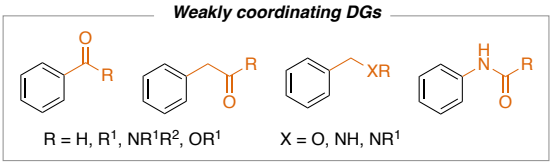

Scheme 1.24. Commonly used weakly DGs

In 2016, an annulation reaction directed by ester group under Cp*Co^{III} catalysis was reported by the Li group. Cp*Co(CO)I_2 was employed as precatalyst in combination with a silver salt as additive (**Scheme 1.25**a).[71] Furthermore, $Zn(OAc)_2$ was utilized to enhance the reactivity through metal coordination with the ester moiety. Notably, HFIP demonstrated superior performance in terms of product yields compared to TFE and DCE as solvents. Besides, amides could be also used as DG, as demonstrated by the Matsunaga group in 2016. They disclosed a HFIP-promoted Cp*Co(III)-catalyzed dehydrative C−H allylation of benzamides with allyl alcohols **65** (Scheme 1.25b).[72] HFIP was proposed to facilitate the formation of active species by promoting the dissociation of ligands from the cobalt catalyst. Similarly, a pivalamide DG was utilized in Cp*Co^{III}-catalyzed alkenylated reaction of indolines by Ravikumar in 2020 (Scheme 1.25c).[73] This methodology allowed the successful coupling of a range of activated alkenes, yet aliphatic alkenes and styrenes turned to be ineffective coupling partners in this context. The same group also demonstrated that an acetyl group could act as an DG in Cp*Co^{III}-catalyzed C-4 olefination of 3-acetyl indoles with activated olefins. Selective C(4)−H functionalization has been achieved using diverse Michael acceptors (acrylate and maleimide) simply by switching the additive from copper acetate to silver carbonate. Further the formation of a cobaltacycle intermediate was also detected through HRMS for mechanistic insight. HFIP was demonstrated as the best solvent, while THF, Toluene or dioxane did not give any products, and DCM, TFE or trifluorotoluene gave lower yield than HFIP. Furthermore, the same research group exhibited the acetyl group's potential as a DG in a Cp*Co^{III}-catalyzed C-4 olefination

71 Kong, L.; Yang, X.; Zhou, X.; Yu, S.; Li, X. *Org. Chem. Front*. **2016**, *3*, 813.
72 Bunno, Y.; Murakami, N.; Suzuki, Y.; Kanai, M.; Yoshino, T.; Matsunaga, S. *Org. Lett.* **2016**, *18*, 2216.
73 Banjare, S. K.; Biswal, P.; Ravikumar, P. C. *J. Org. Chem.* **2020**, *85*, 5330.

of 3-acetyl indoles with activated olefins **69** (Scheme 1.25d).[74] This approach enables the selective functionalization of the C4−H position using a variety of Michael acceptors, such as acrylate and maleimide. HFIP outperforms traditional organic solvents such as THF, toluene, dioxane, or DCM, and alternative perfluorinated ones, such as TFE, or trifluorotoluene.

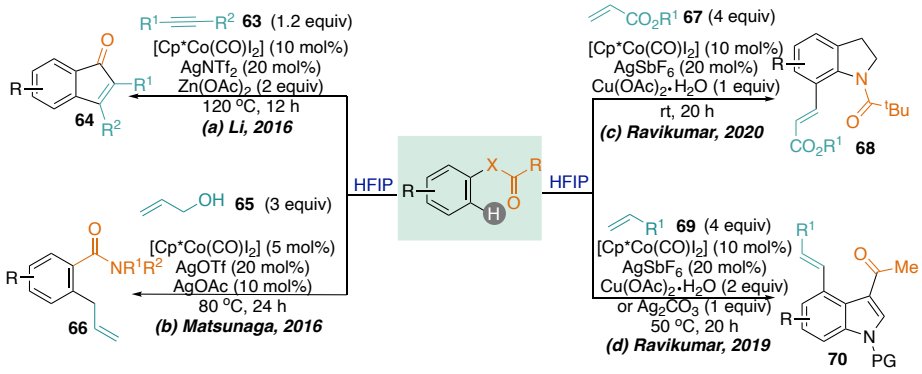

Scheme 1.25. The use of weak DGs in Cp^*Co^{III}-catalyzed C−H functionalizations

The examples summarize in this section highlight the tremendous impact that HFIP has provoked in organometallic chemistry, especially in directed TM-catalyzed C–H functionalization reactions. The widespread use of 1,1,1,3,3,3-hexafluoroisopropanol has primarily arisen from empirical observations, where reactions conducted in this perfluorinated alcohol consistently exhibit enhanced performance when compared to traditional organic solvents. Despite this progress, the exact role of HFIP in these transformations is still obscure. Moreover, its beneficial influence in alternative transformations, such as cross-coupling reactions, or its potential involvement beyond diamagnetic organometallic systems, remain unexplored.

74 Banjare, S. K.; Nanda, T.; Ravikumar, P. C. *Org. Lett.* **2019**, *21*, 8138.

1.4. General Objectives of this Doctoral Thesis

The role of organic solvents in facilitating chemical processes is rarely a point of discussion in organic synthesis, and if mentioned, it is usually approached at a fundamental level. Nonetheless, in recent years, the emergence of innovative organic solvents, especially perfluorinated ones such as HFIP, has led to remarkable breakthroughs in reaction discovery and development. Indeed, this solvent, which was not commonly integrated into the synthetic toolkit, possesses an exceptional attribute: the newly developed reactions either fail to proceed or show minimal activity in its absence. The disclosed reactivity is just the tip of the ice. Therefore, it is of particular interest to further explore whether HFIP could lead to the discovery of new reactivity patterns through reaction pathways that are unattainable with conventional organic solvents.

One of the main interests of our research group is to exploit reaction mechanisms as a reaction design tool for streamlining the development of more sustainable methodologies and unlocking new reaction modes currently unprecedented in organic synthesis. In the last years, we have focused our attention towards gathering a better understanding of the beneficial effect that HFIP exhibits in multiple synthetic fields.

The overall goal of the work presented in this dissertation is to design and develop new HFIP-assisted synthetic protocols by expanding the repertoire of roles that this perfluorinated alcohol can perform in metal-free and TM catalysis. On one hand, we explored the synergistic cooperation between hypervalent iodine(III) reagents and HFIP to circumvent existing synthetic shortcomings related to intramolecular metal-free C(sp^3)–H functionalization reactions. On the other hand, we interrogated, for the first time, whether the utilization of this solvent holds the potential to open up new exciting opportunities within cross-coupling reactions catalyzed by first-row TMs. In both cases, we envisaged to intertwine mechanistic studies & catalysis to investigate the principles that govern the targeted bond-forming events.

Chapter II. HFIP-Assisted Selective Intramolecular Synthesis of Heterocycles Enabled by Single Electron Transfer

2.1. Introduction

Saturated nitrogen-containing heterocycles (SNHets), such as azetidine, pyrrolidine, piperidine, or azepane, are widely present in the chemical space, particularly in medicinal chemistry.[1] These molecular fragments are frequently incorporated into drug-type architectures to enhance their biological activities, resulting in their prevalence in a diverse range of top-selling pharmaceuticals (Scheme 2.1). Intramolecular C(sp^3)–N bond-forming processes have emerged as highly efficient and practical routes for accessing these desirable structural motifs.[2] Although these approaches initially encounter challenges such as the thermodynamic and kinetic stability of C(sp^3)–H bonds or the control of site-selectivity in C–H bond cleavage, the synthetic community has made significant efforts to overcome these obstacles, providing a versatile toolkit for the streamlined construction of these molecules.

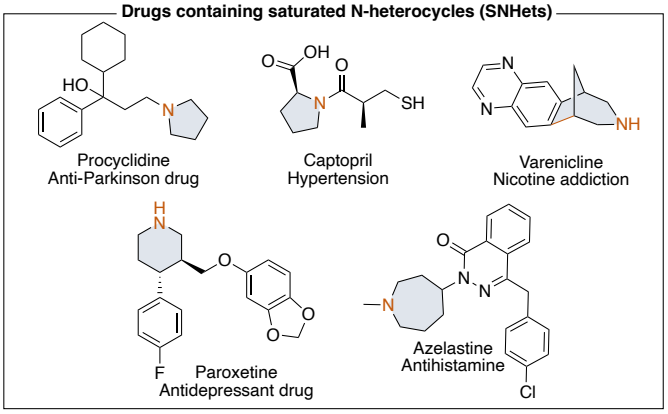

Scheme 2.1. Bioactive molecules containing saturated N-containing heterocycles (SNHets)

1 (a) Horton, D. A.; Bourne, G. T.; Smythe, M. L. *Chem. Rev*. **2003**, 103, 893. (b) Froidevaux, V.; Negrell, C.; Caillol, S.; Pascault, J.-P.; Boutevin, B. *Chem. Rev.* **2016**, *116*, 14181. (c) Tohme, R.; Darwiche, N.; Gali-Muhtasib, H. *Molecules* **2011**, *16*, 9665. (d) O'Hagan, D. *Nat. Prod. Rep*. **2000**, *17*, 435.

2 (a) Trowbridge, A.; Walton, S. M.; Gaunt, M. J.; *Chem. Rev.* **2020**, *120*, 2613. (b) Singh, R.; Mukherjee, A.; *ACS Catal.* **2019**, *9*, 3604. (c) Zhang, M.; Wang, Q.; Peng, Y.; Chen, Z.; Wan, C.; Chen, J.; Zhao, Y.; Zhang, R.; Zhang, A. Q.; *Chem. Commun. 2019*, **55**, 13048. (d) Hayashi, H.; Uchida, T. *Eur. J. Org. Chem.* **2020**, *2020*, 909.

There are three main approaches to achieve intramolecular C(sp^3)–H amination, including (1) transition-metal-catalyzed ligand-assisted C(sp^3)–H activation, (2) transition-metal-catalyzed nitrene C(sp^3)–H insertion, and (3) the Hofmann-Löffler-Freytag (HLF) reaction (Scheme 2.2).[3] Related to the theme of the doctoral thesis, harnessing hypervalent iodine reagent (HIR)-mediated C–H functionalizations emerges as an efficient strategy for constructing C–N bonds, offering enhanced environmental friendliness compared to TM catalysis. In the following sections, we will summarize selected examples of the intramolecular C(sp^3)–H amination via HLF reaction, illustrating their utility and limitations in accessing SNHets.

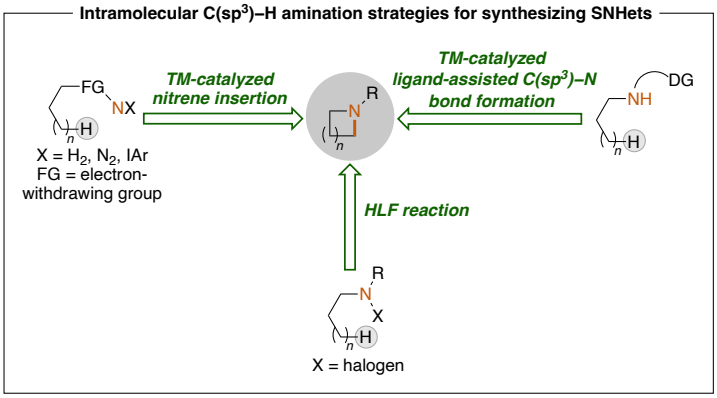

Scheme 2.2. Current synthetic strategies for accessing SNHets via intramolecular C(sp^3)–H amination reactions.

2.1.1. Amination via the Hofmann-Löffler-Freytag (HLF) reaction

The intramolecular amination of remote aliphatic C–H bonds via hydrogen atom transfer (HAT) reactions stands out as a very attracttive and general procedure for generating mainly 5-membered ring saturated N-based heterocycles. [4] These transformations are triggered by the thermal or the photochemical homolysis of the N–X bond of a N-halogenated amine in acidic media.[5] The generated protonated aminyl

[3] (a) S. Minakata, *Acc. Chem. Res*. **2009**, *42*, 1172. (b) J. L. Jeffrey, R. Sarpong, *Chem. Sci*. **2013**, *4*, 4092. (c) T. Xiong, Q. Zhang, *Chem. Soc. Rev*. **2016**, *45*, 3069. (d) D. Šakić, H. Zipse, *Adv. Synth. Catal*. **2016**, *358*, 3983. (e) Y. Park, Y. Kim, S. Chang, *Chem. Rev*. **2017**, *117*, 9247. (f) J. C. K. Chu, T. Rovis, *Angew. Chem. Int. Ed*. **2018**, *57*, 62. (g) L. M. Stateman, K. M. Nakafuku, D. A. Nagib, *Synthesis* **2018**, **50**, 1569.

[4] (a) Mayer, J. M. *Acc. Chem. Res.* **2011**, *44*, 36. (b) Chiba, S.; Chen, H. *Org. Biomol. Chem*. **2014**, *12*, 4051. (c) Zhao, Y.; Xia, W. *Chem. Soc. Rev*. **2018**, *47*, 2591.

[5] (a) Wolff, M. E. *Chem. Rev.* **1963**, *63*, 55. (b) Corey, E. J.; Hertler, W. R. *J. Am. Chem. Soc*. **1960**, *82*, 1657.

radical participates in an intramolecular 1,5-HAT to give a carbon centered radical.[6] Subsequently, this species is trapped by recombination with a caged X• or it participates in a halogen atom abstraction from the protonated starting material to generate usually a δ-halogenated amine. The final cyclization is formed via a S_N2 reaction, usually upon treatment with a base (Scheme 2.3).

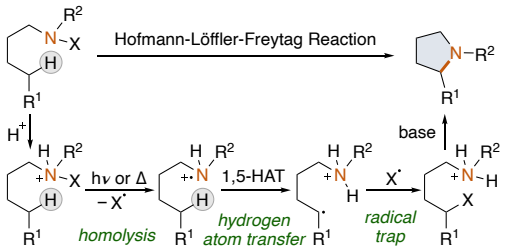

Scheme 2.3. Hofmann-Löffler-Freytag mechanism.

The first example of this transformation was reported in the early 1880s by Hofmann (Scheme 2.4). In this seminal work, the treatment of N-bromo-2-propylpiperidine with hot sulfuric acid, and subsequent basification, afforded the formation of a bicyclic tertiary amine.[7] In 1909, Löffler and Freytag extended the scope to the use of secondary amines, providing a versatile method for the synthesis of pyrrolidines.[8] During the 1960s, Corey and Wawzonek provided the initial experimental evidences that supported the nitrogen to carbon radical relay when no cyclized product was observed in the absence of radical initiators.[9] Despite the significant synthetic progress, the initial reports on HLF protocols were restricted by the need for haloamine pre-formation and/or the utilization of harsh acidic reaction conditions. Within this context, Suárez *et al.* tackled these shortcomings through two significant breakthroughs. First, they were capable of generating the N–halogen bond *in situ* from the corresponding amine, by combining iodine and hypervalent iodine reagents. Second, the introduction of electron-withdrawing groups (such as –CN or –

6 (a) Nechab, M.; Mondal, S.; Bertrand, M. P. *Chem. Eur. J.* **2014**, *20*, 16034. (b) Robertson, J.; Pillai, J.; Lush, R. K. *Chem. Soc. Rev.* **2001**, *30*, 94. (c) Capaldo, L.; Ravelli, D. *Eur. J. Org. Chem*. **2017**, *2017*, 2056.

7 Hofmann, A. W. *Ber. Dtsch. Chem. Ges*. **1883**, *16*, 558.

8 Löffler, K.; Freytag, C. *Ber*. **1909**, *42*, 3427.

9 (a) E. J. Corey, W. R. Hertler, *J. Am. Chem. Soc*. **1960**, *82*, 1657. (b) S. Wawzonek, P. J. Thelen, *J. Am. Chem. Soc*. **1950**, *72*, 2118. (c) S. Wawzonek, M. F. Nelson, P. J. Thelen, *J. Am. Chem. Soc*. **1951**, *73*, 2806. (d) S. Wawzonek, T. P. Culbertson, *J. Am. Chem. Soc*. **1959**, *81*, 3367.

NO_2) onto the nitrogen atom enhanced the reactivity of the resulting N-centered radical, facilitating its participation in the HAT process under neutral conditions. Thanks to these discoveries, it became feasible to apply these methodologies to more complex scaffolds, including starting materials containing acid-sensitive groups or precursors of natural products.

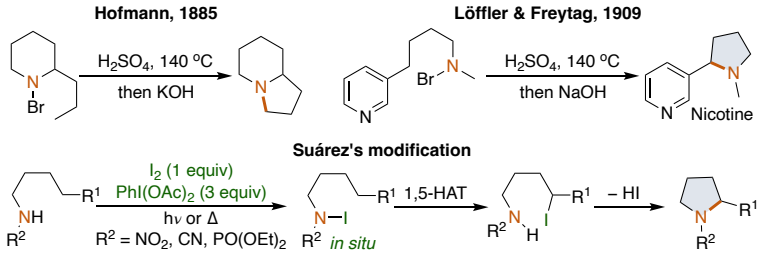

Scheme 2.4. Early examples of HLF reaction

Inspired by these literature precedents, over the past decades, different research groups have contributed to develop more robust and straightforward cyclization events.[3] For example, major accomplishments have been fulfilled developing iodine-catalyzed methodologies (Scheme 2.5). The presence of stoichiometric amounts of I_2 tends to provide undesired oxidation reactions of weaker α-aminyl C–H bonds, which competes with 1,5-HAT processes, due to the AcOI homolysis-derived radicals.[10] In this context, Muñiz and co-workers have designed very elegant strategies to suppress these side-reactions. In 2015, they reported the first example of an HLF reaction using iodine as catalyst (Scheme 2.5). In this work, the authors used 2.5 mol% of I_2 in the presence of a hypervalent iodine oxidant, PhI(*m*CBA)$_2$ (*m*CBA = 3-chlorobenzoate).[11] From a mechanistic perspective, this reaction is proposed to proceed by two interconnected catalytic cycles encompassing a radical chain reaction induced by visible light. Active electrophilic iodine(I) I*m*CBA catalyst is believed to be generated from the comproportionation of molecular iodine and PhI(*m*CBA)$_2$ oxidant. This active catalyst enables the iodination of the starting material to form halogenated sulfonamide **A**. Homolytic cleavage of the N–I bond upon light irradiation generates nitrogen-centered radical **B** which performs a 1,5-HAT to afford carbon-centered radical **C**. Intermediate **C** then triggers a chain-propagation by abstracting an iodine atom from **A**

10 (a) Courtneidge, J. L.; Lusztyk, J.; Pagé, D. *Tetrahedron Lett*. **1994**, *35*, 1003. (b) Wappes, E. A.; Fosu, S. C.; Chopko, T. C.; Nagib, D. A. *Angew. Chem. Int. Ed*. **2016**, *55*, 9974.

11 Martínez, C.; Muñiz, K. *Angew. Chem. Int. Ed.* **2015**, *54*, 8287.

to generate alkyl-iodide **D** and nitrogen-centered radical **B** simultaneously. At this point, a direct intramolecular nucleophilic displacement could be envisioned via oxidation to I(III) reagents. The formation of this alkyl iodine(III) leaving group remains crucial for the kinetics adjustment in this rather complex mechanism thus ensuring the high performance of the reaction and allowing the functionalization at non-activated positions.[12] Intramolecular nucleophilic displacement at **E** yields the final product and regenerates the active iodine(I) catalyst. This method is applicable to the amination of a wide variety of primary, secondary, and tertiary C(sp^3)–H bonds in excellent yields.

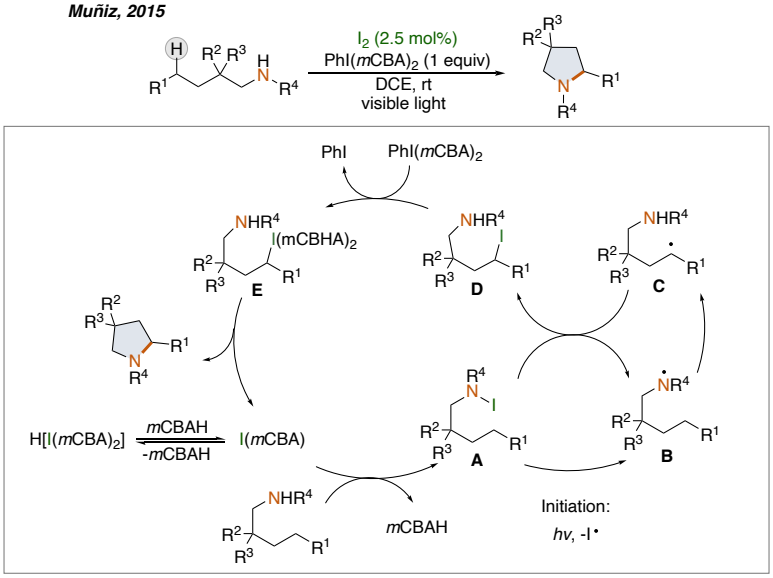

Scheme 2.5. Iodine-catalyzed Hofmann-Löffler reaction mechanism.

Taking into consideration the mechanistic rationale depicted in Scheme 2.5, Muñiz and co-workers developed a series of amination reactions via catalytic HLF reactions (Scheme 2.6). Additional modifications allowed them to perform the reaction using more economical 3-chloro perbenzoic acid (*m*CPBA) as terminal oxidant (Scheme 2.6a).[13] In 2017, the same group reported a dual light-activated cooperative iodine and

12 (a) Okuyama, T.; Takino, T.; Sueda, T.; Ochiai, M. *J. Am. Chem. Soc.* **1995**, *117*, 3360. (b) Ochiai, M. in *Chemistry of Hypervalent Compounds* (Ed.: Akiba, K.), Wiley-VCH, New York, *359*, **1999**.

13 Duhamel, T.; Stein, C. J.; Martínez, C.; Reiher, M.; Muñiz, K. *ACS Catal.* **2018**, *8*, 3918.

photoredox catalysis protocol for the synthesis of 2-arylpyrrolidines (Scheme 2.6b).[14] In this work, the iodine catalyst activates a remote C(sp^3)–H bond (1,5-HAT process) under visible light irradiation, while the organic photoredox catalyst (TPT) allows the regeneration of I_2, after the product release. In a follow-up work, the same group reported a bromine-based catalytic system that effectively promotes selective C(sp^3)–H amination toward pyrrolidines employing a combination of tetrabutylammonium bromide and *m*CPBA (Scheme 2.6c).[15]

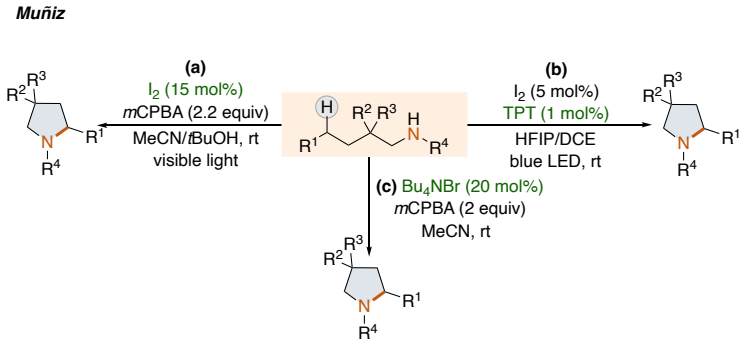

Scheme 2.6. Recent advances of modification of HLF reaction developed by the Muñiz group

At the same time than Muñiz reported the first catalytic HFL methodology, Herrera and co-workers described the chemoselective amination of primary C(sp^3)–H bonds by using sulfonamides as N-centered radical precursors (Scheme 2.7).[16] This work showed the potential of these reactions beyond traditional weak aliphatic C–H bonds (benzylic, tertiary, α-oxy). In addition, it also demonstrated that it is possible to obtain selectively pyrrolidine or 2-pyrrolidinone derivatives, via single or multiple HAT processes (SHAT or MHAT) respectively, by controlling the addition of oxidant. Therefore, this work offers an alternative to avoid undesirable I_2-mediated oxidations.

14 Becker, P.; Duhamel, T.; J. Stein, C. J.; Reiher, M.; Muñiz, K. *Angew. Chem. Int. Ed*. **2017**, *56*, 8004.
15 Becker, P.; Duhamel, T.; Martínez, C.; Muñiz, K. *Angew. Chem. Int. Ed.* **2018**, *57*, 5166.
16 Paz, N. R.; Rodríguez-Sosa, D.; Valdés, H.; Marticorena, R.; Melián, D.; Copano, M. B.; González, C. C.; Herrera, A, J. *Org. Lett*. **2015**, *17*, 2370.

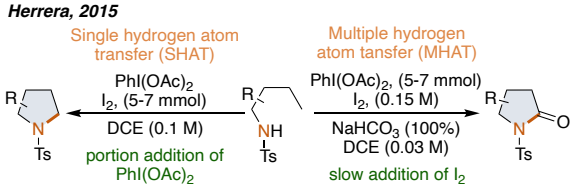

Scheme 2.7. Herrera´s modification for the HLF reaction

In this regard, in 2016, Nagib and co-workers reported another strategy to circumvent the side-reactions associated to the employment of excess of I_2.[10b] The authors described a triiodide-mediated amination strategy where I_3^- acts as a I_2 reservoir (Scheme 2.8). Triiodide is generated *in situ* by the oxidation of NaI to I_2, which in the presence of excess of I^- forms I_3^-. This dynamic equilibrium reduces the amount of available I_2 in the reaction media, attenuating the negative effect of the excess of AcOI in solution.

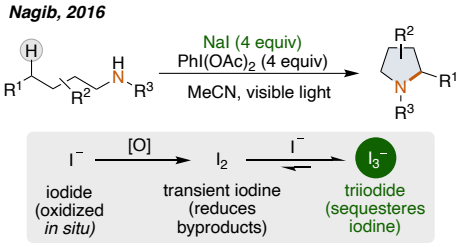

Scheme 2.8. Nagib´s modification for the HLF reaction

In 2015, Yu and co-workers uncovered a protocol for the δ-iodo-γ-lactamization of aliphatic amides by reaction with N-iodosuccinimide (NIS) and trimethyl azide ($TMSN_3$), via 1,5- and 1,6-abstractions (Scheme 2.9).[17] The proposed mechanism, for this *a priori* unexpected transformation, involves the iodination of the starting amide by treatment with NIS to give a N–I intermediate that, following the Suárez-HLF method, provides the corresponding lactam. Subsequently an *in situ* generated azide radical promotes a β-C−N bond scission, to afford a terminal olefin. The final iodinated product is obtained after a radical 5-exo-trig cyclization and the recombination with an iodine free radical. The authors exploited this reactivity not only to synthesize a wide variety of iodolactams, but also to subsequent diversify them into 1,2-amino alcohol

[17] Liu, T.; Mei, T.-S.; Yu, J.-Q. *J. Am. Chem. Soc.* **2015**, *137*, 5871.

and allylic amide derivatives, some of them close related to drug analogues, such as vigabatrin.

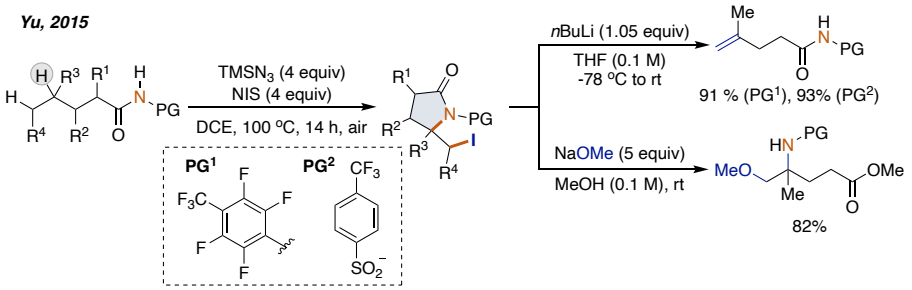

Scheme 2.9. γ,δ,ε-C(sp^3)−H functionalization through directed radical H-abstraction

Over the past years, the use of photochemistry and the implementation of electrochemical strategies have opened innovative and appealing venues in the context of HFL transformations. In 2015, Yu reported a visible light photoredox-mediated protocol for the remote amination of N-chlorosulfonamides (NCSs) (Scheme 2.10a).[18] This methodology proceeds with good to excellent yields at room temperature, under mildly basic conditions, and using very low catalyst loading (0.1 mol%) of $Ir(ppy)_2(dtbbpy)PF_6$. In this transformation, the nitrogen-centered radical is proposed to be generated through an oxidative quenching of the excited state Ir^{III*} with the corresponding NCS. Another major breakthrough in the field was the utilization of electric current as reagent, which has the potential of preventing the use of metal catalysts, halogenated reagents, and/or stoichiometric amounts of chemical oxidants. For example, in 2018 Lei and co-workers disclosed a electrochemical oxidative induced amination of primary, secondary and tertiary C(sp^3)−H bonds (Scheme 2.10b).[19] This site-selective electrosynthetic protocol enables the access to a wide variety of pyrrolidine derivatives and it is compatible with different N-protecting groups. A plausible mechanism for this electro-oxidative HLF reaction involves the generation of the aminyl radical by a single electron oxidation on the anode. After the 1,5-HAT, the corresponding C-centered radical undergoes another anodic oxidation to afford a carbon cation intermediate that provides the desired product after a nucleophilic attack by the sulfonyl group. Recently, Stahl and co-workers have merged photo- and electrochemical strategies for the promoting the intramolecular amination

18 Qin, Q.; Yu, S. *Org. Lett.* **2015**, *17*, 1894.
19 Hu, X.; Zhang, G.; Bu, F.; Nie, L. A. Lei, *ACS Catal.* **2018**, *8*, 9370.

of C(sp^3)–H bonds (Scheme 2.10c).[20] A key feature of this iodide-mediated process is its broad functional group compatibility due to the combination of low applied potentials and the photochemical induced cleavage of intermediate N–I bonds.

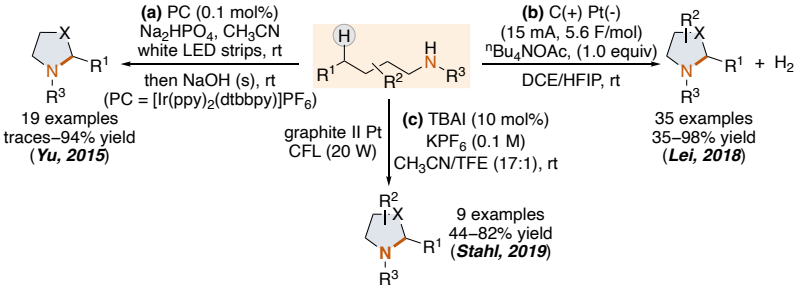

Scheme 2.10. Visible-light and electrochemical-oxidation-induced remote intramolecular C(sp^3)–H aminations

These metal-free HLF protocols enable the transformation of acyclic amines into SNHets through the formation of an amidyl radical that triggers the intramolecular abstraction of δ C−H bonds. Despite significant advances in terms of synthetic applicability and milder nature of the reported reaction conditions due to the exploitation of hypervalent iodine(III) reagent (HIR), such as $PhI(OCOCF_3)_2$ (PIFA) or $PhI(OAc)_2$ (PIDA), there are remaining long-lasting challenges associated to these intramolecular C(sp^3)–H aminations (Scheme 2.11).[3g,21] The high bond-dissociation free energy of N–H bonds (107-110 kcal/mol), hampers the homolytic generation of the N-centred radical.[22] Thus, the efficient in situ generation of this open-shell species requires the presence of iodine or iodide for prefunctionalising the starting material into an N-halogenated amines. Furthermore, the HLF methodology exhibits a high regioselectivity towards 5-membered SNHets formation, as 1,6-HAT processes are kinetically disfavoured even for benzylic positions.[6a] As a result, the access to piperidine derivatives, the most frequent nitrogen heterocycle in medicinal chemistry,[23]

20 Wang, F.; Stahl, S. S. *Angew. Chem. Int. Ed*. **2019**, *58*, 6385.

21 (a) Kandimalla, S. R.; Parvathaneni, S. P.; Sabitha G.; B. V. S. *Eur. J. Org. Chem.* **2019**, 1687. (b) Zhang, J.; Pérez-Temprano, M. H. *Chimia* **2020**, *74*, 895. (c) Guo, W.; Wang, Q.; Zhu, *J. Chem. Soc. Rev*. **2021**, *50*, 7359.

22 (a) Bordwell, F. G.; Ji, G. Z. *J. Am. Chem. Soc.* **1991**, *113*, 8398. (b) Bordwell, F. G.; Zhang, S.; Zhang, X.-M.; Liu, W.-Z. *J. Am. Chem. Soc.* **1995**, *117*, 7092.

23 (a) Horton, D. A.; Bourne, G. T.; Smythe, M. L. *Chem. Rev.* **2003**, *103*, 893. (b) Felpin, F. X.; Lebreton, J. *Eur. J. Org. Chem.* **2003**, 3693. (c) O'Hagan, D. *Nat. Prod. Rep.* **2000**, *17*, 435. (d) Ritchie, T. J.; Macdonald, S. J. F.; Young, R. J.; Pickett, S. D. *Drug Discovery*

is rare and mainly occurs when the formation of pyrrolidines is not viable. Additionally, this reactivity cannot be translating to constructing lactones from carboxylic due to undesired Hunsdiecker decarboxylation processes.[24]

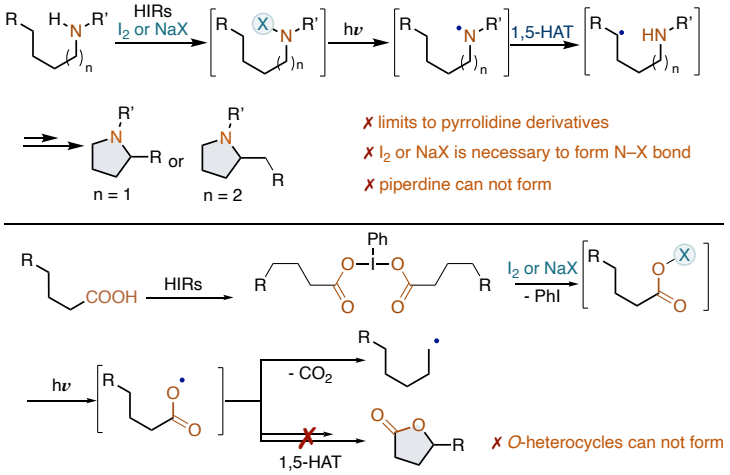

Scheme 2.11. Limitations of HLF reaction

2.1.2. Synthesis of piperidine derivatives through related radical routes

In order to tackle the scarcity of methodologies that enable the access to piperidine derivatives, Muñiz and co-workers fine-tuned the reaction conditions of their previous iodine-catalyzed methodologies,[11] which combines molecular iodine and NBS to allow a radical process involving intermolecular HAT, enabling the selective formation of piperidine over pyrrolidine products (Scheme 2.12).[25] The reaction commenced with the NBS/visible-light-induced creation of a benzylic radical intermediate. Then trapping of this benzyl icradical by iodo radical (I•), generated by the reaction I_2 and NBS afforded the intermediate **D**, which eventually undergoes intramolecular nucleophilic substitution to provide the required products in good to moderate yields.

Today **2011**, *16*, 164. (e) Vitaku, E.; Smith, D. T.; Njardarson, J. T. *J. Med. Chem.* **2014**, *57*, 10257.

24 (a) Hunsdiecker, H.; Hunsdiecker, C. *Chem. Ber.* **1942**, *75*, 291. (b) Johnson, R. G.; Ingham, R. K. *Chem. Rev.* **1956**, *56*, 219. (c) Wilson, C. V. *Org. React.* **1957**, *9*, 341.

25 Zhang, H.; Muñiz, K. *ACS Catal.* **2017**, *7*, 4122.

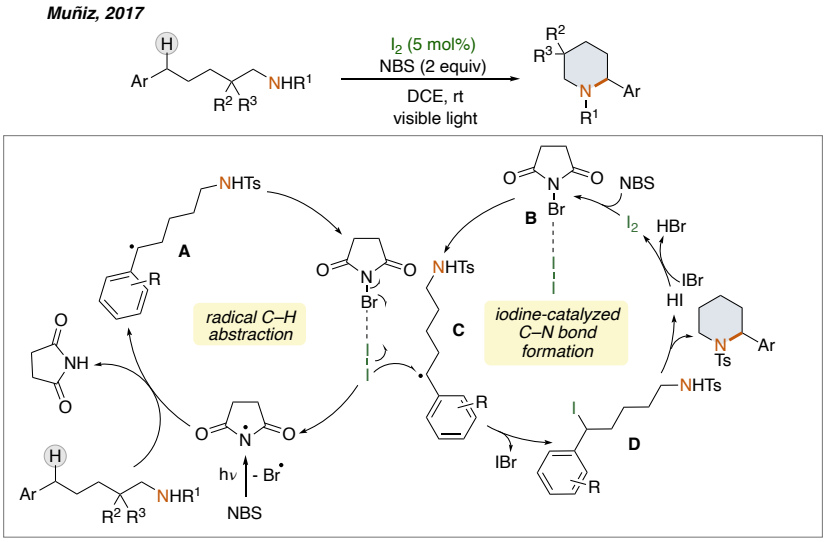

Scheme 2.12. Iodine-catalyzed Csp^3–H amination for the synthesis of piperdines

Besides, they developed an electrochemical benzylic C–H amination strategy to access the important heterocyclic motifs of pyrrolidines and piperidines within a uniform reaction protocol (Scheme 2.13).[26] The mechanism underlying this C–H amination strategy revolves around anodic C–H activation, leading to the formation of a benzylic cation that is effectively captured by a nitrogen nucleophile.

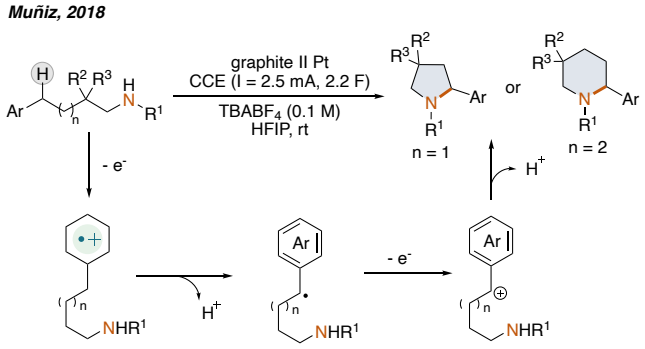

Scheme 2.13. Electrochemical approach for the synthesis of pyrrolidine and piperidine derivatives

Employing transition metals under HLF conditions can facilitate radical relay processes. In these processes, the carbon radical that is formed in situ can either be

26 Herold, S.; Bafaluy, D.; Muñiz, K. *Green Chem*. **2018**, *20*, 3191.

captured or oxidized to form a carbocation. The Muñiz group introduced a Copper-catalyzed N–F bond activation for uniform intramolecular C–H amination yielding pyrrolidines and piperidines (Scheme 2.14).[27] This involves the proposal of substrate coordination on a copper catalyst and further N–F bond cleavage via a single electron transfer with N-centered radical formation, which readily engages in a radical relay, resulting in the formation of the N-heterocycle and the regeneration of the Cu(I) catalyst.

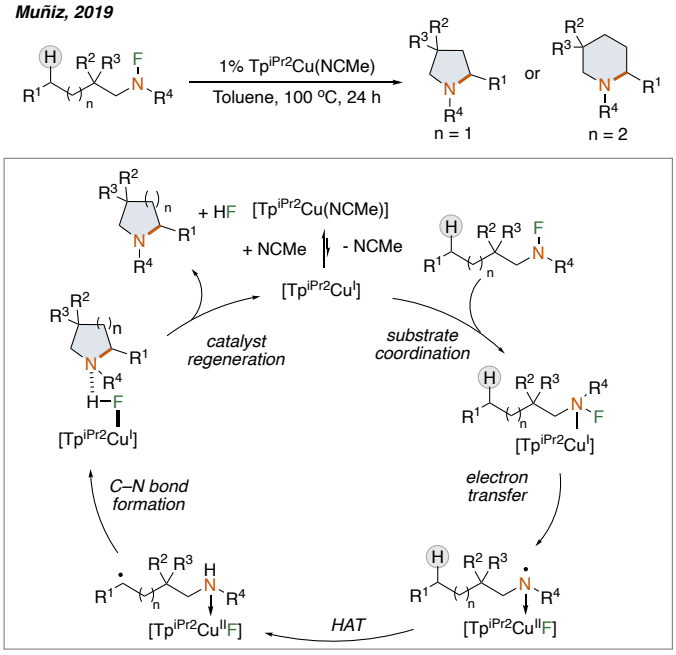

Scheme 2.14. Cu^{I}-catalyzed intramolecular C–H amination for the synthesis of pyrrolidine and piperidine derivatives

Another copper-catalyzed approach of asymmetric HLF variant was reported by Nagib group in the same year. In this method, they intercepted a remote carbon radical using a chiral copper complex and realized a copper-catalyzed enantioselective C–H cyanation (Scheme 2.15a).[28] The resulting aminonitriles underwent cyclization to chiral piperidines in the presence of $^{i}Bu_2Al$-H. Notably, refining the reaction conditions

27 Bafaluy, D.; Muñoz-Molina, J. M.; Funes-Ardoiz, I.; Herold, S.; de Aguirre, A. J.; Zhang, H.; Maseras, F.; Belderrain, T. R.; Pérez, P. J.; Muñiz, K. *Angew. Chem. Int. Ed.* **2019**, *58*, 8912.

28 Zhang, Z.; Zhang, X.; Nagib, D. A. *Chem* **2019**, *5*, 3127.

enabled the first asymmetric synthesis of the anticancer drug Niraparib. Shortly thereafter, they reported a defluorination and remote dehydrogenation strategy for N-fluoro-sulfonamides, employing a combination of Ir and copper catalysts (Scheme 2.15b).[29] This process led to the formation of δ,ε-unsaturated sulfonamides. The transformation initiated with a reduced photocatalyst triggering a single electron reduction of the N-fluoro-sulfonamide, generating an N-centered radical. This radical then underwent a 1,5-HAT resulting in the creation of a carbon-centered radical. The ensuing radical was captured by Cu(II), giving rise to a Cu(III) intermediate. Finally, a β-elimination process led to the formation of δ,ε-unsaturated amines. By utilizing these δ,ε-unsaturated amines, the group achieved the synthesis of both mono- and di-substituted piperidines through 6-endo-trig cyclizations.

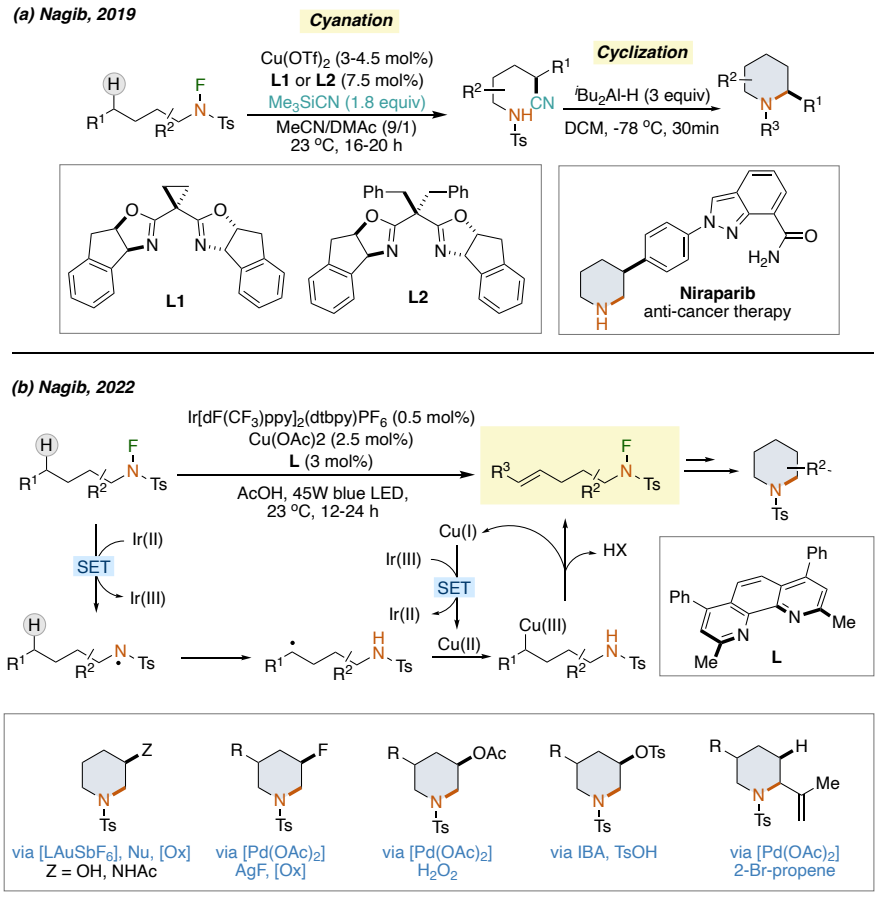

[29] Stateman,L. M.; Dare, R. M.; Paneque, A. N.; Nagib, D. A. *Chem* **2022**, *8,* 210.

Scheme 2.15. Two-Step Synthesis of Piperidine Derivatives

2.2. Objective and Design of the Project

As outlined in the previous sections, the HFL process and its variants have shown a great synthetic potential for the synthesis of pyrrolidine derivatives. However, more than one century after its discovery, these protocols still present shortcomings related to its radical mechanism. In this chapter, we envision to develop a general and mild strategy that could complement the traditional HLF reactivity and additional N to C radical relays[28-29] by the engagement of the hypervalent iodine(III) reagent in a distinct mechanistic paradigm that circumvents the intramolecular HAT process.

Our inspiration for this strategy lies in seminal studies of Kita and co-workers on using hypervalent derivatives to mediate the oxidative nucleophilic C–H functionalization of arenes as we described in the *Chapter I*. These umpolung reactions proceed via radical cations triggered by SET through charge transfer (CT) complexes of HIRs and electron-rich aromatic substrates (Scheme 2.16a).[30] These oxidative SET events have been successfully applied to inter- and intramolecular C(sp^2)–H functionalization reactions with a wide array of nucleophiles.[31] Nonetheless, the translation of this mechanistic concept towards electron-deficient scaffolds or drawing out new C(sp^3)–H functionalization reactions remains unexplored.

Inspired by Kita´s work, we aim to design a SET process between the substrate and the HIR to unlock the access to radical cation intermediates that switch the mechanism of the C(sp^3)–H cleavage by increasing its acidity.[26] If successful, this hypervalent iodine(III)-mediated strategy would deliver a versatile route for the synthesis of valuable 5- and 6-membered saturated heterocycles, which is not achievable under HLF conditions. As detailed in Scheme 2.16b, we envision that while electron-rich arenes can undergo single electron transfer via CT complexation with PIFA, for substrates lacking electron donating groups, the SET process could be promoted by the irradiation

30 (a) Kita, Y.; Tohma, H.; Hatanaka, K.; Takada, T.; Fujita, S.; Mitoh, S.; Sakurai, H.; Oka, S. *J. Am. Chem. Soc*. **1994**, *116*, 3684. (b) Kita,Y.; Takada, T.; Tohma, H. *Pure Appl. Chem.* **1996**, *68*, 627. (c) Kita, Y.; Takada, T.; Mihara, S.; Tohma, H. *Synlett* **1995**, 211. (d) Kita, Y.; Takada, T.; Mihara, S.; Whelan, B. A.; Tohma, H. *J. Org. Chem*. **1995**, *60*, 7144. (e) Kita, Y.; Dohi, T. *Chem. Rec*. **2015**, *15*, 886. (f) Dohi, T.; Yamaoka, N.; Kita, Y. *Tetrahedron* **2010**, *66*, 5775. (g) Shchepochkin, A. V.; Antipin, F. V.; Charushin, V. N.; Chupakhin, O. N. *Dokl. Chem.* **2021**, *499*, 123.

31 Roy, S.; Panja, S.; Sahoo, S. R.; Chatterjeea, S.; Maiti, D. *Chem. Soc. Rev*. **2023**, *52*, 2391.

of visible light. We proposed that HFIP would be the key to promote this intramolecular reactivity by playing a multifunctional role: i) enhancing the oxidation ability of PIFA, ii) facilitating the effective CT-complex formation,[32] or iii) favoring the generation and stabilization of the radical cation intermediates resulted after the SET oxidation,[33] among others. Overall, this strategy would broaden the synthetic utility of hypervalent iodine(III) reagents in metal-free C(sp^3)–H functionalization reactions and intramolecular cyclizations.

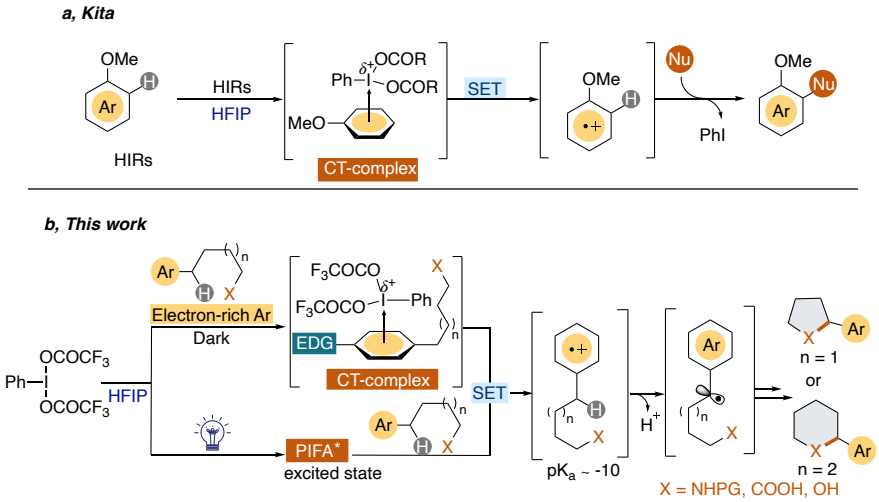

Scheme 2.16. HIR-mediated intramolecular C(sp^3)–H functionalization

2.3. Results and Discussion

2.3.1. Preliminary results

We started our investigation by interrogating the potential formation of a CT-complex between PIFA and a substrate capable to be engaged in an intramolecular C(sp^3)–N bond-forming reaction, such as **1a** by UV-vis spectroscopy. The selection of the starting material was dictated by the works by Kita and co-workers where they demonstrated that the presence of electron-rich aryl moieties promotes the CT

[32] Colomer, I.; Batchelor-McAuley, C.; Odell, B.; Timothy J. Donohoe, T. J.; Compton, R. G. *J. Am. Chem. Soc.* **2016**, *138*, 8855.

[33] (a) Eberson, L.; Hartshorn, M. P.; Persson, O. *Angew. Chem. Int. Ed. Engl.* **1995**, *34*, 2268. (b) Eberson, L.; Hartshornb, M. P.; Perssona, O. *J. Chem. Soc., Chem. Commun.* **1995**, 1131.

complexation with HIRs when using HFIP as solvent.[34] While the solutions of **1a** and PIFA in HFIP are colorless, we were pleased to observe that the mixture of both reagents immediately turned a pale-yellow color (Figure 2.1). Indeed, the analysis of its absorption spectrum exhibited a broad absorption band in the visible region between 400 and 500 nm, which shows good agreement with the reported value for the substituted methoxybenzene radical cation.[32c, 35]

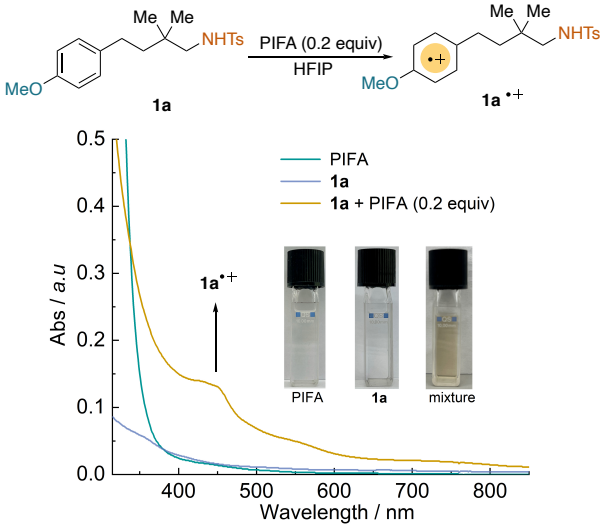

Figure 2.1. UV-vis spectra of **1a** (blue), PIFA (green) and a mixture between **1a** and PIFA (yellow) in HFIP.

Encouraged by these results, we next evaluated whether the formed radical cation could trigger the envisioned mechanistic switch via SET pathways and afford the corresponding pyrrolidine derivative (**Table 2.1**). To our delight, the reaction between **1a** and 1.2 equiv of PIFA in HFIP (0.1 M) afforded the targeted product **2a** in 72% after 14 hours (Table 2.1, entry 1). Interestingly, the application of PIDA did not yield the desired product, likely attributed to the insufficient electron deficiency of the iodine

34 (a) Shchepochkina, A. V.; Antipina, F. V.; Charushina, A. V. N.; Chupakhin, A. O. N. *Doklady Chemistry*, **2021**, *499*, 123. (b) Wang, X.; Studer, A. *Acc. Chem. Res*. **2017**, *50*, 1712. (c) Kits, Y.; Tohma, H.; Hatanaka, K.; Takada, T.; Fujita, S.; Mitoh, S.; Sakurai, H.; Oka, S. *J. Am. Chem. Soc.* **1994**, *116*, 3684. (d) Yasuyuki Kita, Y.; Dohi, T. *Chem. Rec.* **2015**, 15, 886.

35 (a) Ito, M.; Ogawa, C.; Yamaoka, N.; Fujioka, H.; Dohi, T.; Kita, Y. *Molecules* **2010**, *15*, 1918. (b) Huang, J.; Pan, B.; Duan, W.; Wei. X.; Assary, R. S.; Su, L.; Brushett, F. R.; Cheng, L.; Liao, C.; Ferrandon, M. S.; Wang, W.; Zhang, Z.; Burrell, A. K.; Curtiss, L. A.; Shkrob, I. A.; Moore, J. S.; Zhang, L. *Sci. Rep*. **2016**, *6*, 32102.

center to facilitate the formation of a charge-transfer complex with the substrate **1a** (entry 2). Furthermore, the use of 2-propanol or DCM as solvent proved ineffective in producing the 5-membered ring **2a** (entries 3-4).

Table 2.1. Initial reaction conditions screening[a]

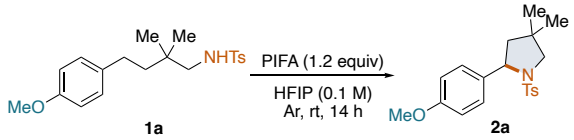

Entry	Changes from the standard conditions	Yield of **2a** (%)
1	Standard conditions	72
2	PIDA instead of PIFA	0
3	2-propanol instead of HFIP	0
4	DCM instead of HFIP	0

[a]Reaction conditions: **1a** (0.05 mmol, 1.0 equiv), HIR (0.06 mmol, 1.2 equiv) in solvent (0.5 mL), at room temperature under argon for 14 h. Yields were determined by crude ^{1}H NMR analysis using 1,1,2,2-tetrachloroethane as the internal standard.

To further confirm that an unconventional SET process is operative in our intramolecular process, we recorded the EPR spectrum of the standard reaction solution at room temperature (Figure 2.2). During the measurement, a signal was detected with a calculated g-value of 2.0028, which differs from the reported N-centered radical in HLF reaction.[36] This result supports the intermediacy of the aromatic cation radical **1a**$^{\bullet+}$ from an intracomplex SET process involving a CT-complex formed between **1a** and PIFA.

36 Bosnidou, A. E.; Duhamel, T.; Muñiz, K. *Eur. J. Org. Chem*. **2020**, *2020*, 6361.

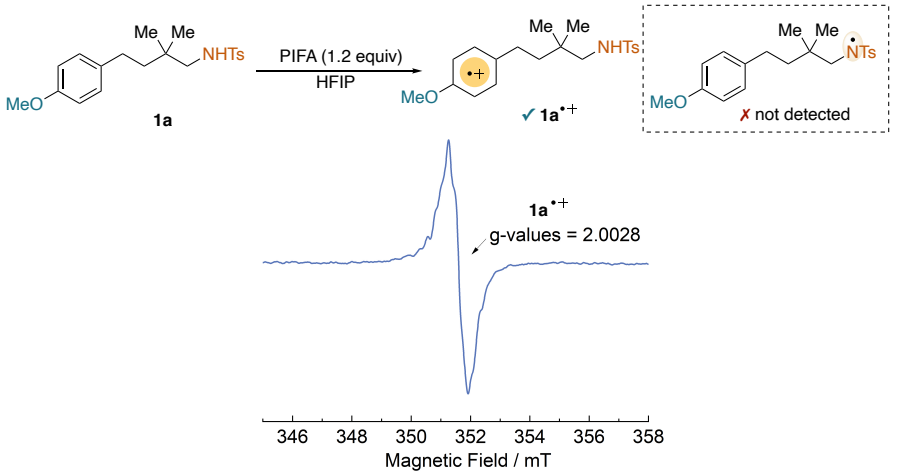

Figure 2.2. EPR measurement of the mixture between **1a** and PIFA in HFIP

2.3.2. Scope of the Reaction with Electron-Rich substrates

With this mechanistic picture in mind, we next determined the generality of our protocol (Scheme 2.17). Adopting the reaction conditions described in Table 2.1, substrates containing alternative electron-donating groups, such as pyrrolidine or aromatic fragments, provided the desired products (**2b-2d**) in moderate to excellent yields. Notably, the gram-scale synthesis of **2c** was also achieved.

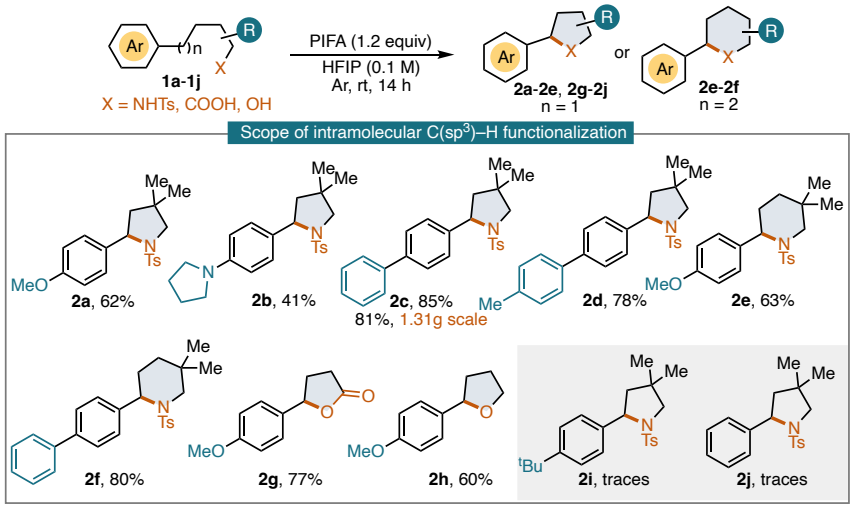

Scheme 2.17. Scope the intramolecular C(sp^3)–H functionalization. Reaction conditions: **1** (0.15 mmol, 1.0 equiv), PIFA (0.18 mmol, 1.2 equiv) in HFIP (0.1 M) at room temperature under argon for 14 h. The yields are isolated yields.

As anticipated, the same strategy successfully enabled the formation of the more challenging piperidine within a six-membered cyclization (**2e-2f**), which was not easily achieved through the kinetically disfavored 1,6-HAT process.[6a] Furthermore, this methodology extends beyond C–H amination, allowing oxygen nucleophiles to capture the benzylic cation and obtain the lactone product **2g** and ether product **2h** with yields of 77% and 60%, respectively. However, when we submitted substrates, such as **1i** or **1j**, that do not contain aromatic fragments with functional groups that increase their electron density through resonance donating effect, only gave traces of the corresponding 5-membered rings.

2.3.3. Photochemical protocol for non-electron rich substrates

2.3.3.1. Mechanistic Studies

The poor yields observed for **1i** and **1j** prompted us to further investigate these systems. Interestingly, we noticed that when **1j** was mixed with PIFA in HFIP, there was no color change of the reaction mixture even when we increased the amount of PIFA to 1.2 equivalents (Figure 2.3). Moreover, the absorption spectra of the reaction mixture (blue line) and PIFA (green line) displayed the same absorption profiles, excluding the formation of a CT-complex between **1j** and PIFA.[37]

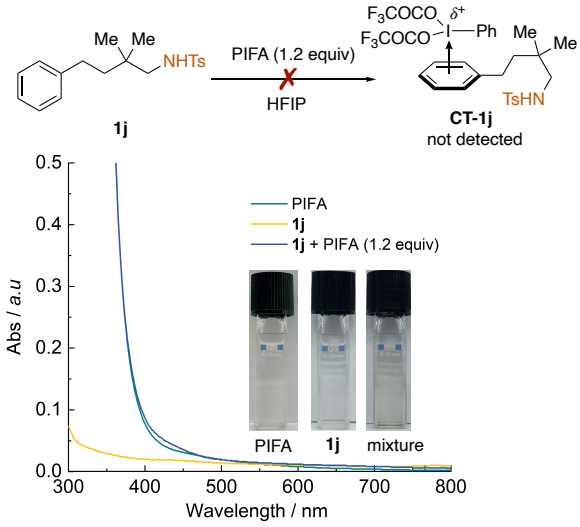

[37] Crisenza, G. E. M.; Mazzarella, D.; Melchiorre, P. "Synthetic Methods Driven by the Photoactivity of Electron Donor–Acceptor Complexes" *J. Am. Chem. Soc.* **2020**, *142*, 5461.

Figure 2.3. UV-vis absorption spectra of **1j** (yellow line), PIFA (green line), **1j** + 1.2 equiv PIFA (blue line).

To gain further insights into the significant influence of the substituents on the aromatic ring, we measured the redox potential of the different substrates in HFIP by cyclic voltammetry. As it is illustrated in Figure 2.4, a clear trend was observed depending on the nature of the functional group. For R = OMe (**1a**), the substrate showcases an irreversible oxidation potential at 1.23 V *vs.* Fc/Fc^{+}—a behavior attributed to its robust charge-transfer donor capability. Comparatively, substrate **1c**, featuring a phenyl substituent, manifests a comparatively weaker charge-transfer donor potential than the methoxy group, evidenced by a 100-mV anodic shift. Nevertheless, this shift remains adequate to activate the charge-transfer complex. While *t*-butyl substituted substrate **1i**, showed a substantial anodic shift of 380 mV compared to **1a**, implying its weaker ability of electron-donating than **1a**. This observation also aligned with the experimental results, as substrate **1i** only offered traces of the desired product **2i** under optimal conditions (Scheme 2.17). It's worth mentioning that, even though substrate **1i** demonstrates a more potent charge-transfer donor ability than substrate **1j**—evident by the latter's 170 mV anodic shift—it similarly exhibits poor reactivity akin to **1i**.

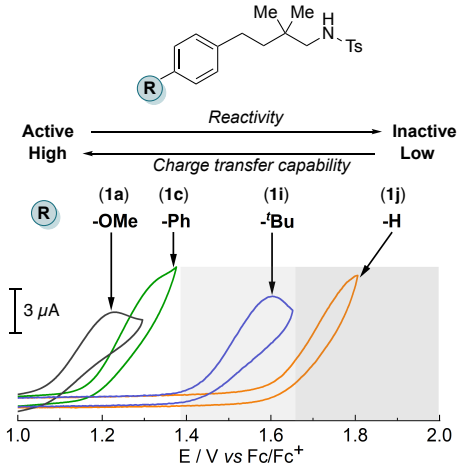

Figure 2.4. Evaluation of the charge transfer capability of the substrates with different substituents by cyclic voltammetry (CV) in HFIP using Fc/Fc^{+} as a reference.

Considering the difference between the charge transfer capability of **1i** and **1j**, we explored whether extending the reaction time could result in noticeable variations in their reactivities. After leaving the reaction mixture for 7 days, **2i** was obtained in 20%

yield while only traces of **2j** were observed (Scheme 2.18). These results indicate that to a certain extent, electron-rich substrates, such **1i**, can form CT-complexes with PIFA. In sharp contrast, substrates lacking EDGs cannot promote SET even at longer reaction times.

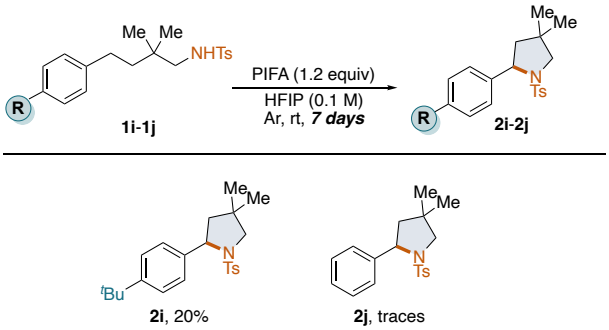

Scheme 2.18. Evaluation of the reactivity of **1i** and **1j** by extending the reaction time. Reaction conditions: **1** (0.05 mmol, 1.0 equiv), PIFA (0.06 mmol, 1.2 equiv) in HFIP (0.1 M) at room temperature under argon for 7 days. Yields were determined by crude ^{1}H NMR analysis using mesitylene as the internal standard.

To further assess the distinct experimental behavior observed for **1a** and **1j**, we performed DFT calculations at the M06-D3/def2-TZVP/SMD//M06-D3/6-31g*-LANL2DZ(I)/SMD level in HFIP solvent (Figure 2.5).[38] In alignment with the UV-vis spectra (Figure 2.1 and Figure 2.2) and the CV measurements (Figure 2.4), the computational studies revealed a viable intramolecular SET process between PIFA and **1a**, leading to an aromatic radical cation **1a**$^{\bullet+}$ with a low energy barrier 8.0 kcal/mol. However, the same process between PIFA and **1j** was determined to be thermodynamically infeasible at ground state, making this SET process unlikely to occur.

[38] The DFT calculations were performed by Jiale Xie from our group and Prof. Feliu Maseras´s group.

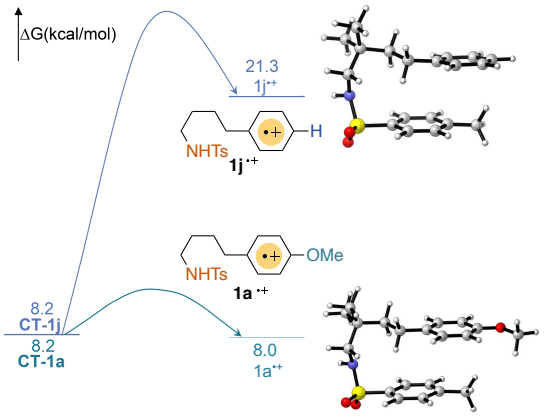

Figure 2.5. Potential energy surface of CT-complex and aromatic radical cation species of **1a** and **1j**.

2.3.3.2. Optimization Studies for 5-membered ring products

Aiming at expand the applicability of our SET process to substrates lacking electron-donating substituents, we wondered whether the reaction could be triggered upon direct excitation by visible-light irradiation. We envisaged to enhance the oxidation capability of PIFA by reaching an electronically excited state.[39] In order to explore the light-absorption capabilities of PIFA, we conducted UV-vis analysis of this HIR in different solvents (Figure 2.6). These measurements revealed that PIFA exhibits a distinct behavior in HFIP when compared to DCM or 2-propanol. When using this perflorinated solvent, we observed a weak absorption band in the visible region that could suggest suggesting that HFIP might play a crucial role in facilitating the photoredox reactions involving PIFA.

[39] Buzzetti, L.; Crisenza, G. E. M.; Melchiorre, P. *Angew. Chem. Int. Ed.* **2019**, *58*, 3730.

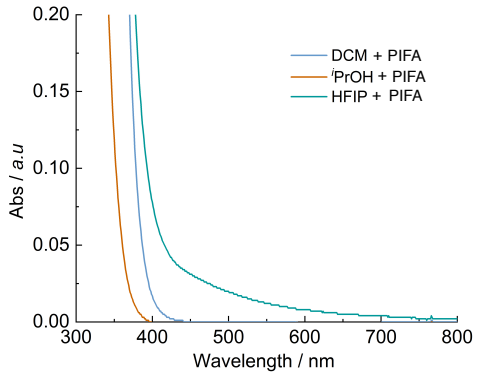

Figure 2.6. Absorption spectra of PIFA in DCM (blue line), ^{i}PrOH (orange line) and HFIP (green line). [PIFA] = $4 \cdot 10^{-2}$ M

Encouraged by these preliminary results, we conducted the intramolecular cyclization of **1j**, in the presence of PIFA, in HFIP at 30-40ºC, under the irradiation by a blue LED strip (λ_{max} = 465 nm). Under these reaction conditions, the corresponding pyrrolidine derivative (**2j**) was afforded in 86% yield. We next performed a solvent screening (Table 2.2), that confirmed that HFIP is the best reaction medium for these transformations.[40] While trifluoroethanol (TFE), perfluoro-*tert*-butanol (PFTB) and DCE provided significant lower yields than HFIP (entries 2, 6, 8), the reactivity was completely shut down when 2-propanol, MeCN, and toluene were used as alternative solvents (entries 3-5). Interestingly, conducting the reaction in Me-HFIP proved ineffective (entry 7), suggesting the protons in the OH and CH groups in HFIP are important for the reaction.

Table 2.2. Screening of the solvents.[a]

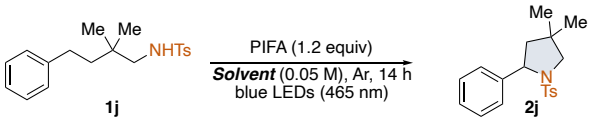

40 Details of the illumination set-up could be found in the experimental section.

Entry	Solvent	Yield of **2j** (%)
1	HFIP	86
2	TFE	35
3	2-Propanol	0
4	MeCN	trace
5	Toluene	0
6	DCE	19
7	Me-HFIP	trace
8	PFTB	33

[a]Reaction conditions: **1j** (0.05 mmol, 1.0 equiv), PIFA (0.06 mmol, 1.2 equiv) in solvent (0.05 M), blue LED strip, 465 nm, at 30~40 ºC under argon for 14 h. Yields were determined by crude ^{1}H NMR analysis using mesitylene as the internal standard.

Subsequently, we proceeded to test the effect of different HIRs (Table 2.3). Upon replacing PIFA with PIDA or PhI(*m*CPBA)$_2$, the yields dramatically decreased (entries 2-3). These results highlight the distinctive reactivity of PIFA specifically in the context of HFIP, underscoring its unique role in the reaction.

Table 2.3. Screening of the HIRs.[a]

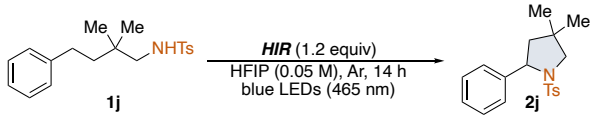

Entry	HIR	Yield of **2j** (%)
1	PIFA	86
2	PIDA	9
3	PhI(*m*CBA)$_2$	7

[a]Reaction conditions: **1j** (0.05 mmol, 1.0 equiv), HIR (0.06 mmol, 1.2 equiv) in HFIP (0.05 M), blue LED strip, 465 nm, at 30~40 ºC under argon for 14 h. Yields were determined by crude ^{1}H NMR analysis using mesitylene as the internal standard.

Next, we turned our attention to examine the impact of the reaction concentration on the process. As we can see in Table 2.4, there was a slight improvement in the yield of product **2j** when working under more diluted reaction conditions (entries 1-4). Based on this observation, we decided to continue our studies using a concentration of 0.03M.

Table 2.4. Screening of the reaction concentrations.[a]

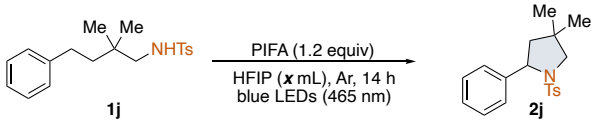

Entry	HFIP (x mL)	Yield of **2j** (%)
1	0.25	82
2	0.5	84
3	1.0	86
4	1.5	88
5	2.0	88

[a]Reaction conditions: **1j** (0.05 mmol, 1.0 equiv), PIFA (0.06 mmol, 1.2 equiv) in HFIP (x mL), blue LED strip, 465 nm, at 30~40 °C under argon for 14 h. Yields were determined by crude ^{1}H NMR analysis using mesitylene as the internal standard.

Our last investigations focused on the fine-tuning of the amount of PIFA (Table 2.5). Employing 1.2 equivalents of PIFA proved to be the most favorable option, as the yield of **2j** obtained was identical to that obtained with 1.5 equivalents (entries 2-3).

Table 2.5. Screening the amount of PIFA.[a]

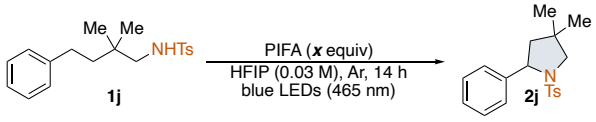

Entry	PIFA (x equiv)	Yield of **2j** (%)
1	0.6	49
2	1.2	88
3	1.5	88

[a]Reaction conditions: **1j** (0.05 mmol, 1.0 equiv), PIFA (x equiv) in HFIP (0.03M), blue LED strip, 465 nm, at 30~40 °C under argon for 14 h. Yields were determined by crude ^{1}H NMR analysis using mesitylene as the internal standard.

We have performed further control experiments to corroborate the role of the different reaction components (Table 2.6). As previously observed, only traces of product **2j** were detected during a control experimental performed in the dark (entry 2), even when the reaction was heated to 40°C (entry 3). Moreover, no reactivity was observed in the absence of PIFA (entry 4). Additionally, conducting the reaction under an air atmosphere led to poor yields, as oxygen had the potential to quench the excited state of PIFA (entry 5).

Table 2.6. Control experiments.[a]

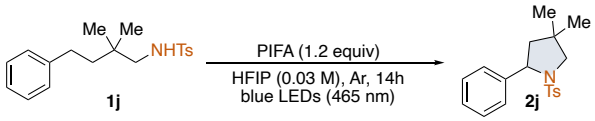

Entry	Changes from the standard conditions	Yield of **2j** (%)
1	Standard conditions	88
2	Without *hv*, rt	trace
3	Without *hv*, 40 °C	trace
4	Without PIFA	0
5	Under air	14

[a]Reaction conditions: **1j** (0.05 mmol, 1.0 equiv), PIFA (1.2 equiv) in HFIP (0.03M), blue LED strip, 465 nm, at 30~40 °C under argon for 14 h. Yields were determined by crude ^{1}H NMR analysis using mesitylene as the internal standard.

2.3.3.3. 5-Membered Ring Scope of the Photoinduced Protocol

Adopting the optimized conditions, we demonstrated the generality of the light-driven intramolecular C(sp^3)–H functionalization protocol by evaluating the formation of wide variety of 5-membered ring products (Scheme 2.19). We first examined substrates containing different protecting groups on the nitrogen atom. Sulfonyl groups, such as tosyl, mesyl, nosyl or triflate, among others, are well-tolerated providing the corresponding pyrrolidine products in excellent yields (**2j**-**2n**). Additionally, benzamide and trifluoroacetamide derivatives also underwent successful transformations, affording pyrrolidines **2o** and **2p** with good yields. The presence of EDGs and EWGs substituents on the aromatic architectures at the *ortho*-, *meta*- or *para*-positions were also tolerated (**2i**, **2q**-**2w**), including halide functionalities which can be further engaged in subsequent diversifications. Moreover, the impact of modifications on the aliphatic backbone was investigated, obtaining the corresponding pyrrolidines in excellent yields (**2x**-**2z**). It is worth noting that an acyclic stereocontrol was achieved when employing substrates with mono-substitution in the alkyl chain, leading to a 2.1:1 diastereomeric ratio in favor of the anti- compound (**2y**). Moreover, the intramolecular cyclization is facile without the presence of geminal alkyl groups, demonstrating well tolerance for substrates without Thorpe-Ingold effect (**2z**). Additionally, the cyclization over tertiary C–H bonds was studied with **1aa**, yielding the desired product **2aa** in an 88% yield. In order to access more intricate molecular frameworks, we incorporated a phenyl backbone into the substrates, leading to the formation of highly desirable isoindoline **2ab** and dioxoisothiazole derivative **2ac** with exceptional yields. The structures **2ac** was confirmed by single-crystal X-ray analysis. Moreover, it is possible to access the tricyclic alkaloid product **2ad** in a moderate yield.

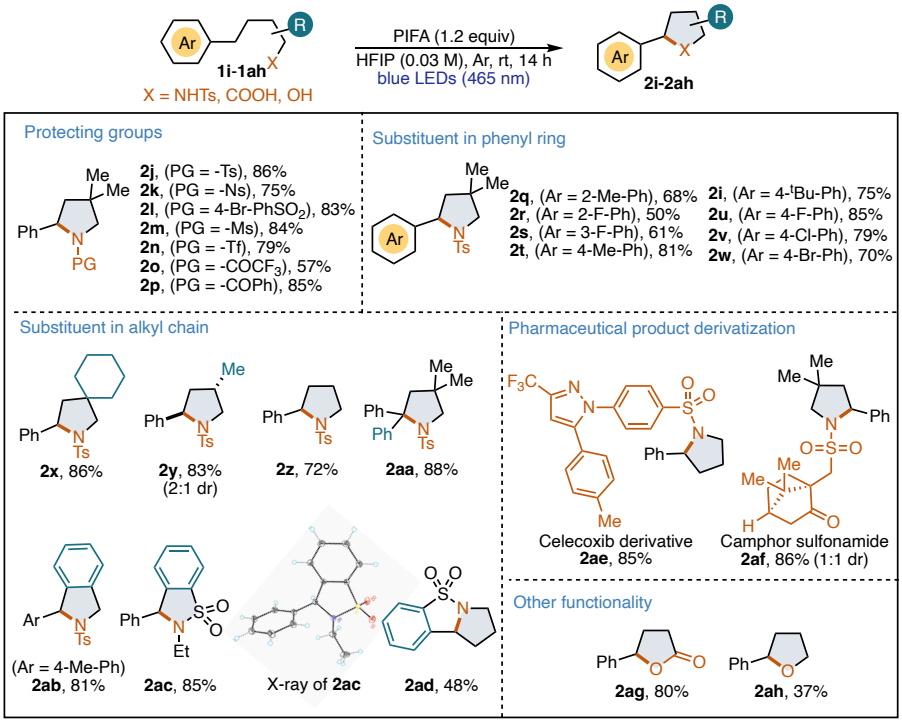

Scheme 2.19. Scope the photoredox intramolecular C(sp^3)–H functionalization. Reaction conditions: **1** (0.15 mmol, 1.0 equiv), PIFA (0.18 mmol, 1.2 equiv) in HFIP (0.03 M), blue LED strip, 465 nm, at 30~40 °C under argon for 14 h. The yields are isolated yields.

To showcase its applicability in late-stage amination of complex pharmaceutical and natural products, we explored its use with celecoxib and camphor derivatives, resulting in the formation of products **2ae** and **2af** with excellent yields. It is worth mentioning that in addition to the amination reactions, this strategy also proved effective in lactonization and etherification processes, delivering the corresponding desired products in moderate to high yields (**2ag-2ah**).

2.3.3.4. Deprotection of 2k to free pyrrolidine 3

Furthermore, we demonstrated the facile removal of the nosyl protecting group, providing the free pyrrolidine **3** with excellent yield.[25] This removal step allows the introduction of other functionalities on the nitrogen atom, opening the door to further applications in key areas such as medicinal chemistry applications (Scheme 2.20).

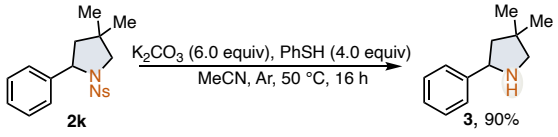

Scheme 2.20. Deprotection of **2k** to free pyrrolidine **3**. Reaction conditions: **2k** (0.15 mmol, 1.0 equiv), K_2CO_3 (0.9 mmol, 6.0 equiv), PhSH (0.6 mmol, 4.0 equiv) in MeCN (0.06 M) at 50 ºC under argon for 16 h. The yield is isolated yield.

2.3.3.5. Re-optimization Studies for 6-Membered Ring Products and Scope

As shown in Scheme 2.19, the formation of 5-membered ring products can be efficiently achieved. However, when we tried to translate the same reaction conditions to the synthesis of piperidine derivatives, such **2ai**, we observed lower yields (Scheme 2.21). Therefore, we decided to re-optimize the reaction conditions for this type of substrates.

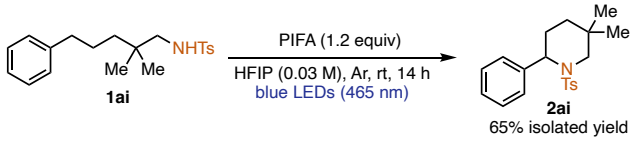

Scheme 2.21. Photoredox intramolecular C(sp^3)–H functionalization for the formation of 6-membered ring product. Reaction conditions: 1ai (0.15 mmol, 1.0 equiv), PIFA (0.18 mmol, 1.2 equiv) in HFIP (0.03 M), blue LED strip, 465 nm, at 30~40 ºC under argon for 14 h.

The previous studies identified the suitable reaction conditions for the synthesis of 5-membered heterocycles. Using them as starting point, we further investigated other reaction parameters, including temperature, concentration, amount of PIFA, and time (Table 2.7). While altering the concentration did not lead to any significant changes in the reactivity (entries 1-2), we observed slightly better results when the reaction was performed at lower temperature (5-10 ºC) and longer reaction times (24-30 hours) (entries 3-4). The addition of increasing amounts of PIFA (1.3 equiv) resulted in 78% yield (entry 5), yet the presence of 1.4 equivalents of the HIR (entry 6) or a shortening of the reaction time to 18 h resulted in lower yields (entry 7).

Table 2.7. Optimization of photoredox intramolecular C(sp^3)–H functionalization for the formation of 6-membered ring product.[a]

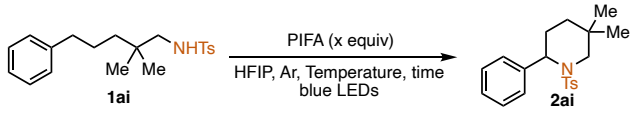

Entry	Temperature (ºC)	HFIP (mL)	PIFA (equiv)	Time (h)	Yield of **2ai** (%)
1[b]	30-40	1.5	1.2	14	65
2[b]	30-40	1.0	1.2	14	65
3[c]	10	1.0	1.2	24	71
4[c]	5	1.0	1.2	30	72
5[c]	5	1.0	1.3	30	78
6[c]	5	1.0	1.4	30	72
7[c]	5	1.0	1.3	18	75

[a]Reaction condition: **1ai** (0.05 mmol), PIFA (x equiv), HFIP (y mL) under argon atmosphere. Yields were determined by ^{1}H NMR analysis of the crude mixture using mesitylene as the internal standard. [b]The reaction was performed using blue LED strip, 465 nm, (the illumination set-up 1 in Figure 2.10, left). [c]The reaction was performed using a 900 mA blue LED, 470 nm, (the illumination set-up 2 in Figure 2.11)

With the optimal conditions in hand, we then expanded the substrate scope of our methodology for the synthesis of piperidine derivatives (Scheme 2.22), which represent the most prevalent heterocyclic scaffold in medicinal chemistry.[23] The cyclization process was successful for substrates containing various nitrogen-protecting groups (**2ai**-**2al**). As expected, our methodology exhibited excellent tolerance towards the inclusion of common functional groups at the 2-, 3-, and 4-positions of the arene group (**2am**-**2as**), including a heteroaromatic derivative **2as**, showcasing the wide applicability of this transformation. Moreover, modifying the backbone of the substrate was also amenable, resulting in the formation of product **2at** with a yield of 68%. Additionally, the reaction proceeded smoothly with a dibenzylic derivative, yielding the crucial tetrahydrosioquinoline core with a high yield (**2au**). Moreover, utilizing this process, we were able to obtain the desired lactone product **2av** with a remarkable yield.

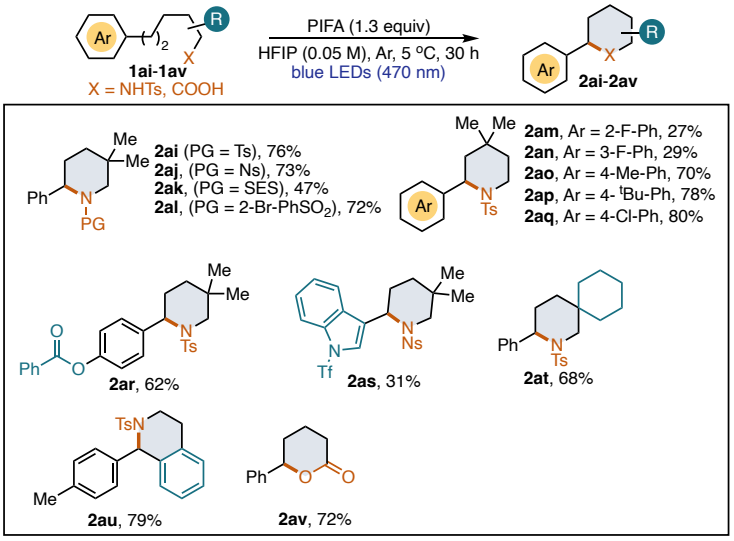

Scheme 2.22. Scope the photoredox intramolecular C(sp^3)–H functionalization for the formation of 6-membered ring products. Reaction conditions: **1** (0.15 mmol, 1.0 equiv), PIFA (0.19 mmol, 1.3 equiv) in HFIP (0.05 M) at 5 °C under illumination by a 900 mA blue LED (λ_{max} = 470 nm) for 30 h. The yields are isolated yields.

2.3.3.6. Scope Limitations

In this chapter, we have engineered an alternative SET mechanism that enables the access to a wide range of 5- and 6-membered heterocycles via C(sp^3)–H functionalization. However, our approach also shows some synthetic limitations (Scheme 2.23). No product is detected when subjecting substrates bearing electron-withdrawing group such as 4-acetyl or 4-CF_3, presumably by their high oxidation potentials (**4a**, **4b**, **4o**). Additionally, the presence of 4-phenylethynyl group was not compatible with the reaction conditions (**4c**). Substrates with electron-rich groups and low oxidation potentials (**4d**-**4f**), decomposed in all cases. Another limitation of this protocol is that it requires an activated benzylic position in the substrate. Substrates with tertiary (**4g**) and secondary (**4h**) aliphatic positions, or those bearing an α-heteroatom (**4i**), remained unreactive. Furthermore, the use of certain substituents in the alkyl chain adversely affected the reaction. For instance, substrate **4j**, **4k**, and **4r** resulted in low yields of the products (lower than 25%). Substrates **4p** and **4q** were unreactive. For the piperidine formation, the reaction did not yield any product when there was an absence of substituent in the alkyl chain (**4s**). This indicates that a Thorpe-Ingold effect is required for this transformation. It is worth mentioning that although this protocol could access 5- and 6-membered ring heterocycles, larger cycles like

azacycloheptanes or smaller ring size products like azetidines could not be accessed by the current methodology (**4l** and **4m**). Finally, the substrate without protecting group in the nitrogen atom (**4n**) exhibited unproductive results. This could likely be attributed to the interaction of the nucleophilic amine with PIFA, resulting in the suppression of reactivity.

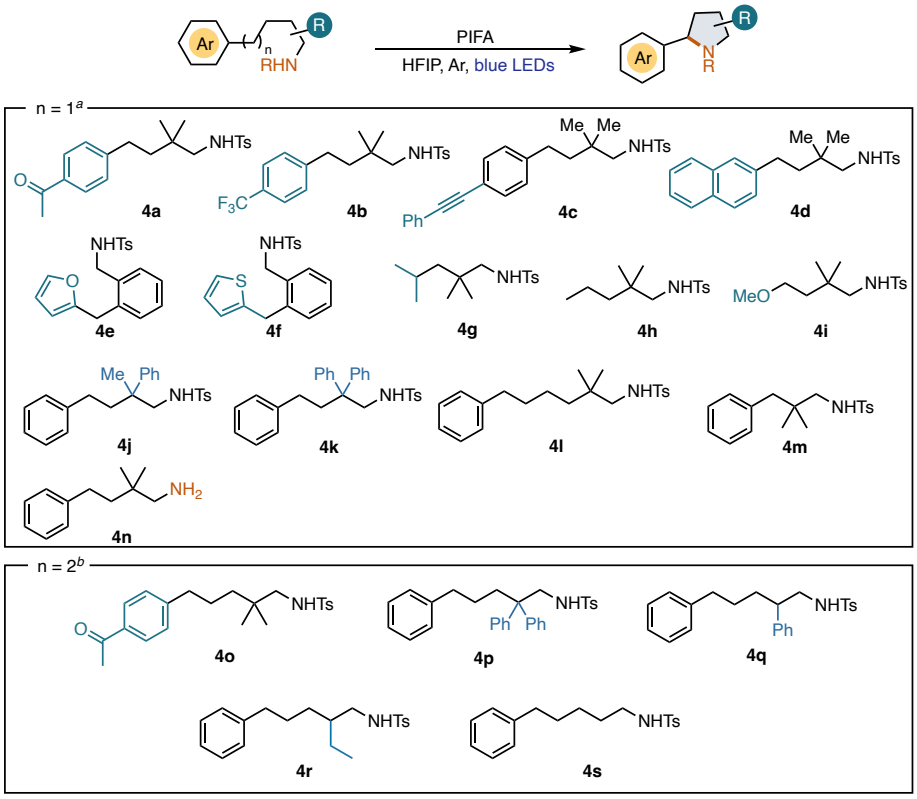

Scheme 2.23. Unsuccessful substrates. [a]Reaction conditions: **4** (0.05 mmol, 1.0 equiv), PIFA (1.2 equiv) in HFIP (0.03M), blue LED strip, 465 nm, at 30~40 °C under argon for 14 h. [b]Reaction conditions: **4** (0.05 mmol, 1.0 equiv), PIFA (0.065 mmol, 1.3 equiv) in HFIP (0.05 M) at 5 °C under illumination by a 900 mA blue LED (λ_{max} = 470 nm) for 30 h.

2.3.4. Mechanistic Studies on the Light-Driven Intramolecular Protocol

Finally, we sought to gain further mechanistic insights of the light-assisted approach. In this context, two possible pathways could be operative. On one hand, an arene oxidation by the excited PIFA (Scheme 2.24, pathway 1), through a SET would lead to the formation of an aromatic radical cation **1j**$^{\bullet+}$. At this stage, the acidity of the benzylic hydrogen atom is dramatically increased (the pK_a is about -10), being easily deprotonated to afford the benzylic radical **I**. Therefore, the KIE should be closer to

1.[41] On the other hand, the radical **I** could also be formed through a traditional HAT mechanism from a an amidyl radical (pathway 2).

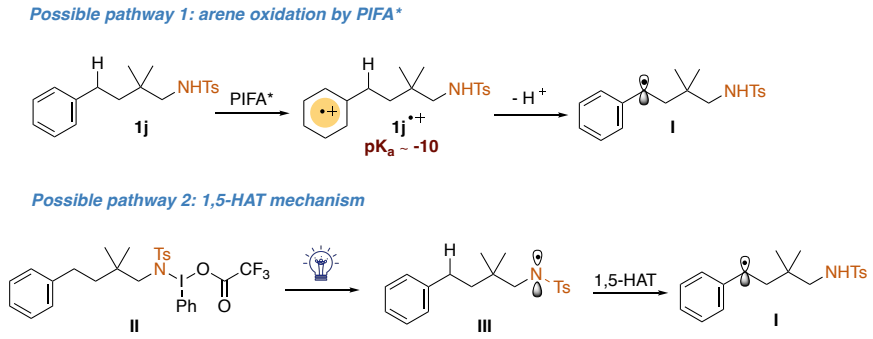

Scheme 2.24. Plausible pathways for the photoredox intramolecular C(sp^3)–H functionalization.

With these two options in hand, we first determined the kinetic isotope effect by comparing the initial reaction rates with **1j** to that with **1j-*d*$_2$** (Scheme 2.25). A KIE of 1.0 was obtained from these experiments. These results indicate that the C–H bond cleavage,[42] that is the benzylic deprotonation (Scheme 2.24, pathway 1) or the 1,5-HAT (Scheme 2.24, pathway 2)[43] is not the rate-determining step of the overall process. These results support Pathway 1, since the high acidity of the benzylic C(sp^3)–H bond of the radical cation should provide KIE closer to 1.[44] Moreover, the 1,5-HAT process often represents the rate-determining step in the HLF reaction (pathway 2).[11] However, we cannot completely rule out Pathway 2 based on the isotope labelling experiments.

41 (a) Schmittel, M.; Burghart, A. *Angew. Chem. Int. Ed.* **1997**, *36*, 2550. (b) Albini, A.; Mella, M.; Freccero, M. *Tetrahedron*, **1994**, *50*, 575. (c) Nicholas, A. M. P.; Arnold, D. R. *Can. J. Chem.* **1982**, *60*, 2165.

42 Simmons, E. M.; Hartwig, J. F. *Angew. Chem. Int. Ed.* **2012**, *51*, 3066.

43 Tang, N.; Wu, X.; Zhu, C. *Chem. Sci*. **2019**, *10*, 6915.

44 (a) Schmittel, M.; Burghart, A. *Angew. Chem. Int. Ed.* **1997**, *36*, 2550. (b) Albini, A.; Mella, M.; Freccero, M. *Tetrahedron*, **1994**, *50*, 575. (c) Nicholas, A. M. P.; Arnold, D. R. *Can. J. Chem.* **1982**, *60*, 2165.

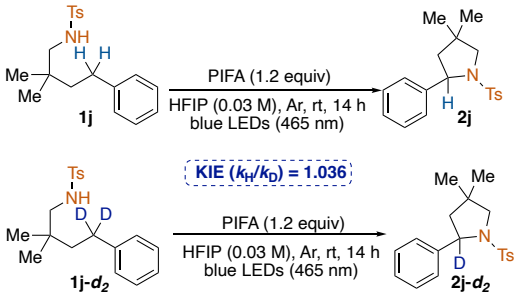

Scheme 2.25. Isotope labelling experiments. Reaction conditions: **1** (0.15 mmol, 1.0 equiv), PIFA (0.18 mmol, 1.2 equiv) in HFIP (0.03 M), blue LED strip, 465 nm, at 30~40 °C under argon for 14 h.

Another indirect evidence that support Pathway 1 is the exclusive formation of a piperidine derivative **2ai** when using **1ai** as starting material. Through the HLF mechanism both **2ai** and **2ai´** could be formed (Scheme 2.26),[11] since the 1,5-HAT is more favourable than 1,6-HAT.[6a]

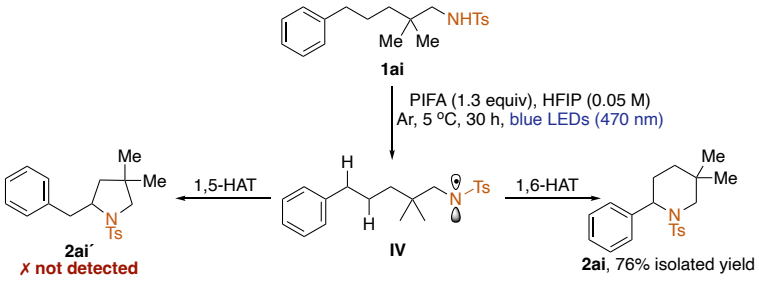

Scheme 2.26. Assessing the feasibility of an HLF mechanism for substrate **1ai**

To gather further supporting evidence for the arene oxidation mechanism under light irraditation, we investigated by UV-vis spectroscopy whether a SET process could generate the aromatic radical cation intermediate. Upon irradiation of the mixture of **1j** and PIFA in HFIP with blue LEDs for 15 minutes, the UV-vis spectra showed an absorption band in the range of 400 to 500 nm (Figure 2.7), similar to the absorption band we observed in Figure 2.1. This observation indicates that a rapid SET process occurred between PIFA and **1j** upon irradiation, leading to the formation of aromatic radical cationic intermediates **1j**$^{\bullet+}$.

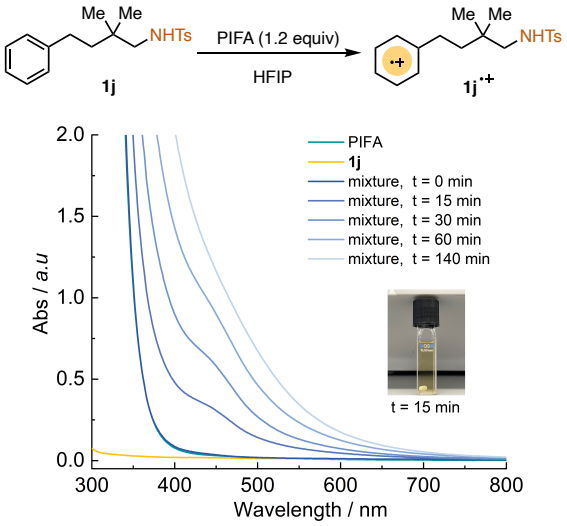

Figure 2.7. UV-vis absorption spectra of **1j** and PIFA (1.2 equiv) in HFIP (0.03M) upon irradiation with blue LED strip (λ_{max} = 465 nm).

To further understand the reaction mechanism, Stern-Volmer quenching experiments were performed. It is useful to study and quantify the effect of a compound (the quencher) on the fluorescence of an excited-state species.[45] The fluorescence of a molecule occurs when it absorbs energy (typically through the absorption of light) and then emits light of a longer wavelength. However, in the presence of certain quenching agents (Q), the excited state energy of the fluorophore can be deactivated through processes like collisional interactions or energy transfer, resulting in reduced or quenched fluorescence. The Stern-Volmer equation is used to describe the relationship between the fluorescence intensity of the fluorophore in the absence of the quenching agent (I_0) and its intensity in the presence of the quenching agent (I):

$$I_0/I = 1 + K_{SV}[Q] \qquad \text{(Eq. 1)}$$

where K_{SV} is usually referred to as the Stern-Volmer constant, which is related to the rate of quenching. [Q] is the concentration of the quenching agent. The equation assumes that the quenching process is dynamic and follows a collisional model, where the rate of quenching is proportional to the collision frequency between the fluorophore

45 (a) Lakowicz, J. R. "Principles of Fluorescence Spectroscopy" New York: Springer, 2006; (b) Balzani, V. Ceroni, P. Juris, A. "Photochemistry and Photophysics: Concept, Research and Applications" Weinheim, Wiley-VCH, 2014.

and the quenching molecule. By measuring the decrease of emission intensity over addition of an increasing concentration of quencher, the Stern-Volmer constant can be deduced. The Stern-Volmer constant *Ksv* can provide information about the nature of the quenching interaction. A large *Ksv* indicates a strong quenching interaction, while a small *Ksv* suggests a weaker interaction.

We conducted emission quenching investigations involving the excited state of PIFA, employing substrate **1j** as the quencher. Experimentally, a solution of PIFA at a concentration of 3.3×10^{-5} M was prepared in dry HFIP. Upon excitation with 332 nm light, PIFA exhibited an emission maximum at 410 nm. Subsequently, the Sequential addition of a solution containing **1j** led to a reduction in emission intensity (Figure 2.8, left panel). A Stern-Volmer plot was then constructed (Figure 2.8, right panel), revealing a linear relationship between I_0/I and the concentration of **1j**. Based on this data, a Stern-Volmer constant (KSV) of 1595 M^{-1} was determined.

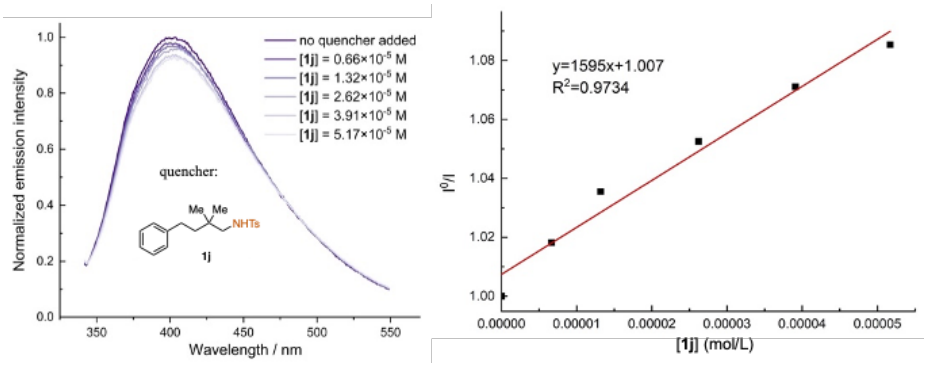

Figure 2.8. Quenching of PIFA emission (3.3×10^{-5} M in HFIP) in the presence of increasing amounts of substrate **1j**.

No change in the absorption spectrum of PIFA was observed upon additions of **1j** (see Figure 2.3), thus excluding a possible ground-state association between these two species, which would lead to a decrease in emission intensity. These results support the excited-state role of PIFA, which likely oxidizes **1j** in a SET event under irradiation, securing the generation of the radical cation in the reaction.

Estimation of the excited-state potential of PIFA

The excited-state potential of PIFA could be estimated using the Rehm-Weller equation (Figure 2.9, Equation 2).[39] This value was calculated from the ground-state

potential E(PIFA/PIFA$^{\bullet-}$) and the excited-state energy E_{00}(PIFA*/PIFA) which could be estimated by including the long wavelength tail of the absorption spectrum (λ_{tail}, obtained spectroscopically) into Equation 3.[46]

Rehm-Weller formalism:

$$E^*(\text{PIFA}^*/\text{PIFA}^{\bullet-}) = E(\text{PIFA}/\text{PIFA}^{\bullet-}) + E_{00}(\text{PIFA}^*/\text{PIFA}) \qquad \text{(Eq. 2)}$$

- *ground-state potentioal*: E(PIFA/PIFA$^{\bullet-}$) ⟹ from cyclic voltammetry
- *excited-state energy*: E_{00}(PIFA*/PIFA) ⟹ from UV-vis (tail of absorption, λ_{tail})
  $E_{00} = hc/\lambda_{tail}$ (Eq. 3)

Figure 2.9. Determination of the excited-state potential of PIFA using the Rehm-Weller equation. *h*: Planck's constant.

E(PIFA/PIFA$^{\bullet-}$) = -0.45 V *vs.* Fc/Fc$^+$ in HFIP was reported by Donohoe and Compton.[31] Using UV-vis spectroscopy, λ_{tail} was found at 354 nm, which translates into an excited-state energy E_{00}(PIFA*/PIFA) = 3.54 V.

Using these data, the following potential was calculated for the excited PIFA using Equation 2:

$$E(\text{PIFA}/\text{PIFA}^{\bullet-}) = -0.45 + 3.54 = 3.09 \text{ V } (vs.\ \text{Fc}/\text{Fc}^+)$$

This value indicates that SET oxidation of substrate **1j** to the aromatic radical cation **1j**$^{\bullet+}$ by PIFA* is highly exergonic ($E_{1/2}$ (**1j**/**1j**$^{\bullet+}$) = 1.78 V *vs.* Fc/Fc$^+$ in HFIP, see Scheme 3.19).

2.3.5. Proposed mechanism

Our proposed mechanism is depicted in Scheme 2.27. The reaction is initiated by a SET between the substrate and PIFA, resulting in the formation of the aromatic radical cation **A**. For electron-rich substrates, **A** is formed through an intracomplex SET of the CT-complex in the ground state. On the other hand, for the substrate in the absence of EDGs, the radical cation is formed after PIFA absorbing visible-light and reaching an electronically excited state capable to oxidize the corresponding substrates via SET. Simultaneously, PIFA receives an electron and releases CF_3 radical along with iodobenzene, OTFA anion, and CO_2.

46 Details about UV-vis studies can be found in the experimental section.

Next, rapid deprotonation occurs, facilitated by the *in-situ* generated OTFA anion, resulting in the formation of the benzylic radical **B** (as mentioned above, due to the significantly increased acidity of benzylic hydrogen atom with a pK_a of about -10). Subsequently, **B** undergoes further single-electron oxidation by a HFIP radical, which is formed through a HAT process involving the CF_3 radical and HFIP. This is supported by experimental data, indicating that HFIP provides a higher yield compared to PFTB (Table 2.2). Furthermore, the generation of the CF_3 radical was confirmed by the detection of CO_2 using gas chromatography after the reaction in both dark and photoredox processes.[47] The oxidation of **B** leads to the formation of the benzylic cation **C**, which is then captured by the nucleophilic fragment, resulting in the formation of the desired product.

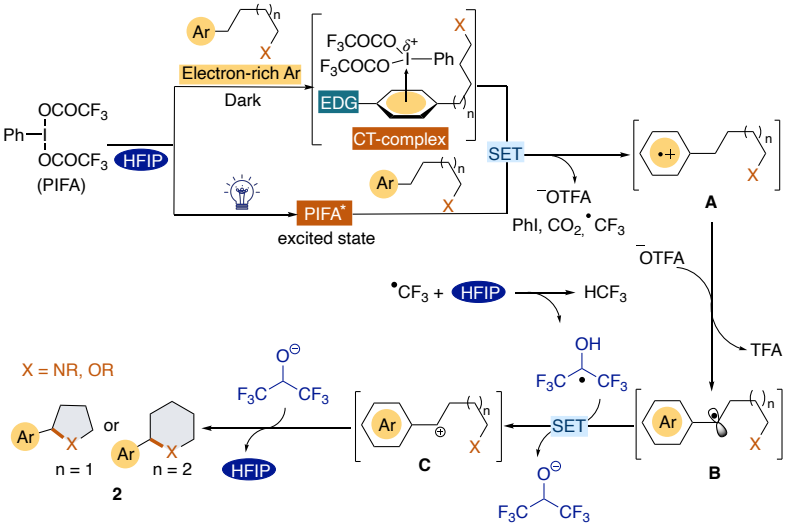

Scheme 2.27. Proposed mechanism of HFIP-assisted intramolecular C(sp^3)–H functionalization.

2.4. Conclusions

In summary, in this chapter we have developed a PIFA-mediated intramolecular C(sp^3)–H functionalization reaction facilitated by HFIP, to access valuable pyrrolidines, piperidines and O-heterocycles (Scheme 2.28). The success of this reaction relies on the SET process, leading to the formation of the aromatic radical cation intermediate. The

47 Details about the detection of CO_2 can be found in the experimental section.

reaction proceeds through two distinct pathways, depending on the electron density of the substrate's arene ring, which confirmed by both mechanism studies and DFT calculations. For electron-rich substrates, the intracomplex SET process takes place via a charge transfer (CT) complex formed between PIFA and the substrate. On the other hand, for the substrates without electron-donating substituents, it occurs under the assistance of the blue light. This protocol features mild reaction conditions and excellent regioselectivity, which achieved, for the first time, the C(sp^3)–H functionalization via the SET process of the CT-complex formed between the electron-rich substrate with HIRs. Furthermore, it opens a new avenue for the functionalization of the substrates which cannot form CT-complexes with HIRs.

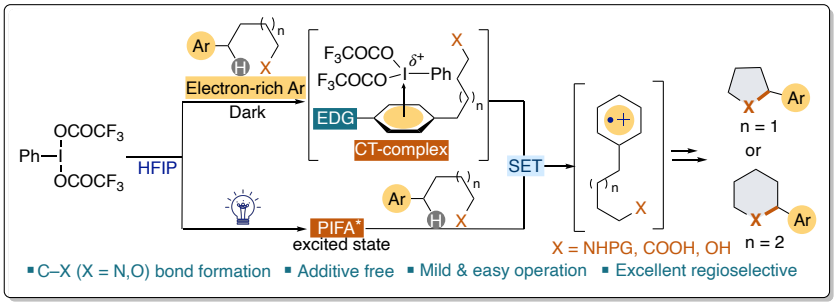

Scheme 2.28. HFIP-assisted PIFA-mediated intramolecular C(sp^3)-H functionalization via a SET process

2.5. Experimental Section

2.5.1. General experimental details

Unless otherwise indicated, reactions were conducted under an argon-filled glove box (mBraun Unilab 4420) with concentrations of O_2 and H_2O < 0.1 ppm or using Schlenk techniques under argon atmosphere. All the glassware was oven-dried at 100 ºC overnight and cooled under vacuum prior use. Synthesis grade solvents were used as purchased. Anhydrous solvents were taken from a commercial SPS solvent dispenser. Chromatographic purification of products was accomplished using force-flow chromatography (FC) on silica gel (40-63 μm). For thin layer chromatography (TLC) analysis throughout this work, Merck pre-coated TLC plates (silica gel 60 F254) were employed. Unless otherwise noted, visualization of developed plates was performed under UV light and/or using basic aqueous potassium permanganate ($KMnO_4$) stain.

Instrumentation

Nuclear magnetic resonance (NMR) spectra were recorded on Bruker AV 400 spectrometer at 400MHz (^{1}H NMR), 100MHz (^{13}C NMR), and 375MHz (^{19}F NMR) using $CDCl_3$ as solvent. 1H, 13C and 19F NMR chemical shifts are reported in parts per million (ppm), relative to tetramethylsilane (TMS) for 1H and 13C with the residual solvent peak used as an internal reference (CDCl3: δH = 7.26 ppm, δC = 77.16 ppm), and relative to CFCl3 (Freon) for 19F. Multiplicities are reported as follows: singlet (s), doublet (d), doublet of doublets (dd), triplet (t), triplet of doublets (td), triplete of triplets (tt) and multiplet (m). NMR yields for optimization studies were obtained by 1H NMR analysis of the crude reaction mixture using mesitylene as an internal standard.

High Resolution Mass Spectrometry (HRMS) data was recorded on a LCT-Premier (Waters) or a MicroTOF Focus (Bruker Daltonics) mass spectrometers using ESI ionization technique and acetonitrile as solvent.

UV-Vis measurements were carried out on a Shimadzu UV-1800PC spectrophotometer equipped with a photomultiplier detector, double beam optics and D^2 and W light sources.

Continuous wave (CW) EPR spectra were acquired at room temperature on a Bruker EMX Micro X-band spectrometer operating at 9.86GHz using a Bruker ER 1164 HS cavity. Individual EPR tubes were placed at the same position of the resonant cavity for EPR spectral acquisition.

The emission spectra were carried out on a Fluorolog Horiba Jobin Yvon spectrofluorimeter equipped with a photomultiplier detector, a double monochromator, and a 350W xenon light source.

Cyclic voltammetry studies were performed with a Biologic SP–150 potentiostat at rt. The working electrode: glassy carbon disk (0.07 cm^2 of surface area); the counter electrode: platinum; the reference electrode: SCE (Saturated Calomel electrode).

Materials

Commercial grade reagents and solvents were purchased from Sigma-Aldrich, Fluka, Alfa Aesar, Fluorochem, SynQuest used without further purification, unless otherwise stated.

Experimental Setup

– ***Set-up 1*** (common to 5-membered ring formation require light)

For reactions performed using a blue LED strip as the light source, a 3D-printed photoreactor was used, consisting of a 9 cm diameter crystallizing dish with a 3D printed support of 10 positions and a hole of 5 cm in the middle to allow ventilation (

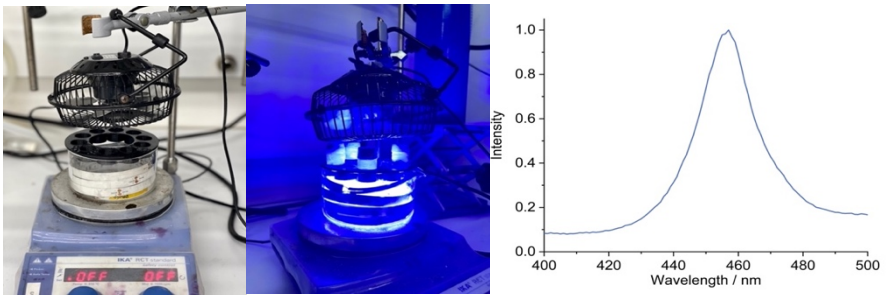

Figure **2.10**, left). A commercial 1-meter LED strip was wrapped around the crystallizing dish, while a fan was used to cool down the reactor (the reaction temperature within the reaction vessel was measured to be between 35-40 ºC). Each of the positions could be used to fit a standard 16 mm diameter vial with a Teflon screw cap. Experiments at 465 nm were conducted using a 1m strip, 14.4W "LEDXON MODULAR 9009083 LED, SINGLE 5050" purchased from Farnell, catalog number 9009083. The emission spectrum of these LEDs is shown in Figure 2.10, right panel.

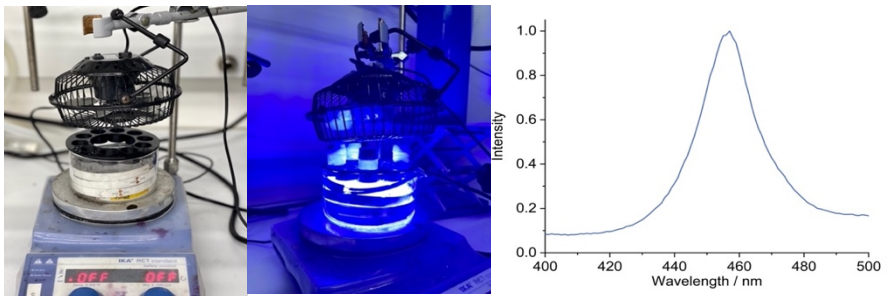

Figure 2.10. *Left and middle panel*: Blue LEDs photoreactor used for reactions. *Right panel*: Emission spectrum of the 465 nm LED strip used in this reactor.

– ***Set-up 2*** (common to 6-membered ring formation require light)

The vials were placed into a parallel photoreactor with 8 positions, fitted with 470 nm OSRAM Oslon SSL 80 blue LEDs on star as controlled by an external power supply. The temperature was kept at 5 °C with a chiller connected to the irradiation plate (the setup is detailed in Figure 2.11).

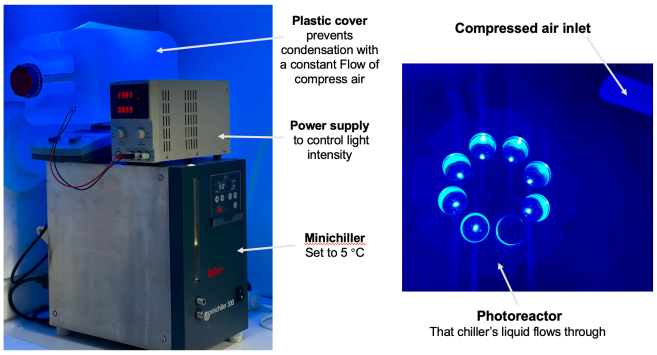

Figure 2.11. Detailed photoreactor setup with 8 parallel reactors. The light source for illuminating the reaction vessel consisted of 470 nm OSRAM Oslon SSL 80 blue LEDs on star.

2.5.2. General protocol for starting materials

The following substrtes were synthesized according to the literature[48] or followed the corresponding general procedures.

[48] (a) Nikolaienko, P.; Jentsch, M.; Kale, A. P.; Cai, Y.; Rueping, M. *Chem. Eur. J.* **2019**, *25*, 7177. (b) Liu, D.; Liu, C.; Li, H.; Lei, A. *Angew. Chem. Int. Ed.* **2013**, *52*, 4453.

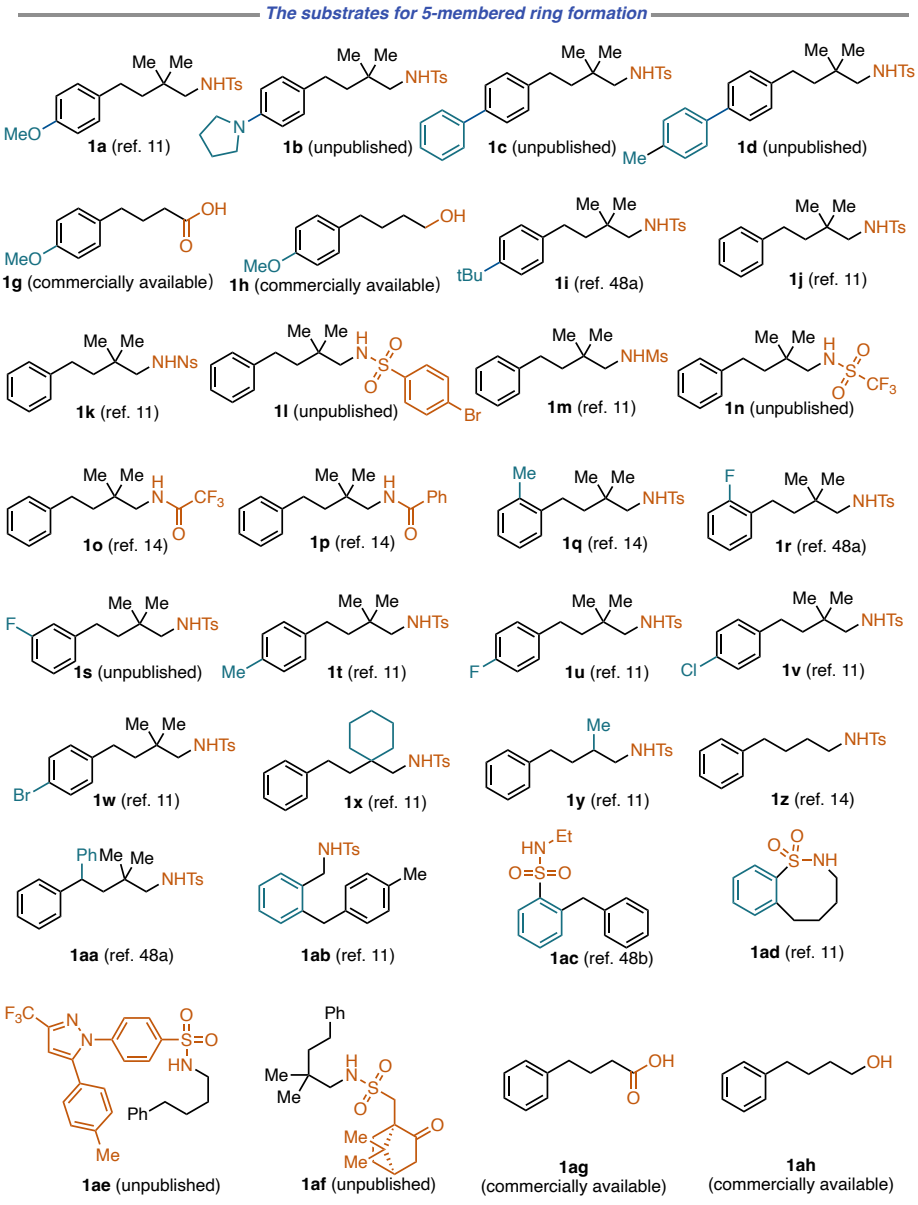

Scheme 2.29. The substrates for 5-membered ring formation

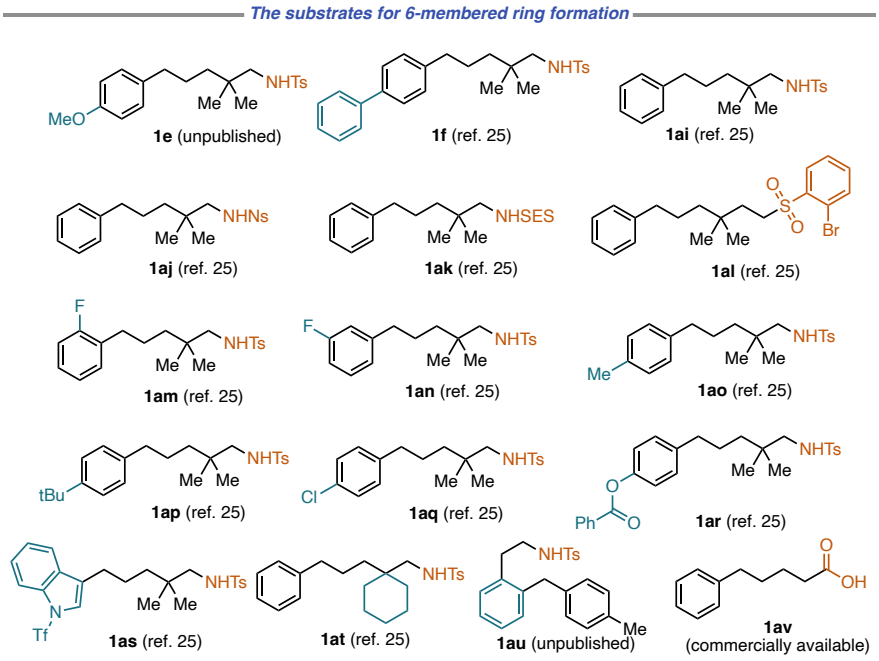

Scheme 2.30. The substrates for 6-membered ring formation

General procedure for the synthesis of the substrates for 5-membered ring formation

General procedure 1 (GP1) for the corresponding starting materials (**1a**, **1j-1q**, **1s-1z**, **1ab**, **1ad**) was performed following the procedure reported in literature[11] and is outlined below.

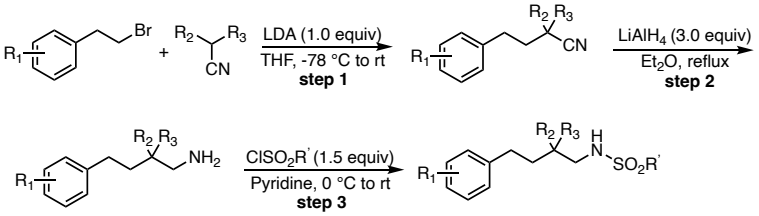

Step 1: The corresponding nitrile compound (1 equiv) was dissolved in dry THF (0.4 M) under an argon atmosphere. The solution was then cooled to -78 °C, and lithium diisopropylamide (LDA) (2 M, 1.0 equiv) was added dropwise at this temperature. The reaction mixture was stirred for 30 minutes at -78 °C. Following this, the corresponding bromide compound (1.2 equiv) was added, and the reaction mixture was warmed to

room temperature and stirred for an additional 12 hours. To quench the reaction, a saturated solution of NH_4Cl was added, and the resulting mixture was extracted with DCM (3 x). The combined organic layers were dried over Na_2SO_4 and the solvent was removed under reduced pressure. The resulting crude product was used in the subsequent step without further purification.

Step 2: A two-neck flask equipped with a stirring bar and a reflux condenser was charged with $LiAlH_4$ (3 equiv based on the nitrile obtained from step 1). Subsequently, Et_2O (0.25 M based on nitrile) was added carefully, and the resulting suspension was cooled to 0 °C. The crude product obtained from step 1 was dissolved in a small volume of Et_2O and added dropwise to the suspension. Then, the reaction mixture was refluxed for 2 hours. After refluxing, the reaction was cooled again to 0 °C and quenched by adding a 10% aqueous solution of NaOH. The mixture was filtered over a pad of Na_2SO_4 and the solvent was removed under reduced pressure to yield the crude amine in quantitative yields.

Step 3: The crude amine from step 2 (1 equiv) was dissolved in pyridine (0.4 M) and the resulting solution was cooled to 0 °C. Subsequently, the corresponding sulfonyl chloride was added in one portion, and the reaction mixture was stirred at room temperature for 12 hours. Then, the mixture was diluted with DCM and washed with a 5% aqueous solution of HCl (3 x). The organic layer was dried over Na_2SO_4 and the solvent was evaporated under reduced pressure. The resulting crude product was further purified by column chromatography on silica gel, employing *n*-hexane and ethyl acetate as eluents.

General procedure 2 (GP2) for the corresponding starting materials (**1c**, **1i**, **1r**, **1aa**) was performed following the procedure reported in literature[48a] and is outlined below:

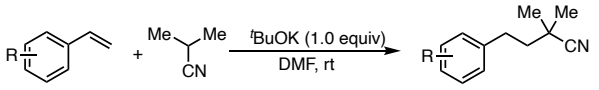

For the synthesis of the required nitriles the first step of GP1 was replaced. To a solution of *t*BuOK (1.0 equiv.) in DMF (0.5 M) was prepared, to which the corresponding vinyl-substituted substrate (1.0 equiv) was added. Subsequently, 1.5 equiv of the nitrile was added to the reaction. The resulting solution exhibited a distinct color and was stirred at room temperature overnight. The reaction mixture was then poured into cold water

(5-fold excess to the DMF volume) and extracted with diethyl ether (3 x). The combined organic phase was washed with water and brine, dried over Na_2SO_4, and the solvent was evaporated under reduced pressure. The resulting crude product was used in the subsequent step without further purification.

Characterization of new starting materials for 5-membered ring formation

N-(2,2-dimethyl-4-(4-(pyrrolidin-1-yl)phenyl)butyl)-4-methylbenzenesulfonamide (1b)

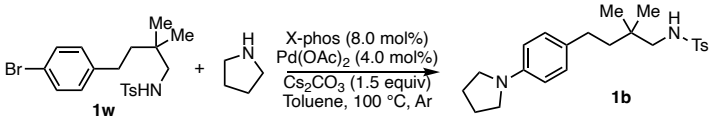

According to a literature procedure[3], in a 50 mL Schlenk flask equipped with a magnetic stirrer, $Pd(OAc)_2$ (13.5 mg, 0.06 mmol, 4.0 mol%), 2-dicyclohexylphosphino-2',4',6'-tri-iso-propylbiphenyl (57.2 mg, 0.12 mmol, 8.0 mol%), Cs_2CO_3 (0.73 g, 2.25 mmol, 1.5 equiv), **1w** (0.61 g, 1.50 mmol, 1.0 equiv) was added. The Schlenk flask was connected to a vacuum condenser and the total system was purged with an argon atmosphere. Then, toluene (7.5 mL) and pyrrolidine (0.21 g, 3.0 mmol, 2.0 equiv) were added to the mixture, and the reaction flask was stirred at 100 °C for 16 hours. After cooling to room temperature, the reaction mixture was filtration over celite and extracted with ethyl acetate (3x). The combined organic layers were dried over Na_2SO_4 and the solvents were evaporated under reduced pressure. The resulting crude product was purified by chromatography on silica gel (*n*-hexane/ethyl acetate 10:1). This afforded the pure title compound **1b** as white solid in 76% yield.

mp: 135–137 °C; TLC (Hexane/EtOAc, 6:1 v/v): $R_f = 0.19$.

^{1}H NMR (400 MHz, $CDCl_3$): δ 7.72 (d, J = 8.3 Hz, 2H), 7.29 (d, J = 7.8 Hz, 2H), 6.98 (d, J = 8.5 Hz, 2H), 6.50 (d, J = 8.2 Hz, 2H), 4.43 (t, J = 6.9 Hz, 1H), 3.26 (t, J = 6.6 Hz, 4H), 2.71 (d, J = 6.9 Hz, 2H), 2.42 (s, 3H), 2.41–2.36 (m, 2H), 2.02–1.97 (m, 4H), 1.48–1.42 (m, 2H), 0.91 (s, 6H).

^{13}C NMR (100 MHz, $CDCl_3$): δ 143.4, 137.2, 129.8, 129.0, 127.2, 112.0, 53.0, 48.0, 42.1, 34.1, 29.3, 25.6, 25.1, 21.6.

IR ν (cm^{-1}): 3263, 2924, 1521, 1319, 1070, 886, 800, 661.

HRMS(ESI) *m/z*: Calcd. for $[C_{23}H_{33}N_2O_2S]^+$: 401.2257; Found: 401.2256.

N-(4-([1,1'-biphenyl]-4-yl)-2,2-dimethylbutyl)-4-methylbenzenesulfonamide (1c)

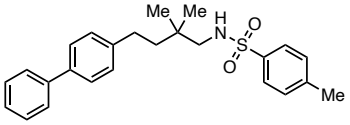

Following the GP2 to give **1c** as a white solid in 65% yield.

mp: 133–135 °C; TLC (Hexane/EtOAc, 6:1 v/v): R_f = 0.18.

^{1}H NMR (400 MHz, $CDCl_3$): δ 7.74 (d, J = 8.3 Hz, 2H), 7.60–7.55 (m, 2H), 7.50 (d, J = 8.4 Hz, 2H), 7.43 (t, J = 7.5 Hz, 2H), 7.36–7.31 (m, 1H), 7.28 (d, J = 7.9 Hz, 2H), 7.21 (d, J = 8.5 Hz, 2H), 4.49 (t, J = 6.9 Hz, 1H), 2.76 (d, J = 6.9 Hz, 2H), 2.59–2.51 (m, 2H), 2.41 (s, 3H), 1.60–1.49 (m, 2H), 0.95 (s, 6H).

^{13}C NMR (100 MHz, $CDCl_3$): δ 143.5, 141.8, 141.2, 138.9, 137.2, 129.9, 128.9, 128.9, 127.3, 127.2, 127.2, 127.1, 53.0, 41.6, 34.2, 30.0, 25.1, 21.7.

IR ν (cm^{-1}): 3261, 1424, 1319, 1160, 1071, 810, 755, 697.

HRMS(ESI) *m/z*: Calcd. for $[C_{25}H_{29}NNaO_2S]^+$: 430.1811; Found: 430.1822.

N-(2,2-dimethyl-4-(4'-methyl-[1,1'-biphenyl]-4-yl)butyl)-4-methylbenzene-sulfonamide (1d)

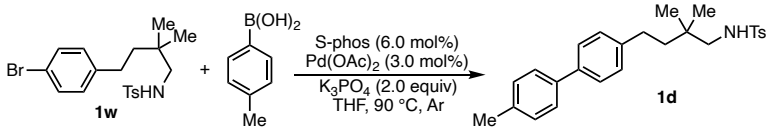

According to a literature procedure4, in a 25 mL Schlenk flask equipped with a magnetic stir bar, **1w** (0.61 g, 1.50 mmol, 1.0 equiv.), Pd(OAc)2 (10.1 mg, 0.045 mmol, 3.0 mol%), S-Phos (37.0 mg, 0.09 mmol, 6 mol%), 4-methylphenyl boronic acid (0.24 g, 1.8 mmol, 1.2 equiv.) and K_3PO_4 (0.64 g, 3.0 mmol, 2.0 equiv.) was added. The reaction mixture was connected to a vacuum condenser and purged with an argon atmosphere. This process was repeated three times. Then, 4.5 mL of THF was added to the mixture under argon. The reaction mixture was stirred for 24 hours at 90 °C. After cooling the reaction mixture to room temperature, it was extracted with ethyl acetate (3 ×) through a celite filter. The organic layer was collected and dried over

Na_2SO_4, the solvents were then evaporated under reduced pressure. The resulting crude product was purified by chromatography on silica gel (*n*-hexane/ethyl acetate 10:1). This afforded the pure title compound **1d** as white solid in 75% yield.

mp: 152–154 °C; TLC (Hexane/EtOAc, 6:1 v/v): $R_f = 0.19$.

^{1}H NMR (400 MHz, $CDCl_3$): δ 7.73 (d, J = 8.4 Hz, 2H), 7.48 (d, J = 7.8 Hz, 4H), 7.28 (d, J = 7.8 Hz, 2H), 7.24 (d, J = 7.8 Hz, 2H), 7.19 (d, J = 8.4 Hz, 2H), 4.46 (t, J = 7.1 Hz, 1H), 2.76 (d, J = 6.9 Hz, 2H), 2.59–2.49 (m, 2H), 2.41 (s, 3H), 2.40 (s, 3H), 1.57–1.51 (m, 2H), 0.94 (s, 6H).

^{13}C NMR (100 MHz, $CDCl_3$): δ 143.5, 141.5, 138.8, 138.3, 137.1, 136.9, 129.9, 129.6, 128.8, 127.2, 127.1, 127.0, 53.0, 41.6, 34.2, 30.0, 25.1, 21.7, 21.2.

IR ν (cm^{-1}): 3265, 2924, 1497, 1422, 1319, 1068, 809, 660.

HRMS(ESI) *m/z*: Calcd. for $[C_{26}H_{31}NNaO_2S]^+$: 444.1968; Found: 444.1958.

4-bromo-N-(2,2-dimethyl-4-phenylbutyl)benzenesulfonamide (1l)

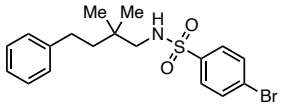

Following the GP1 to give **1l** as a white solid in 63% yield.

mp: 108–110 °C; TLC (Hexane/EtOAc, 8:1 v/v): $R_f = 0.20$.

^{1}H NMR (400 MHz, $CDCl_3$): δ 7.71 (d, J = 8.6 Hz, 2H), 7.63 (d, J = 8.6 Hz, 2H), 7.30–7.24 (m, 2H), 7.21–7.15 (m, 1H), 7.13 (d, J = 7.0 Hz, 2H), 4.64 (t, J = 6.8 Hz, 1H), 2.75 (d, J = 6.8 Hz, 2H), 2.56–2.47 (m, 2H), 1.54–1.46 (m, 2H), 0.93 (s, 6H).

^{13}C NMR (100 MHz, $CDCl_3$): δ 142.5, 139.2, 132.5, 128.7, 128.6, 128.4, 127.7, 126.0, 53.1, 41.6, 34.2, 30.4, 25.0.

IR ν (cm^{-1}): 3273, 2964, 1573, 1323, 1154, 819, 739, 697.

HRMS(ESI) *m/z*: Calcd. for $[C_{18}H_{23}BrNO_2S]^+$: 396.0627; Found: 396.0630.

N-(2,2-dimethyl-4-phenylbutyl)-1,1,1-trifluoromethanesulfonamide (1n)

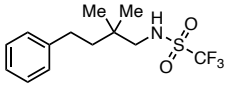

Following the GP1 to give **1n** as a white solid in 56% yield.

mp: 68–70 °C; TLC (Hexane/EtOAc, 10:1 v/v): R_f = 0.27.

^{1}H NMR (400 MHz, $CDCl_3$): δ 7.33–7.27 (m, 2H), 7.23–7.16 (m, 3H), 4.92 (t, J = 6.5 Hz, 1H), 3.12 (d, J = 6.4 Hz, 2H), 2.62–2.56 (m, 2H), 1.63–1.50 (m, 2H), 1.02 (s, 6H).

^{13}C NMR (100 MHz, $CDCl_3$): δ 142.2, 128.7, 128.4, 126.1, 119.9 (q, J = 319.6 Hz), 54.23, 41.45, 34.37, 30.36, 24.68.

^{19}F NMR (375 MHz, $CDCl_3$): δ -76.94 (s, 3F).

IR ν (cm^{-1}): 3306, 2948, 1602, 1438, 1361, 857, 737 699.

HRMS(ESI) *m/z*: Calcd. for $[C_{13}H_{18}F_3NNaO_2S]^+$: 332.0903; Found: 332.0890.

N-(4-(3-fluorophenyl)-2,2-dimethylbutyl)-4-methylbenzenesulfonamide (1s)

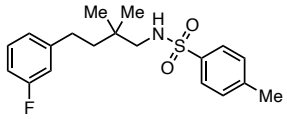

Following the GP1 to give **1s** as a yellow solid in 68% yield.

mp: 114–116 °C; TLC (Hexane/EtOAc, 6:1 v/v): R_f = 0.19.

^{1}H NMR (400 MHz, $CDCl_3$): δ 7.74 (d, J = 8.3 Hz, 2H), 7.30 (d, J = 7.9 Hz, 2H), 7.21 (td, J = 7.9, 6.1 Hz, 1H), 6.90 (d, J = 7.6 Hz, 1H), 6.88–6.78 (m, 2H), 4.53 (t, J = 6.8 Hz, 1H), 2.74 (d, J = 7.2 Hz, 2H), 2.52–2.45 (m, 2H), 2.42 (s, 3H), 1.52–1.44 (m, 2H), 0.92 (s, 6H).

^{13}C NMR (100 MHz, $CDCl_3$): δ 163.0 (d, J = 244.0 Hz), 145.3 (d, J = 7.2 Hz), 143.6, 137.1, 129.9 (d, J = 8.3 Hz), 129.9, 127.2, 124.1 (d, J = 2.7 Hz), 115.2 (d, J = 20.8 Hz), 112.7 (d, J = 21.0 Hz), 53.0, 41.2, 34.1, 30.2 (d, J = 1.7 Hz), 25.0, 21.6.

^{19}F NMR (375 MHz, $CDCl_3$): δ -113.89 (td, 1F).

IR ν (cm^{-1}): 3267, 2941, 1587, 1424, 1320, 1066, 870, 662.

HRMS(ESI) *m/z*: Calcd. for $[C_{19}H_{24}FNNaO_2S]^+$: 372.1404; Found: 372.1412.

N-(4-phenylbutyl)-4-(5-(p-tolyl)-3-(trifluoromethyl)-1H-pyrazol-1-yl)benzenesulfon-amide (1ae)

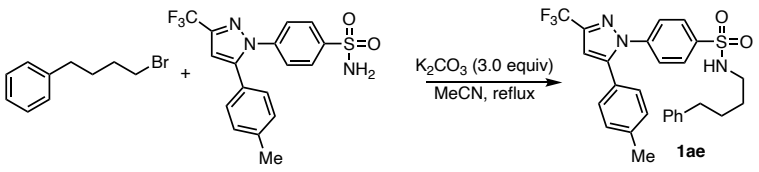

According to a literature procedure[5], in a solution of (4-bromobutyl)benzene (0.21 g, 1.0 mmol, 1.0 equiv) in MeCN (4.0 mL), K_2CO_3 (0.42 g, 3.0 mmol, 3.0 equiv) was added, followed by the addition of benzenesulfonamide (0.76 g, 2.0 mmol, 2.0 equiv.). The resulting solution was heated to reflux and stirred for 5 hours. After completion of the reaction, the mixture was filtrated through Celite and concentrated in vacuo. The desired product **1ae** was afforded after purification by flash column chromatography using silica gel (*n*-hexane/ethyl acetate 4:1). This afforded the pure title compound **1ae** as white solid in 82% yield.

mp: 142–144 °C; TLC (Hexane/EtOAc, 4:1 v/v): $R_f = 0.18$.

^{1}H NMR (400 MHz, $CDCl_3$): δ 7.82 (d, J = 8.9 Hz, 2H), 7.46 (d, J = 8.9 Hz, 2H), 7.29–7.21 (m, 2H), 7.20–7.14 (m, 3H), 7.14–7.08 (m, 4H), 6.75 (s, 1H), 4.56 (s, 1H), 2.96 (q, J = 6.4 Hz, 2H), 2.57 (t, J = 7.2 Hz, 2H), 2.37 (s, 3H), 1.65–1.55 (m, 2H), 1.54–1.44 (m, 2H).

^{13}C NMR (100 MHz, $CDCl_3$): δ 145.4, 144.2 (q, J = 38.2 Hz), 142.6, 141.7, 139.9, 139.6, 129.9, 128.8, 128.5, 128.5, 128.2, 126.1, 125.8, 125.7, 120.1 (q, J = 267.7 Hz), 106.4, 43.3, 35.3, 29.2, 28.3, 21.4.

^{19}F NMR (375 MHz, $CDCl_3$): δ -62.54 (s, 3F).

IR ν (cm^{-1}): 3254, 2927, 1596, 1235, 1094, 974, 814, 698.

HRMS(ESI) *m/z*: Calcd. for $[C_{27}H_{26}F_3N_3NaO_2S]^+$: 536.1590; Found: 536.1577.

1-((*1S*,*4R*)-7,7-dimethyl-2-oxobicyclo[2.2.1]heptan-1-yl)-N-(2,2-dimethyl-4-phenylbutyl)methane-sulfonamide (1af)

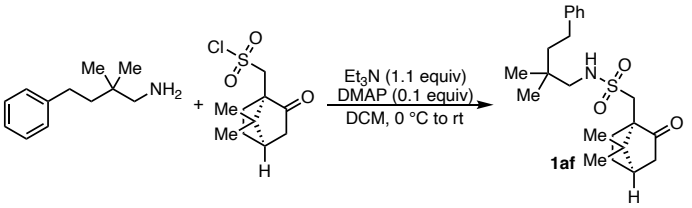

According to a literature procedure14, the third step of GP1 was adjusted. 2,2-dimethyl-4-phenylbutan-1-amine (0.89 g, 5.0 mmol, 1.0 equiv) was dissolved in DCM (25 mL), and Et_3N (0.76 mL, 5.5 mmol, 1.1 equiv) and DMAP (61.1 mg, 0.5 mmol, 0.1 equiv.) was added to the solution. The solution was then cooled to 0 °C, and sulfonyl chloride (1.9 g, 7.5 mmol, 1.5 equiv.) was added dropwise. After stirring at room temperature for 12 hours, the solution was extracted with DCM and washed with saturated $NaHCO_3$ solution and water. The organic phase was dried over anhydrous Na_2SO_4, and the solvent was removed under reduced pressure. The product **1af** was isolated by flash column chromatography using a *n*-hexane:ethyl acetate 4:1 as the eluent. This afforded the pure title compound **1af** as white solid in 74% yield.

mp: 109–111 °C; TLC (Hexane/EtOAc, 4:1 v/v): $R_f = 0.21$.

^{1}H NMR (400 MHz, $CDCl_3$): δ 7.31–7.23 (m, 2H), 7.22–7.13 (m, 3H), 5.32 (dd, J = 8.8, 5.2 Hz, 1H), 3.35 (d, J = 14.8 Hz, 1H), 3.04 (dd, J = 12.1, 8.8 Hz, 1H), 2.93 (dd, J = 12.1, 5.2 Hz, 1H), 2.92 (d, J = 14.8 Hz, 1H), 2.66–2.52 (m, 2H), 2.45–2.34 (m, 1H), 2.25–2.15 (m, 1H), 2.13 (t, J = 4.4 Hz, 1H), 2.08–1.96 (m, 2H), 1.93 (d, J = 18.6 Hz, 1H), 1.65–1.53 (m, 2H), 1.50–1.39 (m, 1H), 1.02 (s, 3H), 1.02 (s, 3H), 1.02 (s, 3H), 0.92 (s, 3H).

^{13}C NMR (100 MHz, $CDCl_3$): δ 217.4, 142.8, 128.4, 128.4, 125.7, 59.4, 53.3, 49.4, 49.0, 43.0, 42.8, 41.8, 34.2, 30.4, 27.1, 27.0, 25.0, 25.0, 20.0, 19.5.

IR ν (cm^{-1}): 3239, 2964, 1727, 1455, 1324, 1073, 838, 742.

HRMS(ESI) *m/z*: Calcd. for $[C_{22}H_{33}NNaO_3S]^+$: 414.2073; Found: 414.2083

General procedure for the synthesis of the substrates for 6-membered ring formation

General procedure 3 (GP3) for the corresponding starting materials (**1e**, **1f**, **1ai-1at**) for the 6-membered ring formation was performed following the procedure reported in literature[11, 25] and is outlined below.

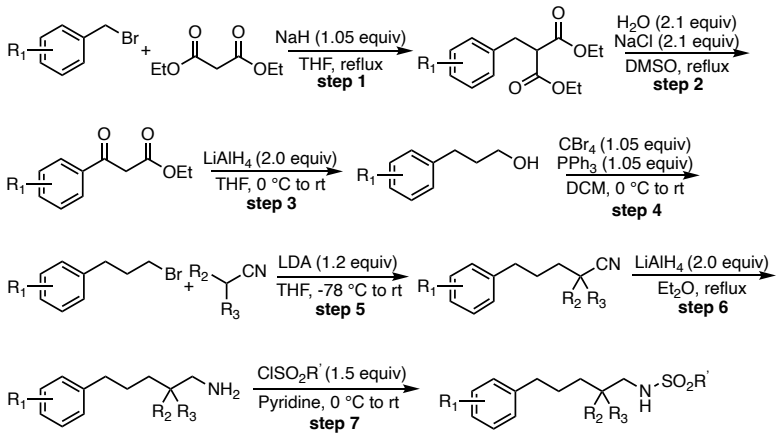

Step 1: Diethyl malonate (1.05 equiv) was added dropwise to a suspension of NaH (60% on mineral oil, 1.05 equiv) in dry THF at 0 °C and stirred for 15 minutes. Subsequently, the corresponding benzyl bromide was added in one portion, resulting in a milky mixture, which was then stirred at reflux for 1 hour. The reaction mixture was cooled and quenched by the addition of water. The THF solvent was removed under reduced pressure, and the resulting crude product was dissolved in Et_2O and washed with water. The aqueous layer was extracted with Et_2O (4 x), and the combined organics layers were washed with brine, dried over Na_2SO_4 and filtered. The solvent was evaporated under reduced pressure, and the crude product was directly used for the subsequent step without further purification.

Step 2: A solution containing the diester (1.0 equiv), NaCl (2.1 equiv.), and H_2O (2.1 equiv) in DMSO (30 mL) was heated at reflux for 8 hours. After completion of the reaction, the mixture was cooled to 25 °C and diluted with a 3M HCl solution. The resulting mixture was extracted with ethyl acetate (3 x 20 mL). The combined organic layers were washed with water (5 x 50 mL), followed by brine (1 x 100 mL) and dried over Na_2SO_4. The crude product, appearing as a brown oil, was then filtered through a pad of silica to obtain the desired ester in a quantitative yield.

Step 3: A THF solution of the ester (1.0 equiv) was prepared and maintained at 0 °C. To this solution, $LiAlH_4$ (2.0 equiv) was slowly added, followed by stirring at room temperature for 2 hours. After that, a solution of NaOH (10% in water) was added carefully until a white solid precipitated. The reaction mixture was then filtered over Na_2SO_4, and the solvent was evaporated to yield the crude amine in quantitative yields.

Step 4: A solution of propanol (1.0 equiv) in CH_2Cl_2 was prepared and cooled to at 0 °C. To this solution, CBr_4 (1.05 equiv) was added, followed by the portion wise addition of triphenylphosphine (1.05 equiv). The reaction mixture was allowed to warm up to 25 °C and monitored by TLC. After 3 hours, no starting material was detected. The organic layer was dried over Na_2SO_4, and the solvent was removed under reduced pressure. The crude product was purified using chromatography on silica gel with *n*-hexane as the eluent, resulting in the isolation of the pure bromide product.

Step 5: A Schlenk tube equipped with a stirrer bar was charged with the corresponding nitrile compound (1.2 equiv) and THF (20 mL). LDA (1.2 equiv) was added dropwise at

-78 °C and the solution was stirred for 30 minutes. After this period, the corresponding bromide (1.0 equiv) was added in a single portion, and the mixture was stirred at room temperature for 12 hours. To quench the reaction, a saturated aqueous solution of NH_4Cl was added, and the resulting mixture was extracted with DCM (3 x). The organic layer was then dried over Na_2SO_4, and the solvent was evaporated under reduced pressure. The resulting crude product was utilized directly for the subsequent reduction step.

Step 6: A flame dried Schlenk flask equipped with a stirrer bar and a reflux condenser was charged with $LiAlH_4$ (3 equiv), Et_2O was carefully added while the mixture was cooled to 0 °C with an external ice/water cooling bath. The crude nitrile (1 equiv) was dissolved in a small volume of Et_2O and added carefully to the suspension of $LiAlH_4$. The mixture was then heated to reflux for 2 hours and cooled back to 0 °C afterwards. A solution of NaOH (10% in water) was added carefully until a white solid precipitated. After filtration over Na_2SO_4 and evaporation of the solvent, the crude amine was obtained in quantitative yields.

Step 7: The crude amine obtained from step 6 (1 equiv) was dissolved in pyridine (20 mL) and the respective sulfonyl chloride (1.5 equiv) was added to the solution at 0 °C. The resulting solution was stirred overnight at 25 °C. DCM was subsequently added, and the mixture was washed three times with a hydrochloride solution (10% HCl in water). The organic layer was dried over Na_2SO_4 and the solvent was then evaporated under reduced pressure. The crude material was purified by chromatography (silica gel, *n*-hexane/ethyl acetate) to give the pure product.

Characterization of new starting materials for 6-membered ring formation

N-(5-(4-methoxyphenyl)-2,2-dimethylpentyl)-4-methylbenzenesulfonamide (1e)

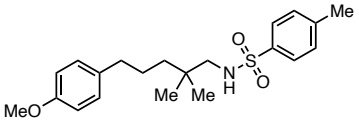

Following the GP3 to give **1e** as a white solid in 56% yield.

mp: 72–74 °C; TLC (Hexane/EtOAc, 6:1 v/v): R_f = 0.19.

^{1}H NMR (400 MHz, $CDCl_3$): δ 7.73 (d, J = 8.3 Hz, 2H), 7.30 (d, J = 7.9 Hz, 2H), 7.05 (d, J = 8.8 Hz, 2H), 6.82 (d, J = 8.8 Hz, 2H), 4.40 (s, 1H), 3.79 (s, 3H), 2.66 (d, J = 6.0 Hz, 2H), 2.47 (t, J = 7.6 Hz, 2H), 2.42 (s, 3H), 1.50–1.39 (m, 2H), 1.23–1.17 (m, 2H), 0.82 (s, 6H).

^{13}C NMR (100 MHz, $CDCl_3$): δ 157.9, 143.4, 137.2, 134.6, 129.8, 129.3, 127.2, 113.9, 55.4, 53.0, 39.0, 35.7, 33.9, 26.0, 25.0, 21.6.

IR ν (cm^{-1}): 3273, 2930, 1610, 1509, 1320, 1246, 818, 676.

HRMS(ESI) *m/z*: Calcd. for $[C_{21}H_{29}NNaO_3S]^+$: 398.1760; Found: 398.1763.

N-(5-(4-methoxyphenyl)-2,2-dimethylpentyl)-4-methylbenzenesulfonamide (1au)

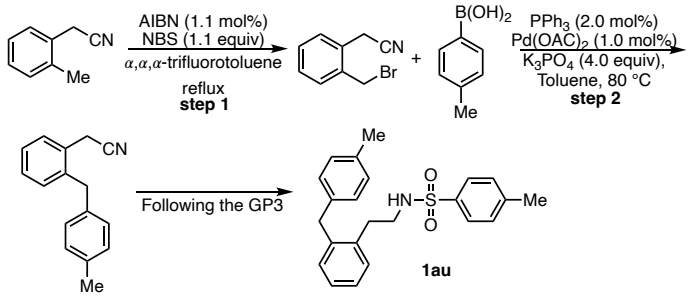

For the synthesis of the requisite nitrile for the preparation of compound **1au** the first four step of GP3 was replaced[6].

Step 1: In a flame-dried Schlenk tube, 2-(2-methylphenyl)acetonitrile (1 mL, 7.7 mmol, 1 equiv.) was dissolved in *α,α,α*-trifluorotoluene (20 mL). To this solution were added *N*-bromosuccinimide (NBS) (1.5 g, 1.1 equiv) and azobisisobutyronitrile (AIBN) (14 mg). The mixture was heated under reflux for 2 hours. Subsequently, water was added

to quench the reaction and the organic phase was extracted. The organic phase was dried over Na_2SO_4 and concentrated under reduced pressure. The crude product obtained was directly used in the subsequent step without further purification.

Step 2: $Pd(OAc)_2$ (11.2 mg, 0.05 mmol, 1.0 mol%), PPh_3 (26.2 mg, 0.1 mmol, 2.0 mol%), arylboronic acid (1.5 equiv) and K_3PO_4 (4.25 g, 20.0 mmol, 4.0 equiv) were added to a pre-dried flask. After protecting the reaction mixture with argon, dry toluene (15 mL) followed by 2-(bromomethyl)benzonitrile (980.3 mg, 5.0 mmol, 1.0 equiv.) were added. The mixture was stirred at 80 °C until all starting material was consumed (9 hours) and then quenched with water. The solution was extracted with Et_2O and the organic phase was washed with water, NaOH solution (1 M), brine and dried over anhydrous Na_2SO_4. The solvent was removed and the product was isolated by flash column chromatography (Hexane/EtOAc, 4:1 v/v).

Subsequently, the requisite nitrile was obtained, and then following the GP3 to give **1au** as a white solid in 37% yield.

mp: 99–101 °C; TLC (Hexane/EtOAc, 6:1 v/v): $R_f = 0.14$.

^{1}H NMR (400 MHz, $CDCl_3$): δ 7.64 (d, J = 8.4 Hz, 2H), 7.26 (d, J = 7.8 Hz, 2H), 7.20–7.09 (m, 3H), 7.08–7.01 (m, 3H), 6.92 (d, J = 8.2 Hz, 2H), 4.24 (s, 1H), 3.89 (s, 2H), 3.05 (q, J = 7.0 Hz, 2H), 2.75 (t, J = 7.3 Hz, 2H), 2.41 (s, 3H), 2.30 (s, 3H).

^{13}C NMR (100 MHz, $CDCl_3$): δ 143.5, 139.2, 137.5, 137.1, 136.2, 135.8, 131.1, 129.8, 129.8, 129.3, 128.6, 127.2, 127.2, 127.0, 43.5, 38.7, 33.0, 21.7, 21.1.

IR ν (cm^{-1}): 3264, 2853, 1430, 1324, 1153, 1094, 811, 771.

HRMS(ESI) *m/z*: Calcd. for $[C_{21}H_{29}NNaO_3S]^+$: 380.1679; Found: 380.1684.

2.5.3. General protocol for C(sp^3)–H functionalization without light irradiation

Optimization studies

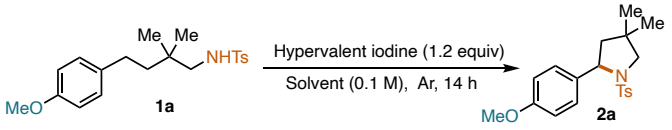

The sulfonamide **1a** (0.05 mmol, 1.0 equiv) and hypervalent iodine (0.06 mmol, 1.2 equiv) were added to a reaction vial equipped with a stir bar. This reaction vial was

then brought into an argon-filled glovebox. Inside the glovebox, 0.5 mL of dry solvent were added to the mixture, and the reaction vial was sealed with a cap equipped with a Teflon-septa. The sealed vial was removed from the glovebox and stirred at room temperature for 14 hours. After completion of the reaction, volatiles were evaporated under reduced pressure and the residue was dissolved in $CDCl_3$ and analyzed by ^1H NMR using 1,1,2,2-tetrachloroethane as the internal standard.

Table 2.8. Optimization for C(sp^3)–H functionalization without light[a]

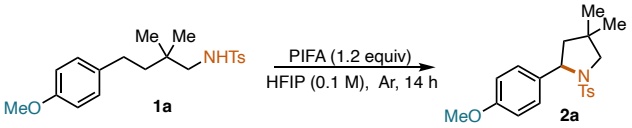

Entry	Variation from standard condition	Yield of **2j** (%)
1	none	72
2	PIDA instead of PIFA	NR
3	DCM instead of HFIP	NR
4	2-Propanol instead of HFIP	NR

[a] Standard reaction condition: **1a** (0.05 mmol), PIFA (1.2 equiv), HFIP (0.5 mL) under argon atmosphere for 14 hours. Yields were determined by ^1H NMR analysis of the crude mixture using 1,1,2,2-tetrachloroethane as the internal standard.

General synthetic procedure (GP4)

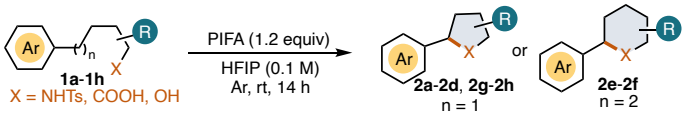

The sulfonamide **1a-1h** (0.15 mmol, 1.0 equiv) and PIFA (0.18 mmol, 1.2 equiv) were added to a vial equipped with a stir bar. This vial was then brought into an argon-filled glovebox. Inside the glovebox, 1.5 mL of dry HFIP were added to the mixture, and the vial was sealed with a cap equipped with a Teflon-septa. The sealed vial was removed from the glovebox and stirred at room temperature for 14 hours. After completion of the reaction, volatiles were evaporated under reduced pressure and the resulting crude product was purified by chromatography (silica gel, *n*-hexane/ethyl acetate) to obtain the pure product **2a-2h**.

Characterization of the resulting products following GP4

2-(4-methoxyphenyl)-4,4-dimethyl-1-tosylpyrrolidine (2a)

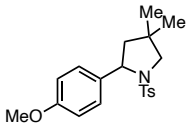

Following the GP4. Column chromatography was performed using a Hexane/EtOAc (15:1) as eluent to afford product as a white solid (33.7 mg, 0.094 mmol, 62% yield). TLC (Hexane/EtOAc, 8:1 v/v): R_f = 0.21. The NMR spectra match those previously described in literature.[11]

^{1}H NMR (400 MHz, $CDCl_3$): δ 7.51 (d, J = 8.4 Hz, 2H), 7.23–7.15 (m, 4H), 6.79 (d, J = 8.7 Hz, 2H), 4.66 (dd, J = 9.5, 7.2 Hz, 1H), 3.79 (s, 3H), 3.43 (dd, J = 10.3, 1.5 Hz, 1H), 3.32 (d, J = 10.3 Hz, 1H), 2.39 (s, 3H), 1.99 (ddd, J = 12.8, 7.2, 1.5 Hz, 1H), 1.71 (dd, J = 12.8, 9.5 Hz, 1H), 1.05 (s, 3H), 0.77 (s, 3H).

^{13}C NMR (100 MHz, $CDCl_3$): δ 158.8, 143.0, 136.1, 135.0, 129.4, 127.9, 127.5, 113.8, 63.4, 61.9, 55.4, 51.6, 38.1, 26.3, 25.8, 21.6.

4,4-dimethyl-2-(4-(pyrrolidin-1-yl)phenyl)-1-tosylpyrrolidine (2b)

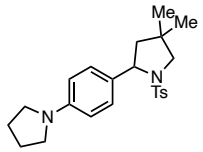

Following the GP4. Column chromatography was performed using a Hexane/EtOAc (15:1) as eluent to afford product as a white solid (24.7 mg, 0.062 mmol, 41% yield).

mp: 115–117 °C; TLC (Hexane/EtOAc, 8:1 v/v): R_f = 0.13.

^{1}H NMR (400 MHz, $CDCl_3$): δ 7.51 (d, J = 8.2 Hz, 2H), 7.18 (d, J = 8.0 Hz, 2H), 7.10 (d, J = 8.6 Hz, 2H), 6.45 (d, J = 8.6 Hz, 2H), 4.60 (dd, J = 9.5, 7.1 Hz, 1H), 3.41 (dd, J = 10.2, 1.5 Hz, 1H), 3.31 (d, J = 10.2 Hz, 1H), 3.29–3.21 (m, 4H), 2.38 (s, 3H), 2.03–1.92 (m, 5H), 1.74 (dd, J = 12.8, 9.5 Hz, 1H), 1.06 (s, 3H), 0.78 (s, 3H).

^{13}C NMR (100 MHz, $CDCl_3$): δ 147.4, 142.6, 136.3, 129.3, 129.1, 127.8, 127.5, 111.5, 63.8, 61.9, 51.5, 47.8, 37.8, 26.4, 25.9, 25.6, 21.6.

IR ν (cm^{-1}): 2877, 1495, 1335, 1155, 1092, 1054, 756, 687.

HRMS(ESI) *m/z*: Calcd. for $[C_{23}H_{31}N_2O_2S]^+$: 399.2101; Found: 399.2105.

2-([1,1'-biphenyl]-4-yl)-4,4-dimethyl-1-tosylpyrrolidine (2c)

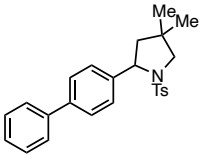

Following the GP4. Column chromatography was performed using a Hexane/EtOAc (15:1) as eluent to afford product as a white solid (51.9 mg, 0.128 mmol, 85% yield).

mp: 176–178 °C; TLC (Hexane/EtOAc, 8:1 v/v): $R_f = 0.23$.

^{1}H NMR (400 MHz, $CDCl_3$): δ 7.61–7.52 (m, 4H), 7.50–7.40 (m, 4H), 7.37–7.30 (m, 3H), 7.20 (d, J = 8.0 Hz, 2H), 4.76 (dd, J = 9.4, 7.3 Hz, 1H), 3.48 (dd, J = 10.4, 1.4 Hz, 1H), 3.37 (d, J = 10.4 Hz, 1H), 2.39 (s, 3H), 2.06 (ddd, J = 12.8, 7.3, 1.4 Hz, 1H), 1.77 (dd, J = 12.8, 9.4 Hz, 1H), 1.08 (s, 3H), 0.80 (s, 3H).

^{13}C NMR (100 MHz, $CDCl_3$): δ 143.1, 142.1, 141.1, 140.2, 136.0, 129.4, 128.8, 127.5, 127.3, 127.2, 127.2, 127.1, 63.7, 62.0, 51.6, 38.3, 26.2, 25.8, 21.6.

IR ν (cm^{-1}): 3028, 2866, 1593, 1485, 1340, 1150, 1053, 771.

HRMS(ESI) *m/z*: Calcd. for $[C_{25}H_{27}NNaO_2S]^+$: 428.1655; Found: 428.1652.

4,4-dimethyl-2-(4'-methyl-[1,1'-biphenyl]-4-yl)-1-tosylpyrrolidine (2d)

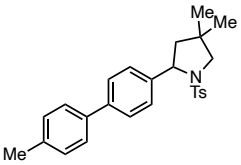

Following the GP4. Column chromatography was performed using a Hexane/EtOAc (15:1) as eluent to afford product as a white solid (49.1 mg, 0.117 mmol, 78% yield).

mp: 131–133 °C; TLC (Hexane/EtOAc, 8:1 v/v): $R_f = 0.18$.

^{1}H NMR (400 MHz, $CDCl_3$): δ 7.55 (d, J = 8.3 Hz, 2H), 7.50–7.42 (m, 4H), 7.31 (d, J = 8.2 Hz, 2H), 7.24 (d, J = 7.7 Hz, 2H), 7.20 (d, J = 7.9 Hz, 2H), 4.75 (dd, J = 9.4, 7.3 Hz, 1H), 3.48 (dd, J = 10.4, 1.4 Hz, 1H), 3.37 (d, J = 10.4 Hz, 1H), 2.40 (s, 3H),

2.38 (s, 3H), 2.05 (ddd, J = 12.8, 7.3, 1.4 Hz, 1H), 1.77 (dd, J = 12.8, 9.4 Hz, 1H), 1.08 (s, 3H), 0.80 (s, 3H).

^{13}C NMR (100 MHz, $CDCl_3$): δ 143.1, 141.7, 140.1, 138.2, 137.1, 136.1, 129.6, 129.4, 127.5, 127.1, 127.0, 127.0, 63.7, 62.0, 51.6, 38.3, 26.2, 25.8, 21.6, 21.2.

IR ν (cm^{-1}): 2876, 1496, 1342, 1154, 1092, 808, 687, 659.

HRMS(ESI) *m/z*: Calcd. for $[C_{26}H_{29}NNaO_2S]^+$: 442.1811; Found: 442.1815.

2-(4-methoxyphenyl)-5,5-dimethyl-1-tosylpiperidine (2e)

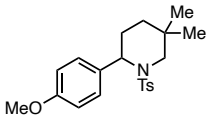

Following the GP4. Column chromatography was performed using a Hexane/EtOAc (15:1) as eluent to afford product as a white solid (35.1 mg, 0.095 mmol, 63% yield). mp: 104–106 °C; TLC (Hexane/EtOAc, 8:1 v/v): R_f = 0.21.

^{1}H NMR (400 MHz, $CDCl_3$): δ 7.64 (d, J = 8.3 Hz, 2H), 7.22 (d, J = 7.8 Hz, 2H), 7.07 (d, J = 8.1 Hz, 2H), 6.77 (d, J = 8.8 Hz, 2H), 5.16 (t, J = 4.0 Hz, 1H), 3.77 (s, 3H), 3.37 (d, J = 13.6 Hz, 1H), 2.84 (d, J = 13.6 Hz, 1H), 2.39 (s, 3H), 2.10–1.99 (m, 2H), 1.33–1.15 (m, 2H), 0.79 (s, 3H), 0.78 (s, 3H).

^{13}C NMR (100 MHz, $CDCl_3$): δ 158.5, 142.8, 138.7, 130.9, 129.5, 128.3, 127.1, 113.9, 55.3, 55.1, 52.5, 32.6, 30.5, 28.7, 25.8, 24.3, 21.6.

IR ν (cm^{-1}): 2924, 1508, 1324, 1154, 1093, 976, 907, 749.

HRMS(ESI) *m/z*: Calcd. for $[C_{21}H_{28}NO_3S]^+$: 374.1784; Found: 374.1776.

2-([1,1'-biphenyl]-4-yl)-5,5-dimethyl-1-tosylpiperidine (2f)

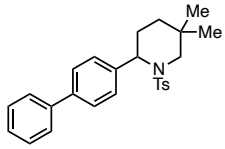

Following the GP4. Column chromatography was performed using a Hexane/EtOAc (15:1) as eluent to afford product as a white solid (50.5 mg, 0.120 mmol, 80% yield).

TLC (Hexane/EtOAc, 19:1 v/v): R_f = 0.24. The NMR spectra match those previously described in literature.[25]

^{1}H NMR (400 MHz, $CDCl_3$): δ 7.67 (d, J = 8.3 Hz, 2H), 7.56 (dd, J = 8.4, 1.3 Hz, 2H). 7.49–7.40 (m, 4H), 7.36–7.31 (m, 1H), 7.25–7.19 (m, 4H), 5.26 (t, J = 4.4 Hz, 1H), 3.44 (d, J = 13.6 Hz, 1H), 2.91 (d, J = 13.6 Hz, 1H), 2.40 (s, 3H), 2.16–2.05 (m, 2H), 1.33–1.20 (m, 2H), 0.82 (s, 6H).

^{13}C NMR (100 MHz, $CDCl_3$): δ 142.9, 140.8, 139.7, 138.7, 138.2, 129.6, 128.9, 127.6, 127.4, 127.2, 127.2, 127.1, 55.4, 52.7, 32.7, 30.5, 28.8, 25.9, 24.3, 21.6.

5-(4-methoxyphenyl)dihydrofuran-2(3H)-one (2g)

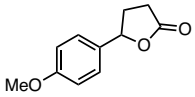

Following the GP4. Column chromatography was performed using a Hexane/EtOAc (5:1) as eluent to afford product as a colorless liquid, (22.3 mg, 0.116 mmol, 77% yield).

mp: 53–55 °C; TLC (Hexane/EtOAc, 2:1 v/v): R_f = 0.34.

^{1}H NMR (400 MHz, $CDCl_3$): δ 7.26 (d, J = 8.3 Hz, 2H), 6.91 (d, J = 8.7 Hz, 2H), 5.45 (dd, J = 8.5, 6.1 Hz, 1H), 3.81 (s, 3H), 2.68–2.54 (m, 3H), 2.27–2.13 (m, 1H).

^{13}C NMR (100 MHz, $CDCl_3$): δ 177.1, 159.9, 131.3, 127.1, 114.2, 81.5, 55.5, 31.0, 29.3.

IR ν (cm^{-1}): 3502, 1609, 1514, 1246, 1176, 1014, 833, 804.

HRMS(ESI) *m/z*: Calcd. for $[C_{11}H_{12}NaO_3]^+$: 215.0679; Found: 215.0678.

2-(4-methoxyphenyl)tetrahydrofuran (2h)

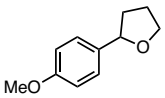

Following the GP4. Column chromatography was performed using a Hexane/EtOAc (10:1) as eluent to afford product as a colorless liquid, (16.04 mg, 0.090 mmol, 60%

yield). TLC (Hexane/EtOAc, 4:1 v/v): R_f = 0.32. The NMR spectra match those previously described in literature.[48b]

^{1}H NMR (400 MHz, $CDCl_3$): δ 7.26 (d, J = 8.3 Hz, 2H), 6.87 (d, J = 8.8 Hz, 2H), 4.83 (t, J = 7.2 Hz, 1H), 4.12–4.04 (m, 1H), 3.95–3.87 (m, 1H), 3.80 (s, 3H), 2.32–2.22 (m, 1H), 2.10–1.93 (m, 2H), 1.85–1.73 (m, 1H).

^{13}C NMR (100 MHz, $CDCl_3$): δ 159.0, 135.5, 127.1, 113.8, 80.6, 68.6, 55.4, 34.6, 26.2.

2.5.4. Gram-scale synthesis of 2c

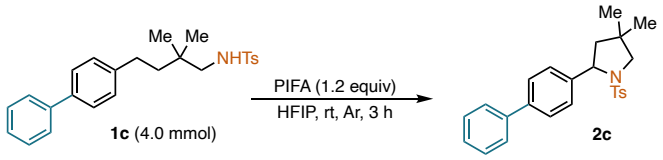

In a Schlenk flask equipped with a magnetic stir bar, N-(4-([1,1'-biphenyl]-4-yl)-2,2-dimethylbutyl)-4-methylbenzenesulfonamide **1c** (1.63 g, 4.0 mmol) and PIFA (2.06 g, 4.8 mmol) were added. The reaction mixture was connected to a vacuum condenser, and the entire system was purged with an argon atmosphere. Subsequently, 40 mL of HFIP was added to the reaction mixture under an inert atmosphere. The reaction mixture was stirred for 3 hours, and then the solvent was evaporated. The crude product was purified by chromatography using silica gel and a mixture of n-hexane and ethyl acetate as the eluent. This purification step afforded product **2c** as a white solid (1.31 g, 81% yield).

2.5.5. General protocol for C(sp^3)–H functionalization under light irradiation

Optimization studies for the 5-membered ring formation

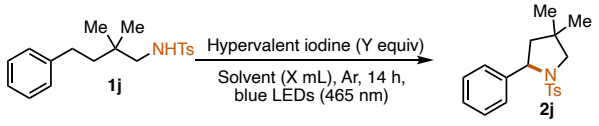

Reactions performed using **set-up 1** in Figure 2.10. The sulfonamide **1j** (0.05 mmol, 1.0 equiv) and hypervalent iodine (Y equiv) were added to a reaction vial equipped with a stir bar. Subsequently, this reaction vial was brought into an argon-filled glovebox, X mL of dry solvent were added to the mixture, and the reaction vial was

sealed with a Teflon-septa equipped cap. The vial was carefully taken outside of the glovebox and subjected to irradiation under stirring for 14 hours. After completion of the reaction, volatiles were evaporated under reduced pressure and the residue was dissolved in $CDCl_3$ and analyzed by ^1H NMR using mesitylene as the internal standard

Table 2.9. Solvent optimization[a]

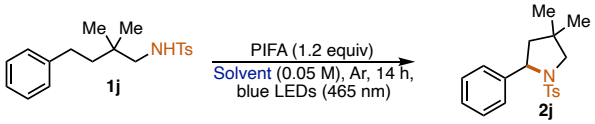

Entry	Solvent	Yield of **2j** (%)
1	HFIP	86
2	TFE	35
3	2-Propanol	0
4	MeCN	trace
5	Toluene	0
6	DCE	19
7	Me-HFIP	trace
8	PFTB	33

[a]Reaction condition: **1j** (0.05 mmol), PIFA (1.2 equiv), solvent (1 mL) under argon atmosphere for 14 hours, blue LEDs, 465 nm, 30~40 °C. Yield determined by ^1H NMR analysis of the crude mixture using mesitylene as the internal standard.

Table 2.10. Hypervalent iodine reagent optimization[a]

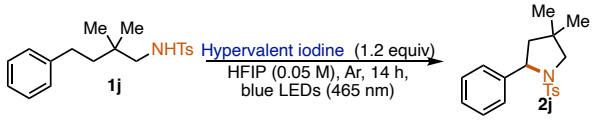

Entry	HIR	Yield of **2j** (%)
1	PIFA	86
2	PIDA	9
3	PhI(*m*CBA)$_2$	7

[a]Reaction condition: **1j** (0.05 mmol), Hypervalent iodine (1.2 equiv), HFIP (1 mL) under argon atmosphere for 14 hours, blue LEDs, 465 nm, 30~40 °C. Yield determined by ^1H NMR analysis of the crude mixture using mesitylene as the internal standard.

Table 2.11. Concentration optimization[a]

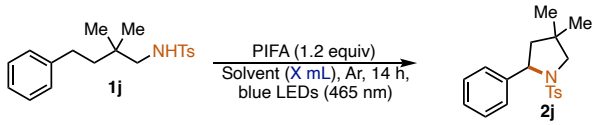

Entry	HFIP (x mL)	Yield of **2j** (%)
1	0.25	82
2	0.5	84
3	1.0	86
4	1.5	88
5	2.0	88

[a]Reaction condition: **1j** (0.05 mmol), PIFA (1.2 equiv), HFIP (X mL) under argon atmosphere for 14 hours, blue LEDs, 465 nm, 30~40 ºC. Yield determined by ^{1}H NMR analysis of the crude mixture using mesitylene as the internal standard.

Table 2.12. Screening the amount of PIFA[a]

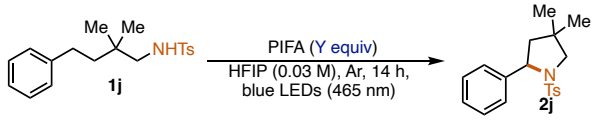

Entry	PIFA (x equiv)	Yield of **2j** (%)
1	0.6	49
2	1.2	88
3	1.5	88

[a]Reaction condition: **1j** (0.05 mmol), PIFA (Y equiv), HFIP (1.5 mL) under argon atmosphere for 14 hours, blue LEDs, 465 nm, 30~40 ºC. Yield determined by ^{1}H NMR analysis of the crude mixture using mesitylene as the internal standard.

Table 2.13. Control experiments[a]

Entry	Changes from the standard conditions	Yield of **2j** (%)
1	Standard conditions	88
2	Without *hv*, rt	trace
3	Without *hv*, 40 ºC	trace
4	Without PIFA	0
5	Under air	14

[a]Standard reaction condition: **1j** (0.05 mmol), PIFA (1.2 equiv), HFIP (1.5 mL) under argon atmosphere for 14 hours, blue LEDs, 465 nm, 30~40 ºC. Yield determined by ^{1}H NMR analysis of the crude mixture using mesitylene as the internal standard.

Optimization studies for the 6-membered ring formation

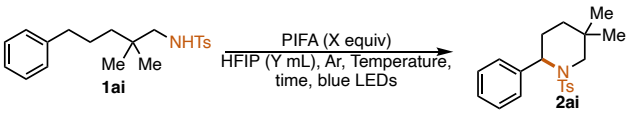

Reactions performed using **set-up 1** (Figure 2.10) or **set-up 2** in (Figure 2.11) The sulfonamide **1ai** (0.05 mmol, 1.0 equiv) and PIFA (X equiv) were added to a reaction vial equipped with a stir bar. Subsequently, this reaction vial was brought into an argon-filled glovebox, Y mL of dry HFIP were added to the mixture, and the reaction vial was sealed with a Teflon-septa equipped cap. The vial was carefully taken outside of the glovebox and subjected to irradiation under stirring different temperature for some hours. After completion of the reaction, volatiles were evaporated under reduced pressure and the residue was dissolved in $CDCl_3$ and analyzed by ^1H NMR using mesitylene as the internal standard.

Table 2.14. Optimization of photoredox intramolecular C(sp^3)–H functionalization for the formation of 6-membered ring product.[a]

Entry	Temperature (°C)	HFIP (mL)	PIFA (equiv)	Time (h)	Yield of **2ai** (%)
1[b]	30-40	1.5	1.2	14	65
2[b]	30-40	1.0	1.2	14	65
3[c]	10	1.0	1.2	24	71
4[c]	5	1.0	1.2	30	72
5[c]	5	1.0	1.3	30	78
6[c]	5	1.0	1.4	30	72
7[c]	5	1.0	1.3	18	75

[a]Reaction condition: **1ai** (0.05 mmol), PIFA (x equiv), HFIP (y mL) under argon atmosphere. Yields were determined by ^1H NMR analysis of the crude mixture using mesitylene as the internal standard. [b]The reaction was performed using blue LED strip, 465 nm, (the illumination set-up 1 in Figure 2.10). [c]The reaction was performed using a 900 mA blue LED, 470 nm, (the illumination set-up 2 in (Figure 2.11).

General procedure (GP5) for the 5-membered ring formation

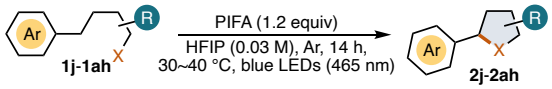

Reactions performed using **set-up 1** in Figure 2.10. The sulfonamide **1j-1ah** (0.15 mmol, 1.0 equiv) and PIFA (0.16 mmol, 1.2 equiv.) were added to a reaction vial

equipped with a stir bar. Subsequently, this reaction vial was brought into an argon-filled glovebox, 4.5 mL of dry HFIP were added to the mixture, and the reaction vial was sealed with a Teflon-septa equipped cap. The vial was carefully taken outside of the glovebox and subjected to irradiation under stirring for 14 hours. After completion of the reaction, volatiles were evaporated under reduced pressure and the resulting crude product was purified by chromatography (silica gel, *n*-hexane/ethyl acetate) to obtain the pure product **2j-2ah**.

Characterization of 5-membered ring products

4,4-dimethyl-2-phenyl-1-tosylpyrrolidine (2j)

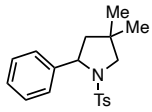

Following the GP5. Column chromatography was performed using a Hexane/EtOAc (20:1) as eluent to afford product as a white solid (42.4 mg, 0.129 mmol, 86% yield). TLC (Hexane/EtOAc, 19:1 v/v): R_f = 0.31. The NMR spectra match those previously described in literature.[11]

^{1}H NMR (400 MHz, $CDCl_3$): δ 7.53 (d, J = 8.3 Hz, 2H), 7.30–7.24 (m, 4H), 7.23–7.17 (m, 3H), 4.70 (dd, J = 9.4, 7.3 Hz, 1H), 3.44 (dd, J = 10.3, 1.5 Hz, 1H), 3.34 (d, J = 10.4 Hz, 1H), 2.39 (s, 3H), 2.02 (ddd, J = 12.8, 7.3, 1.5 Hz, 1H), 1.72 (dd, J = 12.8, 9.4 Hz, 1H), 1.05 (s, 3H), 0.76 (s, 3H).

^{13}C NMR (100 MHz, $CDCl_3$): δ 143.1, 143.0, 135.9, 129.4, 128.4, 127.5, 127.1, 126.6, 63.9, 62.0, 51.6, 38.2, 26.2, 25.8, 21.6.

4,4-dimethyl-1-((4-nitrophenyl)sulfonyl)-2-phenylpyrrolidine (2k)

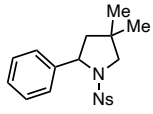

Following the GP5. Column chromatography was performed using a Hexane/EtOAc (20:1) as eluent to afford product as a white solid (40.8 mg, 0.113 mmol, 75% yield). TLC (Hexane/EtOAc, 9:1 v/v): R_f = 0.21. The NMR spectra match those previously described in literature.[11]

^{1}H NMR (400 MHz, $CDCl_3$): δ 8.11 (d, J = 8.8 Hz, 2H), 7.58 (d, J = 8.9 Hz, 2H), 7.22–7.14 (m, 3H), 7.13–7.07 (m, 2H), 4.86 (dd, J = 9.8, 7.2 Hz, 1H), 3.65 (dd, J = 10.0, 1.7 Hz, 1H), 3.30 (d, J = 10.0 Hz, 1H), 2.14 (ddd, J = 12.9, 7.2, 1.7 Hz, 1H), 1.78 (dd, J = 12.9, 9.8 Hz, 1H), 1.13 (s, 3H), 1.02 (s, 3H).

^{13}C NMR (100 MHz, $CDCl_3$): δ 149.5, 145.9, 141.4, 128.5, 128.1, 127.7, 127.2, 123.8, 64.1, 61.8, 51.3, 38.5, 25.7, 25.7.

1-((4-bromophenyl)sulfonyl)-4,4-dimethyl-2-phenylpyrrolidine (2l)

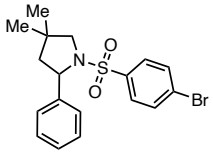

Following the GP5. Column chromatography was performed using a Hexane/EtOAc (20:1) as eluent to afford product as a white solid (48.8 mg, 0.124 mmol, 83% yield). mp: 113–115 °C; TLC (Hexane/EtOAc, 8:1 v/v): R_f = 0.28.

^{1}H NMR (400 MHz, $CDCl_3$): δ 7.48 (d, J = 8.6 Hz, 2H), 7.40 (d, J = 8.6 Hz, 2H), 7.25–7.14 (m, 5H), 4.76 (dd, J = 9.6, 7.2 Hz, 1H), 3.52 (dd, J = 10.2, 1.6 Hz, 1H), 3.31 (d, J = 10.2 Hz, 1H), 2.08 (ddd, J = 12.9, 7.2, 1.6 Hz, 1H), 1.75 (dd, J = 12.9, 9.6 Hz, 1H), 1.09 (s, 3H), 0.90 (s, 3H).

^{13}C NMR (100 MHz, $CDCl_3$): δ 142.2, 138.6, 131.9, 128.7, 128.4, 127.4, 127.1, 126.8, 64.0, 61.9, 51.5, 38.3, 25.9, 25.8.

IR ν (cm^{-1}): 3257, 2958, 1573, 1465, 1349, 1088, 817, 756.

HRMS(ESI) *m/z*: Calcd. for $[C_{18}H_{21}BrNO_2S]^+$: 394.0471; Found: 394.0475.

4,4-dimethyl-1-(methylsulfonyl)-2-phenylpyrrolidine (2m)

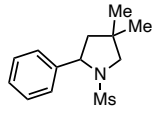

Following the GP5. Column chromatography was performed using a Hexane/EtOAc (20:1) as eluent to afford product as a white solid (32.1 mg, 0.127 mmol, 84% yield). TLC (Hexane/EtOAc, 9:1 v/v): R_f = 0.17. The NMR spectra match those previously described in literature.[14]

^{1}H NMR (400 MHz, $CDCl_3$): δ 7.39–7.30 (m, 4H), 7.30–7.23 (m, 1H), 4.90 (dd, J = 9.8, 7.3 Hz, 1H), 3.66 (dd, J = 10.2, 1.7 Hz, 1H), 3.28 (d, J = 10.2 Hz, 1H), 2.52 (s, 3H), 2.19 (ddd, J = 12.8, 7.3, 1.7 Hz, 1H), 1.83 (dd, J = 12.8, 9.7 Hz, 1H), 1.18 (s, 3H), 1.14 (s, 3H).

^{13}C NMR (100 MHz, $CDCl_3$): δ 142.6, 128.8, 127.8, 126.9, 63.6, 61.5, 51.6, 40.7, 38.5, 25.8, 25.8.

4,4-dimethyl-2-phenyl-1-((trifluoromethyl)sulfonyl)pyrrolidine (2n)

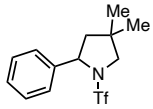

Following the GP5. Column chromatography was performed using a Hexane/EtOAc (10:1) as eluent to afford product as a white liquid (36.4 mg, 0.118 mmol, 79% yield). TLC (Hexane/EtOAc, 10:1 v/v): R_f = 0.40.

^{1}H NMR (400 MHz, $CDCl_3$): δ 7.38–7.32 (m, 2H), 7.32–7.26 (m, 3H), 5.07 (dd, J = 9.7, 7.3 Hz, 1H), 3.68 (dd, J = 10.4, 1.8 Hz, 1H), 3.45 (d, J = 10.5 Hz, 1H), 2.27 (ddd, J = 13.0, 7.3, 1.8 Hz, 1H), 1.91 (dd, J = 12.8, 9.8 Hz, 1H), 1.21 (s, 3H), 1.18 (s, 3H).

^{13}C NMR (100 MHz, $CDCl_3$): δ 141.3, 128.7, 128.1, 126.8, 119.9 (q, J = 321 Hz), 65.2, 62.8, 51.2, 39.0, 25.5, 25.4.

^{19}F NMR (375 MHz, $CDCl_3$): δ -77.6 (s, 3F).

IR ν (cm^{-1}): 2962, 1467, 1378, 1223, 1137, 1050, 770, 698.

HRMS(ESI) *m/z*: Calcd. for $[C_{13}H_{16}F_3NNaO_2S]^+$: 330.0746; Found: 330.0741.

1-(4,4-dimethyl-2-phenylpyrrolidin-1-yl)-2,2,2-trifluoroethan-1-one (2o)

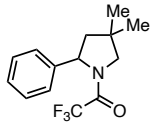

Following the GP5. Column chromatography was performed using a Hexane/EtOAc (20:1) as eluent to afford product as a white solid (23.1 mg, 0.085 mmol, 57% yield). Traces of the other diastereomeric species were visible in NMR. TLC (Hexane/EtOAc, 19:1 v/v): R_f = 0.31. The NMR spectra match those previously described in literature.[14]

^{1}H NMR (400 MHz, $CDCl_3$): δ 7.36–7.30 (m, 2H), 7.27–7.22 (m,1H), 7.25–7.18 (m, 2H), 5.11 (dd, J = 9.9, 7.7 Hz, 1H), 3.71 (dt, J = 10.9, 1.9 Hz, 1H), 3.51 (d, J = 10.9 Hz, 1H), 2.23 (ddd, J = 13.0, 7.8, 1.7 Hz, 1H), 1.74 (dd, J = 13.0, 9.8 Hz, 1H), 1.19 (s, 3H), 1.12 (s, 3H).

^{13}C NMR (100 MHz, $CDCl_3$): δ 155.9 (d, J = 36.4 Hz), 141.7, 128.9, 127.5, 125.7, 116.4 (q, J = 288.0 Hz), 62.7, 60.6 (d, J = 2.9 Hz), 48.6, 39.0, 25.6, 25.5.

^{19}F NMR (375 MHz, $CDCl_3$): δ -72.00 (d, J = 2.4 Hz, 3F).

(4,4-dimethyl-2-phenylpyrrolidin-1-yl)(phenyl)methanone (2p)

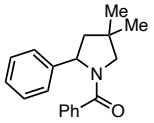

Following the GP5. Column chromatography was performed using a Hexane/EtOAc (15:1) as eluent to afford product as a white solid (35.5 mg, 0.127 mmol, 85% yield). Traces of another diastereomeric species were visible in NMR. TLC (Hexane/EtOAc, 9:1 v/v): R_f = 0.12. The NMR spectra match those previously described in literature.[14]

^{1}H NMR (400 MHz, $CDCl_3$): δ 7.65–7.57 (m, 2H), 7.47–7.37 (m, 3H), 7.37–7.27 (m, 4H), 7.24–7.18 (m, 1H), 5.33 (dd, J = 10.2, 7.7 Hz, 1H), 3.58 (d, J = 10.4 Hz, 1H), 3.37 (dd, J = 10.4, 1.9 Hz, 1H), 2.23 (ddd, J = 12.8, 7.6, 1.9 Hz, 1H), 1.77 (dd, J = 12.7, 10.2 Hz, 1H), 1.10 (s, 3H), 1.03 (s, 3H).

^{13}C NMR (100 MHz, $CDCl_3$): δ 170.3, 143.7, 136.8, 130.4, 128.7, 128.3, 127.9, 126.9, 125.8, 64.2, 60.9, 49.4, 39.1, 25.7, 25.5.

4,4-dimethyl-2-(o-tolyl)-1-tosylpyrrolidine (2q)

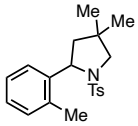

Following the GP5. Column chromatography was performed using a Hexane/EtOAc (20:1) as eluent to afford product as a white solid (34.9 mg, 0.102 mmol, 68% yield). TLC (Hexane/EtOAc, 9:1 v/v): R_f = 0.35. The NMR spectra match those previously described in literature.[48a]

^{1}H NMR (400 MHz, $CDCl_3$): δ 7.54 (d, J = 8.3 Hz, 2H), 7.32–7.27 (m, 1H), 7.21 (d, J = 7.8 Hz, 2H), 7.13–7.02 (m, 3H), 4.99 (dd, J = 9.4, 7.4 Hz, 1H), 3.49 (dd, J = 10.4, 1.5 Hz, 1H), 3.34 (d, J = 10.5 Hz, 1H), 2.39 (s, 3H), 2.35 (s, 3H), 2.06 (ddd, J = 12.7, 7.4, 1.5 Hz, 1H), 1.61 (dd, J = 12.7, 9.4 Hz, 1H), 1.07 (s, 3H), 0.80 (s, 3H).

^{13}C NMR (100 MHz, $CDCl_3$): δ 143.1, 141.2, 136.1, 134.2, 130.3, 129.4, 127.5, 126.8, 126.4, 126.3, 61.8, 60.6, 50.0, 38.4, 26.2, 25.9, 21.6, 19.4.

2-(2-fluorophenyl)-4,4-dimethyl-1-tosylpyrrolidine (2r)

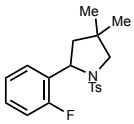

Following the GP5. Column chromatography was performed using a Hexane/EtOAc (20:1) as eluent to afford product as a white solid (26.1 mg, 0.075 mmol, 50% yield). TLC (Hexane/EtOAc, 9:1 v/v): R_f = 0.31. The NMR spectra match those previously described in literature.[48a]

^{1}H NMR (400 MHz, $CDCl_3$): δ 7.60 (d, J = 8.3 Hz, 2H), 7.48 (td, J = 7.7, 1.9 Hz, 1H), 7.24 (d, J = 7.9 Hz, 2H), 7.21–7.15 (m, 1H), 7.09 (td, J = 7.5, 1.2 Hz, 1H), 6.93 (ddd, J = 10.8, 8.1, 1.2 Hz, 1H), 4.96 (dd, J = 9.1, 7.5 Hz, 1H), 3.37 (s, 2H), 2.40 (s, 3H), 2.05 (dd, J = 12.7, 7.5 Hz, 1H), 1.74 (dd, J = 12.7, 9.0 Hz, 1H), 1.05 (s, 3H), 0.70 (s, 3H).

^{13}C NMR (100 MHz, $CDCl_3$): δ 160.2 (d, J = 246.5 Hz), 143.3, 135.3, 130.0 (d, J = 12.2 Hz), 129.53, 128.8 (d, J = 4.2 Hz), 128.7 (d, J = 8.3 Hz), 127.56, 124.2 (d, J = 3.5 Hz), 115.3 (d, J = 21.7 Hz), 61.6, 58.0 (d, J = 2.6 Hz), 49.3, 38.4, 26.2, 25.8, 21.6.

^{19}F NMR (375 MHz, $CDCl_3$): δ -119.52–-119.74 (m,1F).

2-(3-fluorophenyl)-4,4-dimethyl-1-tosylpyrrolidine (2s)

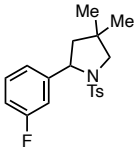

Following the GP5. Column chromatography was performed using a Hexane/EtOAc (20:1) as eluent to afford product as a white solid (31.8 mg, 0.092 mmol, 61% yield). mp: 83–85 °C; TLC (Hexane/EtOAc, 8:1 v/v): R_f = 0.25.

^{1}H NMR (400 MHz, $CDCl_3$): δ 7.56 (d, J = 8.4 Hz, 2H), 7.25–7.18 (m, 3H), 7.06 (d, J = 7.7 Hz, 1H), 6.96–6.84 (m, 2H), 4.69 (dd, J = 9.3, 7.3 Hz, 1H), 3.44 (dd, J = 10.4, 1.5 Hz, 1H), 3.33 (d, J = 10.5 Hz, 1H), 2.40 (s, 3H), 2.02 (ddd, J = 12.8, 7.3, 1.5 Hz, 1H), 1.68 (dd, J = 12.8, 9.3 Hz, 1H), 1.05 (s, 3H), 0.75 (s, 3H).

^{13}C NMR (100 MHz, $CDCl_3$): δ 163.0 (d, J = 245.6 Hz), 145.9 (d, J = 6.9 Hz), 143.4, 135.7, 129.9 (d, J = 8.2 Hz), 129.5, 127.5, 122.2 (d, J = 2.7 Hz), 114.1 (d, J = 21.3 Hz), 113.5 (d, J = 22.2 Hz), 63.4 (d, J = 2.0 Hz), 62.0, 51.5, 38.3, 26.2, 25.8, 21.6.

^{19}F NMR (375 MHz, $CDCl_3$): δ -113.45 (td, 1F).

IR ν (cm^{-1}): 3066, 2960, 1592, 1341, 1156, 1089, 776, 691.

HRMS(ESI) *m/z*: Calcd. for $[C_{19}H_{23}FNO_2S]^+$: 348.1428; Found: 348.1433.

4,4-dimethyl-2-(p-tolyl)-1-tosylpyrrolidine (2t)

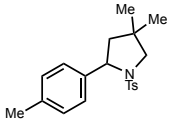

Following the GP5. Column chromatography was performed using a Hexane/EtOAc (20:1) as eluent to afford product as a white solid (41.6 mg, 0.121 mmol, 81% yield). TLC (Hexane/EtOAc, 19:1 v/v): R_f = 0.25. The NMR spectra match those previously described in literature.[11]

^{1}H NMR (400 MHz, $CDCl_3$): δ 7.55 (d, J = 8.2 Hz, 2H), 7.21 (d, J = 7.9 Hz, 2H), 7.17 (d, J = 8.1 Hz, 2H), 7.07 (d, J = 7.9 Hz, 2H), 4.65 (dd, J = 9.4, 7.2 Hz, 1H), 3.42 (dd, J = 10.4, 1.4 Hz, 1H), 3.34 (d, J = 10.4 Hz, 1H), 2.40 (s, 3H), 2.32 (s, 3H), 1.99 (ddd, J = 12.8, 7.2, 1.4 Hz, 1H), 1.72 (dd, J = 12.8, 9.4 Hz, 1H), 1.05 (s, 3H), 0.74 (s, 3H).

^{13}C NMR (100 MHz, $CDCl_3$): δ 143.1, 140.0, 136.8, 135.9, 129.4, 129.1, 127.5, 126.6, 63.7, 62.0, 51.6, 38.1, 26.2, 25.8, 21.6, 21.2.

2-(4-(tert-butyl)phenyl)-4,4-dimethyl-1-tosylpyrrolidine (2i)

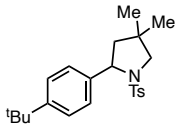

Following the GP5. Column chromatography was performed using a Hexane/EtOAc (20:1) as eluent to afford product as a white solid (43.6 mg, 0.113 mmol, 75% yield). TLC (Hexane/EtOAc, 9:1 v/v): R_f = 0.38. The NMR spectra match those previously described in literature.[48a]

^{1}H NMR (400 MHz, $CDCl_3$): δ 7.47 (d, J = 8.3 Hz, 2H), 7.23 (d, J = 8.6 Hz, 2H), 7.14 (d, J = 8.1 Hz, 4H), 4.71 (dd, J = 9.5, 7.2 Hz, 1H), 3.49 (dd, J = 10.3, 1.5 Hz, 1H), 3.33 (d, J = 10.3 Hz, 1H), 2.37 (s, 3H), 2.02 (ddd, J = 12.8, 7.2, 1.5 Hz, 1H), 1.74 (dd, J = 12.8, 9.5 Hz, 1H), 1.30 (s, 9H), 1.06 (s, 3H), 0.82 (s, 3H).

^{13}C NMR (100 MHz, $CDCl_3$): δ 150.0, 142.8, 139.6, 136.4, 129.3, 127.4, 126.5, 125.2, 63.5, 61.9, 51.6, 38.2, 34.5, 31.5, 26.2, 25.8, 21.6.

2-(4-fluorophenyl)-4,4-dimethyl-1-tosylpyrrolidine (2u)

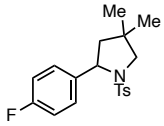

Following the GP5. Column chromatography was performed using a Hexane/EtOAc (20:1) as eluent to afford product as a white solid (44.5 mg,0.128 mmol, 85% yield). TLC (Hexane/EtOAc, 19:1 v/v): R_f = 0.27. The NMR spectra match those previously described in literature.[11]

^{1}H NMR (400 MHz, $CDCl_3$): δ 7.53 (d, J = 8.3 Hz, 2H), 7.25–7.19 (m, 4H), 6.94 (t, J = 8.7 Hz, 2H), 4.67 (dd, J = 9.4, 7.2 Hz, 1H), 3.43 (dd, J = 10.4, 1.5 Hz, 1H), 3.33 (d, J = 10.4 Hz, 1H), 2.40 (s, 3H), 2.00 (ddd, J = 12.8, 7.2, 1.5 Hz, 1H), 1.68 (dd, J = 12.8, 9.4 Hz, 1H), 1.05 (s, 3H), 0.75 (s, 3H).

^{13}C NMR (100 MHz, $CDCl_3$): δ 162.0 (d, J = 245.1 Hz), 143.3, 138.8 (d, J = 3.2 Hz), 135.8, 129.5, 128.2 (d, J = 8.1 Hz), 127.5, 115.2 (d, J = 21.4 Hz). 63.3, 61.9, 51.7, 38.2, 26.2, 25.8, 21.6.

^{19}F NMR (375 MHz, $CDCl_3$): δ -115.96 (tt, 1F).

2-(4-chlorophenyl)-4,4-dimethyl-1-tosylpyrrolidine (2v)

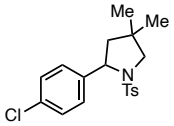

Following the GP5. Column chromatography was performed using a Hexane/EtOAc (20:1) as eluent to afford product as a white solid (43.2 mg, 0.119 mmol, 79% yield). TLC (Hexane/EtOAc, 19:1 v/v): R_f = 0.23. The NMR spectra match those previously described in literature.[11]

^{1}H NMR (400 MHz, $CDCl_3$): δ 7.54 (d, J = 8.4 Hz, 2H), 7.25–7.18 (m, 6H), 4.65 (dd, J = 9.3, 7.3 Hz, 1H), 3.42 (dd, J = 10.4, 1.4 Hz, 1H), 3.33 (d, J = 10.4 Hz, 1H), 2.40 (s, 3H), 1.99 (ddd, J = 12.8, 7.3, 1.4 Hz, 1H), 1.66 (dd, J = 12.9, 9.5 Hz, 1H), 1.04 (s, 3H), 0.73 (s, 3H).

^{13}C NMR (100 MHz, $CDCl_3$): δ 143.4, 141.7, 135.6, 132.8, 129.5, 128.5, 128.0, 127.5, 63.3, 62.0, 51.5, 38.2, 26.2, 25.7, 21.6.

2-(4-bromophenyl)-4,4-dimethyl-1-tosylpyrrolidine (2w)

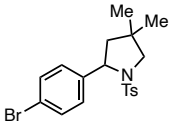

Following the GP5. Column chromatography was performed using a Hexane/EtOAc (20:1) as eluent to afford product as a white solid (42.8 mg, 0.105 mmol, 70% yield). TLC (Hexane/EtOAc, 19:1 v/v): R_f = 0.23. The NMR spectra match those previously described in literature.[11]

^{1}H NMR (400 MHz, $CDCl_3$): δ 7.54 (d, J = 8.3 Hz, 2H), 7.37 (d, J = 8.4 Hz, 2H), 7.23 (d, J = 7.9 Hz, 2H), 7.15 (d, J = 8.4 Hz, 2H), 4.63 (dd, J = 9.3, 7.3 Hz, 1H), 3.42 (dd, J = 10.4, 1.4 Hz, 1H), 3.33 (d, J = 10.5 Hz, 1H), 2.41 (s, 3H), 2.00 (ddd, J = 12.8, 7.3, 1.4 Hz, 1H), 1.66 (dd, J = 12.8, 9.4 Hz, 1H), 1.04 (s, 3H), 0.74 (s, 3H).

^{13}C NMR (100 MHz, $CDCl_3$): δ 143.4, 142.2, 135.6, 131.5, 129.5, 128.3, 127.5, 120.9, 63.3, 62.0, 51.4, 38.2, 26.2, 25.7, 21.6.

3-phenyl-2-tosyl-2-azaspiro[4.5]decane (2x)

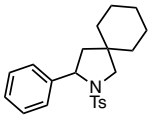

Following the GP5. Column chromatography was performed using a Hexane/EtOAc (20:1) as eluent to afford product as a white solid (47.9 mg, 0.130 mmol, 86% yield). TLC (Hexane/EtOAc, 19:1 v/v): R_f = 0.23. The NMR spectra match those previously described in literature.[11]

^{1}H NMR (400 MHz, $CDCl_3$): δ 7.60 (d, J = 8.3 Hz, 2H), 7.35–7.27 (m, 4H), 7.27–7.20 (m, 3H), 4.64 (dd, J = 9.4, 7.3 Hz, 1H), 3.64 (dd, J = 10.7, 1.4 Hz, 1H), 3.33 (d, J = 11.0 Hz, 1H), 2.42 (s, 3H), 2.13 (ddd, J = 13.0, 7.3, 1.4 Hz, 1H), 1.68 (dd, J = 12.9, 9.4 Hz, 1H), 1.53–1.40 (m, 3H), 1.39–1.23 (m, 5H), 1.12 – 0.94 (m, 2H).

^{13}C NMR (100 MHz, $CDCl_3$): δ 143.2, 143.1, 135.6, 129.4, 128.4, 127.5, 127.1, 126.5, 63.1, 59.4, 49.6, 42.1, 36.4, 34.0, 26.0, 23.9, 22.9, 21.6.

4-methyl-2-phenyl-1-tosylpyrrolidine (2y)

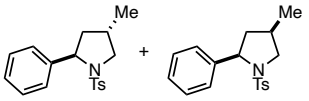

Following the GP5. Column chromatography was performed using a Hexane/EtOAc (20:1) as eluent to afford product as a white solid (39.1 mg, 0.123 mmol, 83% yield, *d.r.* = 2:1). TLC (Hexane/EtOAc, 9:1 v/v): R_f = 0.21. The NMR data of the major diastereoisomer (*anti*) is given which match those previously reported.[11]

^{1}H NMR (400 MHz, $CDCl_3$): δ 7.68 (d, J = 8.3 Hz, 0.69H), 7.61 (d, J = 8.3 Hz, 1.31H), 7.34–7.19 (m, 7H), 4.85 (dd, J = 8.4, 2.5 Hz, 0.33H), 4.64 (dd, J = 9.5, 7.2 Hz, 0.67H), 3.84 (ddd, J = 11.1, 7.3, 1.4 Hz, 0.67H), 3.74 (ddd, J = 9.4, 6.9, 0.8 Hz, 0.34H), 3.09 (t, J = 10.8 Hz, 0.66H), 2.88 (t, J = 9.2 Hz, 0.34H), 2.43 (s, 1H), 2.41 (s, 2H), 2.40–2.30 (m, 1H), 1.93–1.76 (m, 1H), 1.62–1.55 (m, 0.34H), 1.55–1.42 (m, 0.69H), 0.95 (d, J = 6.5 Hz, 2H), 0.88 (d, J = 6.6 Hz, 1H).

^{13}C NMR (100 MHz, $CDCl_3$): δ 143.4, 143.1, 135.7, 129.6, 128.4, 127.5, 127.2, 126.4, 64.7, 56.8, 45.7, 33.5, 21.6, 16.6.

2-phenyl-1-tosylpyrrolidine (2z)

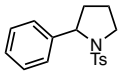

Following the GP5. Column chromatography was performed using a Hexane/EtOAc (20:1) as eluent to afford product as a white solid (32.6 mg, 0.108 mmol, 72% yield). TLC (Hexane/EtOAc, 8:1 v/v): R_f = 0.33. The NMR spectra match those previously described in literature.[11]

^{1}H NMR (400 MHz, $CDCl_3$): δ 7.67 (d, J = 8.3 Hz, 2H), 7.35–7.19 (m, 7H), 4.79 (dd, J = 8.0, 3.6 Hz, 1H), 3.66–3.57 (m, 1H), 3.47–3.38 (m, 1H), 2.42 (s, 3H), 2.03–1.93 (m, 1H), 1.90–1.77 (m, 2H), 1.71–1.61 (m, 1H).

^{13}C NMR (100 MHz, $CDCl_3$): δ 143.4, 143.2, 135.3, 129.7, 128.4, 127.6, 127.1, 126.3, 63.4, 49.5, 35.9, 24.1, 21.6.

4,4-dimethyl-2,2-diphenyl-1-tosylpyrrolidine (2aa)

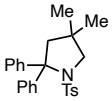

Following the GP5. Column chromatography was performed using a Hexane/EtOAc (20:1) as eluent to afford product as a white solid (53.6 mg, 0.132 mmol, 88% yield). TLC (Hexane/EtOAc, 9:1 v/v): R_f = 0.38. The NMR spectra match those previously described in literature.[48a]

^{1}H NMR (400 MHz, $CDCl_3$): δ 7.38–7.31 (m, 4H), 7.28–7.20 (m, 6H), 6.99 (d, J = 7.8 Hz, 2H), 6.82 (d, J = 8.3 Hz, 2H), 3.52 (s, 2H), 2.69 (s, 2H), 2.35 (s, 3H), 1.06 (s, 6H).

^{13}C NMR (100 MHz, $CDCl_3$): δ 144.5, 142.3, 136.7, 129.7, 128.8, 127.5, 127.3, 126.9, 76.9, 63.5, 61.3, 37.1, 28.1, 21.6.

1-(p-tolyl)-2-tosylisoindoline (2ab)

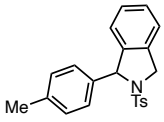

Following the GP5. Column chromatography was performed using a Hexane/EtOAc (20:1) as eluent to afford product as a white solid (44.0 mg, 0.121 mmol, 81% yield).

TLC (Hexane/EtOAc, 9:1 v/v): R_f = 0.31. The NMR spectra match those previously described in literature.[14]

^{1}H NMR (400 MHz, $CDCl_3$): δ 7.55 (d, J = 8.3 Hz, 2H), 7.24–7.20 (m, 2H), 7.19–7.13 (m, 3H), 7.13–7.03 (m, 4H), 6.88 (d, J = 7.6 Hz, 1H), 5.86 (s, 1H), 4.88–4.76 (m, 2H), 2.36 (s, 3H), 2.32 (s, 3H).

^{13}C NMR (100 MHz, $CDCl_3$): δ 143.3, 141.3, 139.1, 137.7, 135.5, 135.2, 129.6, 129.3, 128.1, 128.0, 127.7, 127.6, 123.8, 122.5, 69.4, 54.1, 21.6, 21.3.

2-ethyl-3-phenyl-2,3-dihydrobenzo[d]isothiazole 1,1-dioxide (2ac)

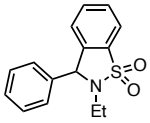

Following the GP5. Column chromatography was performed using a Hexane/EtOAc (15:1) as eluent to afford product as a white solid (35.0 mg, 0.128 mmol, 85% yield). TLC (Hexane/EtOAc, 6:1 v/v): R_f = 0.18. The NMR spectra match those previously described in literature.[13]

^{1}H NMR (400 MHz, $CDCl_3$): δ 7.88–7.78 (m, 1H), 7.54–7.45 (m, 2H), 7.43–7.30 (m, 5H), 7.10–6.99 (m, 1H), 5.40 (s, 1H), 3.39 (dq, J = 14.7, 7.4 Hz, 1H), 3.17 (dq, J = 14.2, 7.1 Hz, 1H), 1.25 (t, J = 7.2 Hz, 3H).

^{13}C NMR (100 MHz, $CDCl_3$): δ 138.4, 137.5, 134.3, 133.0, 129.4, 129.3, 129.1, 128.1, 125.1, 121.1, 64.9, 37.0, 13.6.

1,2,3,9b-tetrahydrobenzo[d]pyrrolo[1,2-b]isothiazole 5,5-dioxide (2ad)

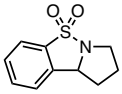

Following the GP5. Column chromatography was performed using a Hexane/EtOAc (10:1) as eluent to afford product as a white solid (15.1 mg, 0.072 mmol, 48% yield). TLC (Hexane/EtOAc, 4:1 v/v): R_f = 0.30. The NMR spectra match those previously described in literature.[11]

^{1}H NMR (400 MHz, $CDCl_3$): δ 7.74 (d, J = 7.8 Hz, 1H), 7.60 (td, J = 7.5, 1.2 Hz, 1H), 7.53–7.48 (m, 1H), 7.36 (dd, J = 7.7, 0.9 Hz, 1H), 4.99 (t, J = 6.8 Hz, 1H), 3.86–3.74 (m, 1H), 3.39–3.36 (m, 1H), 2.52–2.36 (m, 1H), 2.07–1.80 (m, 3H).

^{13}C NMR (100 MHz, $CDCl_3$): δ 140.1, 136.4, 133.3, 129.5, 124.0, 121.7, 65.2, 48.5, 32.6, 26.2.

1-(4-((2-phenylpyrrolidin-1-yl)sulfonyl)phenyl)-5-(p-tolyl)-3-(trifluoromethyl)-1H-pyrazole (2ae)

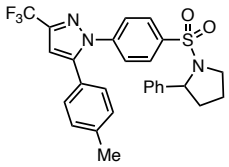

Following the GP5. Column chromatography was performed using a Hexane/EtOAc (10:1) as eluent to afford product as a white solid (65.5 mg, 0.127 mmol, 85% yield). TLC (Hexane/EtOAc, 6:1 v/v): R_f = 0.26. The NMR spectra match those previously described in literature.[49]

^{1}H NMR (400 MHz, $CDCl_3$): δ 7.73 (d, J = 8.9 Hz, 2H), 7.43 (d, J = 8.9 Hz, 2H), 7.33–7.21 (m, 5H), 7.17 (d, J = 7.9 Hz, 2H), 7.09 (d, J = 8.3 Hz, 2H), 6.75 (s, 1H), 4.79 (dd, J = 7.9, 3.8 Hz, 1H), 3.66–3.56 (m, 1H), 3.49–3.38 (m, 1H), 2.38 (s, 3H), 2.10–1.98 (m, 1H), 1.98–1.79 (m, 2H), 1.78–1.65 (m, 1H).

^{13}C NMR (100 MHz, $CDCl_3$): δ 145.4, 144.2 (q, J = 38.6 Hz), 142.6, 142.5, 139.9, 138.0, 129.8, 128.8, 128.5, 128.5, 127.4, 126.3, 125.8, 125.6, 121.2 (q, J = 269.0 Hz), 106.3, 63.7, 49.5, 36.0, 24.2, 21.4.

^{19}F NMR (375 MHz, $CDCl_3$): δ -62.49 (s, 3F).

1-(((4,4-dimethyl-2-phenylpyrrolidin-1-yl)sulfonyl)methyl)-7,7-dimethylbicyclo-[2.2.1]heptan-2-one (2af)

[49] Murray, P. R. D.; Leibler, I. N.; Hell, S. M.; Villalona, E.; Doyle, A. G.; Knowles, R. R. *ACS Catal.* **2022**, *12*, 13732.

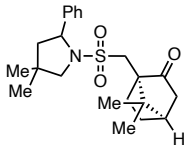

Following the GP5. Column chromatography was performed using a Hexane/EtOAc (15:1) as eluent to afford product as a white solid (50.3 mg, 0.129 mmol, 86% yield, *d.r.* =1:1). mp: 94–96 °C; TLC (Hexane/EtOAc, 6:1 v/v): R_f = 0.19.

^{1}H NMR (400 MHz, $CDCl_3$): δ 7.41–7.30 (m, 4H), 7.29 –7.21 (m, 1H), 4.99–4.88 (m, 1H), 3.72–3.62 (m, 1H), 3.30 (d, J = 10.4 Hz, 1H), 3.17 (d, J = 14.4 Hz, 0.5H), 2.96 (d, J = 14.4 Hz, 0.5H), 2.63 (d, J = 14.8 Hz, 0.5H), 2.44–2.13 (m, 3H), 2.15 (d, J = 14.8 Hz, 0.5H), 2.01–1.76 (m, 3.5H), 1.62–1.52 (m, 0.5H), 1.38–1.23 (m, 2H), 1.18 (s, 3H), 1.15 (s, 1.5H), 1.14 (s, 1.5H), 0.98 (s, 1.5H), 0.82 (s, 1.5H), 0.75 (s, 1.5H), 0.48 (s, 1.5H).

^{13}C NMR (100 MHz, $CDCl_3$): δ 215.2, 214.9, 142.7, 142.6, 128.7, 128.7, 127.8, 127.7, 127.6, 127.3, 63.5, 63.5, 61.6, 61.4, 58.4, 51.4, 51.2, 50.4, 49.7, 47.8, 47.7, 43.0, 42.7, 42.6, 42.5, 38.6, 38.5, 27.1, 27.0, 25.8, 25.7, 25.6, 25.0, 24.8, 20.1, 19.9, 19.7, 19.5.

IR ν (cm^{-1}): 2954, 1741, 1457, 1049, 1024, 964, 770, 702.

HRMS(ESI) *m/z*: Calcd. for $[C_{22}H_{32}NO_3S]^+$: 390.2097; Found: 390.2098.

5-phenyldihydrofuran-2(3H)-one (2ag)

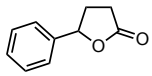

Following the GP5. Column chromatography was performed using a Hexane/EtOAc (10:1) as eluent to afford product as a colorless liquid (19.5 mg, 0.129 mmol, 80% yield). TLC (Hexane/EtOAc, 6:1 v/v): R_f = 0.15. The NMR spectra match those previously described in literature.[26]

^{1}H NMR (400 MHz, $CDCl_3$): δ 7.43–7.37 (m, 2H), 7.36–7.30 (m, 3H), 5.57–5.46 (m, 1H), 2.72–2.61 (m, 3H), 2.27–2.12 (m, 1H).

^{13}C NMR (100 MHz, $CDCl_3$): δ 177.0, 139.5, 128.9, 128.6, 125.4, 81.3, 31.1, 29.1.

2-phenyltetrahydrofuran (2ah)

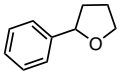

Following the GP5. Column chromatography was performed using a Hexane/EtOAc (20:1) as eluent to afford product as a colorless liquid (8.2 mg, 0.056 mmol, 37% yield). TLC (Hexane/EtOAc, 10:1 v/v): R_f = 0.31. The NMR spectra match those previously described in literature.[26]

^{1}H NMR (400 MHz, $CDCl_3$): δ 7.37–7.30 (m, 4H), 7.29–7.23 (m, 1H), 4.90 (t, J = 7.2 Hz, 1H), 4.16–4.06 (m, 1H), 4.00–3.90 (m, 1H), 2.39–2.27 (m, 1H), 2.06–1.96 (m, 2H), 1.87–1.76 (m, 1H).

^{13}C NMR (100 MHz, $CDCl_3$): δ 143.6, 128.4, 127.2, 125.8, 80.8, 68.8, 34.7, 26.2.

General procedure (GP6) for 6-membered ring formation

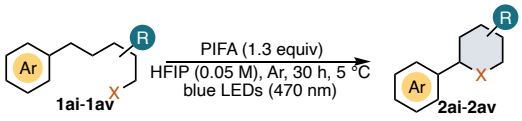

Reactions performed using ***set-up 2*** *in* Figure 2.11. The sulfonamide **1ai-1av** (0.15 mmol, 1.0 equiv.) and PIFA (0.195 mmol, 1.3 equiv.) were added to a reaction vial equipped with a stir bar. Subsequently, this reaction vial was brought into an argon-filled glovebox, 3.0 mL of dry HFIP were added to the mixture, and the reaction vial was sealed with a Teflon-septa equipped cap. The vial was carefully taken outside of the glovebox and subjected to irradiation under stirring at 5 °C for 30 hours. After completion of the reaction, volatiles were evaporated under reduced pressure and the resulting crude product was purified by chromatography (silica gel, *n*-hexane/ethyl acetate) to obtain the pure product **2ai-2av**.

Characterization of 6-membered ring products

5,5-dimethyl-2-phenyl-1-tosylpiperidine (2ai)

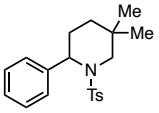

Following the GP6. Column chromatography was performed using a Hexane/EtOAc (20:1) as eluent to afford product as a white solid (39.1 mg, 0.116 mmol, 76% yield). TLC (Hexane/EtOAc, 19:1 v/v): R_f = 0.23. The NMR spectra match those previously described in literature.[25]

^{1}H NMR (400 MHz, $CDCl_3$): δ 7.66 (d, J = 8.3 Hz, 2H), 7.28–7.14 (m, 7H), 5.23 (t, J = 4.1 Hz, 1H), 3.42 (d, J = 13.5 Hz, 1H), 2.86 (d, J = 13.5 Hz, 1H), 2.40 (s, 3H), 2.14–2.06 (m, 2H), 1.28–1.20 (m, 2H), 0.80 (s, 3H), 0.79 (s, 3H).

^{13}C NMR (100 MHz, $CDCl_3$): δ 142.9, 139.0, 138.7, 129.5, 128.5, 127.1, 127.0, 126.8, 55.5, 52.7, 32.6, 30.4, 28.7, 25.8, 24.2, 21.6.

5,5-dimethyl-1-((4-nitrophenyl)sulfonyl)-2-phenylpiperidine (2aj)

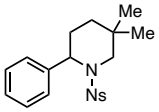

Following the GP6. Column chromatography was performed using a Hexane/EtOAc (20:1) as eluent to afford product as a white solid (41.2 mg, 0.110 mmol, 73% yield). TLC (Hexane/EtOAc, 19:1 v/v): R_f = 0.18. The NMR spectra match those previously described in literature.[25]

^{1}H NMR (400 MHz, $CDCl_3$): δ 8.22 (d, J = 8.8 Hz, 2H), 7.86 (d, J = 8.8 Hz, 2H), 7.24–7.14 (m, 3H), 7.12–7.03 (m, 2H), 5.24 (t, J = 4.4 Hz, 1H), 3.47 (d, J = 13.3 Hz, 1H), 2.94 (d, J = 13.3 Hz, 1H), 2.14–2.05 (m, 2H), 1.34–1.21 (m, 2H), 0.85 (s, 6H).

^{13}C NMR (100 MHz, $CDCl_3$): δ 149.6, 147.0, 138.5, 128.7, 128.2, 127.3, 126.9, 124.1, 56.2, 53.2, 32.4, 30.6, 28.6, 26.2, 24.4.

5,5-dimethyl-2-phenyl-1-((2-(trimethylsilyl)ethyl)sulfonyl)piperidine (2ak)

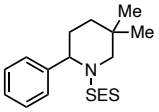

Following the GP6. Column chromatography was performed using a Hexane/EtOAc (20:1) as eluent to afford product as a yellow oil (24.8 mg, 0.070 mmol, 47% yield). TLC (Hexane/EtOAc, 19:1 v/v): R_f = 0.25. The NMR spectra match those previously described in literature.[25]

^{1}H NMR (400 MHz, $CDCl_3$): δ 7.41–7.33 (m, 4H), 7.30–7.23 (m, 1H), 5.08 (dd, J = 5.8, 3.0 Hz, 1H), 3.38 (d, J = 13.5 Hz, 1H), 3.00 (d, J = 13.5 Hz, 1H), 2.84–2.73 (m, 2H), 2.28–2.17 (m, 1H), 2.14–2.06 (m, 1H), 1.40–1.29 (m, 2H), 1.10 (s, 3H), 1.07–1.00 (m, 1H), 1.00–0.92 (m, 1H), 0.87 (s, 3H), -0.03 (s, 9H).

^{13}C NMR (100 MHz, $CDCl_3$): δ 139.9, 128.8, 127.2, 127.1, 55.8, 53.2, 49.7, 32.8, 30.6, 28.8, 26.4, 24.4, 10.6, -1.9.

1-((2-bromophenyl)sulfonyl)-5,5-dimethyl-2-phenylpiperidine (2al)

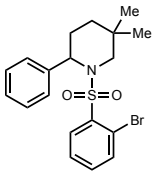

Following the GP6. Column chromatography was performed using a Hexane/EtOAc (20:1) as eluent to afford product as a white solid (44.2 mg, 0.108 mmol, 72% yield). TLC (Hexane/EtOAc, 19:1 v/v): R_f = 0.23. The NMR spectra match those previously described in literature.[25]

^{1}H NMR (400 MHz, $CDCl_3$): δ 8.10 (dd, *J* = 7.6, 2.1 Hz, 1H), 7.72 (dd, *J* = 7.3, 1.8 Hz, 1H), 7.39–7.27 (m, 6H), 7.22–7.15 (m, 1H), 5.31 (dd, *J* = 5.5, 2.9 Hz, 1H), 3.30 (d, *J* = 13.6 Hz, 1H), 3.01 (d, *J* = 13.5 Hz, 1H), 2.44–2.30 (m, 1H), 2.23–2.13 (m, 1H), 1.33–1.20 (m, 2H), 0.79 (s, 3H), 0.74 (s, 3H).

^{13}C NMR (100 MHz, $CDCl_3$): δ 139.9, 139.1, 135.5, 133.3, 132.4, 128.7, 127.6, 127.0, 126.9, 120.5, 56.4, 53.4, 32.8, 30.7, 28.7, 25.6, 23.9.

2-(2-fluorophenyl)-4,4-dimethyl-1-tosylpiperidine (2am)

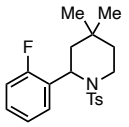

Following the GP6. Column chromatography was performed using a Hexane/EtOAc (20:1) as eluent to afford product as a yellow oil (14.6 mg, 0.0405 mmol, 27% yield). TLC (Hexane/EtOAc, 19:1 v/v): R_f = 0.21. The NMR spectra match those previously described in literature.[25]

^{1}H NMR (400 MHz, $CDCl_3$): δ 7.52(d, J = 8.3 Hz, 2H), 7.20–7.12 (m, 3H), 7.11–7.04 (m, 1H), 7.00–6.82 (m, 2H), 5.25 (t, J = 5.1 Hz, 1H), 3.37 (d, J = 13.0 Hz, 1H), 3.17 (d, J = 12.9 Hz, 1H), 2.37 (s, 3H), 2.09–1.91 (m, 2H), 1.30–1.17 (m, 2H), 0.94 (s, 3H), 0.88 (s, 3H).

^{13}C NMR (100 MHz, $CDCl_3$): δ 160.0 (d, J = 246.2 Hz), 142.9, 137.6, 129.4, 129.1 (d, J = 4.2 Hz), 128.6 (d, J = 8.5 Hz), 128.1 (d, J = 12.6 Hz), 127.2, 123.7 (d, J = 3.5 Hz), 115.8 (d, J = 22.7 Hz), 54.4, 52.2, 33.3, 30.5, 28.2, 27.3 (d, J = 3.9 Hz), 24.9, 21.6.

^{19}F NMR (375 MHz, $CDCl_3$): δ -115.06–-115.31 (m, 1F).

2-(3-fluorophenyl)-4,4-dimethyl-1-tosylpiperidine (2an)

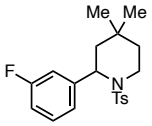

Following the GP6. Column chromatography was performed using a Hexane/EtOAc (20:1) as eluent to afford product as a yellow oil (14.9 mg, 0.0412 mmol, 29% yield). TLC (Hexane/EtOAc, 19:1 v/v): R_f = 0.21. The NMR spectra match those previously described in literature.[25]

^{1}H NMR (400 MHz, $CDCl_3$): δ 7.66 (d, J = 8.3 Hz, 2H), 7.28–7.16 (m, 3H), 6.97–6.93 (m, 1H), 6.91–6.84 (m, 1H), 6.83–6.74 (m, 1H), 5.21 (t, J = 4.0 Hz, 1H), 3.42 (d, J = 13.5 Hz, 1H), 2.82 (d, J = 13.5 Hz, 1H), 2.40 (s, 3H), 2.13–2.00 (m, 2H), 1.27–1.15 (m, 2H), 0.80 (s, 3H), 0.79 (s, 3H).

^{13}C NMR (100 MHz, $CDCl_3$): δ 163.2 (d, J = 245.5 Hz), 143.2, 142.0 (d, J = 6.4 Hz), 138.5, 130.1 (d, J = 8.1 Hz), 129.6, 127.1, 122.7 (d, J = 2.7 Hz), 114.2 (d, J = 22.6 Hz), 113.8 (d, J = 21.0 Hz), 55.1 (d, J = 1.8 Hz), 52.7, 32.6, 30.4, 28.8, 25.9, 24.1, 21.6.

^{19}F NMR (375 MHz, $CDCl_3$): δ -110.97–-117.19 (m, 1F).

4,4-dimethyl-2-(p-tolyl)-1-tosylpiperidine (2ao)

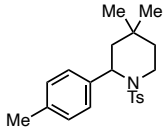

Following the GP6. Column chromatography was performed using a Hexane/EtOAc (20:1) as eluent to afford product as a white solid (37.3 mg, 0.104 mmol, 70% yield). TLC (Hexane/EtOAc, 19:1 v/v): R_f = 0.25. The NMR spectra match those previously described in literature.[25]

^{1}H NMR (400 MHz, $CDCl_3$): δ 7.66 (d, J = 8.3 Hz, 2H), 7.22 (d, J = 7.9 Hz, 2H), 7.04 (m, 4H), 5.19 (t, J = 4.0 Hz, 1H), 3.39 (d, J = 13.5 Hz, 1H), 2.85 (d, J = 13.5 Hz, 1H), 2.40 (s, 3H), 2.30 (s, 3H), 2.15–1.98 (m, 2H), 1.32–1.15 (m, 2H), 0.80 (s, 3H), 0.79 (s, 3H).

^{13}C NMR (100 MHz, $CDCl_3$): δ 142.8, 138.7, 136.4, 135.9, 129.5, 129.2, 127.1, 127.0, 55.3, 52.6, 32.6, 30.5, 28.7, 25.8, 24.2, 21.6, 21.0.

2-(4-(tert-butyl)phenyl)-4,4-dimethyl-1-tosylpiperidine (2ap)

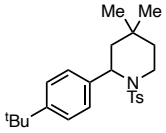

Following the GP6. Column chromatography was performed using a Hexane/EtOAc (20:1) as eluent to afford product as a white oil (46.7 mg, 0.117 mmol, 78% yield). TLC (Hexane/EtOAc, 19:1 v/v): R_f = 0.27. The NMR spectra match those previously described in literature.[25]

^{1}H NMR (400 MHz, $CDCl_3$): δ 7.61 (d, J = 8.3 Hz, 2H), 7.22 (d, J = 8.5 Hz, 2H), 7.19 (d, J = 7.9 Hz, 2H), 7.07 (d, J = 8.0 Hz, 2H), 5.18 (t, J = 4.2 Hz, 1H), 3.40 (d, J = 13.4 Hz, 1H), 2.88 (d, J = 13.4 Hz, 1H), 2.39 (s, 3H), 2.11–2.02 (m, 2H), 1.29 (s, 9H), 1.38–1.17 (m, 2H), 0.81 (s, 6H).

^{13}C NMR (100 MHz, $CDCl_3$): δ 149.7, 142.7, 138.7, 136.1, 129.4, 127.2, 126.8, 125.4, 55.4, 52.7, 34.5, 32.7, 31.5, 30.5, 28.8, 25.9, 24.3, 21.6.

2-(4-chlorophenyl)-4,4-dimethyl-1-tosylpiperidine (2aq)

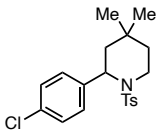

Following the GP6. Column chromatography was performed using a Hexane/EtOAc (20:1) as eluent to afford product as a yellow solid (45.3 mg, 0.120 mmol, 80% yield). TLC (Hexane/EtOAc, 19:1 v/v): R_f = 0.24. The NMR spectra match those previously described in literature.[25]

^{1}H NMR (400 MHz, CDCl$_3$): δ 7.64 (d, J = 8.3 Hz, 2H), 7.24 (d, J = 7.8 Hz, 2H), 7.21 (d, J = 8.6 Hz, 2H), 7.09 (d, J = 7.9 Hz, 2H), 5.17 (t, J = 4.0 Hz, 1H), 3.39 (d, J = 13.4 Hz, 1H), 2.80 (d, J = 13.5 Hz, 1H), 2.41 (s, 3H), 2.11–1.99 (m, 2H), 1.25–1.15 (m, 2H), 0.79 (s, 3H), 0.77 (s, 3H).

^{13}C NMR (100 MHz, CDCl$_3$): δ 143.1, 138.5, 137.6, 132.8, 129.6, 128.7, 128.6, 127.1, 55.1, 52.7, 32.6, 30.5, 28.7, 25.8, 24.2, 21.6.

4-(5,5-dimethyl-1-tosylpiperidin-2-yl)phenyl benzoate (2ar)

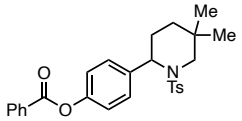

Following the GP6. Column chromatography was performed using a Hexane/EtOAc (20:1) as eluent to afford product as a white solid (43.1 mg, 0.093 mmol, 62% yield). TLC (Hexane/EtOAc, 19:1 v/v): R_f = 0.17. The NMR spectra match those previously described in literature.[25]

^{1}H NMR (400 MHz, CDCl$_3$): δ 8.19 (dd, J = 8.5, 1.4 Hz, 2H), 7.67 (d, J = 8.2 Hz, 2H), 7.63 (d, J = 7.4 Hz, 1H), 7.51 (t, J = 7.6 Hz, 2H), 7.25 (d, J = 7.8 Hz, 2H), 7.20 (d, J = 8.0 Hz, 2H), 7.10 (d, J = 8.7 Hz, 2H), 5.24 (t, J = 4.2 Hz, 1H), 3.43 (d, J = 13.6 Hz, 1H), 2.86 (d, J = 13.5 Hz, 1H), 2.41 (s, 3H), 2.16–2.07 (m, 2H), 1.31–1.19 (m, 2H), 0.82 (s, 6H).

^{13}C NMR (100 MHz, CDCl$_3$): δ 165.2, 149.8, 143.0, 138.6, 136.7, 133.8, 130.3, 129.6, 129.6, 128.7, 128.2, 127.1, 121.7, 55.1, 52.6, 32.6, 30.5, 28.7, 25.8, 24.2, 21.6.

3-(5,5-dimethyl-1-((4-nitrophenyl)sulfonyl)piperidin-2-yl)-1-((trifluoromethyl)-sulfonyl)-1H-indole (2as)

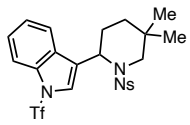

Following the GP6. Column chromatography was performed using a Hexane/EtOAc (20:1) as eluent to afford product as a white oil (25.4 mg, 0.046 mmol, 31% yield). TLC (Hexane/EtOAc, 19:1 v/v): R_f = 0.19. The NMR spectra match those previously described in literature.[25]

^{1}H NMR (400 MHz, $CDCl_3$): δ 8.12 (d, J = 8.7 Hz, 2H), 7.83 (d, J = 7.9 Hz, 1H), 7.74 (d, J = 8.7 Hz, 2H), 7.66 (d, J = 7.2 Hz, 1H), 7.50–7.35 (m, 2H), 6.74 (s, 1H), 5.55 (d, J = 4.2 Hz, 1H), 3.56 (d, J = 12.7 Hz, 1H), 2.97 (d, J = 12.8 Hz, 1H), 2.32–2.18 (m, 1H), 2.06–1.97 (m, 1H), 1.42–1.27 (m, 2H), 1.04 (s, 3H), 0.99 (s, 3H).

^{13}C NMR (100 MHz, $CDCl_3$): δ 150.0, 146.0, 135.2, 129.4, 128.1, 126.7, 125.2, 124.1, 123.0, 122.9, 120.5, 119.5 (q, J = 320.8 Hz), 114.1, 53.5, 49.4, 32.5, 30.7, 28.8, 26.2, 23.7.

^{19}F NMR (375 MHz, $CDCl_3$): δ -75.05 (s, 3F).

3-phenyl-2-tosyl-2-azaspiro[5.5]undecane (2at)

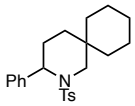

Following the GP6. Column chromatography was performed using a Hexane/EtOAc (20:1) as eluent to afford product as a yellow oil (39.1 mg, 0.102 mmol, 68% yield). TLC (Hexane/EtOAc, 19:1 v/v): R_f = 0.19. The NMR spectra match those previously described in literature.[25]

^{1}H NMR (400 MHz, $CDCl_3$): δ 7.65 (d, J = 8.3 Hz, 2H), 7.25–7.12 (m, 7H), 5.21 (t, J = 4.3 Hz, 1H), 3.73 (d, J = 13.2 Hz, 1H), 2.78 (d, J = 13.6 Hz, 1H), 2.39 (s, 3H), 2.09–1.99 (m, 2H), 1.43–1.24 (m, 8H), 1.21–1.02 (m, 4H).

^{13}C NMR (100 MHz, $CDCl_3$): δ 142.8, 139.2, 138.7, 129.5, 128.5, 127.2, 127.1, 126.8, 56.1, 50.3, 38.0, 32.7, 32.0, 30.9, 26.6, 25.1, 21.7, 21.6, 21.5.

1-(p-tolyl)-2-tosyl-1,2,3,4-tetrahydroisoquinoline (2au)

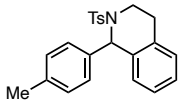

Following the GP6. Column chromatography was performed using a Hexane/EtOAc (20:1) as eluent to afford product as a white solid (44.8 mg, 0.119 mmol, 79% yield). TLC (Hexane/EtOAc, 19:1 v/v): R_f = 0.19. The NMR spectra match those previously described in literature.[50]

^{1}H NMR (400 MHz, $CDCl_3$): δ 7.55 (d, J = 8.3 Hz, 2H), 7.15–7.10 (m, 2H), 7.10–7.05 (m, 6H), 7.01–6.94 (m, 2H), 6.20 (s, 1H), 3.80–3.71 (m, 1H), 3.38-3.24 (m, 1H), 2.73–2.61 (m, 1H), 2.60-2.51 (m, 1H), 2.32 (s, 3H), 2.31 (s, 3H).

^{13}C NMR (100 MHz, $CDCl_3$): δ 143.1, 138.8, 137.9, 137.5, 134.4, 133.9, 129.4, 129.1, 129.0, 128.8, 128.5, 127.2, 127.1,126.2, 59.1, 39.1, 26.8, 21.6, 21.2.

6-phenyltetrahydro-2H-pyran-2-one (2av)

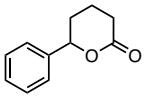

Following the GP6. Column chromatography was performed using a Hexane/EtOAc (8:1) as eluent to afford product as a yellow liquid (19.0 mg, 0.108 mmol, 72% yield). TLC (Hexane/EtOAc, 6:1 v/v): R_f = 0.15. The NMR spectra match those previously described in literature.[51]

^{1}H NMR (400 MHz, $CDCl_3$): δ 7.42–7.29 (m, 5H), 5.36 (dd, J = 10.4, 3.4 Hz, 1H), 2.77–2.67 (m, 1H), 2.64–2.51 (m, 1H). 2.22–2.13 (m, 1H), 2.04–1.95 (m, 2H), 1.91–1.82 (m, 1H).

^{13}C NMR (100 MHz, $CDCl_3$): δ 171.5, 139.9, 128.7, 128.4, 125.8, 81.8, 30.7, 29.6, 18.7.

2.5.6. X-Ray crystallography

[50] Zhang, J.; Zhang, Z. M.; Wu, Q.; Zhang, J. *Adv. Synth. Catal.* **2022**, *364*, 4075.

[51] Bergamaschi, E.; Lunic, D.; McLean, L. A.; Hohenadel, M.; Chen, Y. K.; Teskey, C. J. *Angew. Chem. Int. Ed.* **2022**, *61*, e202114482.

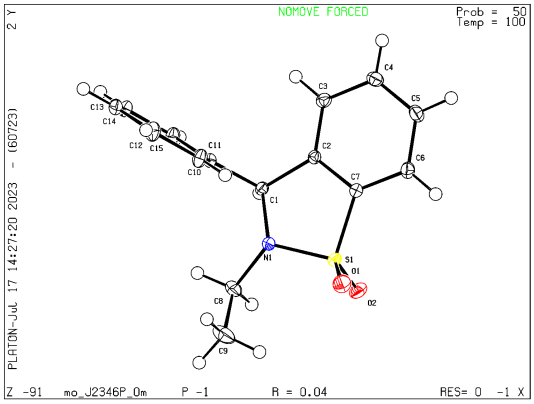

Figure 2.12. ORTEP drawing (thermal ellipsoids set at 50% probability) of **2ac**

Table 2.15. Crystal data and structure refinement for **2ac** (CCDC: 2282188)

Identification code	mo_J2346P_0m
Empirical formula	$C_{15}H_{15}NO_2S$
Formula weight	273.34
Temperature	100(2)K
Wavelength	0.71073 Å
Crystal system	triclinic
Space group	P -1
Unit cell dimensions	a = 8.4061(15)Å a=107.475(3)°. b = 9.3059(16)Å b=105.031(3)°. c = 10.2652(18)Å. g=109.077(3)°.
Volume	664.5(2) $Å^3$
Z	2
Density (calculated)	1.366 Mg/m^{-3}
Absorption coefficient	0.240 mm^{-1}

F(000)	288
Crystal size	0.500 x 0.500 x 0.400 mm^3
Theta range for data collection	2.266 to 32.066°.
Index ranges	-12<=h<=12,-13<=k<=13,-15<=l<=15
Reflections collected	12709
Independent reflections	4521[R(int) = 0.0406]
Completeness to theta =32.066°	97.2%
Absorption correction	Multi-scan
Max. and min. transmission	0.74 and 0.68
Refinement method	Full-matrix least-squares on F^2
Data / restraints / parameters	4521/ 0/ 173
Goodness-of-fit on F^2	1.042
Final R indices [I>2sigma(I)]	R1 = 0.0364, wR2 = 0.0974
R indices (all data)	R1 = 0.0414, wR2 = 0.1012
Largest diff. peak and hole	0.469 and -0.440 e.$Å^{-3}$

2.5.7. Deprotection of 2k to free pyrrolidine 3

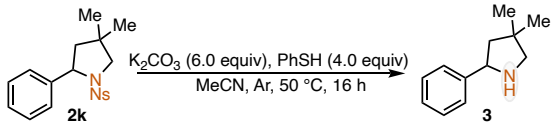

A flame-dried pressure tube equipped with a magnetic stir bar was charged with compound **2k** (54.0 mg, 0.15 mmol, 1.0 equiv.) and K_2CO_3 (124.4 mg, 0.9 mmol, 6.0 equiv). The reaction tube was purged with argon atmosphere, then MeCN (2.5 mL) and PhSH (61 µL, 0.6 mmol, 4.0 equiv) was added via syringe. The tube was sealed, and the reaction mixture was stirred at 50 °C for 16 hours. DCM was added and the resulting solution was washed with saturated aqueous solutions of $NaHCO_3$ and extracted with

DCM (3x). The combined organic layers were dried over Na_2SO_4 and solvents were evaporated under reduced pressure. The crude product was purified by chromatography (silica gel, n-hexane/ethyl acetate 2/1, v/v) to give the pure product **3** as colorless liquid with a yield of 90% (25.8 mg, 0.135 mmol). TLC (Hexane/EtOAc, 4:1 v/v): $R_f = 0.21$. The NMR spectra match those previously described in literature.[52]

^{1}H NMR (400 MHz, $CDCl_3$): δ 7.39–7.35 (m, 2H), 7.34–7.28 (m, 2H), 7.25–7.19 (m, 1H), 4.30 (dd, J = 9.7, 7.1 Hz, 1H), 2.92 (d, J = 10.1 Hz, 1H), 2.80 (d, J = 10.1 Hz, 1H), 2.11 (s, 1H). 1.98 (dd, J = 12.5, 7.1 Hz, 1H), 1.55 (dd, J = 12.5, 9.7 Hz, 1H), 1.15 (s, 3H), 1.15 (s, 3H).

^{13}C NMR (100 MHz, $CDCl_3$): δ 145.3, 128.5, 126.8, 126.6, 62.6, 61.4, 50.2, 39.8, 28.7, 28.0.

2.5.8. Mechanistic experiments

Absorption spectroscopy Analysis (UV-vis)

- *Absorption spectra of the substrates **1a**, PIFA and the mixture*

For the solutions of PIFA: A 10 mL glass vial containing PIFA (25.8 mg, 0.06 mmol) was sealed with a rubber plug, vacuumed and backfilled with argon for 3 times, then degassed HFIP (10 mL) was added via syringe ($6 \cdot 10^{-3}$ M solution). A 3 mL of the solution was transferred into an argon filled quartz cuvette (10 x 10 mm light path) equipped with a septum.

For the solutions of substrate **1a**: A 10 mL volumetric flask containing substrate **1a** (18.1 mg, 0.05 mmol) was sealed with a rubber plug, vacuumed and backfilled with argon for 3 times, then degassed HFIP (10 mL) was added via syringe ($5 \cdot 10^{-3}$ M solution). 3 mL of the solution was transferred into an argon filled quartz cuvette (10 x 10 mm light path) equipped with a septum.

For the solution containing a mixture of substrate **1a** and PIFA: following the completion of substrate **1a** measurement, a 10 μL of the 0.3 M PIFA solution was injected into the argon filled quartz cuvette using a hamilton. The resulting mixture was then thoroughly mixed.

52 Yuan, Q.; Liu, D.; Zhang, W. *Org. Lett.* **2017**, *19*, 1144.

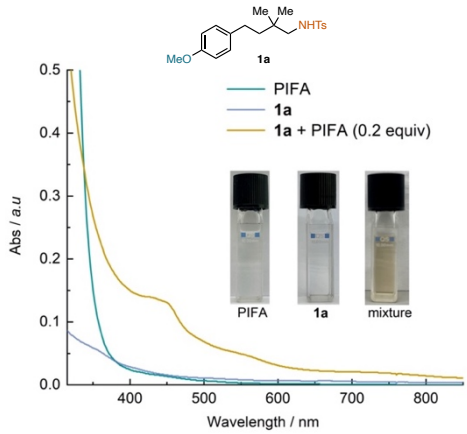

Figure 2.13. Absorption spectra of the substrates **1a**, PIFA and the mixture of **1a** and PIFA (0.2 equiv.) in HFIP. [**1a**] = $5 \cdot 10^{-3}$ M, [PIFA] = $6 \cdot 10^{-3}$ M.

- *The influence of solvents on PIFA*

For the solutions of PIFA: A 5 mL glass vial containing PIFA (86.0 mg, 0.2 mmol) was sealed with a rubber plug, vacuumed and backfilled with argon for 3 times, then degassed DCM (5 mL), ^{i}PrOH (5 mL) or HFIP (5 mL) was added via syringe ($4 \cdot 10^{-2}$ M solution). 3 mL of the solution was transferred into an argon filled quartz cuvette (10 x 10 mm light path) equipped with a septum.

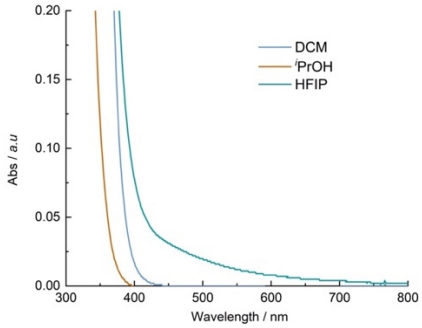

Figure 2.14. Absorption spectra of PIFA in DCM, ^{i}PrOH and HFIP. [PIFA] = $4 \cdot 10^{-2}$ M.

*Absorption spectra of the substrates **1j**, PIFA and the mixture*

For the solutions of PIFA: A 5 mL glass vial containing PIFA (86.0 mg, 0.2 mmol) was sealed with a rubber plug, vacuumed and backfilled with argon for 3 times, then degassed HFIP (5 mL) was added via syringe ($4 \cdot 10^{-2}$ M solution). A 3 mL of the

solution was transferred into an argon filled quartz cuvette (10 x 10 mm light path) equipped with a septum.

For the solutions of substrate **1j**: A 5 mL volumetric flask containing substrate **1j** (55.2 mg, 0.16 mmol) was sealed with a rubber plug, vacuumed and backfilled with argon for 3 times, then degassed HFIP (5 mL) was added via syringe ($3.3 \cdot 10^{-2}$ M solution). 3 mL of the solution was transferred into an argon filled quartz cuvette (10 x 10 mm light path) equipped with a septum.

For the solutions of the mixture of **1j** and PIFA: A 5 mL glass vial containing substrate **1j** (55.2 mg, 0.16 mmol) and PIFA (86.0 mg, 0.2 mmol) was sealed with a rubber plug, vacuumed and backfilled with argon for 3 times, then degassed HFIP (5 mL) was added via syringe ($6 \cdot 10^{-3}$ M solution). The resulting mixture was then thoroughly mixed. 3 mL of the solution was transferred into an argon filled quartz cuvette (10 x 10 mm light path) equipped with a septum.

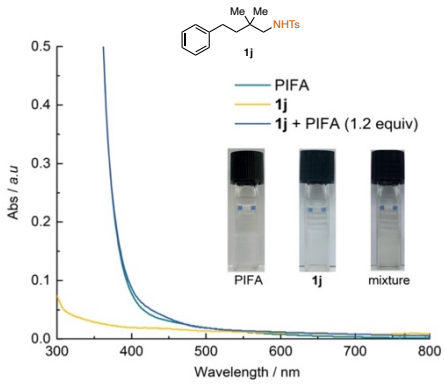

Figure 2.15. Absorption spectra of the substrates **1j**, PIFA, and the mixture of **1j** and PIFA (1.2 equiv.) in HFIP. [**1j**] = $3.3 \cdot 10^{-2}$ M, [PIFA] = $4 \cdot 10^{-2}$ M.

*Absorption spectra evolution of the mxture of **1j** and PIFA upon irradiation*

A 3 mL glass vial containing substrate **1j** (33.1 mg, 0.1mmol) and PIFA (51.6 mg, 0.12 mmol) was sealed with a rubber plug, vacuumed and backfilled with argon for 3 times, then degassed HFIP (3 mL) was added via syringe ($6 \cdot 10^{-3}$ M solution). The resulting mixture was then thoroughly mixed. Subsequently, 3 mL of the solution was transferred into an argon filled quartz cuvette (10 x 10 mm light path) equipped with a stirring bar

and a septum. The cuvette was then subjected to irradiation using ***set-up 1*** in Figure S1 and the absorption spectra were recorded over time.

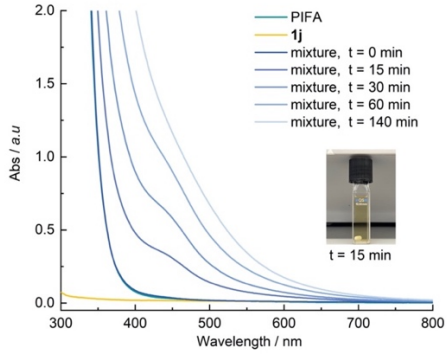

Figure 2.16. Absorption spectra of the substrates **1j**, PIFA, and the mixture of **1j** and PIFA (1.2 equiv.) upon irradiation in HFIP. [**1j**] = $3 \cdot 10^{-2}$ M, [PIFA] = $4 \cdot 10^{-2}$ M. The cuvette was irradiated at 465 nm and the absorption spectra were recorded over time.

Absorption spectra of PIFA in HFIP with low concentration.

A 5 mL glass vial containing PIFA (2.1 mg, $5 \cdot 10^{-3}$ mmol) was sealed with a rubber plug, vacuumed and backfilled with argon for 3 times, then degassed HFIP (5 mL) was added via syringe. A 0.1 mL of the solution was transferred into an argon filled quartz cuvette (10 x 10 mm light path) equipped with a septum and degassed HFIP (2.9 mL) was added via syringe ($3.3 \cdot 10^{-5}$ M solution).

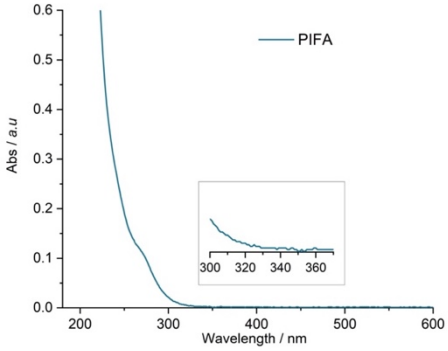

Figure 2.17. Absorption spectra of PIFA in HFIP. [PIFA] = $3.3 \cdot 10^{-5}$ M

Electron paramagnetic Resonance (EPR)

To gain further understanding of the mechanism, electron paramagnetic resonance (EPR) experiments were conducted (Figure S9). A single clean signal at 3516.3 G was

observed with a *g*-value of 2.0028, which provided conclusive evidence for the existence of radicals. Interestingly, the peak shape and g-value of the observed signal differed from the nitrogen radical signal previously reported in the literature.[36] The result suggests that the experimental mechanism likely involves a radical cation **1a**$^{\bullet+}$.[35a,53]

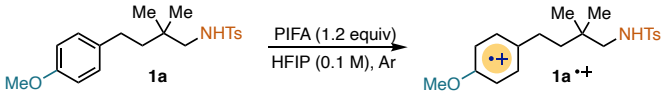

In two reaction vials were added respectively the sulfonamide **1a** (18.08 mg, 0.05 mmol, 1.0 equiv.) in the first, and PIFA (25.80 mg, 0.06 mmol, 1.2 equiv.) in the second. The reaction vials were then brought into an argon-filled glovebox, and dry HFIP (0.5 mL) followed by PIFA was added to the first vial. Immediately the stock solution was transferred to the capillary via a 100 µL hamilton, and then placed the capillary in the EPR tube. The spectral data was collected at 298 K with the following spectrometer settings: g-factor = 1.999000, microwave power = 2.066 mW; center field = 3510.25 G, sweep width = 200.0 G, sweep time = 30.00 s, modulation frequency = 100.00 KHz, modulation amplitude = 1.00 G, power attenuation = 20.00 dB, time constant = 0.01 ms, conversion time = 15.00 ms, gain = 30.00 dB.

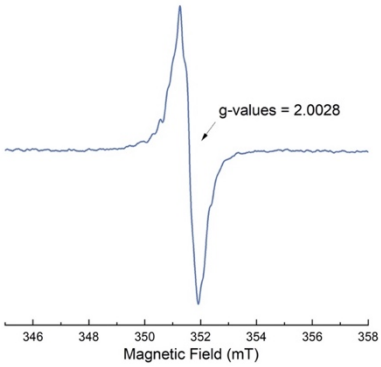

Figure 2.18. EPR experiment of sulfonamide **1a** (g-factor 2.0028)

Cyclic voltammetry studies (CV)

53 Dohi, T.; Ito, M.; Yamaoka, N.; Morimoto, K.; Fujioka, H.; Kita, Y. *Angew. Chem. Int. Ed. 2010,* **49**, 3334.

For all cyclic voltammetry (CV) measurements of sulfonamide substrate **1a**, **1c**, **1i**, **1j** and **1v** were performed in a 3-electrode cell set up consisting of a glassy carbon disk (0.07 cm^2 of surface area) as working electrode and platinum as a counter electrode and SCE (Saturated Calomel Electrode) as the reference electrode. The electrodes were previously polished with diamond abrasive slurries (DIAPAT-M, 39-321-M, Netkon) in an order of 3 μm and 1 μm diameter particle-based slurries (2 minutes in each). Synthetic nap based polishing pads (METAPO-B, polishing cloth, self- adhesive back, diamond 3-1 μm, Netkon) were used for diamond polishing.

The substrates were measured at concentration of 3 mM in HFIP with $TBAPF_6$ (0.1 M) as electrolyte at the scan rate is 100 mV/s with Fc/Fc^+ as a reference.

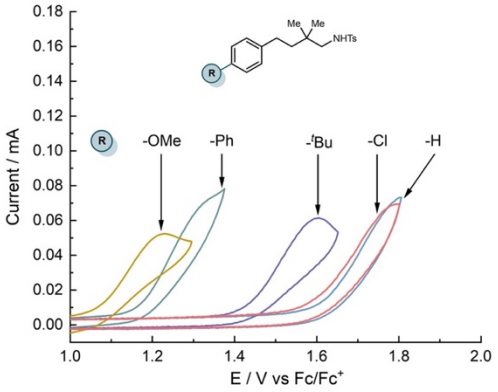

Figure 2.19. Cyclic voltammetry of **1a** (yellow line), **1c** (green line), **1i** (purple line), **1j** (blue line) and **1v** (red line).

Kinetic isotope effect (KIE) studies

Reactions performed using set-up 1 in Figure 2.10. In the reaction vials with previously placed stir bars were charged **1j** (16.6 mg, 0.05 mmol, 1.0 equiv.) or **1j-*d*₂** (16.7 mg, 0.05 mmol, 1.0 equiv.), PIFA (25.8 mg, 0.06 mmol, 1.2 equiv.). The reaction vials were then brought into an argon-filled glovebox. Inside the glovebox, 1.5 mL of dry HFIP were added to the mixture, and the reaction vials were sealed with a Teflon-septa equipped cap. The vials were carefully taken outside of the glovebox and subjected to irradiation under stirring for different time. After completion of the reaction, volatiles were evaporated under reduced pressure, and the yield of **2j** and **2j-*d*₂** were determined by crude ^1H NMR using mesitylene as internal standard to determine the intermolecular

KIE value. The KIE value of the C–H activation process was 1.036, revealing that the C–H cleavage is fast and not involved as a rate-determining step.

Table 2.16. kinetic isotope effect

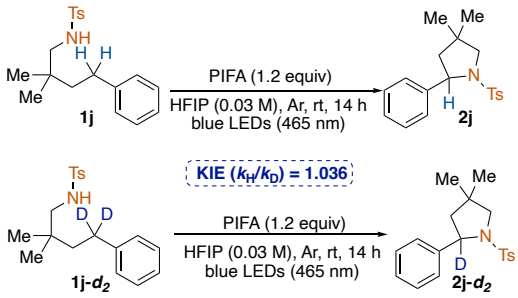

Time (h)	**2j** yield (%)	**D-2j** yield (%)
0	0	0
0.5	5	5
1	18	18
2		26
2.4	43	
3	65	62
4	80	78

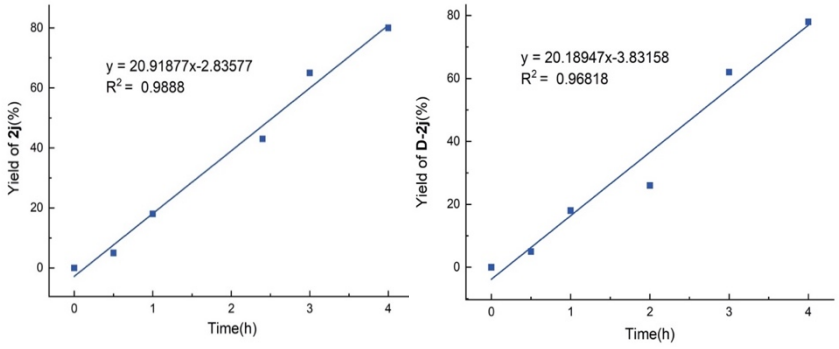

Emission spectrum and Stern-Volmer quenching studies

Emission spectrum of [PIFA]*

The emission spectra were recorded in a Fluorolog Horiba Jobin Yvon spectrofluorimeter equipped with a photomultiplier detector, a double monochromator, and a 350W xenon light source. In the glovebox, 3 mL of a 0.033 mM solution of PIFA in degassed HFIP were placed in a 10 x10 mm light path quartz fluorescence cuvette equipped with Silicone/PTFE 3.2 mm septum under an argon atmosphere. The excitation wavelength was fixed at 332 nm (incident light slit regulated to 5 mm), while the emission light was acquired from 342 nm to 549 nm (emission light slit regulated to 5 mm).

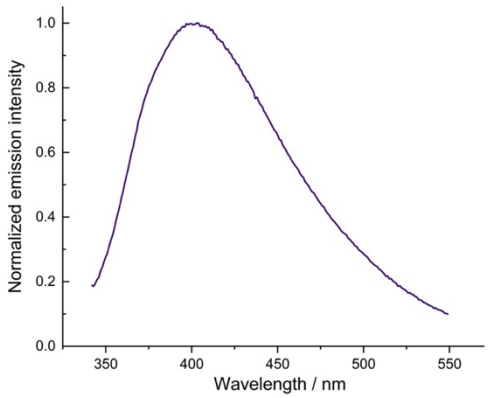

Figure 2.20. Emission spectrum of [PIFA]* upon 332 nm irradiation in HFIP.

– Stern-Volmer Quenching Studies using **1j** as the quencher

In the glovebox, a solution of sulfonamide **1j** in HFIP was prepared with a concentration of 1.6 mM. This stock solution, 12 μL were added to the solution of PIFA, prepared as described above. The addition of this solution of **1j** was repeated five consecutive times. After each addition, an absorption spectrum and an emission spectrum of the solution were recorded. The excitation wavelength was fixed at 332 nm (incident light slit regulated to 5 mm); the emission light was acquired from 342 nm to 549 nm (emission light slit regulated to 5 mm). The excitation wavelength was chosen in order to avoid saturation of the emission detector. The results, showed in Figure S12, clearly demonstrate that sulfonamide **1j** effectively quenches the excited state of PIFA and its emission.

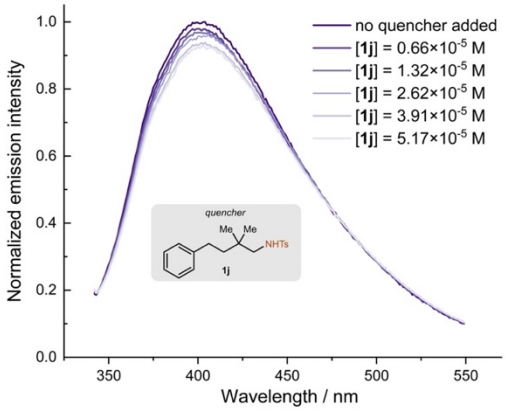

Figure 2.21. Quenching of the emission of [PIFA]* (0.033 mM in HFIP) in the presence of increasing amounts of **1j**.

The Stern-Volmer plot, reported in Figure S13, shows a linear correlation between the amounts of **1j** and the ratio I^0/I. Based on the following Equation 1, it is possible to calculate the Stern-Volmer constant K_{SV}.[54]

$$I^0/I = 1 + K_{SV}[Q] \qquad \text{[Eq. 1]}$$

We calculated a Stern-Volmer quenching constant of **1595 M^{-1}**.

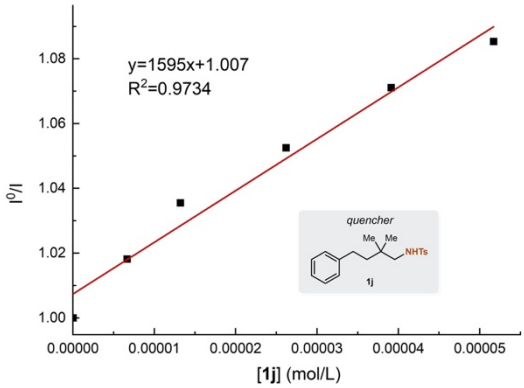

Figure 2.22. Stern-Volmer quenching plot using **1j** as a quencher.

54 Lakovicz, J. R. *Principles of Fluorescence Spectroscopy* (Springer, 2006).

Evaluation of the excited-state potential of [PIFA]*

Using the data from the absorption spectra (Figure S8) of **PIFA** and the cyclic voltammetry (CV) studies those previously described in literature[19], the oxidation potential relative to its excited state **[PIFA]*** could be estimated, by means of the following Equation 2[20]:

$$E(\mathbf{PIFA}^{\bullet-}/\mathbf{[PIFA]}^*) = E(\mathbf{PIFA}^{\bullet-}/\mathbf{PIFA}) + E_{0\text{-}0}(\mathbf{[PIFA]}^*)/\mathbf{PIFA}) \quad \text{[Eq. 2]}$$

$E(\mathbf{PIFA}^{\bullet-}/\mathbf{PIFA})$ was provided by the reported cyclic voltammetry (CV) studies,[32] is *-0.45* V vs. Fc/Fc+ in HFIP. $E_{0\text{-}0}(\mathbf{[PIFA]}^*)/\mathbf{PIFA})$, which is the excited state energy of **PIFA**, was estimated spectroscopically from the position of the long wavelength tail of the absorption spectrum recorded in degassed HFIP (354 nm, Figure S8), which translates into an $E_{0\text{-}0}(\mathbf{[PIFA]}^*)/\mathbf{PIFA})$ of *3.54* eV.

$$E(\mathbf{PIFA}^{\bullet-}/\mathbf{[PIFA]}^*) = -0.45 + 3.54 = 3.09 \text{ V (vs Fc/ Fc}^+)$$

Detection of CO_2

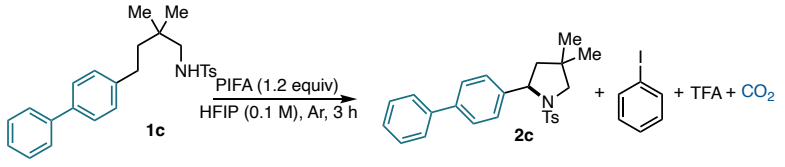

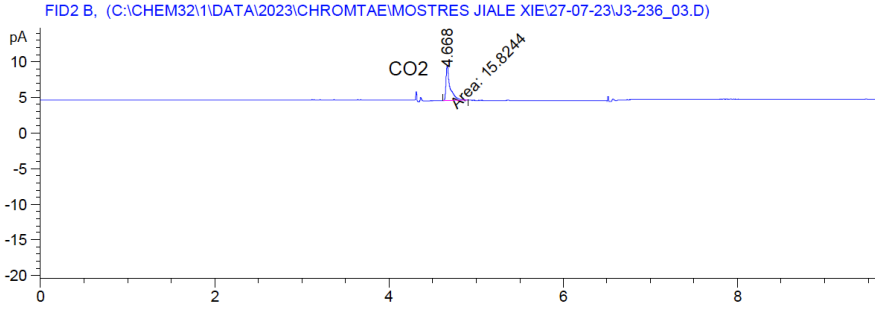

The sulfonamide **1c** (20.4 mg, 0.05 mmol, 1.0 equiv) and PIFA (25.8 mg, 0.06 mmol, 1.2 equiv) were added to a reaction vial equipped with a stir bar. This reaction vial was then brought into an argon-filled glovebox. Inside the glovebox, the reaction vial was sealed with a cap equipped with a Teflon-septa and0.5 mL of dry HFIP were added to the mixture via the hamilton. The sealed vial was removed from the glovebox and stirred at room temperature. After 3 hours, a gas sample was taken from the head space of the sealed reaction vial via a syringe with valve for measurement.

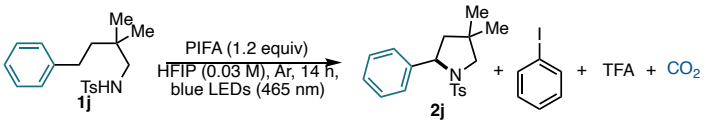

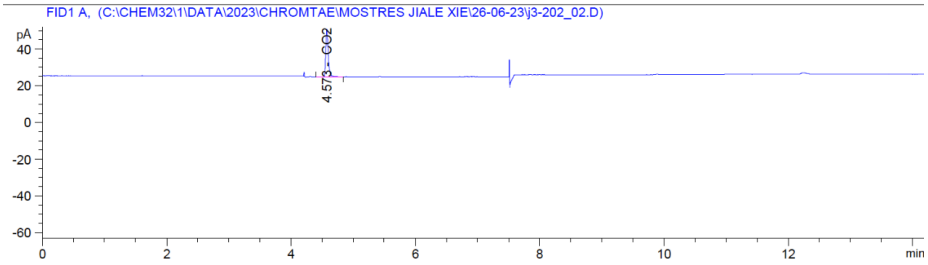

The sulfonamide **1j** (16.6 mg, 0.05 mmol, 1.0 equiv) and PIFA (25.8 mg, 0.06 mmol, 1.2 equiv) were added to a reaction vial equipped with a stir bar. This reaction vial was then brought into an argon-filled glovebox. Inside the glovebox, 1.5 mL of dry HFIP were added to the mixture, and the reaction vial was sealed with a cap equipped with a Teflon-septa. The sealed vial was removed from the glovebox and stirred at room temperature. After 14 hours, a gas sample was taken from the head space of the sealed reaction vial via a syringe with valve for measurement.

Detection of TEMPO-adduct 4

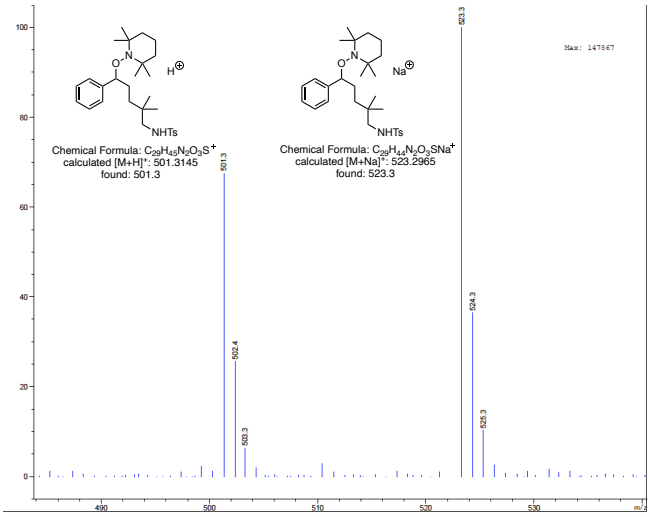

The sulfonamide **1ai** (17.3 mg, 0.05 mmol, 1.0 equiv) and PIFA (27.9 mg, 0.06 mmol, 1.2 equiv) were added to a reaction vial equipped with a stirrer. This reaction vial was then brought into an argon-filled glovebox. Inside the glovebox, 1.0 mL of dry HFIP were added to the mixture, and the reaction vial was sealed with a cap equipped with a Teflon-septa. The sealed vial was removed from the glovebox and stirred at 5 ºC under irradiation. After 4 hours, the reaction was taken into the glovebox and TEMPO (15.6 mg, 0.1 mmol, 2.0 equiv) was added. The vail was sealed and removed from the glovebox and stirred at 5 ºC under irradiation for another 14 hours. Then the sample was injected to HFLC-MS analysis (Column: Sunfire-C18 100*4.6 mm, 5µm; H_2O/MeOH 1:1, 50% MeOH up to 100% in 10´, hold 5´; 1 mL/min; ESI +/-). TEMPO-adduct **4** was detected indicate that the benzylic radical was involve in the reaction.

Proposed mechanisms

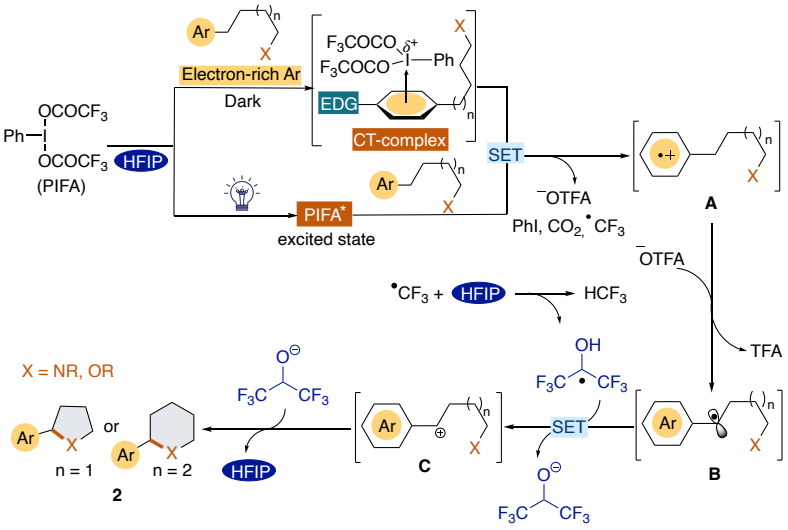

Scheme 2.31. Proposed mechanism of HFIP-assisted intramolecular C(sp^3)–H functionalization

The reaction commences with the substrate undergoing a SET process with PIFA, resulting in the formation of the aromatic radical cation **A**. In the case of the electron-rich substrate, **A** is formed through an intracomplex SET of the CT-complex in the ground state. On the other hand, PIFA oxidizes substrate into the aromatic radical cation **A**. And PIFA acquires one electron from the substrate **1a**, leading to the generation of OTFA anion, CF_3 radical, PhI, and CO_2. Next, rapid deprotonation occurs, facilitated by the *in-situ* generated OTFA anion, resulting in the formation of the benzylic radical **B**. Subsequently, intermediate **B** undergoes further single-electron oxidation by the HFIP radical, which is formed through a HAT process involving the CF3 radical and HFIP. The oxidation of intermediate **B** leads to the formation of the benzylic cation **C**, which is then captured by the nucleophilic tosylamide, resulting in the formation of the desired product.

2.5.9. DFT calculations

Computational details

DFT calculations were performed using the Gaussian16[55] package with the M06-D3 functional[56], where D3 stands for Grimme's empirical dispersion[57]. Geometry optimizations of all the compounds and transition states were carried out with LANL2DZ as the basis set for iodine,[58] and 6-31g*[59]for the remaining atoms. Implicit solvent was modeled through the SMD method.[60] As the solvent, hexafluoroisopropanol, is not included in Gaussian, we defined the solvent by including the dielectric constant and the refracting index. The keywords used were: (solvent=generic, eps=16.7, epsinf=1.625625). Frequencies were computed at the same level of theory to obtain the free energies and to confirm whether the structures are minima (no imaginary frequency) or transition states (only one imaginary frequency). All the potential energies were refined with single-point calculations using the M06-D3 functional and a def2-TZVP[61] basis set with the above-mentioned solvation models. The CYL View software was employed to show the 3D structures of the studied species[62]. All the computational data are deposited in the ioChem-BD repository.[63]

Possible reaction pathways for SET

---

55 Gaussian 16; Revision A. 03; Frisch, M. J.; Trucks, G. W.; Schlegel, H. B.; Scuseria, G. E.; Robb, M. A.; Cheeseman, J. R.; Scalmani, G.; Barone, V.; Petersson, G. A.; Nakatsuji, H.; Li, X.; Caricato, M.; Marenich, A. V.; Bloino, J.; Janesko, B. G.; Gomperts, R.; Mennucci, B.; Hratchian, H. P.; Ortiz, J. V.; Izmaylov, A. F.; Sonnenberg, J. L.; Williams-Young, D.; Ding, F.; Lipparini, F.; Egidi, F.; Goings, J.; Peng, B.; Petrone, A.; Henderson, T.; Ranasinghe, D.; Zakrzewski, V. G.; Gao, J.; Rega, N.; Zheng, G.; Liang, W.; Hada, M.; Ehara, M.; Toyota, K.; Fukuda, R.; Hasegawa, J.; Ishida, M.; Nakajima, T.; Honda, Y.; Kitao, O.; Nakai, H.; Vreven, T.; Throssell, K.; Montgomery, J. A. Jr.; Peralta, J. E.; Ogliaro, F.; Bearpark, M. J.; Heyd, J. J.; Brothers, E. N.; Kudin, K. N.; Staroverov, V. N.; Keith, T. A.; Kobayashi, R.; Normand, J.; Raghavachari, K.; Rendell, A. P.; Burant, J. C.; Iyengar, S. S.; Tomasi, J.; Cossi, M.; Millam, J. M.; Klene, M.; Adamo, C.; Cammi, R.; Ochterski, J. W.; Martin, R. L.; Morokuma, K.; Farkas, O.; Foresman, J. B.; Fox, D. J.; Gaussian, Inc. Wallingford CT, 2016.

56 Zhao, Y.*;* Truhlar, D. G. *Theor. Chem. Account.* **2008***, 120*, 215.

57 Grimme, S. *J. Comput. Chem.* **2006***, 27*, 1787.

58 Dunning Jr. T. H.*;* Hay, P. J. Modern Theoretical Chemistry, Ed. Schaefer III, H. F. Vol. 3 (Plenum, New York, 1977) 1–28

59 (a) Hehre, W. J.; Ditchfield, R.; Pople, J. A. *J. Chem. Phys.***1972***, 56*, 2257. (b) Dill, J. D.; Pople, J. A. *J. Chem. Phys.* **1975***, 62*, 2921. (c) Francl, M. M.*;* Pietro, W. J.; Hehre, W. J.; Binkley, J. S.; Gordon, M. S.; DeFrees, D.J.; Pople, J. A. *J. Chem. Phys.* **1982***, 77*, 3654.

60 Marenich, A. V.; Cramer, C. J.; Truhlar, D. G. *J. Phys. Chem. B* **2009**, *113*, 6378.

61 Weigend, F.; Ahlrichs, R. *Phys. Chem. Chem. Phys.* **2005***, 7*, 3297.

62 C. Y. Legault, CYLview, 1.0b. Université de Sherbrooke. (http://www.cylview.org) (2009).

63 Alvarez-Moreno, M.; de Graaf, C.; Lopez, N.; Maseras, F.; Poblet, J. M.; Bo, C. *J. Chem. Inf. Model.* **2015***, 55*, 95.

To investigate the single electron transfer (SET) process in detail, we explored four pathways (Scheme 2.32). The results indicated that Path3 is the most probable among the four, where PIFA acquires one electron from the electron-rich substrate **1a**, leading to the generation of OTFA anion, CF_3 radical, PhI, and CO_2. The corresponding free energies are shown in Scheme 2.14.

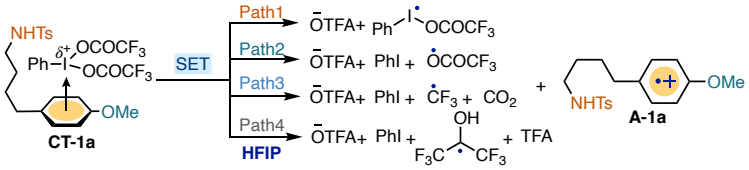

Scheme 2.32. Potential pathways for SET process from CT-complex

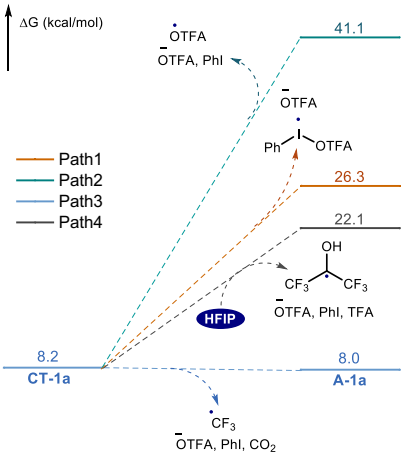

Scheme 2.33. Free energy profile of the potential pathways for SET process from CT-complex.

The fate of the CF_3 radical

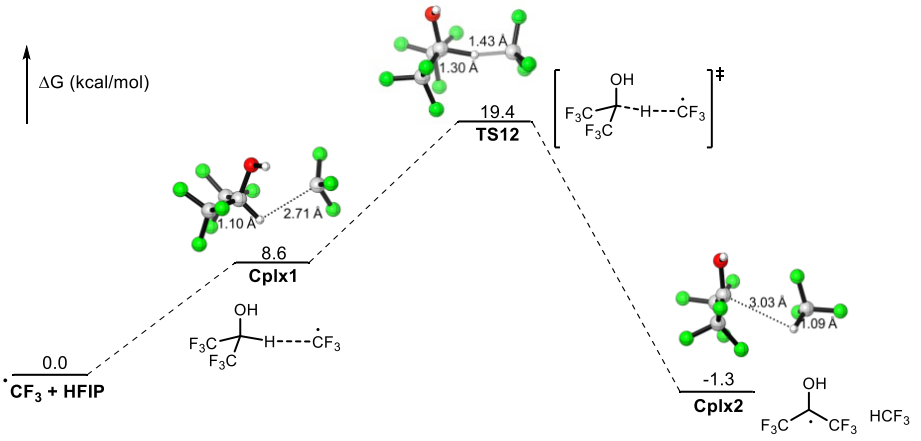

Scheme 2.34. Free energy profile of the process of converting CF_3 radical into HCF_3.

Reaction mechanism: computational analysis

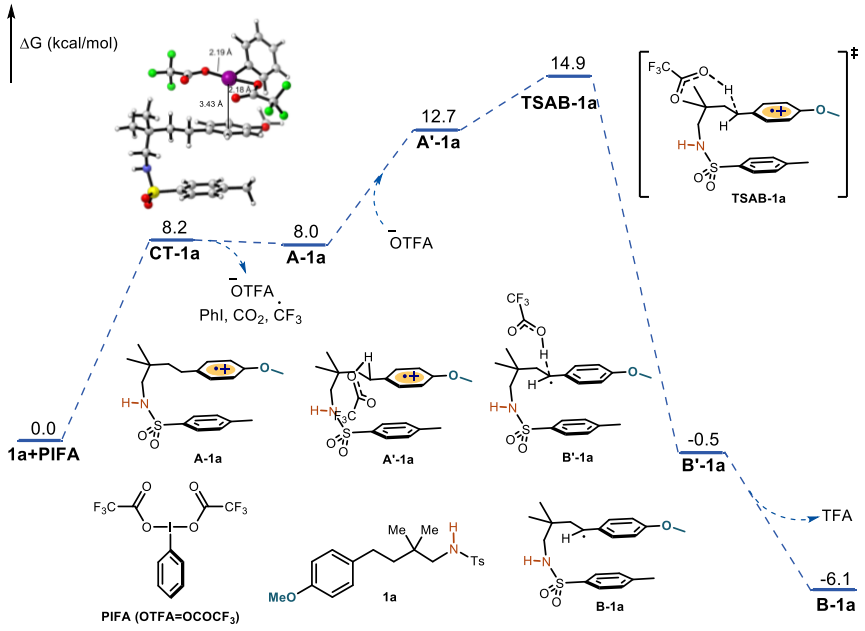

Scheme 2.35. Free energy profile of the C(sp^3)–H functionalization with substrate **1a** and PIFA in HFIP (part1).

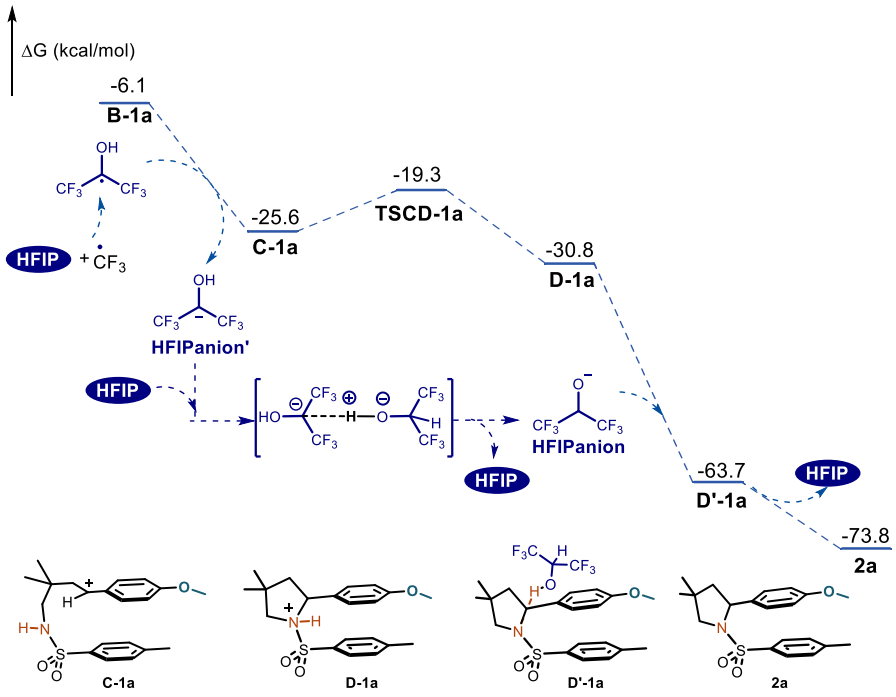

Scheme 2.36. Free energy profile of the C(sp^3)–H functionalization with substrate **1a** and PIFA in HFIP (part2).

Comparing the SET process of substrate **1a** and substrate **1j**

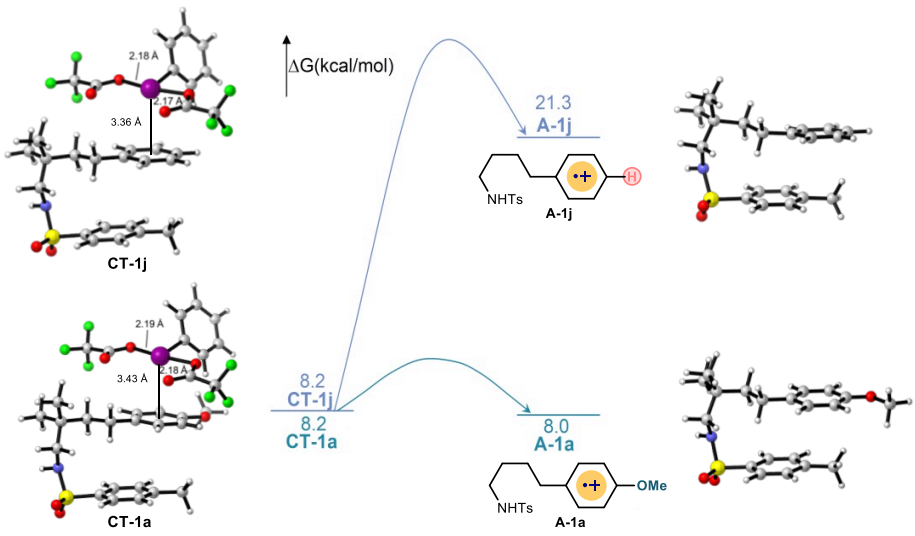

Scheme 2.37. Free energy profile of CT-complex and aromatic radical cation species of substrate **1a** and substrate **1j**.

Gibbs-free energies for the Calculated Structures

Table 2.17. Summary of Gibbs-free energies for the C(sp^3)–H functionalization

Structure Name	G (hartree) [6-31g* & LANL2DZ] +SMD(HFIP)]	G (hartree) [def2tzvp +SMD(HFIP)]	imaginary frequency (cm^{-1}) [6-31g* & LANL2DZ] +SMD(HFIP)]
1a	-1455.821499	-1456.305361	None
1j	-1341.387170	-1341.825001	None
2a	-1454.637826	-1455.115561	None
PIFA	-1294.682104	-1581.641012	None
CT-1a	-2750.498248	-3037.933382	None
CT-1j	-2636.062952	-2923.452902	None
PIFAanion	-1294.832412	-1581.800599	None
A-1a	-1455.620662	-1456.098882	None
A-1j	-1341.165979	-1341.597327	None
OTFAanion	-526.133677	-526.3752866	None
IPhOTFAradical	-768.698534	-1055.430279	None
PhI	-242.765143	-529.2629028	None
OTFAradical	-525.916940	-526.1438540	None
CO_2	-188.505639	-188.5917025	None
CF_3radical	-337.450997	-337.6048109	None
HFIP	-789.497551	-789.8416152	None
HFIPradical	-788.851118	-789.1946534	None
TFA	-526.589326	-526.8211115	None

A'-1a	-1981.75997	-1982.466729	None
TSAB-1a	-1981.753904	-1982.463188	-601.22
B'-1a	-1981.775748	-1982.487823	None
B-1a	-1455.192016	-1455.675633	None
HCF_3	-338.118409	-338.2727126	None
HFIPanion	-789.003297	-789.3602762	None
HFIPanion'	-788.976470	-789.3360898	None
C-1a	-1455.042386	-1455.520035	None
TSCD-1a	-1455.035063	-1455.510016	-72.64
D-1a	-1455.055267	-1455.527930	None
D'-1a	-2244.129180	-2244.941087	None
Cplx1	-1126.939246	-1127.432769	None
TS12	-1126.921957	-1127.415438	-1983.34
Cplx2	-1126.955269	-1127.448525	None

2.5.10. NMR spectra

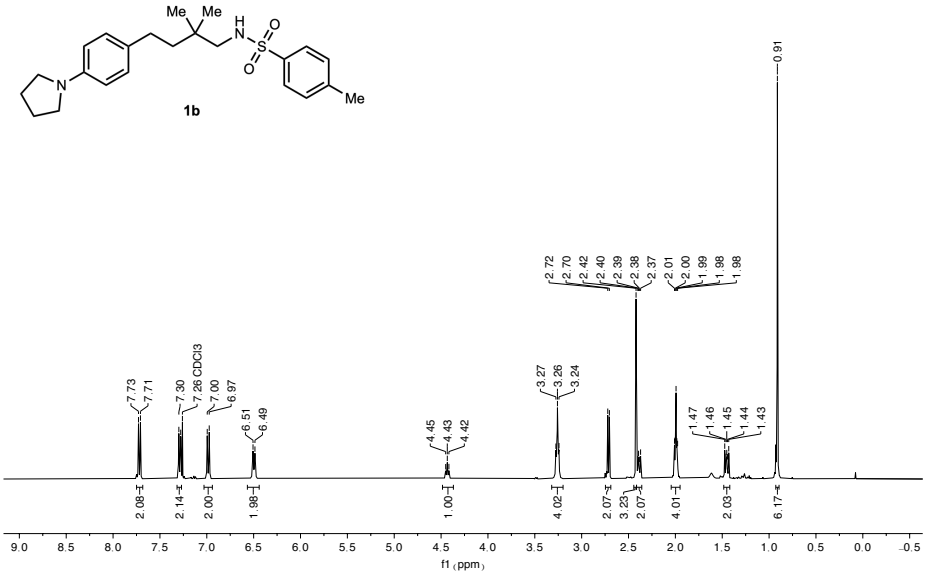
Me
Me
H
N
S
O
O
Me
N
1b
0.91
2.72
2.70
2.42
2.40
2.39
2.38
2.37
2.01
2.00
1.99
1.98
1.98
7.73
7.71
7.30
7.26 CDCl3
7.00
6.97
6.51
6.49
4.45
4.43
4.42
3.27
3.26
3.24
1.47
1.46
1.45
1.44
1.43
2.08
2.14
2.00
1.98
1.00
4.02
2.07
3.23
2.07
4.01
2.03
6.17
f1 (ppm)

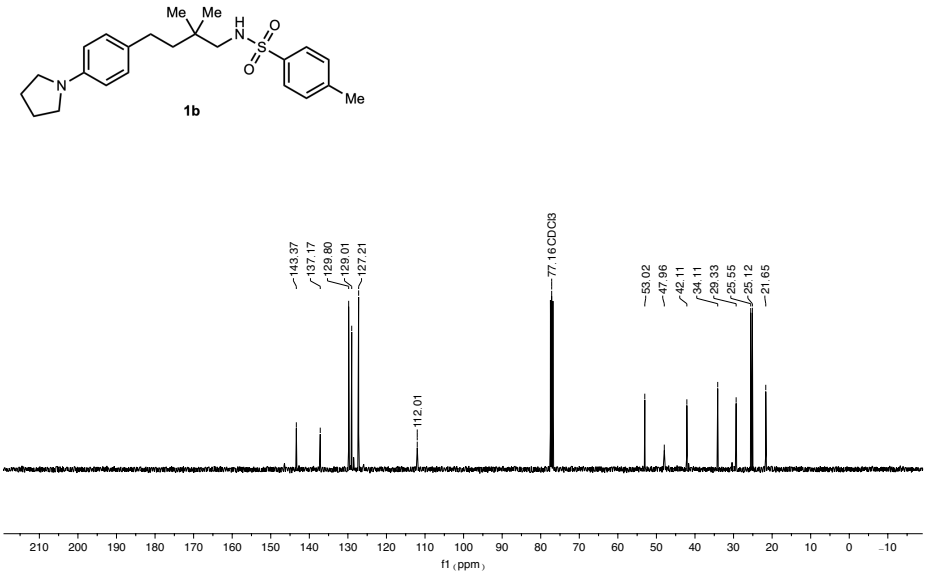
Me
Me
H
N
S
O
O
Me
N
1b
143.37
137.17
129.80
129.01
127.21
112.01
77.16 CDCl3
53.02
47.96
42.11
34.11
29.33
25.55
25.12
21.65
f1 (ppm)

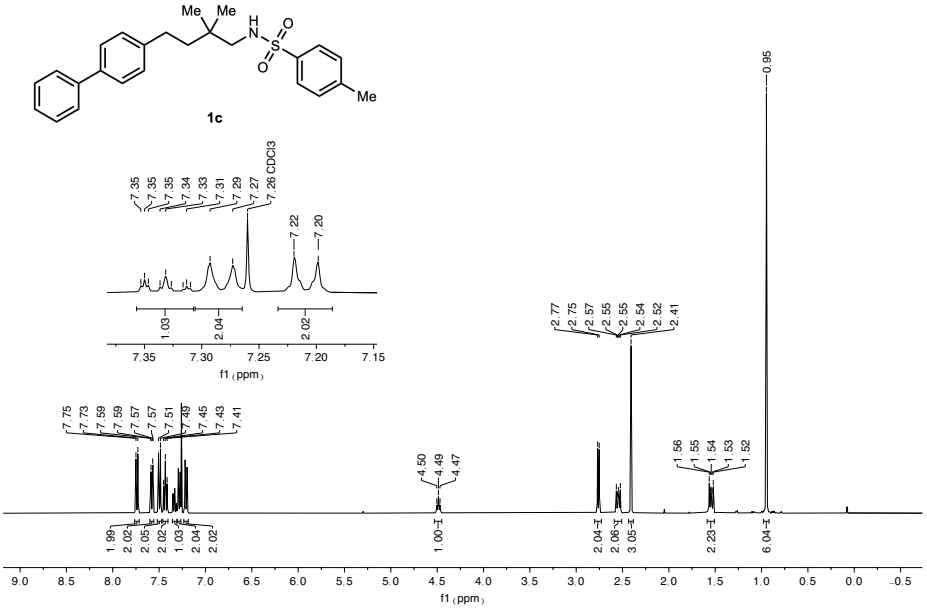
Me
Me
H
N
O
S
O
O
Me
1c
7.35
7.35
7.35
7.34
7.33
7.31
7.29
7.27
7.26 CDCl3
7.22
7.20
1.03
2.04
2.02
7.35
7.30
7.25
7.20
7.15
f1 (ppm)
7.75
7.73
7.59
7.59
7.57
7.57
7.51
7.49
7.45
7.43
7.41
4.50
4.49
4.47
2.77
2.75
2.57
2.55
2.55
2.54
2.52
2.41
1.56
1.55
1.54
1.53
1.52
0.95
1.99
2.02
2.05
2.02
1.03
2.04
2.02
1.00
2.04
2.06
3.05
2.23
6.04
9.0
8.5
8.0
7.5
7.0
6.5
6.0
5.5
5.0
4.5
4.0
3.5
3.0
2.5
2.0
1.5
1.0
0.5
0.0
-0.5
f1 (ppm)

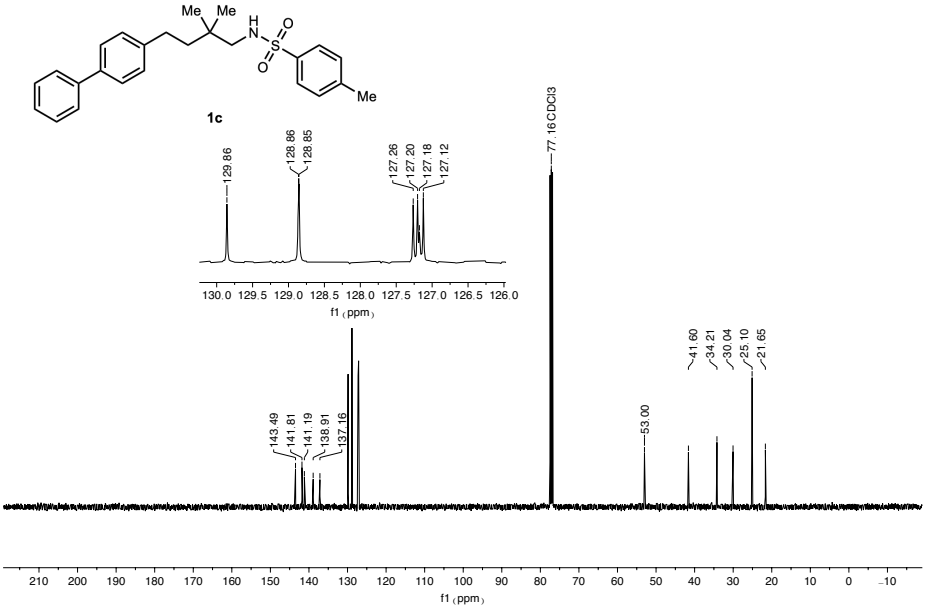
Me
Me
H
N
O
S
O
O
Me
1c
129.86
128.86
128.85
127.26
127.20
127.18
127.12
130.0
129.5
129.0
128.5
128.0
127.5
127.0
126.5
126.0
f1 (ppm)
77.16 CDCl3
143.49
141.81
141.19
138.91
137.16
53.00
41.60
34.21
30.04
25.10
21.65
210
200
190
180
170
160
150
140
130
120
110
100
90
80
70
60
50
40
30
20
10
0
-10
f1 (ppm)

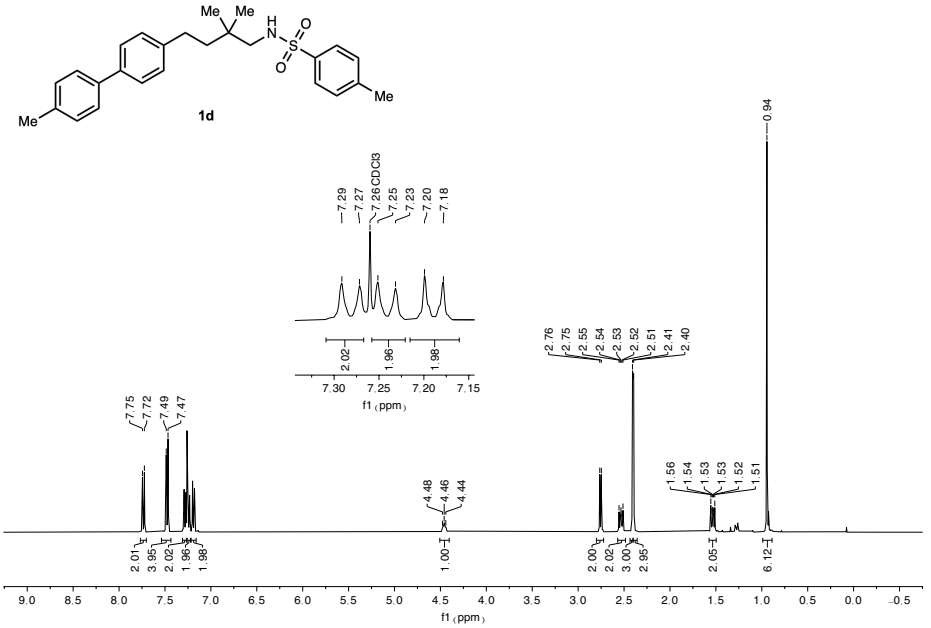
Me
Me
H
N
S
O
O
Me
Me
1d
7.29
7.27
7.26 CDCl3
7.25
7.23
7.20
7.18
2.02
1.96
1.98
7.30
7.25
7.20
7.15
f1 (ppm)
0.94
2.76
2.75
2.55
2.54
2.53
2.52
2.51
2.41
2.40
7.75
7.72
7.49
7.47
4.48
4.46
4.44
1.56
1.54
1.53
1.53
1.52
1.51
2.01
3.95
2.02
1.96
1.98
1.00
2.00
2.02
3.00
2.95
2.05
6.12
9.0
8.5
8.0
7.5
7.0
6.5
6.0
5.5
5.0
4.5
4.0
3.5
3.0
2.5
2.0
1.5
1.0
0.5
0.0
-0.5
f1 (ppm)

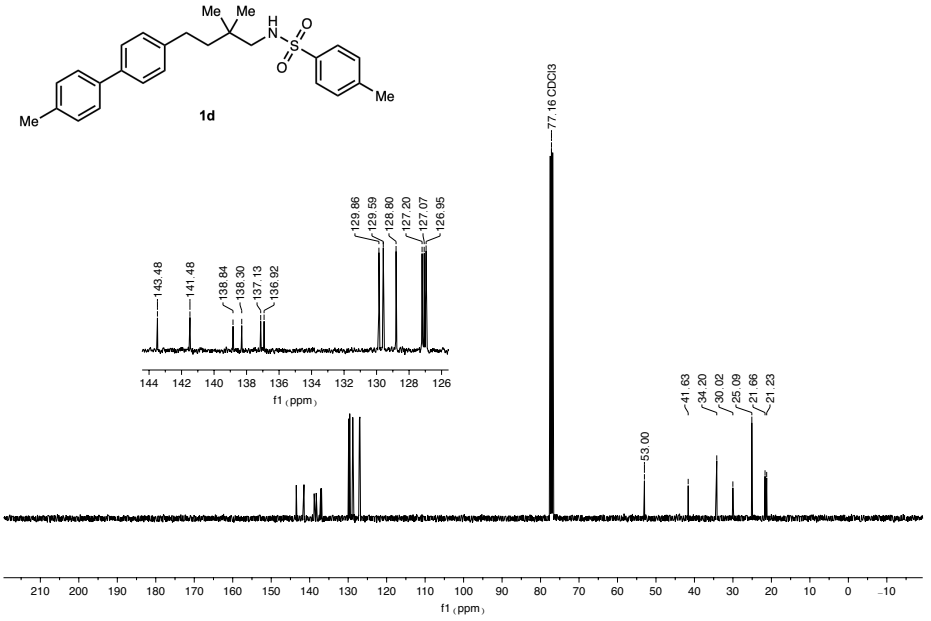
Me
Me
H
N
S
O
O
Me
Me
1d
77.16 CDCl3
129.86
129.59
128.80
127.20
127.07
126.95
143.48
141.48
138.84
138.30
137.13
136.92
144
142
140
138
136
134
132
130
128
126
f1 (ppm)
41.63
34.20
30.02
25.09
21.66
21.23
53.00
210
200
190
180
170
160
150
140
130
120
110
100
90
80
70
60
50
40
30
20
10
0
-10
f1 (ppm)

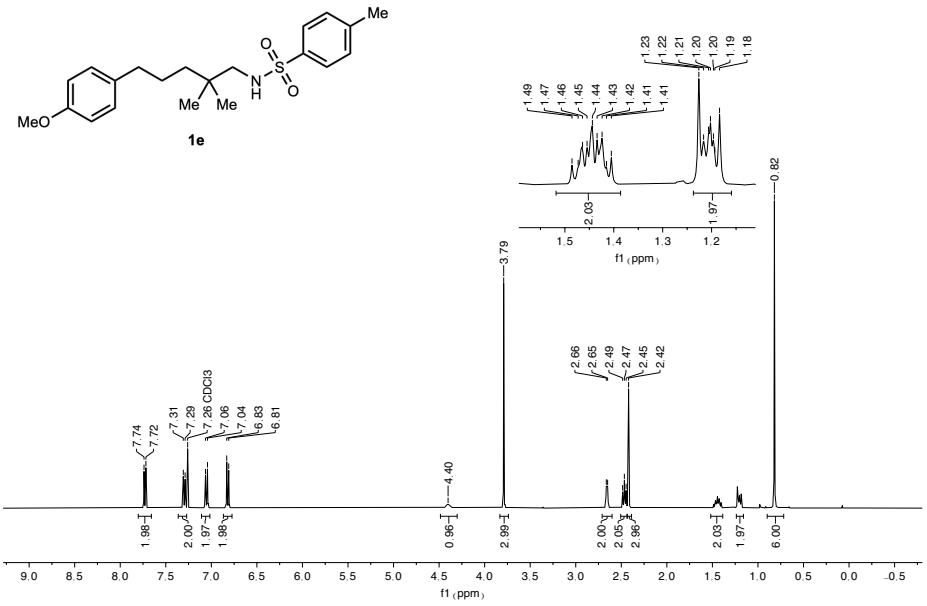
Me
O
S
N
H
O
Me Me
MeO
1e
7.74
7.72
7.31
7.29
7.26 CDCl3
7.06
7.04
6.83
6.81
4.40
3.79
2.66
2.65
2.49
2.47
2.45
2.42
1.49
1.47
1.46
1.45
1.44
1.43
1.42
1.41
1.41
1.23
1.22
1.21
1.20
1.20
1.19
1.18
0.82
1.98
2.00
1.97
1.96
0.96
2.99
2.00
2.05
2.96
2.03
1.97
6.00
f1 (ppm)

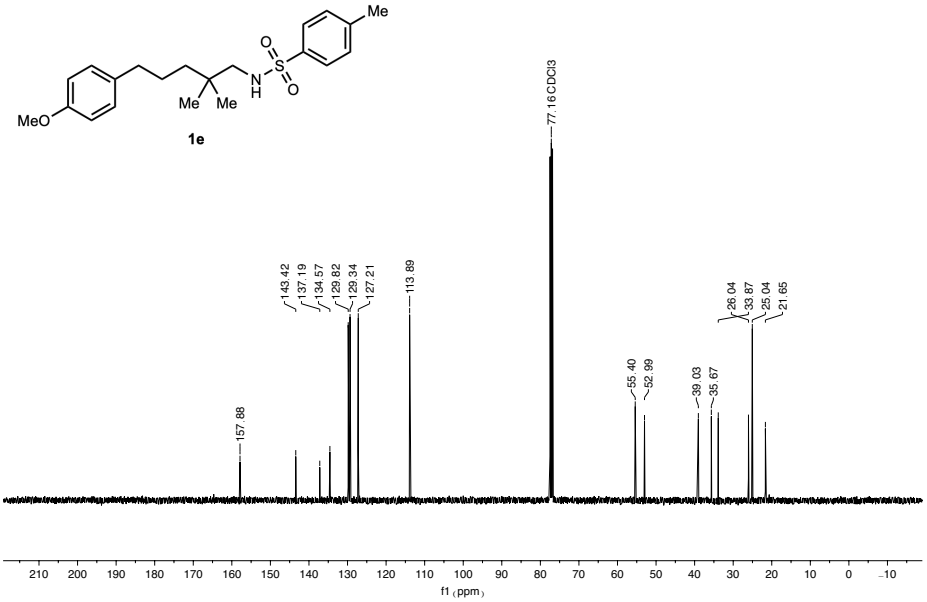
Me
O
S
N
H
O
Me Me
MeO
1e
157.88
143.42
137.19
134.57
129.82
129.34
127.21
113.89
77.16 CDCl3
55.40
52.99
39.03
35.67
26.04
33.87
25.04
21.65
f1 (ppm)

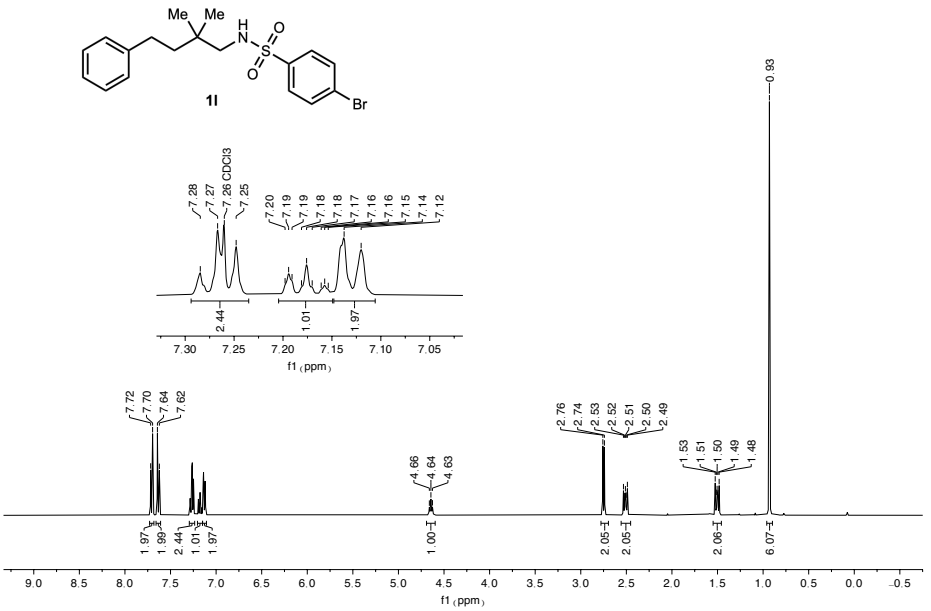
Me
Me
H
N
O
S
O
Br
1l
7.28
7.27
7.26 CDCl3
7.25
7.20
7.19
7.19
7.18
7.18
7.17
7.16
7.16
7.15
7.14
7.12
2.44
1.01
1.97
7.30
7.25
7.20
7.15
7.10
7.05
f1 (ppm)
0.93
7.72
7.70
7.64
7.62
4.66
4.64
4.63
2.76
2.74
2.53
2.52
2.51
2.50
2.49
1.53
1.51
1.50
1.49
1.48
1.97
1.99
2.44
1.01
1.97
1.00
2.05
2.05
2.06
6.07
9.0
8.5
8.0
7.5
7.0
6.5
6.0
5.5
5.0
4.5
4.0
3.5
3.0
2.5
2.0
1.5
1.0
0.5
0.0
-0.5
f1 (ppm)

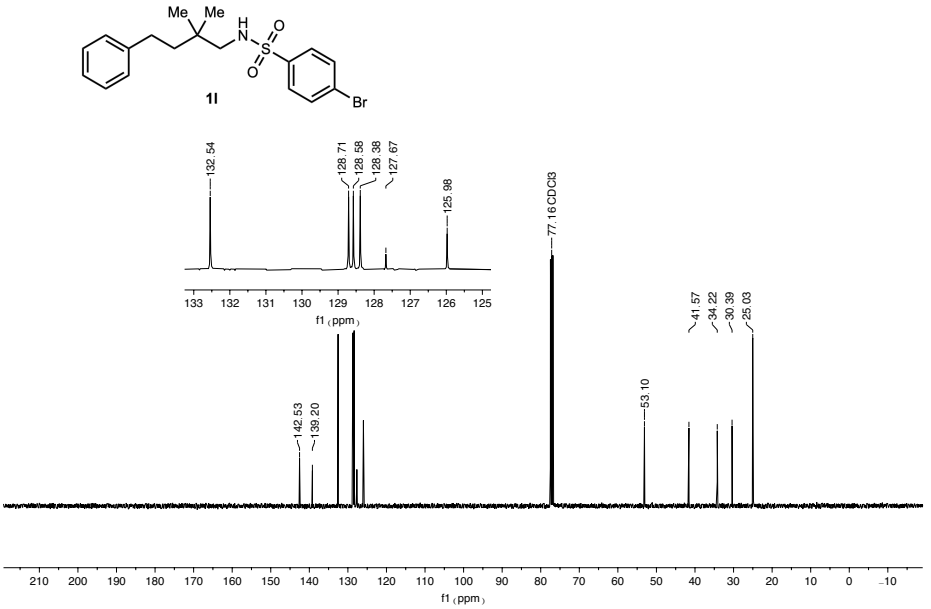
Me
Me
H
N
O
S
O
Br
1l
132.54
128.71
128.58
128.38
127.67
125.98
77.16 CDCl3
41.57
34.22
30.39
25.03
53.10
142.53
139.20
133
132
131
130
129
128
127
126
125
f1 (ppm)
210
200
190
180
170
160
150
140
130
120
110
100
90
80
70
60
50
40
30
20
10
0
-10
f1 (ppm)

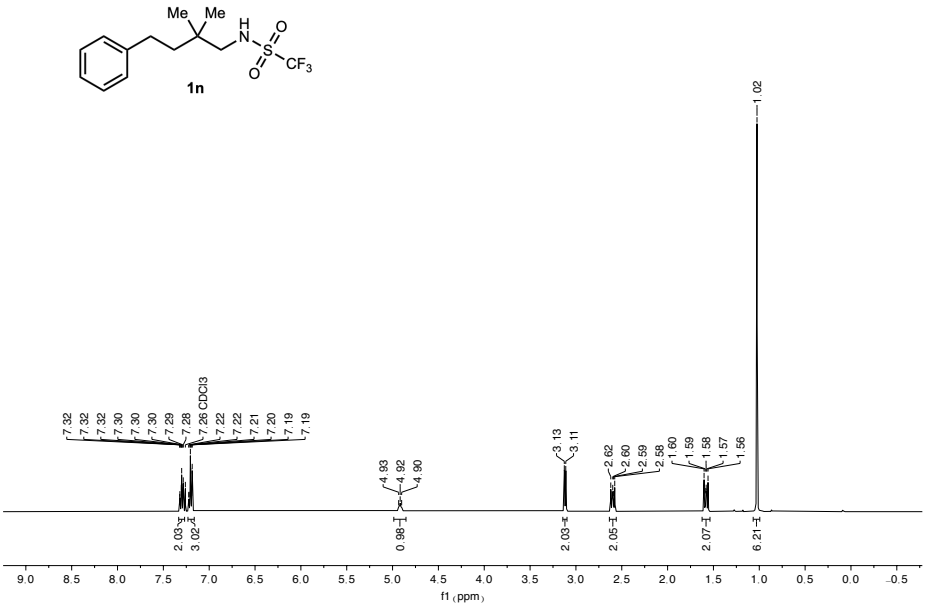
Me
Me
H
N
O
S
O
CF3
1n
1.02
7.32
7.32
7.32
7.30
7.30
7.30
7.29
7.28
7.26 CDCl3
7.22
7.22
7.21
7.20
7.19
7.19
4.93
4.92
4.90
3.13
3.11
2.62
2.60
2.59
2.58
1.60
1.59
1.58
1.57
1.56
2.03
3.02
0.98
2.03
2.05
2.07
6.21
f1 (ppm)

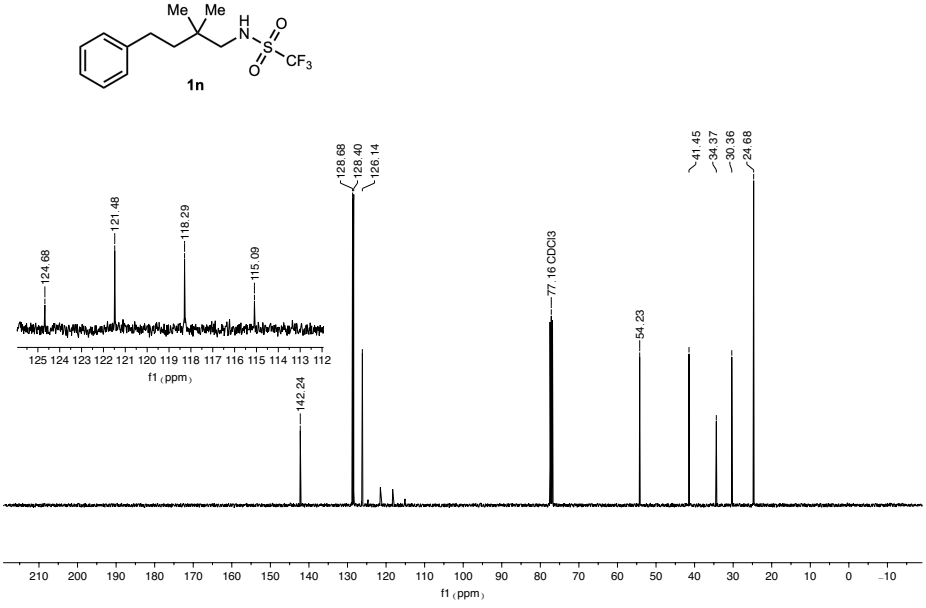
Me
Me
H
N
O
S
O
CF3
1n
128.68
128.40
126.14
121.48
118.29
124.68
115.09
41.45
34.37
30.36
24.68
77.16 CDCl3
54.23
142.24
f1 (ppm)
f1 (ppm)

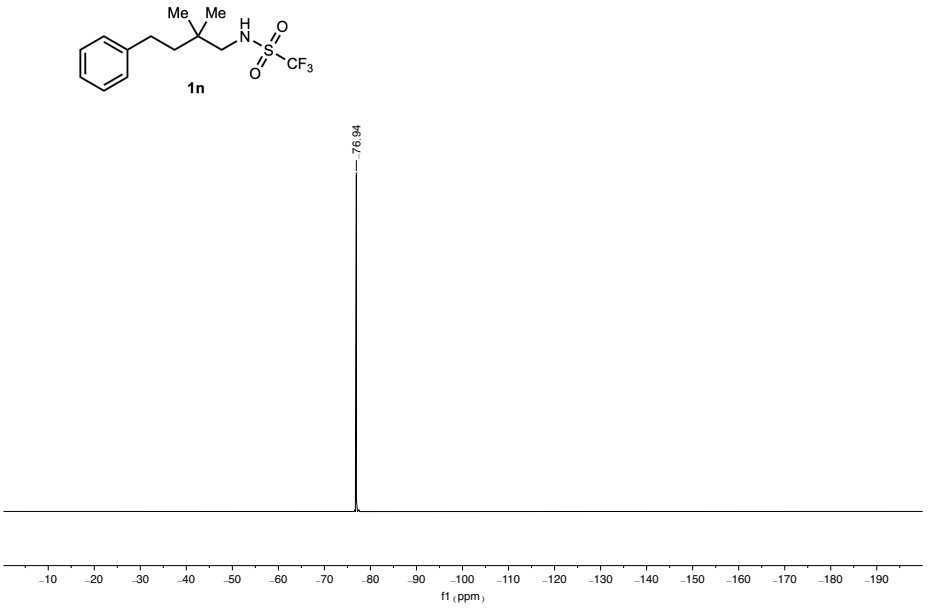
Me
Me
H
N
O
S
O
CF3
1n
-76.94
-10 -20 -30 -40 -50 -60 -70 -80 -90 -100 -110 -120 -130 -140 -150 -160 -170 -180 -190
f1 (ppm)

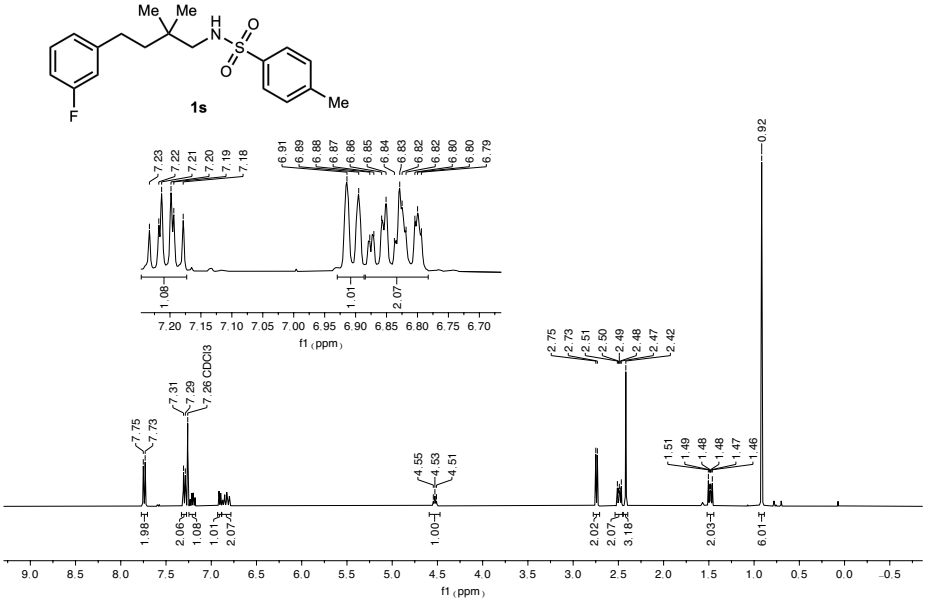
Me
Me
H
N
O
S
O
F
Me
1s
7.23 7.22 7.21 7.20 7.19 7.18
6.91 6.89 6.88 6.87 6.86 6.85 6.84 6.83 6.82 6.82 6.80 6.80 6.79
1.08
1.01
2.07
7.20 7.15 7.10 7.05 7.00 6.95 6.90 6.85 6.80 6.75 6.70
f1 (ppm)
0.92
2.75 2.73 2.51 2.50 2.49 2.48 2.47 2.42
1.51 1.49 1.48 1.48 1.47 1.46
7.75 7.73
7.31 7.29 7.26 CDCl3
4.55 4.53 4.51
1.98
2.06
1.08
1.01
2.07
1.00
2.02
2.07
3.18
2.03
6.01
9.0 8.5 8.0 7.5 7.0 6.5 6.0 5.5 5.0 4.5 4.0 3.5 3.0 2.5 2.0 1.5 1.0 0.5 0.0 -0.5
f1 (ppm)

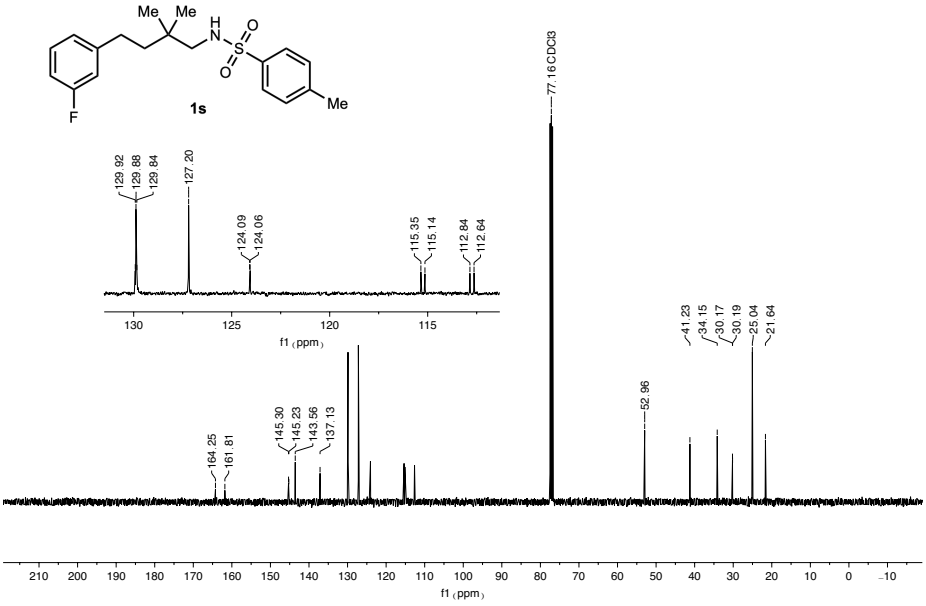
Me
Me
H
N
S
O
O
F
Me
1s
77.16CDCl3
129.92
129.88
129.84
127.20
124.09
124.06
115.35
115.14
112.84
112.64
130
125
120
115
f1 (ppm)
41.23
34.15
30.17
30.19
25.04
21.64
52.96
145.30
145.23
143.56
137.13
164.25
161.81
210 200 190 180 170 160 150 140 130 120 110 100 90 80 70 60 50 40 30 20 10 0 -10
f1 (ppm)

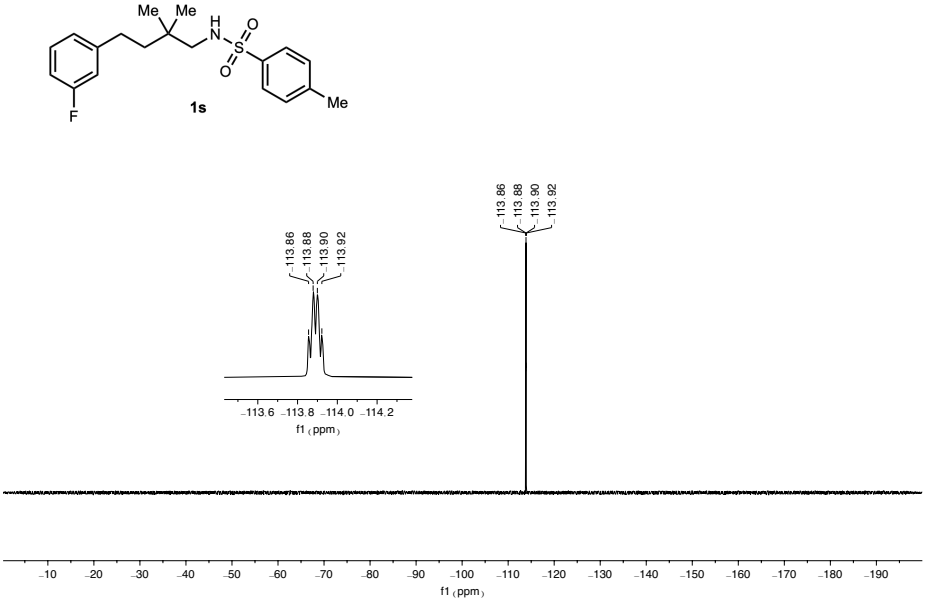
Me
Me
H
N
S
O
O
F
Me
1s
113.86
113.88
113.90
113.92
113.86
113.88
113.90
113.92
-113.6 -113.8 -114.0 -114.2
f1 (ppm)
-10 -20 -30 -40 -50 -60 -70 -80 -90 -100 -110 -120 -130 -140 -150 -160 -170 -180 -190
f1 (ppm)

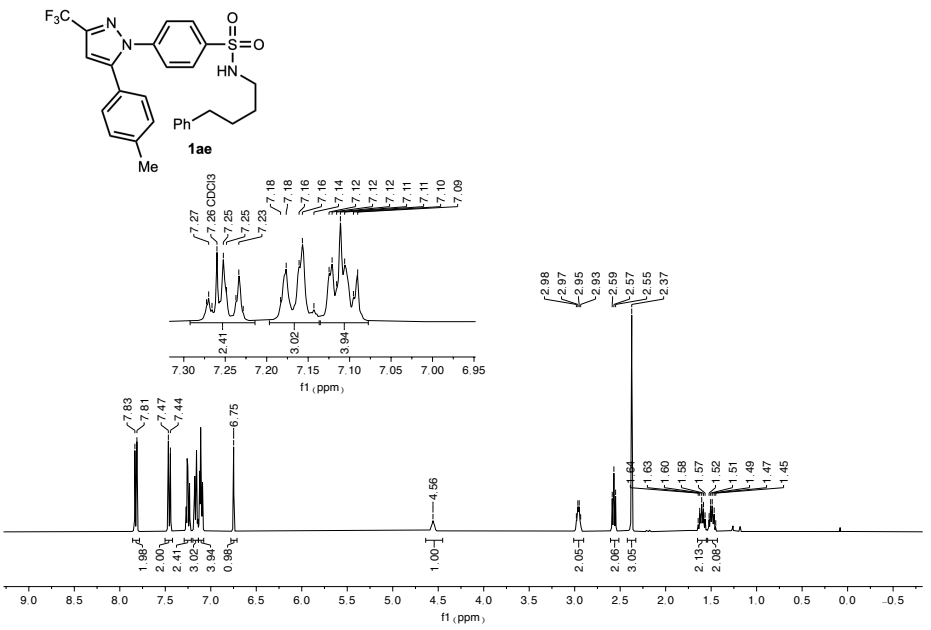
F3C
N
N
O
S=O
HN
Ph
Me
1ae
7.27
7.26 CDCl3
7.25
7.25
7.23
7.18
7.18
7.16
7.16
7.14
7.12
7.12
7.12
7.11
7.11
7.10
7.09
2.41
3.02
3.94
7.30 7.25 7.20 7.15 7.10 7.05 7.00 6.95
f1 (ppm)
2.98
2.97
2.95
2.93
2.59
2.57
2.55
2.37
7.83
7.81
7.47
7.44
6.75
4.56
1.64
1.63
1.60
1.58
1.57
1.52
1.51
1.49
1.47
1.45
1.98
2.00
2.41
3.02
3.94
0.98
1.00
2.05
2.06
3.05
2.13
2.08
9.0 8.5 8.0 7.5 7.0 6.5 6.0 5.5 5.0 4.5 4.0 3.5 3.0 2.5 2.0 1.5 1.0 0.5 0.0 -0.5
f1 (ppm)

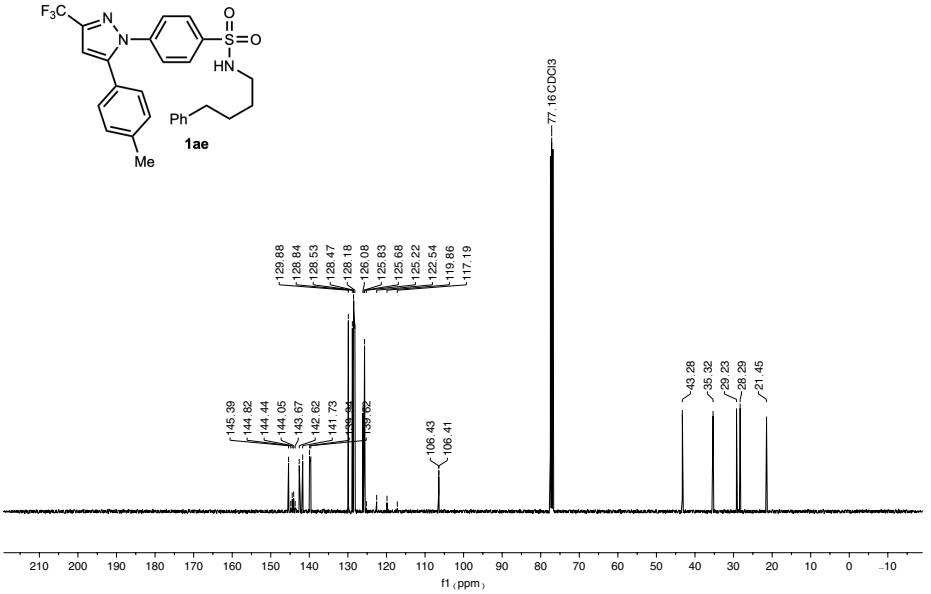
F3C
N
N
O
S=O
HN
Ph
Me
1ae
77.16 CDCl3
129.88
128.84
128.53
128.47
128.18
126.08
125.83
125.68
125.22
122.54
119.86
117.19
145.39
144.82
144.44
144.05
143.67
142.62
141.73
133.31
107.62
106.43
106.41
43.28
35.32
29.23
28.29
21.45
210 200 190 180 170 160 150 140 130 120 110 100 90 80 70 60 50 40 30 20 10 0 -10
f1 (ppm)

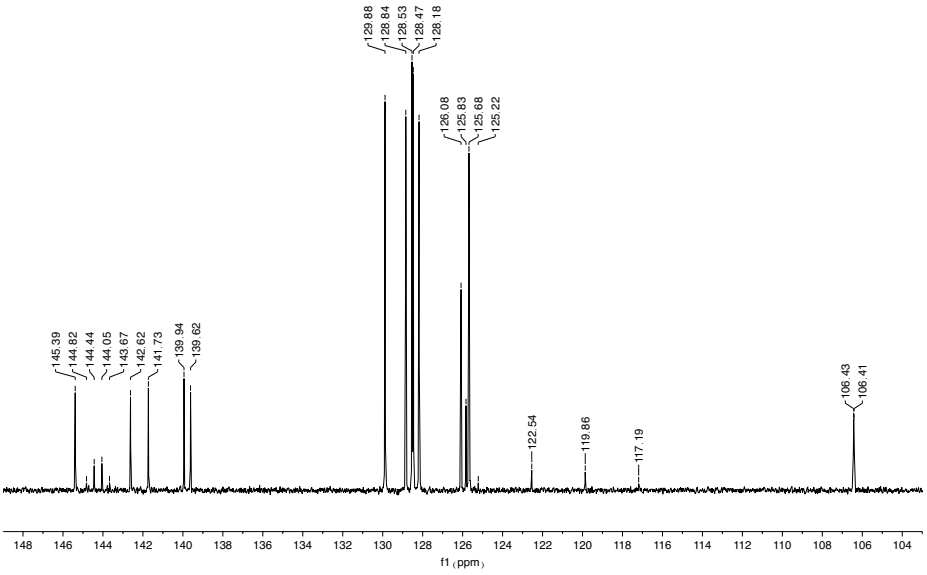
129.88
128.84
128.53
128.47
128.18
126.08
125.83
125.68
125.22
145.39
144.82
144.44
144.05
143.67
142.62
141.73
139.94
139.62
122.54
119.86
117.19
106.43
106.41
148 146 144 142 140 138 136 134 132 130 128 126 124 122 120 118 116 114 112 110 108 106 104
f1 (ppm)

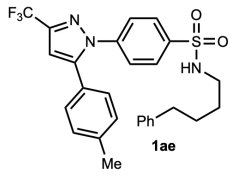
F3C
N
N
O
S=O
HN
Ph
Me

1ae

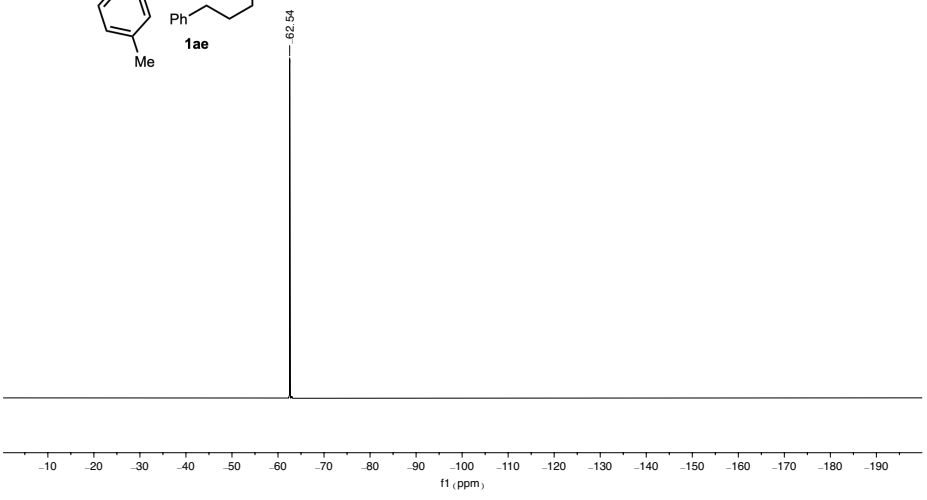
-62.54
-10 -20 -30 -40 -50 -60 -70 -80 -90 -100 -110 -120 -130 -140 -150 -160 -170 -180 -190
f1 (ppm)

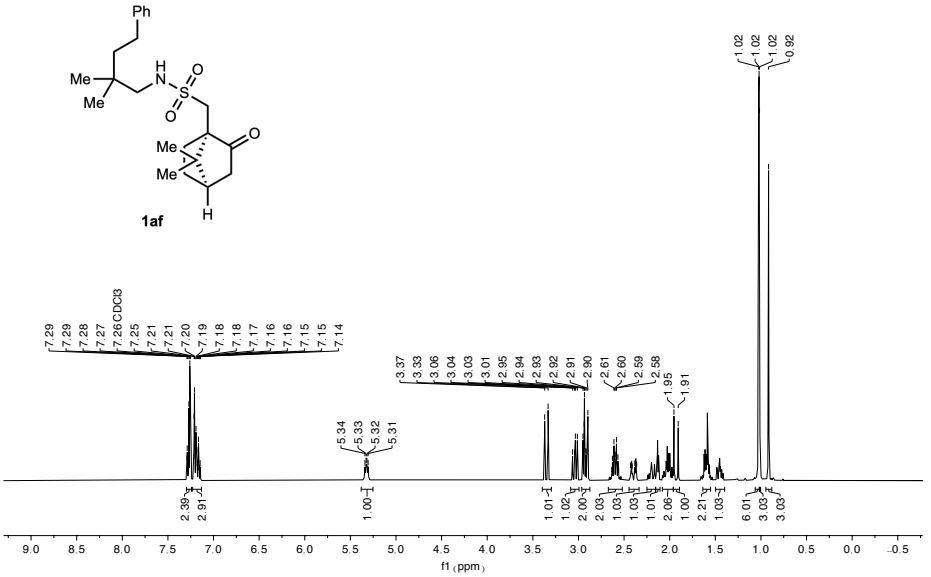
Ph
Me
Me
H
N
O
S
O
O
Me
Me
O
H
1af
f1 (ppm)

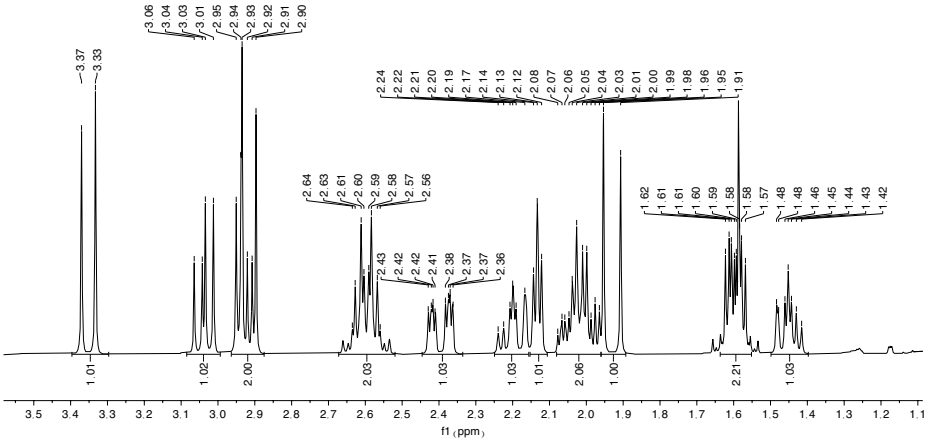
f1 (ppm)

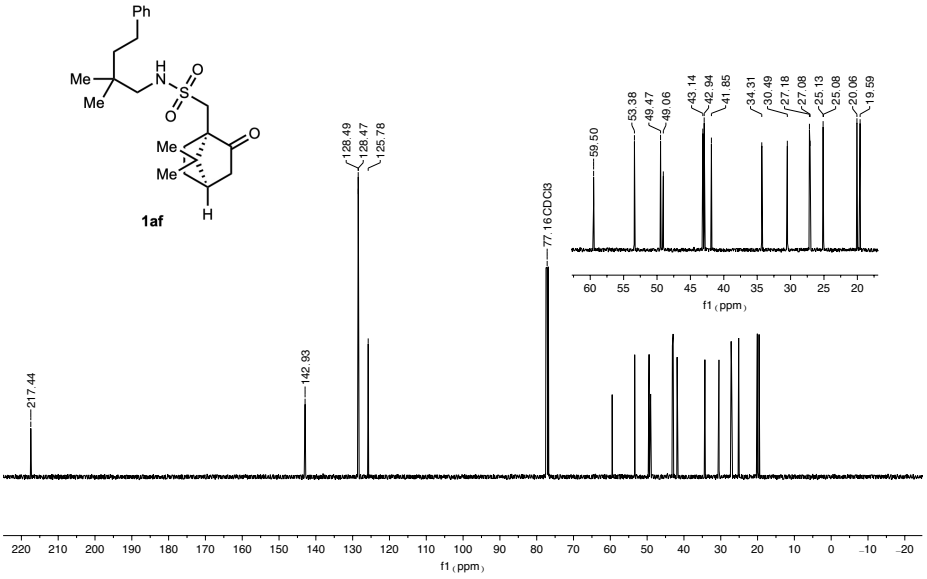
Ph
Me
Me
H
N
S
O
O
O
Me
Me
H
1af
217.44
142.93
128.49
128.47
125.78
77.16 CDCl3
59.50
53.38
49.47
49.06
43.14
42.94
41.85
34.31
30.49
27.18
27.08
25.13
25.08
20.06
19.59
f1 (ppm)

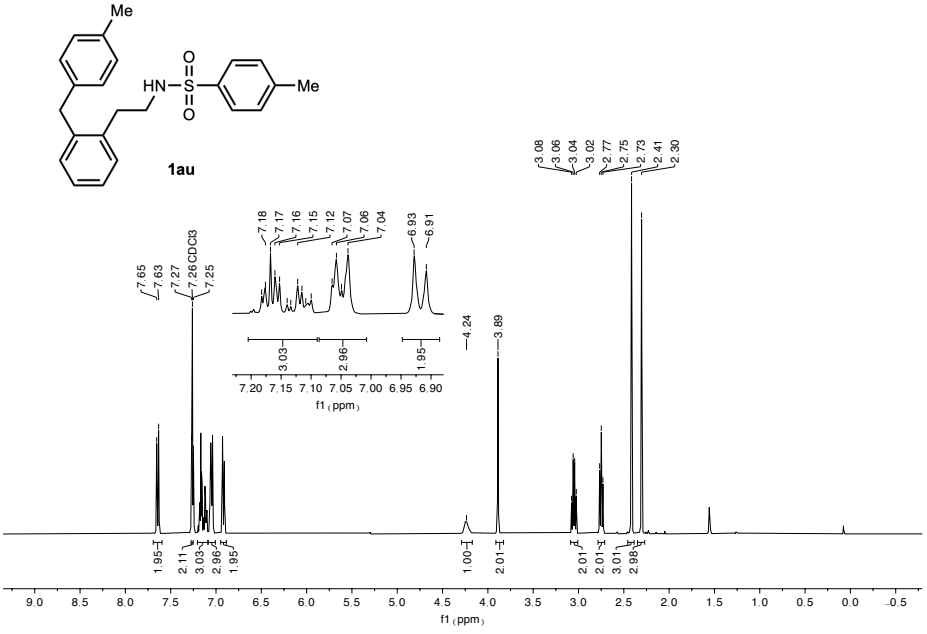
Me
HN
S
O
O
Me
1au
7.65
7.63
7.27
7.26 CDCl3
7.25
7.18
7.17
7.16
7.15
7.12
7.07
7.06
7.04
6.93
6.91
3.03
2.96
1.95
4.24
3.89
3.08
3.06
3.04
3.02
2.77
2.75
2.73
2.41
2.30
1.95
2.11
3.03
2.96
1.95
1.00
2.01
2.01
2.01
3.01
2.98
f1 (ppm)

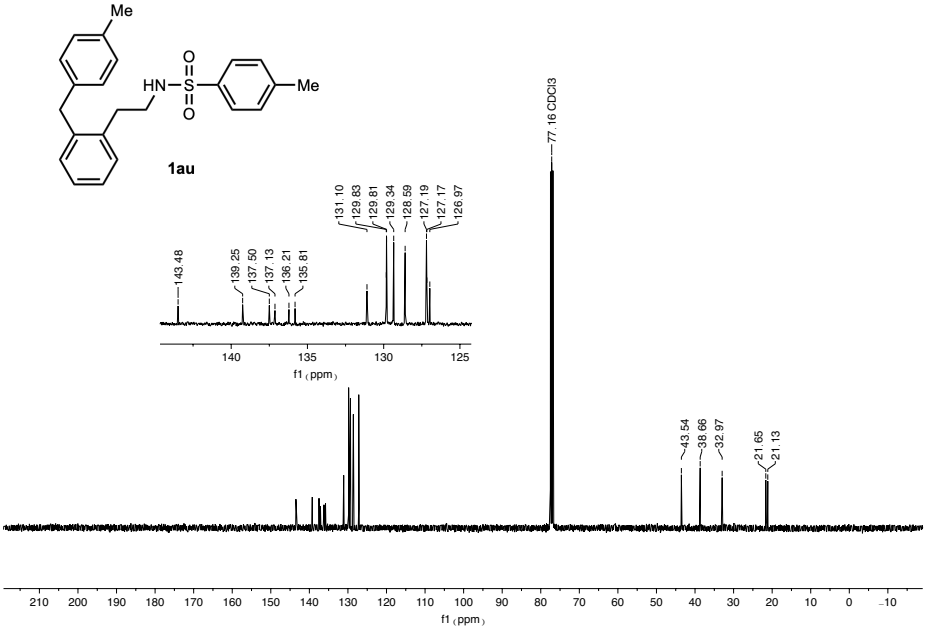
Me
HN
S
O
O
Me
1au
77.16 CDCl3
131.10
129.83
129.81
129.34
128.59
127.19
127.17
126.97
143.48
139.25
137.50
137.13
136.21
135.81
43.54
38.66
32.97
21.65
21.13
f1 (ppm)

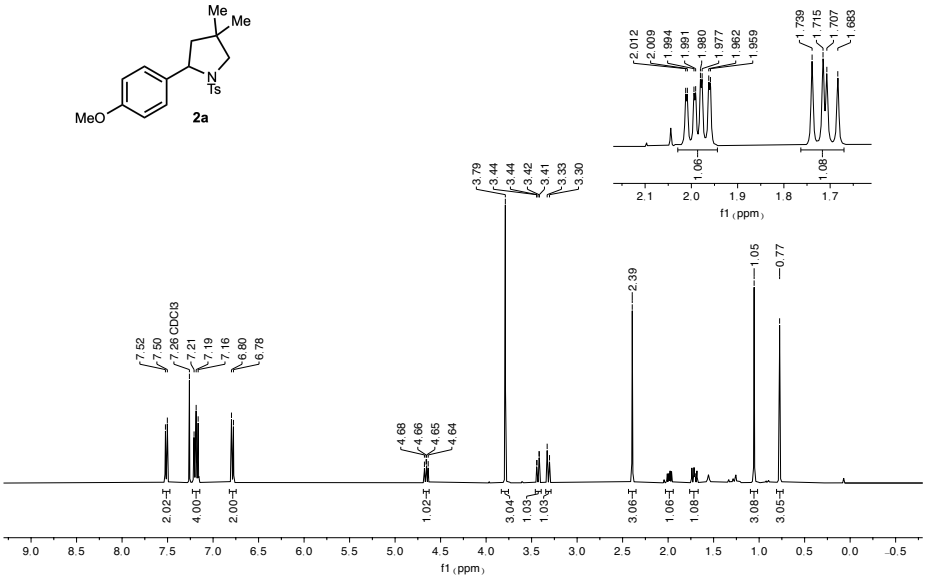
Me
Me
N
Ts
MeO
2a
2.012
2.009
1.994
1.991
1.980
1.977
1.962
1.959
1.739
1.715
1.707
1.683
1.06
1.08
3.79
3.44
3.44
3.42
3.41
3.33
3.30
7.52
7.50
7.26 CDCl3
7.21
7.19
7.16
6.80
6.78
4.68
4.66
4.65
4.64
2.39
1.05
0.77
2.02
4.00
2.00
1.02
3.04
1.03
1.03
3.06
1.06
1.08
3.08
3.05
f1 (ppm)

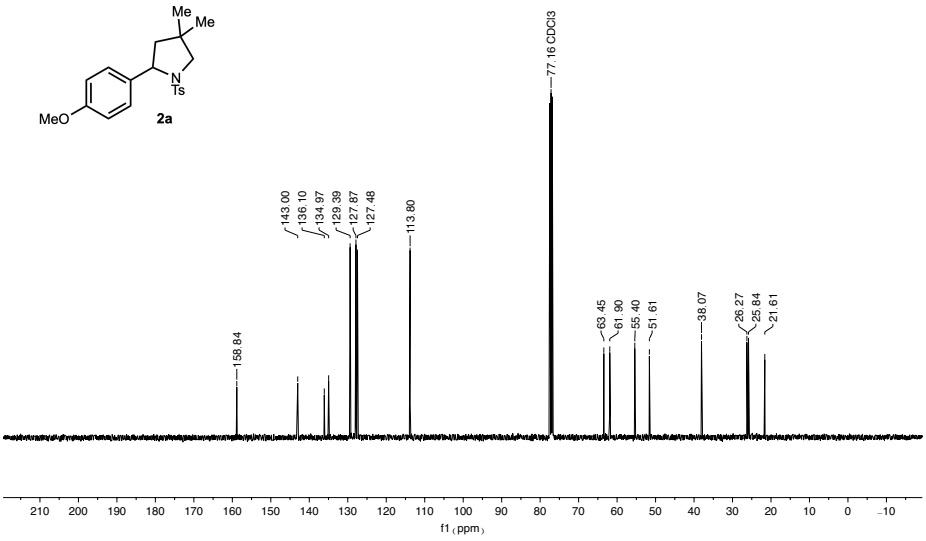
Me
Me
N
Ts
MeO
2a
158.84
143.00
136.10
134.97
129.39
127.87
127.48
113.80
77.16 CDCl3
63.45
61.90
55.40
51.61
38.07
26.27
25.84
21.61
f1 (ppm)

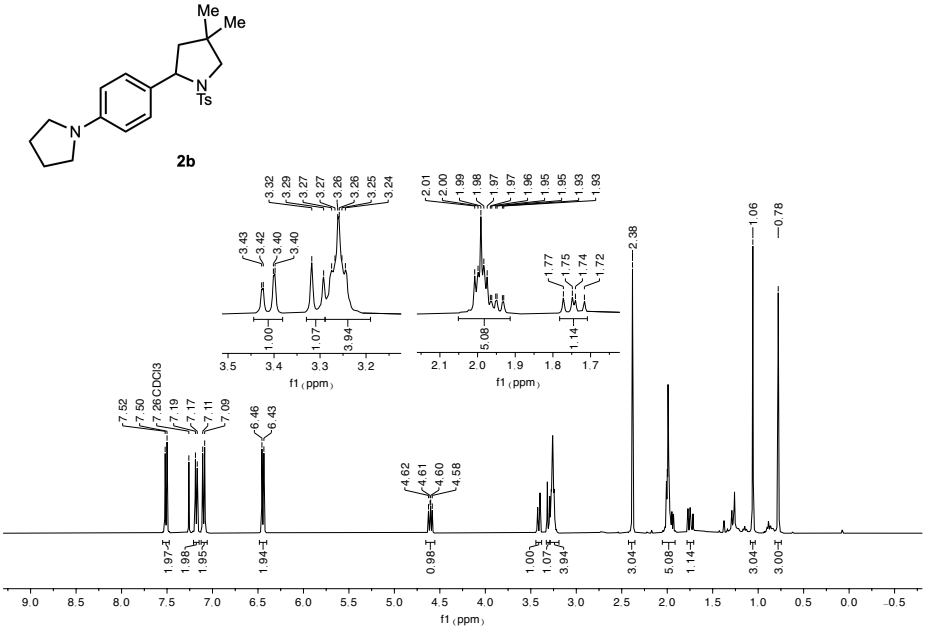
Me
Me
N
Ts
N
2b
3.32
3.29
3.27
3.27
3.26
3.26
3.25
3.24
3.43
3.42
3.40
3.40
1.00
1.07
3.94
2.01
2.00
1.99
1.98
1.97
1.97
1.96
1.95
1.95
1.93
1.93
1.77
1.75
1.74
1.72
5.08
1.14
2.38
1.06
0.78
7.52
7.50
7.26 CDCl3
7.19
7.17
7.11
7.09
6.46
6.43
4.62
4.61
4.60
4.58
1.97
1.98
1.95
1.94
0.98
1.00
1.07
3.94
3.04
5.08
1.14
3.04
3.00
f1 (ppm)

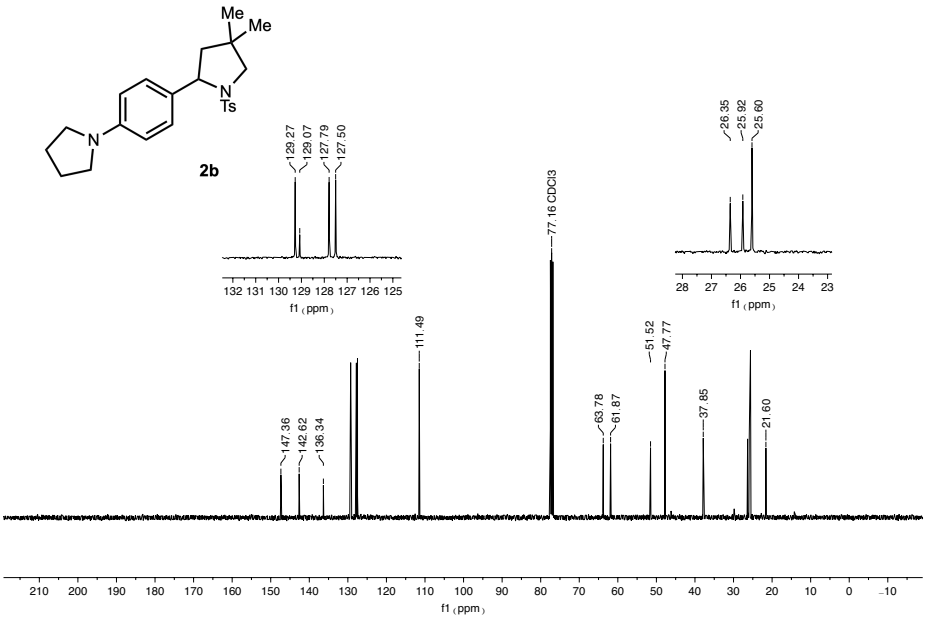
Me
Me
N
Ts
N
2b
129.27
129.07
127.79
127.50
77.16 CDCl3
26.35
25.92
25.60
111.49
147.36
142.62
136.34
63.78
61.87
51.52
47.77
37.85
21.60
f1 (ppm)

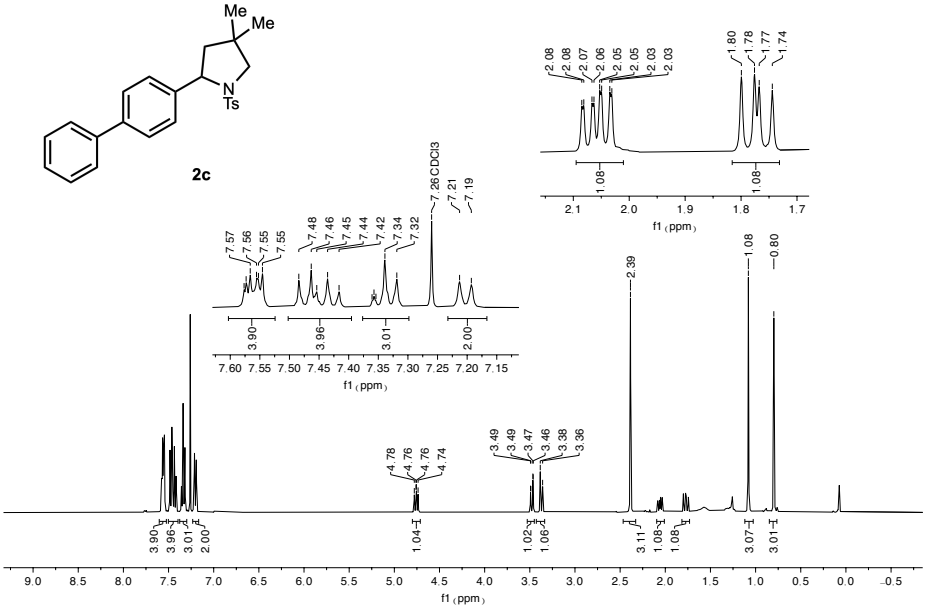
Me
Me
N
Ts
2c
7.26 CDCl3
7.57
7.56
7.55
7.55
7.48
7.46
7.45
7.44
7.42
7.34
7.32
7.21
7.19
2.08
2.08
2.07
2.06
2.05
2.05
2.03
2.03
1.80
1.78
1.77
1.74
2.39
1.08
0.80
4.78
4.76
4.76
4.74
3.49
3.49
3.47
3.46
3.38
3.36
f1 (ppm)

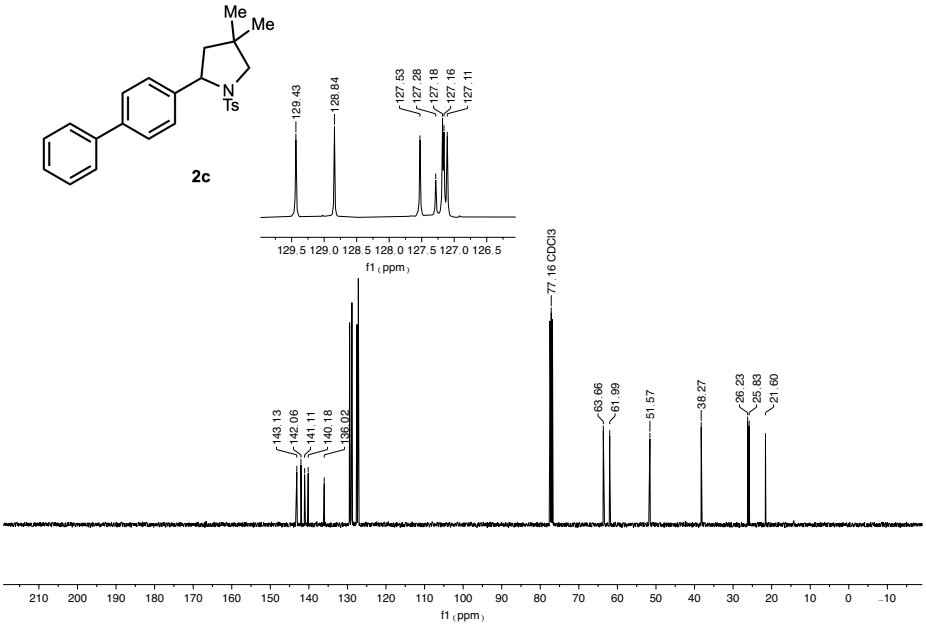
Me
Me
N
Ts
2c
129.43
128.84
127.53
127.28
127.18
127.16
127.11
129.5 129.0 128.5 128.0 127.5 127.0 126.5
f1 (ppm)
77.16 CDCl3
143.13
142.06
141.11
140.18
136.02
63.66
61.99
51.57
38.27
26.23
25.83
21.60
210 200 190 180 170 160 150 140 130 120 110 100 90 80 70 60 50 40 30 20 10 0 -10
f1 (ppm)

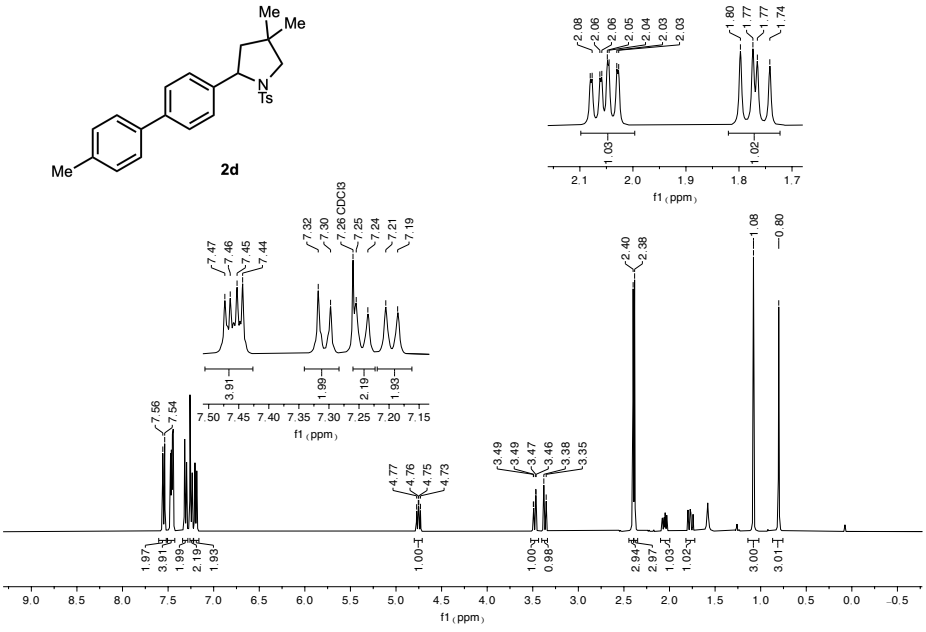
Me
Me
N
Ts
Me
2d
2.08
2.06
2.06
2.05
2.04
2.03
2.03
1.80
1.77
1.77
1.74
1.03
1.02
2.1 2.0 1.9 1.8 1.7
f1 (ppm)
7.47
7.46
7.45
7.44
7.32
7.30
7.26 CDCl3
7.25
7.24
7.21
7.19
3.91
1.99
2.19
1.93
7.50 7.45 7.40 7.35 7.30 7.25 7.20 7.15
f1 (ppm)
7.56
7.54
4.77
4.76
4.75
4.73
3.49
3.49
3.47
3.46
3.38
3.35
2.40
2.38
1.08
0.80
1.97
3.91
1.99
2.19
1.93
1.00
1.00
0.98
2.94
2.97
1.03
1.02
3.00
3.01
9.0 8.5 8.0 7.5 7.0 6.5 6.0 5.5 5.0 4.5 4.0 3.5 3.0 2.5 2.0 1.5 1.0 0.5 0.0 -0.5
f1 (ppm)

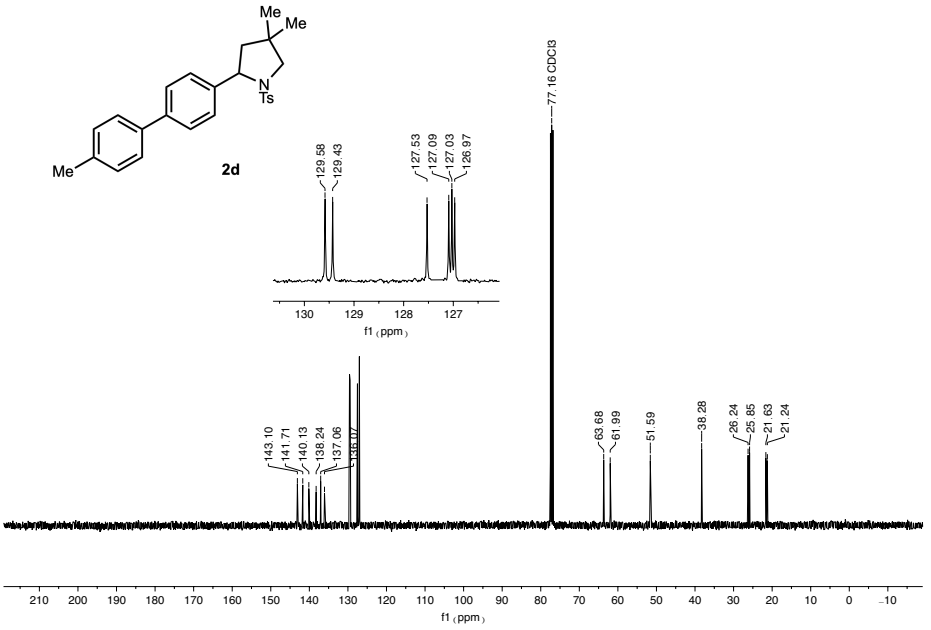
Me
Me
N
Ts
Me
2d
129.58
129.43
127.53
127.09
127.03
126.97
77.16 CDCl3
143.10
141.71
140.13
138.24
137.06
135.07
63.68
61.99
51.59
38.28
26.24
25.85
21.63
21.24
f1 (ppm)

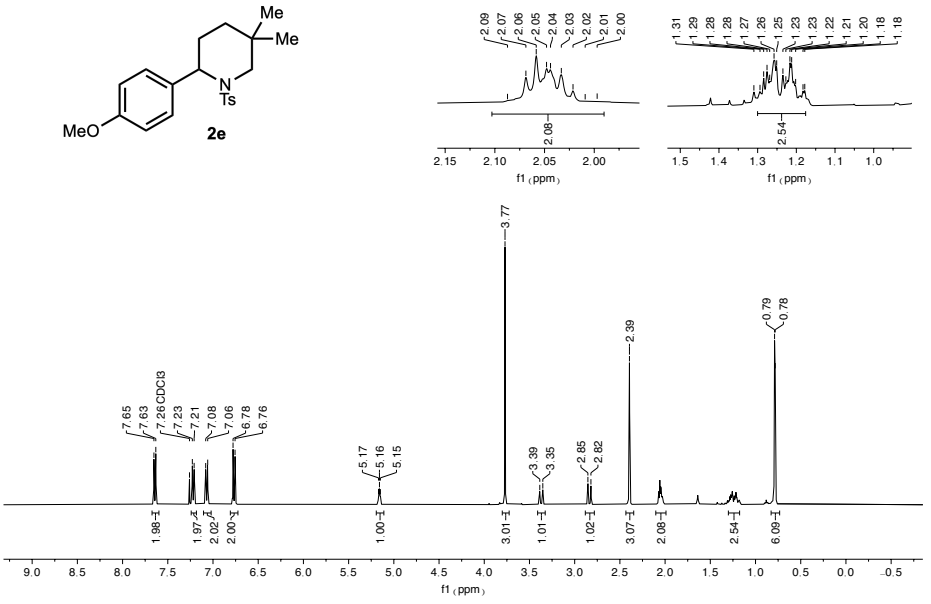
Me
Me
N
Ts
MeO
2e
2.09
2.07
2.06
2.05
2.04
2.03
2.02
2.01
2.00
2.08
1.31
1.29
1.28
1.28
1.27
1.26
1.25
1.23
1.23
1.22
1.21
1.20
1.18
1.18
2.54
f1 (ppm)
7.65
7.63
7.26 CDCl3
7.23
7.21
7.08
7.06
6.78
6.76
5.17
5.16
5.15
3.77
3.39
3.35
2.85
2.82
2.39
0.79
0.78
1.98
1.97
2.02
2.00
1.00
3.01
1.01
1.02
3.07
2.08
2.54
6.09
f1 (ppm)

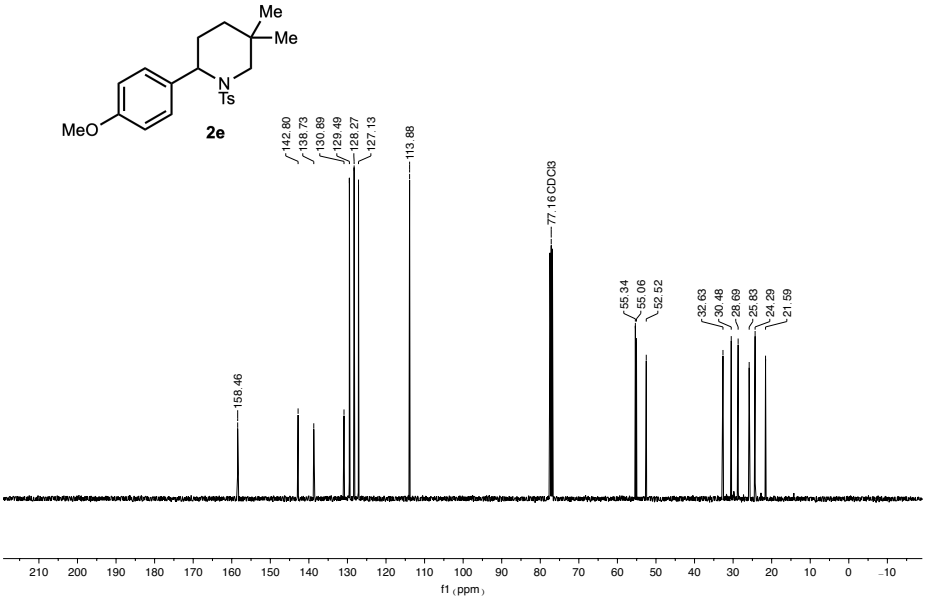
Me
Me
N
Ts
MeO
2e
142.80
138.73
130.89
129.49
128.27
127.13
113.88
77.16 CDCl3
55.34
55.06
52.52
32.63
30.48
28.69
25.83
24.29
21.59
158.46
210 200 190 180 170 160 150 140 130 120 110 100 90 80 70 60 50 40 30 20 10 0 -10
f1 (ppm)

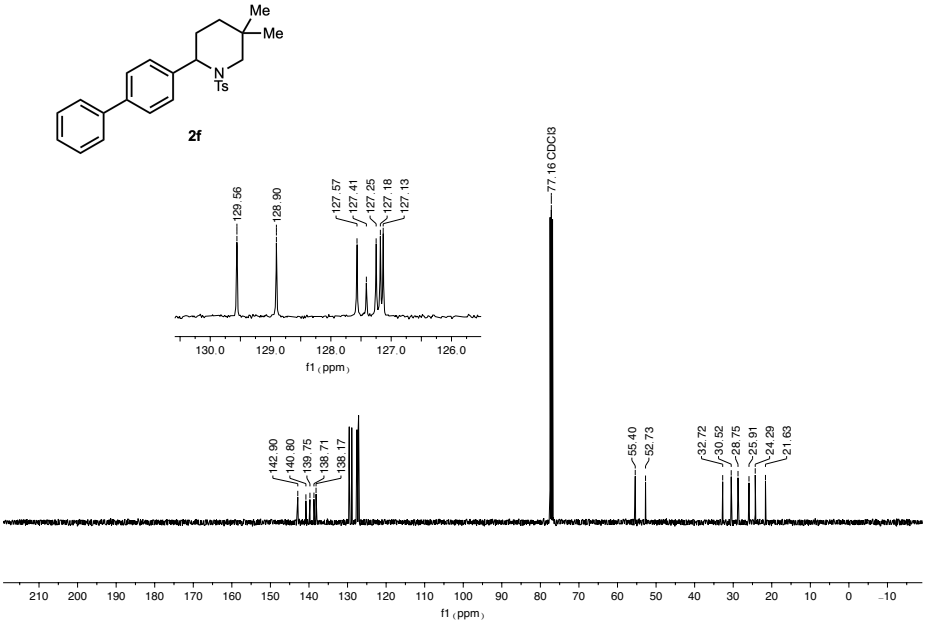
Me
Me
N
Ts
2f
129.56
128.90
127.57
127.41
127.25
127.18
127.13
77.16 CDCl3
130.0 129.0 128.0 127.0 126.0
f1 (ppm)
142.90
140.80
139.75
138.71
138.17
55.40
52.73
32.72
30.52
28.75
25.91
24.29
21.63
210 200 190 180 170 160 150 140 130 120 110 100 90 80 70 60 50 40 30 20 10 0 -10
f1 (ppm)

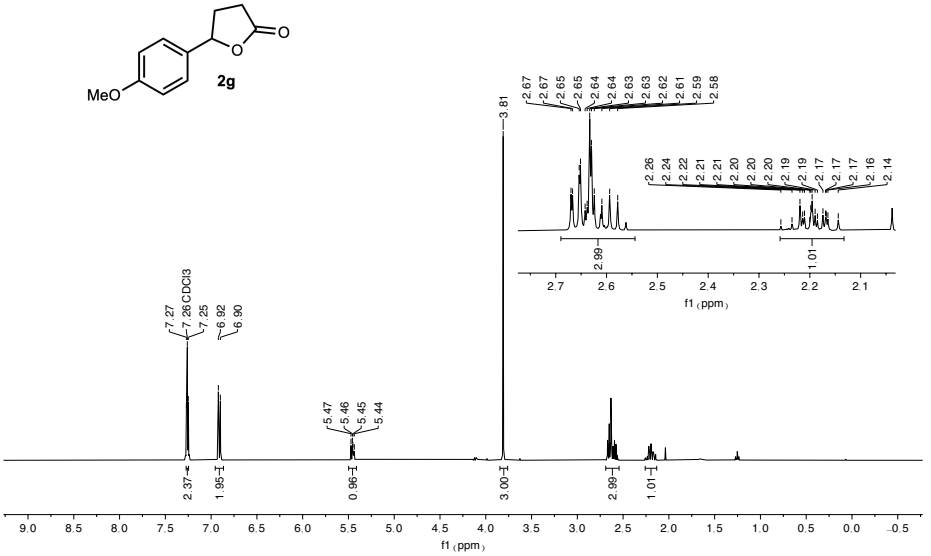
2g
MeO
O
O
7.27
7.26 CDCl3
7.25
6.92
6.90
5.47
5.46
5.45
5.44
3.81
2.67
2.67
2.65
2.65
2.64
2.64
2.63
2.63
2.62
2.61
2.59
2.58
2.26
2.24
2.22
2.21
2.21
2.20
2.20
2.20
2.19
2.19
2.17
2.17
2.17
2.16
2.14
2.37
1.95
0.96
3.00
2.99
1.01
2.99
1.01
f1 (ppm)

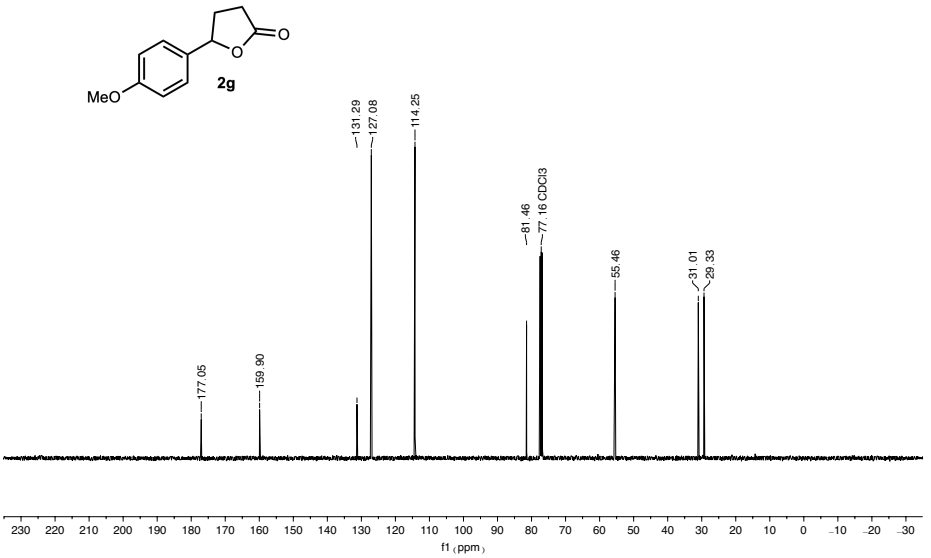
2g
MeO
O
O
131.29
127.08
114.25
81.46
77.16 CDCl3
55.46
31.01
29.33
177.05
159.90
f1 (ppm)

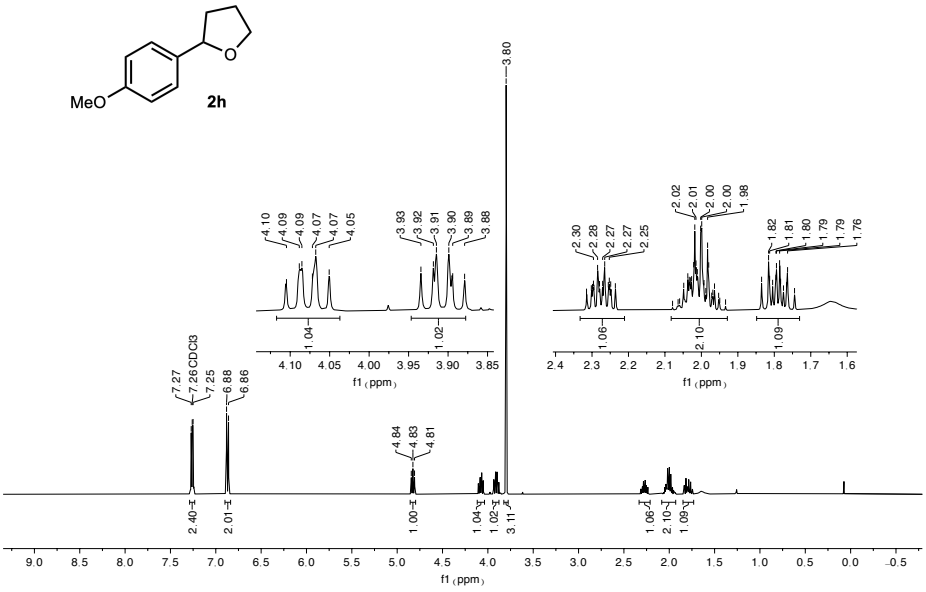
MeO
2h
7.27
7.26 CDCl3
7.25
6.88
6.86
4.84
4.83
4.81
3.80
4.10
4.09
4.09
4.07
4.07
4.05
3.93
3.92
3.91
3.90
3.89
3.88
2.30
2.28
2.27
2.27
2.25
2.02
2.01
2.00
2.00
1.98
1.82
1.81
1.80
1.79
1.79
1.76
2.40
2.01
1.00
1.04
1.02
3.11
1.06
2.10
1.09
f1 (ppm)

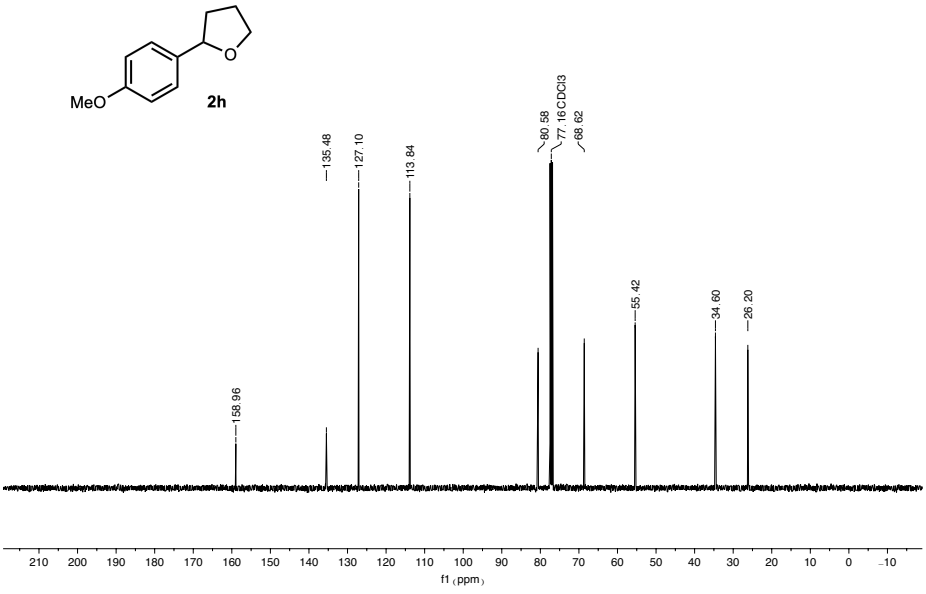
MeO
2h
158.96
135.48
127.10
113.84
80.58
77.16 CDCl3
68.62
55.42
34.60
26.20
f1 (ppm)

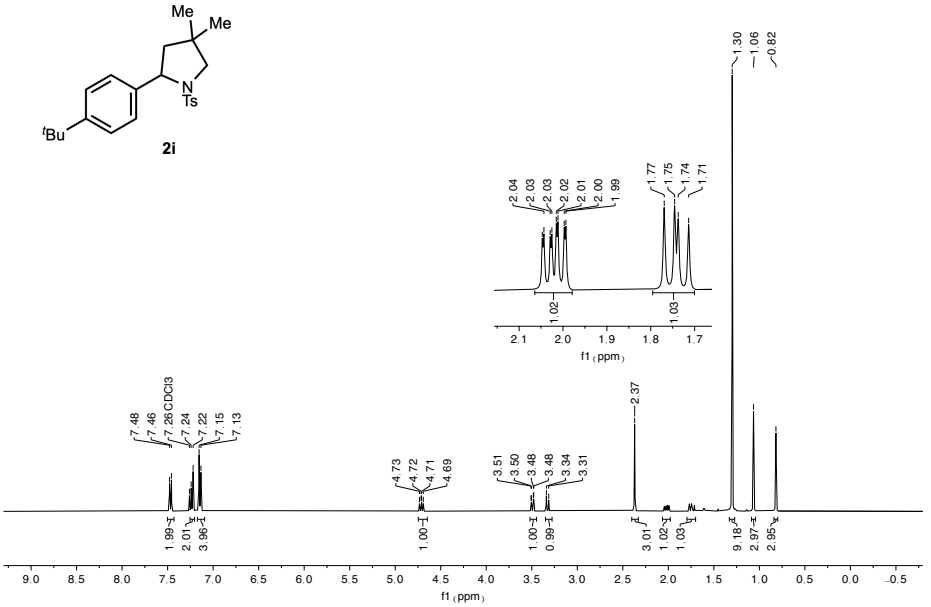
Me
Me
N
Ts
tBu
2i
1.30
1.06
0.82
2.04
2.03
2.03
2.02
2.01
2.00
1.99
1.77
1.75
1.74
1.71
1.02
1.03
2.1 2.0 1.9 1.8 1.7
f1 (ppm)
7.48
7.46
7.26 CDCl3
7.24
7.22
7.15
7.13
4.73
4.72
4.71
4.69
3.51
3.50
3.48
3.48
3.34
3.31
2.37
1.99
2.01
3.96
1.00
1.00
0.99
3.01
1.02
1.03
9.18
2.97
2.95
9.0 8.5 8.0 7.5 7.0 6.5 6.0 5.5 5.0 4.5 4.0 3.5 3.0 2.5 2.0 1.5 1.0 0.5 0.0 -0.5
f1 (ppm)

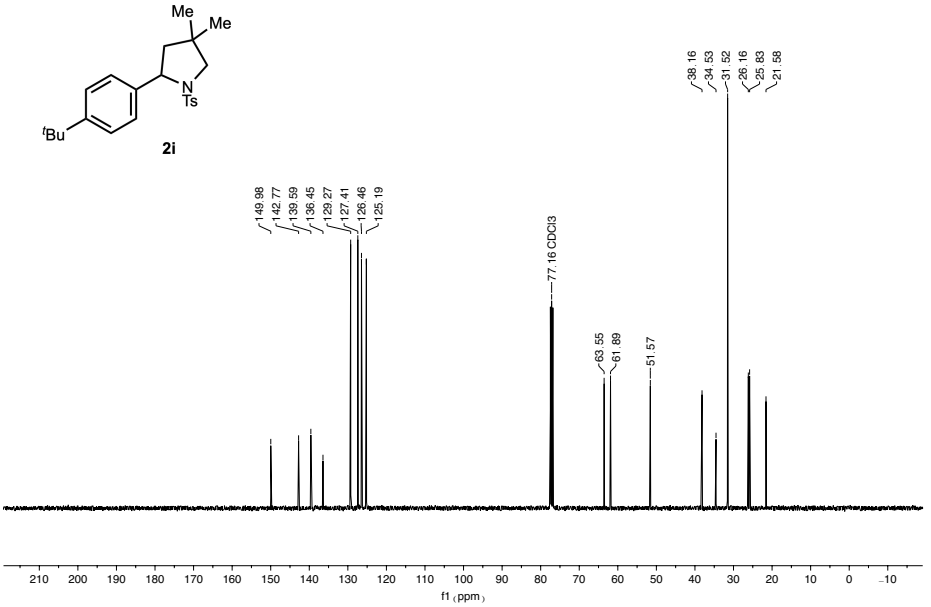
Me
Me
N
Ts
tBu
2i
38.16
34.53
31.52
26.16
25.83
21.58
149.98
142.77
139.59
136.45
129.27
127.41
126.46
125.19
77.16 CDCl3
63.55
61.89
51.57
210 200 190 180 170 160 150 140 130 120 110 100 90 80 70 60 50 40 30 20 10 0 -10
f1 (ppm)

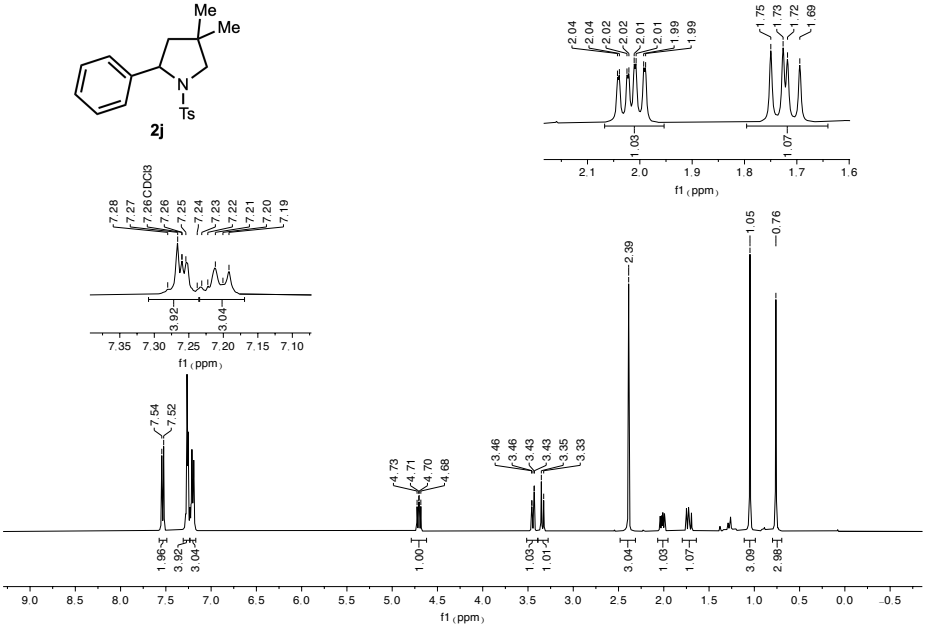
Me
Me
N
Ts
2j
f1 (ppm)

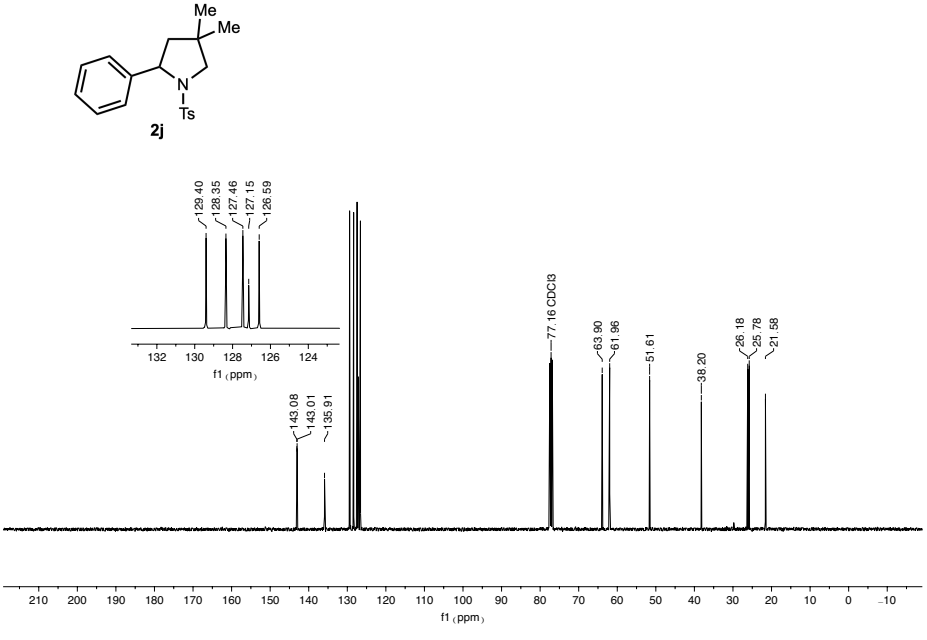
Me
Me
N
Ts
2j
f1 (ppm)

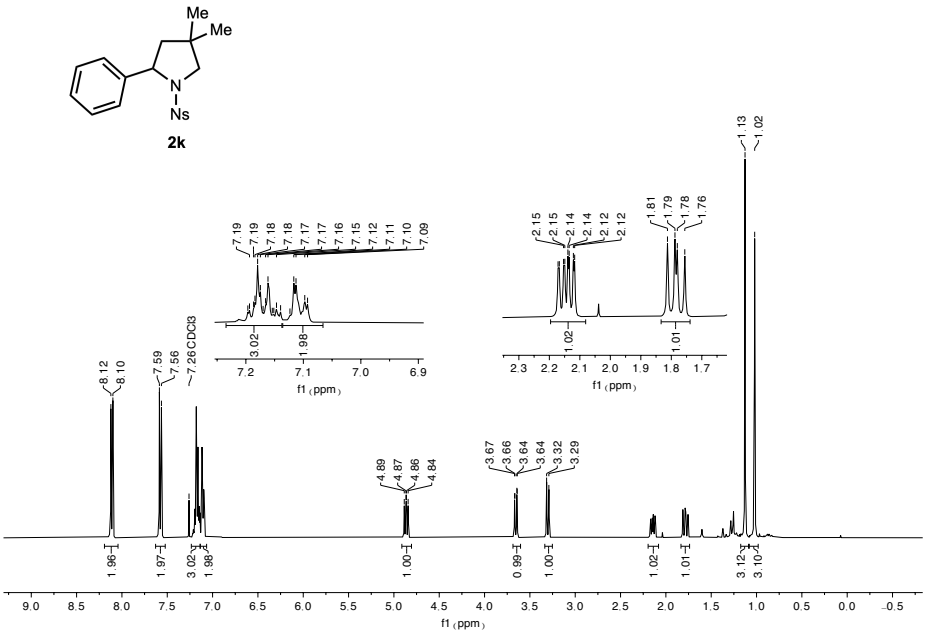
Me
Me
N
Ns
2k
8.12
8.10
7.59
7.56
7.26 CDCl3
7.19
7.18
7.17
7.16
7.15
7.12
7.11
7.10
7.09
4.89
4.87
4.86
4.84
3.67
3.66
3.64
3.64
3.32
3.29
2.15
2.14
2.12
1.81
1.79
1.78
1.76
1.13
1.02
f1 (ppm)

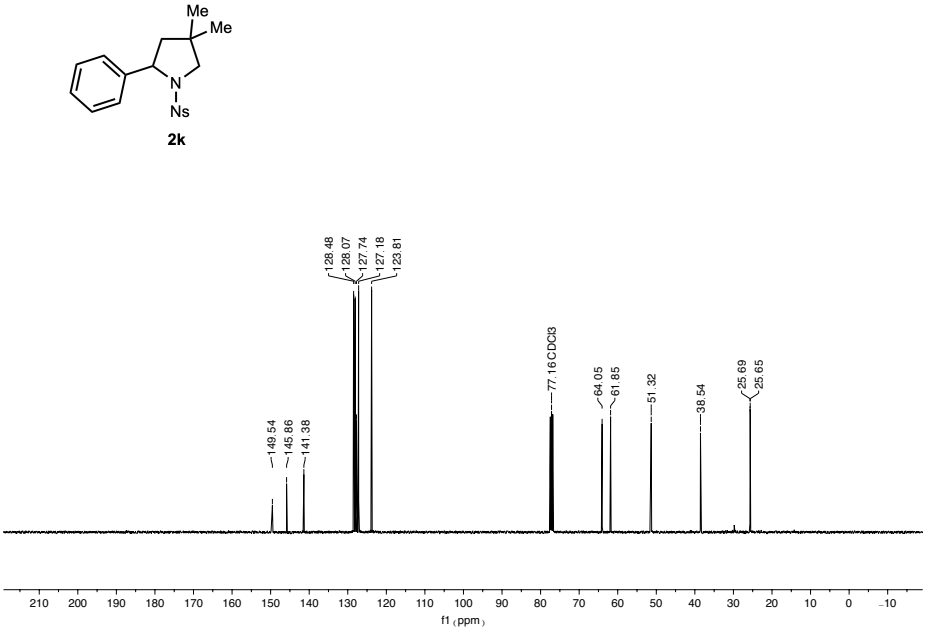
Me
Me
N
Ns
2k
149.54
145.86
141.38
128.48
128.07
127.74
127.18
123.81
77.16 CDCl3
64.05
61.85
51.32
38.54
25.69
25.65
f1 (ppm)

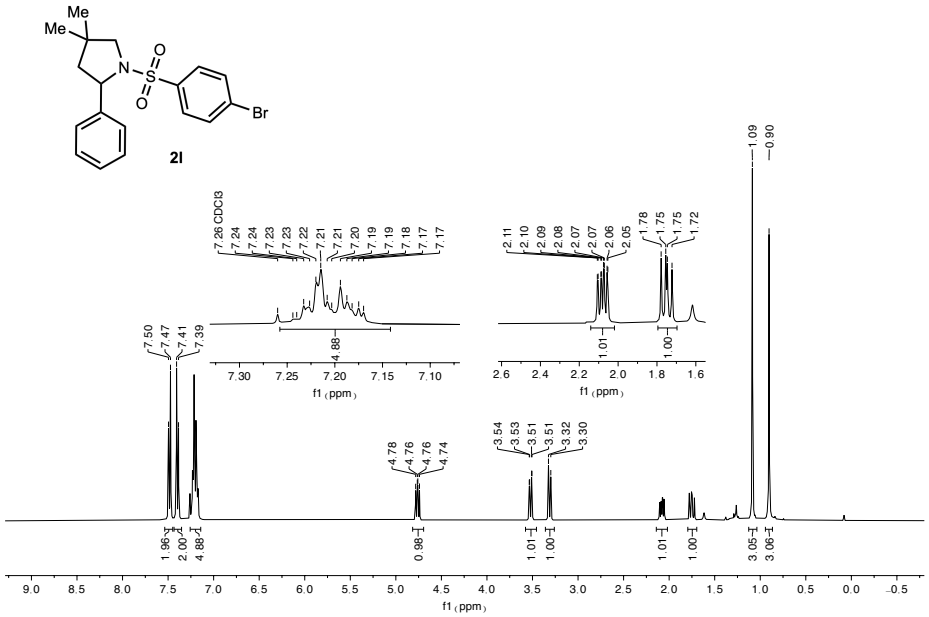
Me
Me
N
S
O
O
Br
2l
7.26 CDCl3
7.50
7.47
7.41
7.39
4.78
4.76
4.74
3.54
3.53
3.51
3.51
3.32
3.30
2.11
2.10
2.09
2.08
2.07
2.07
2.06
2.05
1.78
1.75
1.75
1.72
1.09
0.90
1.96
2.00
4.88
0.98
1.01
1.00
1.01
1.00
3.05
3.06
f1 (ppm)

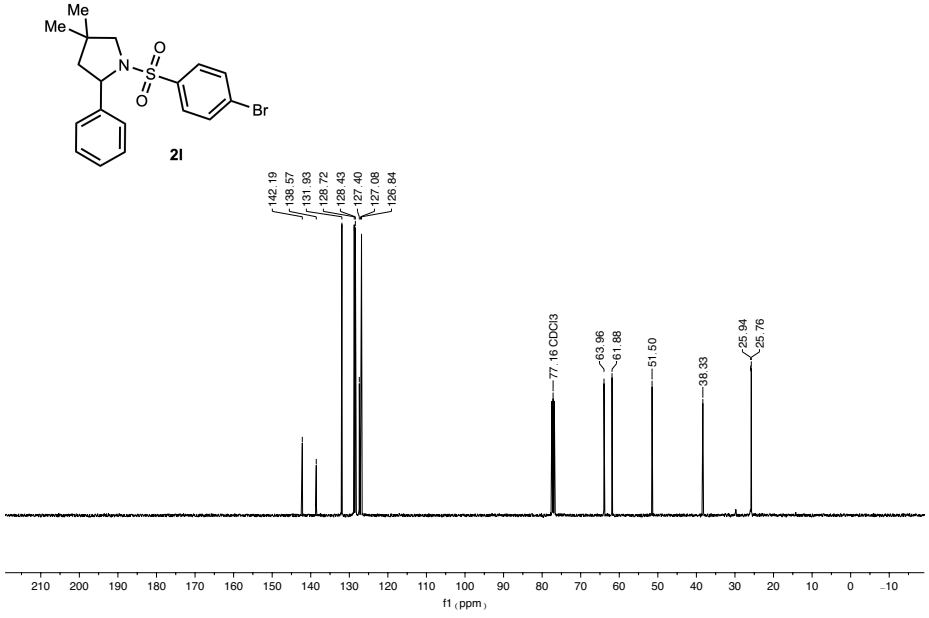
Me
Me
N
S
O
O
Br
2l
142.19
138.57
131.93
128.72
128.43
127.40
127.08
126.84
77.16 CDCl3
63.96
61.88
51.50
38.33
25.94
25.76
f1 (ppm)

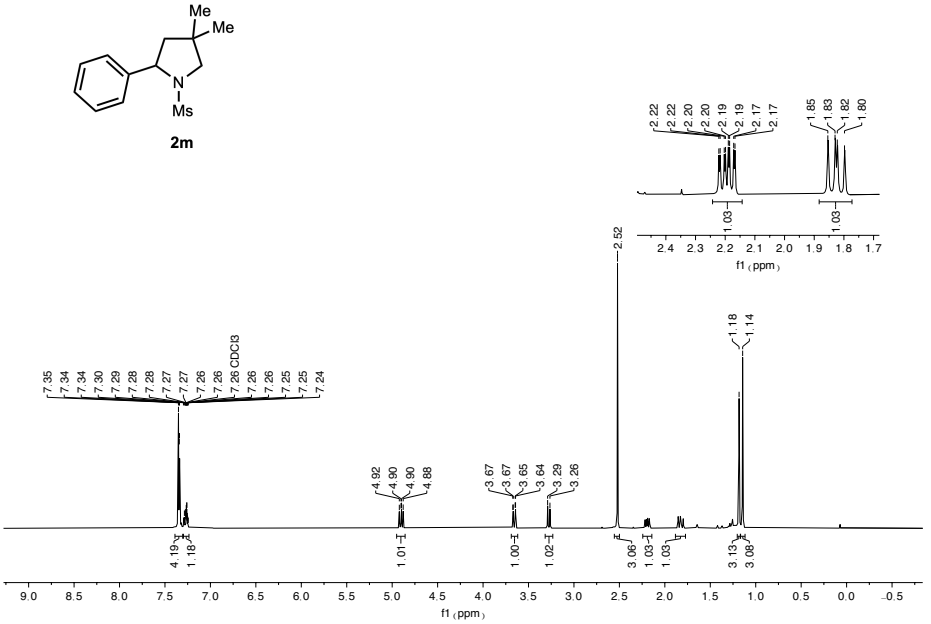
Me
Me
N
Ms
2m
2.22
2.22
2.20
2.20
2.19
2.19
2.17
2.17
1.85
1.83
1.82
1.80
1.03
1.03
2.52
1.18
1.14
7.35
7.34
7.34
7.30
7.29
7.28
7.28
7.27
7.27
7.26
7.26
7.26 CDCl3
7.26
7.26
7.25
7.25
7.24
4.92
4.90
4.90
4.88
3.67
3.67
3.65
3.64
3.29
3.26
4.19
1.18
1.01
1.00
1.02
3.06
1.03
1.03
3.13
3.08
f1 (ppm)

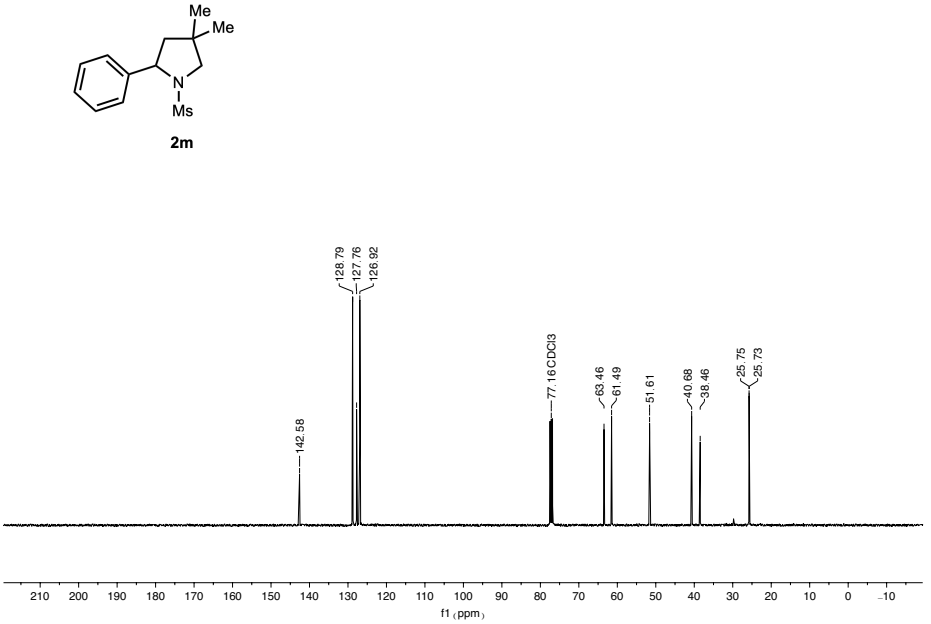
Me
Me
N
Ms
2m
128.79
127.76
126.92
142.58
77.16 CDCl3
63.46
61.49
51.61
40.68
38.46
25.75
25.73
f1 (ppm)

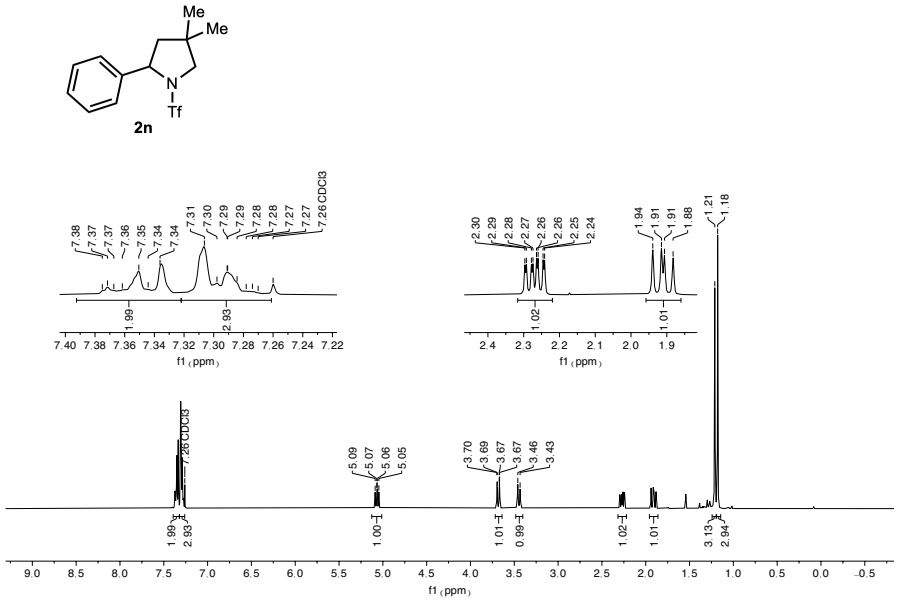
Me
Me
N
Tf
2n
7.38
7.37
7.37
7.36
7.35
7.34
7.34
7.31
7.30
7.29
7.29
7.28
7.28
7.27
7.27
7.26 CDCl3
1.99
2.93
f1 (ppm)
2.30
2.29
2.28
2.27
2.26
2.26
2.25
2.24
1.94
1.91
1.91
1.88
1.21
1.18
1.02
1.01
f1 (ppm)
7.26 CDCl3
5.09
5.07
5.06
5.05
3.70
3.69
3.67
3.67
3.46
3.43
1.99
2.93
1.00
1.01
0.99
1.02
1.01
3.13
2.94
f1 (ppm)

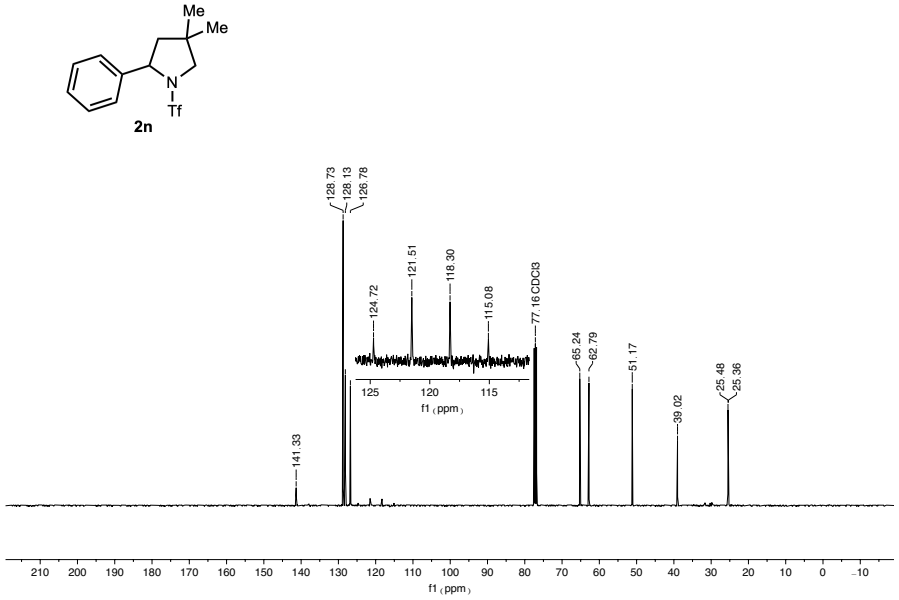
Me
Me
N
Tf
2n
128.73
128.13
126.78
124.72
121.51
118.30
115.08
77.16 CDCl3
65.24
62.79
51.17
39.02
25.48
25.36
141.33
125
120
115
f1 (ppm)
f1 (ppm)

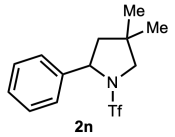

2n

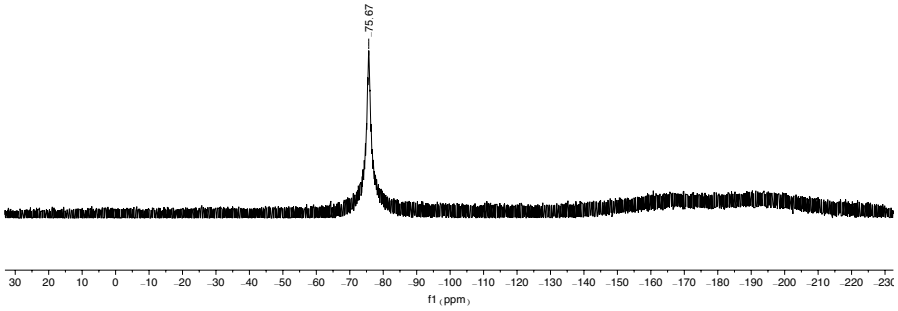

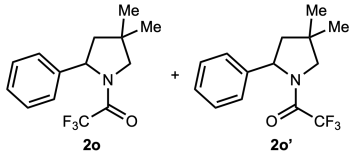

2o

+

2o'

The diastereomeric species were visible

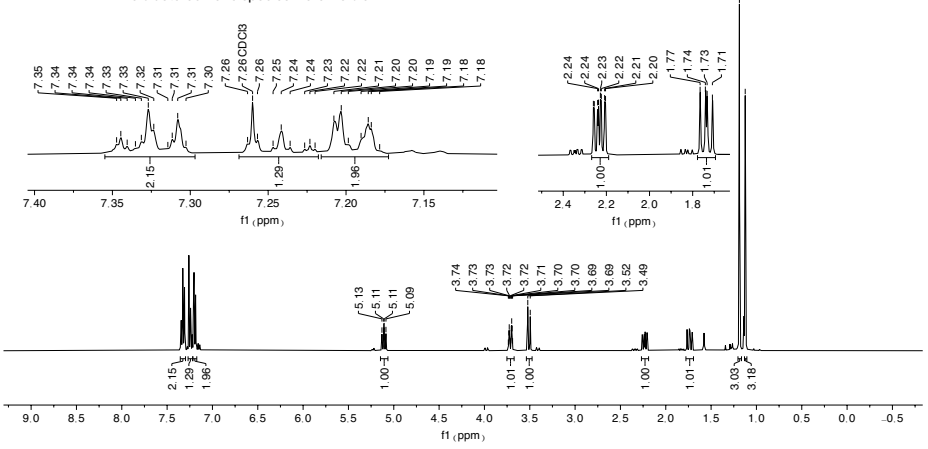

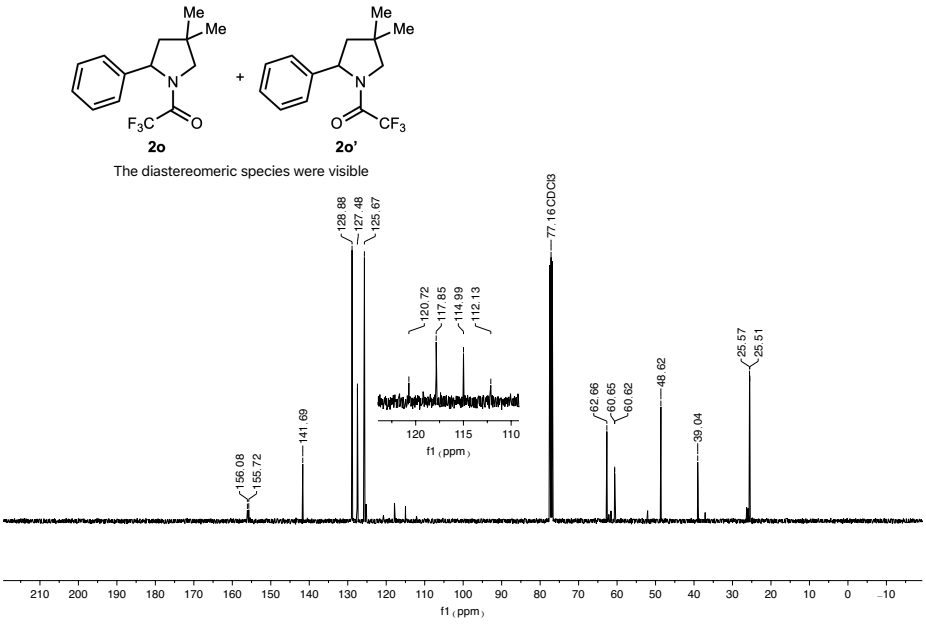
Me
Me
N
F3C
O
2o
+
Me
Me
N
O
CF3
2o'
The diastereomeric species were visible
128.88
127.48
125.67
77.16CDCl3
120.72
117.85
114.99
112.13
25.57
25.51
48.62
62.66
60.65
60.62
39.04
156.08
155.72
141.69
f1 (ppm)

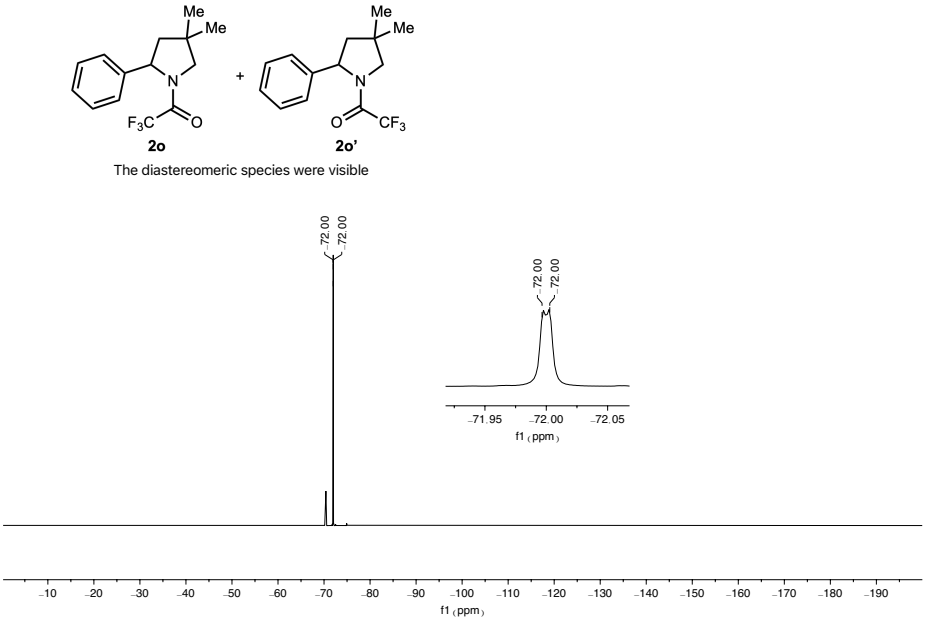
Me
Me
N
F3C
O
2o
+
Me
Me
N
O
CF3
2o'
The diastereomeric species were visible
-72.00
-72.00
f1 (ppm)

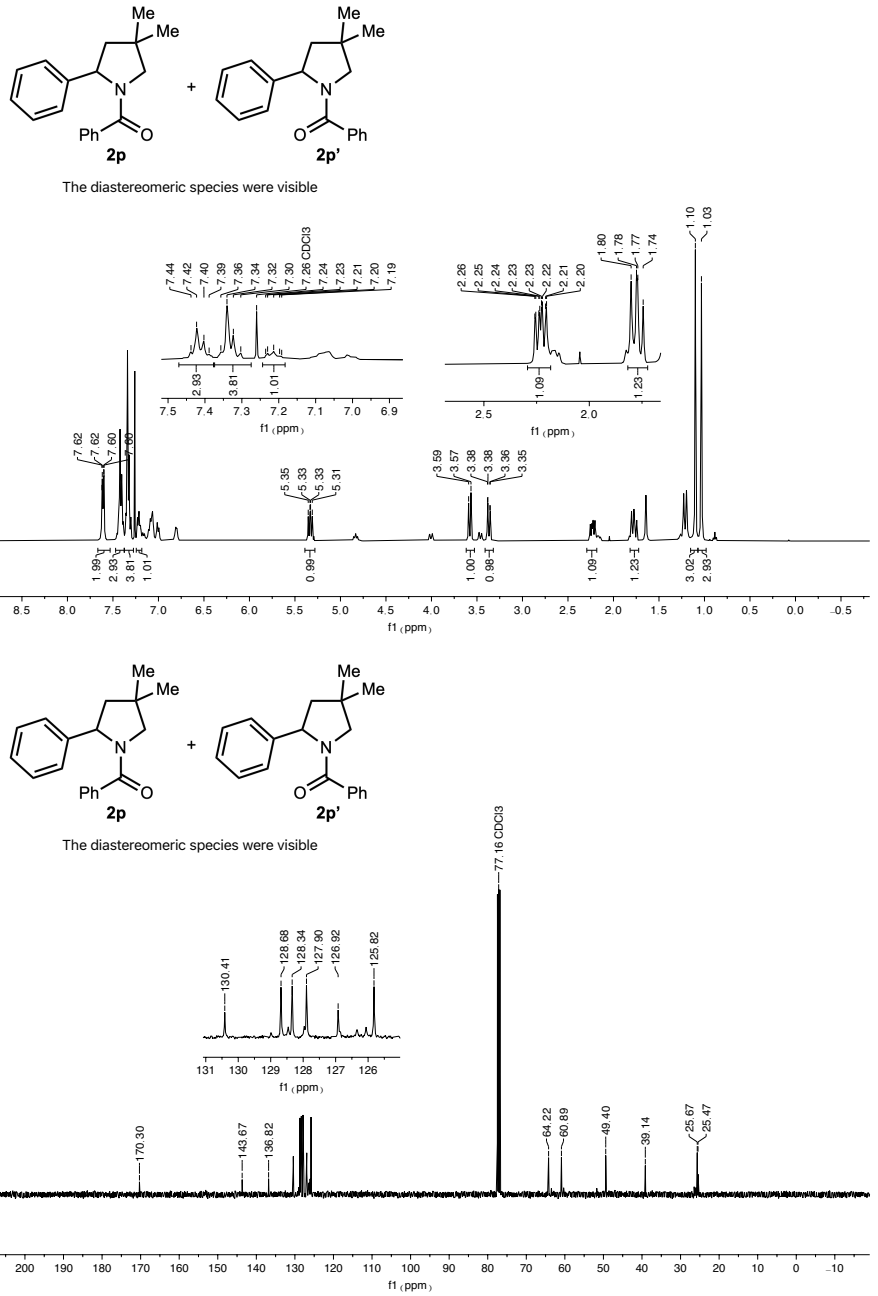
Me
Me
N
Ph
O
2p
2p'
The diastereomeric species were visible
CDCl3
f1 (ppm)
77.16 CDCl3

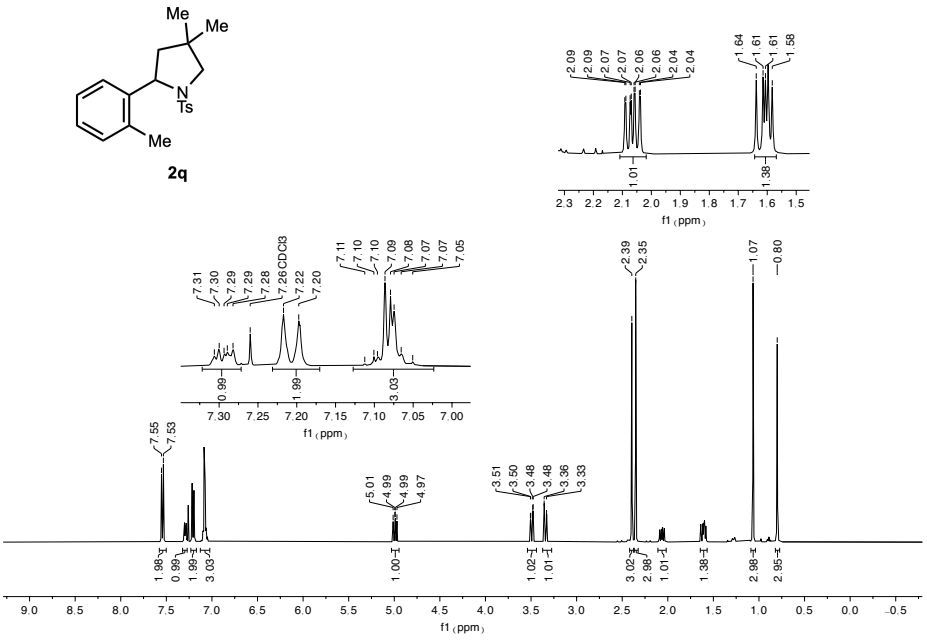
Me
Me
N
Ts
Me
2q
f1 (ppm)

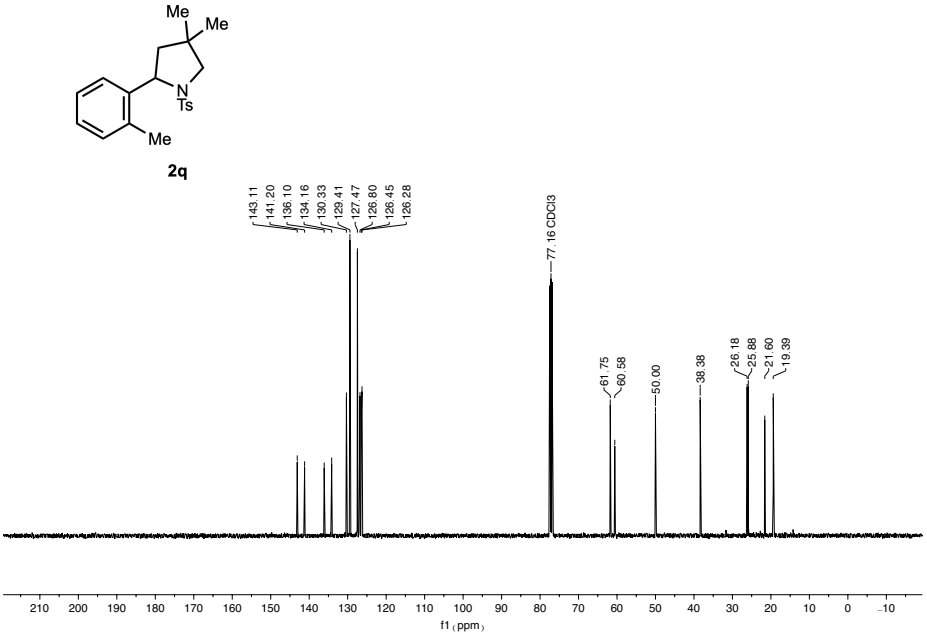
Me
Me
N
Ts
Me
2q
f1 (ppm)

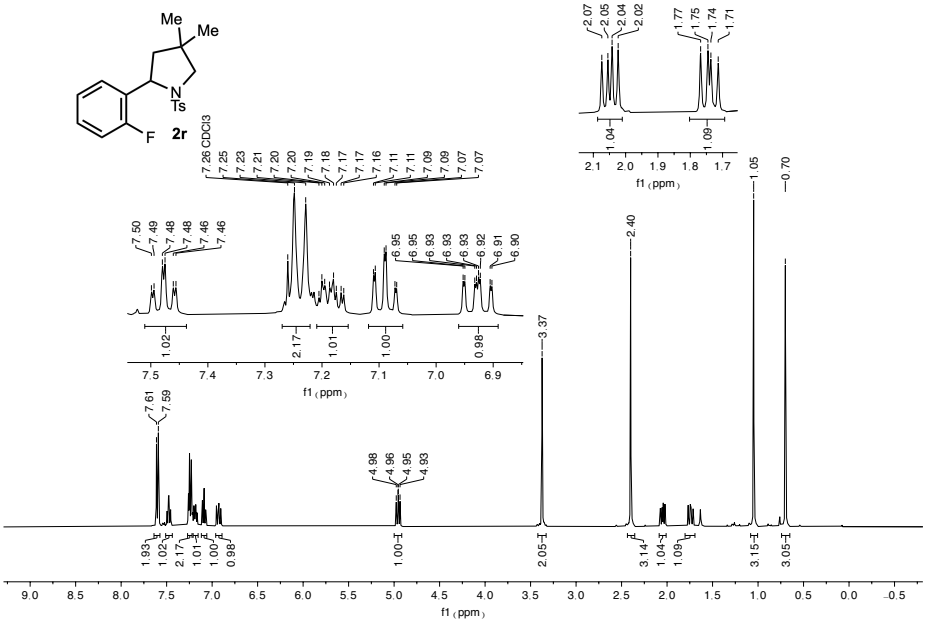
Me
Me
N
Ts
F
2r
7.26 CDCl3
2.07
2.05
2.04
2.02
1.77
1.75
1.74
1.71
1.04
1.09
f1 (ppm)
7.50
7.49
7.48
7.48
7.46
7.46
6.95
6.95
6.93
6.93
6.93
6.92
6.91
6.90
1.02
2.17
1.01
1.00
0.98
3.37
2.40
1.05
0.70
7.61
7.59
4.98
4.96
4.95
4.93
1.93
1.02
2.17
1.01
1.00
0.98
1.00
2.05
3.14
1.04
1.09
3.15
3.05

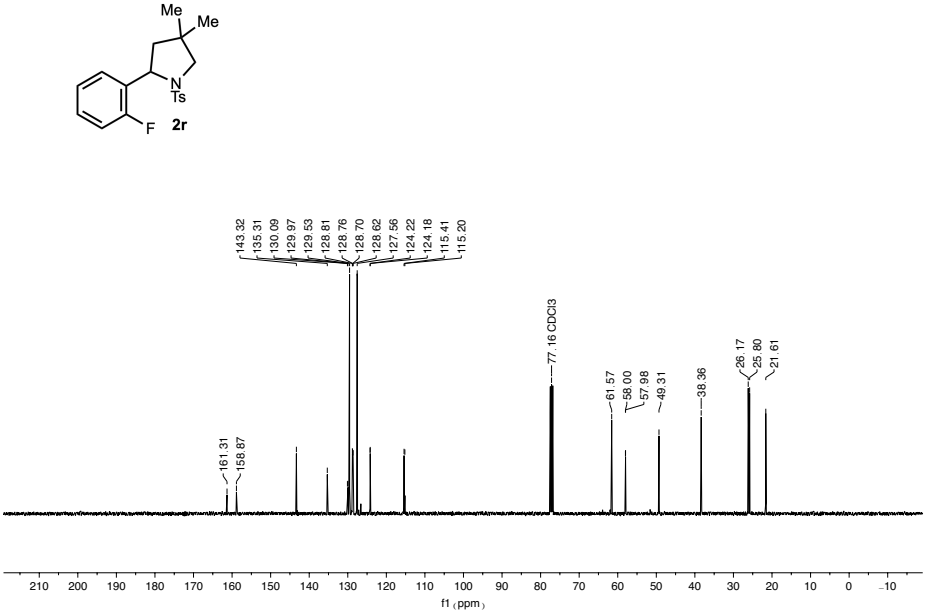
Me
Me
N
Ts
F
2r
143.32
135.31
130.09
129.97
129.53
128.81
128.76
128.70
128.62
127.56
124.22
124.18
115.41
115.20
77.16 CDCl3
61.57
58.00
57.98
49.31
38.36
26.17
25.80
21.61
161.31
158.87
f1 (ppm)

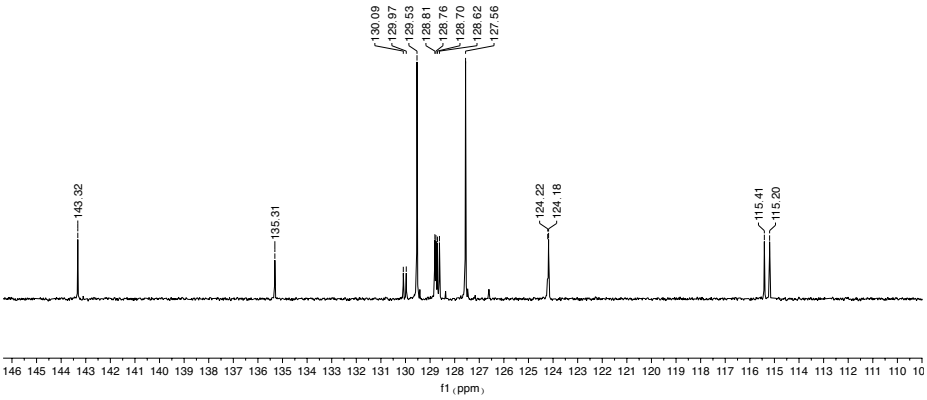
130.09
129.97
129.53
128.81
128.76
128.70
128.62
127.56
143.32
135.31
124.22
124.18
115.41
115.20
146 145 144 143 142 141 140 139 138 137 136 135 134 133 132 131 130 129 128 127 126 125 124 123 122 121 120 119 118 117 116 115 114 113 112 111 110
f1 (ppm)

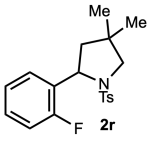
Me
Me
N
Ts
F

2r

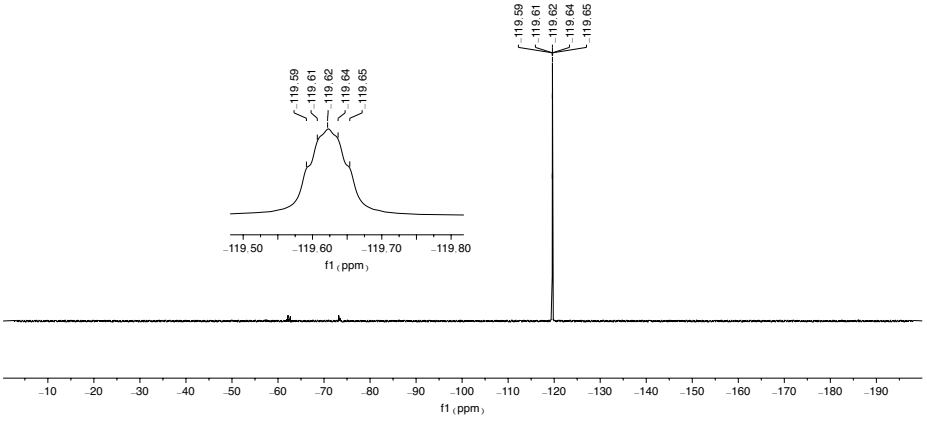
119.59
119.61
119.62
119.64
119.65
119.59
119.61
119.62
119.64
119.65
119.50
119.60
119.70
119.80
f1 (ppm)
-10 -20 -30 -40 -50 -60 -70 -80 -90 -100 -110 -120 -130 -140 -150 -160 -170 -180 -190
f1 (ppm)

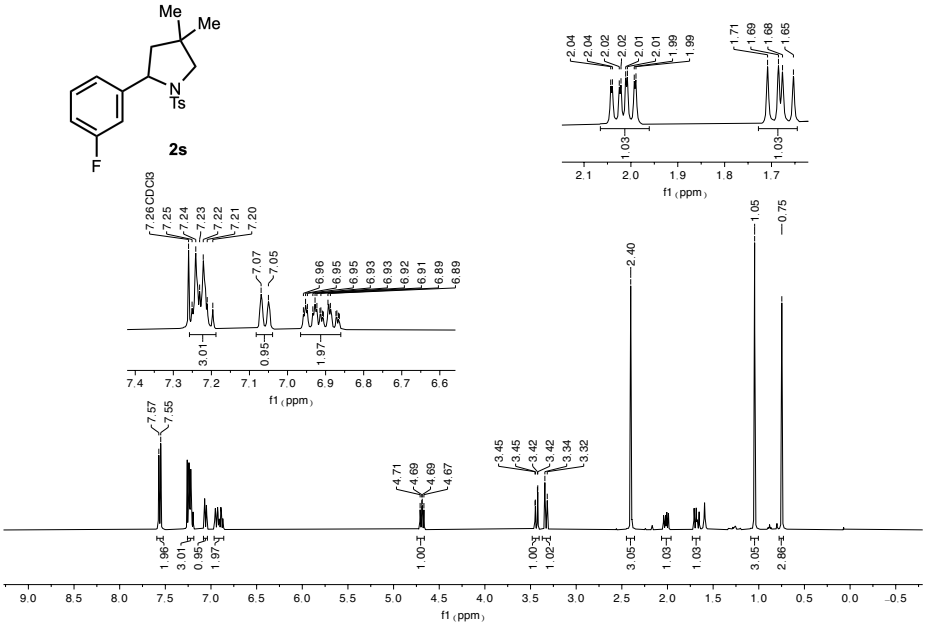
Me
Me
N
Ts
F
2s
f1 (ppm)

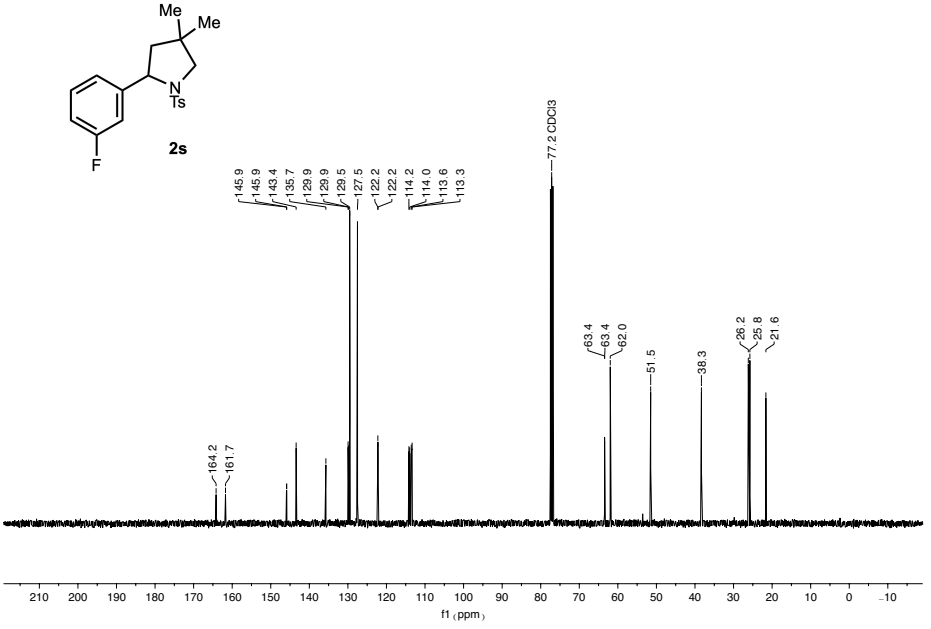
Me
Me
N
Ts
F
2s
77.2 CDCl3
f1 (ppm)

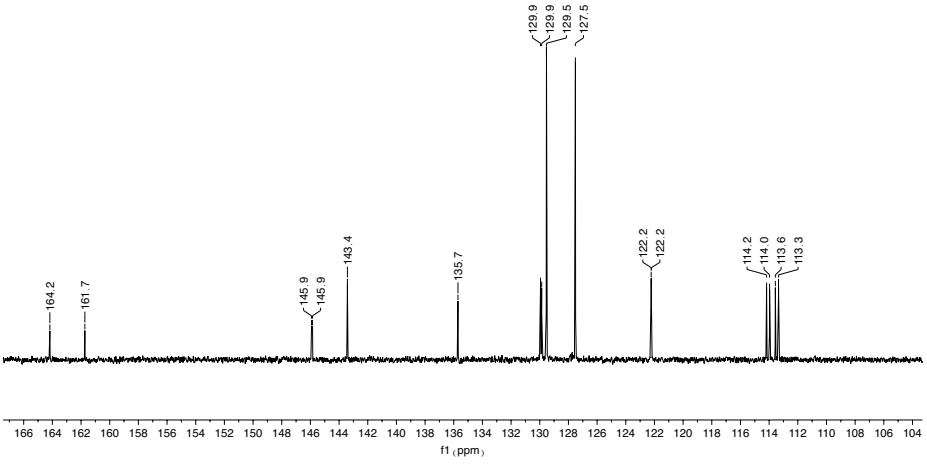
164.2
161.7
145.9
145.9
143.4
135.7
129.9
129.9
129.5
127.5
122.2
122.2
114.2
114.0
113.6
113.3
166 164 162 160 158 156 154 152 150 148 146 144 142 140 138 136 134 132 130 128 126 124 122 120 118 116 114 112 110 108 106 104
f1 (ppm)

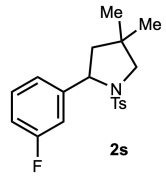
Me
Me
N
Ts
F

2s

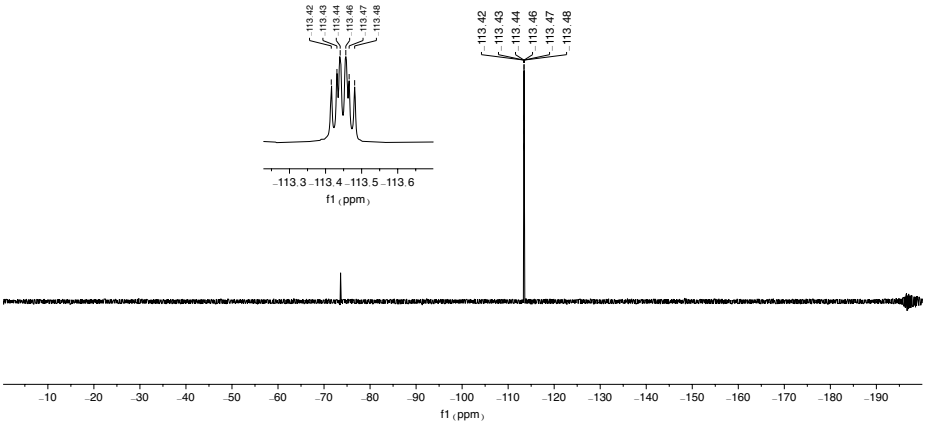
113.42
113.43
113.44
113.46
113.47
113.48
113.3 113.4 113.5 113.6
f1 (ppm)
10 20 30 40 50 60 70 80 90 100 110 120 130 140 150 160 170 180 190
f1 (ppm)

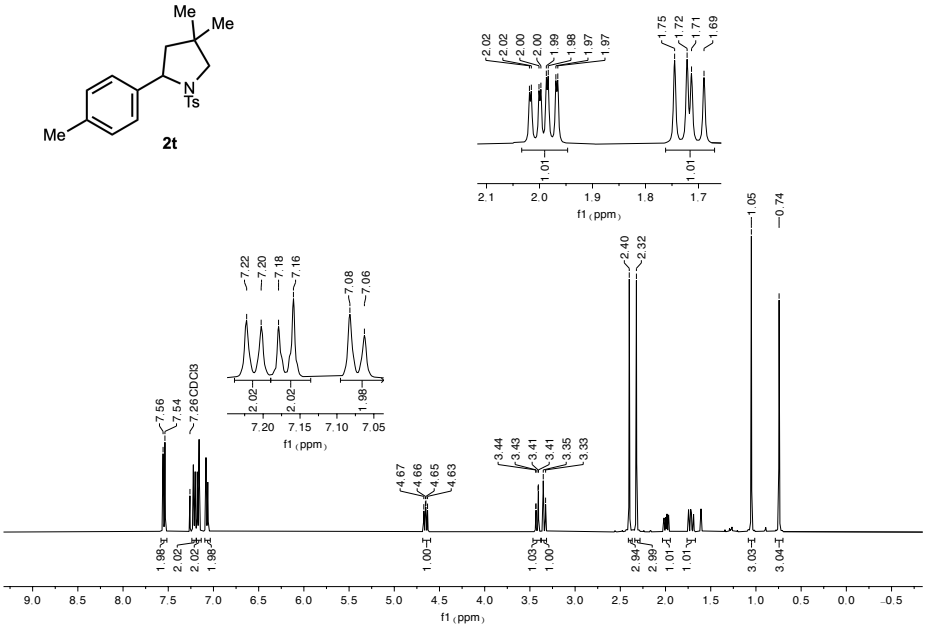
Me
Me
N
Ts
Me
2t
2.02
2.02
2.00
2.00
1.99
1.98
1.97
1.97
1.75
1.72
1.71
1.69
1.01
1.01
2.1
2.0
1.9
1.8
1.7
f1 (ppm)
7.22
7.20
7.18
7.16
7.08
7.06
2.02
2.02
1.98
7.20
7.15
7.10
7.05
f1 (ppm)
7.56
7.54
7.26 CDCl3
4.67
4.66
4.65
4.63
3.44
3.43
3.41
3.41
3.35
3.33
2.40
2.32
1.05
0.74
1.98
2.02
2.02
1.98
1.00
1.03
1.00
2.94
2.99
1.01
1.01
3.03
3.04
9.0
8.5
8.0
7.5
7.0
6.5
6.0
5.5
5.0
4.5
4.0
3.5
3.0
2.5
2.0
1.5
1.0
0.5
0.0
−0.5
f1 (ppm)

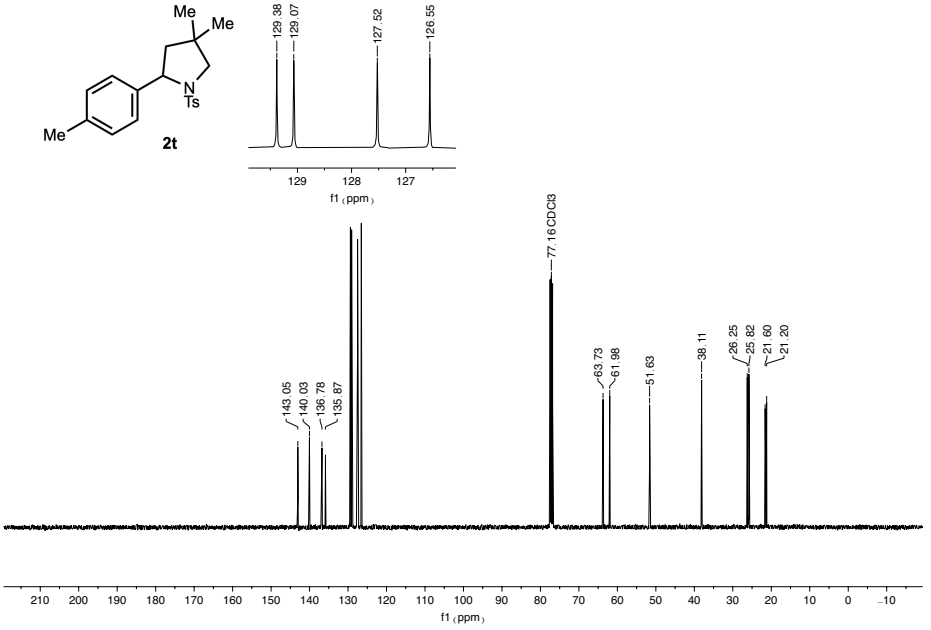
Me
Me
N
Ts
Me
2t
129.38
129.07
127.52
126.55
129
128
127
f1 (ppm)
77.16 CDCl3
143.05
140.03
136.78
135.87
63.73
61.98
51.63
38.11
26.25
25.82
21.60
21.20
210
200
190
180
170
160
150
140
130
120
110
100
90
80
70
60
50
40
30
20
10
0
−10
f1 (ppm)

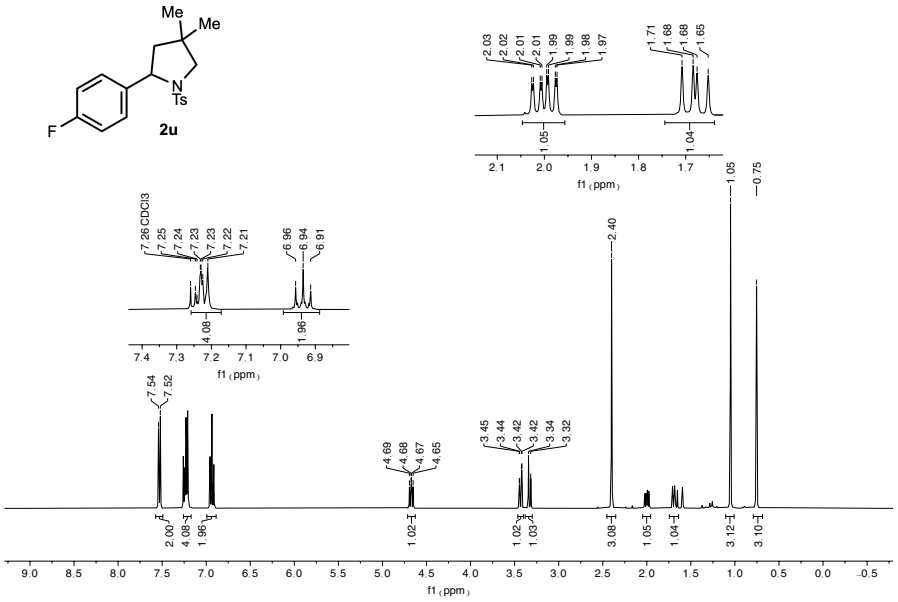
Me
Me
N
Ts
F
2u
2.03
2.02
2.01
2.01
1.99
1.99
1.98
1.97
1.71
1.68
1.68
1.65
1.05
1.04
2.1
2.0
1.9
1.8
1.7
f1 (ppm)
7.26 CDCl3
7.25
7.24
7.23
7.23
7.22
7.21
6.96
6.94
6.91
4.08
1.96
7.4
7.3
7.2
7.1
7.0
6.9
f1 (ppm)
7.54
7.52
4.69
4.68
4.67
4.65
3.45
3.44
3.42
3.42
3.34
3.32
2.40
1.05
0.75
2.00
4.08
1.96
1.02
1.02
1.03
3.08
1.05
1.04
3.12
3.10
9.0
8.5
8.0
7.5
7.0
6.5
6.0
5.5
5.0
4.5
4.0
3.5
3.0
2.5
2.0
1.5
1.0
0.5
0.0
-0.5
f1 (ppm)

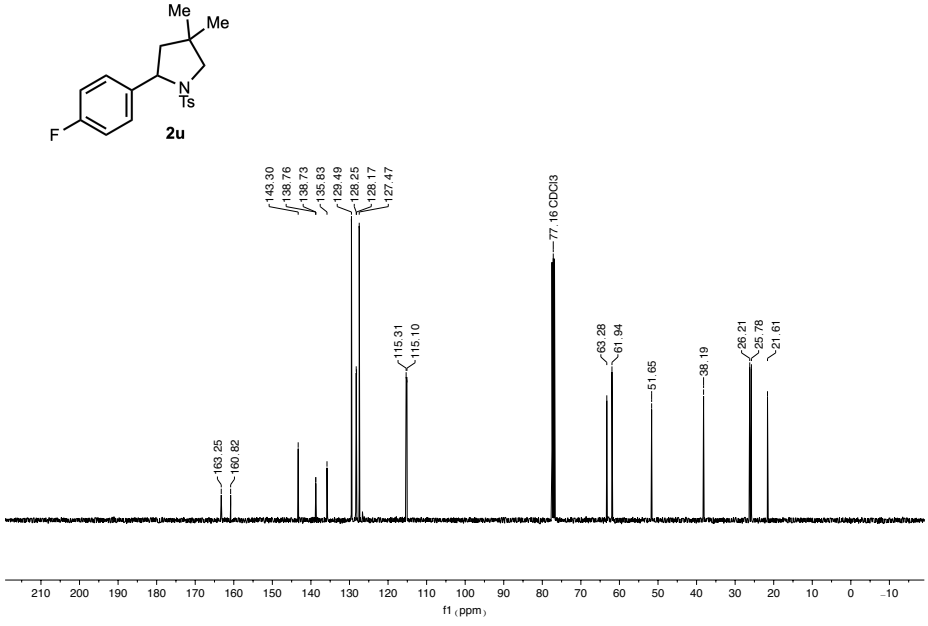
Me
Me
N
Ts
F
2u
143.30
138.76
138.73
135.83
129.49
128.25
128.17
127.47
77.16 CDCl3
115.31
115.10
63.28
61.94
51.65
38.19
26.21
25.78
21.61
163.25
160.82
210
200
190
180
170
160
150
140
130
120
110
100
90
80
70
60
50
40
30
20
10
0
-10
f1 (ppm)

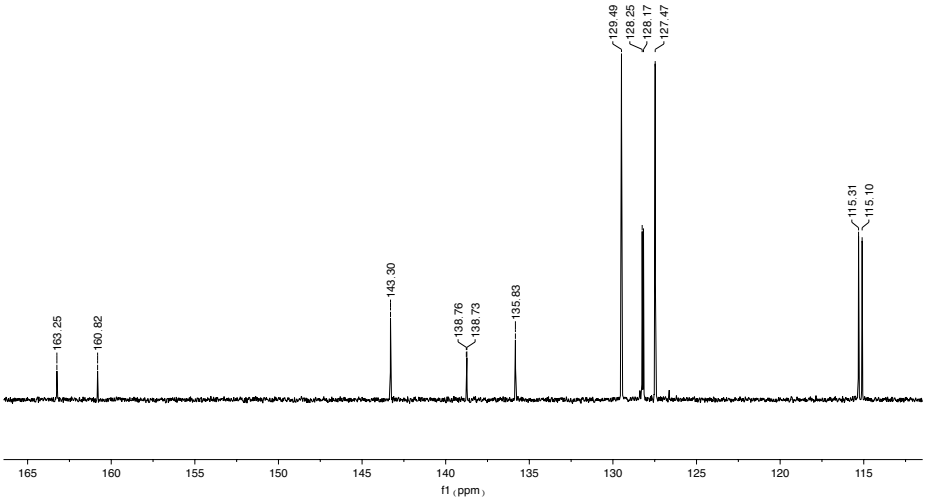
129.49
128.25
128.17
127.47
115.31
115.10
143.30
138.76
138.73
135.83
163.25
160.82
165
160
155
150
145
140
135
130
125
120
115
f1 (ppm)

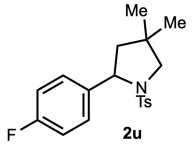
Me
Me
N
Ts
F

2u

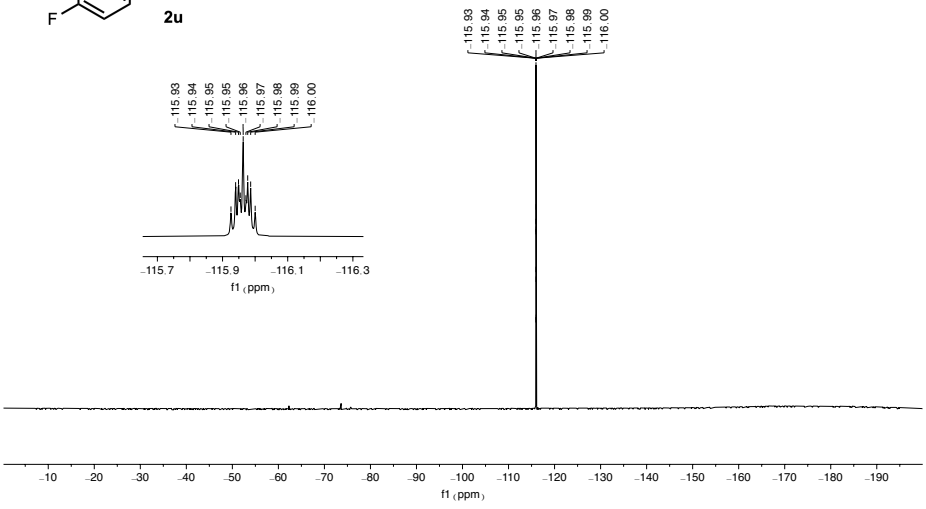
115.93
115.94
115.95
115.95
115.96
115.97
115.98
115.99
116.00
−115.7
−115.9
−116.1
−116.3
f1 (ppm)
−10
−20
−30
−40
−50
−60
−70
−80
−90
−100
−110
−120
−130
−140
−150
−160
−170
−180
−190
f1 (ppm)

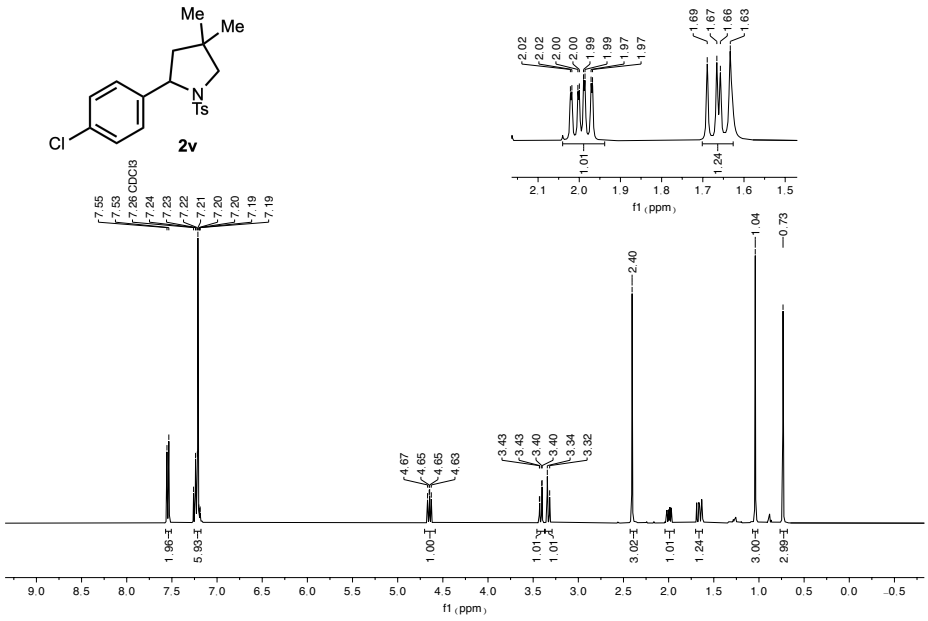
Me
Me
N
Ts
Cl
2v
7.55
7.53
7.26 CDCl3
7.24
7.23
7.22
7.21
7.20
7.20
7.19
7.19
4.67
4.65
4.65
4.63
3.43
3.43
3.40
3.40
3.34
3.32
2.40
1.04
0.73
1.96
5.93
1.00
1.01
1.01
3.02
1.01
1.24
3.00
2.99
f1 (ppm)
2.02
2.02
2.00
2.00
1.99
1.97
1.97
1.69
1.67
1.66
1.63
1.01
1.24
f1 (ppm)

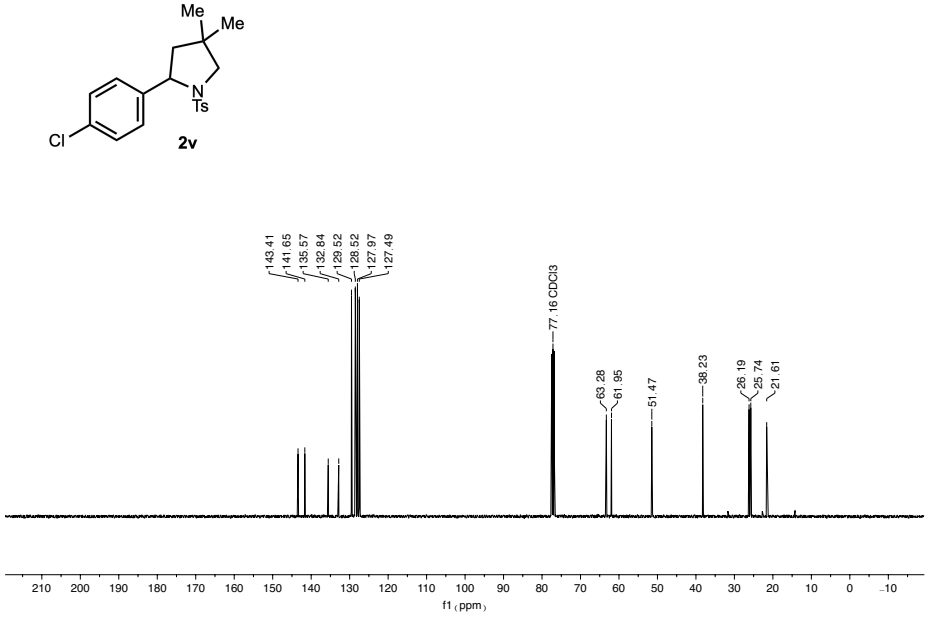
Me
Me
N
Ts
Cl
2v
143.41
141.65
135.57
132.84
129.52
128.52
127.97
127.49
77.16 CDCl3
63.28
61.95
51.47
38.23
26.19
25.74
21.61
f1 (ppm)

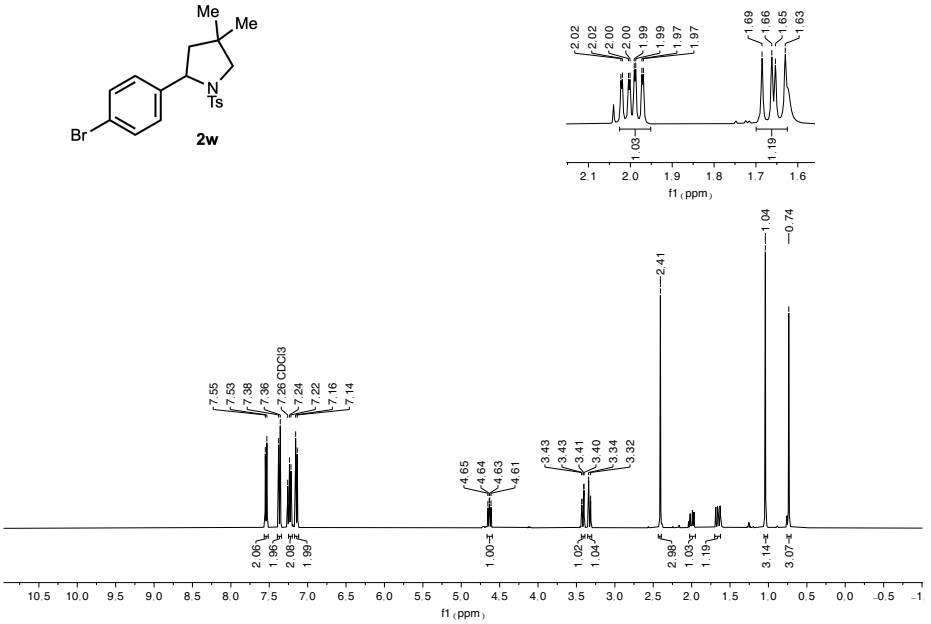
Me
Me
N
Ts
Br
2w
7.55
7.53
7.38
7.36
7.26 CDCl3
7.24
7.22
7.16
7.14
4.65
4.64
4.63
4.61
3.43
3.43
3.41
3.40
3.34
3.32
2.41
1.04
0.74
f1 (ppm)

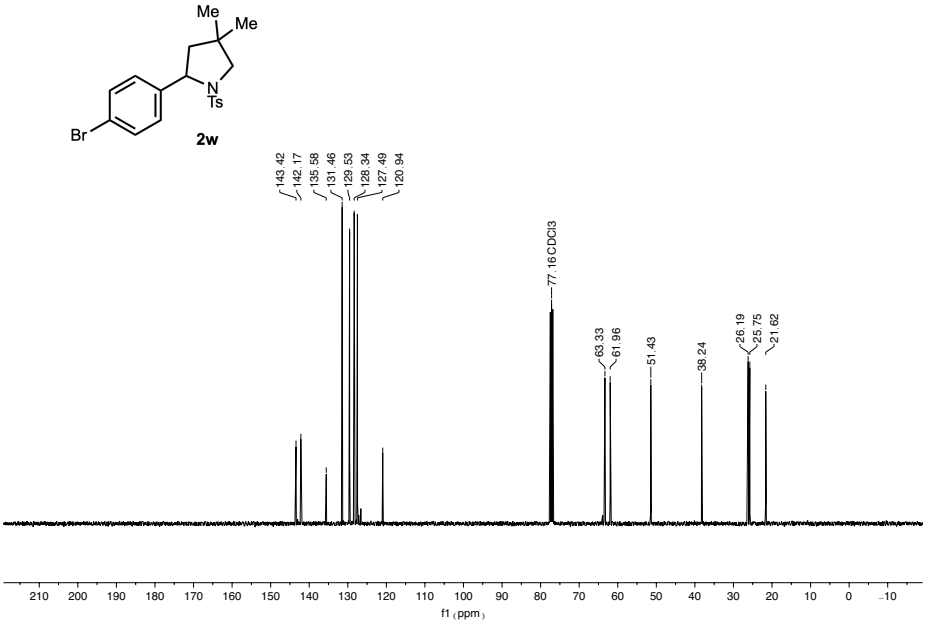
Me
Me
N
Ts
Br
2w
143.42
142.17
135.58
131.46
129.53
128.34
127.49
120.94
77.16 CDCl3
63.33
61.96
51.43
38.24
26.19
25.75
21.62
f1 (ppm)

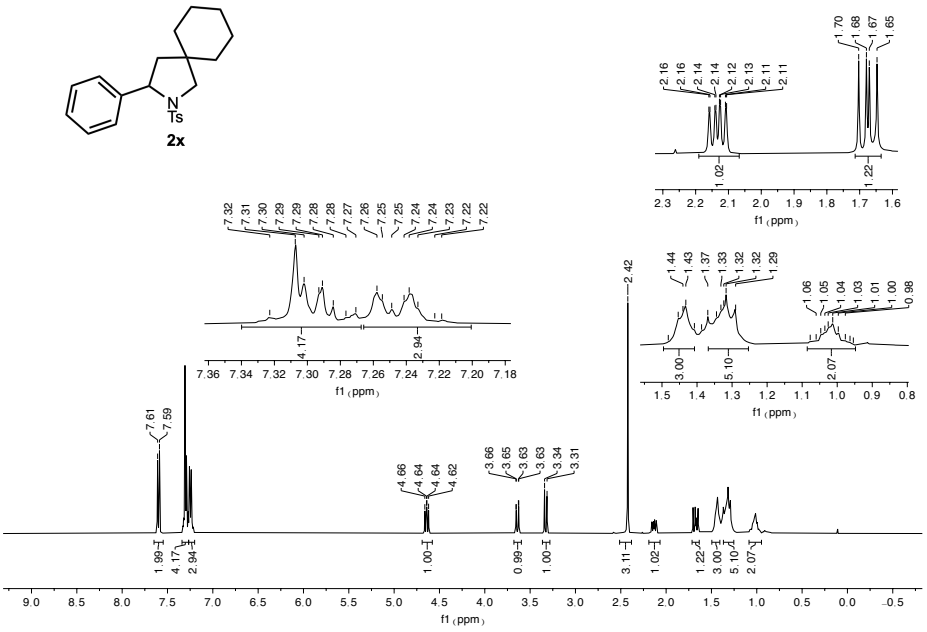
N
Ts
2x
f1 (ppm)

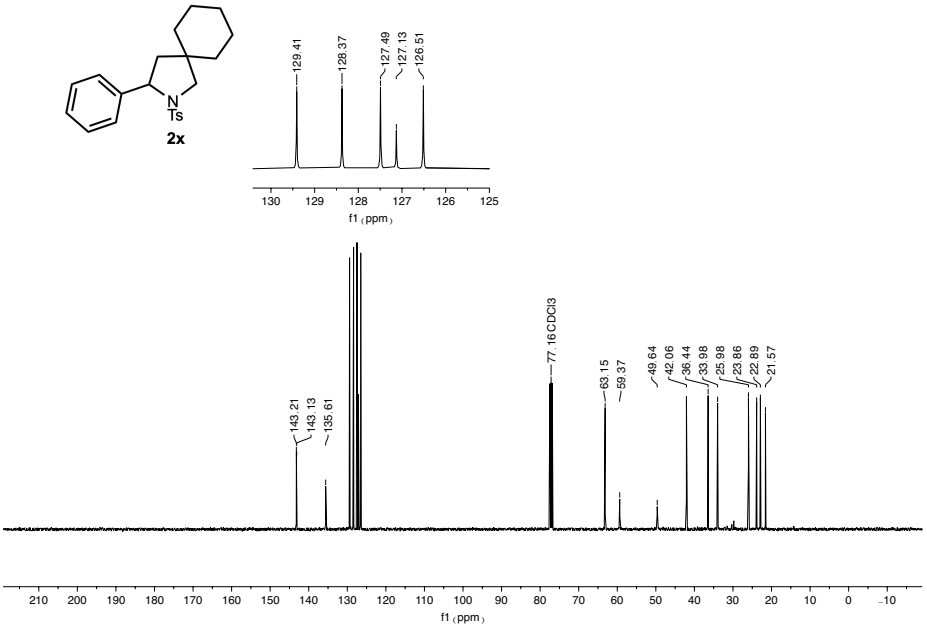
N
Ts
2x
129.41
128.37
127.49
127.13
126.51
143.21
143.13
135.61
77.16CDCl3
63.15
59.37
49.64
42.06
36.44
33.98
25.98
23.86
22.89
21.57
f1 (ppm)

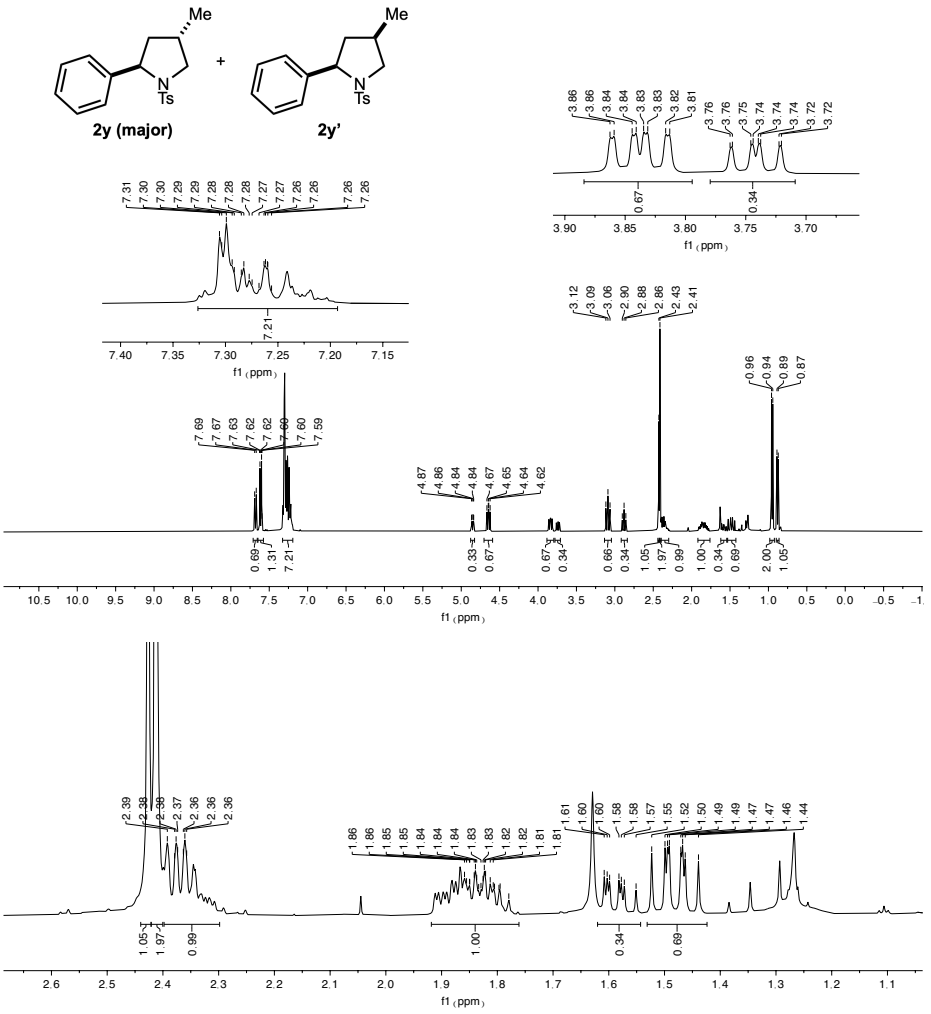
Me
N
Ts
2y (major)
+
Me
N
Ts
2y'
f1 (ppm)

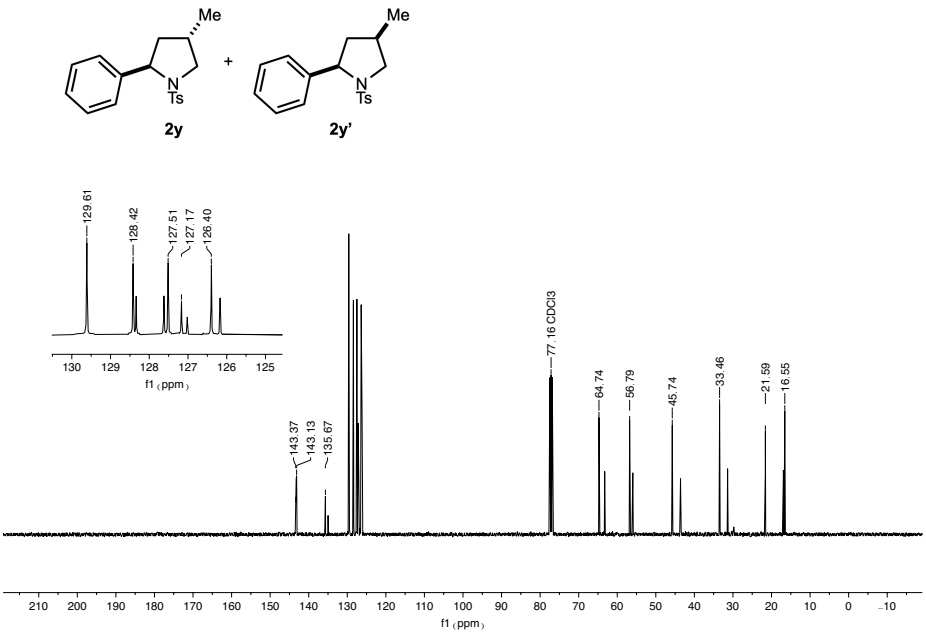
Me
N
Ts
2y
+
Me
N
Ts
2y'
129.61
128.42
127.51
127.17
126.40
143.37
143.13
135.67
77.16 CDCl3
64.74
56.79
45.74
33.46
21.59
16.55
f1 (ppm)

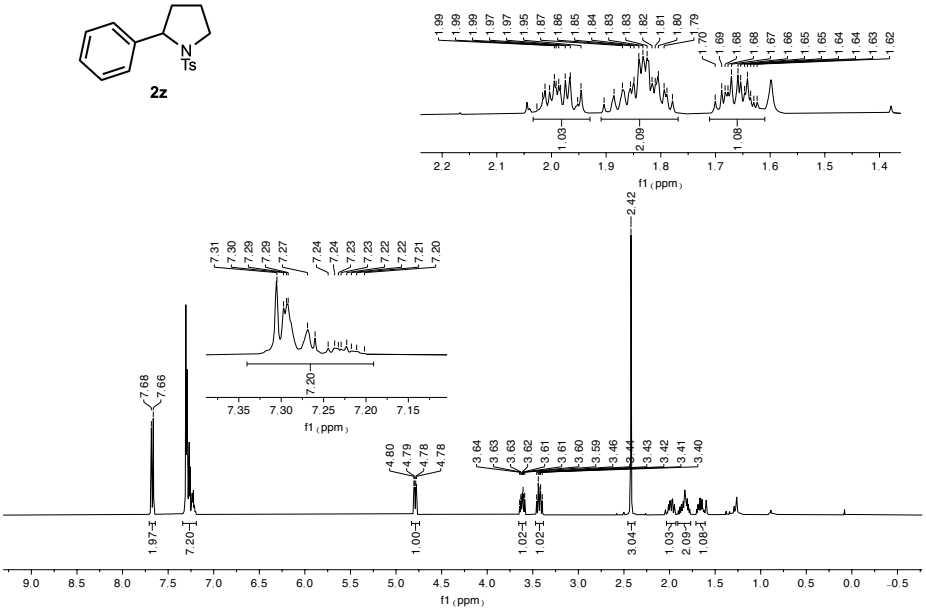
N
Ts
2z
1.03
2.08
1.08
f1 (ppm)
2.42
7.68
7.66
7.20
4.80
4.79
4.78
4.78
1.97
7.20
1.00
1.02
1.02
3.04
1.03
2.09
1.08
f1 (ppm)

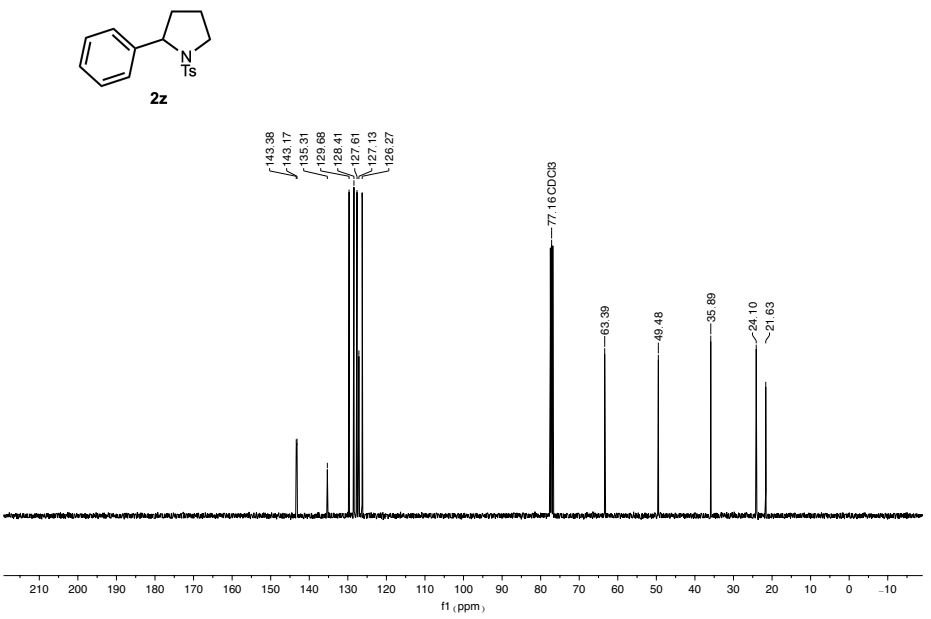
N
Ts
2z
143.38
143.17
135.31
129.68
128.41
127.61
127.13
126.27
77.16 CDCl3
63.39
49.48
35.89
24.10
21.63
f1 (ppm)

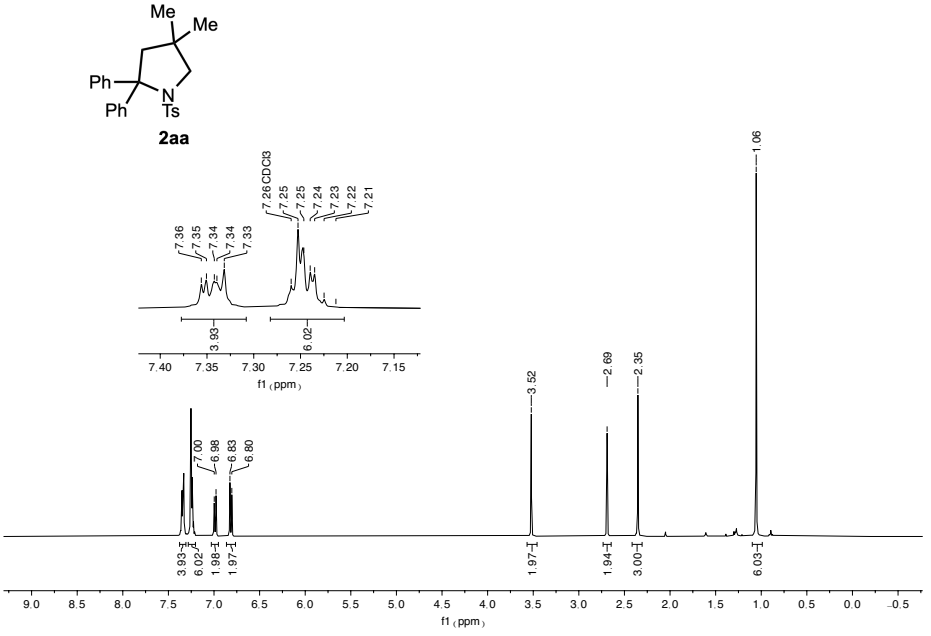
Me
Me
Ph
Ph
N
Ts
2aa
7.26 CDCl3
7.36
7.35
7.34
7.34
7.33
7.25
7.25
7.24
7.23
7.22
7.21
3.93
6.02
7.40
7.35
7.30
7.25
7.20
7.15
f1 (ppm)
7.00
6.98
6.83
6.80
3.52
2.69
2.35
1.06
3.93
6.02
1.98
1.97
1.97
1.94
3.00
6.03
f1 (ppm)

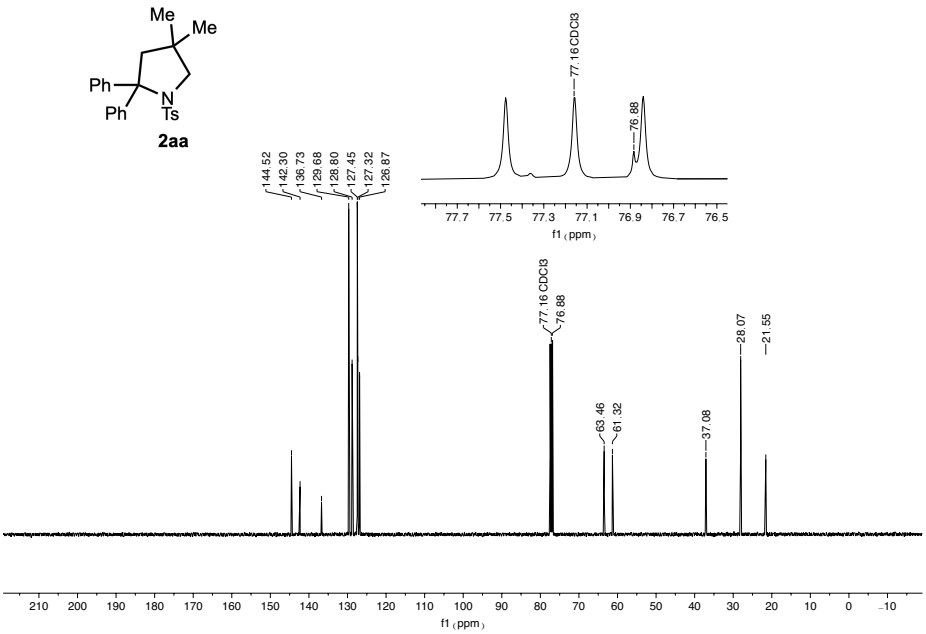
Me
Me
Ph
Ph
N
Ts
2aa
144.52
142.30
136.73
129.68
128.80
127.45
127.32
126.87
77.16 CDCl3
76.88
63.46
61.32
37.08
28.07
21.55
f1 (ppm)

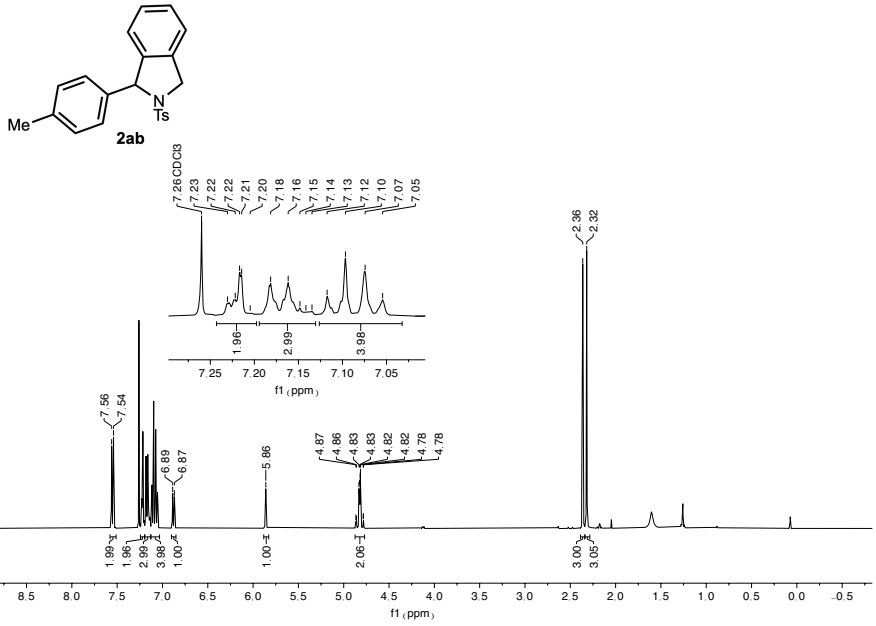
N
Ts
Me
2ab
7.26 CDCl3
7.56
7.54
6.89
6.87
5.86
4.87
4.86
4.83
4.82
4.78
2.36
2.32
1.99
1.96
2.99
3.98
1.00
2.06
3.00
3.05
f1 (ppm)

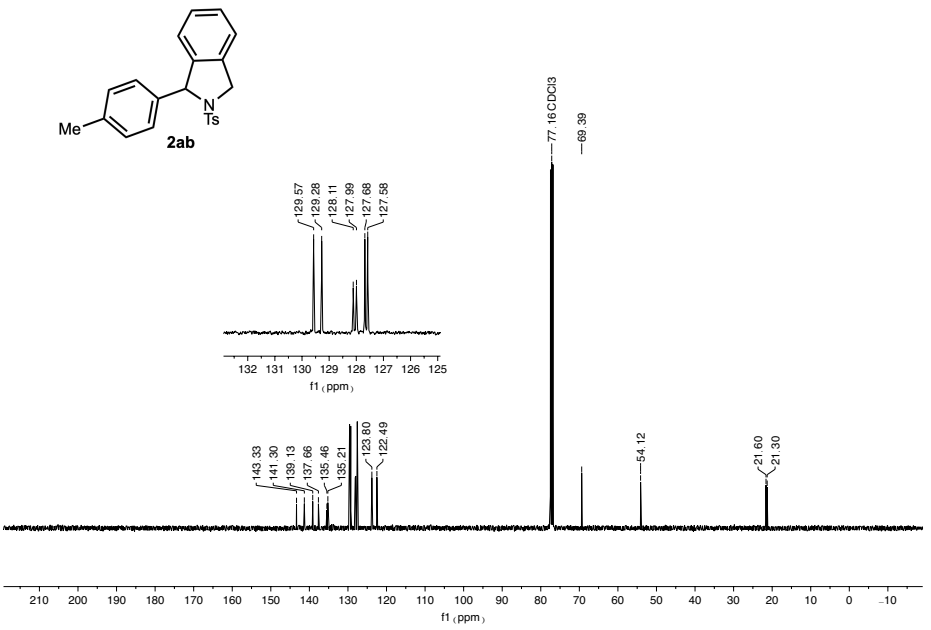
Me
N
Ts
2ab
77.16 CDCl3
69.39
129.57
129.28
128.11
127.99
127.68
127.58
143.33
141.30
139.13
137.66
135.46
135.21
123.80
122.49
54.12
21.60
21.30
f1 (ppm)

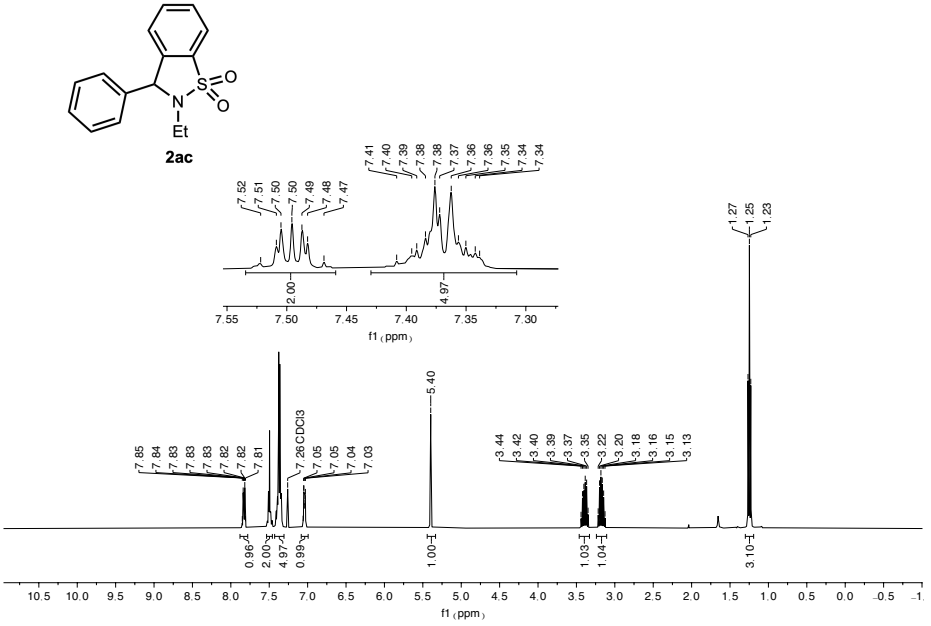
S
O
O
N
Et
2ac
7.41
7.40
7.39
7.38
7.38
7.37
7.36
7.36
7.35
7.34
7.34
7.52
7.51
7.50
7.50
7.49
7.48
7.47
2.00
4.97
1.27
1.25
1.23
7.85
7.84
7.83
7.83
7.83
7.82
7.82
7.81
7.26 CDCl3
7.05
7.05
7.04
7.03
5.40
3.44
3.42
3.40
3.39
3.37
3.35
3.22
3.20
3.18
3.16
3.15
3.13
0.96
2.00
4.97
0.99
1.00
1.03
1.04
3.10
f1 (ppm)

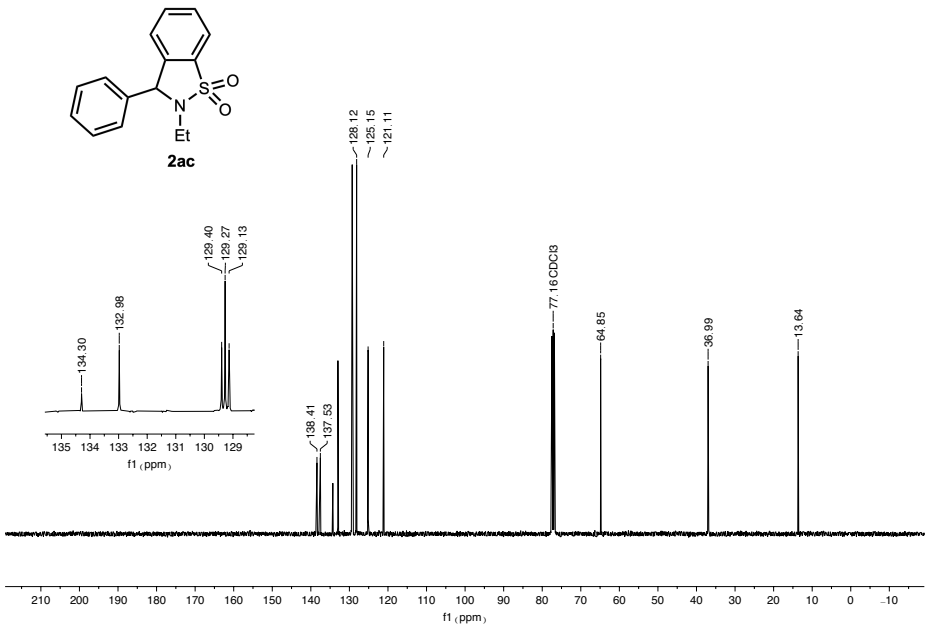
Et
2ac
134.30
132.98
129.40
129.27
129.13
138.41
137.53
128.12
125.15
121.11
77.16 CDCl3
64.85
36.99
13.64
f1 (ppm)

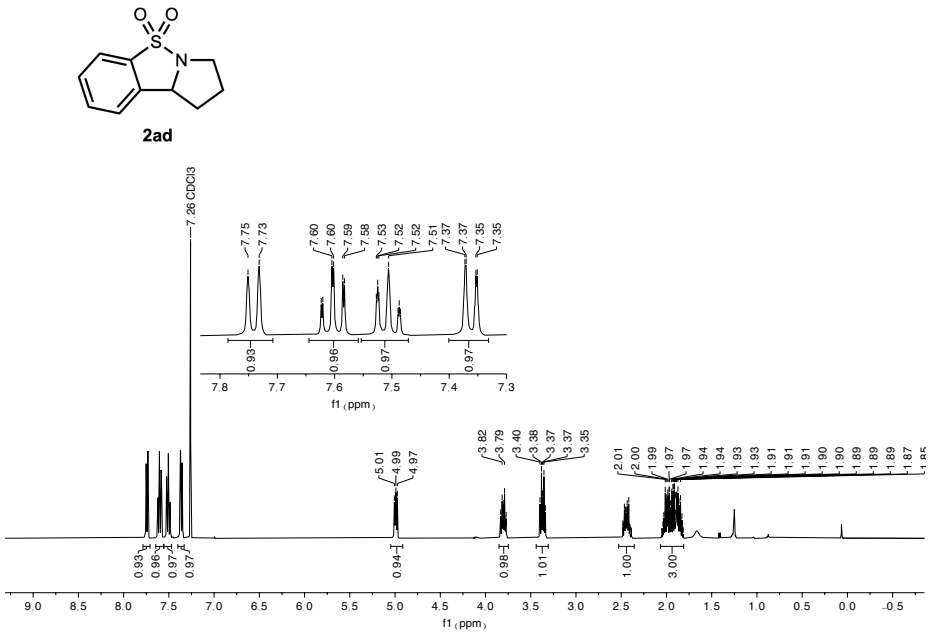
2ad
7.26 CDCl3
7.75
7.73
7.60
7.60
7.59
7.58
7.53
7.52
7.52
7.51
7.37
7.37
7.35
7.35
5.01
4.99
4.97
3.82
3.79
3.40
3.38
3.37
3.37
3.35
2.01
2.00
1.99
1.97
1.97
1.94
1.94
1.93
1.93
1.91
1.91
1.91
1.90
1.90
1.89
1.89
1.89
1.87
0.93
0.96
0.97
0.97
0.94
0.98
1.01
1.00
3.00
f1 (ppm)

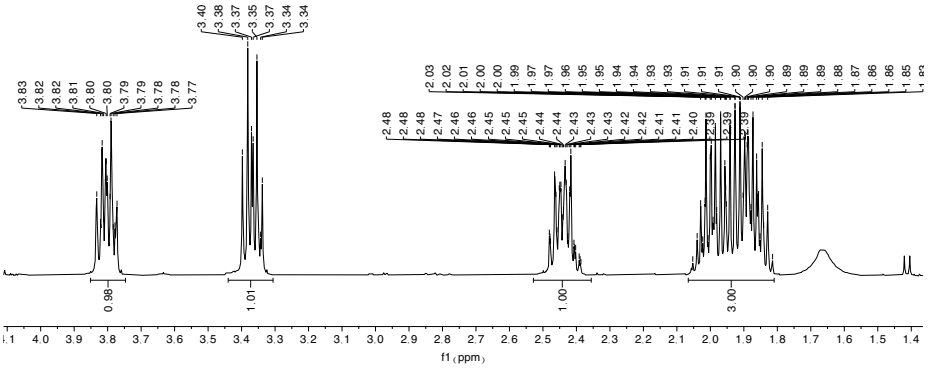
3.83
3.82
3.82
3.81
3.80
3.80
3.79
3.79
3.78
3.78
3.77
3.40
3.38
3.37
3.35
3.37
3.34
3.34
2.48
2.48
2.48
2.47
2.46
2.46
2.46
2.45
2.45
2.45
2.44
2.44
2.43
2.43
2.43
2.42
2.42
2.41
2.41
2.40
2.39
2.39
2.39
2.03
2.02
2.01
2.00
2.00
1.99
1.97
1.97
1.96
1.95
1.95
1.94
1.94
1.93
1.93
1.91
1.91
1.91
1.90
1.90
1.90
1.89
1.89
1.89
1.88
1.87
1.86
1.86
1.85
0.98
1.01
1.00
3.00
f1 (ppm)

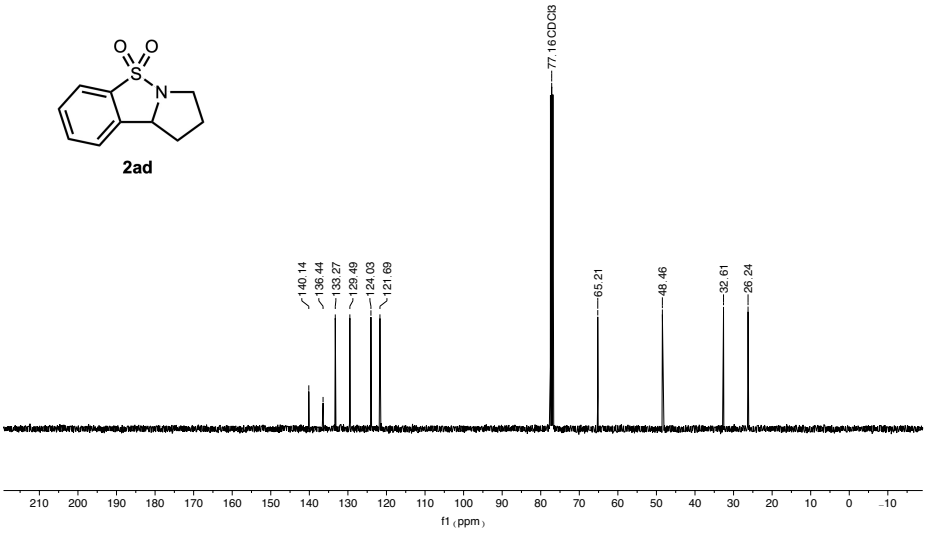
O
O
S
N
2ad
140.14
136.44
133.27
129.49
124.03
121.69
77.16 CDCl3
65.21
48.46
32.61
26.24
f1 (ppm)

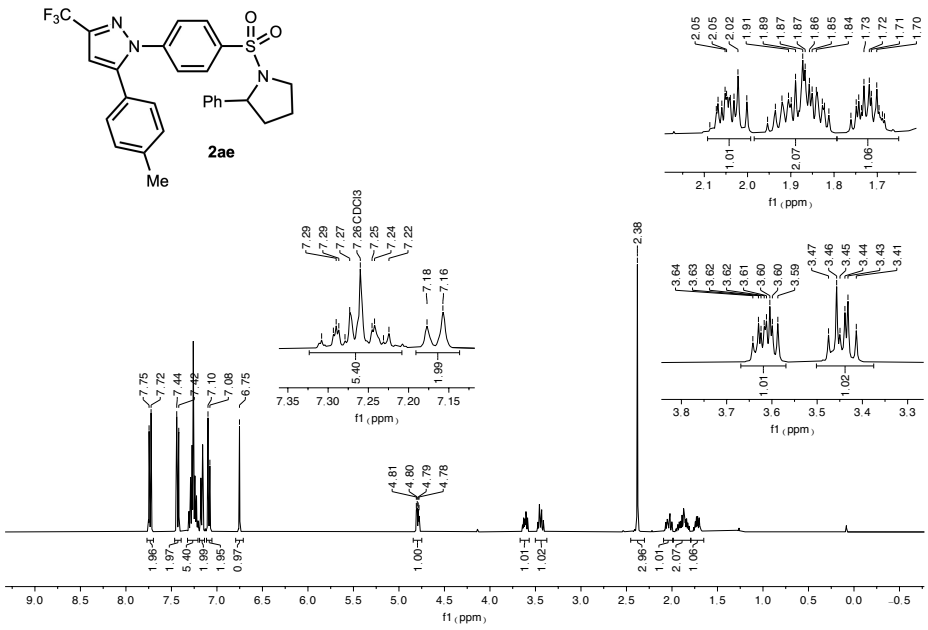
2ae
Me
Ph
f1 (ppm)

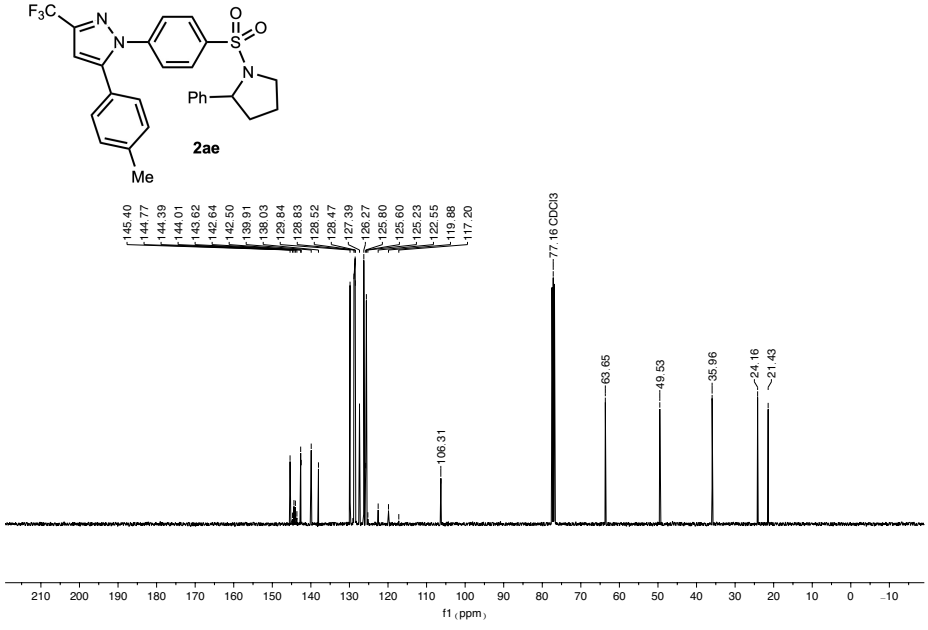
2ae
Me
Ph
77.16 CDCl3
f1 (ppm)

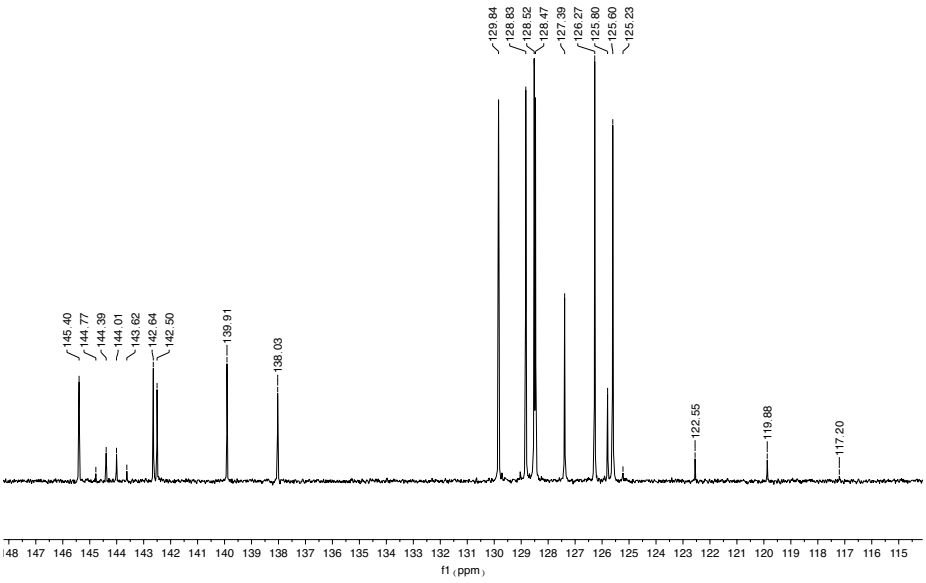
129.84
128.83
128.52
128.47
127.39
126.27
125.80
125.60
125.23
145.40
144.77
144.39
144.01
143.62
142.64
142.50
139.91
138.03
122.55
119.88
117.20
f1 (ppm)

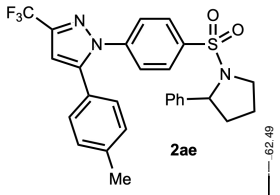
F3C
N
N
O
S
O
N
Ph
Me

2ae

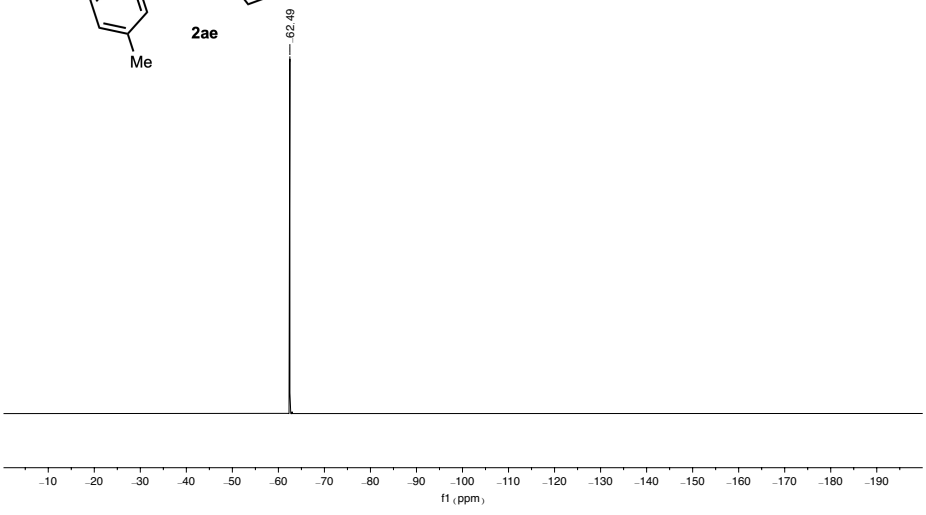
62.49
f1 (ppm)

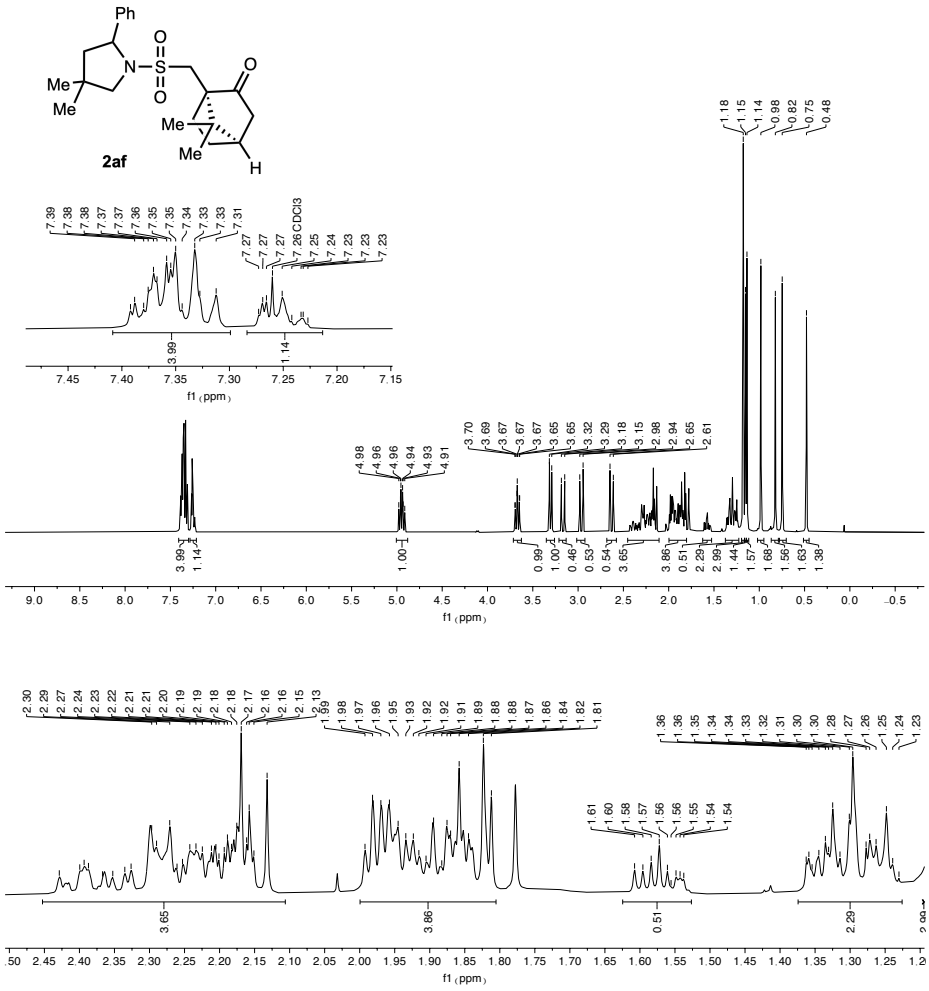
Ph
O
N
S
O
O
Me
Me
Me
Me
H
2af
7.39
7.38
7.38
7.37
7.37
7.36
7.35
7.35
7.34
7.33
7.33
7.31
7.27
7.27
7.27
7.26 CDCl3
7.25
7.24
7.23
7.23
7.23
3.99
1.14
f1 (ppm)
1.18
1.15
1.14
0.98
0.82
0.75
0.48
4.98
4.96
4.96
4.94
4.93
4.91
3.70
3.69
3.67
3.67
3.67
3.65
3.65
3.32
3.29
3.18
3.15
2.98
2.94
2.65
2.61
3.99
1.14
1.00
0.99
1.00
0.46
0.53
0.54
3.65
3.86
0.51
2.29
2.99
1.44
1.57
1.68
1.56
1.63
1.38
f1 (ppm)
2.30
2.29
2.27
2.24
2.23
2.22
2.21
2.21
2.20
2.19
2.19
2.18
2.18
2.17
2.16
2.16
2.15
2.13
1.99
1.98
1.97
1.96
1.95
1.93
1.92
1.92
1.91
1.89
1.88
1.88
1.87
1.86
1.84
1.82
1.81
1.61
1.60
1.58
1.57
1.56
1.56
1.55
1.54
1.54
1.36
1.36
1.35
1.34
1.34
1.33
1.32
1.31
1.30
1.30
1.28
1.27
1.26
1.25
1.24
1.23
3.65
3.86
0.51
2.29
f1 (ppm)

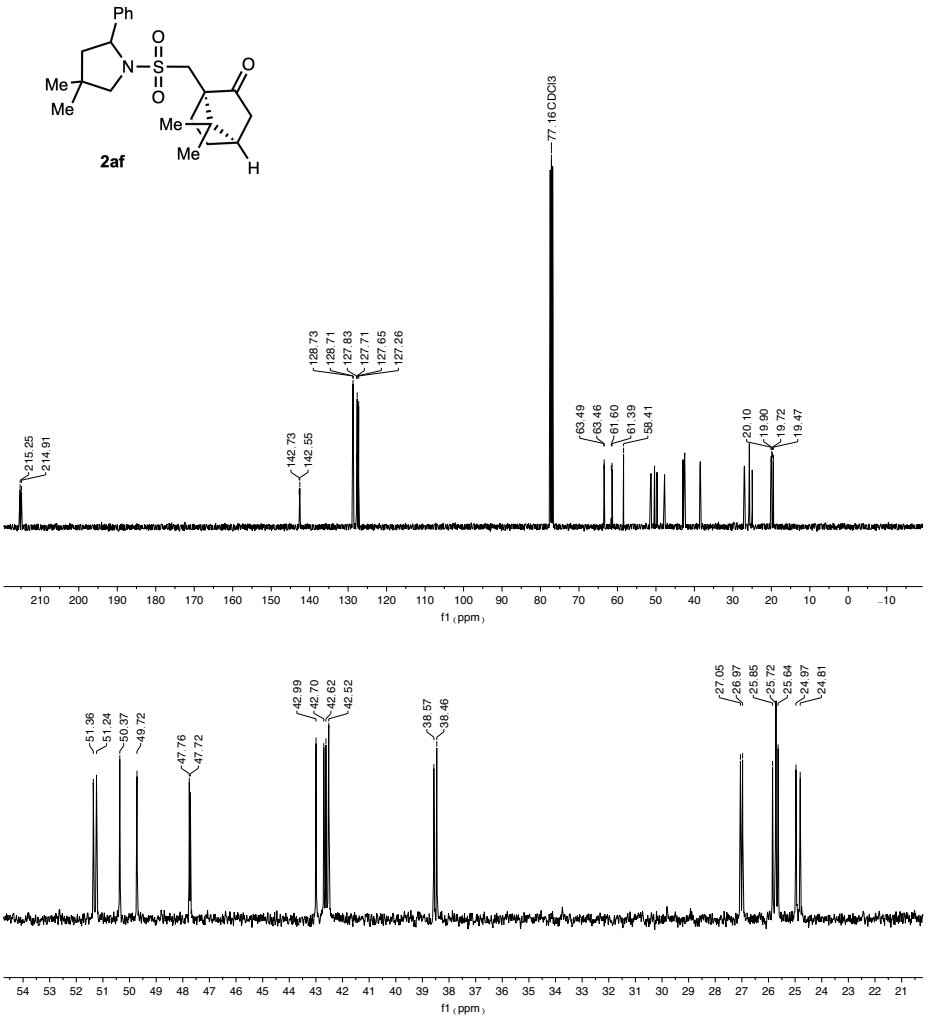
Ph
O
N
S
O
O
Me
Me
Me
Me
O
H
2af
77.16 CDCl3
128.73
128.71
127.83
127.71
127.65
127.26
215.25
214.91
142.73
142.55
63.49
63.46
61.60
61.39
58.41
20.10
19.90
19.72
19.47
f1 (ppm)
51.36
51.24
50.37
49.72
47.76
47.72
42.99
42.70
42.62
42.52
38.57
38.46
27.05
26.97
25.85
25.72
25.64
24.97
24.81
f1 (ppm)

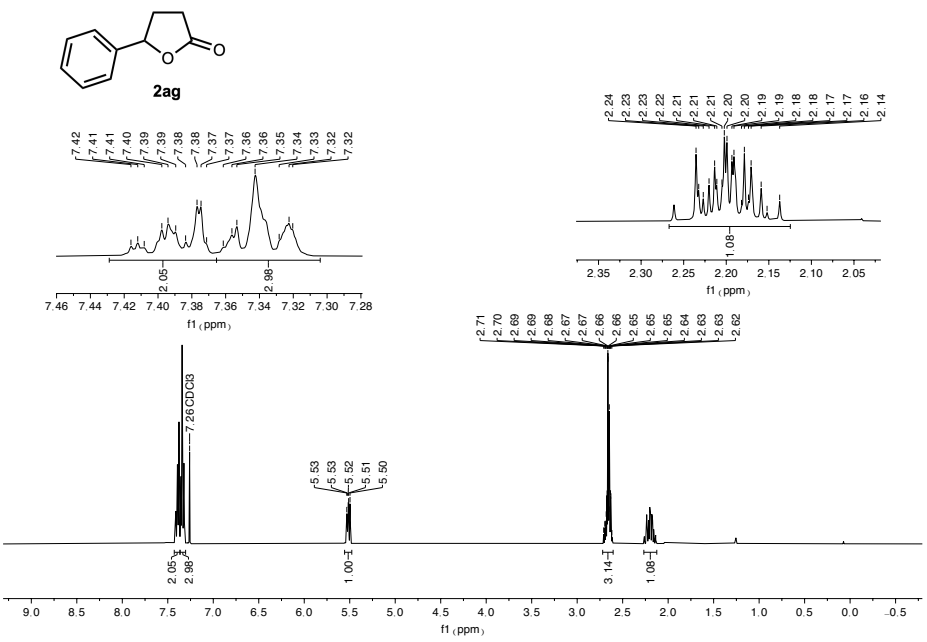
2ag
7.42
7.41
7.41
7.40
7.39
7.39
7.38
7.38
7.37
7.37
7.36
7.36
7.35
7.34
7.33
7.32
7.32
2.05
2.98
7.46 7.44 7.42 7.40 7.38 7.36 7.34 7.32 7.30 7.28
f1 (ppm)
2.24
2.23
2.23
2.22
2.21
2.21
2.21
2.20
2.20
2.19
2.19
2.18
2.18
2.17
2.17
2.16
2.14
1.08
2.35 2.30 2.25 2.20 2.15 2.10 2.05
f1 (ppm)
2.71
2.70
2.69
2.69
2.68
2.67
2.67
2.66
2.66
2.65
2.65
2.65
2.64
2.63
2.63
2.62
7.26 CDCl3
5.53
5.53
5.52
5.51
5.50
2.05
2.98
1.00
3.14
1.08
9.0 8.5 8.0 7.5 7.0 6.5 6.0 5.5 5.0 4.5 4.0 3.5 3.0 2.5 2.0 1.5 1.0 0.5 0.0 -0.5
f1 (ppm)

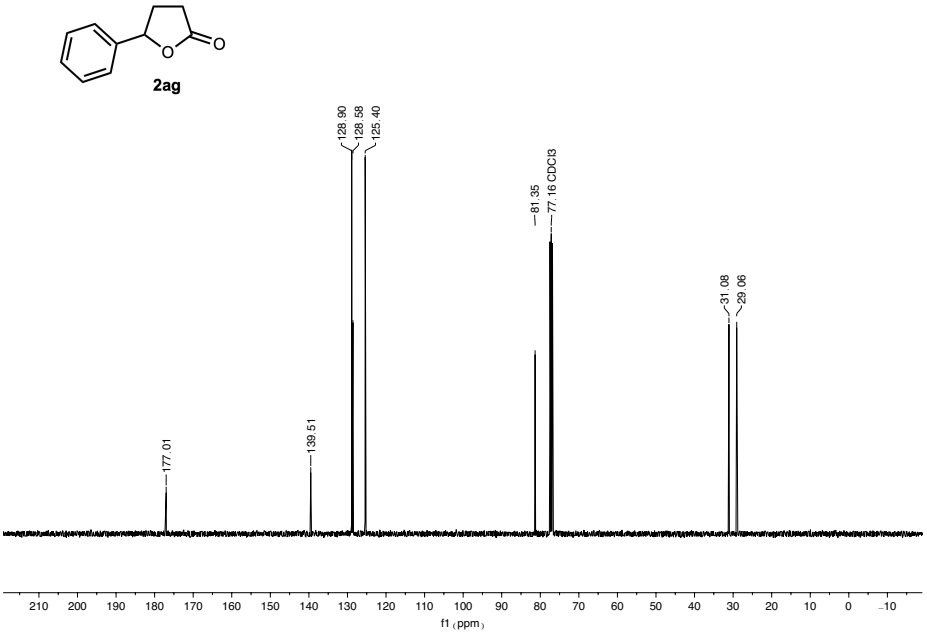
2ag
128.90
128.58
125.40
81.35
77.16 CDCl3
31.08
29.06
177.01
139.51
210 200 190 180 170 160 150 140 130 120 110 100 90 80 70 60 50 40 30 20 10 0 -10
f1 (ppm)

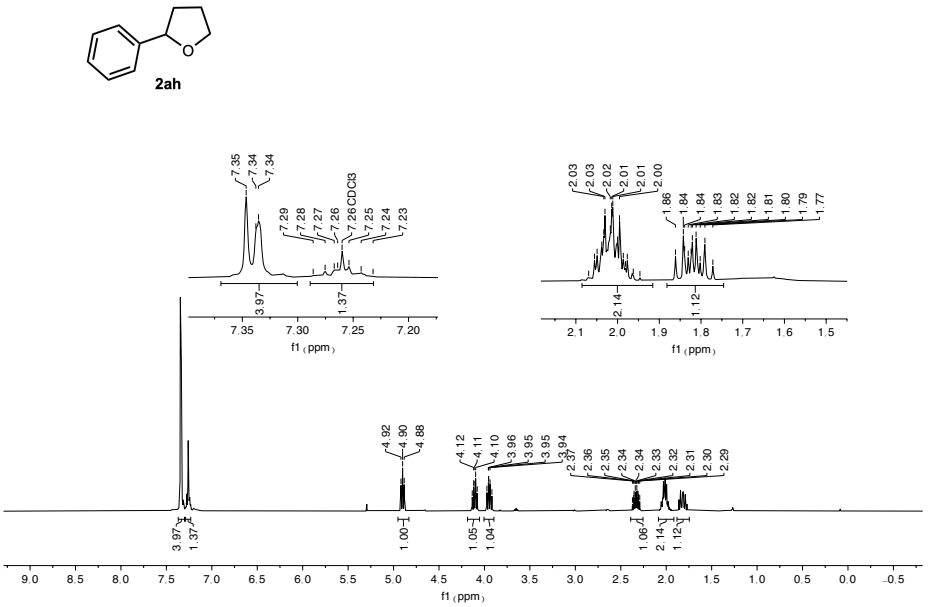
2ah
7.35
7.34
7.34
7.29
7.28
7.27
7.26
7.26 CDCl3
7.25
7.24
7.23
3.97
1.37
f1 (ppm)
2.03
2.03
2.02
2.01
2.01
2.00
1.86
1.84
1.84
1.83
1.82
1.82
1.81
1.80
1.79
1.77
2.14
1.12
f1 (ppm)
4.92
4.90
4.88
4.12
4.11
4.10
3.96
3.95
3.95
3.94
2.37
2.36
2.35
2.34
2.34
2.33
2.32
2.31
2.30
2.29
3.97
1.37
1.00
1.05
1.04
1.06
2.14
1.12
f1 (ppm)

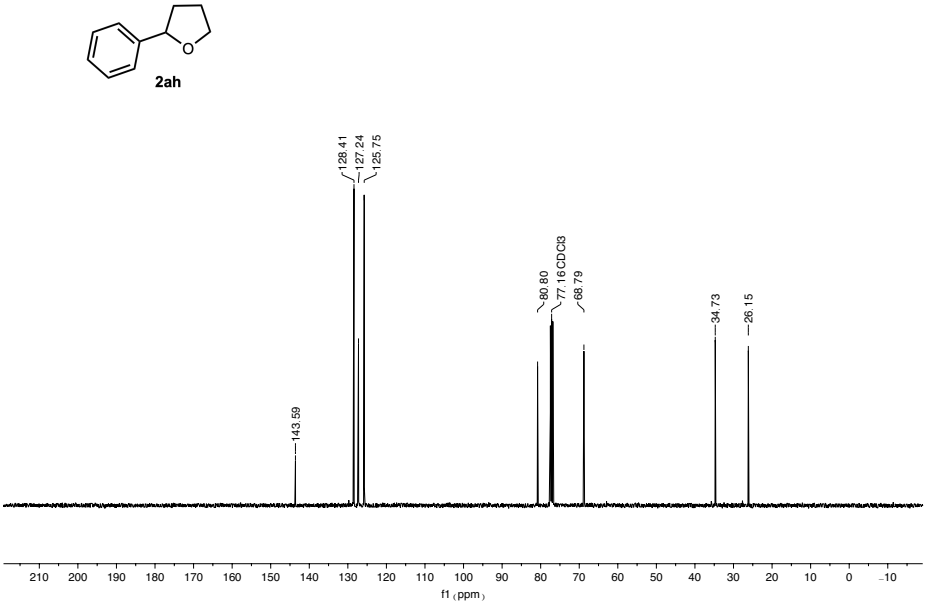
2ah
128.41
127.24
125.75
80.80
77.16 CDCl3
68.79
34.73
26.15
143.59
f1 (ppm)

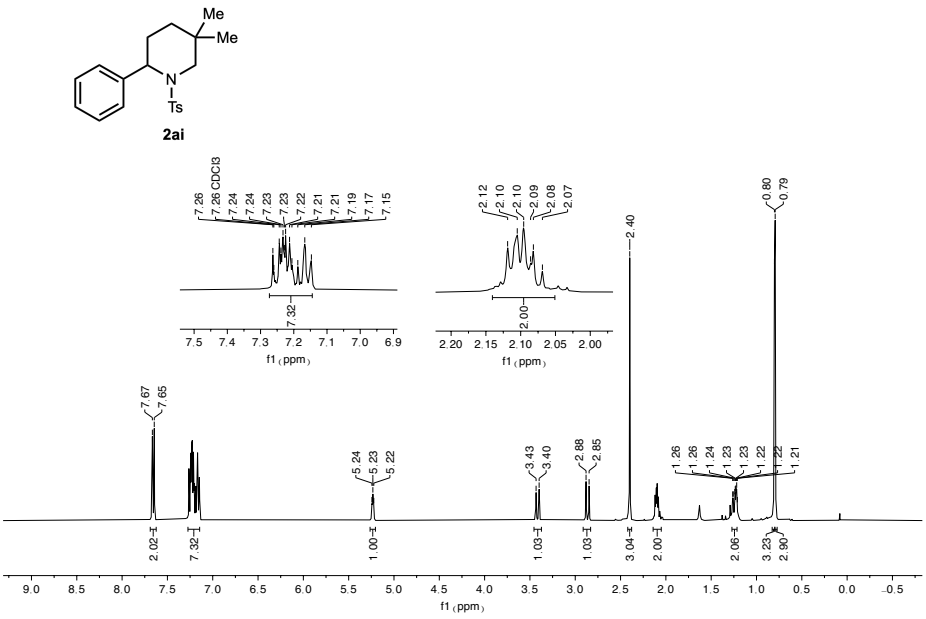
Me
Me
N
Ts
2ai
7.26
7.26 CDCl3
7.24
7.24
7.23
7.23
7.22
7.21
7.21
7.19
7.17
7.15
7.32
f1 (ppm)
2.12
2.10
2.10
2.09
2.08
2.07
2.00
2.40
0.80
0.79
7.67
7.65
5.24
5.23
5.22
3.43
3.40
2.88
2.85
1.26
1.26
1.24
1.23
1.23
1.22
1.22
1.21
2.02
7.32
1.00
1.03
1.03
3.04
2.00
2.06
3.23
2.90

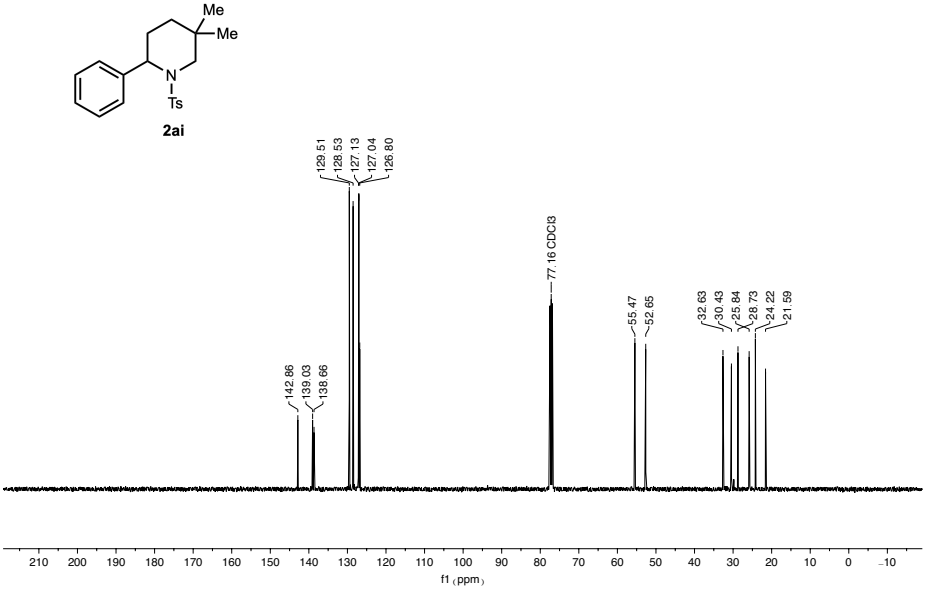
Me
Me
N
Ts
2ai
129.51
128.53
127.13
127.04
126.80
77.16 CDCl3
55.47
52.65
32.63
30.43
25.84
28.73
24.22
21.59
142.86
139.03
138.66
f1 (ppm)

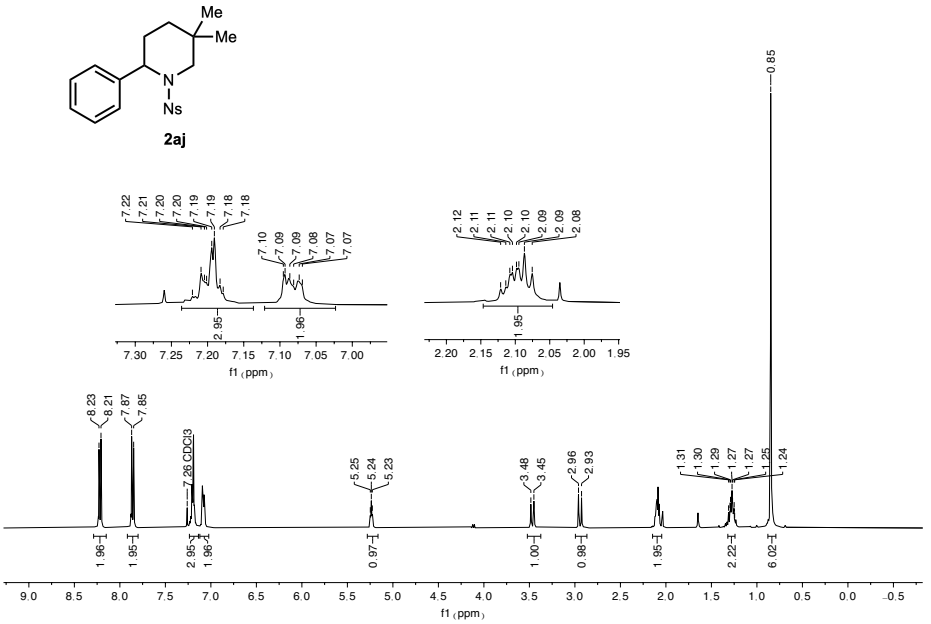
Me
Me
N
Ns
2aj
0.85
7.22
7.21
7.20
7.20
7.19
7.19
7.18
7.18
7.10
7.09
7.09
7.08
7.07
7.07
2.95
1.96
2.12
2.11
2.11
2.10
2.10
2.09
2.09
2.08
1.95
f1 (ppm)
8.23
8.21
7.87
7.85
7.26 CDCl3
5.25
5.24
5.23
3.48
3.45
2.96
2.93
1.31
1.30
1.29
1.27
1.27
1.25
1.24
1.96
1.95
2.95
1.96
0.97
1.00
0.98
1.95
2.22
6.02

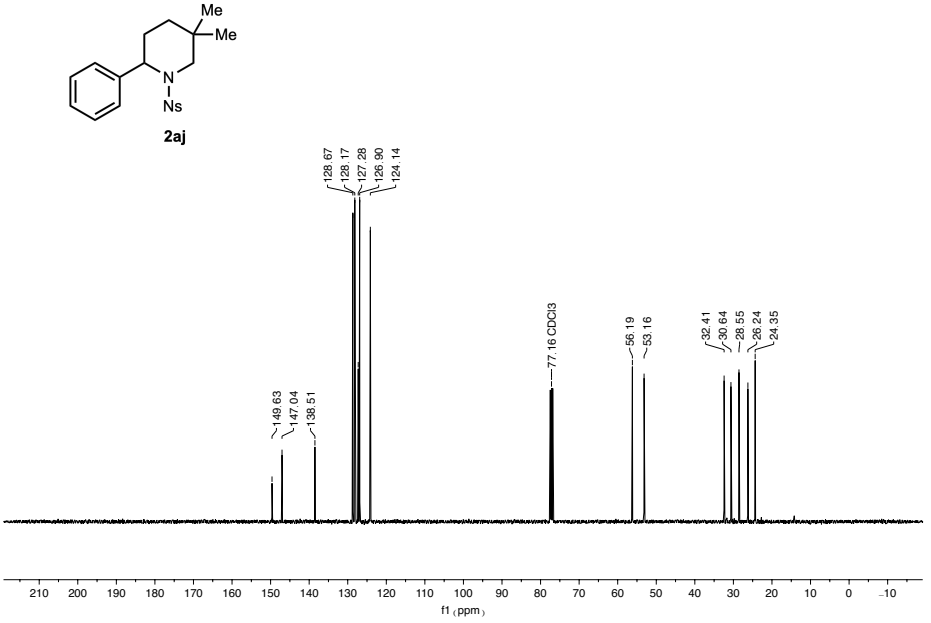
Me
Me
N
Ns
2aj
128.67
128.17
127.28
126.90
124.14
149.63
147.04
138.51
77.16 CDCl3
56.19
53.16
32.41
30.64
28.55
26.24
24.35
f1 (ppm)

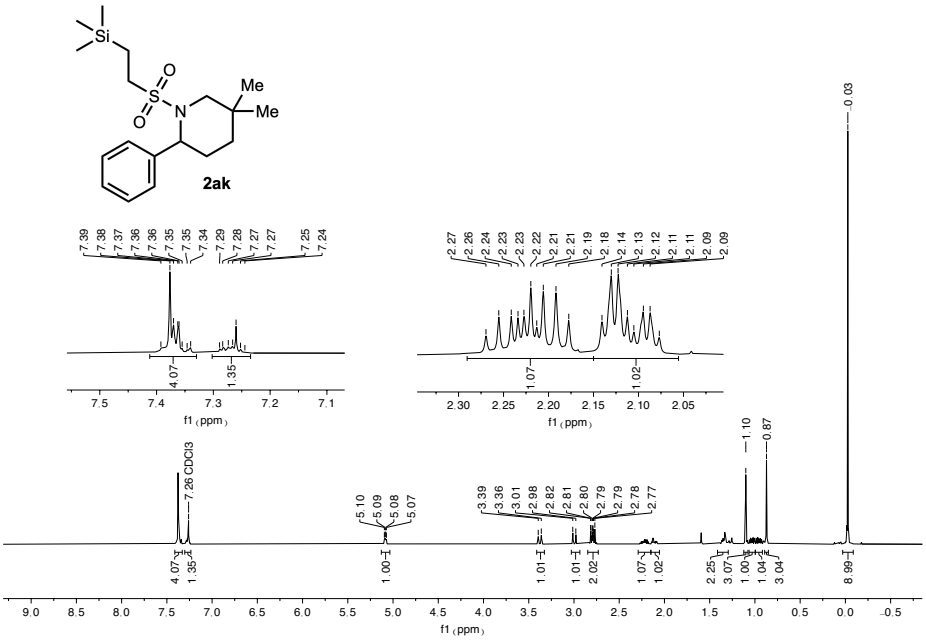
Si
O
S
O
N
Me
Me
2ak
7.26 CDCl3
f1 (ppm)

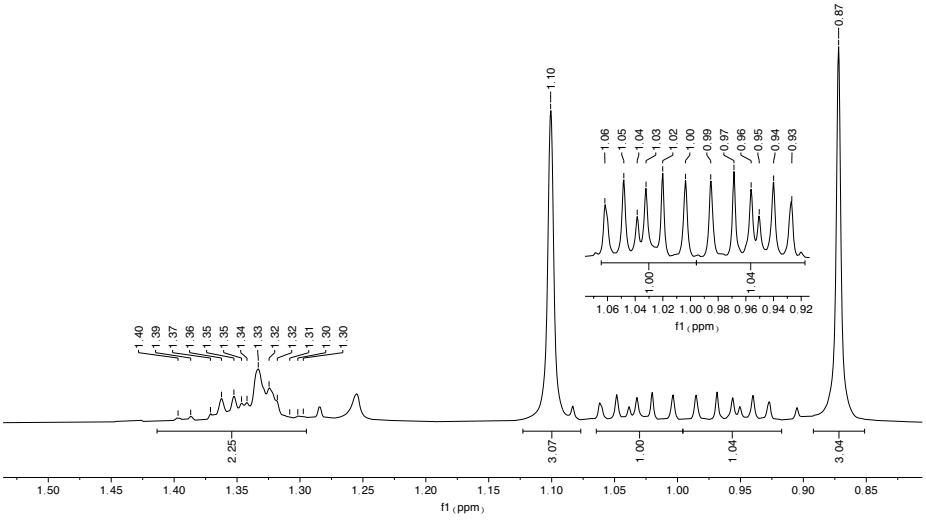
1.10
0.87
f1 (ppm)

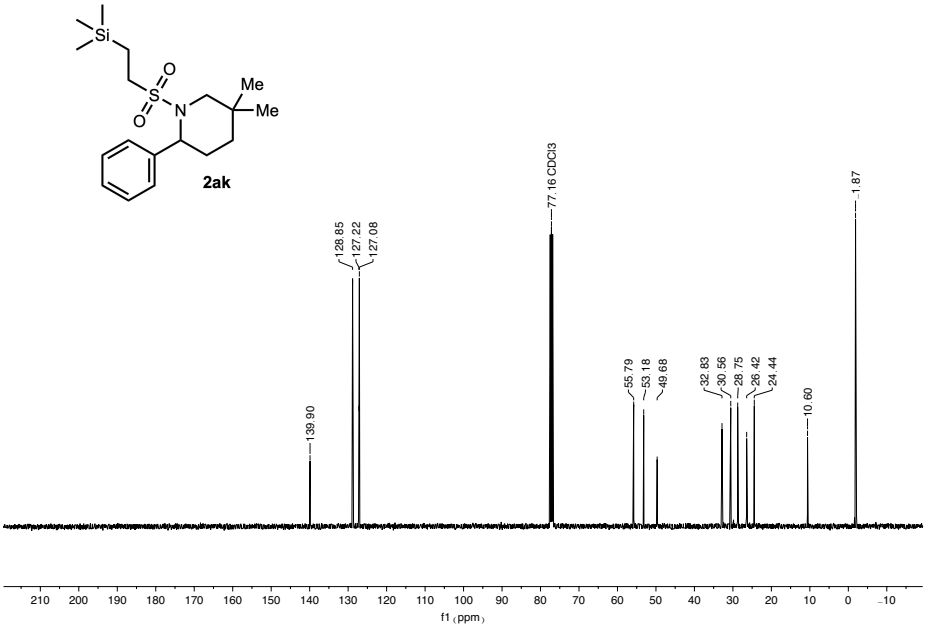
Si
O
S
O
N
Me
Me
2ak
139.90
128.85
127.22
127.08
77.16 CDCl3
55.79
53.18
49.68
32.83
30.56
28.75
26.42
24.44
10.60
1.87
f1 (ppm)

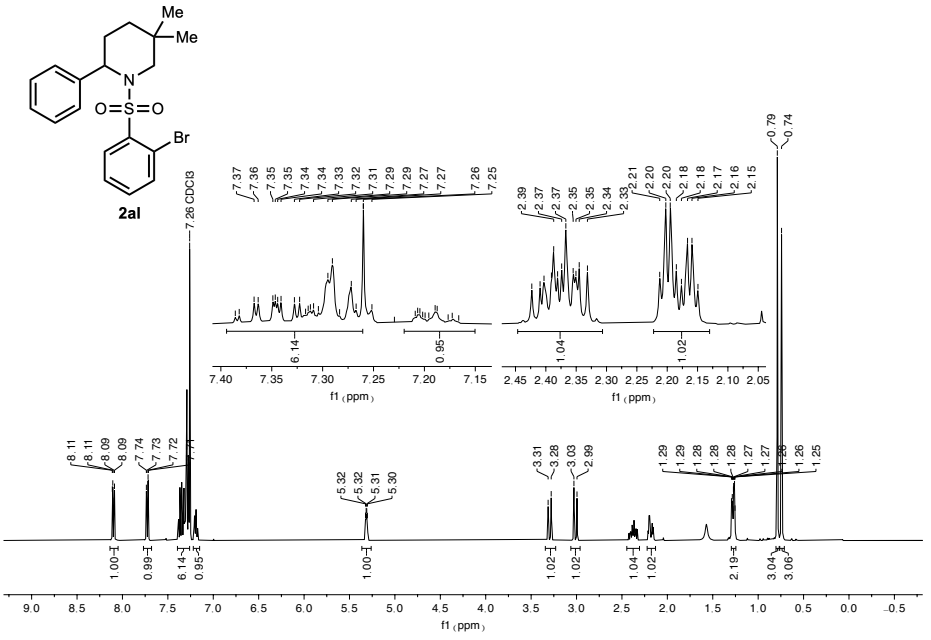
Me
Me
N
O=S=O
Br
2al
7.26 CDCl3
0.79
0.74
6.14
0.95
1.04
1.02
f1 (ppm)

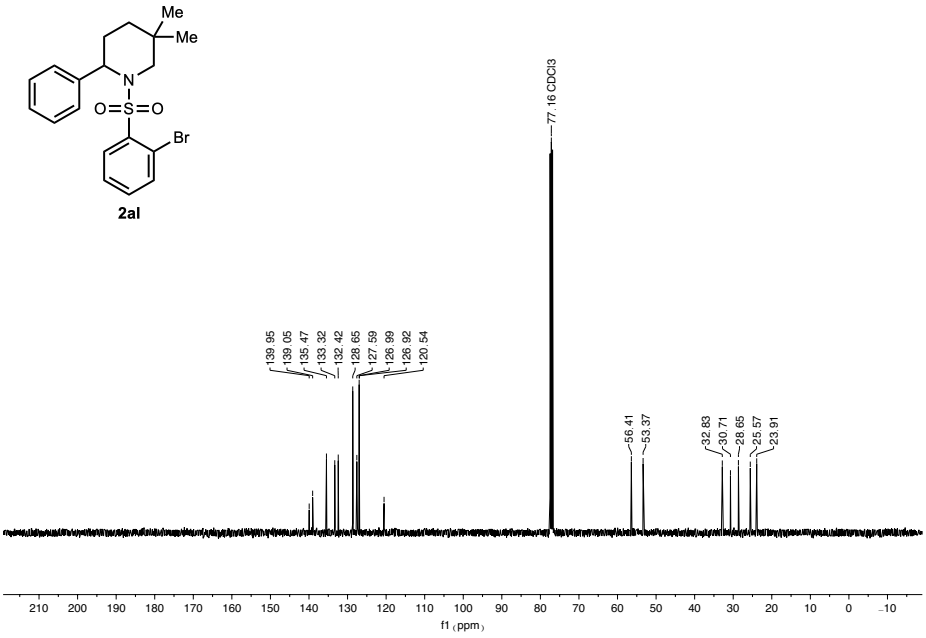
Me
Me
N
O=S=O
Br
2al
77.16 CDCl3
139.95
139.05
135.47
133.32
132.42
128.65
127.59
126.99
126.92
120.54
56.41
53.37
32.83
30.71
28.65
25.57
23.91
f1 (ppm)

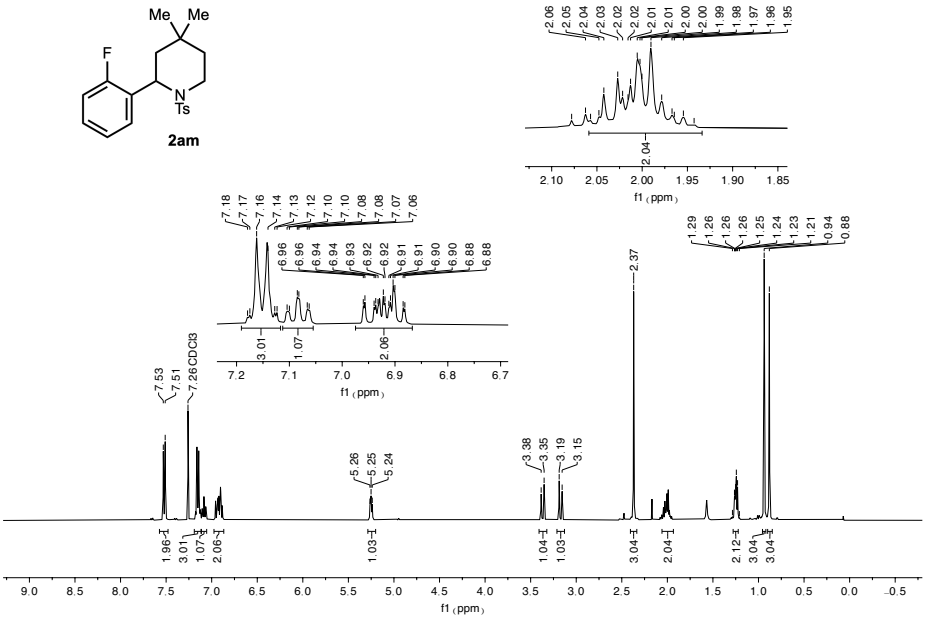
Me
Me
F
N
Ts
2am
2.06
2.05
2.04
2.03
2.02
2.02
2.01
2.01
2.00
2.00
1.99
1.98
1.97
1.96
1.95
2.04
f1 (ppm)
7.18
7.17
7.16
7.14
7.13
7.12
7.10
7.10
7.08
7.08
7.07
7.06
6.96
6.96
6.94
6.94
6.93
6.92
6.92
6.91
6.91
6.90
6.90
6.88
6.88
3.01
1.07
2.06
f1 (ppm)
7.53
7.51
7.26 CDCl3
5.26
5.25
5.24
3.38
3.35
3.19
3.15
2.37
1.29
1.26
1.26
1.26
1.25
1.24
1.23
1.21
0.94
0.88
1.96
3.01
1.07
2.06
1.03
1.04
1.03
3.04
2.04
2.12
3.04
3.04
f1 (ppm)

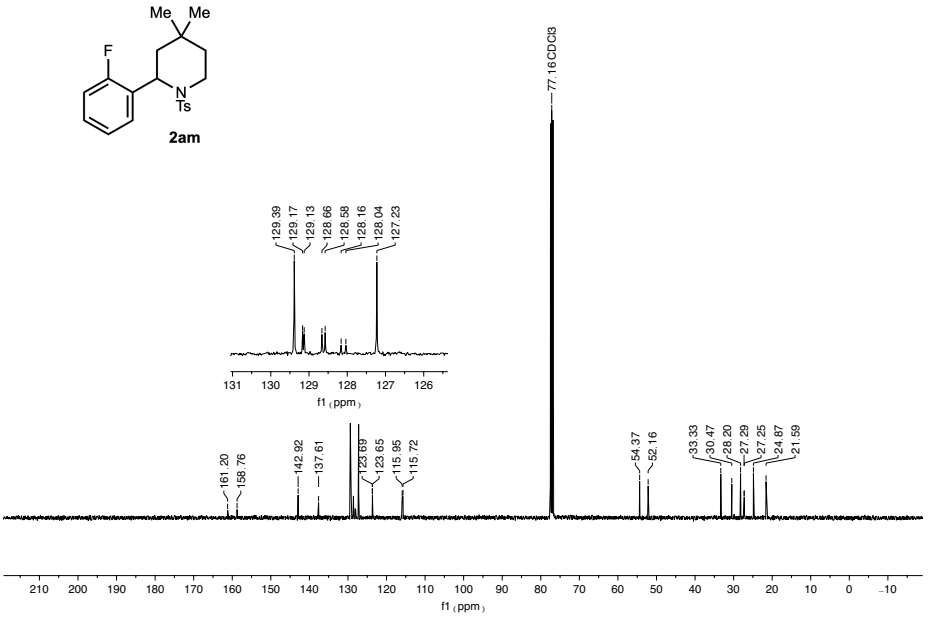
Me
Me
F
N
Ts
2am
77.16 CDCl3
129.39
129.17
129.13
128.66
128.58
128.16
128.04
127.23
161.20
158.76
142.92
137.61
123.69
123.65
115.95
115.72
54.37
52.16
33.33
30.47
28.20
27.29
27.25
24.87
21.59
f1 (ppm)

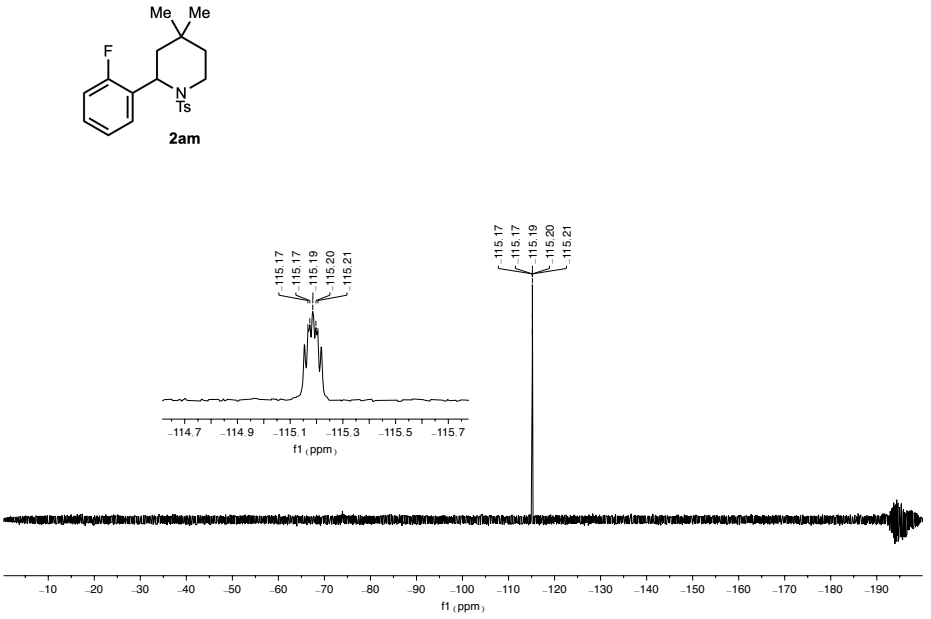
Me
Me
F
N
Ts
2am
-115.17
-115.17
-115.19
-115.20
-115.21
f1 (ppm)

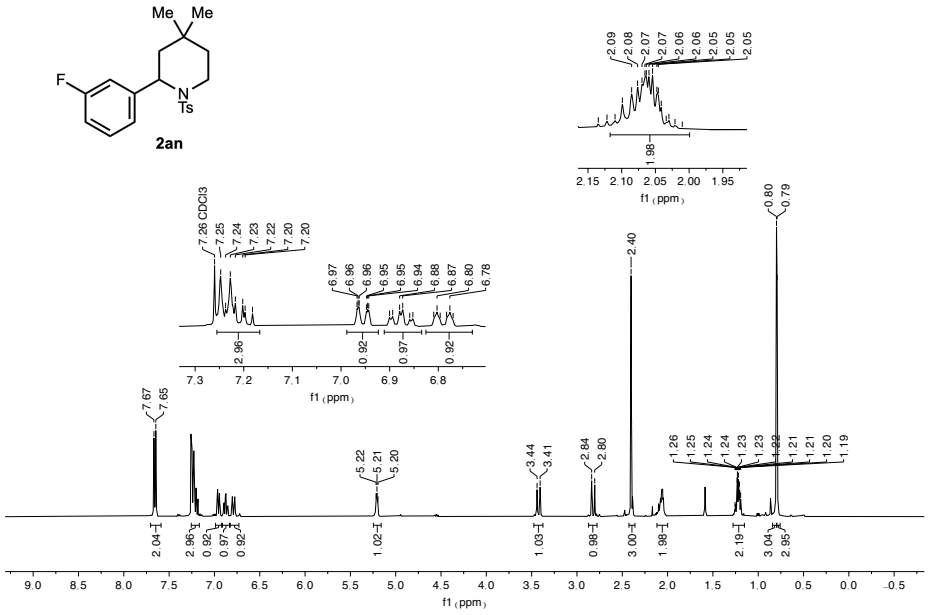
Me Me
F
N
Ts
2an
7.67
7.65
7.26 CDCl3
7.25
7.24
7.23
7.22
7.20
7.20
6.97
6.96
6.96
6.95
6.95
6.94
6.88
6.87
6.80
6.78
5.22
5.21
5.20
3.44
3.41
2.84
2.80
2.40
2.09
2.08
2.07
2.07
2.06
2.06
2.05
2.05
2.05
1.26
1.25
1.24
1.24
1.23
1.23
1.22
1.21
1.21
1.20
1.19
0.80
0.79
f1 (ppm)

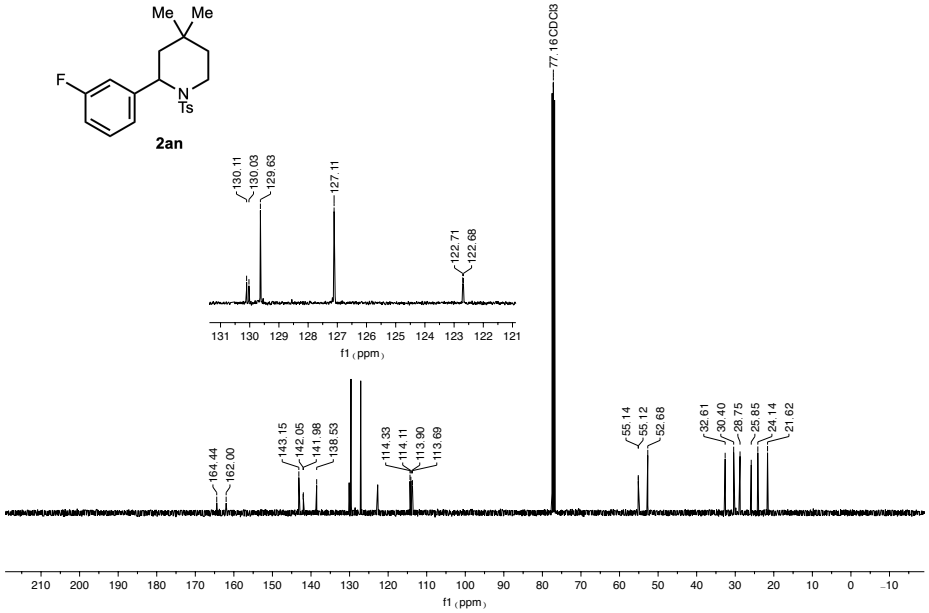
Me Me
F
N
Ts
2an
77.16 CDCl3
130.11
130.03
129.63
127.11
122.71
122.68
164.44
162.00
143.15
142.05
141.98
138.53
114.33
114.11
113.90
113.69
55.14
55.12
52.68
32.61
30.40
28.75
25.85
24.14
21.62
f1 (ppm)

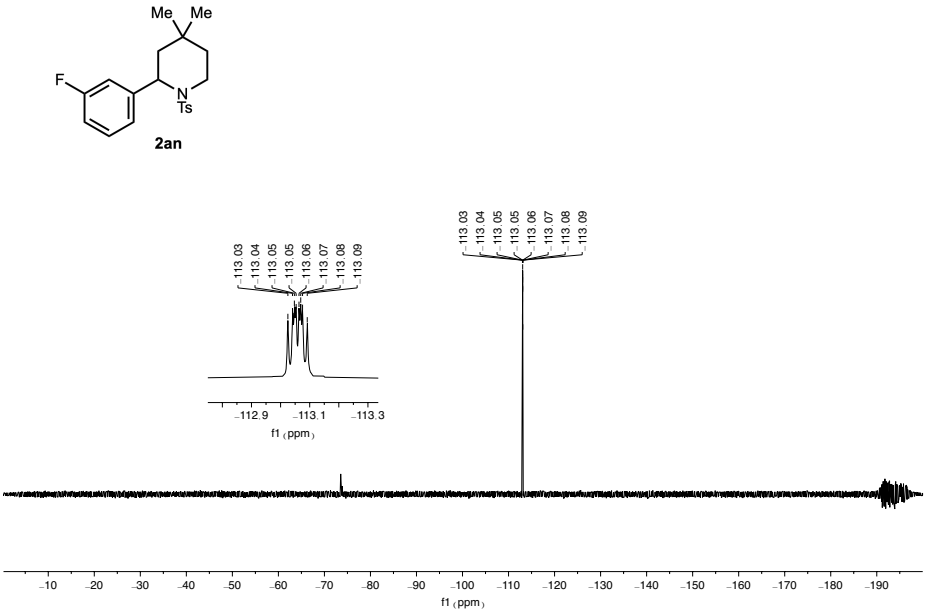
Me
Me
F
N
Ts
2an
113.03
113.04
113.05
113.06
113.07
113.08
113.09
112.9
113.1
113.3
f1 (ppm)
10
20
30
40
50
60
70
80
90
100
110
120
130
140
150
160
170
180
190

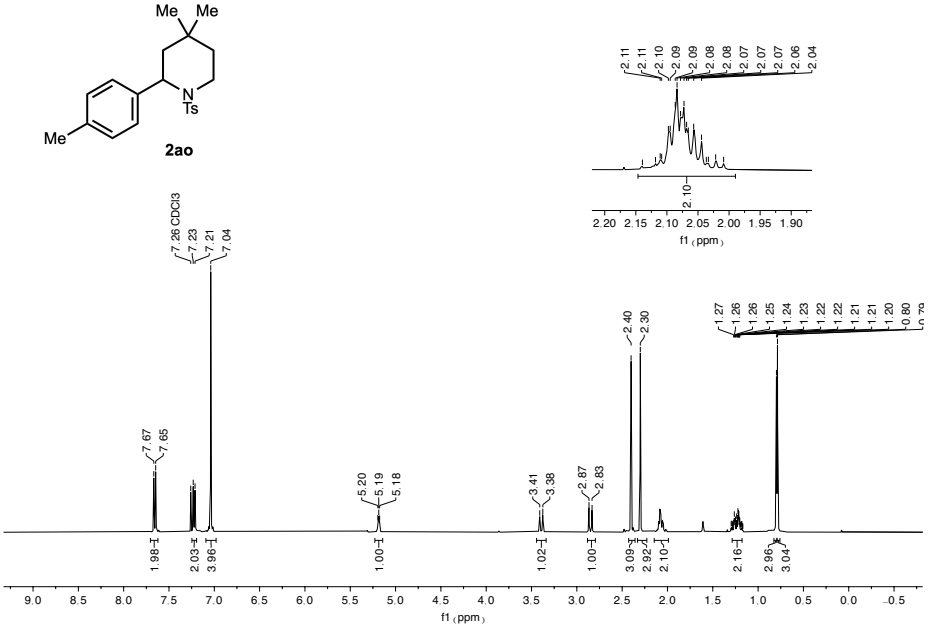
Me
Me
N
Ts
Me
2ao
2.11
2.10
2.09
2.08
2.07
2.06
2.04
2.10
2.20
2.15
2.10
2.05
2.00
1.95
1.90
f1 (ppm)
7.26 CDCl3
7.67
7.65
7.23
7.21
7.04
5.20
5.19
5.18
3.41
3.38
2.87
2.83
2.40
2.30
1.27
1.26
1.25
1.24
1.23
1.22
1.22
1.21
1.21
1.20
0.80
1.98
2.03
3.96
1.00
1.02
1.00
3.09
2.92
2.10
2.16
2.96
3.04
9.0
8.5
8.0
7.5
7.0
6.5
6.0
5.5
5.0
4.5
4.0
3.5
3.0
2.5
2.0
1.5
1.0
0.5
0.0
-0.5
f1 (ppm)

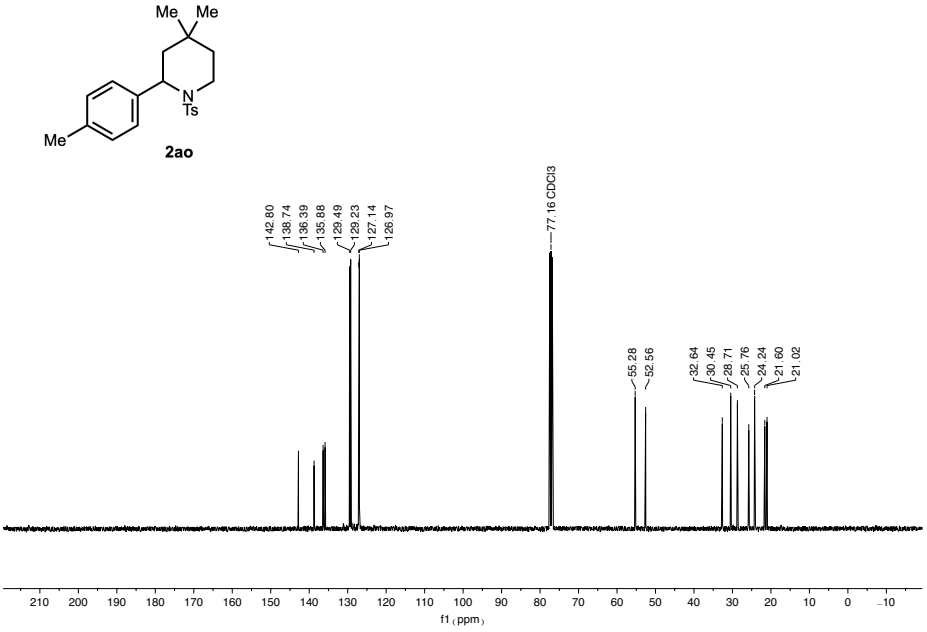
Me
Me
N
Ts
Me
2ao
142.80
138.74
136.39
135.88
129.49
129.23
127.14
126.97
77.16 CDCl3
55.28
52.56
32.64
30.45
28.71
25.76
24.24
21.60
21.02
f1 (ppm)

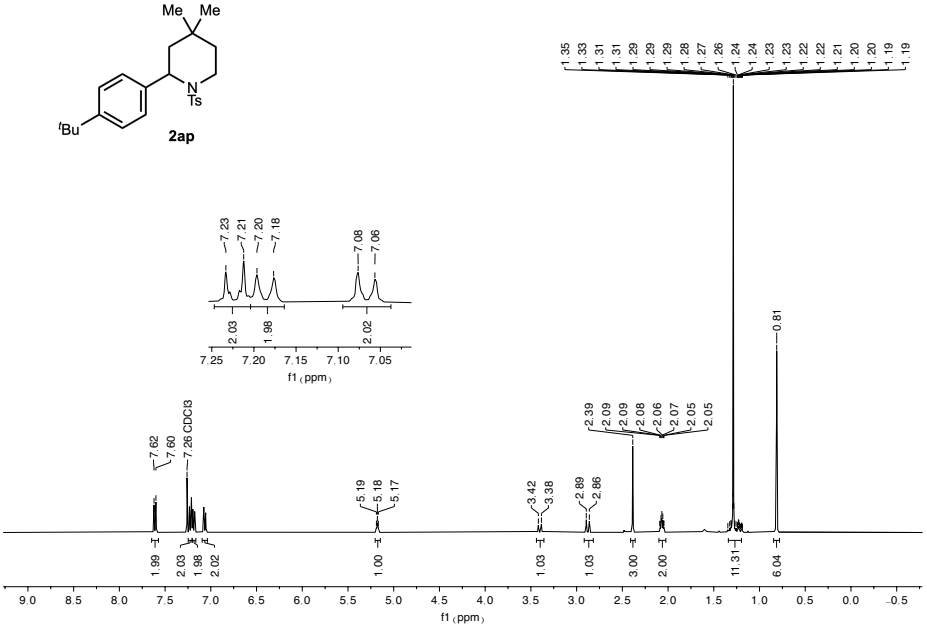
Me
Me
N
Ts
tBu
2ap
1.35
1.33
1.31
1.31
1.29
1.29
1.29
1.28
1.27
1.26
1.24
1.24
1.24
1.23
1.23
1.22
1.22
1.21
1.20
1.20
1.19
1.19
7.23
7.21
7.20
7.18
7.08
7.06
2.03
1.98
2.02
f1 (ppm)
7.62
7.60
7.26 CDCl3
5.19
5.18
5.17
3.42
3.38
2.89
2.86
2.39
2.09
2.09
2.08
2.06
2.07
2.05
2.05
0.81
1.99
2.03
1.98
2.02
1.00
1.03
1.03
3.00
2.00
11.31
6.04
f1 (ppm)

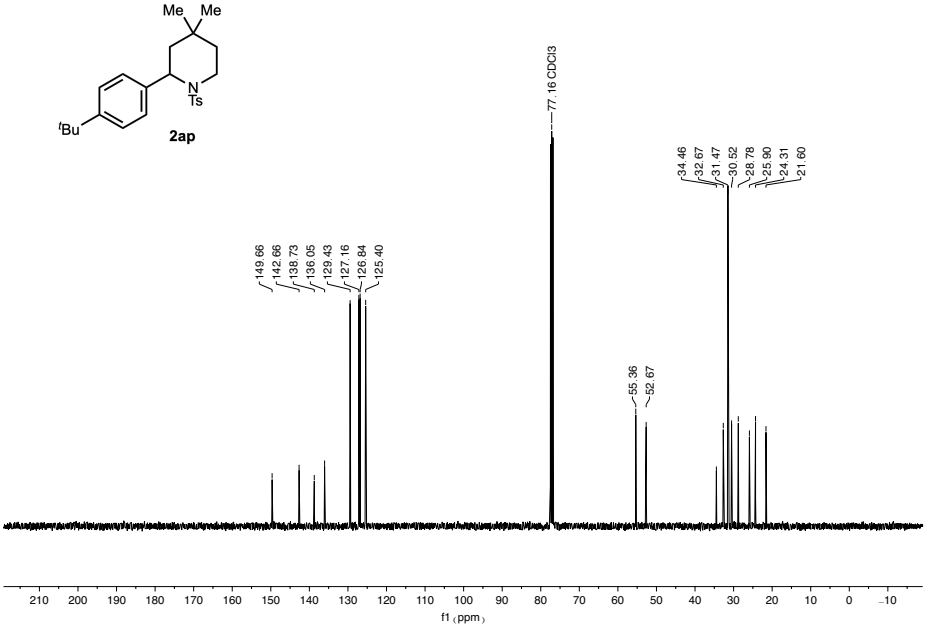
Me Me
N
Ts
tBu
2ap
77.16 CDCl3
149.66
142.66
138.73
136.05
129.43
127.16
126.84
125.40
55.36
52.67
34.46
32.67
31.47
30.52
28.78
25.90
24.31
21.60
f1 (ppm)

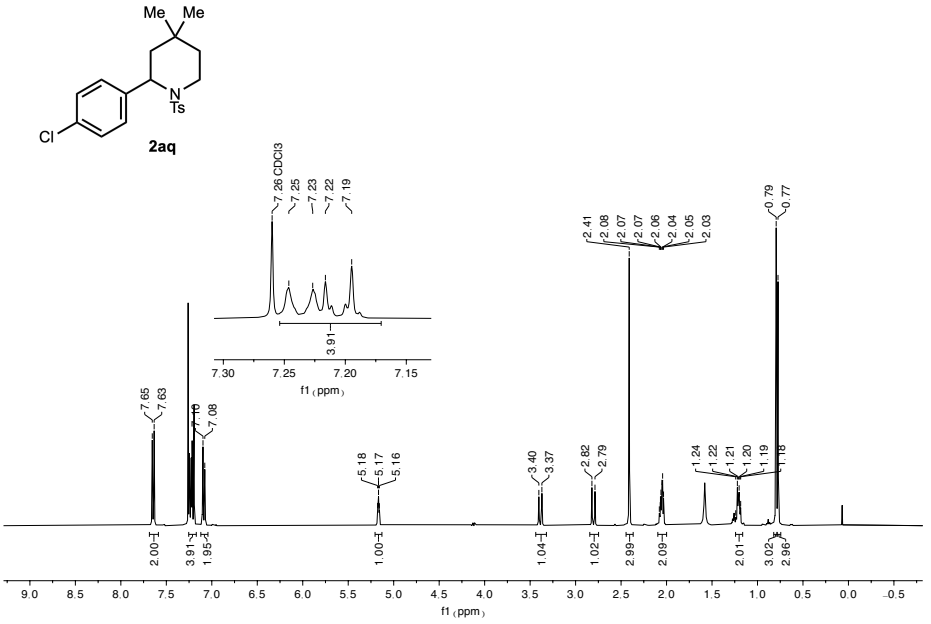
Me Me
N
Ts
Cl
2aq
7.26 CDCl3
7.25
7.23
7.22
7.19
3.91
7.30
7.25
7.20
7.15
f1 (ppm)
7.65
7.63
7.08
5.18
5.17
5.16
3.40
3.37
2.82
2.79
2.41
2.08
2.07
2.07
2.06
2.04
2.05
2.03
1.24
1.22
1.21
1.20
1.19
0.79
0.77
2.00
3.91
1.95
1.00
1.04
1.02
2.99
2.09
2.01
3.02
2.96
f1 (ppm)

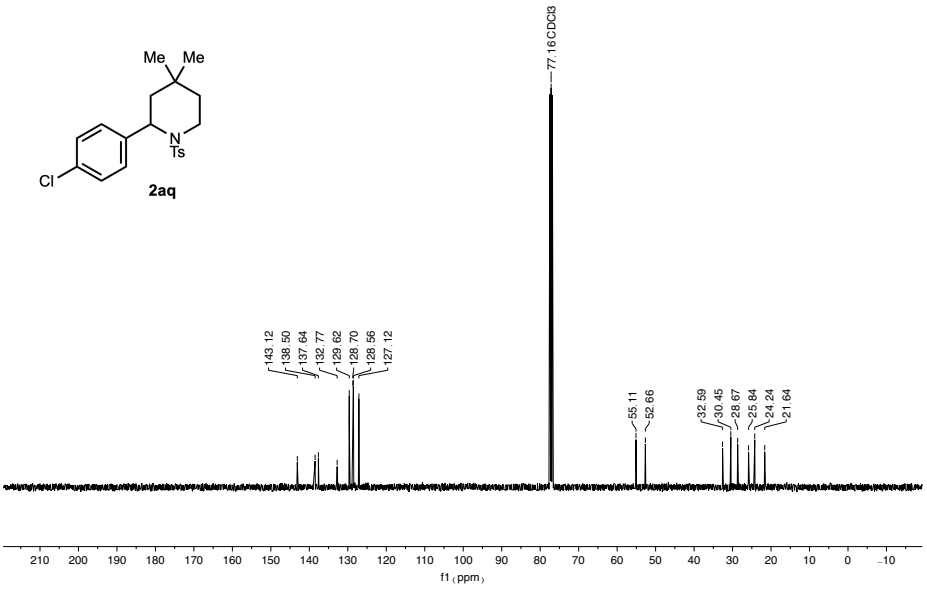
Me
Me
N
Ts
Cl
2aq
77.16 CDCl3
143.12
138.50
137.64
132.77
129.62
128.70
128.56
127.12
55.11
52.66
32.59
30.45
28.67
25.84
24.24
21.64
f1 (ppm)

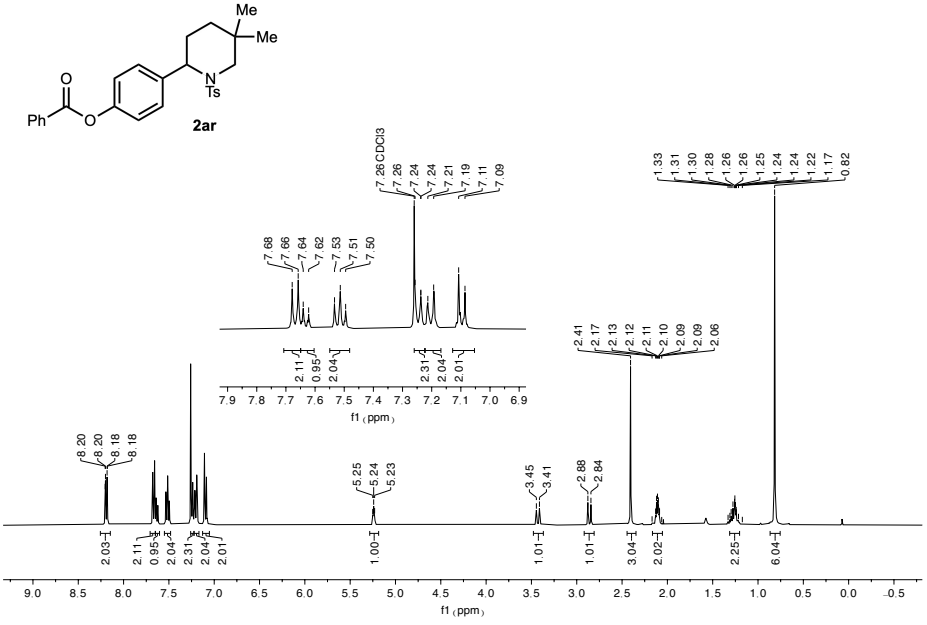
Me
Me
O
N
Ts
Ph
O
2ar
7.26 CDCl3
7.68
7.66
7.64
7.62
7.53
7.51
7.50
7.26
7.24
7.24
7.21
7.19
7.11
7.09
1.33
1.31
1.30
1.28
1.26
1.26
1.25
1.24
1.24
1.22
1.17
0.82
2.41
2.17
2.13
2.12
2.11
2.10
2.09
2.09
2.06
8.20
8.20
8.18
8.18
5.25
5.24
5.23
3.45
3.41
2.88
2.84
f1 (ppm)

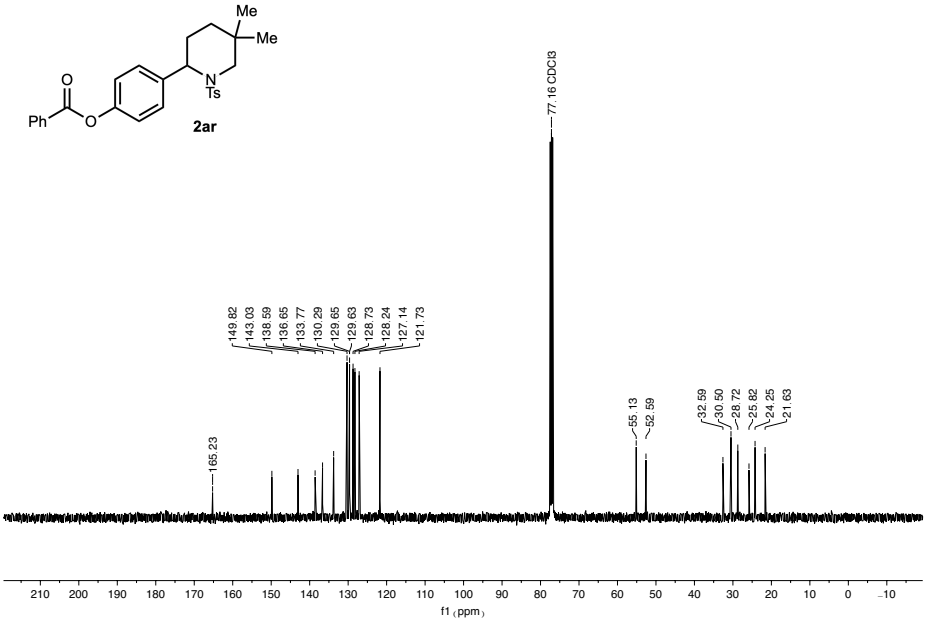
Me
Me
N
Ts
O
Ph
O
2ar
77.16 CDCl3
149.82
143.03
138.59
136.65
133.77
130.29
129.65
129.63
128.73
128.24
127.14
121.73
165.23
55.13
52.59
32.59
30.50
28.72
25.82
24.25
21.63
f1 (ppm)

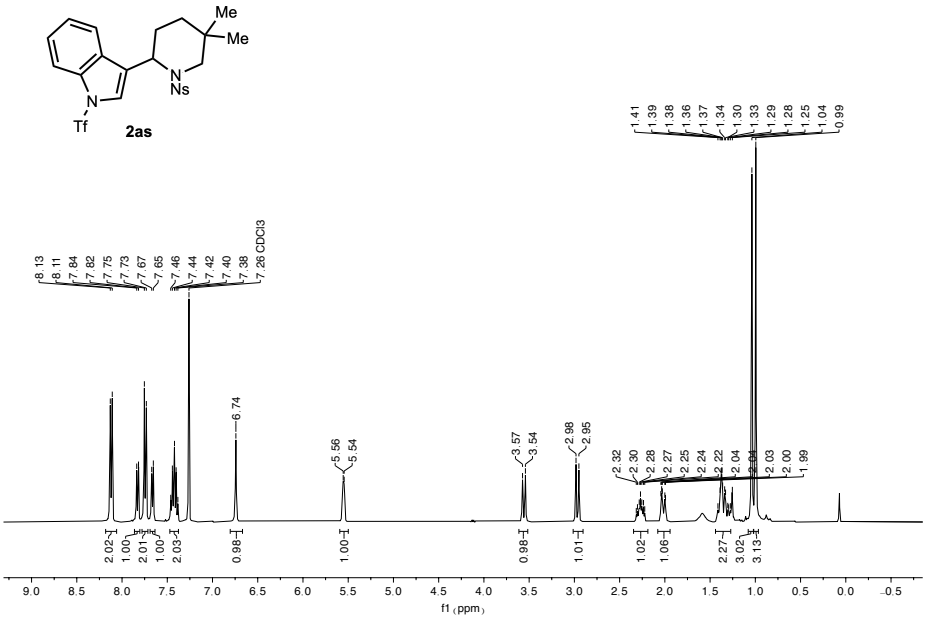
Me
Me
N
Ns
N
Tf
2as
1.41
1.39
1.38
1.36
1.37
1.34
1.30
1.33
1.29
1.28
1.25
1.04
0.99
8.13
8.11
7.84
7.82
7.75
7.73
7.67
7.65
7.46
7.44
7.42
7.40
7.38
7.26 CDCl3
6.74
5.56
5.54
3.57
3.54
2.98
2.95
2.32
2.30
2.28
2.27
2.25
2.24
2.22
2.04
2.03
2.00
1.99
2.02
1.00
2.01
1.00
2.03
0.98
1.00
0.98
1.01
1.02
1.06
2.27
3.02
3.13
f1 (ppm)

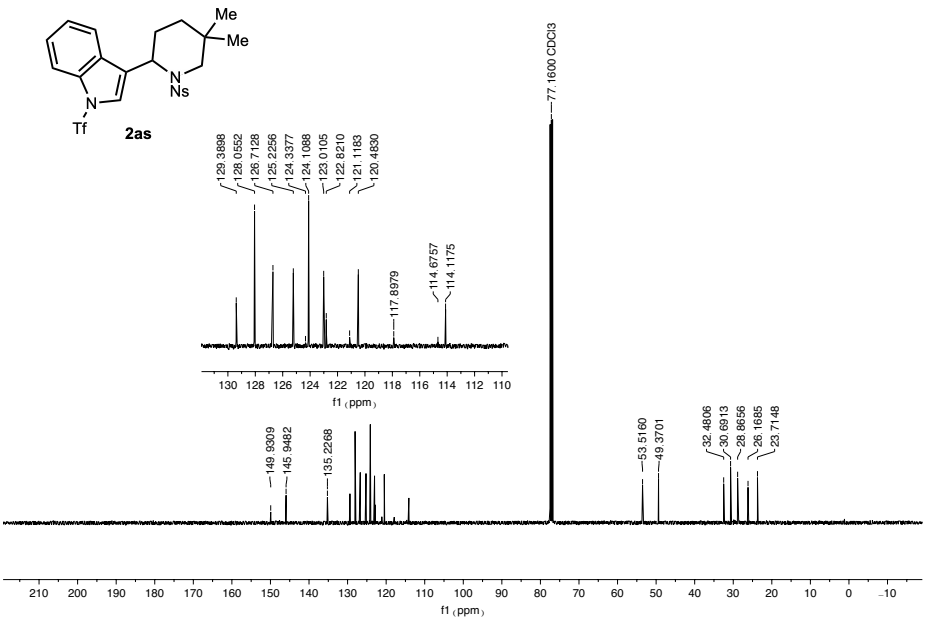
Me
Me
N
Ns
N
Tf
2as
129.3898
128.0552
126.7128
125.2256
124.3377
124.1068
123.0105
122.8210
121.1183
120.4830
117.8979
114.6757
114.1175
77.1600 CDCl3
149.9309
145.9482
135.2268
53.5160
49.3701
32.4806
30.6913
28.8656
26.1685
23.7148
f1 (ppm)

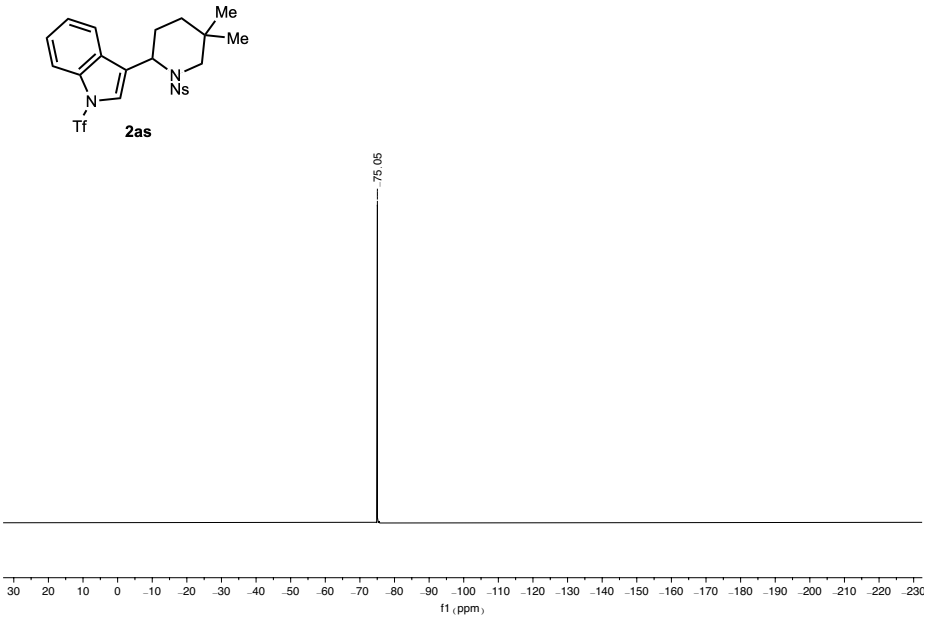
Me
Me
N
Ns
N
Tf
2as
75.05
f1 (ppm)

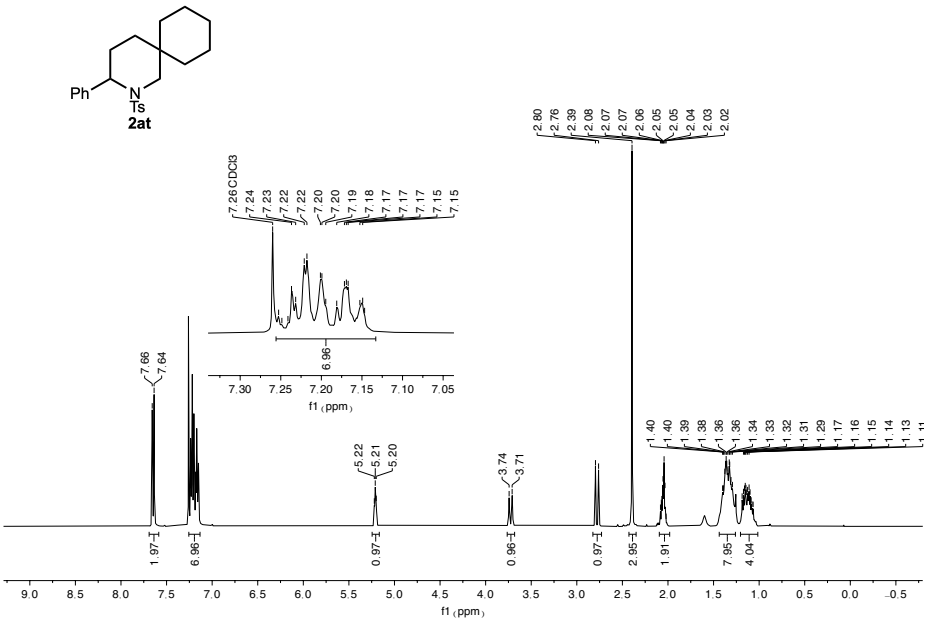
Ph
N
Ts
2at
7.26 CDCl3
7.66
7.64
5.22
5.21
5.20
3.74
3.71
2.80
2.76
2.39
2.08
2.07
2.07
2.06
2.05
2.05
2.04
2.03
2.02
1.40
1.40
1.39
1.38
1.36
1.36
1.34
1.33
1.32
1.31
1.29
1.17
1.16
1.15
1.14
1.13
1.97
6.96
0.97
0.96
0.97
2.95
1.91
7.95
4.04
f1 (ppm)

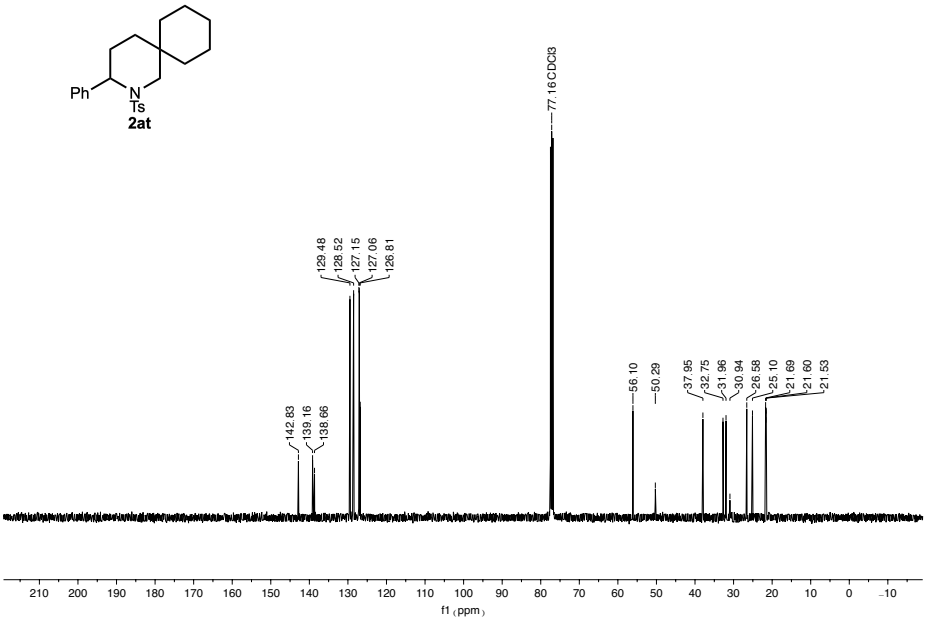
Ph
N
Ts
2at
77.16 CDCl3
129.48
128.52
127.15
127.06
126.81
142.83
139.16
138.66
56.10
50.29
37.95
32.75
31.96
30.94
26.58
25.10
21.69
21.60
21.53
f1 (ppm)

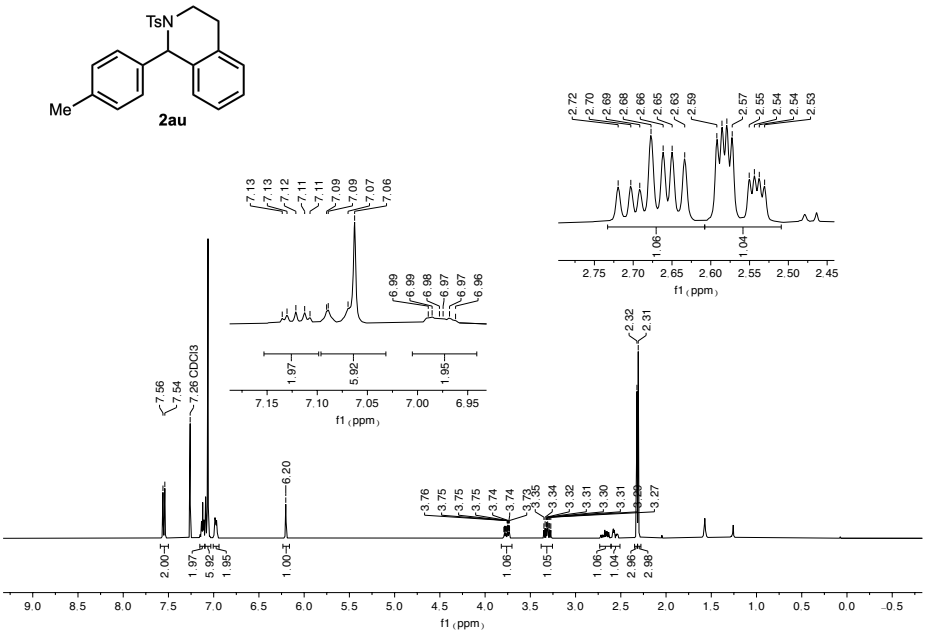
TsN
Me
2au
7.56
7.54
7.26 CDCl3
6.20
2.32
2.31
f1 (ppm)

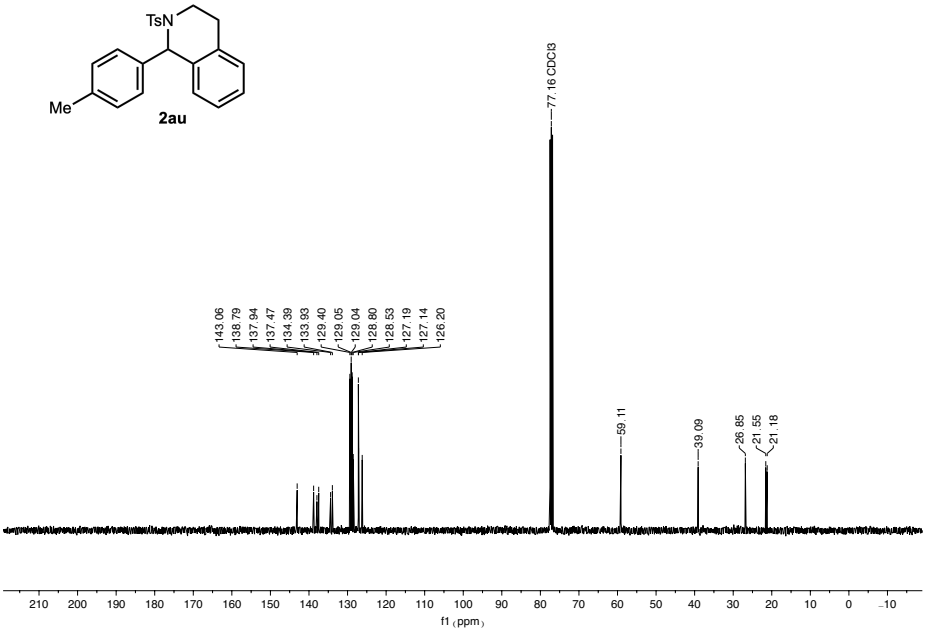
TsN
Me
2au
77.16 CDCl3
59.11
39.09
26.85
21.55
21.18
f1 (ppm)

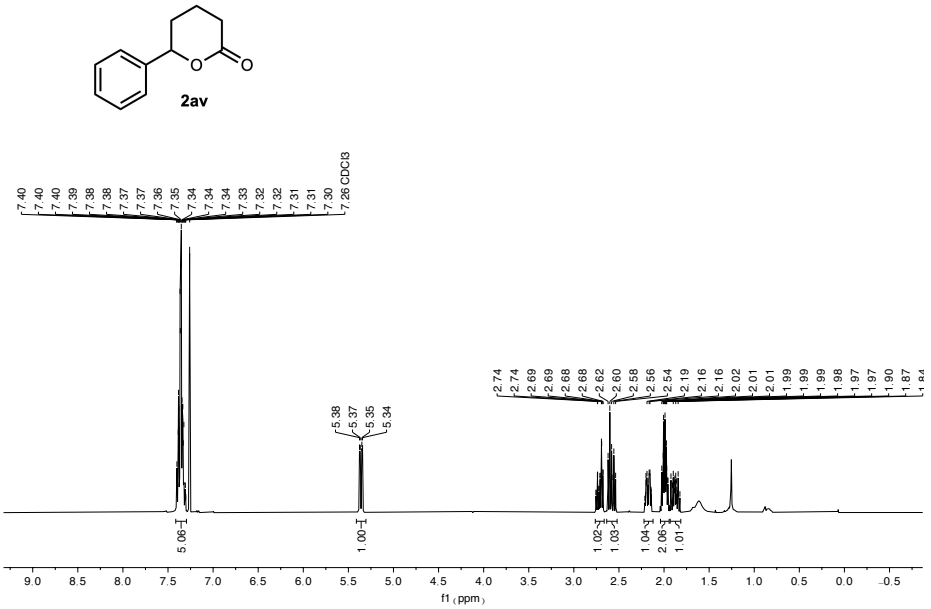
2av
7.40
7.40
7.40
7.39
7.38
7.38
7.37
7.37
7.36
7.35
7.34
7.34
7.34
7.33
7.32
7.31
7.31
7.30
7.26 CDCl3
5.38
5.37
5.35
5.34
2.74
2.74
2.69
2.69
2.68
2.68
2.62
2.60
2.58
2.56
2.54
2.19
2.16
2.16
2.02
2.01
2.01
1.99
1.99
1.99
1.98
1.97
1.97
1.90
1.87
5.06
1.00
1.02
1.03
1.04
2.06
1.01
f1 (ppm)

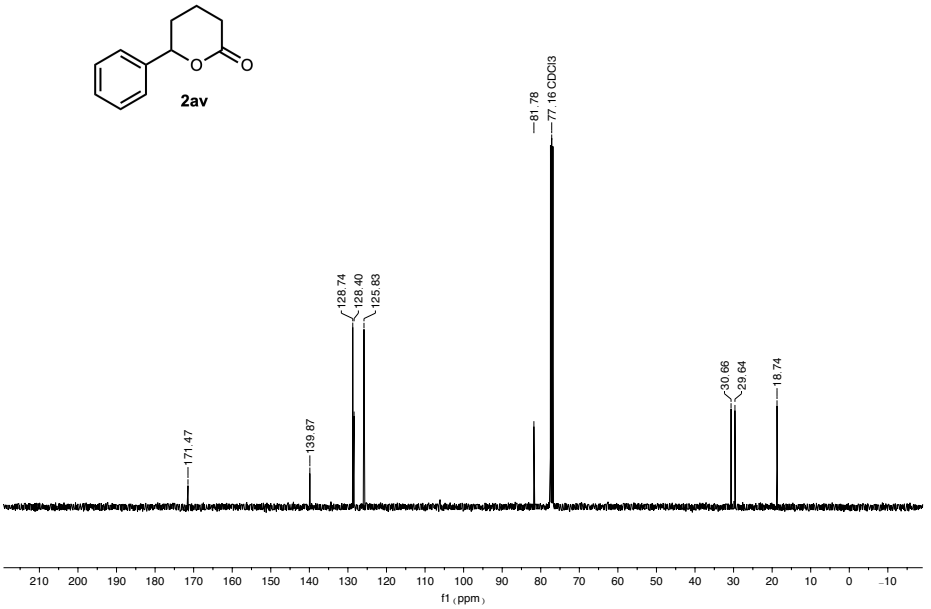
2av
171.47
139.87
128.74
128.40
125.83
81.78
77.16 CDCl3
30.66
29.64
18.74
f1 (ppm)

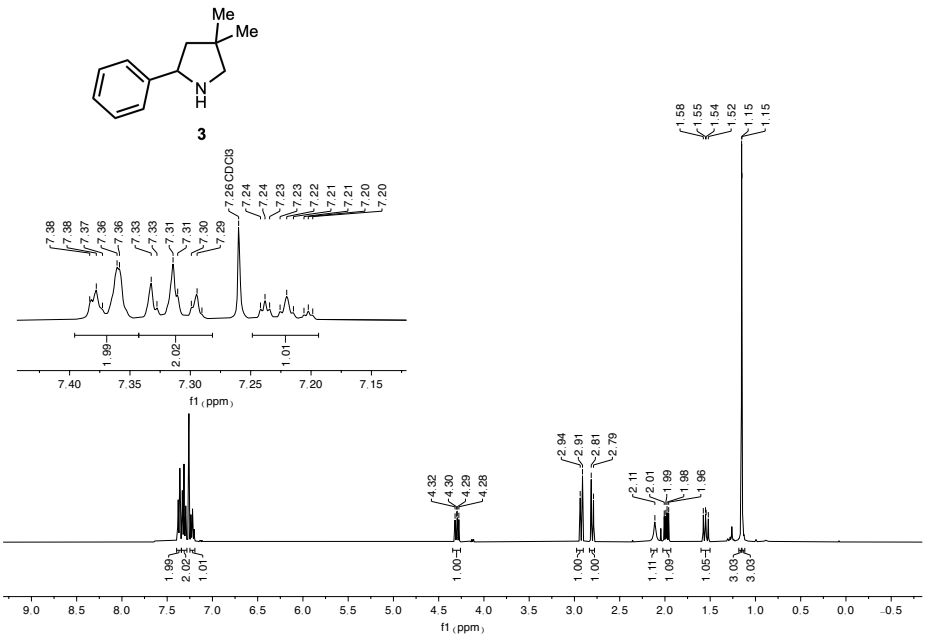

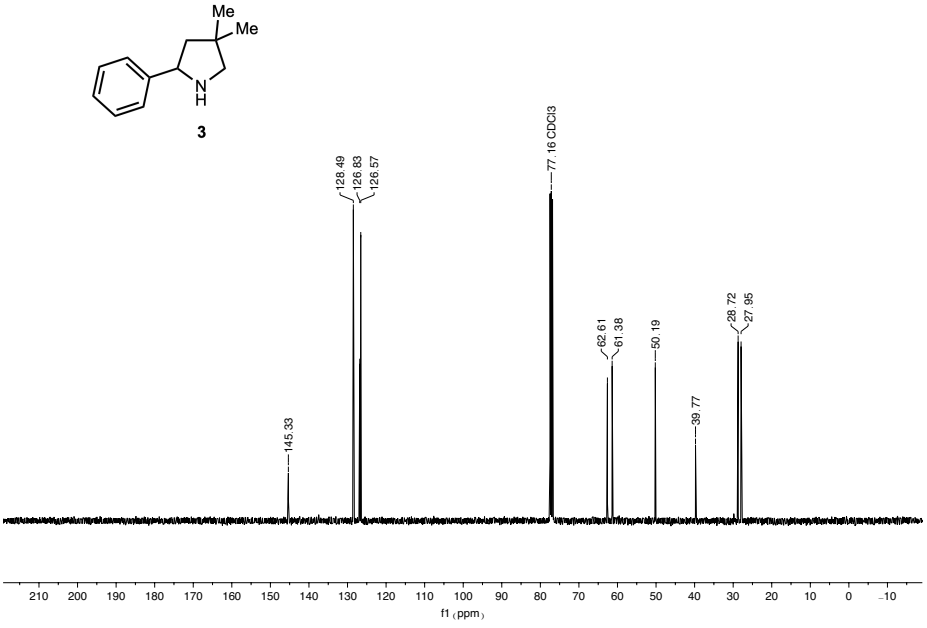

2.5.11. Cartesian coordinates of the optimized structures

1a

Atom	X	Y	Z

1	C	-0.9106	-2.1049	1.4552
2	C	0.4630	-2.2462	1.2543
3	C	1.0159	-2.3600	-0.0226
4	C	0.1378	-2.3088	-1.1126
5	C	-1.2309	-2.1688	-0.9361
6	C	-1.7681	-2.0851	0.3529
7	O	-3.1181	-1.9990	0.4306
8	C	-3.7017	-1.9491	1.7144
9	H	-4.7821	-1.8728	1.5586
10	H	-3.3594	-1.0732	2.2859
11	H	-3.4838	-2.8601	2.2912
12	H	-1.9107	-2.1411	-1.7874
13	H	0.5402	-2.3885	-2.1244
14	C	2.4959	-2.5837	-0.2097
15	C	3.4245	-1.4720	0.2903
16	C	3.5196	-0.1777	-0.5361
17	C	4.5812	0.7148	0.1045
18	H	4.3461	0.9311	1.1552
19	H	5.5669	0.2286	0.0702
20	H	4.6590	1.6751	-0.4270
21	C	3.9345	-0.4833	-1.9745
22	H	3.1540	-1.0256	-2.5273
23	H	4.8489	-1.0942	-1.9939
24	H	4.1400	0.4474	-2.5233
25	C	2.1925	0.5846	-0.6115
26	N	1.6877	0.9583	0.7136

27	S	0.6557	2.2585	0.8260
28	O	0.3601	2.4076	2.2468
29	O	1.2702	3.3498	0.0778
30	C	-0.8486	1.7955	0.0059
31	C	-1.9539	1.4250	0.7717
32	C	-3.1129	1.0174	0.1289
33	C	-3.1759	0.9377	-1.2666
34	C	-2.0573	1.3202	-2.0116
35	C	-0.8955	1.7601	-1.3862
36	H	-0.0394	2.0798	-1.9781
37	H	-2.0988	1.2758	-3.0999
38	C	-4.4168	0.4252	-1.9277
39	H	-5.2974	1.0158	-1.6400
40	H	-4.3343	0.4442	-3.0208
41	H	-4.6130	-0.6111	-1.6165
42	H	-3.9889	0.7415	0.7168
43	H	-1.9012	1.4696	1.8581
44	H	1.2964	0.1691	1.2371
45	H	2.3660	1.5164	-1.1669
46	H	1.4432	-0.0028	-1.1669
47	H	4.4442	-1.8873	0.3418
48	H	3.1612	-1.2181	1.3311
49	H	2.6991	-2.7947	-1.2699
50	H	2.7746	-3.5014	0.3321
51	H	1.1182	-2.2911	2.1271
52	H	-1.2987	-2.0326	2.4688

1j

	Atom	X	Y	Z
1	C	3.6407	0.3536	-1.1419
2	C	2.3561	0.5619	-0.6510
3	C	2.0738	1.6362	0.1982
4	C	3.1112	2.5078	0.5353
5	C	4.4002	2.3069	0.0441
6	C	4.6702	1.2277	-0.7934
7	H	5.6785	1.0672	-1.1732
8	H	5.1981	2.9951	0.3213
9	H	2.9048	3.3516	1.1960
10	C	0.6731	1.8446	0.7027
11	C	-0.2532	2.3684	-0.3960
12	C	-1.7259	2.5627	-0.0082
13	C	-1.8587	3.4993	1.1919
14	H	-2.9137	3.7497	1.3752
15	H	-1.3171	4.4390	1.0098
16	H	-1.4602	3.0520	2.1133
17	C	-2.4601	3.1842	-1.1962
18	H	-2.0803	4.1969	-1.3933
19	H	-3.5396	3.2634	-0.9975
20	H	-2.3225	2.5990	-2.1169
21	C	-2.3905	1.2379	0.3799
22	N	-2.4113	0.2782	-0.7309
23	S	-2.6378	-1.3325	-0.3522

24	O	-3.3827	-1.4828	0.8966
25	O	-3.1442	-1.9461	-1.5772
26	C	-0.9826	-1.8994	-0.0632
27	C	-0.2149	-2.3117	-1.1493
28	C	1.0895	-2.7381	-0.9300
29	C	1.6415	-2.7382	0.3550
30	C	0.8466	-2.3195	1.4283
31	C	-0.4651	-1.9073	1.2311
32	H	-1.0855	-1.6027	2.0723
33	H	1.2650	-2.3218	2.4351
34	C	3.0612	-3.1531	0.5874
35	H	3.1231	-3.9777	1.3105
36	H	3.5454	-3.4756	-0.3420
37	H	3.6466	-2.3206	1.0032
38	H	1.6984	-3.0662	-1.7728
39	H	-0.6374	-2.3066	-2.1526
40	H	-3.0648	0.5211	-1.4781
41	H	-3.4113	1.4335	0.7481
42	H	-1.8382	0.7750	1.2098
43	H	0.1371	3.3377	-0.7514
44	H	-0.2025	1.6835	-1.2583
45	H	0.2875	0.8856	1.0864
46	H	0.6891	2.5442	1.5514
47	H	1.5500	-0.1239	-0.9202
48	H	3.8396	-0.4972	-1.7946

2a

	Atom	X	Y	Z
1	C	-1.9745	-1.6600	1.0001
2	C	-0.6120	-1.4680	0.8656
3	C	0.0014	-1.5096	-0.3936
4	C	-0.7934	-1.7709	-1.5040
5	C	-2.1696	-1.9762	-1.3893
6	C	-2.7671	-1.9047	-0.1308
7	O	-4.0933	-2.0409	0.1015
8	C	-4.9459	-2.1698	-1.0164
9	H	-5.9651	-2.2189	-0.6233
10	H	-4.8591	-1.3024	-1.6882
11	H	-4.7360	-3.0876	-1.5848
12	H	-2.7597	-2.1649	-2.2831
13	H	-0.3341	-1.7918	-2.4940
14	C	1.4703	-1.2200	-0.5497
15	N	1.8556	0.0812	0.0575
16	S	1.4561	1.4809	-0.7291
17	O	2.3135	2.5332	-0.1868
18	O	1.4246	1.2491	-2.1738
19	C	-0.2121	1.7913	-0.2043
20	C	-0.4467	2.0951	1.1353
21	C	-1.7535	2.2678	1.5696
22	C	-2.8302	2.1344	0.6843
23	C	-2.5640	1.8538	-0.6588
24	C	-1.2610	1.6778	-1.1100

25	H	-1.0559	1.4406	-2.1520
26	H	-3.3943	1.7525	-1.3588
27	H	-1.9485	2.4979	2.6171
28	H	0.3859	2.1808	1.8340
29	C	3.0708	-0.0293	0.8824
30	C	3.6800	-1.3654	0.4482
31	C	4.5039	-1.1739	-0.8226
32	H	4.8214	-2.1438	-1.2319
33	H	3.9423	-0.6445	-1.6062
34	H	5.4071	-0.5842	-0.6101
35	C	4.5353	-1.9795	1.5432
36	H	5.3927	-1.3341	1.7839
37	H	3.9549	-2.1318	2.4645
38	H	4.9313	-2.9551	1.2265
39	C	2.4157	-2.1847	0.1675
40	H	2.6069	-3.0843	-0.4329
41	H	1.9656	-2.5031	1.1214
42	H	2.7947	-0.0487	1.9502
43	H	3.7420	0.8210	0.7156
44	H	1.7065	-1.1996	-1.6251
45	H	-0.0115	-1.2452	1.7497
46	H	-2.4623	-1.6012	1.9724
47	C	-4.2432	2.2367	1.1693
48	H	-4.6644	1.2336	1.3353
49	H	-4.3091	2.7819	2.1186
50	H	-4.8869	2.7367	0.4345

PIFA

	Atom	X	Y	Z
1	I	-0.0002	-0.2479	-0.0024
2	O	-2.1559	0.0351	0.0067
3	C	-2.7642	-1.1075	0.0493
4	O	-2.2579	-2.2111	0.0704
5	C	-4.2922	-0.9153	0.0653
6	F	-4.9197	-2.0802	0.1364
7	F	-4.6565	-0.1735	1.1113
8	F	-4.6884	-0.2882	-1.0426
9	O	2.1557	0.0347	-0.0095
10	C	2.7635	-1.1081	-0.0552
11	O	2.2566	-2.2113	-0.0812
12	C	4.2916	-0.9167	-0.0684
13	F	4.6866	-0.2917	1.0411
14	F	4.6579	-0.1735	-1.1128
15	F	4.9185	-2.0819	-0.1404
16	C	0.0002	1.8460	0.0021
17	C	-0.4204	2.5062	1.1522
18	C	-0.4202	3.8981	1.1414
19	C	0.0019	4.5904	0.0086
20	C	0.4231	3.9029	-1.1274
21	C	0.4218	2.5111	-1.1447
22	H	0.7425	1.9622	-2.0278
23	H	0.7500	4.4485	-2.0104

24	H	0.0026	5.6789	0.0112
25	H	-0.7464	4.4399	2.0270
26	H	-0.7417	1.9536	2.0328

CT-1a

	Atom	X	Y	Z
1	C	6.1790	0.1255	1.7059
2	C	6.1082	0.2029	0.3117
3	C	4.8900	0.2420	-0.3618
4	C	3.7209	0.2110	0.4147
5	C	3.7675	0.1468	1.7969
6	C	5.0043	0.0926	2.4533
7	H	2.8567	0.1373	2.3955
8	H	2.7514	0.2510	-0.0866
9	C	4.7709	0.3391	-1.8628
10	C	6.0864	0.2198	-2.6156
11	C	6.0050	0.2400	-4.1482
12	C	5.3023	1.5011	-4.6480
13	H	5.3676	1.5738	-5.7436
14	H	5.7699	2.3964	-4.2144
15	H	4.2369	1.5151	-4.3775
16	C	7.4305	0.2235	-4.7008
17	H	7.9647	1.1398	-4.4112
18	H	7.4297	0.1683	-5.8000
19	H	8.0105	-0.6272	-4.3151
20	C	5.2294	-0.9664	-4.6871

21	N	5.8682	-2.2368	-4.3248
22	S	4.9041	-3.5910	-4.2486
23	O	3.8541	-3.5765	-5.2672
24	O	5.8341	-4.7175	-4.2029
25	C	4.1227	-3.3969	-2.6685
26	C	4.9123	-3.3944	-1.5193
27	C	4.2971	-3.2877	-0.2797
28	C	2.9045	-3.1907	-0.1722
29	C	2.1385	-3.1804	-1.3423
30	C	2.7374	-3.2868	-2.5920
31	H	2.1420	-3.2846	-3.5028
32	H	1.0543	-3.0911	-1.2698
33	C	2.2392	-3.1062	1.1666
34	H	1.7360	-4.0526	1.4117
35	H	2.9615	-2.8974	1.9649
36	H	1.4684	-2.3238	1.1817
37	H	4.9043	-3.2708	0.6263
38	H	5.9968	-3.4678	-1.5961
39	H	6.7034	-2.4609	-4.8691
40	H	5.1210	-0.8805	-5.7810
41	H	4.2121	-0.9724	-4.2687
42	H	6.7458	1.0495	-2.3131
43	H	6.6007	-0.7051	-2.3075
44	H	4.0658	-0.4408	-2.1991
45	H	4.2895	1.3014	-2.1080
46	H	7.0433	0.2366	-0.2457

47	H	7.1532	0.0956	2.1883
48	I	4.7346	3.6304	0.9091
49	O	2.8881	3.5412	2.0551
50	C	1.9360	3.1804	1.2552
51	O	2.0122	3.0188	0.0524
52	C	0.6235	2.9372	2.0214
53	F	-0.3626	2.6280	1.1924
54	F	0.7817	1.9299	2.8831
55	F	0.2731	4.0197	2.7139
56	O	6.7856	3.7251	0.1543
57	C	6.7373	3.5999	-1.1313
58	O	5.7389	3.5124	-1.8225
59	C	8.1425	3.5289	-1.7561
60	F	8.7326	2.3841	-1.3980
61	F	8.9088	4.5342	-1.3430
62	F	8.0745	3.5640	-3.0810
63	C	5.5920	4.1975	2.7375
64	C	5.4706	3.3369	3.8237
65	C	6.0346	3.7278	5.0351
66	C	6.7115	4.9408	5.1354
67	C	6.8210	5.7826	4.0309
68	C	6.2495	5.4214	2.8140
69	H	6.3183	6.0792	1.9498
70	H	7.3451	6.7327	4.1138
71	H	7.1559	5.2348	6.0845
72	H	5.9469	3.0718	5.8998

73	H	4.9401	2.3894	3.7408
74	O	4.9536	0.0341	3.8102
75	C	6.1783	-0.0809	4.5055
76	H	5.9269	-0.1131	5.5696
77	H	6.7099	-1.0036	4.2302
78	H	6.8367	0.7806	4.3166

CT-1j

	Atom	X	Y	Z
1	C	5.8021	0.3785	1.7739
2	C	5.8967	0.4219	0.3819
3	C	4.7482	0.4532	-0.4130
4	C	3.5020	0.4639	0.2283
5	C	3.4020	0.4306	1.6139
6	C	4.5569	0.3763	2.3959
7	H	4.4830	0.3383	3.4826
8	H	2.4197	0.4477	2.0872
9	H	2.5957	0.5000	-0.3805
10	C	4.7813	0.4813	-1.9212
11	C	6.1656	0.3988	-2.5407
12	C	6.2256	0.3463	-4.0736
13	C	5.4723	1.5189	-4.6997
14	H	5.6504	1.5600	-5.7843
15	H	5.8058	2.4689	-4.2600
16	H	4.3868	1.4416	-4.5447
17	C	7.6940	0.4271	-4.4921

18	H	8.1193	1.3985	-4.2012
19	H	7.8032	0.3231	-5.5821
20	H	8.3018	-0.3525	-4.0104
21	C	5.5985	-0.9407	-4.6184
22	N	6.2703	-2.1428	-4.1124
23	S	5.3851	-3.5523	-4.0712
24	O	4.4856	-3.6698	-5.2189
25	O	6.3629	-4.6097	-3.8236
26	C	4.3855	-3.3092	-2.6266
27	C	5.0060	-3.2471	-1.3797
28	C	4.2226	-3.0886	-0.2449
29	C	2.8288	-2.9938	-0.3383
30	C	2.2346	-3.0431	-1.6035
31	C	3.0030	-3.2060	-2.7502
32	H	2.5406	-3.2528	-3.7342
33	H	1.1511	-2.9576	-1.6885
34	C	1.9823	-2.8531	0.8887
35	H	1.4647	-3.7965	1.1148
36	H	2.5838	-2.5860	1.7660
37	H	1.2053	-2.0886	0.7536
38	H	4.6964	-3.0332	0.7357
39	H	6.0904	-3.3172	-1.2995
40	H	7.1762	-2.3360	-4.5438
41	H	5.6069	-0.9202	-5.7208
42	H	4.5435	-0.9951	-4.3121
43	H	6.7497	1.2757	-2.2205

44	H	6.6979	-0.4802	-2.1433
45	H	4.1478	-0.3458	-2.2861
46	H	4.2832	1.4070	-2.2523
47	H	6.8827	0.4332	-0.0821
48	H	6.7117	0.3500	2.3739
49	I	4.6478	3.8733	0.9996
50	O	2.9991	3.8128	2.4109
51	C	1.8930	3.5209	1.8036
52	O	1.7203	3.3813	0.6100
53	C	0.7461	3.3316	2.8135
54	F	-0.4040	3.1061	2.1954
55	F	1.0093	2.2900	3.6073
56	F	0.6091	4.4099	3.5835
57	O	6.6038	4.0104	0.0452
58	C	6.4973	3.8571	-1.2338
59	O	5.4790	3.6933	-1.8780
60	C	7.8828	3.8762	-1.9085
61	F	8.5718	2.7896	-1.5425
62	F	8.5817	4.9481	-1.5454
63	F	7.7750	3.8728	-3.2315
64	C	5.7261	4.4965	2.6851
65	C	5.9040	3.6024	3.7348
66	C	6.6155	4.0362	4.8497
67	C	7.1362	5.3276	4.8901
68	C	6.9472	6.2016	3.8219
69	C	6.2286	5.7936	2.7018

70	H	6.0669	6.4699	1.8646
71	H	7.3528	7.2108	3.8589
72	H	7.6946	5.6570	5.7645
73	H	6.7657	3.3560	5.6858
74	H	5.4973	2.5936	3.6861

PIFAanion

	Atom	X	Y	Z
1	I	-0.0104	-0.0902	0.0127
2	O	-2.7622	0.2295	0.1235
3	C	-3.0524	-0.9902	0.0900
4	O	-2.3354	-1.9943	0.0237
5	C	-4.5851	-1.2250	0.1548
6	F	-4.9249	-2.5117	0.0596
7	F	-5.0854	-0.7659	1.3122
8	F	-5.2161	-0.5732	-0.8324
9	O	2.7247	0.2181	-0.0584
10	C	3.0352	-0.9979	-0.0854
11	O	2.3359	-2.0150	-0.0652
12	C	4.5733	-1.1995	-0.1388
13	F	5.1501	-0.7207	0.9743
14	F	5.1128	-0.5423	-1.1751
15	F	4.9327	-2.4794	-0.2514
16	C	0.0048	2.0014	0.0024
17	C	-0.6096	2.6944	1.0450
18	C	-0.6036	4.0863	1.0249

19	C	0.0152	4.7712	-0.0188
20	C	0.6288	4.0657	-1.0520
21	C	0.6239	2.6739	-1.0509
22	H	1.1037	2.1169	-1.8535
23	H	1.1133	4.5993	-1.8683
24	H	0.0189	5.8600	-0.0274
25	H	-1.0844	4.6360	1.8326
26	H	-1.0947	2.1532	1.8550

A-1a

	Atom	X	Y	Z
1	C	3.7356	1.0039	-1.4688
2	C	2.4239	1.3064	-1.2346
3	C	1.9346	1.4027	0.0939
4	C	2.8389	1.1720	1.1765
5	C	4.1552	0.8751	0.9677
6	C	4.6221	0.7753	-0.3720
7	H	4.8262	0.7096	1.8060
8	H	2.4537	1.2476	2.1929
9	C	0.5308	1.7486	0.4297
10	C	-0.3950	2.0838	-0.7266
11	C	-1.8280	2.4717	-0.3290
12	C	-1.8327	3.6641	0.6265
13	H	-2.8583	4.0264	0.7859
14	H	-1.2435	4.4955	0.2130
15	H	-1.4182	3.4103	1.6125

16	C	-2.5844	2.8560	-1.5995
17	H	-2.1407	3.7529	-2.0549
18	H	-3.6386	3.0785	-1.3773
19	H	-2.5545	2.0538	-2.3504
20	C	-2.5527	1.3206	0.3766
21	N	-2.6950	0.1384	-0.4798
22	S	-2.6325	-1.3623	0.2362
23	O	-3.1927	-1.3497	1.5862
24	O	-3.1743	-2.2832	-0.7593
25	C	-0.8822	-1.6188	0.3852
26	C	-0.1266	-1.7422	-0.7806
27	C	1.2381	-1.9621	-0.6772
28	C	1.8596	-2.0699	0.5765
29	C	1.0810	-1.9233	1.7283
30	C	-0.2907	-1.7046	1.6420
31	H	-0.9003	-1.6029	2.5380
32	H	1.5556	-1.9947	2.7070
33	C	3.3198	-2.3796	0.6679
34	H	3.4890	-3.4637	0.5906
35	H	3.8811	-1.9173	-0.1567
36	H	3.7480	-2.0502	1.6229
37	H	1.8397	-2.0643	-1.5809
38	H	-0.6042	-1.6631	-1.7565
39	H	-3.4848	0.1689	-1.1266
40	H	-3.5405	1.6661	0.7213
41	H	-1.9983	1.0232	1.2783

42	H	0.0316	2.9242	-1.2990
43	H	-0.4441	1.2276	-1.4181
44	H	0.1394	0.8981	1.0227
45	H	0.5741	2.5749	1.1614
46	H	1.7506	1.4749	-2.0714
47	H	4.1385	0.9205	-2.4757
48	O	5.8479	0.4626	-0.7063
49	C	6.8254	0.1613	0.3043
50	H	6.5023	-0.7076	0.8885
51	H	7.7422	-0.0698	-0.2391
52	H	6.9782	1.0306	0.9526

A-1j

	Atom	X	Y	Z
1	C	3.7520	0.8353	-1.3377
2	C	2.4107	1.0635	-1.1236
3	C	1.9063	1.2159	0.20328
4	C	2.8027	1.0660	1.29895
5	C	4.1386	0.8439	1.08217
6	C	4.6247	0.7304	-0.2424
7	H	5.6860	0.5571	-0.4113
8	H	4.8296	0.7563	1.91729
9	H	2.4077	1.1657	2.30945
10	C	0.4992	1.5679	0.50015
11	C	-0.3851	1.9899	-0.6609
12	C	-1.7961	2.4621	-0.2733

13	C	-1.7365	3.6900	0.63447
14	H	-2.7446	4.0959	0.80052
15	H	-1.1278	4.4817	0.17476
16	H	-1.3094	3.4622	1.62134
17	C	-2.5359	2.8365	-1.5564
18	H	-2.0340	3.6757	-2.059
19	H	-3.5691	3.1446	-1.3385
20	H	-2.5709	1.9983	-2.2668
21	C	-2.5817	1.3808	0.47761
22	N	-2.7678	0.1604	-0.3132
23	S	-2.6155	-1.3242	0.40122
24	O	-2.9620	-1.2862	1.81891
25	O	-3.2883	-2.2604	-0.4929
26	C	-0.8583	-1.6009	0.30153
27	C	-0.2610	-1.6287	-0.9579
28	C	1.1008	-1.8614	-1.0468
29	C	1.8751	-2.0921	0.1118
30	C	1.2455	-2.0457	1.368
31	C	-0.1150	-1.8078	1.46937
32	H	-0.6123	-1.7841	2.43678
33	H	1.8371	-2.2225	2.26586
34	C	3.3190	-2.4181	0.00092
35	H	3.5859	-3.2660	0.64562
36	H	3.6122	-2.6425	-1.0305
37	H	3.9374	-1.5699	0.34821
38	H	1.5855	-1.9000	-2.0218

39	H	-0.8557	-1.4651	-1.8555
40	H	-3.5554	0.1609	-0.9616
41	H	-3.5623	1.7849	0.77354
42	H	-2.0697	1.1111	1.41191
43	H	0.1035	2.8139	-1.2064
44	H	-0.4781	1.1569	-1.3753
45	H	0.0758	0.6808	1.02024
46	H	0.5171	2.3333	1.29528
47	H	1.7286	1.1588	-1.9658
48	H	4.1385	0.7376	-2.3492

OTFAanion

	Atom	X	Y	Z
1	O	-1.8145	1.7706	-0.3050
2	C	-1.0337	2.7275	-0.1888
3	O	-0.3910	3.1779	0.7754
4	C	-0.7735	3.5399	-1.4934
5	F	-1.0321	4.8535	-1.3284
6	F	-1.4982	3.1459	-2.5534
7	F	0.5206	3.4580	-1.8708

IPhOTFAradical

	Atom	X	Y	Z
1	I	-0.1293	-0.0807	0.3217
2	O	-2.7016	0.1203	-0.0637
3	C	-2.9993	-1.1064	0.0265
4	O	-2.2874	-2.0835	0.2363

5	C	-4.5241	-1.3287	-0.1675
6	F	-4.8533	-2.6134	-0.0956
7	F	-5.2121	-0.6732	0.7710
8	F	-4.9167	-0.8679	-1.3576
9	C	0.0399	1.9870	0.1789
10	C	-0.0537	2.7591	1.3403
11	C	0.0667	4.1402	1.2377
12	C	0.2730	4.7362	-0.0057
13	C	0.3599	3.9544	-1.1569
14	C	0.2426	2.5717	-1.0746
15	H	0.3072	1.9541	-1.9682
16	H	0.5193	4.4228	-2.1264
17	H	0.3658	5.8183	-0.0783
18	H	-0.0016	4.7529	2.1348
19	H	-0.2168	2.2858	2.3066

PhI

	Atom	X	Y	Z
1	C	0.8644	-1.2145	0.0000
2	C	2.2571	-1.2130	0.0005
3	C	2.9608	-0.0107	0.0000
4	C	2.2526	1.1896	-0.0010
5	C	0.8591	1.2029	-0.0015
6	C	0.1695	-0.0076	-0.0009
7	H	0.3199	-2.1570	0.0004
8	H	2.8066	-2.1529	0.0012

9	H	4.0493	-0.0104	0.0004
10	H	0.3152	2.1456	-0.0022
11	H	-0.9193	-0.0015	-0.0013
12	I	3.3088	3.0185	-0.0016

OTFAradical

	Atom	X	Y	Z
1	O	3.4837	0.4781	0.1163
2	C	4.5257	1.1233	-0.1104
3	O	5.4711	0.8579	0.6649
4	C	4.6277	2.1483	-1.2410
5	F	3.7286	3.1034	-1.0480
6	F	4.3751	1.5513	-2.3979
7	F	5.8399	2.6745	-1.2657

CO_2

	Atom	X	Y	Z
1	O	-2.4831	1.0020	0.5123
2	C	-2.4051	0.8413	-0.6386
3	O	-2.3268	0.6806	-1.7895

CF_3radical

	Atom	X	Y	Z
1	C	-2.0986	0.1708	0.0296
2	F	-1.6422	0.8164	1.0805
3	F	-1.6420	-1.0621	-0.0040
4	F	-3.4130	0.1904	-0.0039

HFIP

	Atom	X	Y	Z
1	C	-2.3097	-0.8807	0.0284
2	H	-1.9492	-0.4025	-0.8961
3	O	-1.8695	-0.2591	1.1916
4	H	-1.9165	0.7023	1.0661
5	C	-1.7374	-2.2886	0.0513
6	C	-3.8330	-0.8661	-0.0247
7	F	-4.3771	-1.5597	0.9746
8	F	-4.2950	-1.3602	-1.1730
9	F	-4.2555	0.3980	0.0809
10	F	-2.0319	-2.9272	1.1821
11	F	-0.4101	-2.2391	-0.0532
12	F	-2.2074	-3.0113	-0.9670

HFIPradical

	Atom	X	Y	Z
1	C	1.2590	-0.9849	0.1883
2	O	1.9466	-0.0883	0.8998
3	H	1.4291	0.7341	0.9995
4	C	1.8892	-2.3264	0.1214
5	C	-0.1993	-0.8186	-0.0628
6	F	-0.9329	-1.7176	0.6082
7	F	-0.5143	-0.9531	-1.3522
8	F	-0.5809	0.4028	0.3319
9	F	1.9020	-2.9377	1.3171

10	F	3.1584	-2.2454	-0.2813
11	F	1.2199	-3.1120	-0.7244

TFA

	Atom	X	Y	Z
1	O	-1.9729	2.0202	-0.3330
2	C	-0.7680	2.5685	-0.3916
3	O	0.1697	2.3349	0.3194
4	C	-0.7301	3.5859	-1.5418
5	F	-1.6484	4.5314	-1.3515
6	F	-0.9898	2.9812	-2.6996
7	F	0.4612	4.1555	-1.6147
8	H	-1.9828	1.3732	0.4029

A'-1a

	Atom	X	Y	Z
1	C	3.1908	-0.2948	-2.6501
2	C	1.9150	0.1156	-2.3815
3	C	1.5288	0.4211	-1.0515
4	C	2.4922	0.2843	0.0011
5	C	3.7751	-0.1132	-0.2527
6	C	4.1409	-0.4171	-1.5890
7	H	4.4963	-0.2051	0.5553
8	H	2.1507	0.5005	1.0200
9	C	0.1831	0.8882	-0.6673
10	C	-0.8477	1.0871	-1.7611
11	C	-2.2077	1.6097	-1.2685

12	C	-2.0550	2.9572	-0.5623
13	H	-3.0431	3.3742	-0.3170
14	H	-1.5434	3.6769	-1.2187
15	H	-1.4845	2.8825	0.3744
16	C	-3.1193	1.7901	-2.4810
17	H	-2.7156	2.5605	-3.1537
18	H	-4.1262	2.1095	-2.1725
19	H	-3.2180	0.8622	-3.0623
20	C	-2.8572	0.6411	-0.2739
21	N	-3.1570	-0.6616	-0.8792
22	S	-3.0772	-2.0165	0.0880
23	O	-3.4168	-1.7123	1.4759
24	O	-3.8304	-3.0407	-0.6326
25	C	-1.3492	-2.4115	0.0265
26	C	-0.8313	-2.9513	-1.1534
27	C	0.5189	-3.2520	-1.2169
28	C	1.3622	-3.0222	-0.1175
29	C	0.8208	-2.4578	1.0386
30	C	-0.5354	-2.1519	1.1224
31	H	-0.9405	-1.6839	2.0173
32	H	1.4672	-2.2358	1.8869
33	C	2.8100	-3.3912	-0.1964
34	H	2.9374	-4.4828	-0.1593
35	H	3.2563	-3.0591	-1.1457
36	H	3.3837	-2.9622	0.6344
37	H	0.9385	-3.6737	-2.1309

38	H	-1.4829	-3.1311	-2.0075
39	H	-4.0254	-0.6908	-1.4156
40	H	-3.7737	1.0949	0.1374
41	H	-2.1927	0.4736	0.5858
42	H	-0.4629	1.8043	-2.5056
43	H	-1.0072	0.1376	-2.2981
44	H	-0.1702	0.1718	0.1012
45	H	0.3255	1.7996	-0.0518
46	H	1.1931	0.2061	-3.1900
47	H	3.5193	-0.5406	-3.6577
48	O	5.3282	-0.8374	-1.9567
49	C	6.3524	-1.0519	-0.9739
50	H	6.0277	-1.8100	-0.2518
51	H	7.2199	-1.4094	-1.5300
52	H	6.5916	-0.1125	-0.4637
53	O	0.6547	0.3628	2.5626
54	C	-0.0050	1.4192	2.5544
55	O	0.2366	2.5322	2.0534
56	C	-1.3554	1.3600	3.3194
57	F	-1.2472	1.9792	4.5103
58	F	-1.7832	0.1149	3.5660
59	F	-2.3466	1.9800	2.6547

TSAB-1a

	Atom	X	Y	Z
1	C	3.7440	1.04551	-1.251

2	C	2.4504	1.42553	-1.0039
3	C	1.9036	1.33262	0.30374
4	C	2.7504	0.86722	1.34733
5	C	4.0545	0.49931	1.11589
6	C	4.5641	0.57962	-0.1962
7	H	4.6763	0.14843	1.93555
8	H	2.3449	0.82898	2.3587
9	C	0.5829	1.79283	0.64385
10	C	-0.4212	2.13557	-0.4356
11	C	-1.8690	2.32177	0.04585
12	C	-1.9648	3.29367	1.22107
13	H	-3.0185	3.51472	1.44489
14	H	-1.4580	4.24138	0.99485
15	H	-1.5153	2.88139	2.13586
16	C	-2.6928	2.87302	-1.1167
17	H	-2.3639	3.8909	-1.3701
18	H	-3.7606	2.92051	-0.8554
19	H	-2.5886	2.25682	-2.021
20	C	-2.4578	0.98745	0.51355
21	N	-2.5509	0.01134	-0.5767
22	S	-2.4387	-1.6018	-0.1814
23	O	-3.0042	-1.8814	1.13753
24	O	-2.9545	-2.3148	-1.3477
25	C	-0.6843	-1.84	-0.0767
26	C	0.0735	-1.7553	-1.2456
27	C	1.4345	-2.0118	-1.1851

28	C	2.0499	-2.3586	0.02583
29	C	1.2726	-2.406	1.1858
30	C	-0.0956	-2.1554	1.14305
31	H	-0.7045	-2.2108	2.04339
32	H	1.7456	-2.6545	2.13606
33	C	3.5075	-2.6983	0.06202
34	H	3.6721	-3.7314	-0.2775
35	H	4.0914	-2.0494	-0.6059
36	H	3.9156	-2.618	1.07724
37	H	2.0364	-1.9552	-2.0926
38	H	-0.4022	-1.4971	-2.1911
39	H	-3.3510	0.14384	-1.1977
40	H	-3.4466	1.15618	0.96993
41	H	-1.8196	0.55743	1.2994
42	H	-0.1050	3.06314	-0.9431
43	H	-0.4182	1.35197	-1.2131
44	H	0.1775	1.27196	1.52445
45	H	0.8666	2.86951	1.19509
46	H	1.8290	1.78526	-1.822
47	H	4.1710	1.09042	-2.251
48	O	5.8007	0.23418	-0.5446
49	C	6.6953	-0.2426	0.45697
50	H	6.3133	-1.1634	0.91611
51	H	7.6350	-0.453	-0.0577
52	H	6.8595	0.51981	1.22869
53	O	0.8984	2.96119	3.70846

54	C	0.8924	3.99017	3.04738
55	O	1.0476	4.16349	1.79346
56	C	0.5874	5.32928	3.75605
57	F	1.4579	6.2868	3.42049
58	F	0.5997	5.21751	5.08251
59	F	-0.6339	5.75409	3.39569

B'-1a

	Atom	X	Y	Z
1	C	3.7810	1.2260	-1.0005
2	C	2.4371	1.4647	-0.8139
3	C	1.8097	1.2007	0.4370
4	C	2.6363	0.7022	1.4790
5	C	3.9881	0.4697	1.2971
6	C	4.5722	0.7225	0.0470
7	H	4.5806	0.0832	2.1233
8	H	2.1817	0.4999	2.4503
9	C	0.4330	1.4306	0.6666
10	C	-0.5033	2.0046	-0.3445
11	C	-1.9484	2.1999	0.1367
12	C	-2.0006	3.1214	1.3546
13	H	-3.0420	3.3196	1.6463
14	H	-1.5294	4.0896	1.1276
15	H	-1.4910	2.6896	2.2277
16	C	-2.7571	2.8328	-0.9933
17	H	-2.3724	3.8361	-1.2262

18	H	-3.8152	2.9364	-0.7101
19	H	-2.7058	2.2367	-1.9154
20	C	-2.5731	0.8601	0.5374
21	N	-2.6468	-0.0718	-0.5925
22	S	-2.4945	-1.7002	-0.2842
23	O	-3.0266	-2.0569	1.0303
24	O	-3.0253	-2.3593	-1.4755
25	C	-0.7352	-1.9193	-0.2291
26	C	0.0039	-1.7170	-1.3959
27	C	1.3702	-1.9497	-1.3761
28	C	2.0101	-2.3945	-0.2105
29	C	1.2493	-2.5687	0.9477
30	C	-0.1230	-2.3366	0.9473
31	H	-0.7172	-2.4843	1.8471
32	H	1.7398	-2.8969	1.8644
33	C	3.4766	-2.6973	-0.2230
34	H	3.6706	-3.6551	-0.7273
35	H	4.0418	-1.9297	-0.7696
36	H	3.8811	-2.7718	0.7940
37	H	1.9590	-1.7918	-2.2803
38	H	-0.4892	-1.3805	-2.3073
39	H	-3.4436	0.0730	-1.2143
40	H	-3.5744	1.0288	0.9656
41	H	-1.9708	0.3879	1.3264
42	H	-0.1289	2.9851	-0.6989
43	H	-0.5156	1.3685	-1.2490

44	H	0.0491	1.1385	1.6470
45	H	1.2917	3.2133	1.3471
46	H	1.8420	1.8478	-1.6423
47	H	4.2583	1.4160	-1.9609
48	O	5.8710	0.5067	-0.2502
49	C	6.7040	-0.0281	0.7598
50	H	6.3510	-1.0157	1.0907
51	H	7.6971	-0.1329	0.3148
52	H	6.7668	0.6434	1.6280
53	O	0.8042	3.2169	3.6561
54	C	1.0234	4.1636	2.9475
55	O	1.3253	4.1516	1.6626
56	C	0.9661	5.6160	3.4428
57	F	2.1282	6.2305	3.2280
58	F	0.6942	5.6593	4.7369
59	F	0.0168	6.2812	2.7833

B-1a

	Atom	X	Y	Z
1	C	3.7329	0.9392	-1.3775
2	C	2.4198	1.3233	-1.2036
3	C	1.8625	1.4864	0.0961
4	C	2.7273	1.2426	1.1940
5	C	4.0494	0.8651	1.0245
6	C	4.5635	0.7033	-0.2696
7	H	4.6718	0.6872	1.8989

8	H	2.3296	1.3559	2.2040
9	C	0.5208	1.8657	0.3111
10	C	-0.4388	2.2020	-0.7788
11	C	-1.8705	2.5222	-0.3249
12	C	-1.8865	3.7117	0.6337
13	H	-2.9194	3.9964	0.8818
14	H	-1.3997	4.5830	0.1722
15	H	-1.3676	3.4968	1.5780
16	C	-2.7071	2.8747	-1.5532
17	H	-2.3296	3.7937	-2.0240
18	H	-3.7589	3.0463	-1.2788
19	H	-2.6760	2.0795	-2.3114
20	C	-2.4891	1.3266	0.4042
21	N	-2.6238	0.1576	-0.4716
22	S	-2.5241	-1.3507	0.2253
23	O	-3.0410	-1.3532	1.5934
24	O	-3.1025	-2.2624	-0.7595
25	C	-0.7730	-1.6168	0.3104
26	C	-0.0586	-1.7609	-0.8798
27	C	1.2967	-2.0459	-0.8207
28	C	1.9488	-2.1994	0.4104
29	C	1.2150	-2.0221	1.5856
30	C	-0.1461	-1.7351	1.5458
31	H	-0.7212	-1.6131	2.4617
32	H	1.7176	-2.1192	2.5483
33	C	3.3972	-2.5761	0.4564

34	H	3.5237	-3.6508	0.2599
35	H	3.9772	-2.0414	-0.3080
36	H	3.8364	-2.3677	1.4398
37	H	1.8660	-2.1612	-1.7436
38	H	-0.5623	-1.6524	-1.8398
39	H	-3.4352	0.1813	-1.0914
40	H	-3.4673	1.6091	0.8264
41	H	-1.8497	1.0391	1.2511
42	H	-0.0671	3.0720	-1.3553
43	H	-0.4814	1.3757	-1.5125
44	H	0.1987	1.9562	1.3512
45	H	1.7960	1.4953	-2.0805
46	H	4.1534	0.8076	-2.3739
47	O	5.8291	0.3142	-0.5524
48	C	6.7007	0.0634	0.5299
49	H	6.3306	-0.7520	1.1689
50	H	7.6578	-0.2334	0.0921
51	H	6.8502	0.9625	1.1454

HCF_3

	Atom	X	Y	Z
1	C	-2.0947	0.1757	0.0209
2	F	-1.6669	0.7821	1.1283
3	F	-1.6669	-1.0866	0.0499
4	F	-3.4272	0.1593	0.0498
5	H	-1.7309	0.6915	-0.8722

HFIPanion

	Atom	X	Y	Z
1	C	-2.2750	-0.8356	0.1193
2	H	-1.9852	-0.4227	-0.9108
3	O	-1.8604	-0.2223	1.1885
4	C	-1.7402	-2.2804	0.0270
5	C	-3.8143	-0.8564	0.0144
6	F	-4.4040	-1.4365	1.0734
7	F	-4.3034	-1.4812	-1.0815
8	F	-4.2806	0.4028	-0.0394
9	F	-2.0979	-3.0403	1.0759
10	F	-0.3967	-2.2638	0.0085
11	F	-2.1181	-2.9599	-1.0804

HFIPanion'

	Atom	X	Y	Z
1	C	-2.3799	-0.8616	0.0359
2	O	-1.9948	-0.2140	1.2666
3	H	-1.4921	0.5666	1.0051
4	C	-1.7707	-2.1871	0.0291
5	C	-3.8371	-0.8831	-0.0067
6	F	-4.4941	-1.4706	1.0610
7	F	-4.3316	-1.5333	-1.0872
8	F	-4.3678	0.3669	-0.0343
9	F	-2.0773	-3.0339	1.0813
10	F	-0.4152	-2.1257	0.0761

11	F	-2.0826	-2.9159	-1.0697

C-1a

	Atom	X	Y	Z
1	C	3.7791	0.9860	-1.3371
2	C	2.4624	1.3154	-1.2373
3	C	1.8343	1.4146	0.0481
4	C	2.6240	1.1503	1.2107
5	C	3.9502	0.8259	1.1203
6	C	4.5394	0.7334	-0.1614
7	H	4.5314	0.6310	2.0169
8	H	2.1458	1.2177	2.1873
9	C	0.5052	1.7348	0.2146
10	C	-0.4668	2.0344	-0.8542
11	C	-1.8602	2.4785	-0.3893
12	C	-1.7658	3.7492	0.4516
13	H	-2.7679	4.0955	0.7407
14	H	-1.2824	4.5543	-0.1193
15	H	-1.1900	3.5971	1.3759
16	C	-2.7060	2.7600	-1.6282
17	H	-2.2750	3.5871	-2.2098
18	H	-3.7287	3.0459	-1.3430
19	H	-2.7658	1.8841	-2.2893
20	C	-2.5213	1.3882	0.4590
21	N	-2.6972	0.1406	-0.2891
22	S	-2.5060	-1.3056	0.5138

23	O	-2.8664	-1.1920	1.9256
24	O	-3.1773	-2.2938	-0.3259
25	C	-0.7510	-1.5598	0.4290
26	C	-0.1553	-1.7195	-0.8236
27	C	1.2013	-1.9951	-0.8937
28	C	1.9710	-2.1319	0.2709
29	C	1.3511	-1.9573	1.5112
30	C	-0.0088	-1.6755	1.5999
31	H	-0.4944	-1.5512	2.5658
32	H	1.9433	-2.0489	2.4221
33	C	3.4232	-2.4806	0.1788
34	H	3.5547	-3.5670	0.0694
35	H	3.8941	-2.0158	-0.6982
36	H	3.9713	-2.1763	1.0799
37	H	1.6794	-2.1177	-1.8659
38	H	-0.7507	-1.6265	-1.7314
39	H	-3.5409	0.0965	-0.8618
40	H	-3.4890	1.7533	0.8366
41	H	-1.9086	1.1715	1.3463
42	H	-0.0380	2.8013	-1.5230
43	H	-0.5577	1.1327	-1.4880
44	H	0.1544	1.7627	1.2511
45	H	1.8804	1.5046	-2.1373
46	H	4.2806	0.8998	-2.2982
47	O	5.7952	0.4079	-0.3702
48	C	6.6495	0.1047	0.7396

49	H	6.2638	-0.7591	1.2938
50	H	7.6203	-0.1365	0.3040
51	H	6.7420	0.9731	1.4015

TSCD-1a

	Atom	X	Y	Z
1	C	-1.6122	-3.1571	1.9887
2	C	-0.4330	-2.7190	1.4381
3	C	-0.3664	-2.3100	0.0820
4	C	-1.5501	-2.3731	-0.7045
5	C	-2.7228	-2.8391	-0.1743
6	C	-2.7729	-3.2099	1.1861
7	O	-3.9629	-3.5809	1.6346
8	C	-4.1013	-3.9862	2.9962
9	H	-3.5042	-4.8846	3.1951
10	H	-5.1611	-4.2100	3.1330
11	H	-3.8036	-3.1794	3.6775
12	H	-3.6371	-2.8965	-0.7609
13	H	-1.5067	-2.0475	-1.7438
14	C	0.8007	-1.8030	-0.5002
15	C	2.1790	-1.9308	0.0019
16	C	3.1128	-0.7649	-0.4141
17	C	4.1462	-0.5657	0.6908
18	H	4.8842	0.1935	0.3974
19	H	3.6729	-0.2380	1.6286
20	H	4.6829	-1.5030	0.8937
21	C	3.8166	-1.0733	-1.7308

22	H	3.0957	-1.3395	-2.5174
23	H	4.5192	-1.9094	-1.6106
24	H	4.3859	-0.1991	-2.0776
25	C	2.2782	0.5189	-0.5982
26	N	1.0698	0.4205	0.2310
27	S	-0.1205	1.5984	-0.0555
28	O	0.3780	2.9090	0.3519
29	O	-0.5579	1.3951	-1.4311
30	C	-1.3715	1.0638	1.0698
31	C	-1.1638	1.2122	2.4427
32	C	-2.1456	0.7727	3.3172
33	C	-3.3367	0.2069	2.8411
34	C	-3.5197	0.0850	1.4615
35	C	-2.5429	0.5086	0.5675
36	H	-2.6863	0.4100	-0.5067
37	H	-4.4412	-0.3570	1.0812
38	C	-4.3998	-0.2383	3.7960
39	H	-4.9983	0.6183	4.1383
40	H	-5.0885	-0.9519	3.3264
41	H	-3.9668	-0.7028	4.6912
42	H	-1.9939	0.8736	4.3918
43	H	-0.2488	1.6661	2.8228
44	H	1.2892	0.3890	1.2341
45	H	2.8765	1.4090	-0.3524
46	H	1.9377	0.6143	-1.6381
47	H	2.5766	-2.8683	-0.4283

48	H	2.1853	-2.0755	1.0909
49	H	0.6966	-1.4487	-1.5316
50	H	0.4537	-2.6588	2.0666
51	H	-1.6477	-3.4423	3.0363

D-1a

	Atom	X	Y	Z
1	C	-1.6795	-2.9961	1.8669
2	C	-0.5403	-2.3768	1.3662
3	C	-0.4552	-1.9905	0.0275
4	C	-1.5284	-2.2784	-0.8226
5	C	-2.6593	-2.9185	-0.3462
6	C	-2.7508	-3.2652	1.0071
7	O	-3.9063	-3.8432	1.3891
8	C	-4.0681	-4.1666	2.7567
9	H	-3.3256	-4.9066	3.0874
10	H	-5.0696	-4.5936	2.8543
11	H	-3.9940	-3.2706	3.3902
12	H	-3.5001	-3.1424	-1.0002
13	H	-1.4755	-1.9852	-1.8716
14	C	0.7494	-1.2862	-0.5098
15	C	2.0978	-1.9722	-0.3440
16	C	3.1774	-0.8677	-0.4398
17	C	4.1565	-0.9757	0.7231
18	H	4.9350	-0.2032	0.6549
19	H	3.6434	-0.8598	1.6894

20	H	4.6485	-1.9580	0.7192
21	C	3.9184	-0.9217	-1.7696
22	H	3.2157	-0.9132	-2.6152
23	H	4.5208	-1.8380	-1.8332
24	H	4.5947	-0.0622	-1.8790
25	C	2.3823	0.4525	-0.3475
26	N	1.0334	0.0527	0.1839
27	S	-0.2277	1.3944	-0.0723
28	O	0.5166	2.5821	0.2933
29	O	-0.6993	1.1620	-1.4211
30	C	-1.4342	1.0111	1.1334
31	C	-1.1381	1.2811	2.4737
32	C	-2.0838	0.9576	3.4301
33	C	-3.3126	0.3848	3.0684
34	C	-3.5777	0.1408	1.7172
35	C	-2.6454	0.4491	0.7358
36	H	-2.8551	0.2563	-0.3136
37	H	-4.5297	-0.3047	1.4292
38	C	-4.3160	0.0490	4.1241
39	H	-4.6518	0.9570	4.6436
40	H	-5.1968	-0.4489	3.7031
41	H	-3.8763	-0.6073	4.8874
42	H	-1.8753	1.1551	4.4811
43	H	-0.1894	1.7333	2.7592
44	H	1.1010	-0.1029	1.2044
45	H	2.8234	1.2009	0.3161

46	H	2.2076	0.8953	-1.3369
47	H	2.2185	-2.7471	-1.1108
48	H	2.1374	-2.4704	0.6350
49	H	0.5929	-1.0027	-1.5603
50	H	0.2891	-2.1759	2.0490
51	H	-1.7240	-3.2624	2.9199

D'-1a

	Atom	X	Y	Z
1	C	-1.6169	-2.4089	2.3690
2	C	-0.6441	-1.6726	1.6995
3	C	-0.4850	-1.7666	0.3166
4	C	-1.3181	-2.6437	-0.3848
5	C	-2.2844	-3.3942	0.2668
6	C	-2.4479	-3.2742	1.6508
7	O	-3.4308	-4.0220	2.2010
8	C	-3.6433	-3.9104	3.5932
9	H	-2.7584	-4.2266	4.1645
10	H	-4.4791	-4.5740	3.8312
11	H	-3.9071	-2.8816	3.8799
12	H	-2.9381	-4.0721	-0.2799
13	H	-1.2103	-2.7312	-1.4670
14	C	0.5819	-1.0159	-0.4301
15	C	1.9984	-1.5101	-0.1590
16	C	2.9234	-0.4067	-0.6966
17	C	4.1731	-0.2520	0.1624

18	H	4.8245	0.5421	-0.2311
19	H	3.9144	0.0024	1.1994
20	H	4.7510	-1.1874	0.1711
21	C	3.3207	-0.7023	-2.1402
22	H	2.4387	-0.8721	-2.7750
23	H	3.9536	-1.5998	-2.1897
24	H	3.8864	0.1363	-2.5713
25	C	2.0415	0.8642	-0.6457
26	N	0.7292	0.4291	-0.0616
27	S	-0.5049	1.4909	-0.5941
28	O	-0.0194	2.8207	-0.2336
29	O	-0.8255	1.1957	-1.9898
30	C	-1.9130	1.1105	0.4019
31	C	-1.9673	1.5867	1.7096
32	C	-3.0688	1.2753	2.4934
33	C	-4.1241	0.5123	1.9806
34	C	-4.0532	0.0692	0.6553
35	C	-2.9533	0.3603	-0.1399
36	H	-2.8954	0.0036	-1.1663
37	H	-4.8686	-0.5278	0.2467
38	C	-5.3136	0.1868	2.8284
39	H	-5.0430	0.1168	3.8893
40	H	-6.0825	0.9680	2.7403
41	H	-5.7758	-0.7597	2.5213
42	H	-3.1120	1.6278	3.5240
43	H	-1.1615	2.1964	2.1126

44	H	1.3136	0.5362	1.6602
45	H	2.4629	1.6576	-0.0188
46	H	1.8950	1.2713	-1.6577
47	H	2.1769	-2.4831	-0.6359
48	H	2.1318	-1.6433	0.9257
49	H	0.3743	-1.0781	-1.5129
50	H	-0.0202	-0.9953	2.2843
51	H	-1.7241	-2.2901	3.4448
52	C	1.6996	1.8322	3.0586
53	H	1.0969	2.5251	2.4470
54	O	1.8336	0.5703	2.5006
55	C	0.9969	1.6973	4.4031
56	C	3.0870	2.4506	3.1713
57	F	3.9466	1.6385	3.7846
58	F	3.0614	3.6074	3.8351
59	F	3.5686	2.6903	1.9470
60	F	1.7130	0.9806	5.2703
61	F	-0.1733	1.0747	4.2354
62	F	0.7516	2.8878	4.9519

Cplx1

	Atom	X	Y	Z
1	C	-0.6507	-1.4612	4.0368
2	F	0.1733	-0.8477	4.8527
3	F	-0.8439	-2.7086	4.4046
4	F	-1.7961	-0.8139	3.9441

5	H	-0.7666	0.5286	1.9256
6	O	0.1501	0.2156	1.8436
7	C	0.1589	-0.9267	1.0490
8	C	-0.1113	-0.5573	-0.4052
9	F	-0.2328	-1.6371	-1.1745
10	F	0.8481	0.2128	-0.9152
11	F	-1.2590	0.1261	-0.4673
12	C	1.5215	-1.5725	1.2423
13	F	2.5129	-0.7159	1.0121
14	F	1.6707	-2.6135	0.4235
15	F	1.6483	-2.0119	2.4964
16	H	-0.5982	-1.6766	1.3383

TS12

	Atom	X	Y	Z
1	C	-0.9226	-1.6761	3.3841
2	F	-0.4733	-0.8486	4.3132
3	F	-0.5188	-2.9068	3.6420
4	F	-2.2406	-1.6314	3.3365
5	H	-0.0528	1.2009	1.6646
6	O	0.7415	0.6376	1.6943
7	C	0.4251	-0.6279	1.2889
8	C	-0.3377	-0.6822	-0.0175
9	F	-0.8698	-1.8832	-0.2210
10	F	0.4346	-0.3867	-1.0657
11	F	-1.3279	0.2167	0.0230

12	C	1.6828	-1.4659	1.3294
13	F	2.6682	-0.9377	0.6064
14	F	1.4398	-2.6943	0.8748
15	F	2.1080	-1.5622	2.5910
16	H	-0.3313	-1.2118	2.1631

Cplx2

	Atom	X	Y	Z
1	C	-1.1681	-2.0226	3.4784
2	F	-0.7796	-0.7727	3.7407
3	F	-0.1489	-2.8354	3.7540
4	F	-2.1725	-2.3222	4.2990
5	H	0.2208	1.4793	1.3779
6	O	0.9058	0.8359	1.6437
7	C	0.6329	-0.3685	1.1366
8	C	-0.2578	-0.4928	-0.0545
9	F	-1.1221	-1.5053	0.0544
10	F	0.4309	-0.6976	-1.1855
11	F	-0.9595	0.6374	-0.2004
12	C	1.7038	-1.3723	1.3797
13	F	2.8149	-1.1050	0.6753
14	F	1.2889	-2.5911	1.0268
15	F	2.0554	-1.3922	2.6642
16	H	-1.4715	-2.1214	2.4311

Chapter III. HFIP-Enabled Spin Catalysis

3.1. Introduction

Still now, the underutilization of earth-abundant first-row transition metals (TMs), such as cobalt, iron or manganese, remains a long-standing challenge among practitioners of organometallic catalysis.[1] This is particularly surprising given their pivotal role in the initial breakthroughs of transformative TM catalytic processes like cross-coupling or C–H activation reactions.[2,3] Nevertheless, over the past five decades, these 3d TMs have been overshadowed by the robustness and efficiency of noble metals in these reactions. Metals like Pd, Rh, or Ru have revolutionized the way chemists approach synthesis, offering new opportunities for creating chemical bonds in a predictable and selective manner through the direct interaction of the TM center with organic fragments.[4] The maturity of these noble metals has been achieved through a profound understanding of reaction mechanisms, the nature of reactive intermediates, and the identification of factors governing their catalytic performance. In fact, noble metals have played a decisive role in shaping the current mechanistic landscape in organometallic chemistry, which is built on closed-shell paradigms.[5]

In recent years, the global focus towards increasing the sustainability of chemical processes has sparked renewed interest in incorporating first-row TMs into the organometallic toolkit.[6] However, the widespread adoption of these metals in coupling reactions is far from being trivial, and Co, Fe, and Mn are still in their early stages (Figure 3.1).[7] A extended approach is to use these metals as cost-effective alternatives to Pd, Rh, or Ru by promoting the formation of low-spin diamagnetic organometallic

1 Ludwig, J. R.; Schindler, C. S. *Chem* **2017**, *2*, 313.
2 Kharasch, M. S.; Fuchs, C. F. *J. Am. Chem. Soc.* **1943**, *65*, 504.
3 Murahashi, S. *J. Am. Chem. Soc.***1955**, *77*, 6403.
4 (a) Miyaura, N.; Suzuki, A. *Chem. Rev.* **1995**, *95*, 2457. (b) Labinger, J. A.; Bercaw, J. E. *Nature* **2002**, *417,* 507–514. (c) Colby, D. A.; Bergman, R. G.; Ellman, J. A. *Chem. Rev.* **2010**, *110*, 624. (d) Lyons, T. W.; Sanford, M. S. *Chem. Rev.* **2010**, *110*, 1147. (e) Arockiam, P. B.; Bruneau, C.; Dixneuf, P. H. *Chem. Rev.* **2012**, *112*, 5879. (f) Campeau, L.-C.; Hazari, N. *Organometallics* **2019**, *38*, 3.
5 (a) Hartwig, J. F. Organotransition Metal Chemistry: From Bonding to Catalysis, 1st ed.; Palgrave Macmillan, 2009. (b) Crabtree, R. H. The Organometallic Chemistry of the Transition Metals. 7th ed.; Crabtree, R. H. (Ed.); Wiley, 2019.
6 Anastas, P.; Eghbali, N. *Chem Soc Rev* **2010**, *39*, 301.
7 Kaplaneris, N.; Ackermann, L. *Beilstein J. Org. Chem.* **2022**, *18*, 86.

species that mimic the behavior of traditional noble metals.[8] Despite significant progress, these 3d TMs should not be considered just as a cheap replacement for noble metals. Their closed-shell reactivity is just the tip of the iceberg in terms of their reactivity patterns.[9] Indeed, these metals can offer a rich manifold of open-shell catalytic transformations that could lead to a new dimension in organometallic chemistry, currently unexplored.[10] It is ironic that the same intrinsic and distinctive properties – dynamic redox and spin-state chemistry – that will enable the discovery of new reaction modes and catalytic cycles are also preventing their mainstream use due to their perceived unpredictability and uncontrollability. Fine-tuning ligand design and an increased mechanistic understanding have enabled to start the translation of Ni singularity into new opportunities for reaction discovery.[11] However, Co, Fe and Mn lag far behind. Catalytic advances exploiting their great redox activity through 1 or 2 electron processes have been mostly driven by serendipitous discoveries or extensive screenings since the underlying reaction mechanisms remain highly speculative.[9d,12] The poor knowledge at molecular level is associated to the formation of paramagnetic species that are difficult to isolate and characterize. Moreover, the involvement of spin changes along the catalytic cycles is usually completely neglected when using this type of transition metals. Therefore, the lack of fundamental understanding on the principles behind their redox and spin-state changes is limiting the creation of a new mechanistic playground with the potential to untap new reaction modes and synthetic opportunities in key catalytic organometallic transformations.

---

8 (a) Hu, Y.; Zhou, B.; Wang, C. *Acc. Chem. Res.* **2018**, *51* (3), 816. (b) Arevalo, R.; Chirik, P. J. *J. Am. Chem. Soc.* **2019**, *141*, 9106. (c) Lukasevics, L.; Cizikovs, A.; Grigorjeva, L. *Chem. Commun.* **2021**, *57*, 10827.

9 (a) Sherry, B. D.; Fürstner, A. *Acc. Chem. Res.* **2008**, *41*, 1500. (b) Su, B.; Cao, Z.-C.; Shi, Z.-J. *Acc. Chem. Res.* **2015**, *48*, 886. (c) Chirik, P. J. *Angew. Chem. Int. Ed.* **2017**, *56*, 5170. (d) Liu, X.; Jaroschik, F.; Taillefer, M. *Manganese Catalysis in Organic Synthesis*; Sortais, J., Ed.; Wiley, 2021; pp 257.

10 (a) Poli, R. *Chem. Rev.* **1996**, *96*, 2135. (b) Poli, R. *J. Organomet. Chem.* **2004**, *689*, 4291. (c) Riedel, S.; Kaupp, M. *Coord. Chem. Rev.* **2009**, *253*, 606. (d) Swart, M.; Gruden, M. *Acc. Chem. Res.* **2016**, *49*, 2690.

11 (a) Tasker, S. Z.; Standley, E. A.; Jamison, T. F. *Nature* **2014**, *509*, 299. (b) Chan, A. Y.; Perry, I. B.; Bissonnette, N. B.; Buksh, B. F.; Edwards, G. A.; Frye, L. I.; Garry, O. L.; Lavagnino, M. N.; Li, B. X.; Liang, Y.; Mao, E.; Millet, A.; Oakley, J. V.; Reed, N. L.; Sakai, H. A.; Seath, C. P.; MacMillan, D. W. C. *Chem. Rev.* **2022**, *122*, 1485.

12 (a) Sears, J. D.; Neate, P. G. N.; Neidig, M. L. *J. Am. Chem. Soc.* **2018**, *140*, 11872. (b) Gallego, D.; Baquero, E. A. *Open Chem.* **2018**, *16*, 1001. (c) Neidig, M. L.; Carpenter, S. H.; Curran, D. J.; DeMuth, J. C.; Fleischauer, V. E.; Iannuzzi, T. E.; Neate, P. G. N.; Sears, J. D.; Wolford, N. J. *Acc. Chem. Res.* **2019**, *52*, 140.

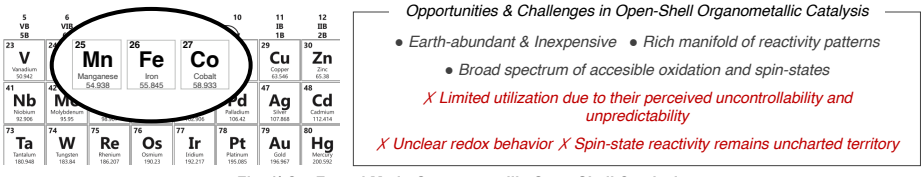

Figure 3.1. Co, Fe, and Mn in organometallic open-shell catalysis

3.1.1. Spin Reactivity

The formation of paramagnetic species within catalytic cycles is usually associated to redox changes. However, it is often dismissed that spin state changes can also play a key role unlocking the open-shell world.[10a] Maybe this still remains rather overlooked because noble metal catalysis has been traditionally built on the paradigm of spin conservation ("Single-State Reactivity," SSR). The reactive TM intermediates involved in the elementary steps of traditional organometallic reactions are usually diamagnetic species that do not experience any spin change due to the large energy splitting of their d-orbitals. This reliable and predictable low-spin behavior has been key to foster the widespread use of precious metals in synthetic organic chemistry. In sharp contrast, 3d TMs present a rich spin state landscape due to multiple energetically close-lying states.[13] This opens the door to access excited spin state or to promote spin-crossover (SCO) events that lead to catalytic two-state (or multistate) reactivity (TSR or MSR)[14] by intersystem crossing (ISC) (Figure 3.2a).[15] These so-called "spin-forbidden" events are not uncommon in organometallic chemistry due to strong spin-orbit couplings and they hold the potential to accelerate reaction rates and unlock bond-breaking/forming processes that otherwise would not be easily available at the single-state reactivity (SSR) of "closed-shell behavior."[16] They can be triggered by external stimuli (temperature, pressure of light irradiation) or molecular changes along the elementary steps of organometallic catalytic cycles (e.g., coordination number, geometry, electron count, ligands with different donor strengths). For a long time, these

13 Dzik, W. I.; Böhmer, W.; de Bruin, B. Multiple Spin-State Scenarios in Organometallic Reactivity. In *Spin States in Biochemistry and Inorganic Chemistry*; Swart, M., Costas, M., Eds.; John Wiley & Sons, Ltd: Oxford, UK, 2015; pp 103–129.
14 Schröder, D.; Shaik, S.; Schwarz, H. *Acc. Chem. Res.* **2000**, *33*, 139.
15 Penfold, T. J.; Gindensperger, E.; Daniel, C.; Marian, C. M. *Chem. Rev.* **2018**, *118*, 6975.
16 Poli, R.; Harvey, J. N. *Chem. Soc. Rev.* **2003**, *32*, 1.

events have been mainly object of fundamental study, especially from a computational perspective due to the complexity associate to the experimental study of organometallic species in multiple spin states. However, the recent widespread use of photocatalytic strategies in organometallic catalysis has brought a renaissance in the field of spin-state catalysis (Figure 3.2b). Excited-state TM species and intersystem crossing events can be triggered by the direct photoexcitation of the organometallic system[17] or by an energy transfer (EnT)[18] pathway from exogeneous photosensitizers.

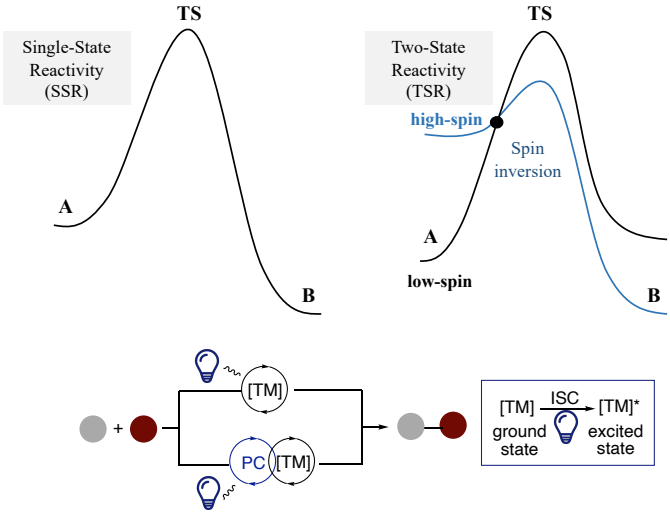

Figure 3.2. (a) Reaction energy profile of SSR and TSR, and (b) light-induced ISC processes.

These phenomena can drive elementary steps involved in organometallic reaction pathways with different transition metal-based systems. Indeed, the photoinduced ligand dissociation from TM carbonyl complexes to generate coordinatively unsaturated organometallic compounds that trigger oxidative addition events has been a subject of great interest in organometallic chemistry. Interestingly, different studies have shown that upon irradiation of $CpCo(CO)_2$ with UV light, the organometallic complex loses a CO ligand to afford a short-live time 16-electron species, [CpCo(CO)],

[17] (a) Prier, C. K.; Rankic, D. A.; MacMillan, D. W. C., *Chem. Rev.* **2013,** *113* , 5322. (b)Shaw, M. H.; Twilton, J.; MacMillan, D. W. C., *J. Org. Chem*. **2016**, 81, 6898.

[18] Strieth-Kalthoff, F.; James, M. J.; Teders, M.; Pitzer, L.; Glorius, F. *Chem. Soc. Rev.* **2018**, 47, 7190.

that exhibit a triplet electronic ground state (Figure 3.3a).[19,20] While it is well-established that this type of intermediates can participate in Si–H bond activations or ligand exchanges (Figure 3.3b),[20] their utilization as catalytically active intermediates in the context of coupling reactions remains underexplored. Moreover, there is an important barrier that compromises the potential implementation of light-enabled CpCo-induced transformations: the requirement for UV irradiation for the in-situ photogeneration of the triplet cobalt(I) species. The use of this high-energy light usually leads to unselective processes and limits the synthetic applicability, which could be avoided by developing alternative strategies to facilitate the CO dissociation.

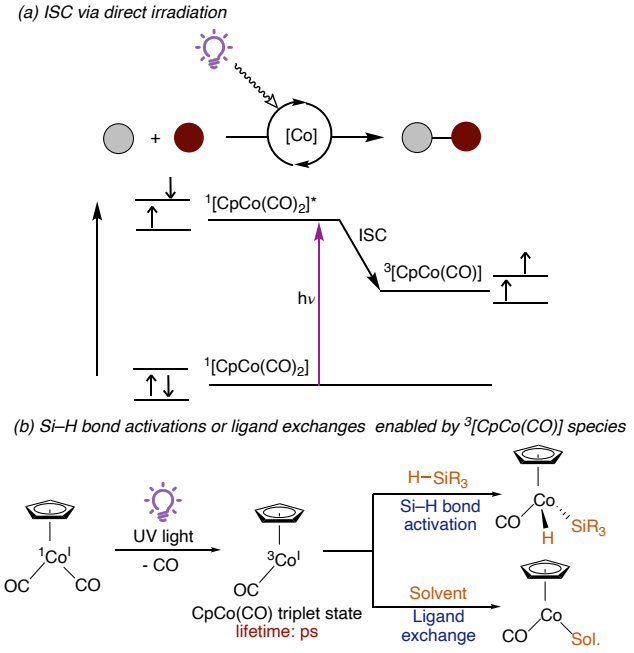

19 (a) Lee, W.-S.; Brintzinger, H. H. *J. Organomet. Chem.* **1977**, *127*, 87. (b) Wasserman, E. P.; Bergman, R. G.; Moore, C. B. *J. Am. Chem. Soc*. **1988**, *110*, 6076. (c) Hofmann, P.; Padmanabhan, M. *Organometallics* **1983**, *2*, 1273. (d) Bengali, A. A.; Robert G. Bergman, R. G.; Moore, C. B. *J. Am. Chem. Soc.* **1995**, *117,* 3879.

20 (a) Lomont, J. P.; Nguyen, S. C.; Harris, C. B. *Organometallics* **2012**, *31*, 3947. (b) Lomont, J. P.; Nguyen, S. C.; Zoerb, M. C.; Hill, A. D.; Schlegel, J. P.; Harris, C. B. *Organometallics* **2012**, *31*, 3582. (c) Lomont, J. P.; Nguyen, S. C.; Schlegel, J. P.; Zoerb, M. C.; Hill, A. D.; Harris, C. B. *J. Am. Chem. Soc*. **2012**, *134*, 3120. (d) Gandon, V.; Agenet, N.; Vollhardt, P. C.; Malacria, M.; Aubert, C. *J. Am. Chem. Soc*. **2009**, *131*, 3007. (e) Snee, P. T.; Payne, C. K.; Kotz, K. T.; Yang, H.; Harris, C. B. *J. Am. Chem. Soc.* **2001**, *123*, 2255. (f) Zhang, Z.-F.; Su, M.-D. *RSC Adv.* **2018**, *8*, 24641.

Figure 3.3. (a) ISC via direct irradiation (b) SiH bond activations or ligand exchanges enabled by ^{3}[CpCo(CO)] species

3.2. Objective and Design of the Project

Despite literature precedents have shown exciting reactivity patterns via photoinduced singlet-triplet intersystem crossing events, these phenomena are still very elusive in organometallic catalysis. Still now, there are more open questions than answers on the effect of spin changes on organometallic reactivity or whether there are alternative strategies that trigger SCO events in the absence of light.

In this chapter, we aim to explore whether it is possible to promote "non-excited" spin-crossover events in Cp*Co^{I} systems by the assistance of HFIP. We anticipated that the successful realization of this strategy could offer very exciting venues for cross-coupling reactions.

To achieve this, the following objectives were pursued (Scheme 3.1):

- Explore the secondary-coordination sphere interaction between HFIP and Cp*Co(CO)$_2$ species using a range of analytical techniques.
- Establish a site-selective cobalt-catalyzed Mizoroki-Heck catalysis and delving into the ISC process.
- Investigate the scope and generality of the cobalt-catalyzed Mizoroki-Heck protocol by examining a diverse range of substrate candidates.

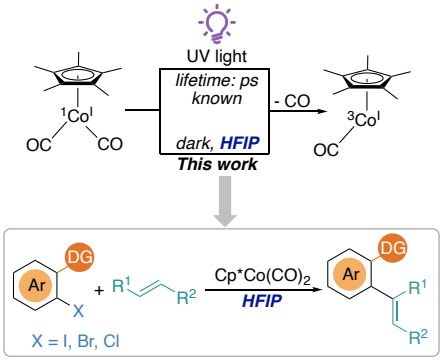

Scheme 3.1. Objectives

3.2. Results and discussion

3.2.1. Initial Investigations on Solvent-Assisted Spin-State Change

We initiated the validation of our above-mentioned proposal by investigating whether it is possible to trigger spin-state changes in TM systems simply through second-sphere interactions with solvents. In particular, we analyzed by EPR spectroscopy the potential formation of paramagnetic species when dissolving $Cp^*Co(CO)_2$ in a wide variety of solvents (Figure 3.1, top). While we did not observe the generation of any open-shell species in DCM or 2-propanol (green line), we were very pleased to detect a long-lived paramagnetic signal when using perfluorinated alcohols such as TFE (blue line), HFIP (black line) or PFBT (red line), giving HFIP the signal with the highest intensity.[21] The calculated g-value, 2.04, and the shape of the signal differs significantly from carbon centered radicals,[22] suggesting that observed species belongs to a cobalt paramagnetic species that it is formed after a redox process (Co^0 or Co^{II}) or a change in the spin state (Co^I triplet species) (Figure 3.1, below). Interestingly, when we dissolved the cobalt(I) compound in 1,1,1,3,3,3-hexafluoroisopropyl methyl ether (Me-HFIP), any signal was detected by EPR spectroscopy. These results strongly suggest that both the trifluoromethyl (CF_3–) and the hydroxyl (–OH) groups are important for the generation of a paramagnetic system.

21 A similar signal was observed when $CpCo^I(CO)_2$ was dissolved in HFIP. See experimental section for further details.

22 Woodward J. R. *Progress in Reaction Kinetics and Mechanism* **2002**, *27*, 165.

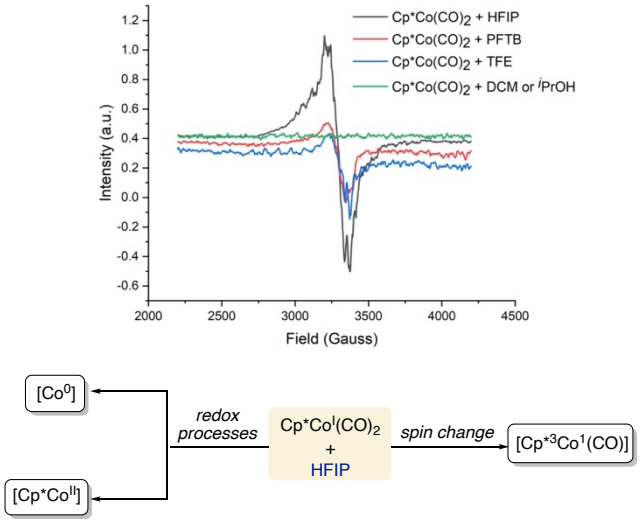

Figure 3.4. (top) EPR measurements of the solution of $Cp^*Co(CO)_2$ in different solvents. (below) Possible species could be formed in solution by interaction with the solvent

EPR quantification studies show that the concentration of the solution in HFIP affects the degree of paramagnetism of the reaction mixture. Specifically, the lower % of paramagnetic species was observed in more concentrated solutions (Figure 3.2a). This observation gained further insight through HRMS analysis, which detected an organometallic species, likely pertaining to a dimeric compound (Figure 3.2b). The explanation for the decreased paramagnetic species percentage in more concentrated solutions can be attributed to the quenching effect induced by dimer formation, leading to the rationalization of this phenomenon.

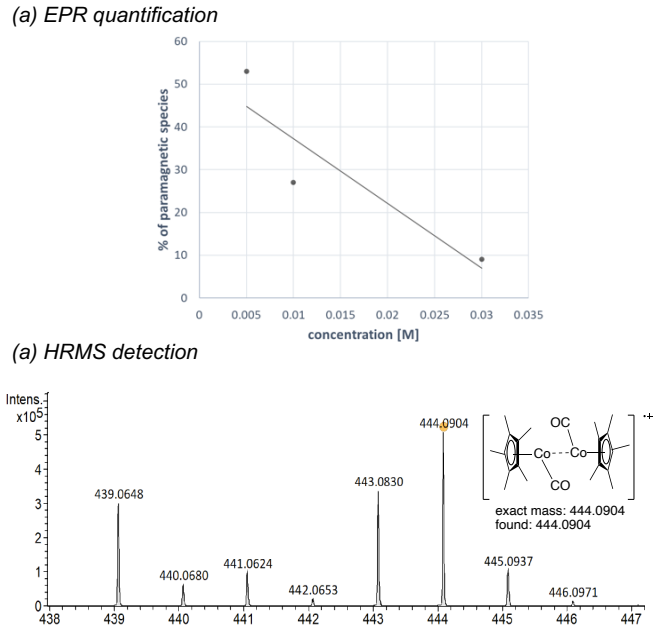

Figure 3.5. (a) EPR quantification of paramagnetic species in HFIP different concentrations. (b) HRMS measurements of $Cp^*Co(CO)_2$/ HFIP solution [0.01M].

Additionally, an examination was conducted on the solution of $Cp^*Co(CO)_2$ in different solvents through the utilization of UV-vis spectroscopy. Interestingly, a discernible divergence in behavior was distinctly observed when HFIP was employed as the solvent. Notably, the emergence of an orange color in the $Cp^*Co(CO)_2$/HFIP solution, accompanied by prominent absorption peaks within the visible light spectrum, specifically at approximately 460 nm and 590 nm. This phenomenon stood in stark contrast to the absence of such features in the solution when other solvents were used for examination. (Figure 3.6).

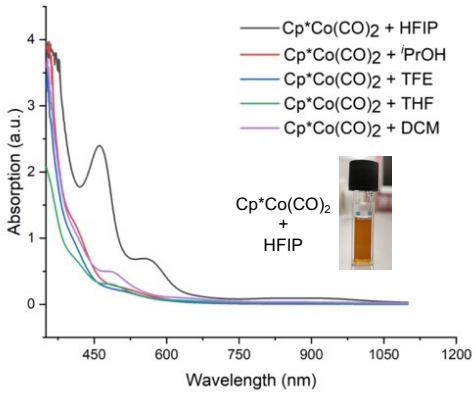

Figure 3.6. UV-vis absorption of $Cp^*Co(CO)_2$ in different solvents. [$Cp^*Co(CO)_2$ = 0.002M]

Encouraged by these results, next we aimed to uncover further details on the nature of the observed open-shell species when dissolving Cp*Co(CO) in HFIP. First, we evaluated by cyclic voltammetry whether the cobalt(I) compound is redox active in the presence of HFIP. The CV measurement of $Cp^*Co(CO)_2$ in DCM served as reference as the compound remains stable, that is without changing its oxidation or spin state, in this solvent.[23] When we compared the cyclic voltammograms in both solvents (Figure 3.7), we observed an irreversible oxidation peak at +0.08 V *vs.* Fc/Fc^+ (Fc = ferrocene) in DCM, which we assigned it to a $Co^{I/II}$ redox couple, while the cobalt(I) shows two oxidative waves at approximately –0.13 V and +0.06 V *vs.* Fc/Fc^+ in HFIP.

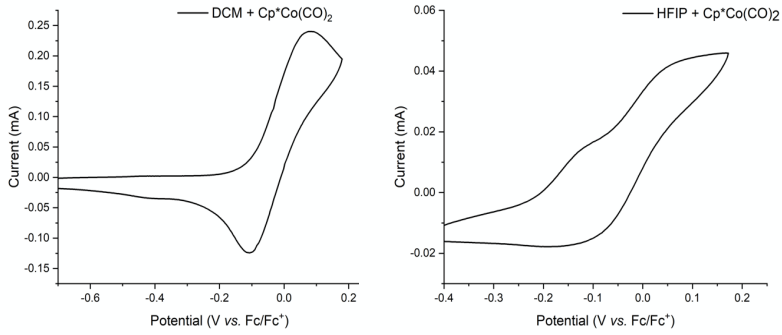

[23] DCM is the solvent used for the synthesis of $Cp^*Co(CO)_2$: Chan, N. H.; Roache, J. H.; Jones, W. D. *Inorganica Chimica Acta* **2015**, *437*, 36.

Figure 3.7. Cyclic voltammograms of complex $Cp^*Co(CO)_2$. [Co] = 0.01 M in DCM (top) and HFIP (below); $[TBAPF_6]$ = 0.1 M ; Scan rate = 200 mV/s. Glassy carbon working electrode, SCE reference electrode, Pt wire auxiliary electrode.

Intrigued by the electrochemical analysis of our targeted Co^I compound in HFIP, we carried out differential pause voltammetry (DPV) measurements. This electrochemical technique merges features of chronoamperometry and linear sweep voltammetry and provides high selectivity and sensitivity due to the minimization of background charging currents, allowing to compare the concentration of species in solution.[24] The waveform in DPV comprises a sequence of pulses where a baseline potential is held for a specified period of time prior to the application of a potential pulse (Figure 3.8). The current is measured before and at the end of the application of each and at the end of each pulse, and the difference between the currents is calculated and expressed in terms of potential. Thus, the oxidation of a compound produces a sharp peak, where its height is normally proportional to the corresponding concentration in the solution.

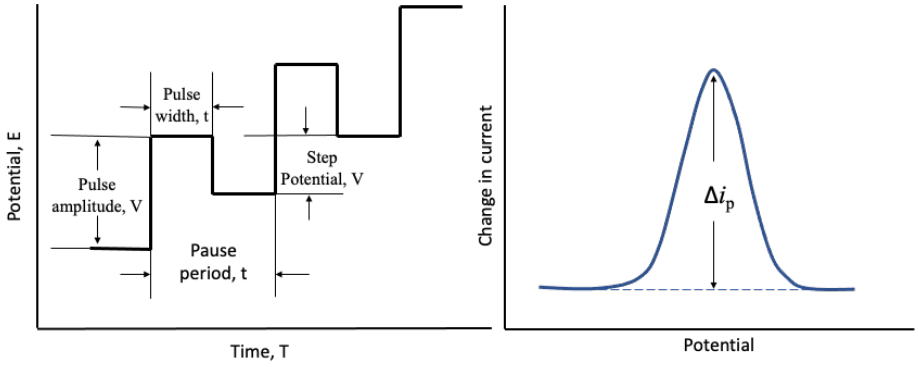

Figure 3.8. DPV excitation signal potential and its voltammogram

The analysis of the DPV voltammogram (Figure 3.9) indicates that the relevance of the species associated to –0.13 V is practically negligible when compared to one at +0.06 V. By analogy to the CV in DCM, we proposed that the oxidative wave at more positive potentials belongs to the $Co^{I/II}$ transition. These results suggest that the

[24] (a) Laborda, E.; González, J.; Molina, Á. *Electrochem. Commun.* **2014**, *43*, 25. (b) García-Armada, P.; Losada, J.; Vicente-Pérez S. *J. Chem. Educ.* **1996**, *73*, 544.

paramagnetic behavior observed by EPR spectroscopy when dissolving $Cp^*Co(CO)_2$ in HFIP is not related to a change in its oxidation state.

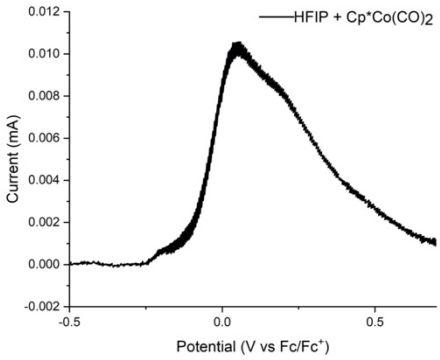

Figure 3.9. Differential pulse voltammetry of complex $Cp^*Co(CO)_2$. [Co] = 0.01 M in HFIP; [$TBAPF_6$] = 0.1 M; Scan rate = 200 mV/s. Glassy carbon working electrode, SCE reference electrode, Pt wire auxiliary electrode.

After ruling out the involvement of 1-electron reduction or oxidation processes between the cobalt(I) compound and HFIP, we next interrogated whether HFIP could provide alternative ways to produce open-shell cobalt(I) species in triplet state. As mentioned in the introduction of this chapter, it is well-established that short-lived $Cp^XCo^I(CO)$ intermediates can be generated after CO dissociation upon irradiation with UV light. However, the possibility that analogous triplet 16-electron compounds can be formed through second-coordination sphere interactions with the reaction solvent has not been contemplated in the literature to date. First, we performed NMR and IR spectroscopy studies to establish if HFIP can promote the CO loss from $Cp^*Co^I(CO)_2$, yet we could not observe free carbon monoxide with either of both techniques.[25] In view of these results, we decided to explore an indirect approach to determine if CO can be dissociated from the starting cobalt(I) singlet compound. Specifically, we exploited an elegant two-chamber reactor connected by a bridge, called COware that

[25] See experimental section for further details.

was released by the Skrydstrup group in 2011.[26] This research group introduced this technology to alleviate the safety issues associated to handling gaseous reagents, such as CO, in organic synthesis.[26] This simple set-up comprises in one chamber a stable solid or liquid gas surrogates that *in situ* generates stoichiometric amounts of the targeted gas. After its diffusion through the bridge to the secondary chamber, the gas participates as reagent in TM-catalyzed reactions.

Inspired by these literature examples, we selected one of the carbonylation reactions (chamber B)[26b] employed by the Skrydstrup group as benchmark to test if CO can be released from a solution of $Cp^*Co(CO)_2$ in HFIP (chamber A). Gratifyingly, the formation of the mono-carbonation product **3** was determined by ^1H NMR spectroscopy in 25% yield after 2 hours at room temperatura (Figure 3.10),[27] confirming the feasibility of the CO release from a solution of $Cp^*Co(CO)_2$ in HFIP.

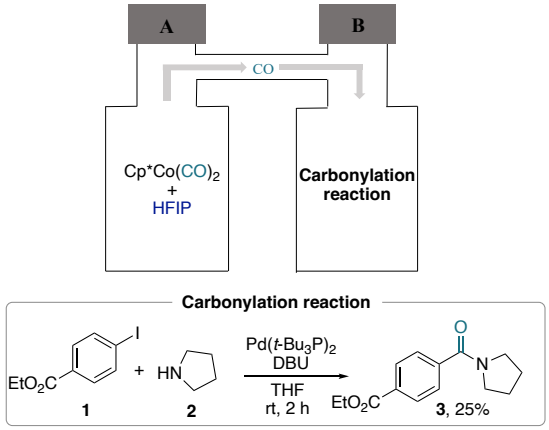

Figure 3.10. The capture of dissociated CO by using two-chamber system

In the absence of HFIP as solvent, we could only observe the formation of carbonylation products (**3** (10% yield) and **4** (25% yield), chamber B) when we the

[26] (a) Hermange, P.; Lindhardt, A. T.; Taaning, R. H.; Bjerglund, K.; Lupp, D.; Skrydstrup, T. *J. Am. Chem. Soc.* **2011**, *133*, 6061. (b) Friis, S. D.; Taaning, R. H.; Lindhardt, A. T.; Skrydstrup, T. *J. Am. Chem. Soc.* **2011**, *133*, 18114.

[27] This result slightly differed from the reported carbonylation by the Skrydstrup group, where they also observed the formation of a double carbonation product (**4**). See Figure 3.11.

dissociation of CO was photoinduced from a solution of the cobalt(I) compound in ethyl ether (Et_2O) (Figure 3.11).[28] In this case, we observed a color change in chamber A upon irradiation with UV light from dark red (before the reaction) to dark green (after the reaction). We tried to confirmed the formation of the triplet Cp*Co(CO) species upon UV irradiation by EPR spectroscopy, but as expected from literature precedents, its short lifetime hampered its detection.[20e,f] This experimental outcome highlights that HFIP is crucial not only for generating the paramagnetic organometallic compound but also for increasing its effective lifetime presumably due to the unique capability of this perfluorinated alcohol to stabilize radical intermediates and establish supramolecular network aggregations.[29]

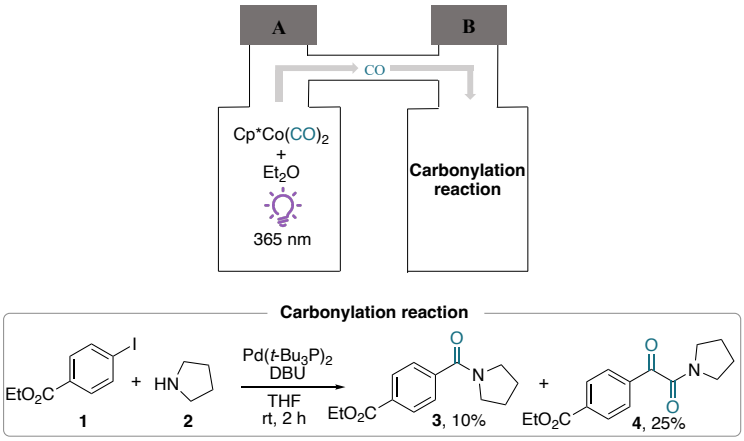

Figure 3.11. CO dissociation promoted by UV light irradiation with non-fluorinated solvents

3.2.2 Preliminary Results on HFIP-enabled Spin Catalysis

As mentioned above, the spin-crossover phenomenon is both appealing and intriguing in the realm of organometallic chemistry. These events can be caused by modifications on the molecular structure of key reactive intermediates along the course of a reaction or by external factors such as changes in temperature, or light irradiation. Strikingly, the major external component of chemical reactions, the surrounding

[28] No product formation is detected without irradiation.

[29] (a) Berkessel, A.; Adrio, J. A.; Hüttenhain, D.; Neudörfl, J. M. *J. Am. Chem. Soc.* **2006**, *128*, 8421. (b) Arnold, A. M.; Philipp Dullinger, P.; Biswas, A.; Jandl, C.; Horinek, D.; Gulder, T. *Nat. Commun.* **2023**, *14*, 813.

solvent, have not been yet considered to play a decisive role for promoting SCO in organometallic catalysis. Our investigations on cobalt chemistry have led to the discovery of an unconventional strategy to generate Cp*Co^{I} species in triplet state, triggered by HFIP, without the necessity of irradiating UV light. Despite this perfluorinated alcohol is receiving special attention by many research groups, including ours, for its unique behavior promoting organic and organometallic transformations, its participation in spin-crossover events had not been contemplated.

Encouraged by these findings, we wondered whether this unconventional phenomenon could provoke a SCO paradigm change in organometallic catalysis enabling transformations that otherwise would not be easily available at the single-state reactivity (SSR) of "closed-shell behavior." In order to test this hypothesis, we seeked for transformations in which the singlet-triplet intersystem crossing (ISC) events in cobalt(I) systems could accelerate reaction rates and unlock bond-breaking/forming processes. Specifically, we envisioned to exploit this solvent-induced SCO to promote the functionalization aryl halides. The idea of using these organic electrophiles as starting materials relies on previous studies from our group. In 2020, we uncovered the facile participation of Cp*Co^{I} complexes in ligand-assisted oxidative addition events when using substrates containing weakly directing groups (Scheme 3.2a).[30] As a proof-of-concept, we reported the first example of a directed functionalization of a benzamide derivative by a Cp*Co^{I}-based system (Scheme 3.2b). These results are particularly relevant since these oxidative addition strategies hold the potential to complement, synthetically and mechanistically, the scarcity of Cp*Co-catalyzed directed C–H functionalization reactions when using arenes containing these prevalent functional groups.

[30] Martínez de Salinas, S.; Sanjosé-Orduna, J.; Odena, C.; Barranco, S.; Benet-Buchholz, J.; Pérez-Temprano, M. H. *Angew. Chem. Int. Ed.* **2020**, *59*, 6239.

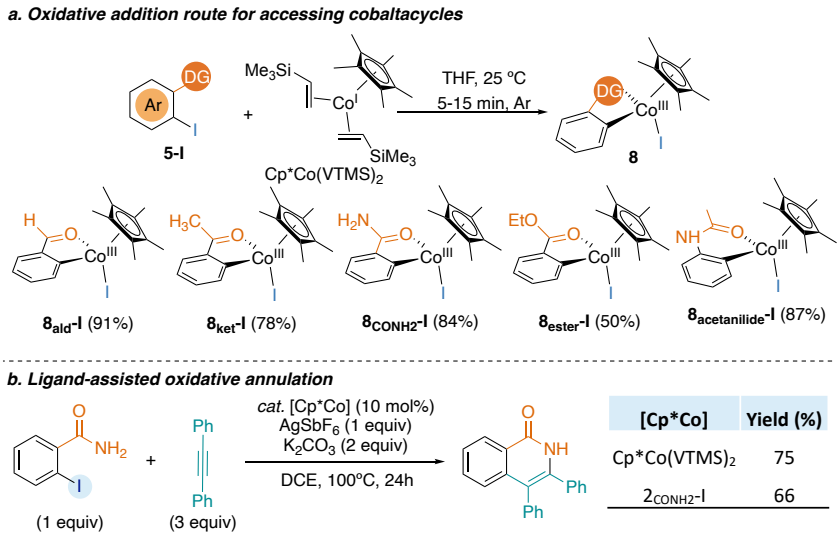

Scheme 3.2. (a) Oxidative addition route for accessing cobaltacycles. (b) Ligand-assisted oxidative annulation between benzamide derivative and diphenylacetylene.

Aiming at establishing the catalytic utility of "non-excited" singlet-triplet intersystem crossing (ISC) via second-coordination sphere interactions (SCSI), we focused our attention on the Mizoroki-Heck cross-coupling. This reaction has proven its versatility and applicability by palladium catalysts using as coupling partners olefins, readily available building blocks in organic synthesis. Yet its use in cobalt catalysis remains practically unexplored. Under appropriate reaction conditions, we anticipated that the *in situ* generated triplet state Cp^*Co^{I} by HFIP might exhibit a higher reactivity towards aryl halides than $Cp^*Co(CO)_2$. Thus, the acceleration of the C–X bond-cleavage might enable the coupling of more accessible aryl bromides and chlorides. From a mechanistic standpoint (Scheme 3.3), a similar scenario to traditional Pd-catalyzed Mizoroki-Heck couplings, in terms of elementary steps, could be foreseen. After the oxidative addition event, a halide abstraction facilitates the coordination and migratory insertion of the olefin into the cobalt–carbon bond, generating an alkyl–cobalt intermediate **II**. A β-hydride elimination would take place affording the olefination product and a cobalt hydride **III** that undergoes reductive elimination after reaction with a base.

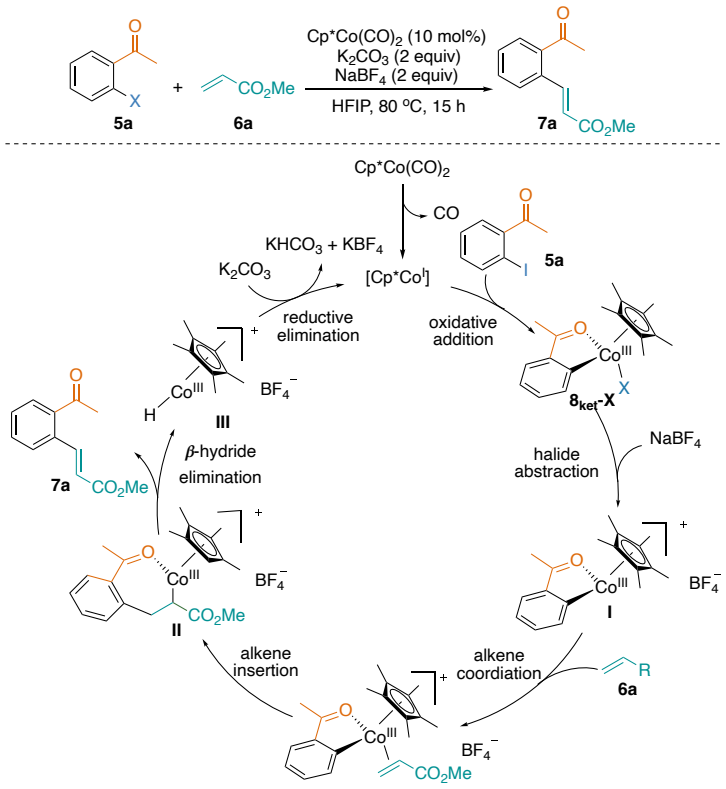

Scheme 3.3. Traditional mechanism

Our initial synthetic efforts towards the ligand-assisted Cp*Co-catalyzed olefination of aryl halides was made using ketone derivatives as starting materials. This selection was performed based on our previous studies on the oxidative addition of aryl iodides to Cp^*Co^I and the stability of the resulting metalacyclic intermediate, key for facilitating the mechanistic investigation of the process. According to the rationale depicted in Scheme 3.3, we speculated that the utilization of a halide abstractor and a base should be key for the overall catalytic efficiency. When we performed the reaction between 2-iodoacetophenone (**5a-I**) and methyl acrylate (**6a**), using 10 mol% of $Cp^*Co(CO)_2$ as the catalyst, in conjunction with $NaBF_4$ (2 equiv) and K_2CO_3 (2 equiv) in HFIP, quantitative formation of the desired product (**7a**) with an excellent *E/Z* selectivity was afforded with after 15 hours at 80 ºC (Scheme 3.4). Notably, when we extended this reactivity to more challenging substrates, such as 2-chloroacetophenone (**5a-Cl**), the olefination reaction was successfully accomplished, yielding **7a** with an impressive 92% yield (Scheme 3.4).

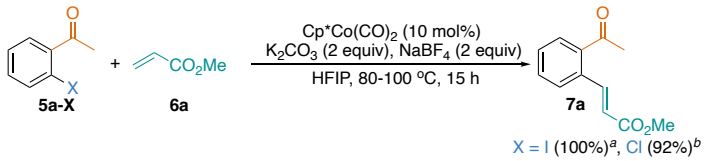

Scheme 3.4. Initial experiments for developing a ligand-assisted Cp*Co-catalyzed Mizoroki-Heck coupling protocol. Reaction conditions: **5a-X** (0.05 mmol, 1.0 equiv), **6a** (0.1 mmol, 2.0 equiv), $Cp^*Co(CO)_2$ (10 mol%), $NaBF_4$ (0.1 mmol, 2.0 equiv), K_2CO_3 (0.1 mmol, 2.0 equiv), HFIP (0.5 mL) at 80 °C for 15 h. The yields were determined by analysis of the crude mixture by ^1H NMR spectroscopy by using CH_2Br_2 as an internal standard. [a]The reaction was performed at 80 °C. [b]The reaction was performed at 100 °C.

With these promising results in hand, we carried out control experiments to corroborate the involvement of the proposed triplet cobalt(I) species within the catalytic transformation (Tables 3.1 and 3.2). Our attempts to employ alternative catalyst/solvent combinations proved to be ineffective, confirming the unique reactivity observed with $Cp^*Co(CO)_2$ in HFIP. First, we explored other group 9 Cp^XTM^I catalysts (Table 3.1). Despite we observed the formation of a paramagnetic species when dissolving $CpCo(CO)_2$ in hexafluoroisopropanol, we rationalized the lack of catalytic activity to the lower electron donating ability of the cyclopentadienyl ligand, which less to organometallic compounds less prone to participate in oxidative addition events (entry 2). In sharp contrast to our previous reported example in 2020, when we used $Cp^*Co(VTMS)_2$ as catalyst, we do not observed the olefinated product (entry 3). Instead, we observed the formation of the corresponding Hiyama product leading to catalyst degradation.[31] Additionally, when we used $Cp^*Rh(CO)_2$, direct analogue of the cobalt(I) compound, no conversion was detected (entry 4). This result reassures that first-row transition metals are more than merely cost-effective alternative to precious metals and they can unlock new reaction modes/pathways currently unprecedented in TM catalysis. As expected, in the absence of $Cp^*Co^I(CO)_2$ no product formation was observed (entry 5).

Table 3.1. Control experiments: Evaluation of the catalyst effect[a]

[31] This initial hit has been further explored by our research group, leading to the development of an alternative olefination protocol.

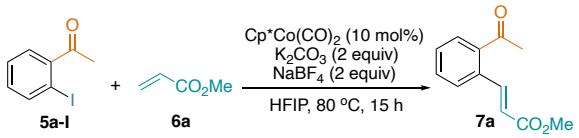

Entry	Changes from the standard conditions	Yield of **7a** (%)
1	none	100
2	$CpCo(CO)_2$ instead of $Cp^*Co(CO)_2$	0
3	$Cp^*Co(VTMS)_2$ instead of $Cp^*Co(CO)_2$	traces
4	$Cp^*Rh(CO)_2$ instead of $Cp^*Co(CO)_2$	0
5	Without $Cp^*Co(CO)_2$	0

[a]Reaction conditions: **5a-I** (0.05 mmol, 1.0 equiv), **6a** (0.1 mmol, 2.0 equiv), $Cp^*Co(CO)_2$ (10 mol%), $NaBF_4$ (0.1 mmol, 2.0 equiv), K_2CO_3 (0.1 mmol, 2.0 equiv), solvent (0.5 mL) at 80 °C for 15 h. The yields were determined by analysis of the crude mixture by ^1H NMR spectroscopy by using CH_2Br_2 as an internal standard.

We next evaluated the solvent influence (Table 3.2). In alignment with our preliminary EPR study, only the employment of perfluorinated solvents led to the formation of **7a**. While TFE only affords **7a** in 13% yield (entry 2), perfluoro-tert-butanol (PFTB) gives the desired product in quantitative yields (entry 3). The presence of the CF_3- and OH- groups in the solvent is pivotal, given the ineffectiveness of 2-propanol or MeOH (entries 4-5) and 1,1,1,3,3,3-hexafluoroisopropyl methyl ether (Me-HFIP) (entry 6). Commonly used non-perfluorinated organic solvents are not suitable for facilitating this olefination reaction (entries 7-10).

Table 3.2. Control experiments: Evaluating solvent effects[a]

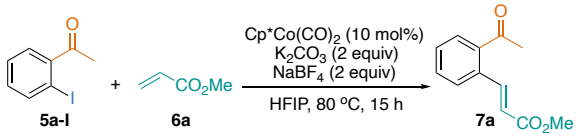

Entry	Changes from the standard conditions	Yield of 7a (%)
1	None	100
2	TFE instead of HFIP	13
3	PFTB instead of HFIP	100
4	2-Propanol instead of HFIP	0
5	MeOH instead of HFIP	0
6	HFIPMe instead of HFIP	0
7	Toluene instead of HFIP	0
8	DCE instead of HFIP	0
9	THF instead of HFIP	0
10	Dioxane instead of HFIP	0

[a]Reaction conditions: **5a-I** (0.05 mmol, 1.0 equiv), **6a** (0.1 mmol, 2.0 equiv), Cp*Co(CO)$_2$ (10 mol%), $NaBF_4$ (0.1 mmol, 2.0 equiv), K_2CO_3 (0.1 mmol, 2.0 equiv), solvent (0.5 mL) at 80 °C for 15 h. The yields were determined by analysis of the crude mixture by ^1H NMR spectroscopy by using CH_2Br_2 as an internal standard.

At this point, the gathered experimental outcomes suggested that the *in-situ* generation of open-shell Cp*Co^I species in HFIP, after CO dissociation, is key for the successful realization of the olefination reaction. Given the well-established ability of UV light to enable the access to triplet Cp^{X}Co(CO) intermediates, we decided to test the feasibility of a photoinduced methodology (Scheme 3.5). The reaction between **5a-Cl** and **6a** in 2-propanol at room temperature, using 30 mol% of Cp*Co(CO)$_2$ and UV light, turned to be considerable worse in terms of yield (37%) and *E/Z* regioselectivity (1:1.5). Thus, our "non-excited" route enabled by HFIP offers exciting opportunities to complement photochemical methodologies and expand the applicability of open-shell TM catalysis.

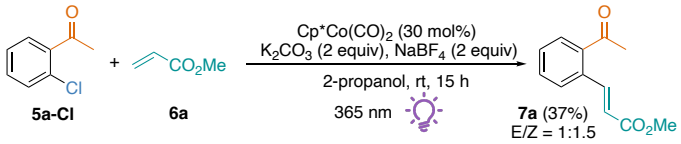

Scheme 3.5. UV light-promoted Cp*Co-catalyzed Mizoroki-Heck coupling

3.2.3 Scope of the reaction

Aryl Halide Scope

Adopting the optimized conditions reported in the previous section, we next explored the generality of our Cp*Co(I)-catalyzed Heck-type coupling. We first evaluated the scope of the aryl halides. As shown in Scheme 3.6, the reaction displayed compatibility not only with iodo substrates but also their bromo or chloro counterparts, as exemplified by the yield achieved with 2-bromoacetophenone (**7a**). Sterically hindered (2-chlorophenyl)(phenyl)methanone was also successfully coupled in a great yield (**7b**). Our method exhibited exceptional selectivity, yielding a quantitative amount of **7c** when an additional chlorine atom was present in the substrate. Additionally, extending beyond ketones, successful implementation of esters as DG yielded the desired product **7d** in a substantial yield. The different substituents in the phenyl ring of methyl 2-bromobenzoate were investigated (**7e**-**7n**). The reaction was tolerated to either electron rich or electron deficient substituents, as well as some valuable functional groups such as free amine, -F, -Cl, -I. Extension of this reaction to heterocyclic methyl esters turned out to be successful. Methyl 5-bromo-1H-indazole-6-carboxylate and methyl 4-bromo-7-methoxy-1,3-benzodioxole-5-carboxylate could also react with methyl acrylate **6a** to afford corresponding products in moderate yields (**7o** and **7p**). Substitution of methyl with ethyl group delivered the product **7q** in high yield. Notably, the primary amides which usually are not capable in TM-catalyzed C–H functionalization reactions worked well in our catalysis and gave desired product **7r** in great yield.[32] Besides, not only primary amides, secondary amides (**7s**-**7v**) and tertiary amides (**7w**-**7y**), also proved to be suitable substrates to give the corresponding products in good to great yields. It is worth noting that Flubendiamide, a synthetic petrochemical pesticide underwent tandem heck coupling and Michael addition to give lactam product **7v** in 65% yield. The more electron rich substrates 2-I- and 2-Br-acetanilide could afford **7z** in great yield. Moreover, the benzoic acid substrates with different substituetions underwent tandem heck coupling and Michael addition to give

[32] few examples of primary amides in C-H oxidative olefination: (a) Baghel, A. S.; Aghi, A.; Kumar, A. *J. Org. Chem.* **2021**, *86*, 9744. (b) Patureau, F. W.; Besset, T.; Glorius, F. *Angew. Chem., Int. Ed*. **2011**, 50, 1064. (c) Bao, R.-P.; Chen, X.; Li, C.; Wang D.-H. *Org. Lett.* **2019**, *21*, 8116. (d) Zhang, Y.; Struwe, J.; Ackermann L. *Angew. Chem. Int. Ed.* **2020**, *59*, 15076. (e) Jambu, S.; Shambhavi, C. N.; Jeganmohan, M. *Org. Lett*. **2021**, *23*, 2964.

the lactone products in moderate to excellent yields (**7aa**-**7ad**). In order to have the Heck product instead of lactone product **7aa** with carboxylic acid as DG, *tert*-butyl 2-bromobenzoate was chosen as substrate, since HFIP could cleave *tert*-butyl esters under thermolytic conditions.[33] As we expected, it afforded corresponding deprotection product **7ae** in an excellent yield. Heterocyclic carboxylic acids were also examined. For example, both 3-bromo-2-thiophenecarboxylic acid and 2-bromo-3-furancarboxylic acid were compatible with the reaction conditions, giving the corresponding heck products (**7af**-**7ag**).

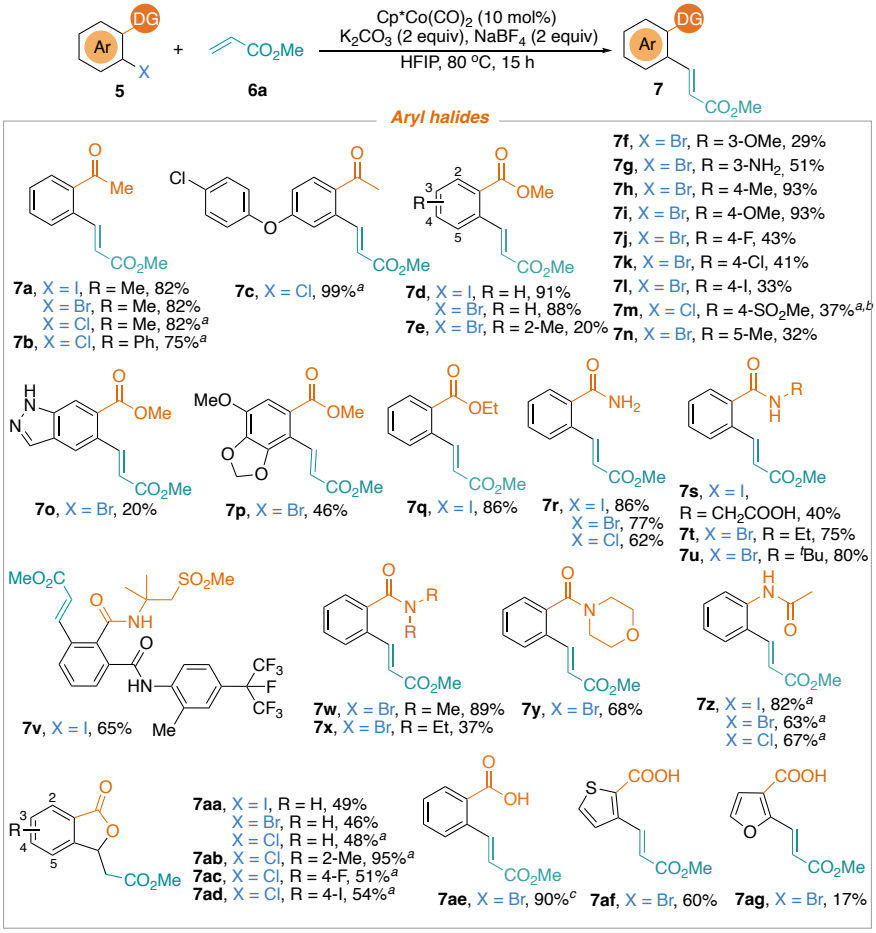

Scheme 3.6. Scope of the aryl iodides and bromides. Reaction conditions: **5** (0.15 mmol, 1.0 equiv), **6a** (0.3 mmol, 2.0 equiv), $Cp^*Co(CO)_2$ (10 mol%), $NaBF_4$ (0.3 mmol, 2.0 equiv), K_2CO_3 (0.3 mmol, 2.0 equiv), HFIP (1.5 mL) at 80 °C for 15 h. The yields are isolated yields.

[33] Choy, J.; Jaime-Figueroa, S.; Lara-Jaime, T. *Tetrahedron Lett.* **2010**, *51*, 2244.

[a]The reactions were performed at 100 ºC. [b]An esterification reaction was performed after the reaction, details see *Experimental Section*. [c]The product was obtained from *tert*-butyl 2-bromobenzoate.

Alkene Scope

Subsequently, we proceeded to assess the diversity of alkene substrates. Specifically, we selected as model organic electrophile an ester derivative, 2-iodobenzoate. The ester group can be commonly found in synthetically relevant organic compounds, since it can be easily transformed it into other functional groups, such as carboxylic acid, amide, ketone, aldehyde, among others.[34] However, in the context of directed TM-catalyzed C–H functionalizations, the exploitation of esters as DGs remains challenging, especially in Cp*Co catalysis.[35] Therefore, our orthogonal methodology could surmount certain existing synthetic limitations.

As shown in Scheme 3.7, the activated or electronically biased alkenes such as the *t*-butyl and benzyl acrylates were effective to furnish the corresponding alkenylated products (**9a-9b**). When phenyl acrylate was used as coupling partner, the reaction delivered **9c** in 38% isolated yield, accompanied by the formation of by-products, which likely due to the alcoholysis of phenyl acrylate **6c** with the HFIP solvent.[36] Isobornyl group was compatible in this Heck coupling and delivered the desired product **9d** in 68% yield. Acrylamide was tolerated but only gave product **9e** in 23% yield. Vinyl sulfone could give a moderate yield of the desired product **9f** at 100 ºC, accompanied by the formation of the Michael addition by-product **6f-1** in 50% yield.

The utilization of unactivated olefins in TM-catalyzed oxidative C–H olefination reactions has been limited due to their inherent low reactivity. Encouragingly, our olefination protocol exhibits remarkable efficacy when applied to non-activated alkenes. This was evidenced by the successful coupling of vinylcyclohexane **6g**, affording the desired product **9g** in a high yield. Further underscoring the versatility of our approach, the coupling of the allylic alcohol, 3-buten-1-ol, yielded product **9h** in

34 (a)Esters, Organic. Ullmann's Encyclopedia of Industrial Chem-istry; Riemenschneider, W., Bolt, H. M., Eds.; Wiley-VCH: Weinheim, 2005. (b) Veitch, G. E.; Bridgwood, K. L.; Ley, S. V. *Org. Lett.* **2008**, *10*, 3623. (c) Cao, P.; Raleigh, D. P. *J. Am. Chem. Soc*. **2010**, *132*, 4052.

35 (a) Yu, W.; Zhang, W.; Liu, Z.; Zhang, Y. *Chem. Commun*. **2016**, *52*, 6837. (b) Kong, L.; Yang, X.; Zhou, X.; Yu, S.; Li, X. *Org. Chem. Front.* **2016**, *3*, 813.

36 Shao, N.-Q.; Chen, Y.-H.; Li, C.; Wang, D.-H. *Org. Lett.* **2020**, *22*, 7141.

an impressive 83% yield with an E/Z ratio of 2.2:1. Notably, the commercially available vinyl cyclic carbonate **6i** showcased its potential by undergoing decarboxylative Heck coupling, yielding the corresponding allylic alcohol product **9i** (30% yield, E:Z = 1:1). The industrially significant alkene, ethylene, readily engaged in the reaction, yielding the terminal olefin **9j** with a notable 85% yield. Expanding the scope to encompass less reactive internal alkenes, coupling with methyl 2-iodobenzoate **5b** led to the formation of trisubstituted alkenes (**9k-9l**) in moderate yields. Notably, an array of styrene derivatives, regardless of substitution patterns on the aryl ring, proved amenable to standard conditions, delivering the targeted products in good to excellent yields (**9m-9x**). Remarkably, this reaction showcased compatibility with various functional groups commonly found on the aromatic ring of styrenes—fluoro, chloro, bromo, aldehyde, cyano, trifluoromethyl substituents. This characteristic opens avenues for further coupling strategies, enabling the synthesis of more intricate and multifaceted molecules.

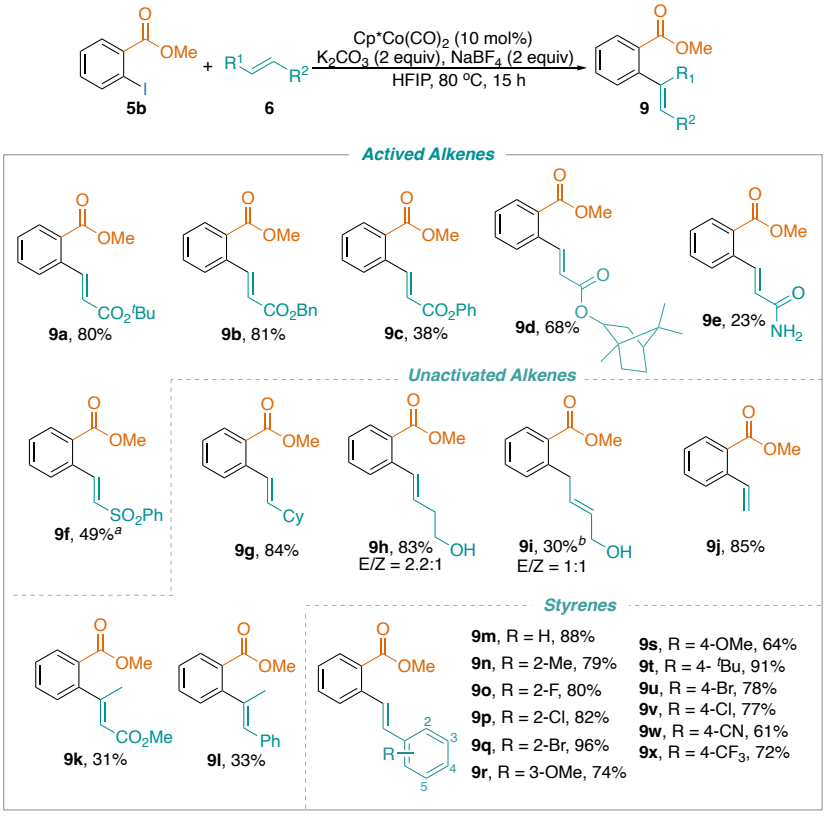

Scheme 3.7. Scope of the unactivated alkenes and styrenes. Reaction conditions: **5b** (0.15 mmol, 1.0 equiv), **6** (0.3 mmol, 2.0 equiv), $Cp^*Co(CO)_2$ (10 mol%), $NaBF_4$ (0.3 mmol, 2.0 equiv), K_2CO_3 (0.3 mmol, 2.0 equiv), HFIP (1.5 mL) at 80 °C for 15 h. The yields are isolated yields. [a]The reaction was performed at 100 °C. [b]4-Vinyl-1,3-dioxolan-2-onewas used as coupling partner.

Furthermore, the high functional group tolerance of our Heck coupling was highlighted by its application in late-stage functionalization of natural products (Scheme 3.8). For example, substrates derived from drugs or natural products, such as Vitamin E, Diacetine-D-glucose, Bezafibrate, Indomethacin, Oxaprozin, and Naproxen were all suitable for the transformations to give desired products in good to excellent yields (**9y-9ad**). For the alkene substrates bearing an aliphatic chain, the 1,1-insertion product **9-1** was also produced (**9z-1**, **9aa-1**, **9ac-1**, **9ad-1**).

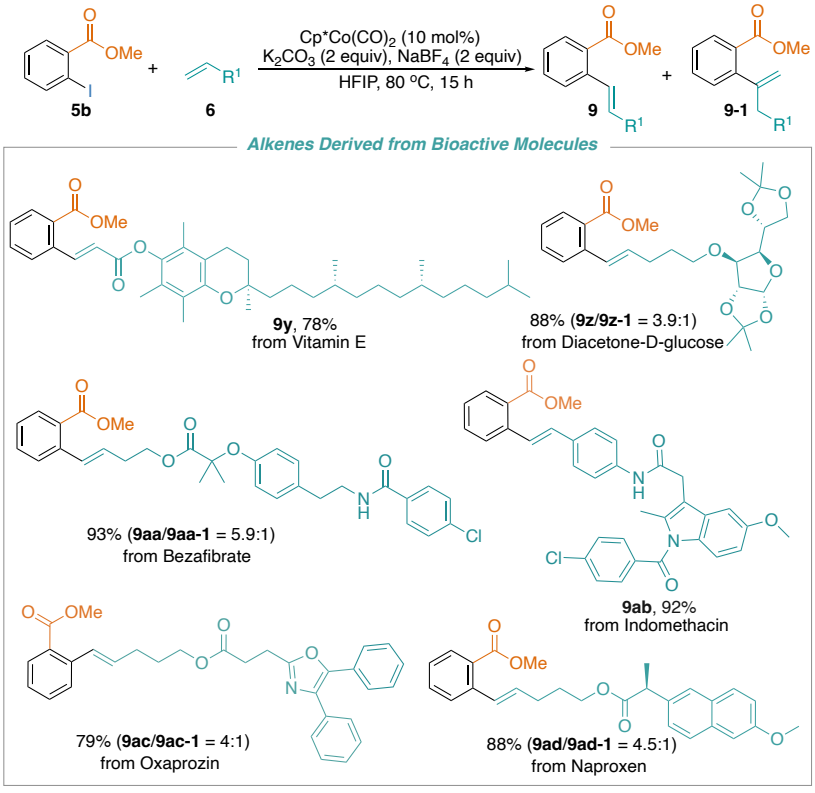

Scheme 3.8. Scope of the drug derivative alkenes. Reaction conditions: **5b** (0.15 mmol, 1.0 equiv), **6** (0.3 mmol, 2.0 equiv), $Cp^*Co(CO)_2$ (10 mol%), $NaBF_4$ (0.3 mmol, 2.0 equiv), K_2CO_3 (0.3 mmol, 2.0 equiv), HFIP (1.5 mL) at 80 °C for 15 h. The yields are isolated yields.

Scope Limitations

It is worth noting that some of the tested aryl halides and alkenes did not work or gave the desired product in low yields (Scheme 3.9 to 3.11). In terms of DGs, Aldehyde derivative (**5ah**) only gave traces amount of the heck product, even when using aniline as additive to form an imine as transient directing group. Sulfonamide (**5ai**) and trifluoroacetophenone (**5aj**) are not good directing groups, probably because of their weakly coordinated abilities. Surprisingly, using strong directing groups such as pyridine (**5ak**), the most prevalent in C–H functionalization reactions in Cp*Co chemistry, did not deliver any product. Phenol (**5al**), aniline (**5am**), benzonitrile (**5an**) are not good substrates, presumably due to the difficulties associated to the formation of the corresponding four-membered cobaltacycles after the oxidative addition. Moreover, substrate **5ao** which could form six-membered cobaltacycle is also unreactive. Additionally, C–F, C–O bonds cannot be activated in this methodology (**5ap-5ar**).

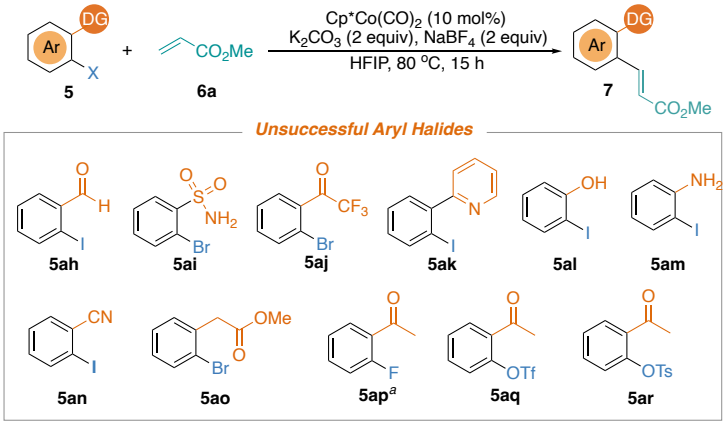

Scheme 3.9. The scope of unsuccessful aryl halides. Reaction conditions: **5** (0.15 mmol, 1.0 equiv), **6a** (0.3 mmol, 2.0 equiv), $Cp^*Co(CO)_2$ (10 mol%), $NaBF_4$ (0.3 mmol, 2.0 equiv), K_2CO_3 (0.3 mmol, 2.0 equiv), HFIP (1.5 mL) at 80 °C for 15 h. The yields were determined by analysis of the crude mixture by ^1H NMR spectroscopy by using CH_2Br_2 as an internal standard. [a]The reaction was performed at 100 °C.

We have also explored if the olefination protocol could be extended to additional organic halides. For example, we did not observe product formation when using the vinyl iodide substrate **5as**.[37] Instead, an air stable three-membered cobaltacycle **7as-1** was obtained (Scheme 3.10). This result suggests that **5as** can undergo oxidative

[37] We chose styrene **6m** instead of methyl acrylate **6a** as the coupling reagent to facilitate the further analysis process due to the fluorescent of the aromatic ring of the olefin.

addition but the subsequent the alkene coordinating and/or insertion process seems not favored.

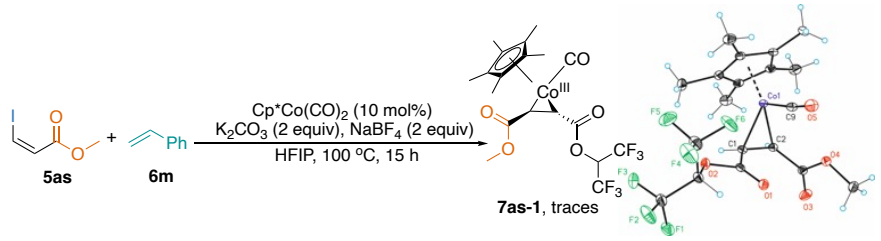

Scheme 3.10. Heck coupling of vinyl iodide **5as** and styrene **6m**. Reaction conditions: **5as** (0.15 mmol, 1.0 equiv), **6m** (0.3 mmol, 2.0 equiv), $Cp^*Co(CO)_2$ (10 mol%), $NaBF_4$ (0.3 mmol, 2.0 equiv), K_2CO_3 (0.3 mmol, 2.0 equiv), HFIP (1.5 mL) at 100 °C for 15 h. The yields was determined by analysis of the crude mixture by ^1H NMR spectroscopy by using CH_2Br_2 as an internal standard.

Attempts to carry out non-directed olefination reactions turned out to be unsuccessful. When we employed **5at** as starting material, instead of the desired product, we detected that the Cp* acted as coupling partner (Scheme 3.11).[38]

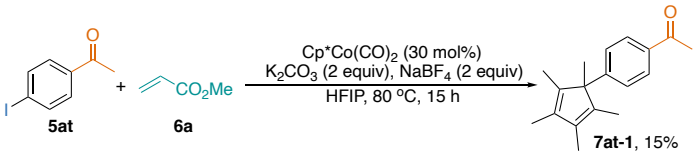

Scheme 3.11. Heck coupling of 4-iodoacetophenone **5at** and methyl acrylate **6a**. Reaction conditions: **5at** (0.05 mmol, 1.0 equiv), **6a** (0.1 mmol, 2.0 equiv), $Cp^*Co(CO)_2$ (30 mol%), $NaBF_4$ (0.1 mmol, 2.0 equiv), K_2CO_3 (0.1 mmol, 2.0 equiv), HFIP (0.5 mL) at 80 °C for 15 h. The yields are isolated yields.

A survey of low yielding and unsuccessful alkene substrates is also provided in Scheme 3.12. 1,1-disubstituted alkenes **6ae-6ag** are not tolerated. The internal alkenes substrates **6ah-6ak** are inefficient due to their low reactivity. Alkenes **6al** – **6ao** failed to afford the targeted products, probably due to the hindrance. Electron rich alkenes such as **6ap-6as** had lower reactivity compared to electron deficient alkenes, which cannot be coupled in this methodology. –Br, –CHO and $–NO_2$ were not tolerated in this catalytic transformation (**6at-6av**). Phenyl(vinyl)sulfane **6aw** exhibits a notable preference for Markovnikov addition with HFIP, rather than undergoing cross-coupling with methyl 2-iodobenzoate **5b.**

[38] See supporting information for further details.

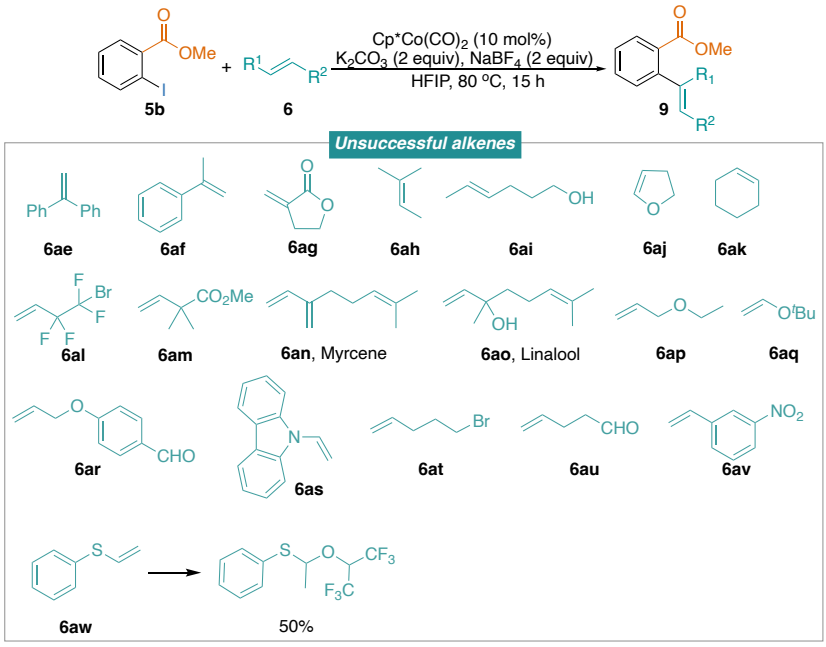

Scheme 3.12. Scope of the unsuccessful alkenes. Reaction conditions: **5b** (0.15 mmol, 1.0 equiv), **6** (0.3 mmol, 2.0 equiv), $Cp^*Co(CO)_2$ (10 mol%), $NaBF_4$ (0.3 mmol, 2.0 equiv), K_2CO_3 (0.3 mmol, 2.0 equiv), HFIP (1.5 mL) at 80 °C for 15 h. The yields were determined by analysis of the crude mixture by ^1H NMR spectroscopy by using CH_2Br_2 as an internal standard.

There are also olefines that, instead of the alkenylation product, favor the alkylated one (Scheme 3.13), presumably due to the participation of HFIP as proton source.

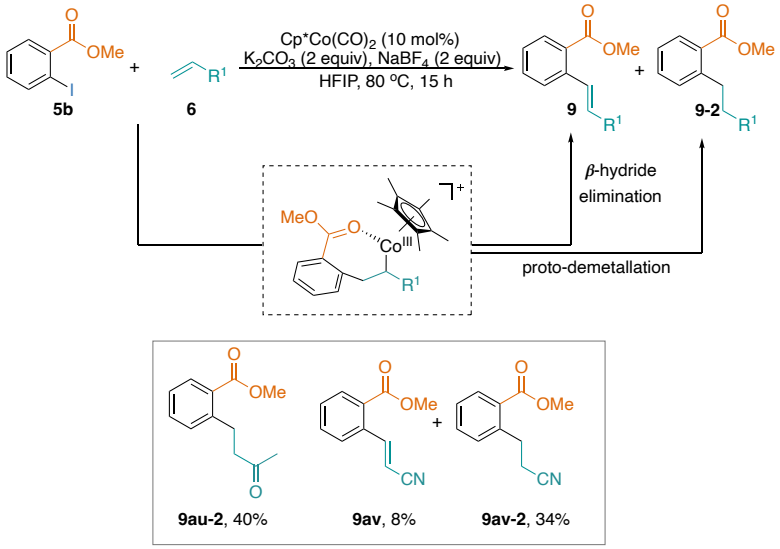

Scheme 3.13. Heck coupling of **5b** with vinyl ketone and acrylonitrile. Reaction conditions: **5b** (0.15 mmol, 1.0 equiv), **6** (0.3 mmol, 2.0 equiv), $Cp^*Co(CO)_2$ (10 mol%), $NaBF_4$ (0.3 mmol, 2.0 equiv), K_2CO_3 (0.3 mmol, 2.0 equiv), HFIP (1.5 mL) at 80 ºC for 15 h. The yields are isolated yields.

3.2.4. Mechanistic Studies

To gain further information about the mechanistic intricacies of the reaction, we first decided to follow our traditional approach and test the catalytic performance of proposed reaction intermediates. In particular, we decided to evaluate the reactivity of the oxidative addition process to access the metallacycle, as proposed in Scheme 3.3. We focused our attention on the more challenging aryl chloride substrate **5a-Cl**, as we expected, the oxidative addition of **5a-Cl** and $Cp^*Co(CO)_2$ proceeded smoothly, leading to the $\mathbf{8_{ket}}$**-Cl** in a 40% isolated yield (Scheme 3.14). This outcome strongly suggests the feasibility of facial C–X bond cleavage, facilitated by the Cp*Co(CO) triplet state species.

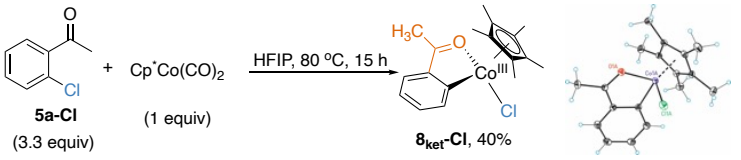

Scheme 3.14. Oxidative addition process between 2-chloroacetophenone and $Cp^*Co(CO)_2$

Next, we envaulted the activity of the metallacyclic compounds that were expected to be formed after the oxidative addition step, as proposed in Scheme 3.3. Strikingly, when we employed $\mathbf{8_{ket}}$**-X** as catalysts, instead of obtaining comparable results to the ones with $Cp^*Co(CO)_2$, we only observed traces of the desired product (Scheme 3.15). These results clearly indicate that $\mathbf{8_{ket}}$**-X** are not intermediates within the catalytic cycle, suggesting a more complex mechanistic scenario than originally anticipated.

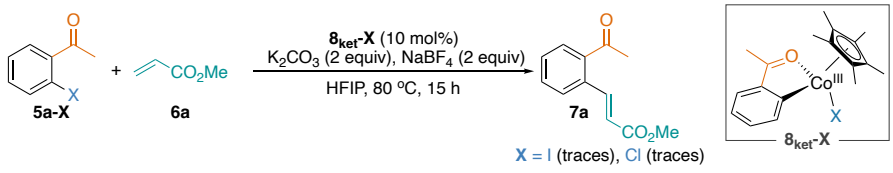

Scheme 3.15. Catalytic activity of $\mathbf{8_{ket}}$**-X** complexes

Intrigued by these results, computational studies have been performed by Dr. Ignacio Funes (Universidad de La Rioja) to interrogate the lack of catalytic activity

observed when using **8$_{ket}$-X**. In alignment with our experimental results, DFT calculations at CPCM M06/Def2TZVPP//wB97xD/Def2SVP level in HFIP solvent revealed that **8$_{ket}$-CO** in the singlet spin state is formed after the oxidative addition event instead of the expected **8$_{ket}$-X** intermediate (Scheme 3.16). Moreover, these studies support the participation of ISC events along the C–X bond cleavage, observing lower energy barriers for the transition state of oxidative addition process in the triplet spin state, regardless of whether iodide (21.2 kcal/mol) or chloride (21.0 kcal/mol) was employed.

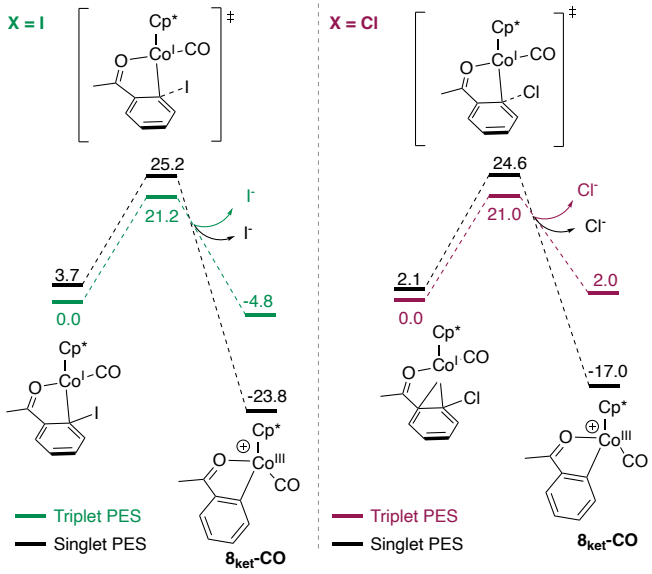

Scheme 3.16. DFT calculations

In order to confirm the catalytic intermediacy of **8$_{ket}$-CO**, we synthesized independently this complex by the treatment of **8$_{ket}$-CO** with $AgBF_4$ in the presence of CO atmosphere (Scheme 3.17a). The corresponding cationic metalacyclic compound was isolated in 59% yield and fully characterized by NMR spectroscopy and X-ray crystallography. With this synthesis in hand, we subsequently employed the isolated **8$_{ket}$-CO** as a pre-catalyst for the Heck coupling, and we were pleased to observe a quantitative yield of **7a** after 15 hours (Scheme 3.17b). These outcomes strongly imply that **8$_{ket}$-CO** indeed functions as an intermediate within the catalytic cycle. Interstingly, when the same reaction was conducted in 2-propanol or TFE, only trace amounts of **7a** were produced. This underscores the significance of HFIP, not only in the generation

of the Cp*Co(CO) triplet state species and the oxidative addition process, but also in the subsequent crucial steps of the reaction.

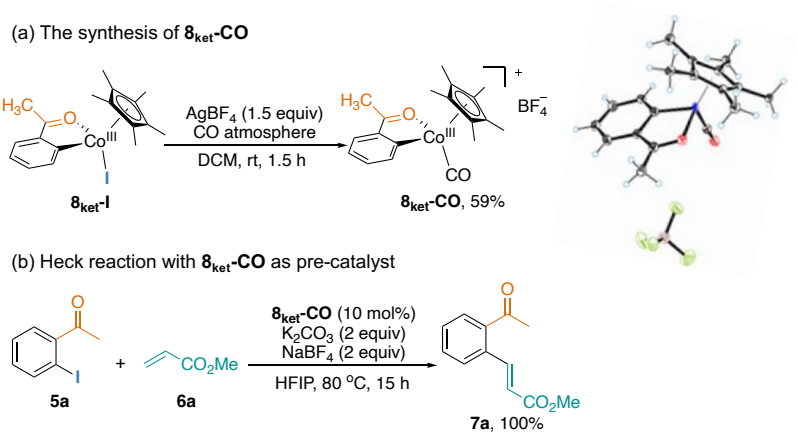

Scheme 3.17. (a) The synthesis of **8_{ket}-CO.** (b) Heck reaction with **8_{ket}-CO** as pre-catalyst

In an effort to further elucidate the nature of the species formed along the ligand-assisted Mizoroki-Heck coupling, we performed preliminary high-resolution mass spectrometry (HRMS) studies (Scheme 3.18). To ensure adequate intermediate concentrations for detection, a catalyst loading of 30 mol% was employed. The results revealed the possible presence of intermediates **In-I** and **II**.

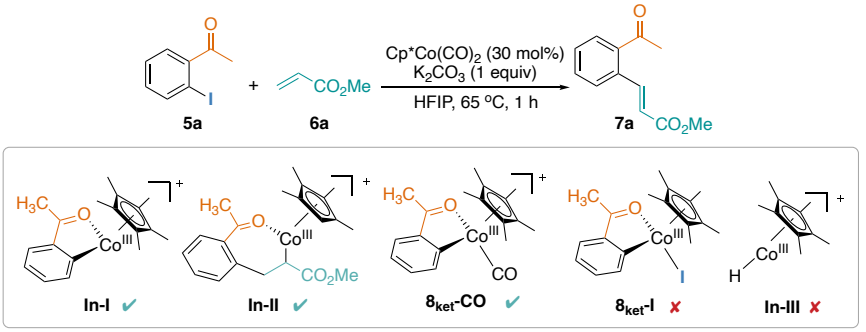

Scheme 3.18. Possible intermediates detected by HRMS of a catalytic experiment.

In order to investigate the possibility that the reaction underwent a radical mechanism, a standard reaction was conducted in the presence of the two most commonly utilized radical scavengers, 2,6-di-tert-butyl-4-methylphenol (BHT) and 2,2,6,6-tetramethylpiperidine 1-oxyl (TEMPO; Table 3.3). No change in the yield of product **7a** (entry 1) was observed upon addition of BHT, however, when two

equivalents of TEMPO were used, no product was detected (entry 2). To test if the TEMPO had inhibited the catalyst, 10 mol% of TEMPO was added to the reaction, resulting in a product yield of 8% (entry 3). These results suggest that TEMPO poisoned the Cp*Co(CO)$_2$ catalyst, as reported by Harris.[39]

Table 3.3 Radical tapping experiments[a]

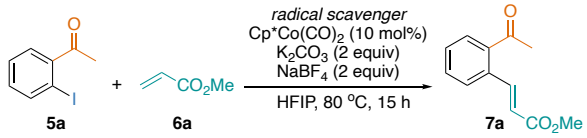

Entry	Radical scavenger	Yield of 7a (%)
1	BHT (2 equiv)	100
2	TEMPO (2 equiv)	0
3	TEMPO (10 mol%)	8

[a]Reaction conditions: **5a** (0.05 mmol, 1.0 equiv), **6a** (0.1 mmol, 2.0 equiv), Cp*Co(CO)$_2$ (10 mol%), $NaBF_4$ (0.1 mmol, 2.0 equiv), K_2CO_3 (0.1 mmol, 2.0 equiv), radical scavenger (x equiv), HFIP (0.5 mL) at 80 °C for 15 h. The yields were determined by analysis of the crude mixture by ^{1}H NMR spectroscopy by using CH_2Br_2 as an internal standard.

To gain further insight, we next performed a radical clock experiment and subjected *cis*-diphenylcyclopropenyl olefin (***cis*-10**) to standard reaction, instead of obtaining any heck product, the starting material **5a** remained in 100%, and the *trans*-olefin was formed in a mixture with the *cis*-isomer in a 6.6:1 ratio, which is a strong indication of radical intermediates (Scheme 3.19).

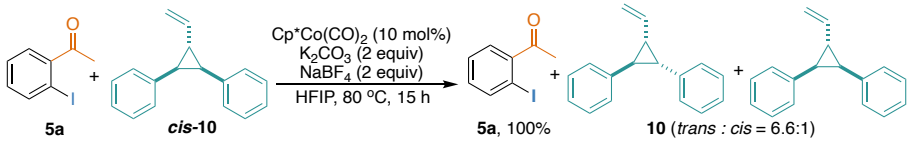

Scheme 3.19. Radical clock experiments. Reaction conditions: **5a** (0.05 mmol, 1.0 equiv), ***cis*-10** (0.1 mmol, 2.0 equiv), Cp*Co(CO)$_2$ (10 mol%), $NaBF_4$ (0.1 mmol, 2.0 equiv), K_2CO_3 (0.1 mmol, 2.0 equiv), HFIP (0.5 mL) at 80 °C for 15 h. The yields were determined by analysis of the crude mixture by ^{1}H NMR spectroscopy by using CH_2Br_2 as an internal standard.

A series of control experiments were meticulously conducted to elucidate the nature of the interaction between HFIP and Cp*Co(CO)$_2$, as outlined in Table 3.4. In the

[39] Lomont, J. P.; Nguyen, S. C.; Harris, C. B. *J. Am. Chem. Soc.* **2013**, *135*, 11266.

scenario where aryl halide **5a** was absent, the ***trans:cis*-10** ratio displayed a resemblance to that observed in the presence of **5a** (entry 1). This observation indicates that the absence of aryl halide **5a** did not significantly alter the ***trans:cis*-10** ratio. Interestingly, employing 2-propanol as the solvent failed to yield the *trans* olefin (entry 2), while in TFE (entry 3), a ***trans:cis*-10** ratio of 1.6:1 was attained, suggesting a notable role of fluorinated solvents in trans olefin formation. These results aligned with our EPR measurements, which indicated that the formation of cobalt paramagnetic species exclusively occurred in fluorinated solvents. Significantly, the reaction was entirely inhibited when carried out without the catalyst (entry 4), effectively dismissing the possibility of a radical mechanism being responsible for the reaction. Neither the additive nor the base exhibited any significant impact on the ***trans:cis*-10** ratio (entry 5). Minor variations in the ratio were observed even when the reaction was conducted at room temperature (entry 6). Noteworthy, $CpCo(CO)_2$ resulted in the formation of ***trans*-10**, albeit with a lower *trans:cis* ratio of 5:1 (entries 7). PFTB, on the other hand, yielded a 6:1 ***trans:cis*-10** ratio (entry 8). These findings collectively indicated that the interaction between Co(I) catalysts and fluorinated solvents could generate paramagnetic species, thus enabling the isomerization process.[40]

Table 3.4. Radical clock control experiments.[a]

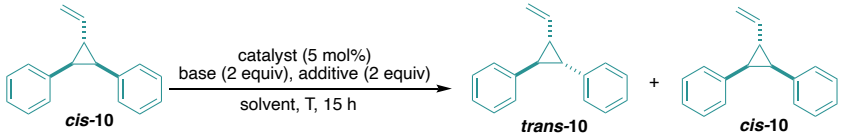

[40] Kapat, A.; Sperger, T.; Guven, S.; Schoenebeck, F. *Science* **2019**, *363*, 391.

Entry	Catalyst	Additive	Base	Solvent	Temperature (°C)	Ratio of ***trans*-10**:***cis*-10**
1	$Cp^*Co(CO)_2$	$NaBF_4$	K_2CO_3	HFIP	80	6.6:1
2	$Cp^*Co(CO)_2$	$NaBF_4$	K_2CO_3	^{i}PrOH	80	0:1
3	$Cp^*Co(CO)_2$	$NaBF_4$	K_2CO_3	TFE	80	1.6:1
4	-	$NaBF_4$	K_2CO_3	HFIP	80	0:1
5	$Cp^*Co(CO)_2$	-	-	HFIP	80	6.3:1
6	$Cp^*Co(CO)_2$	-	-	HFIP	rt	6.6:1
7	$CpCo(CO)_2$	-	-	HFIP	rt	5:1
8	$Cp^*Co(CO)_2$	-	-	PFTB	rt	6:1

[a]Reaction conditions: ***cis*-10** (0.1 mmol, 1.0 equiv), $Cp^*Co(CO)_2$ (5 mol%), additive (0.1 mmol, 1.0 equiv), base (0.1 mmol, 1.0 equiv), solvent (0.5 mL) at T for 15 h. The ratio was determined by analysis of the crude mixture by ^{1}H NMR spectroscopy.

3.2.5. Proposed mechanism

Based on the mechanistic studies, we proposed the mechanistic picture detailed in Scheme 3.20. In the presence of $NaBF_4$ and K_2CO_3, the triplet state Cp*Co(CO) species was generated in situ through the interaction with HFIP. This triplet state underwent oxidative addition with aryl halides **5**, leading to the formation of $\mathbf{8_{DG}}$**-CO**. Subsequently, coordination and migratory insertion of the olefin into the cobalt–carbon bond occur, giving rise to the formation of an alkyl–cobalt intermediate **B**. A subsequent β-hydride elimination event ensues, yielding the olefination product (**7**, **9**) and a cobalt hydride B. The latter undergoes reductive elimination after interacting with a base, where CO re-coordinates to cobalt, thereby regenerating the Cp*Co(CO) triplet state species.

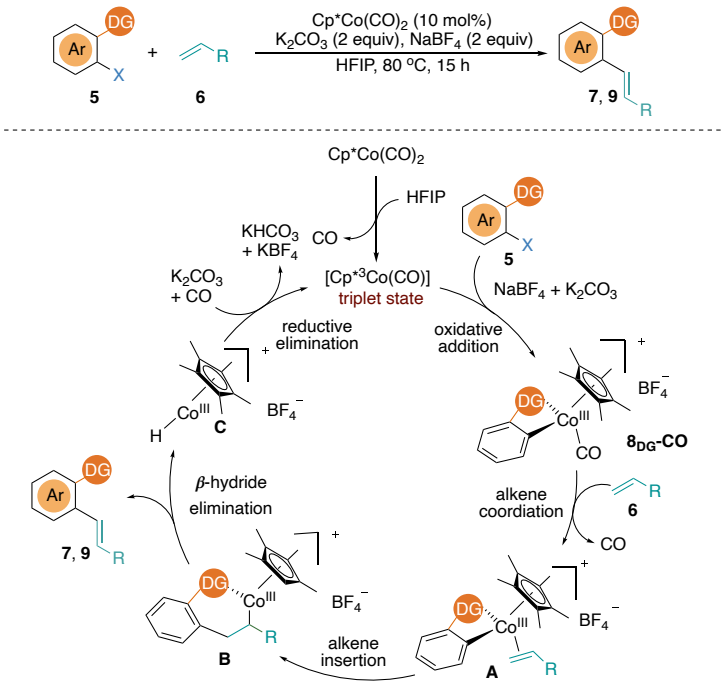

Scheme 3.20. Proposed mechanism

3.3 Conclusions

In conclusion, in this chapter we disclose a "non-excited" ISC process via secondary-coordination sphere interactions with HFIP. We have capitalized on this unusual phenomenon to develop a versatile site-selective cobalt-catalyzed Mizoroki-Heck protocol that includes the activation of inexpensive and readily available aryl chlorides, and late-stage functionalization (LSF) strategies (Scheme 3.21). For the first time, we provide experimental and computational evidence that the solvent-induced SCO is responsible for the C–X bond-cleavage. This opens the door to the design and development of new cross-coupling reactions catalyzed by cobalt and other first-row metals.

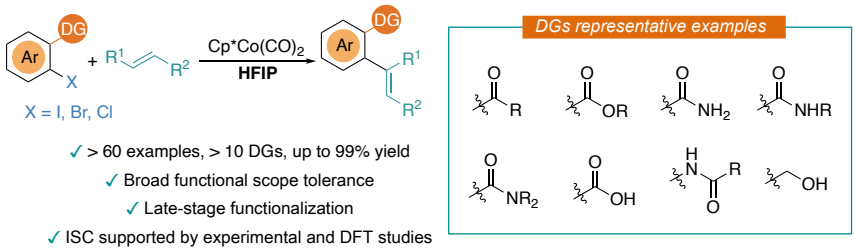

Scheme 3.21. Spin catalysis enabled by secondary-coordination sphere interactions with HFIP

3.4 Experimental Section

3.4.1. General information

Nuclear magnetic resonance (NMR) spectra were recorded on Bruker 400 MHz, 500 MHz or a 500 MHz with cryoprobe spectrometers equipped with probeheads capable of producing gradients in the z direction with a maximum strength of 53.5 G/cm. spectrometers spectrometer. ^{1}H, ^{13}C and ^{19}F NMR chemical shifts are reported in parts per million (ppm). The residual solvent signals were used as references and the chemical shifts converted to the TMS scale (DMSO-d_6: δH = 2.50 ppm, δC = 39.52 ppm; $CDCl_3$: δH = 7.26 ppm, δC = 77.16 ppm; CD_2Cl_2: δH = 5.32 ppm, δC = 53.84 ppm). Multiplicities are reported as follows: singlet (s), doublet (d), doublet of doublets (dd), triplet of doublets (td), triplet (t), doublet of triplets (dt), quartet (q), broad signal (br) and multiplet (m). High resolution mass spectra (HRMS) were obtained from the ICIQ HRMS unit on MicroTOF Focus and Maxis Impact (Bruker Daltonics) with electrospray ionization (ESI). FT-IR measurements were carried out on a Bruker Optics FT-IR Alpha spectrometer equipped with a DTGS detector, KBr beamsplitter at 4 cm^{-1} resolution using a one bounce ATR accessory with diamond windows. UV-Vis measurements were carried out on an Agilent Cary 60 UV-Vis spectrophotometer equipped with two silicon diode detectors, double beam optics and Xenon pulse light. Continuous wave (CW) EPR spectra were acquired on a Bruker EMX X-band Micro EPR spectrometer with an ER 4116 HS cavity. A 150 mL Suprasil offset liquid nitrogen dewar flask (Wilmad-LabGlass) was used for low-temperature measurements (77 K).

General procedures

All reactions were conducted in an argon-filled glovebox (mBraun Unilab 4420) with concentrations of O_2 and H_2O < 0.1 ppm or oven-dried glassware (at 100 ºC

overnight and cooled under vacuum prior use) using Schlenk techniques under argon atmosphere (otherwise mentioned).

Materials and methods

Trifluoroethanol (TFE), methanol, 1,2-dichloroethane (DCE) and 1,1,1,3,3,3-hexafluoroisopropanol (HFIP), 2-propanol were stored under argon with activated 4 Å molecular sieves. If necessary, the solvents (hexane, toluene, THF, CH_2Cl_2) were used from a solvent purification system pure-solv (SPS-400, Innovative Technology) and stored under argon over activated 4 Å molecular sieves. Most of the starting materials used in this study are commercial and were purchased in the highest purity available from Sigma-Aldrich, Fluka, Alfa Aesar, Fluorochem, and used as received, without further purifications.

3.4.2. Synthesis of catalysts and substrate

$Cp^*Co(CO)_2$,[41] $Cp^*Co(VTMS)_2$,[42] $\mathbf{8_{ket}\text{-}I}$,[30] were synthesized according to reported procedures.

The following substrates were synthesized according to previous literature procedures.[43]

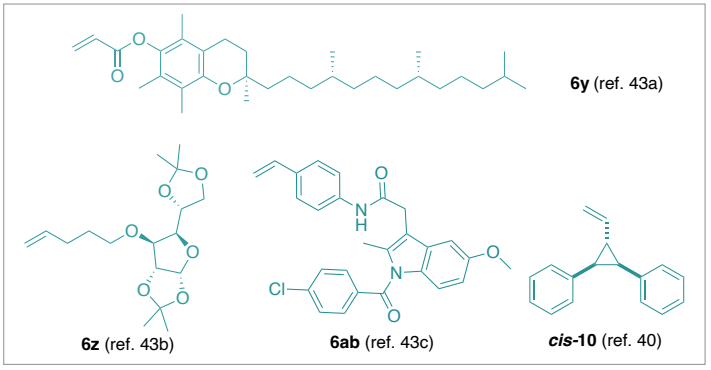

Procedure for the synthesis of substrate 6ac

41 Chan, N. H.; Roache, J. H.; Jones, W. D. *Inorganica Chimica Acta* **2015**, *437*, 36.

42 Sanjosé-Orduna, J.; Gallego, D.; García-Roca, A.; Martin, E.; Benet-Buchholz, J.; Pérez-Temprano, M. H. *Angew. Chem., Int. Ed.* **2017**, *56*, 12137.

43 (a) Xie, H.; Guo, J.; Wang, Y.-Q.; Wang, K.; Guo, P.; Su, P.-F.; Wang, X.; Shu, X.-Z. *J. Am. Chem. Soc.* **2020**, *142*, 16787. (b) Bianchini, R.; Catelani, G.; Riccardo Cecconi, D'Andrea, F.; Guazzelli, L.; Isaad, J.; Rolla, M. *Eur. J. Org. Chem.* **2008**, 444. (c) Liu, K.; Studer, A. *J. Am. Chem. Soc.* **2021**, *143,* 4903.

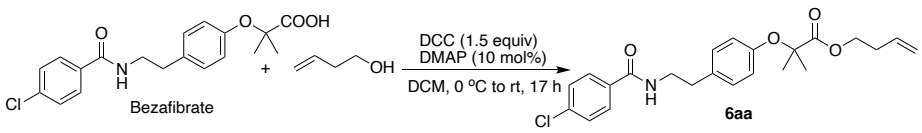

To a solution of Bezafibrate (723.64 mg, 2 mmol, 1.0 equiv) in DCM (5 mL) was added but-3-en-1-ol (216.3 mg, 3 mmol, 1.5 equiv) and DMAP (24.4 mg, 10 mol%) at 0 °C. A solution of DCC (618.9 mg, 3 mmol, 1.5 equiv) in DCM (15 mL) was then added over 20 min. The reaction mixture was stirred at room temperature for 17 h. The reaction was quenched with saturated aqueous solution of NaCl, and extracted with DCM (10 mL × 2). The combined organic layers were dried over anhydrous $MgSO_4$, filtered and concentrated under the reduced pressure. The residue was purified by flash chromatography on silica gel (hexane/ethyl acetate 5:1) to give the resulting product **6aa** 498.18 mg (60%) as white solid.

but-3-en-1-yl 2-(4-(2-(4-chlorobenzamido)ethyl)phenoxy)-2-methylpropanoate (6aa)

^{1}H NMR (400 MHz, $CDCl_3$) δ 7.65 – 7.56 (m, 2H), 7.33 – 7.27 (m, 2H), 7.07 – 6.99 (m, 2H), 6.79 – 6.71 (m, 2H), 6.63 (t, *J* = 5.8 Hz, 1H), 5.67 (ddt, *J* = 17.0, 10.2, 6.7 Hz, 1H), 5.08 – 4.95 (m, 2H), 4.18 (t, *J* = 6.6 Hz, 2H), 3.62 – 3.50 (m, 2H), 2.80 (t, *J* = 7.1 Hz, 2H), 2.34 (qt, *J* = 6.7, 1.4 Hz, 2H), 1.54 (s, 6H).
^{13}C NMR (101 MHz, $CDCl_3$) δ 174.2, 166.5, 154.0, 137.5, 133.6, 133.0, 132.5, 129.4, 128.6, 128.4, 119.5, 117.4, 79.1, 64.3, 41.3, 34.7, 32.9, 25.4.
HRMS-ESI(m/z): $[M+Na]^+$: Calcd for $C_{23}H_{26}ClNNaO_4$, 438.1443; Found, 438.1438.

IR (neat): 3253, 2932, 1732, 1633, 1552, 1510, 1145, 1089.

General procedure for the synthesis of substrate 6ac and 6ad

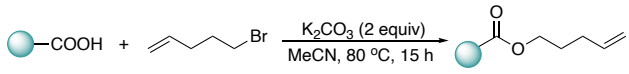

To a solution of acid (1.0 equiv) in MeCN (10 mL) was added K_2CO_3 (2 equiv) and 5-bromopent-1-ene (2 equiv) at room temperature. The reaction mixture was stirred at 80 °C for 15 h. The reaction was quenched with water and extracted with DCM (10 mL × 2). The combined organic layers were dried over anhydrous $MgSO_4$, filtered and concentrated under the reduced pressure. The residue was purified by flash chromatography on silica gel to give the resulting product **6ac** and **6ad**.

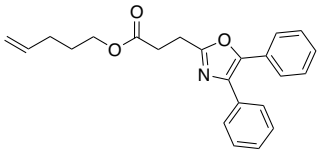

pent-4-en-1-yl 3-(4,5-diphenyloxazol-2-yl)propanoate (6ac)

Oxaprozin (1.0 g, 1.0 equiv), K_2CO_3 (939 mg, 2 equiv) and 5-bromopent-1-ene (804 μL, 2 equiv) were used, affording the title compound as a colorless oil (859 mg, 70% yield) by using Hexane/EtOAc (10:1) as eluent.

^{1}H NMR (400 MHz, $CDCl_3$) δ 7.68 – 7.53 (m, 4H), 7.41 – 7.28 (m, 6H), 5.78 (ddt, *J* = 16.9, 10.2, 6.6 Hz, 1H), 5.08 – 4.93 (m, 2H), 4.15 (t, *J* = 6.6 Hz, 2H), 3.25 – 3.12 (m, 2H), 2.92 (m, 2H), 2.15 – 2.06 (m, 2H), 1.74 (dq, *J* = 8.1, 6.7 Hz, 2H).
^{13}C NMR (101 MHz, $CDCl_3$) δ 172.0, 161.7, 145.4, 137.4, 135.1, 132.4, 129.0, 128.6, 128.5, 128.4, 128.0, 127.9, 126.4, 115.3, 64.2, 31.1, 30.0, 27.7, 23.5.
HRMS-ESI(m/z): $[M+H]^+$: Calcd for $C_{23}H_{24}NO_3$, 362.1751; Found, 362.1744.

IR (neat): 2935, 1671, 1449, 1173, 694, 643.

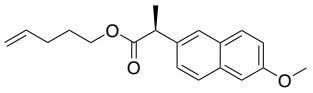

pent-4-en-1-yl (*S*)-2-(6-methoxynaphthalen-2-yl)propanoate (6ad)
Naproxen (1.0 g, 1.0 equiv), K_2CO_3 (1.18 g, 2 equiv) and 5-bromopent-1-ene (1 mL, 2 equiv) were used, affording the title compound as a colorless oil (961 mg, 75% yield) by using Hexane/EtOAc (10:1) as eluent.

^{1}H NMR (400 MHz, $CDCl_3$) δ 7.80 – 7.66 (m, 3H), 7.43 (dd, *J* = 8.5, 1.9 Hz, 1H), 7.21 – 7.09 (m, 2H), 5.74 (ddt, *J* = 17.6, 9.7, 6.7 Hz, 1H), 5.01 – 4.88 (m, 2H), 4.11 (td, *J* = 6.6, 0.9 Hz, 2H), 3.94 (s, 3H), 3.87 (q, *J* = 7.1 Hz, 1H), 2.11 – 1.98 (m, 2H), 1.70 (dq, *J* = 8.3, 6.7 Hz, 2H), 1.60 (d, *J* = 7.2 Hz, 3H).
^{13}C NMR (101 MHz, $CDCl_3$) δ 174.6, 157.6, 137.4, 135.8, 133.6, 129.2, 128.9, 127.1, 126.2, 125.9, 118.9, 115.2, 105.6, 64.1, 55.3, 45.5, 29.9, 27.7, 18.5.
HRMS-ESI(m/z): $[M+Na]^+$: Calcd for $C_{19}H_{22}NaO_3$, 321.1461; Found, 321.1456.

IR (neat): 2937, 1728, 1605, 1714, 1031, 852.

3.4.3. Investigations on solvent-assisted spin-state change

EPR studies

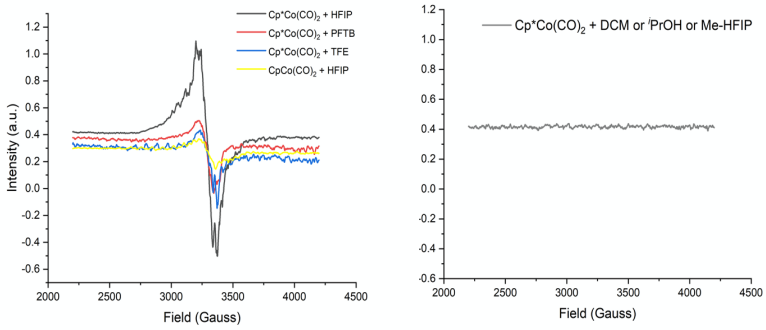

Figure 3.12. EPR measurements of Cp*Co(CO)2 in different solvents

$Cp^*Co(CO)_2$ (3.8 mg, 0.015mmol) or $CpCo(CO)_2$ (2.0 μL, 0.015 mmol) was weighted in a vial equipped with a stir bar inside an argon-filled glovebox. Once the solvent (0.5 mL) was introduced, the solution was stirred at room temperature while still within the glovebox. After 1 hour, the solution was carefully transferred into an EPR tube and the tube was moved out of the glovebox and promptly immersed in liquid nitrogen for rapid cooling. The spectra were collected at 77K with the following spectrometer settings:

g-factor = 2.000000, microwave power = 0.5637 mW; center field = 3200.00 G, sweep width = 2000.0 G, sweep time = 20.00 s, modulation frequency = 100.00 KHz, modulation amplitude = 4.00 G, power attenuation = 25.00 dB, time constant = 0.01 ms, conversion time = 4.00 ms, gain = 20.00 dB.

EPR quantification

The amount of the formed paramagnetic species as a percentage of the initial catalyst loading with different concentrations was determined by EPR spectroscopy using a set of $CuSO_4$ samples of known concentrations dissolved in a 1:1 mixture of water/ethylene glycol.

Procedure of preparing the $CuSO_4$/(water/ethylene glycol=1:1) samples: under air atmosphere, individual amounts of 3.0 mg, 6.4 mg, 9.6 mg, and 12.8 mg of $CuSO_4$ were weighed and placed into separate vials. Subsequently, volumes of 6 mL, 2 mL, 2 mL, and 2 mL of the water/ethylene glycol mixture in a 1:1 ratio were added to the

corresponding vials. The vials were then subjected to a 3-minute ultrasonic treatment to ensure thorough mixing and dissolution. Following the ultrasonic treatment, 0.5 mL of the resulting solution from each vial was carefully transferred into distinct EPR tubes. These tubes, containing the solutions, were rapidly cooled in liquid nitrogen. The EPR spectra of the samples were acquired at a low temperature of 77K. Using the integral values derived from these EPR spectra, a calibration curve was generated as shown in Figure 3.13.

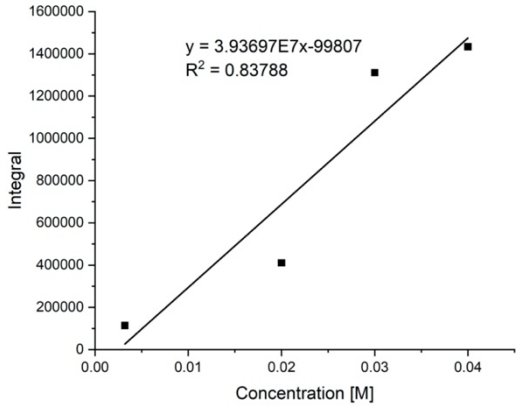

Figure 3.13. Calibration curve

Procedure of preparing the Cp*Co(CO)$_2$/HFIP samples: inside an argon-filled glovebox, in 3 separate vials, each equipped with a stir bar, 3.8 mg of Cp*Co(CO)$_2$ was added to each vial. Subsequently, volumes of 3 mL, 1.5 mL, and 0.5 mL of HFIP were added to the respective vials. The solutions were stirred at room temperature within the glovebox. After 1 hour, 0.5 mL of the resulting solution from each vial was transferred into distinct EPR tubes. These tubes were then taken outside the glovebox and rapidly cooled using liquid nitrogen. Subsequently, the EPR spectra of the samples were acquired at a low temperature of 77K. Utilizing the integral values obtained from these EPR spectra, a quantification process was established in Figure 3.14.

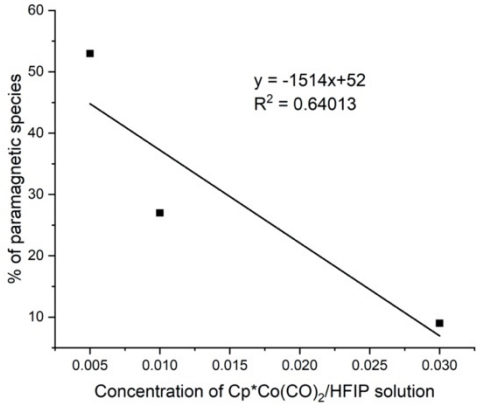

Figure 3.14. EPR quantification of the paramagnetic species

EPR at different temperatures

$Cp^*Co(CO)_2$ (3.8 mg, 0.015mmol) was weighted in a vial equipped with a stir bar inside an argon-filled glovebox. Once HFIP (0.5 mL) was introduced, the solution was stirred at room temperature while still within the glovebox. After 1 hour, the solution was transferred to a capillary via a 100 µL hamilton, and then placed the capillary inside a EPR tube. The sample was measured first at room temperature and then at 77K. At room temperature, a EPR signal was obtained as seen in Figure 3.15 left, black line. However, it is EPR silence at 77K. It is worth noting that the minor signal observed alongside the cobalt paramagnetic species is unrelated to the sample itself; rather, it corresponds to the empty capillary, as depicted in Figure 3.15 (right) by the orange line.

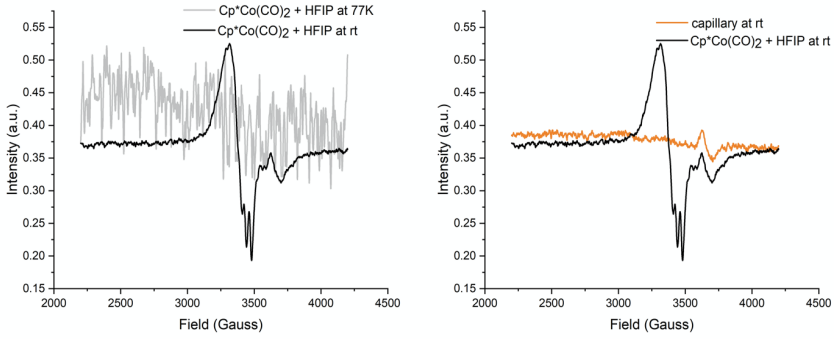

Figure 3.15. EPR measurments at different temperatures

EPR of $Cp^*Co(CO)_2$ in Et_2O after UV irradication

$Cp^*Co(CO)_2$ (3.8 mg, 0.015mmol) was weighted in an EPR tube inside an argon-filled glovebox. Once Et_2O (0.5 mL) was introduced, the tube was sealed and taken out of glovebox. The sample was irradiated under two EvoluChem lamps (365 nm) at room temperature cooling down by a fan (the set-up as shown in Figure 3.16, left). After 1 hour, the sample was transferred into liquid nitrogen immediately and recorded the EPR spectra. However, no signal was observed after irradiation (Figure 3.16, right), probably due to the short lifetime of Cp*Co(CO) triplet state species in Et_2O.

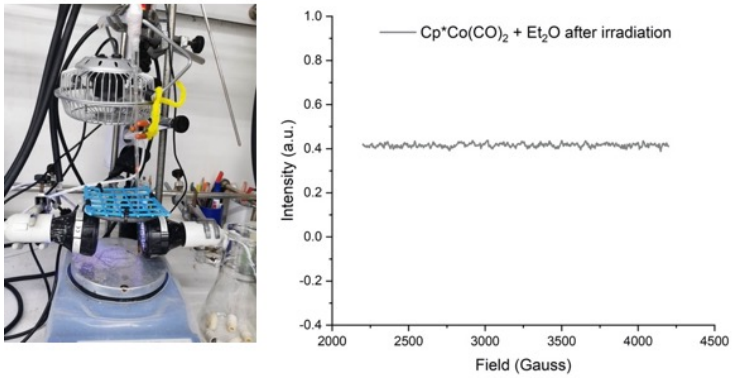

Figure 3.16. EPR of $Cp^*Co(CO)_2$ in Et_2O after UV irradication. Left: the reaction set-up. Right: EPR spectra after irradiation

HRMS studies of $Cp^*Co(CO)_2$/HFIP sample

Inside an argon-filled glovebox, 1.3 mg $Cp^*Co(CO)_2$ was as charged into a 5 mL crimped vial, after HFIP (0.5 mL) was added, The vial was sealed and taken out of the glovebox. The solution was stirred at room temperature for 1 hour and submitted for HRMS analysis. Instead of the Cp*Co(CO) triplet state species, the $[Cp^*Co(CO)]_2$ dimer was detected. HRMS (ESI) m/z calcd for $C_{22}H_{30}Co_2O_2$ $[M]^{\bullet+}$: 444.0904; found: 444.0904.

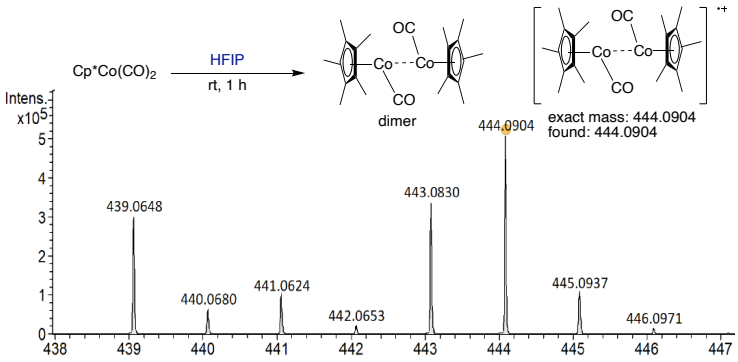

Figure 3.17. HRMS detection of $[Cp^*Co(CO)]_2$ dimer

Cyclic voltammetry studies (CV) and Differential pulse voltammetry (DPV)

For all CV measurements of $Cp^*Co(CO)_2$ in HFIP and DCM were performed in a 3-electrode cell set up consisting of a glassy carbon disk (0.07 cm^2 of surface area) as working electrode and platinum as a counter electrode and SCE (Saturated Calomel Electrode) as the reference electrode. The electrodes were previously polished with diamond abrasive slurries (DIAPAT-M, 39-321-M, Netkon) in an order of 3 μm and 1 μm diameter particle-based slurries (2 minutes in each). Synthetic nap based polishing pads (METAPO-B, polishing cloth, self- adhesive back, diamond 3-1 μm, Netkon) were used for diamond polishing.

The $Cp^*Co(CO)_2$ (12.5 mg, 0.05 mml) were measured at concentration of 10 mM in DCM (5 mL) or HFIP (5 mL) with $TBAPF_6$ (0.1 M) as electrolyte at the scan rate is 200 mV/s with Fc/Fc^+ as a reference.

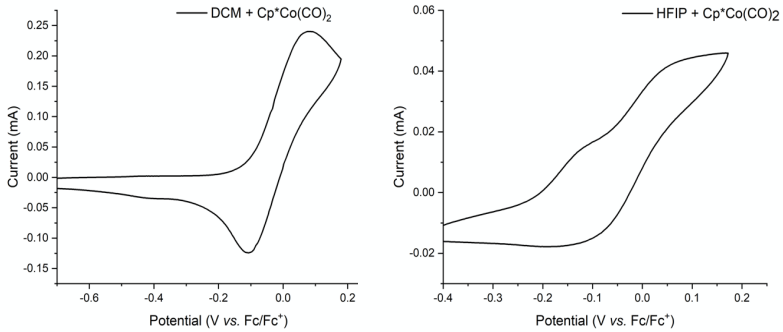

Figure 3.18. Cyclic voltammograms of complex $Cp^*Co(CO)_2$. [Co] = 0.01 M in DCM (left) and HFIP (right); $[TBAPF_6]$ = 0.1 M ; Scan rate = 200 mV/s. Glassy carbon working electrode, SCE reference electrode, Pt wire auxiliary electrode.

After the CV measurements, the same sample of $Cp^*Co(CO)_2$/HFIP (10 mM) solution utilized for performing the DPV measurement.

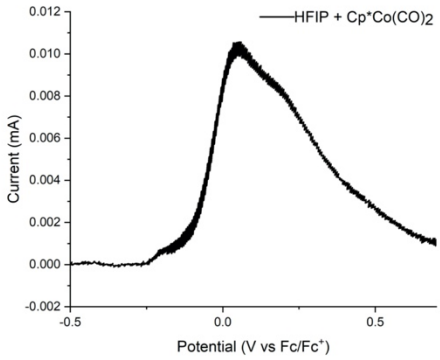

Figure 3.19. Differential pulse voltammetry of complex $Cp^*Co(CO)_2$. [Co] = 0.01 M in HFIP; $[TBAPF_6]$ = 0.1 M; Scan rate = 200 mV/s. Glassy carbon working electrode, SCE reference electrode, Pt wire auxiliary electrode.

UV-vis studies

UV-vis absorption of $Cp^*Co(CO)_2$ in different solvents

To prepare the $Cp^*Co(CO)_2$ solution, 1.3 mg (0.005 mmol) of $Cp^*Co(CO)_2$ was weighed and introduced into a quartz cuvette with dimensions of 10 x 10 mm, all performed within an argon-filled glovebox. Subsequently, 2 mL of the specified solvent was added to the cuvette. The cuvette was sealed, the UV-vis spectra was obtained in Figure 3.20.

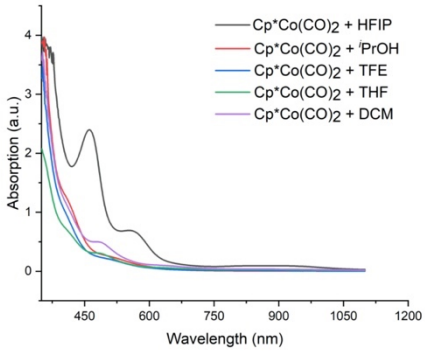

Figure 3.20. UV-vis absorption of $Cp^*Co(CO)_2$ in different solvents. [$Cp^*Co(CO)_2$ = 0.002M]

The capture of dissociated CO by using two-chamber system

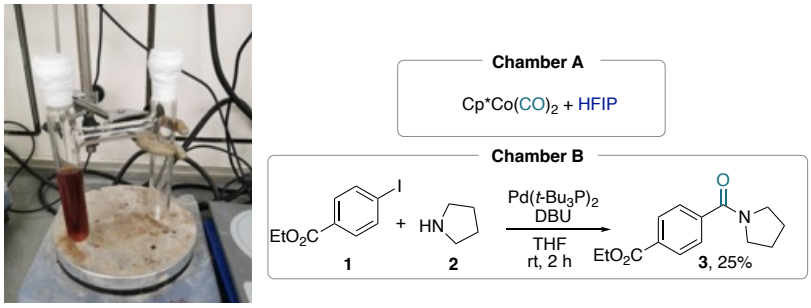

Figure 3.21. Two-chamber system set-up

In an argon-filled glovebox, in a two chamber system, $Cp^*Co(CO)_2$ (37.5 mg, 0.15 mmol) was weighed into chamber A (on the left), and $Pd(t\text{-}Bu_3P)_2$ (0.5 mg, 0.001 mmol) were weighed into chamber B (on the right). Dry THF (0.5 mL) was then added to chamber B, followed by ethyl 4-iodobenzoate **1** (13.8 mg, 0.05 mmol), pyrrolidine **2** (10 μL, 0.122 mmol), and DBU (30 μL, 0.2 mmol). The system was closed with the rubber stoppers, and which was taken out of the glovebox. Dry HFIP (10 mL) was then added to chamber A and the system was stirred at room temperature for 2 h. The reaction mixture in chamber B was filtrated through a small silica plug, and the solvent was removed under vacuum, CH_2Br_2 (22.5 mg, 0.13 mmol) was added as internal standardand (IS) the mixture was analyzed by ^1H NMR. The yield of **3** is 25%, which indicates HFIP does help the dissociation of CO.

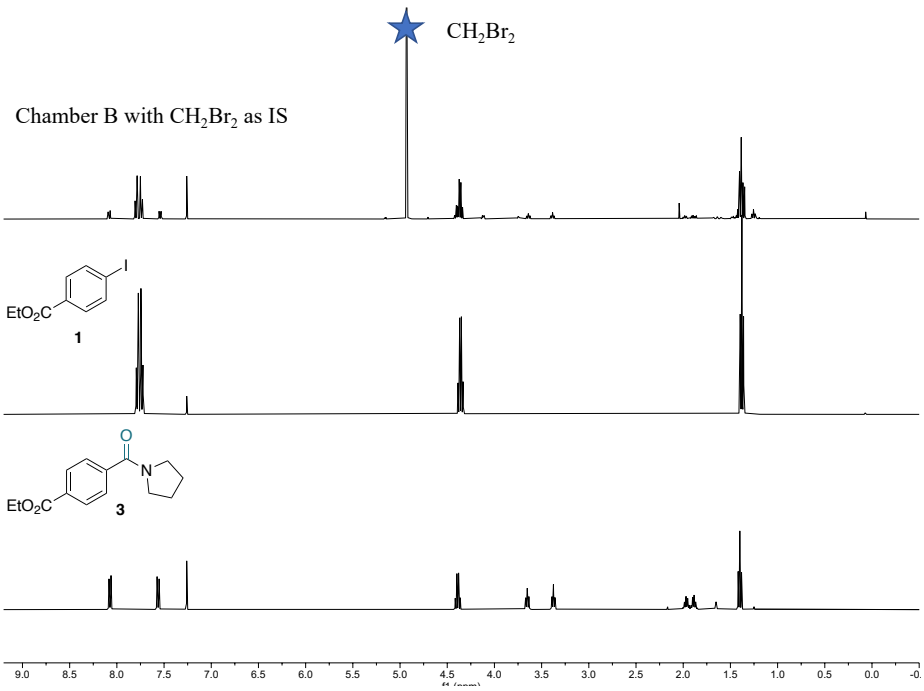

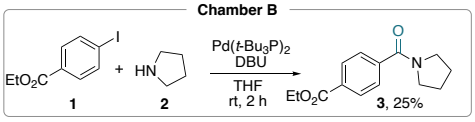

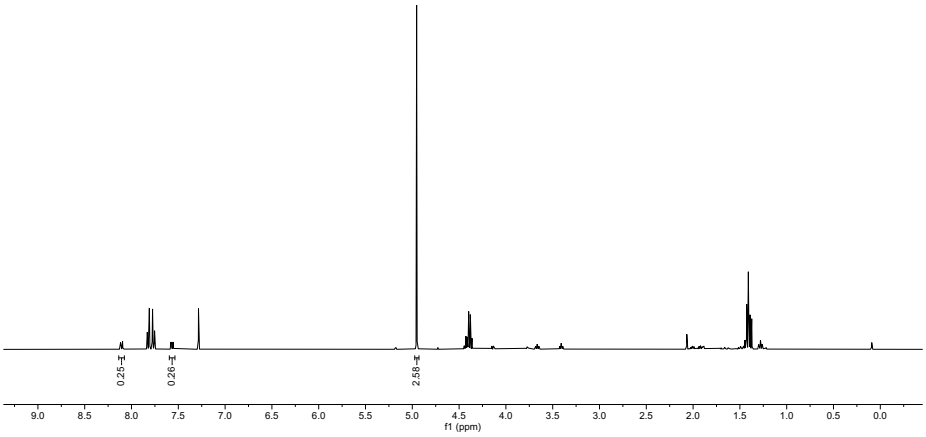

CO dissociation promoted by UV light irradiation with non-fluorinated solvents

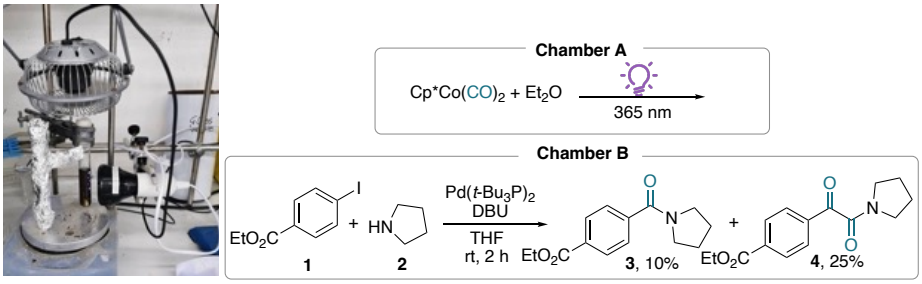

Figure 3.22. CO dissociation promoted by UV light irradiation reaction set-up

In an argon-filled glovebox, in a two chamber system, $Cp^*Co(CO)_2$ (37.5 mg, 0.15 mmol) was weighed into chamber A (on the right), and $Pd(t\text{-}Bu_3P)_2$ (0.5 mg, 0.001 mmol) were weighed into chamber B (on the left). Dry THF (0.5 mL) was then added to chamber B, followed by ethyl 4-iodobenzoate **1** (13.8 mg, 0.05 mmol), pyrrolidine **2** (10 μL, 0.122 mmol), and DBU (30 μL, 0.2 mmol). The system was closed with the rubber stoppers, and which was taken out of the glovebox. Chamber B was covered by aluminum paper. Dry Et_2O (10 mL) was then added to chamber A and the system was stirred under an EvoluChem lamp (365 nm) at room temperature for 2 h. The reaction mixture in chamber B was filtrated through a small silica plug, and the solvent was removed under vacuum, CH_2Br_2 (21.5 mg, 0.12 mmol) was added as internal standardand (IS) the mixture was analyzed by ^1H NMR. Mono-carbonylation product **3** was obtained in 10% yield, and double carbonylation product **4** was observed in 25% yield. The same reaction without UV-light was also performed, neither 3 nor 4 was observed by ^1H NMR. This result indicates UV light could promote the dissociation of CO.

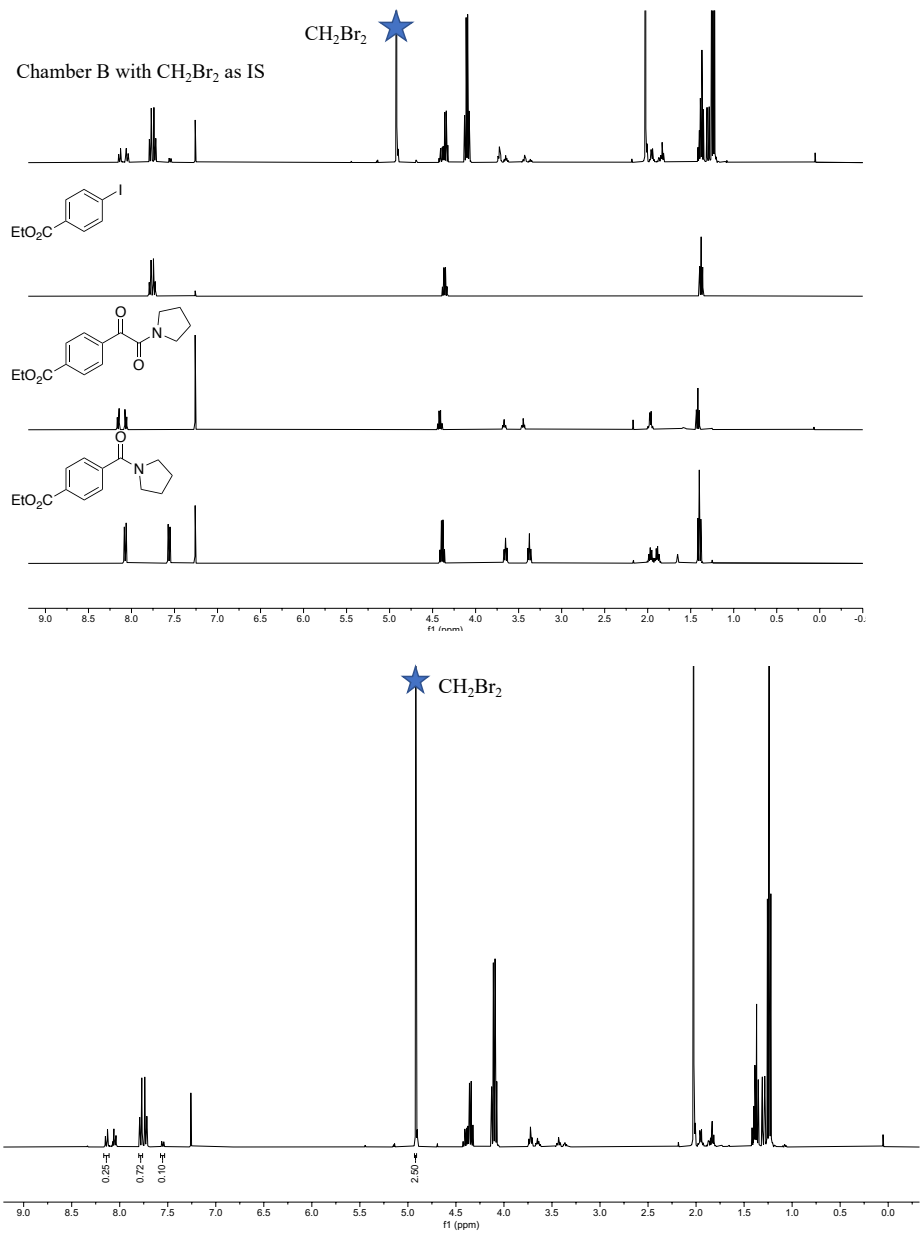

3.4.4. General procedure for the Optimization of the Heck reaction

Base, additive and catalyst were weighted in a vial equipped with a stir bar inside a glovebox, and then the solvent (0.5 mL), 2-iodoacteophenone **5a** (7 µL,0.05 mmol, 1.0 equiv) and methyl acrylate **6a** (9 µL, 0.1 mmol, 2.0 equiv) were then added and the vial was sealed. Outside the glovebox, the reaction mixture was stirred at 80 °C in a sand

bath for 15 hours. After cooling down to room temperature, the reaction mixture was filtrated through a small silica plug, and the solvent was removed under vacuum. Then, CH_2Br_2 was added as internal standard, and the mixture was analyzed by ^1H NMR.

Table 3.5. Optimization of the Heck reaction

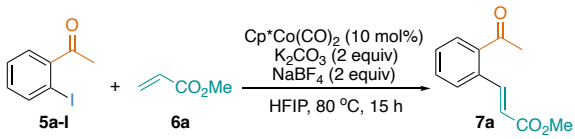

Entry	Changes from the standard conditions	Yield of 7a (%)
1	None	100
2	TFE instead of HFIP	13
3	PFTB instead of HFIP	100
4	2-Propanol instead of HFIP	0
5	MeOH instead of HFIP	0
6	HFIPMe instead of HFIP	0
7	Toluene instead of HFIP	0
8	DCE instead of HFIP	0
9	THF instead of HFIP	0
10	Dioxane instead of HFIP	0

3.4.5. General Procedure for Heck Reaction

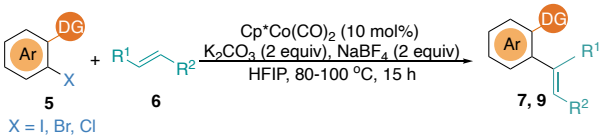

K_2CO_3 (41.5 mg, 0.3 mmol, 2 equiv), $NaBF_4$ (32.9 mg, 0.3 mmol, 2 equiv), and $Cp^*Co(CO)_2$ (3.8 mg, 10 mol%) were weighted in a vial equipped with a stir bar inside an argon-filled glovebox, and then after HFIP (1.5 mL), aryl halide **5** (0.15 mmol, 1.0 equiv) and alkene **6** (0.3 mmol, 2.0 equiv) were added, the vial was sealed (Note: if the substrate is a solid, it was added before the solvent). Outside the glovebox, the reaction mixture was stirred at 80 °C or 100 ºC in the sand bath for 15h. After cooling down to room temperature, the reaction mixture was filtrated through a small silica plug, and the solvent was removed under vacuum. Then the crude residue was purified by column chromatography to afford the corresponding product.

3.4.6. Characterization of products

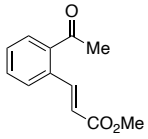

methyl (*E*)-3-(2-acetylphenyl)acrylate (7a) The title compound was obtained from *aryl iodide, bromide and chloride* by column chromatography (Hexane: EtOAc = 5:1) as a colorless oil in 82% (25.0 mg), 82% (25.0 mg) and 82% (25.0 mg) yields, respectively.

^{1}H NMR (400 MHz, $CDCl_3$) δ 8.15 (d, *J* = 15.9 Hz, 1H), 7.74 (dd, *J* = 7.8, 1.4 Hz, 1H), 7.58 (dd, *J* = 7.7, 1.5 Hz, 1H), 7.51 (td, *J* = 7.5, 1.2 Hz, 1H), 7.45 (td, *J* = 7.5, 1.5 Hz, 1H), 6.28 (d, *J* = 15.9 Hz, 1H), 3.80 (s, 3H), 2.61 (s, 3H).

^{13}C NMR (101 MHz, $CDCl_3$) δ 200.9, 167.0, 144.2, 138.3, 134.9, 132.0, 129.5, 129.3, 128.4, 120.6, 51.8, 29.3.

Spectroscopic data were in accordance with previous report.[44]

[44] Fu, Z.; Huang, S.; Su, W.; Hong, M. *Org. Lett.* **2010**, *12*, 4992.

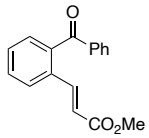

methyl (*E*)-3-(2-benzoylphenyl)acrylate (7b) The title compound was obtained from *aryl chloride* by column chromatography (Hexane: EtOAc = 10:1) as a colorless oil (30.1 mg) in 75% yield

^{1}H NMR (400 MHz, $CDCl_3$) δ 7.86 – 7.67 (m, 4H), 7.64 – 7.50 (m, 2H), 7.45 (m, 4H), 6.38 (d, *J* = 15.9 Hz, 1H), 3.72 (s, 3H).

^{13}C NMR (101 MHz, $CDCl_3$) δ 197.2, 166.8, 142.1, 139.4, 137.4, 134.0, 133.6, 130.8, 130.5, 129.3, 129.2, 128.6, 127.3, 120.6, 51.8.

Spectroscopic data were in accordance with previous report.[45]

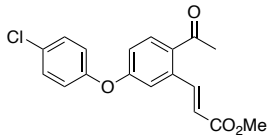

methyl (*E*)-3-(2-acetyl-5-(4-chlorophenoxy)phenyl)acrylate (7c) The title compound was obtained from *aryl chloride* by column chromatography (Hexane: EtOAc = 3:1) as a white solid (49.3 mg) in 99% yield

^{1}H NMR (400 MHz, $CDCl_3$) δ 8.18 (d, *J* = 15.9 Hz, 1H), 7.77 (d, *J* = 8.6 Hz, 1H), 7.39 – 7.31 (m, 2H), 7.09 (d, *J* = 2.5 Hz, 1H), 7.05 – 6.95 (m, 3H), 6.14 (d, *J* = 15.9 Hz, 1H), 3.78 (s, 3H), 2.58 (s, 3H).

^{13}C NMR (101 MHz, $CDCl_3$) δ 199.0, 166.8, 160.4, 153.9, 144.2, 138.1, 132.6, 132.1, 130.3, 130.1, 121.4, 121.1, 117.9, 117.3, 51.9, 28.9.

HRMS-ESI(m/z): $[M+Na]^+$: Calcd for $C_{18}H_{15}ClNaO_4$, 353.0551; Found, 353.0558.

IR (neat): 2951, 1711, 1677, 1483, 1219, 1087.

45 Han, S.; Sharma, S.; Park, J.; Kim, M.; Shin, Y.; Mishra, N. K.; Bae, J. J.; Kwak, J. H.; Jung, Y. H.; Kim, I. S. *J. Org. Chem*. **2015**, *80*, 4223.

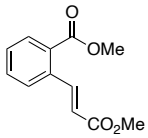

Methyl (*E*)-2-(3-methoxy-3-oxoprop-1-en-1-yl)benzoate (7d) The title compound was obtained from *aryl iodide and bromide* by column chromatography (Hexane: EtOAc = 10:1) as a colorless oil in 91% (30.0 mg), and 88% (29.0 mg) yields, respectively.

^{1}H NMR (400 MHz, $CDCl_3$) δ 8.44 (d, *J* = 15.9 Hz, 1H), 7.96 (dd, *J* = 7.6, 1.2 Hz, 1H), 7.59 (dd, *J* = 7.8, 1.5 Hz, 1H), 7.55 – 7.48 (m, 1H), 7.43 (td, *J* = 7.5, 1.5 Hz, 1H), 6.30 (d, *J* = 15.9 Hz, 1H), 3.93 (s, 3H), 3.81 (s, 3H).

^{13}C NMR (101 MHz, $CDCl_3$) δ 167.2, 167.1, 144.0, 136.5, 132.4, 130.9, 129.9, 129.5, 128.0, 120.8, 52.5, 51.9.

Spectroscopic data were in accordance with previous report.[46]

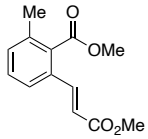

methyl (*E*)-2-(3-methoxy-3-oxoprop-1-en-1-yl)-6-methylbenzoate(7e) The title compound was obtained from *aryl bromide* by column chromatography (Hexane: EtOAc = 10:1) then preparative TLC (Hexane: EtOAc = 20:1) as a colorless oil (7.0 mg) in 20% yield.

^{1}H NMR (400 MHz, $CDCl_3$) δ 7.70 (d, *J* = 15.8 Hz, 1H), 7.46 (d, *J* = 7.9 Hz, 1H), 7.33 (t, *J* = 7.7 Hz, 1H), 7.24 (d, *J* = 7.2 Hz, 1H), 6.37 (d, *J* = 15.8 Hz, 1H), 3.96 (s, 3H), 3.79 (s, 3H), 2.35 (s, 3H).

^{13}C NMR (101 MHz, $CDCl_3$) δ 169.4, 167.0, 142.1, 136.1, 134.2, 132.4, 131.9, 129.9, 124.2, 120.5, 52.5, 51.9, 19.8.

HRMS-ESI(m/z): $[M+Na]^+$: Calcd for $C_{13}H_{14}NaO_4$, 257.0784; Found, 257.0785.

IR (neat): 2952, 1717, 1637, 1268, 1168, 1117, 1072.

46 Callonnec, F. L.; Fouquet, E.; Felpin, F. X. *Org. Lett.* **2011**, *13*, 2646.

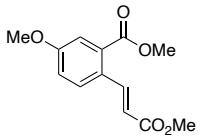

methyl (*E*)-5-methoxy-2-(3-methoxy-3-oxoprop-1-en-1-yl)benzoate (7f) The title compound was obtained from *aryl bromide* by column chromatography (Hexane: EtOAc = 10:1) as a colorless oil (10.8 mg) in 29% yield.

^{1}H NMR (400 MHz, $CDCl_3$) δ 8.38 (d, *J* = 15.9 Hz, 1H), 7.57 (d, *J* = 8.7 Hz, 1H), 7.44 (d, *J* = 2.8 Hz, 1H), 7.06 (ddd, *J* = 8.7, 2.9, 0.7 Hz, 1H), 6.25 (d, *J* = 15.9 Hz, 1H), 3.94 (s, 3H), 3.87 (s, 3H), 3.80 (s, 3H).

^{13}C NMR (101 MHz, $CDCl_3$) δ 167.4, 167.2, 160.5, 143.3, 131.5, 129.3, 128.5, 118.8, 118.6, 115.4, 55.7, 52.6, 51.8.

HRMS-ESI(m/z): $[M+Na]^+$: Calcd for $C_{13}H_{14}NaO_5$, 273.0733; Found, 273.0729.

IR (neat): 2952, 1716, 1601, 1498, 1223, 1168, 1072.

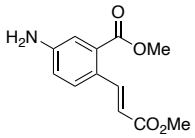

methyl (*E*)-5-amino-2-(3-methoxy-3-oxoprop-1-en-1-yl)benzoate (7g) The title compound was obtained from *aryl bromide* by column chromatography (Hexane: EtOAc = 2:1) as a yellow solid (18.1 mg) in 51% yield.

^{1}H NMR (400 MHz, $CDCl_3$) δ 8.34 (dt, *J* = 15.8, 0.6 Hz, 1H), 7.47 (d, *J* = 8.4 Hz, 1H), 7.18 (d, *J* = 2.5 Hz, 1H), 6.78 (ddd, *J* = 8.4, 2.6, 0.6 Hz, 1H), 6.21 (d, *J* = 15.9 Hz, 1H), 4.01 (s, 2H), 3.91 (s, 3H), 3.78 (s, 3H).

^{13}C NMR (101 MHz, $CDCl_3$) δ 167.7, 167.6, 147.9, 143.4, 131.7, 129.1, 125.5, 118.2, 117.0, 116.2, 52.5, 51.7.

HRMS-ESI(m/z): $[M+Na]^+$: Calcd for $C_{12}H_{13}NNaO_4$, 258.0737; Found, 258.0732.

IR (neat): 3453, 3367, 2950, 1690, 1591, 1433, 1233, 1070.

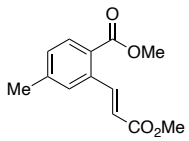

methyl (*E*)-2-(3-methoxy-3-oxoprop-1-en-1-yl)-4-methylbenzoate (7h) The title compound was obtained from *aryl bromide* by column chromatography (Hexane: EtOAc = 10:1) as a white solid (32.6 mg) in 93% yield.

^{1}H NMR (400 MHz, $CDCl_3$) δ 8.46 (d, *J* = 15.9 Hz, 1H), 7.86 (d, *J* = 8.0 Hz, 1H), 7.37 (s, 1H), 7.22 (dd, *J* = 8.0, 1.8 Hz, 1H), 6.27 (d, *J* = 15.9 Hz, 1H), 3.90 (s, 3H), 3.80 (s, 3H), 2.40 (s, 3H).

^{13}C NMR (101 MHz, $CDCl_3$) δ 167.2, 167.1, 144.3, 143.1, 136.6, 131.0, 130.2, 128.7, 127.0, 120.5, 52.3, 51.8, 21.6.

Spectroscopic data were in accordance with previous report.[47]

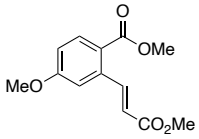

methyl (*E*)-4-methoxy-2-(3-methoxy-3-oxoprop-1-en-1-yl)benzoate (7i) The title compound was obtained from *aryl bromide* by column chromatography (Hexane: EtOAc = 10:1) as a white solid (34.9mg) in 93% yield.

^{1}H NMR (400 MHz, $CDCl_3$) δ 8.51 (d, *J* = 15.9 Hz, 1H), 7.97 (d, *J* = 8.8 Hz, 1H), 7.02 (d, *J* = 2.6 Hz, 1H), 6.92 (dd, *J* = 8.8, 2.6 Hz, 1H), 6.26 (d, *J* = 15.9 Hz, 1H), 3.89 (s, 3H), 3.87 (s, 3H), 3.81 (s, 3H).

^{13}C NMR (101 MHz, $CDCl_3$) δ 167.0, 166.8, 162.7, 144.6, 139.1, 133.2, 121.9, 120.9, 114.7, 113.2, 55.6, 52.2, 51.9.

Spectroscopic data were in accordance with previous report.[48]

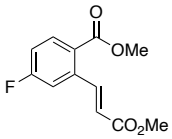

methyl (*E*)-4-fluoro-2-(3-methoxy-3-oxoprop-1-en-1-yl)benzoate (7j) The title compound was obtained from *aryl bromide* by column chromatography (Hexane:

47 Gao, F.; Huang, Y. *Adv. Synth. Catal.* **2014**, *356*, 2422.
48 Graczyk, K.; Ma, W.; Ackermann, L. *Org. Lett.* **2012**, *14*, 4110.

EtOAc = 10:1) then preparative TLC (Hexane: EtOAc = 20:1) as a white solid (15.3 mg) in 43% yield.

^{1}H NMR (400 MHz, $CDCl_3$) δ 8.44 (dd, *J* = 15.9, 1.3 Hz, 1H), 8.01 (dd, *J* = 8.7, 5.8 Hz, 1H), 7.26 (dd, *J* = 9.5, 2.6 Hz, 1H), 7.12 (ddd, *J* = 8.8, 7.7, 2.6 Hz, 1H), 6.28 (d, *J* = 15.9 Hz, 1H), 3.92 (s, 3H), 3.82 (s, 3H).

^{13}C NMR (101 MHz, $CDCl_3$) δ 166.7, 166.2 (d, *J* = 12.9 Hz), 163.6, 143.0 (d, *J* = 1.9 Hz), 139.7 (d, *J* = 8.5 Hz), 133.7 (d, *J* = 9.2 Hz), 125.9 (d, *J* = 3.2 Hz), 121.9, 116.5 (d, *J* = 21.6 Hz), 114.97 (d, *J* = 22.9 Hz), 52.6, 52.0.

^{19}F NMR (376 MHz, $CDCl_3$) δ -106.09 (dt, *J* = 9.1, 6.4 Hz).

HRMS-ESI(m/z): $[M+Na]^+$: Calcd for $C_{12}H_{11}FNaO_4$, 261.0534; Found, 261.0531.

IR (neat): 3099, 2957, 2848, 1713, 1281, 1255, 1079.

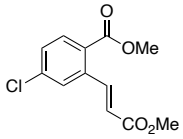

methyl (*E*)-4-chloro-2-(3-methoxy-3-oxoprop-1-en-1-yl)benzoate (7k) The title compound was obtained from *aryl bromide* by column chromatography (Hexane: EtOAc = 10:1) as a colorless oil (15.6 mg) in 41% yield.

^{1}H NMR (400 MHz, $CDCl_3$) δ 8.40 (d, *J* = 15.9 Hz, 1H), 7.92 (d, *J* = 8.4 Hz, 1H), 7.55 (d, *J* = 2.1 Hz, 1H), 7.40 (dd, *J* = 8.4, 2.1 Hz, 1H), 6.29 (d, *J* = 15.9 Hz, 1H), 3.92 (s, 3H), 3.82 (s, 3H).

^{13}C NMR (101 MHz, $CDCl_3$) δ 166.7, 166.4, 142.8, 138.9, 138.4, 132.4, 129.4, 128.1, 128.0, 121.9, 52.6, 52.0.

HRMS-ESI(m/z): $[M+Na]^+$: Calcd for $C_{12}H_{11}ClNaO_4$, 277.0238; Found, 277.0243.

IR (neat): 3103, 2953, 1711, 1433, 1234, 1072.

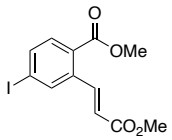

methyl (*E*)-4-iodo-2-(3-methoxy-3-oxoprop-1-en-1-yl)benzoate (7l) The title compound was obtained from *aryl bromide* by column chromatography (Hexane: EtOAc = 10:1) as a white solid (17.7 mg) in 33% yield.

^{1}H NMR (400 MHz, $CDCl_3$) δ 8.34 (d, *J* = 15.9 Hz, 1H), 7.93 (d, *J* = 2.3 Hz, 1H), 7.78 (dd, *J* = 8.3, 1.8 Hz, 1H), 7.67 (d, *J* = 8.3 Hz, 1H), 6.28 (d, *J* = 15.9 Hz, 1H), 3.92 (s, 3H), 3.81 (s, 3H).

^{13}C NMR (101 MHz, $CDCl_3$) δ 166.7, 142.6, 138.4, 138.3, 137.0, 132.2, 129.0, 121.9, 99.8, 52.6, 52.0.

HRMS-ESI(m/z): $[M+Na]^+$: Calcd for $C_{12}H_{11}INaO_4$, 368.9594; Found, 368.9599.

IR (neat): 2952, 1703, 1433, 1266, 1085.

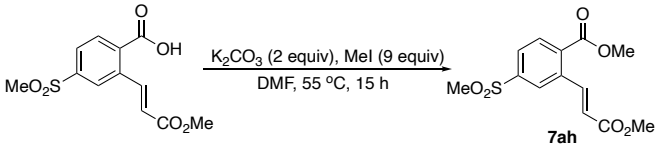

methyl (*E*)-2-(3-methoxy-3-oxoprop-1-en-1-yl)-4-(methylsulfonyl)benzoate (7m) The acid Heck product was obtained from *aryl chloride*, due to the purification issues, an esterification process was performed: After the Heck reaction, HCl was added to the mixture to pH=1. The mixture was extracted with EtOAc (3 x 5 mL) and the combined organic layer dried over Na_2SO_4 and concentrated under reduced pressure. The obtained crude was esterified in DMF (2 mL) by adding anhydrous K_2CO_3 (41.5 mg, 0.3 mmol) and MeI (84 μL, 1.35 mmol) at 55 °C for 15 h. Then the solution was hydrolyzed and extracted with EtOAc (3 x 5 mL), and the combined organic layers were dried over Na_2SO_4 and concentrated under reduced pressure. The crude was purified by column chromatography (Hexane: EtOAc = 1:1) as a white solid (16.7 mg) in 37% yield.

^{1}H NMR (400 MHz, $CDCl_3$) δ 8.37 (d, *J* = 16.0 Hz, 1H), 8.19 – 8.10 (m, 2H), 7.98 (dd, *J* = 8.2, 1.9 Hz, 1H), 6.43 (d, *J* = 16.0 Hz, 1H), 3.98 (s, 3H), 3.83 (s, 3H), 3.10 (s, 3H).

^{13}C NMR (101 MHz, $CDCl_3$) δ 166.4, 165.9, 144.0, 141.6, 137.8, 134.4, 132.0, 127.8, 126.9, 123.2, 53.1, 52.1, 44.4.

HRMS-ESI(m/z): $[M+Na]^+$: Calcd for $C_{13}H_{14}NaO_6S$, 321.0403; Found, 321.0413.

IR (neat): 2954, 1709, 1437, 1269, 1139, 1101.

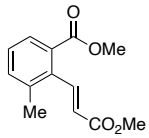

methyl (*E*)-2-(3-methoxy-3-oxoprop-1-en-1-yl)-3-methylbenzoate (7n) The title compound was obtained from *aryl bromide* by column chromatography (Hexane: EtOAc = 10:1) as a colorless oil (11.2 mg) in 32% yield.

^{1}H NMR (400 MHz, $CDCl_3$) δ 8.06 (d, *J* = 16.3 Hz, 1H), 7.71 (dd, *J* = 7.7, 1.9 Hz, 1H), 7.38 (d, *J* = 7.6 Hz, 1H), 7.29 (t, *J* = 7.7 Hz, 1H), 5.92 (d, *J* = 16.3 Hz, 1H), 3.85 (s, 3H), 3.81 (s, 3H), 2.36 (d, *J* = 0.7 Hz, 3H).

^{13}C NMR (101 MHz, $CDCl_3$) δ 168.2, 166.8, 144.3, 137.0, 135.9, 134.1, 130.7, 128.1, 127.9, 123.2, 52.3, 51.8, 20.9.

HRMS-ESI(m/z): $[M+Na]^+$: Calcd for $C_{13}H_{14}NaO_4$, 257.0784; Found, 257.0792.

IR (neat): 2952, 1715, 1435, 1268, 1168, 1134.

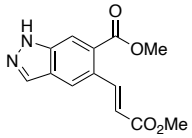

methyl (*E*)-5-(3-methoxy-3-oxoprop-1-en-1-yl)-1*H*-indazole-6-carboxylate (7o) The title compound was obtained from *aryl bromide* by column chromatography (Hexane: EtOAc = 2:1) then preparative TLC (Hexane: EtOAc = 3:1) as a white solid (8.0 mg) in 20% yield.

^{1}H NMR (400 MHz, $CDCl_3$) δ 10.45 (s, 1H), 8.47 (dd, *J* = 15.8, 0.7 Hz, 1H), 8.19 – 8.16 (m, 2H), 8.01 (t, *J* = 0.7 Hz, 1H), 6.32 (d, *J* = 15.8 Hz, 1H), 3.97 (s, 3H), 3.83 (s, 3H).

^{13}C NMR (101 MHz, $CDCl_3$) δ 167.4, 167.3, 144.9, 139.5, 135.7, 129.4, 128.9, 125.3, 121.0, 119.3, 113.2, 52.8, 51.9.

HRMS-ESI(m/z): $[M+Na]^+$: Calcd for C13H12N2NaO4, 283.0689; Found, 283.0689.

IR (neat): 3366, 2955, 1705, 1685, 1276, 1206.

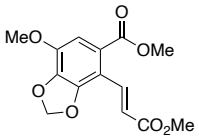

methyl (*E*)-7-methoxy-4-(3-methoxy-3-oxoprop-1-en-1-yl)benzo[*d*][1,3]dioxole-5-carboxylate (7p) The title compound was obtained from *aryl bromide* by column chromatography (Hexane: EtOAc = 5:1) as a white solid (20.4 mg) in 46% yield.

^{1}H NMR (400 MHz, $CDCl_3$) δ 8.28 (d, *J* = 16.2 Hz, 1H), 7.24 (s, 1H), 6.67 (d, *J* = 16.2 Hz, 1H), 6.13 (s, 2H), 3.95 (s, 3H), 3.91 (s, 3H), 3.79 (s, 3H).

^{13}C NMR (101 MHz, $CDCl_3$) δ 167.9, 166.8, 148.6, 143.5, 138.5, 137.5, 124.7, 121.9, 112.8, 111.7, 102.7, 56.7, 52.5, 51.8.

HRMS-ESI(m/z): $[M+H]^+$: Calcd for $C_{14}H_{15}O_7$, 295.0812; Found, 295.0816.

IR (neat): 2952, 1710, 1626, 1492, 1432, 1302, 1157, 1036.

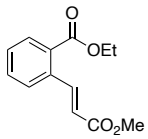

ethyl (*E*)-2-(3-methoxy-3-oxoprop-1-en-1-yl)benzoate (7q) The title compound was obtained from *aryl bromide* by column chromatography (Hexane: EtOAc = 8:1) as a colorless oil (30.1 mg) in 86% yield.

^{1}H NMR (400 MHz, $CDCl_3$) δ 8.45 (d, *J* = 15.8 Hz, 1H), 7.96 (dd, *J* = 8.1, 1.2 Hz, 1H), 7.58 (dd, *J* = 7.8, 1.5 Hz, 1H), 7.52 (td, *J* = 7.5, 1.4 Hz, 1H), 7.43 (td, *J* = 7.5, 1.5 Hz, 1H), 6.29 (d, *J* = 15.9 Hz, 1H), 4.39 (q, *J* = 7.1 Hz, 2H), 3.81 (s, 3H), 1.41 (t, *J* = 7.1 Hz, 3H).

^{13}C NMR (101 MHz, $CDCl_3$) δ 167.1, 166.9, 144.2, 136.3, 132.3, 130.8, 130.3, 129.5, 127.9, 120.6, 61.5, 51.8, 14.3.

Spectroscopic data were in accordance with previous report.[49]

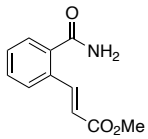

[49] Diebold, C.; Schweizer, S.; Becht, J. M.; Drian, C. L. *Org. Biomol. Chem.* **2010**, *8*, 4834.

Methyl (*E*)-3-(2-carbamoylphenyl)acrylate (**7r**) The title compound was obtained from *aryl iodide, bromide and chloride* by column chromatography (Hexane: EtOAc = 1:2) as a white solid in 86% (26.4 mg), 77% (23.6 mg), 62% (19.0 mg) yields, respectively.

^{1}H NMR (400 MHz, DMSO) δ 7.98 (d, *J* = 16.1 Hz, 2H), 7.92 – 7.85 (m, 1H), 7.59 (s, 1H), 7.52 – 7.45 (m, 3H), 6.59 (d, *J* = 16.0 Hz, 1H), 3.73 (s, 3H).

^{13}C NMR (101 MHz, DMSO) δ 170.5, 167.0, 142.7, 138.5, 131.9, 130.3, 130.2, 128.0, 127.2, 119.4, 52.0.

Spectroscopic data were in accordance with previous report.[50]

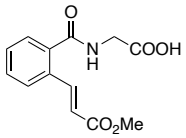

(*E*)-(2-(3-methoxy-3-oxoprop-1-en-1-yl)benzoyl)glycine (7s) The title product was obtained from *aryl iodide,* and the following work-up was performed: After the reaction, HCl was added to the mixture to pH=1. The mixture was extracted with EtOAc (3 x 50 mL) and the combined organic layer dried over Na_2SO_4 and concentrated under reduced pressure. The obtained crude was purified by column chromatography (DCM: MeOH = 5:1 with 0.1% AcOH) to afford the desired product in 40% yield (15.8 mg) as a white solid.

^{1}H NMR (400 MHz, DMSO) δ 12.66 (s, 1H), 8.83 (t, *J* = 6.0 Hz, 1H), 7.98 (d, *J* = 16.1 Hz, 1H), 7.94 – 7.87 (m, 1H), 7.60 – 7.45 (m, 3H), 6.61 (d, *J* = 16.0 Hz, 1H), 3.93 (d, *J* = 6.0 Hz, 2H), 3.72 (s, 3H).

^{13}C NMR (101 MHz, DMSO) δ 171.0, 168.4, 166.4, 142.0, 137.1, 132.0, 130.1, 129.9, 127.8, 126.8, 119.3, 51.4, 41.1.

HRMS-ESI(m/z): $[M-H]^-$: Calcd for $C_{13}H_{12}NO_5$, 262.0721; Found, 262.0719.

IR (neat): 3270, 2925, 1710, 1638, 1199, 1174, 979.

[50] Li, B.; Ma, J.; Wang, N.; Feng, H.; Xu, S.; Wang, B. *Org. Lett.* **2012**, *14*, 736.

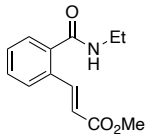

methyl (*E*)-3-(2-(ethylcarbamoyl)phenyl)acrylate (7t) The title compound was obtained from *aryl bromide* by column chromatography (Hexane: EtOAc = 5:1) as a colorless oil (26.3 mg) in 75% yield.

^{1}H NMR (400 MHz, $CDCl_3$) δ 8.01 (d, *J* = 16.0 Hz, 1H), 7.62 (dd, *J* = 7.5, 1.6 Hz, 1H), 7.51 – 7.37 (m, 3H), 6.39 (d, *J* = 16.0 Hz, 1H), 5.79 (s, 1H), 3.79 (s, 3H), 3.51 (qd, *J* = 7.3, 5.7 Hz, 2H), 1.26 (t, *J* = 7.3 Hz, 3H).

^{13}C NMR (101 MHz, $CDCl_3$) δ 168.6, 167.0, 142.2, 137.4, 132.7, 130.4, 130.0, 127.7, 127.2, 120.5, 51.9, 35.2, 15.0.

HRMS-ESI(m/z): $[M+Na]^+$: Calcd for $C_{13}H_{15}NNaO_3$, 256.0944; Found, 256.0951.

IR (neat): 3288, 2978, 2950, 1715, 1627, 1534, 1271, 1162.

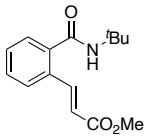

methyl (*E*)-5-methoxy-2-(3-methoxy-3-oxoprop-1-en-1-yl)benzoate (7u) The title compound was obtained from *aryl bromide* by column chromatography (Hexane: EtOAc = 2:1) as a colorless oil (31.5 mg) in 80% yield.

^{1}H NMR (400 MHz, $CDCl_3$) δ 7.98 (d, *J* = 16.0 Hz, 1H), 7.57 (dd, *J* = 7.3, 1.8 Hz, 1H), 7.46 – 7.42 (m, 1H), 7.42 – 7.34 (m, 2H), 6.37 (d, *J* = 16.0 Hz, 1H), 5.62 (s, 1H), 3.78 (s, 3H), 1.47 (s, 9H).

^{13}C NMR (101 MHz, $CDCl_3$) δ 168.2, 167.0, 142.3, 138.5, 132.3, 130.0, 129.9, 127.6, 127.1, 120.2, 52.3, 51.8, 28.8.

HRMS-ESI(m/z): $[M+Na]^+$: Calcd for $C_{15}H_{19}NNaO_3$, 284.1257; Found, 284.1254.

IR (neat): 3296, 2982, 1716, 1636, 1533, 1316, 1170.

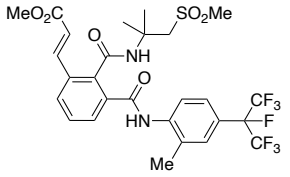

methyl (*E*)-3-(2-((2-methyl-1-(methylsulfonyl)propan-2-yl)carbamoyl)-3-((2-methyl-4-(perfluoropropan-2-yl)phenyl)carbamoyl)phenyl)acrylate (7v) The reaction was carried out with 0.05 mmol scale. The title compound was obtained from *aryl iodide* by column chromatography (Hexane: EtOAc = 1:1), and another column chromatography (DCM: EtOAc = 10:1) as a white solid (20.8 mg) in 65% yield.

^{1}H NMR (400 MHz, DMSO) δ 9.79 (s, 1H), 8.49 (s, 1H), 8.05 (dd, *J* = 8.0, 1.1 Hz, 1H), 7.94 – 7.83 (m, 2H), 7.78 (d, *J* = 7.6 Hz, 1H), 7.63 – 7.51 (m, 3H), 6.69 (d, *J* = 15.9 Hz, 1H), 3.75 (s, 3H), 3.70 (s, 2H), 2.97 (s, 3H), 2.39 (s, 3H), 1.50 (s, 6H).

^{13}C NMR (101 MHz, DMSO) δ 166.8, 166.3, 166.2, 141.2, 139.5, 137.3, 135.4, 132.8, 132.8, 131.7, 129.02 (d, *J* = 9.1 Hz), 128.1, 127.22 (d, *J* = 10.7 Hz), 124.8, 123.39 (d, *J* = 9.4 Hz), 121.33 (d, *J* = 20.4 Hz), 120.1, 60.1, 52.4, 51.6, 43.0, 26.4, 17.9.

^{19}F NMR (376 MHz, DMSO) δ -75.19 (d, *J* = 7.4 Hz, 6F), -181.44 (hept, *J* = 6.8 Hz, 1F).

HRMS-ESI(m/z): $[M+Na]^+$: Calcd for $C_{28}H_{27}F_7N_3NaO_3S$, 641.1554; Found, 641.1548.

IR (neat): 3318, 1729, 1635, 1527, 1217, 1127, 980.

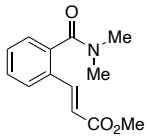

methyl (*E*)-3-(2-(dimethylcarbamoyl)phenyl)acrylate (7w) The title compound was obtained from *aryl bromide* by column chromatography (Hexane: EtOAc = 5:1) as a colorless oil (31.0 mg) in 89% yield.

^{1}H NMR (400 MHz, $CDCl_3$) δ 7.69 – 7.60 (m, 2H), 7.43 – 7.36 (m, 2H), 7.30 – 7.23 (m, 1H), 6.41 (d, *J* = 15.9 Hz, 1H), 3.77 (s, 3H), 3.15 (s, 3H), 2.78 (s, 3H).

^{13}C NMR (101 MHz, $CDCl_3$) δ 170.1, 167.0, 141.3, 137.5, 131.2, 130.3, 129.3, 127.0, 126.9, 120.3, 51.8, 38.7, 34.9.

Spectroscopic data were in accordance with previous report.[51]

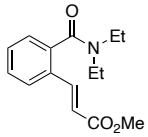

methyl (*E*)-3-(2-(diethylcarbamoyl)phenyl)acrylate (7x) The title compound was obtained from *aryl bromide* by column chromatography (Hexane: EtOAc = 2:1) as a colorless oil (14.4 mg) in 37% yield.

^{1}H NMR (400 MHz, $CDCl_3$) δ 7.68 (d, *J* = 16.0 Hz, 1H), 7.65 – 7.61 (m, 1H), 7.43 – 7.36 (m, 2H), 7.29 – 7.25 (m, 1H), 6.43 (d, *J* = 16.0 Hz, 1H), 3.77 (s, 3H), 3.58 (s, 2H), 3.08 (q, *J* = 7.1 Hz, 2H), 1.30 (t, *J* = 7.1 Hz, 3H), 1.01 (t, *J* = 7.1 Hz, 3H).

^{13}C NMR (101 MHz, $CDCl_3$) δ 169.5, 167.0, 141.3, 138.1, 130.9, 130.2, 129.1, 126.7, 126.6, 120.2, 51.8, 43.0, 39.1, 14.0, 12.8.

HRMS-ESI(m/z): $[M+Na]^+$: Calcd for $C_{15}H_{19}NNaO_3$, 284.1257; Found, 284.1249.

IR (neat): 2974, 1716, 1624, 1429, 1317, 1275, 1171.

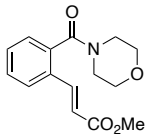

methyl (*E*)-3-(2-(morpholine-4-carbonyl)phenyl)acrylate (7y) The title compound was obtained from *aryl bromide* by column chromatography (Hexane: EtOAc = 5:1) as a colorless oil (28.1 mg) in 68% yield.

^{1}H NMR (400 MHz, $CDCl_3$) δ 7.72 (d, *J* = 16.0 Hz, 1H), 7.68 – 7.62 (m, 1H), 7.44 – 7.38 (m, 2H), 7.32 – 7.27 (m, 1H), 6.43 (d, *J* = 16.0 Hz, 1H), 3.79 (s, 7H), 3.54 (dd, *J* = 5.7, 4.0 Hz, 2H), 3.20 – 3.12 (m, 2H).

^{13}C NMR (101 MHz, $CDCl_3$) δ 168.7, 166.8, 141.1, 136.5, 131.2, 130.4, 129.6, 127.1, 126.8, 120.6, 66.9, 66.8, 51.9, 47.5, 42.3.

HRMS-ESI(m/z): $[M+Na]^+$: Calcd for $C_{15}H_{17}NNaO_4$, 298.1050; Found, 298.1048.

IR (neat): 2954, 2856, 1713, 1629, 1429, 1275, 1173, 1112.

51 Fabry, D. C.; Zoller, J.; Raja, S.; Rueping, M. *Angew. Chem. Int. Ed.* **2014**, *53*, 10228.

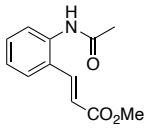

methyl (*E*)-3-(2-acetamidophenyl)acrylate (7z) The title compound was obtained from *aryl iodide, bromide and chloride* by column chromatography (Hexane: EtOAc = 1:2) as a white solid in 82% (26.9 mg), 63% (20.7), 67% (22.0) yields, respectively.

^{1}H NMR (400 MHz, $CDCl_3$) δ 7.81 (d, *J* = 15.9 Hz, 1H), 7.73 (d, *J* = 8.1 Hz, 1H), 7.54 (d, *J* = 7.8 Hz, 1H), 7.38 (t, *J* = 7.6 Hz, 2H), 7.19 (t, *J* = 7.6 Hz, 1H), 6.39 (d, *J* = 15.8 Hz, 1H), 3.80 (s, 3H), 2.23 (s, 3H).

^{13}C NMR (101 MHz, $CDCl_3$) δ 169.0, 167.3, 139.6, 136.0, 131.0, 127.6, 127.2, 126.0, 125.3, 120.3, 52.0, 24.3.

Spectroscopic data were in accordance with previous report.[52]

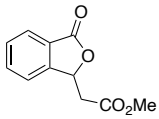

methyl 2-(3-oxo-1,3-dihydroisobenzofuran-1-yl)acetate (7aa) The title compound was obtained from *aryl iodide, bromide and chloride* by column chromatography (Hexane: EtOAc = 4:1) as a colorless oil in 49% (15.0 mg), 46% (14.2 mg), 48% (14.8 mg) yields, respectively.

^{1}H NMR (400 MHz, $CDCl_3$) δ 7.94 (d, *J* = 7.7 Hz, 1H), 7.71 (td, *J* = 7.5, 1.1 Hz, 1H), 7.58 (t, *J* = 7.5 Hz, 1H), 7.52 (dd, *J* = 7.7, 0.9 Hz, 1H), 5.95 – 5.87 (m, 1H), 3.79 (s, 3H), 3.01 – 2.85 (m, 2H).

^{13}C NMR (101 MHz, $CDCl_3$) δ 169.9, 169.8, 148.8, 134.4, 129.7, 126.0, 126.0, 122.2, 77.0, 52.3, 39.5.

Spectroscopic data were in accordance with previous report.[53]

[52] Kim, B. S.; Jang, C.; Lee, D. J. Youn, S. W. *Chem. Asian J.* **2010**, *5*, 2336.

[53] Zhu, Y.-Q.; Li, J.-X.; Han, T.-F.; He, J.-L.; Zhu, K. *Eur. J. Org. Chem*., **2017**, *4*, 806.

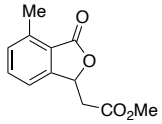

methyl 2-(4-methyl-3-oxo-1,3-dihydroisobenzofuran-1-yl)acetate (7ab) The title compound was obtained from *aryl chloride* by column chromatography (Hexane: EtOAc = 3:1) as a colorless oil (31.5 mg) in 95% yield.

^{1}H NMR (400 MHz, $CDCl_3$) δ 7.52 (t, *J* = 7.6 Hz, 1H), 7.32 – 7.23 (m, 2H), 5.86 – 5.76 (m, 1H), 3.75 (s, 3H), 2.86 (d, *J* = 6.6 Hz, 2H), 2.67 (s, 3H).

^{13}C NMR (101 MHz, $CDCl_3$) δ 170.1, 169.9, 149.3, 140.0, 134.1, 131.2, 123.4, 119.3, 76.1, 52.2, 39.7, 17.4.

Spectroscopic data were in accordance with previous report.[54]

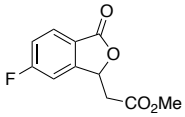

methyl 2-(6-fluoro-3-oxo-1,3-dihydroisobenzofuran-1-yl)acetate (7ac) The title compound was obtained from *aryl chloride* by column chromatography (Hexane: EtOAc = 3:1) as a colorless oil (17.0 mg) in 51% yield

^{1}H NMR (400 MHz, $CDCl_3$) δ 7.90 (dd, *J* = 8.4, 4.8 Hz, 1H), 7.34 – 7.16 (m, 2H), 5.83 (t, *J* = 6.7 Hz, 1H), 3.77 (s, 3H), 3.07 – 2.77 (m, 2H).

^{13}C NMR (101 MHz, $CDCl_3$) δ 169.6, 168.3 (d, *J* = 68.5 Hz), 165.4, 151.6 (d, *J* = 10.2 Hz), 128.3 (d, *J* = 10.4 Hz), 122.1 (d, *J* = 2.0 Hz), 117.9 (d, *J* = 24.1 Hz), 109.9 (d, *J* = 24.8 Hz), 76.3 (d, *J* = 2.9 Hz), 52.4, 39.1.

^{19}F NMR (376 MHz, $CDCl_3$) δ -102.13 (td, *J* = 8.3, 4.7 Hz).

Spectroscopic data were in accordance with previous report.[53]

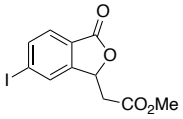

[54] Mandal, A.; Garai, B.; Dana, S.; Bera, R.; and Baidya, M. *Chem. Asian. J.* **2020**, *15*, 4009.

methyl 2-(6-iodo-3-oxo-1,3-dihydroisobenzofuran-1-yl)acetate (7ad) The title compound was obtained from *aryl chloride* by column chromatography (Hexane: EtOAc = 3:1) as a white solid (27.2 mg) in 54% yield.

^{1}H NMR (400 MHz, $CDCl_3$) δ 7.97 – 7.85 (m, 2H), 7.65 – 7.57 (m, 1H), 5.88 – 5.77 (m, 1H), 3.76 (s, 3H), 3.02 – 2.81 (m, 2H).

^{13}C NMR (101 MHz, $CDCl_3$) δ 169.6, 169.1, 150.4, 139.1, 131.8, 127.1, 125.6, 102.2, 76.2, 52.4, 39.1.

HRMS-ESI(m/z): $[M+Na]^+$: Calcd for $C_{11}H_9INaO_4$, 354.9438; Found, 354.9440.

IR (neat): 3087, 1765, 1715, 1584, 1355, 1060, 992.

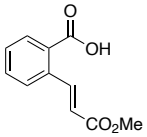

(*E*)-2-(3-methoxy-3-oxoprop-1-en-1-yl)benzoic acid (7ae) The title compound was obtained from *tert*-butyl 2-bromobenzoate without column as a white solid (27.7 mg) in 90% yield.

^{1}H NMR (400 MHz, DMSO) δ 8.38 (d, *J* = 16.0 Hz, 1H), 7.90 (ddd, *J* = 7.7, 1.5, 0.5 Hz, 1H), 7.84 (d, *J* = 7.8 Hz, 1H), 7.65 – 7.58 (m, 1H), 7.53 (td, *J* = 7.5, 1.3 Hz, 1H), 6.52 (d, *J* = 15.9 Hz, 1H), 3.74 (s, 3H), 3.35 (s, 1H).

^{13}C NMR (101 MHz, DMSO) δ 168.0, 166.4, 143.2, 134.6, 132.1, 131.1, 130.3, 129.9, 127.8, 119.9, 51.5.

Spectroscopic data were in accordance with previous report.[55]

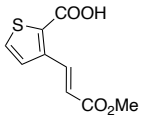

(*E*)-3-(3-methoxy-3-oxoprop-1-en-1-yl)thiophene-2-carboxylic acid (7af) The title compound was obtained from *aryl bromide* by column chromatography (Hexane: EtOAc = 5:1) as a white solid (19.0 mg) in 60% yield.

[55] Arcas, V. A.; Hernandez, F. J.; Bautista, D. *Angew. Chem. Int. Ed.* **2011**, *50*, 6896.

^{1}H NMR (400 MHz, $CDCl_3$) δ 8.52 (d, *J* = 16.2 Hz, 1H), 7.52 (d, *J* = 5.2 Hz, 1H), 7.35 (d, *J* = 5.2 Hz, 1H), 6.37 (d, *J* = 16.0 Hz, 1H), 5.00 (s, 1H), 3.81 (s, 3H).

^{13}C NMR (101 MHz, $CDCl_3$) δ 167.4, 166.5, 142.7, 136.8, 132.0, 131.4, 127.0, 121.9, 52.1.

HRMS-ESI(m/z): $[M+H]^+$: Calcd for $C_9H_7O_4S$, 211.0071; Found, 211.0071.

IR (neat): 3084, 2962, 1714, 1674, 1430, 1314, 1209, 1035.

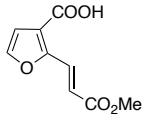

(*E*)-2-(3-methoxy-3-oxoprop-1-en-1-yl)furan-3-carboxylic acid (7ag) The title compound was obtained from *aryl bromide* by column chromatography (Hexane: EtOAc = 5:1 with 0.1% AcOH), and then recrystallized with DCM and hexane as a white solid (5.0 mg) in 17% yield.

^{1}H NMR (400 MHz, DMSO) δ 13.32 (s, 1H), 7.99 (d, J = 16.0 Hz, 1H), 7.91 (d, J = 1.9 Hz, 1H), 6.87 (d, J = 1.9 Hz, 1H), 6.45 (d, J = 16.1 Hz, 1H), 3.74 (s, 3H).

^{13}C NMR (101 MHz, DMSO) δ 166.0, 163.5, 152.1, 145.5, 129.3, 120.5, 118.9, 113.0, 51.8.

HRMS-ESI(m/z): $[M-H]^-$: Calcd for $C_9H_7O_5$, 195.0299; Found, 195.0303.

IR (neat): 2920, 1682, 1262, 1244, 1062.

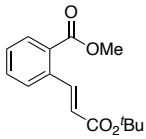

methyl (*E*)-2-(3-(*tert*-butoxy)-3-oxoprop-1-en-1-yl)benzoate (9a) The title compound was obtained by column chromatography (Hexane: EtOAc = 20:1) as a colorless oil (30.0mg) in 80% yield.

^{1}H NMR (400 MHz, $CDCl_3$) δ 8.32 (d, *J* = 15.9 Hz, 1H), 7.93 (dd, *J* = 7.8, 0.9 Hz, 1H), 7.60 (dd, *J* = 7.9, 1.4 Hz, 1H), 7.51 (td, *J* = 7.3, 0.9 Hz, 1H), 7.41 (td, *J* = 7.6, 1.4 Hz, 1H), 6.24 (d, *J* = 15.9 Hz, 1H), 3.93 (s, 3H), 1.54 (s, 9H).

^{13}C NMR (101 MHz, $CDCl_3$) δ 167.4, 166.0, 142.6, 136.5, 132.3, 130.8, 130.0, 129.2, 127.9, 123.1, 80.7, 52.4, 28.3.

Spectroscopic data were in accordance with previous report.[56]

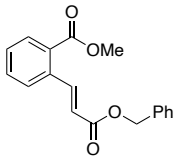

methyl (*E*)-2-(3-(benzyloxy)-3-oxoprop-1-en-1-yl)benzoate (9b) The title compound was obtained by column chromatography (Hexane: EtOAc = 10:1) as a colorless oil (36.1mg) in 81% yield.

^{1}H NMR (400 MHz, $CDCl_3$) δ 8.49 (d, *J* = 15.9 Hz, 1H), 7.96 (ddd, *J* = 7.8, 1.5, 0.5 Hz, 1H), 7.59 (dd, *J* = 7.8, 1.5 Hz, 1H), 7.53 (tdd, *J* = 7.8, 1.5, 0.6 Hz, 1H), 7.47 – 7.30 (m, 6H), 6.36 (d, *J* = 15.9 Hz, 1H), 5.27 (s, 2H), 3.92 (s, 3H).

^{13}C NMR (101 MHz, $CDCl_3$) δ 167.3, 166.4, 144.4, 136.3, 136.2, 132.4, 130.9, 130.0, 129.5, 128.7, 128.3, 128.3, 128.0, 120.8, 66.5, 52.5.

HRMS-ESI(m/z): $[M+Na]^+$: Calcd for $C_{18}H_{16}NaO_4$, 319.0941; Found, 319.0938.

IR (neat): 2951, 1712, 1256, 1157, 1077.

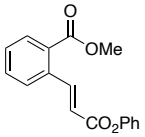

methyl (*E*)-2-(3-oxo-3-phenoxyprop-1-en-1-yl)benzoate (9c) The title compound was obtained by column chromatography (Hexane: EtOAc = 20:1 to 5:1) then preparative TLC (Hexane: EtOAc = 10:1) as a colorless oil (16.1mg) in 38% yield.

^{1}H NMR (400 MHz, $CDCl_3$) δ 8.64 (d, *J* = 15.9 Hz, 1H), 8.00 (dd, *J* = 7.8, 1.5 Hz, 1H), 7.68 (d, *J* = 7.8 Hz, 1H), 7.62 – 7.55 (m, 1H), 7.48 (td, *J* = 7.6, 1.4 Hz, 1H), 7.45 – 7.36 (m, 2H), 7.25 (ddt, *J* = 8.0, 7.0, 1.2 Hz, 1H), 7.22 – 7.17 (m, 2H), 6.50 (d, *J* = 15.9 Hz, 1H), 3.95 (s, 3H).

^{13}C NMR (101 MHz, $CDCl_3$) δ 167.2, 165.1, 150.9, 145.8, 136.2, 132.6, 131.0, 130.1, 129.8, 129.5, 128.1, 125.9, 121.8, 120.3, 52.6.

[56] Peh, G.-R.; Kantchev, E. A. B.; Zhang, C.; Ying, J. Y. *Org. Biomol. Chem*. **2009**, *7*, 2110.

HRMS-ESI(m/z): $[M+Na]^+$: Calcd for $C_{15}H_{12}N_3NaO_3$, 305.0771; Found, 305.0777.

IR (neat): 3084, 2956, 1715, 1476, 1247, 1147, 1073.

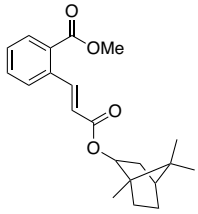

methyl 2-((*E*)-3-oxo-3-(((4*R*)-1,7,7-trimethylbicyclo[2.2.1]heptan-2-yl)oxy)prop-1-en-1-yl)benzoate (9d) The title compound was obtained by column chromatography (Hexane: EtOAc = 10:1) as a colorless oil (35.0 mg) in 68% yield.

^{1}H NMR (400 MHz, $CDCl_3$) δ 8.37 (d, *J* = 15.9 Hz, 1H), 7.94 (ddd, *J* = 7.8, 1.5, 0.5 Hz, 1H), 7.61 (d, *J* = 7.8 Hz, 1H), 7.52 (td, *J* = 7.6, 1.8 Hz, 1H), 7.42 (td, *J* = 7.6, 1.3 Hz, 1H), 6.28 (d, *J* = 16.0 Hz, 1H), 4.80 (dd, *J* = 7.0, 4.5 Hz, 1H), 3.92 (s, 3H), 1.91 – 1.83 (m, 2H), 1.79 – 1.75 (m, 1H), 1.74 – 1.67 (m, 1H), 1.58 (td, *J* = 12.1, 3.9 Hz, 1H), 1.26 – 1.10 (m, 2H), 1.07 (s, 3H), 0.92 (s, 3H), 0.87 (s, 3H).

^{13}C NMR (101 MHz, $CDCl_3$) δ 167.4, 166.1, 143.2, 136.3, 132.3, 130.9, 130.1, 129.4, 127.9, 121.8, 81.3, 52.4, 49.0, 47.1, 45.2, 39.0, 33.9, 27.2, 20.2, 20.1, 11.6.

HRMS-ESI(m/z): $[M+Na]^+$: Calcd for $C_{21}H_{26}NaO_4$, 365.1723; Found, 365.1728.

IR (neat): 2952, 2877, 1708, 1261, 1162, 1077.

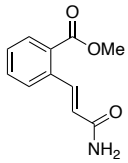

methyl (*E*)-2-(3-amino-3-oxoprop-1-en-1-yl)benzoate (9e) The title compound was obtained by column chromatography (Hexane: EtOAc = 1:1) then preparative TLC (DCM: MeOH = 20:1) as a white solid (7.0 mg) in 23% yield.

^{1}H NMR (400 MHz, $CDCl_3$) δ 8.29 (d, *J* = 15.8 Hz, 1H), 7.96 (dd, *J* = 7.7, 1.9 Hz, 1H), 7.61 – 7.50 (m, 2H), 7.43 (td, *J* = 7.5, 1.5 Hz, 1H), 6.31 (d, *J* = 15.8 Hz, 1H), 5.59 (s, 2H), 3.93 (s, 3H).

^{13}C NMR (101 MHz, $CDCl_3$) δ 167.7, 167.4, 141.0, 136.7, 132.4, 130.9, 129.8, 129.2, 127.9, 123.1, 52.5.

HRMS-ESI(m/z): $[M+Na]^+$: Calcd for $C_{11}H_{11}NNaO_3$, 228.0631; Found, 228.0623.

IR (neat): 3368, 3193, 1718, 1661, 1605, 1254, 1075.

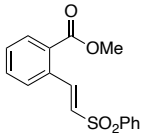

methyl (*E*)-2-(2-(phenylsulfonyl)vinyl)benzoate (9f) The title compound was obtained by column chromatography (Hexane: EtOAc = 5:1) as a colorless oil (22.2 mg) in 49% yield.

^{1}H NMR (400 MHz, $CDCl_3$) δ 8.50 (d, *J* = 15.3 Hz, 1H), 8.09 – 7.97 (m, 3H), 7.68 – 7.46 (m, 6H), 6.74 (d, *J* = 15.3 Hz, 1H), 3.96 (s, 3H).

^{13}C NMR (101 MHz, $CDCl_3$) δ 166.8, 142.7, 140.7, 134.5, 133.5, 132.6, 131.1, 130.3, 130.1, 129.9, 129.4, 128.3, 128.0, 52.6.

HRMS-ESI(m/z): $[M+Na]^+$: Calcd for $C_{16}H_{14}NaO_4S$, 325.0505; Found, 325.0491.

IR (neat): 3059, 3039. 2952, 1715, 1264, 1076.

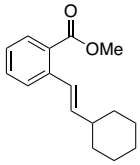

methyl (*E*)-2-(2-cyclohexylvinyl)benzoate (9g) The title compound was obtained by column chromatography (Hexane: EtOAc = 20:1) as a colorless oil (30.6 mg) in 84% yield.

^{1}H NMR (400 MHz, $CDCl_3$) δ 7.86 (dd, *J* = 7.9, 1.5 Hz, 1H), 7.56 (d, *J* = 7.9 Hz, 1H), 7.45 (td, *J* = 7.6, 1.8 Hz, 1H), 7.31 – 7.23 (m, 1H), 7.14 (d, *J* = 15.9 Hz, 1H), 6.11 (dd, *J* = 15.9, 6.8 Hz, 1H), 3.92 (s, 3H), 2.21 (m, 1H), 1.91 – 1.67 (m, 5H), 1.40 – 1.19 (m, 5H).

^{13}C NMR (101 MHz, $CDCl_3$) δ 168.2, 140.0, 139.7, 132.0, 130.4, 128.3, 127.2, 126.5, 126.2, 52.0, 41.3, 33.0, 26.3, 26.1.

Spectroscopic data were in accordance with previous report.[57]

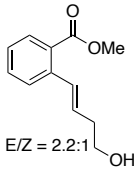

methyl (*E*)-2-(4-hydroxybut-1-en-1-yl)benzoate (9h) The title compound was obtained by column chromatography (Hexane: EtOAc = 1:1) as a colorless oil (25.6 mg) in 83% yield.

^{1}H NMR (400 MHz, $CDCl_3$) δ 7.92 (dd, *J* = 7.7, 1.9 Hz, 0.45H), 7.86 (dd, *J* = 7.9, 1.4 Hz, 1H), 7.56 – 7.40 (m, 2.6H), 7.37 – 7.24 (m, 2H), 7.18 (d, *J* = 15.9 Hz, 1H), 6.96 (d, *J* = 11.5 Hz, 0.46H), 6.04 (dt, *J* = 15.8, 7.1 Hz, 1H), 5.73 (dt, *J* = 11.5, 7.6 Hz, 0.47H), 3.88 (s, 3H), 3.86 (s, 1.43H), 3.76 (t, *J* = 6.1 Hz, 2H), 3.64 (t, *J* = 6.2 Hz, 1H), 2.63 – 2.45 (m, 2H), 2.38 (dtd, *J* = 7.7, 6.2, 1.6 Hz, 1H), 2.03 (s, 1.58H).

^{13}C NMR (101 MHz, $CDCl_3$) δ 168.0, 139.7(E), 138.9(Z), 132.5(Z), 132.2(E), 132.1(E), 131.9(Z), 130.9(Z), 130.5(Z), 130.4(E), 129.3(E), 129.2(Z), 128.2(E), 127.7(Z), 127.6(E), 127.0(Z), 127.0(E), 62.1(Z), 61.8(E), 52.2(E), 52.1(Z), 36.3(E), 31.7(Z).

Spectroscopic data were in accordance with previous report.[58]

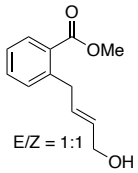

methyl (*E*)-2-(3,3-dimethylbut-1-en-1-yl)benzoate (9i) The title compound was obtained by column chromatography (Hexane: EtOAc = 1:1) then preparative TLC (Hexane: EtOAc = 2:1) as a colorless oil (9.3mg) in 30% yield.

^{1}H NMR (400 MHz, $CDCl_3$) δ 7.96 – 7.87 (m, 1H), 7.47 (m, 1H), 7.30 (td, *J* = 7.7, 2.8 Hz, 2H), 5.92 (m, 0.6H), 5.80 – 5.57 (m, 1.5H), 4.31 (d, *J* = 7.0 Hz, 1H), 4.12 (d, *J* =

57 Woerly, E. M.; Banik, S. M.; Jacobsen, E. N. *J. Am. Chem. Soc.* **2016**, *138,* 13858.
58 Fujita, M.; Mori, K.; Shimogaki, M.; Sugimura, T. *Org. Lett.* **2012**, *14*, 1294.

5.6 Hz, 1H), 3.91 (d, *J* = 1.4 Hz, 3H), 3.83 (d, *J* = 7.2 Hz, 1H), 3.77 (d, *J* = 6.4 Hz, 1H), 2.08 (s, 0.48H), 1.37 (s, 0.56H).

^{13}C NMR (101 MHz, $CDCl_3$) δ 168.1, 142.3(Z), 141.7(E), 132.5(Z), 132.2(E), 131.7(E), 131.2(Z), 131.1(E), 131.0(Z), 130.9(Z), 130.8(E), 130.3(E), 129.7(E), 129.5(Z), 129.1(Z), 126.4(Z), 126.4(E), 63.7(E), 58.4(Z), 52.2(Z), 52.1(E), 37.0(E), 32.6(Z).

HRMS-ESI(m/z): $[M+Na]^+$: Calcd for $C_{12}H_{14}NaO_3$, 229.0835; Found, 229.0831.

IR (neat): 3401, 2951, 1715, 1260, 1078.

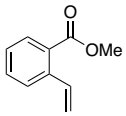

methyl 2-vinylbenzoate (9j) The title compound was obtained by column chromatography (Hexane: EtOAc = 20:1) as a colorless oil (20.7 mg) in 85% yield.
^{1}H NMR (400 MHz, $CDCl_3$) δ 7.88 (dd, *J* = 7.8, 0.9 Hz, 1H), 7.58 (d, *J* = 7.9 Hz, 1H), 7.53 – 7.42 (m, 2H), 7.32 (td, *J* = 7.6, 1.3 Hz, 1H), 5.65 (dd, *J* = 17.4, 1.3 Hz, 1H), 5.36 (dd, *J* = 11.0, 1.3 Hz, 1H), 3.91 (s, 3H).

^{13}C NMR (101 MHz, $CDCl_3$) δ 168.0, 139.7, 136.0, 132.2, 130.4, 128.7, 127.5, 127.3, 116.6, 52.2.

Spectroscopic data were in accordance with previous report.[59]

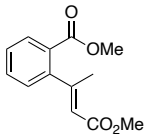

methyl (*E*)-2-(4-methoxy-4-oxobut-2-en-2-yl)benzoate (7k) The title compound was obtained by column chromatography (Hexane: EtOAc = 10:1) and then preparative TLC (Hexane: EtOAc = 20:1) as a colorless oil (11.0 mg) in 31% yield.
^{1}H NMR (400 MHz, $CDCl_3$) δ 7.91 (dd, *J* = 7.8, 1.4 Hz, 1H), 7.50 (td, *J* = 7.6, 1.4 Hz, 1H), 7.39 (td, *J* = 7.6, 1.3 Hz, 1H), 7.19 (dd, *J* = 7.6, 1.3 Hz, 1H), 5.74 (d, *J* = 1.4 Hz, 1H), 3.86 (s, 3H), 3.74 (s, 3H), 2.45 (d, *J* = 1.4 Hz, 3H).

[59] Hemric, B. N.; Chen, A. W.; Wang, Q. *J. Org. Chem.* **2019**, *84*, 1468.

^{13}C NMR (101 MHz, $CDCl_3$) δ 167.4, 167.0, 159.3, 145.6, 132.2, 130.5, 128.6, 128.6, 128.0, 117.5, 52.3, 51.2, 21.3.

HRMS-ESI(m/z): $[M+Na]^+$: Calcd for $C_{13}H_{14}NaO_4$, 257.0784; Found, 257.0780.

IR (neat): 3236, 1719, 1257, 1643, 1064.

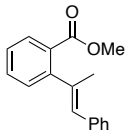

methyl (*E*)-2-(1-phenylprop-1-en-2-yl)benzoate (9l) The title compound was obtained by column chromatography (Hexane: EtOAc = 10:1) and then preparative TLC (Hexane: EtOAc = 20:1) as a colorless oil (12.5 mg) in 33% yield.
^{1}H NMR (400 MHz, $CDCl_3$) δ 7.83 (dd, *J* = 8.1, 1.5 Hz, 1H), 7.53 – 7.45 (m, 1H), 7.40 – 7.31 (m, 6H), 7.26 – 7.21 (m, 1H), 6.35 (d, *J* = 1.5 Hz, 1H), 3.85 (s, 3H), 2.22 (d, *J* = 1.4 Hz, 3H).

^{13}C NMR (101 MHz, $CDCl_3$) δ 168.7, 147.0, 139.5, 138.1, 131.7, 130.0, 130.0, 129.4, 129.0, 128.3, 128.2, 127.0, 126.6, 52.2, 20.2.

HRMS-ESI(m/z): $[M+Na]^+$: Calcd for $C_{17}H_{16}NaO_2$, 275.1043; Found, 275.1042.

IR (neat): 3023, 2949, 1722, 1251, 1093.

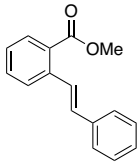

methyl (*E*)-2-styrylbenzoate (9m) The title compound was obtained by column chromatography (Hexane: EtOAc = 20:1) as a yellowish oil (31.3 mg) in 88% yield.
^{1}H NMR (400 MHz, $CDCl_3$) δ 8.03 (d, *J* = 16.2 Hz, 1H), 7.97 (dd, *J* = 7.9, 1.0 Hz, 1H), 7.76 (d, *J* = 7.9 Hz, 1H), 7.62 – 7.50 (m, 3H), 7.45 – 7.27 (m, 4H), 7.05 (d, *J* = 16.3 Hz, 1H), 3.96 (s, 3H).

^{13}C NMR (101 MHz, $CDCl_3$) δ 168.0, 139.3, 137.5, 132.2, 131.5, 130.8, 128.8, 128.7, 127.9, 127.5, 127.2, 127.1, 127.0, 52.2.

Spectroscopic data were in accordance with previous report.[60]

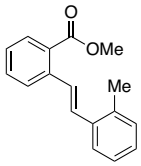

methyl (*E*)-2-(2-methylstyryl)benzoate (9n) The title compound was obtained by column chromatography (Hexane: EtOAc = 20:1) as a colorless oil (30.0 mg) in 79% yield.

^{1}H NMR (400 MHz, $CDCl_3$) δ 7.94 (dd, *J* = 8.0, 1.4 Hz, 1H), 7.85 (d, *J* = 16.1 Hz, 1H), 7.72 (d, *J* = 8.0 Hz, 1H), 7.66 (d, *J* = 6.7 Hz, 1H), 7.53 (td, *J* = 7.6, 1.8 Hz, 1H), 7.33 (td, *J* = 7.6, 1.3 Hz, 1H), 7.25 – 7.16 (m, 4H), 3.93 (d, *J* = 0.6 Hz, 3H), 2.44 (s, 3H).

^{13}C NMR (101 MHz, $CDCl_3$) δ 168.0, 139.7, 136.5, 136.0, 132.3, 130.7, 130.5, 129.4, 128.9, 128.8, 127.8, 127.3, 127.2, 126.4, 126.0, 52.2, 20.0.

HRMS-ESI(m/z): $[M+Na]^+$: Calcd for $C_{17}H_{16}NaO_2$, 275.1043; Found, 275.1043.

IR (neat): 2949, 1715, 1267, 1243, 1075.

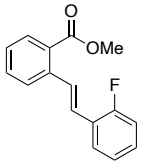

methyl (*E*)-2-(2-fluorostyryl)benzoate (9o) The title compound was obtained by column chromatography (Hexane: EtOAc = 20:1) as a colorless oil (30.8 mg) in 80% yield.

^{1}H NMR (400 MHz, $CDCl_3$) δ 8.05 (d, *J* = 16.4 Hz, 1H), 7.95 (dd, *J* = 8.1, 1.2 Hz, 1H), 7.75 (d, *J* = 7.9 Hz, 1H), 7.69 (td, *J* = 7.7, 1.7 Hz, 1H), 7.53 (m, 1H), 7.34 (td, *J* = 7.6, 1.3 Hz, 1H), 7.28 – 7.12 (m, 3H), 7.07 (ddd, *J* = 10.8, 8.1, 1.3 Hz, 1H), 3.93 (s, 3H).

60 Hemric, B. N.; Shen, K.; Wang, Q. *J. Am. Chem. Soc.* **2016**, *138*, 5813.

^{13}C NMR (101 MHz, $CDCl_3$) δ 167.9, 161.8, 159.4, 139.3, 132.4, 130.8, 129.7 (d, *J* = 4.4 Hz), 129.2 (d, *J* = 8.4 Hz), 128.7, 127.4 (d, *J* = 3.6 Hz), 127.4 (d, *J* = 24.9 Hz), 125.4 (d, *J* = 12.0 Hz), 124.3 (d, *J* = 3.5 Hz), 123.5 (d, *J* = 4.1 Hz), 115.8 (d, *J* = 22.2 Hz), 52.2.

^{19}F NMR (376 MHz, $CDCl_3$) δ -118.36 (ddd, *J* = 10.9, 7.7, 5.3 Hz).

HRMS-ESI(m/z): $[M+Na]^+$: Calcd for $C_{16}H_{13}FNaO_2$, 279.0792; Found, 279.0787.

IR (neat): 3066, 2950, 1715, 1228, 1076.

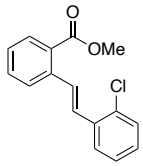

methyl (*E*)-2-(2-chlorostyryl)benzoate (9p) The title compound was obtained by column chromatography (Hexane: EtOAc = 20:1) as a colorless oil (33.4 mg) in 82% yield.

^{1}H NMR (400 MHz, $CDCl_3$) δ 8.04 – 7.92 (m, 2H), 7.77 (dd, *J* = 7.9, 1.4 Hz, 2H), 7.55 (m, 1H), 7.45 – 7.32 (m, 3H), 7.31 – 7.25 (m, 1H), 7.21 (td, *J* = 7.7, 1.7 Hz, 1H), 3.93 (s, 3H).

^{13}C NMR (101 MHz, $CDCl_3$) δ 167.8, 139.2, 135.6, 133.6, 132.4, 130.8, 130.2, 129.8, 128.8, 128.7, 127.6, 127.6, 127.5, 127.1, 127.1, 52.2.

Spectroscopic data were in accordance with previous report.[61]

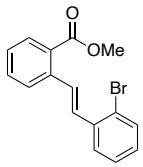

methyl (*E*)-2-(2-bromostyryl)benzoate (9q) The title compound was obtained by column chromatography (Hexane: EtOAc = 20:1) as a colorless oil (45.3 mg) in 96% yield.

61 Shahzad, S. A.; Vivant, C.; Wirt, T. *Org. Lett.* **2010**, *12*, 1364.

^{1}H NMR (400 MHz, $CDCl_3$) δ 7.99 – 7.90 (m, 2H), 7.80 – 7.73 (m, 2H), 7.62 – 7.51 (m, 2H), 7.40 – 7.28 (m, 3H), 7.13 (ddd, *J* = 8.0, 7.3, 1.7 Hz, 1H), 3.93 (s, 3H).

^{13}C NMR (101 MHz, $CDCl_3$) δ 167.8, 139.1, 137.3, 133.1, 132.4, 130.8, 130.4, 130.1, 129.1, 128.7, 127.7, 127.6, 127.6, 127.4, 124.3, 52.2.

HRMS-ESI(m/z): $[M+Na]^+$: Calcd for $C_{16}H_{13}BrNaO_2$, 338.9991; Found, 338.9987.

IR (neat): 3063, 3025, 2951, 1716, 1432, 1244, 1076.

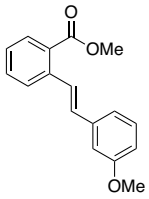

methyl (*E*)-2-(3-methoxystyryl)benzoate (9r) The title compound was obtained by column chromatography (Hexane: EtOAc = 20:1) as a colorless oil (29.7mg) in 74% yield.

^{1}H NMR (400 MHz, $CDCl_3$) δ 8.06 – 7.91 (m, 2H), 7.74 (d, *J* = 8.0 Hz, 1H), 7.54 (td, *J* = 7.6, 1.4 Hz, 1H), 7.41 – 7.25 (m, 2H), 7.19 (d, *J* = 7.6 Hz, 1H), 7.11 (t, *J* = 2.0 Hz, 1H), 7.00 (d, *J* = 16.2 Hz, 1H), 6.86 (ddd, *J* = 8.2, 2.6, 1.0 Hz, 1H), 3.95 (s, 3H), 3.88 (s, 3H).

^{13}C NMR (101 MHz, $CDCl_3$) δ 168.0, 160.0, 139.2, 139.0, 132.2, 131.5, 130.8, 129.7, 128.7, 127.9, 127.3, 127.1, 119.6, 113.6, 112.3, 55.4, 52.2.

HRMS-ESI(m/z): $[M+Na]^+$: Calcd for $C_{17}H_{16}NaO_3$, 291.0992; Found, 291.0987.

IR (neat): 2950, 2835, 1714, 1578, 1236, 1075.

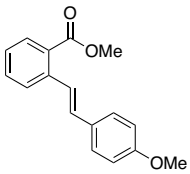

methyl (*E*)-2-(4-methoxystyryl)benzoate (9s) The title compound was obtained by column chromatography (Hexane: EtOAc = 20:1) as a colorless oil (25.7mg) in 64% yield.

^{1}H NMR (400 MHz, $CDCl_3$) δ 7.91 (dd, *J* = 7.9, 1.0 Hz, 1H), 7.86 (d, *J* = 16.2 Hz, 1H), 7.71 (d, *J* = 8.0 Hz, 1H), 7.54 – 7.45 (m, 3H), 7.29 (td, *J* = 7.6, 1.3 Hz, 1H), 6.98 (d, *J* = 16.2 Hz, 1H), 6.94 – 6.87 (m, 2H), 3.93 (s, 3H), 3.83 (s, 3H).

^{13}C NMR (101 MHz, $CDCl_3$) δ 168.1, 159.6, 139.6, 132.2, 131.1, 130.7, 130.4, 128.4, 128.2, 126.8, 126.8, 125.3, 114.2, 55.4, 52.2.

HRMS-ESI(m/z): $[M+Na]^+$: Calcd for $C_{17}H_{16}NaO_3$, 291.0992; Found, 291.0988.

IR (neat): 2994, 2947, 2838, 1716, 1246, 1125, 1077.

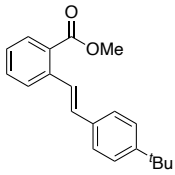

methyl (*E*)-2-(4-(*tert*-butyl)styryl)benzoate (9t) The title compound was obtained by column chromatography (Hexane: EtOAc = 10:1) as a white solid (40.3 mg) in 91% yield.

^{1}H NMR (400 MHz, $CDCl_3$) δ 8.01 – 7.90 (m, 2H), 7.74 (d, *J* = 8.0 Hz, 1H), 7.55 – 7.49 (m, 3H), 7.44 – 7.38 (m, 2H), 7.32 (td, *J* = 7.6, 1.3 Hz, 1H), 7.02 (d, *J* = 16.2 Hz, 1H), 3.94 (s, 3H), 1.36 (s, 9H).

^{13}C NMR (101 MHz, $CDCl_3$) δ 168.0, 151.1, 139.5, 134.8, 132.2, 131.4, 130.7, 128.6, 127.0, 127.0, 126.8, 126.7, 125.7, 52.2, 34.7, 31.4.

HRMS-ESI(m/z): $[M+Na]^+$: Calcd for $C_{20}H_{22}NaO_2$, 317.1512; Found, 317.1527.

IR (neat): 2951, 1722, 1711, 1246, 1076.

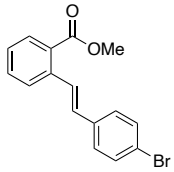

methyl (*E*)-2-(4-bromostyryl)benzoate (9u) The title compound was obtained by column chromatography (Hexane: EtOAc = 10:1) as a white solid (37.2 mg) in 78% yield.

^{1}H NMR (400 MHz, $CDCl_3$) δ 8.04 – 7.91 (m, 2H), 7.70 (d, *J* = 8.0 Hz, 1H), 7.55 – 7.45 (m, 3H), 7.44 – 7.37 (m, 2H), 7.34 (td, *J* = 7.6, 1.3 Hz, 1H), 6.93 (d, *J* = 16.3 Hz, 1H), 3.93 (s, 3H).

^{13}C NMR (101 MHz, $CDCl_3$) δ 167.8, 139.1, 136.5, 132.3, 131.9, 130.8, 130.2, 128.6, 128.4, 128.3, 127.5, 127.1, 121.7, 52.2.

HRMS-ESI(m/z): $[M+Na]^+$: Calcd for $C_{16}H_{13}BrNaO_2$, 338.9991; Found, 338.9986.

IR (neat): 2946, 1719, 1486, 1249, 1070.

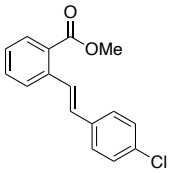

methyl (*E*)-2-(4-chlorostyryl)benzoate (9v) The title compound was obtained by column chromatography (Hexane: EtOAc = 10:1) as a white solid (31.6 mg) in 77% yield.

^{1}H NMR (400 MHz, $CDCl_3$) δ 8.03 – 7.91 (m, 2H), 7.70 (d, *J* = 8.0 Hz, 1H), 7.55 – 7.43 (m, 3H), 7.37 – 7.30 (m, 3H), 6.95 (d, *J* = 16.2 Hz, 1H), 3.93 (s, 3H).

^{13}C NMR (101 MHz, $CDCl_3$) δ 167.9, 139.1, 136.1, 133.5, 132.3, 130.8, 130.2, 128.9, 128.6, 128.2, 128.1, 127.4, 127.1, 52.2.

Spectroscopic data were in accordance with previous report.[62]

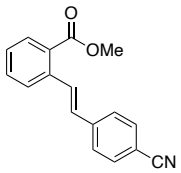

methyl (*E*)-2-(4-cyanostyryl)benzoate (9w) The title compound was obtained by column chromatography (Hexane: EtOAc = 5:1) as a white solid (24.1 mg) in 61% yield.

62 Folgueiras-Amador, A. A.; Philipps, K.; Guilbaud, S.; Poelakker, J.; Wirth, T. *Angew. Chem. Int. Ed.* **2017**, *56*, 15446.

^{1}H NMR (400 MHz, $CDCl_3$) δ 8.14 (d, *J* = 16.2 Hz, 1H), 7.98 (dd, *J* = 7.9, 1.4 Hz, 1H), 7.70 (dd, *J* = 8.0, 1.3 Hz, 1H), 7.66 – 7.59 (m, 4H), 7.54 (td, *J* = 7.6, 1.5 Hz, 1H), 7.38 (td, *J* = 7.6, 1.3 Hz, 1H), 6.97 (d, *J* = 16.2 Hz, 1H), 3.93 (d, *J* = 0.5 Hz, 3H).

^{13}C NMR (101 MHz, $CDCl_3$) δ 167.6, 142.0, 138.5, 132.6, 132.5, 131.5, 131.0, 129.4, 128.8, 128.1, 127.3, 127.3, 119.1, 110.9, 52.3.

HRMS-ESI(m/z): $[M+Na]^+$: Calcd for $C_{17}H_{13}NNaO_2$, 286.0838; Found, 286.0842.

IR (neat): 2951, 2223, 1707, 1251, 1077.

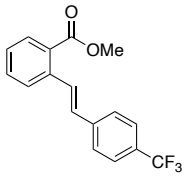

methyl (*E*)-2-(4-(trifluoromethyl)styryl)benzoate (9x) The title compound was obtained by column chromatography (Hexane: EtOAc = 10:1) as a white solid (33.3 mg) in 72% yield.

^{1}H NMR (400 MHz, $CDCl_3$) δ 8.10 (d, *J* = 16.2 Hz, 1H), 7.97 (ddd, *J* = 7.9, 1.5, 0.5 Hz, 1H), 7.72 (d, *J* = 8.0 Hz, 1H), 7.68 – 7.58 (m, 4H), 7.54 (tdd, *J* = 7.9, 1.4, 0.6 Hz, 1H), 7.37 (td, *J* = 7.6, 1.3 Hz, 1H), 7.01 (d, *J* = 16.2 Hz, 1H), 3.94 (s, 3H).

^{13}C NMR (101 MHz, $CDCl_3$) δ 167.8, 141.0(q, *J*=1.4), 138.8, 132.4, 130.9, 130.3, 129.9, 129.6(q, *J*=32.5), 128.8, 127.8, 127.2, 127.0, 125.7(q, *J*=3.9), 124.3(q, *J*=272.7), 52.3.

^{19}F NMR (376 MHz, $CDCl_3$) δ -62.56.

Spectroscopic data were in accordance with previous report.[63]

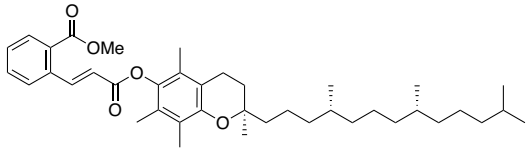

63 Wu, N.; Messinis, A.; Batsanov, A. S.; Yang, Z.; Whiting, A.; Marder, T. B. *Chem. Commun.* **2012**, *48*, 9986.

methyl 2-((*E*)-3-oxo-3-(((*R*)-2,5,7,8-tetramethyl-2-((4*R*,8*R*)-4,8,12-trimethyltridecyl)chroman-6-yl)oxy)prop-1-en-1-yl)benzoate (9y) The title compound was obtained by column chromatography (Hexane: EtOAc = 20:1) as a colorless oil (72.0 mg) in 78% yield.

^{1}H NMR (400 MHz, $CDCl_3$) δ 8.67 (d, *J* = 15.9 Hz, 1H), 7.99 (dd, *J* = 7.8, 1.4 Hz, 1H), 7.72 (d, *J* = 7.4 Hz, 1H), 7.58 (td, *J* = 7.6, 1.4 Hz, 1H), 7.48 (td, *J* = 7.6, 1.3 Hz, 1H), 6.56 (d, *J* = 15.9 Hz, 1H), 3.94 (s, 3H), 2.61 (t, *J* = 6.9 Hz, 2H), 2.11 (s, 3H), 2.08 (s, 3H), 2.04 (s, 3H), 1.88 – 1.72 (m, 2H), 1.56 (m, 2H), 1.53 – 1.49 (m, 1H), 1.45 – 1.35 (m, 4H), 1.27 (m, 11H), 1.17 – 1.05 (m, 6H), 0.86 (m, 12H).

^{13}C NMR (101 MHz, $CDCl_3$) δ 167.3, 165.2, 149.5, 145.2, 140.6, 136.1, 132.5, 131.0, 130.3, 129.7, 128.0, 127.0, 125.2, 123.2, 120.3, 117.5, 75.2, 52.5, 39.5, 37.6, 37.6, 37.4, 32.9, 32.8, 31.2, 28.1, 24.9, 24.6, 22.8, 22.7, 21.2, 20.7, 19.9, 19.8, 13.2, 12.3, 11.9.

HRMS-ESI(m/z): $[M+H]^+$: Calcd for $C_{40}H_{59}O_5$, 619.4357; Found, 619.4374.

IR (neat): 2925, 1721, 1460, 1221, 1143, 1076.

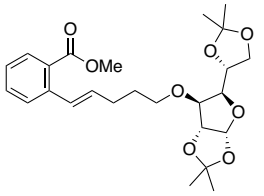

methyl 2-((*E*)-5-(((3a*R*,5*R*,6*S*,6a*R*)-5-((*R*)-2,2-dimethyl-1,3-dioxolan-4-yl)-2,2-dimethyltetrahydrofuro[2,3-*d*][1,3]dioxol-6-yl)oxy)pent-1-en-1-yl)benzoate (9z) After the reaction, the crude mixture was purified by column chromatography (Hexane: EtOAc = 4:1) to afford inseparable products **9z** and **9z-1** as a colorless oil (60.7 mg) in 88% yield with a ratio of 3.9:1. The title compound was further purified by preparative HPLC.

^{1}H NMR (500 MHz, $CDCl_3$) δ 7.84 (dd, *J* = 7.9, 1.4 Hz, 1H), 7.53 (dd, *J* = 8.0, 1.4 Hz, 1H), 7.44 (td, *J* = 7.8, 1.4 Hz, 1H), 7.30 – 7.22 (m, 1H), 7.16 (d, *J* = 15.7 Hz, 1H), 6.12 (dt, *J* = 15.7, 6.9 Hz, 1H), 5.88 (d, *J* = 3.7 Hz, 1H), 4.56 (d, *J* = 3.7 Hz, 1H), 4.33 (dt, *J* = 7.5, 6.0 Hz, 1H), 4.17 – 4.05 (m, 2H), 4.00 (dd, *J* = 8.6, 5.8 Hz, 1H), 3.89 (s, 4H), 3.68 (dt, *J* = 9.3, 6.3 Hz, 1H), 3.59 (dt, *J* = 9.3, 6.2 Hz, 1H), 2.40 – 2.27 (m, 2H), 1.82 – 1.73 (m, 2H), 1.49 (s, 3H), 1.42 (s, 3H), 1.34 (s, 3H), 1.30 (s, 3H).

^{13}C NMR (126 MHz, $CDCl_3$) δ 168.0, 139.6, 132.9, 132.1, 130.4, 129.2, 128.2, 127.3, 126.7, 111.8, 109.0, 105.4, 82.6, 82.3, 81.3, 72.6, 69.8, 67.3, 52.1, 29.7, 29.3, 26.9, 26.9, 26.3, 25.5.

HRMS-ESI(m/z): $[M+H]^+$: Calcd for $C_{25}H_{35}O_8$, 463.2326; Found, 463.2336.

IR (neat): 2987, 1715, 1371, 1251, 1072, 847.

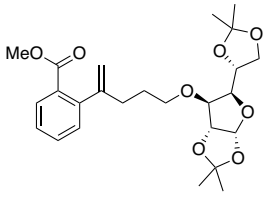

methyl 2-(5-(((3a*R*,5*R*,6*S*,6a*R*)-5-((*R*)-2,2-dimethyl-1,3-dioxolan-4-yl)-2,2-dimethyltetrahydrofuro[2,3-*d*][1,3]dioxol-6-yl)oxy)pent-1-en-2-yl)benzoate (9z-1)

^{1}H NMR (500 MHz, $CDCl_3$) δ 7.80 (dd, *J* = 7.8, 1.4 Hz, 1H), 7.44 (td, *J* = 7.5, 1.4 Hz, 1H), 7.32 (td, *J* = 7.6, 1.3 Hz, 1H), 7.21 (dd, *J* = 7.6, 1.3 Hz, 1H), 5.85 (d, *J* = 3.7 Hz, 1H), 5.12 (q, *J* = 1.4 Hz, 1H), 4.90 (d, *J* = 1.5 Hz, 1H), 4.49 (d, *J* = 3.7 Hz, 1H), 4.29 (dt, *J* = 7.5, 6.0 Hz, 1H), 4.14 – 4.04 (m, 2H), 3.97 (dd, *J* = 8.5, 5.8 Hz, 1H), 3.84 (s, 4H), 3.62 (dt, *J* = 9.3, 6.3 Hz, 1H), 3.52 (dt, *J* = 9.3, 6.3 Hz, 1H), 2.45 (t, *J* = 7.7 Hz, 2H), 1.74 – 1.65 (m, 2H), 1.49 (s, 3H), 1.41 (d, *J* = 0.7 Hz, 3H), 1.34 – 1.29 (m, 6H).

^{13}C NMR (126 MHz, $CDCl_3$) δ 168.4, 150.1, 144.4, 131.5, 130.0, 129.8, 129.8, 127.1, 113.2, 111.8, 109.0, 105.4, 82.5, 82.3, 81.3, 72.6, 70.0, 67.3, 52.1, 33.9, 28.3, 26.9, 26.9, 26.4, 25.5.

HRMS-ESI(m/z): $[M+H]^+$: Calcd for $C_{25}H_{35}O_8$, 463.2326; Found, 463.2313.

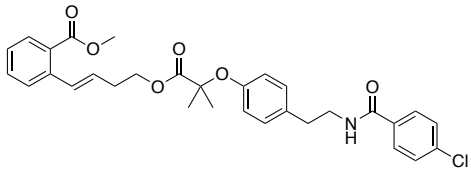

methyl (*E*)-2-(4-((2-(4-(2-(4-chlorobenzamido)ethyl)phenoxy)-2-methylpropanoyl)oxy)but-1-en-1-yl)benzoate (9aa) After the reaction, the crude mixture was purified by column chromatography (Hexane: EtOAc = 10:1) to afford inseparable products **9aa** and **9aa-1** as a white solid (76.9 mg) in 93% yield with a ratio of 5.9:1. The title compound was further purified by preparative HPLC.

^{1}H NMR (400 MHz, $CDCl_3$) δ 7.86 (dt, *J* = 7.8, 0.8 Hz, 1H), 7.66 – 7.59 (m, 2H), 7.48 – 7.42 (m, 2H), 7.41 – 7.34 (m, 2H), 7.32 – 7.28 (m, 1H), 7.24 (dt, *J* = 15.7, 1.5 Hz, 1H), 7.04 (d, *J* = 8.6 Hz, 2H), 6.84 – 6.79 (m, 2H), 6.14 – 6.06 (m, 1H), 5.99 (dt, *J* = 15.7, 7.0 Hz, 1H), 4.34 (t, *J* = 6.5 Hz, 2H), 3.89 (s, 3H), 3.62 (td, *J* = 6.8, 5.9 Hz, 2H), 2.82 (t, *J* = 6.8 Hz, 2H), 2.60 (qd, *J* = 6.6, 1.5 Hz, 2H), 1.61 (s, 6H).

^{13}C NMR (101 MHz, $CDCl_3$) δ 174.3, 167.9, 166.4, 154.3, 139.0, 137.7, 133.1, 132.4, 132.1, 131.4, 130.5, 129.6, 128.9, 128.3, 128.3, 128.3, 127.4, 127.1, 119.4, 79.2, 64.6, 52.1, 41.2, 34.7, 32.6, 25.5.

HRMS-ESI(m/z): $[M+H]^+$: Calcd for $C_{31}H_{33}ClNO_6$, 550.1991; Found, 550.1999.

IR (neat): 2950, 1712, 1508, 1485, 1222, 1133.

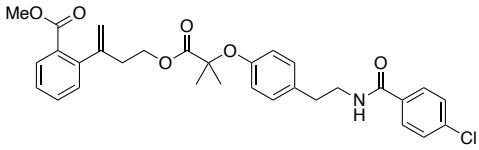

methyl 2-(4-((2-(4-(2-(4-chlorobenzamido)ethyl)phenoxy)-2-methylpropanoyl)oxy)but-1-en-2-yl)benzoate (9aa-1)

^{1}H NMR (500 MHz, $CDCl_3$) δ 7.84 (ddd, *J* = 7.8, 1.4, 0.5 Hz, 1H), 7.60 (d, *J* = 8.6 Hz, 2H), 7.43 (td, *J* = 7.5, 1.4 Hz, 1H), 7.39 – 7.31 (m, 3H), 7.15 (ddd, *J* = 7.6, 1.3, 0.5 Hz, 1H), 7.10 – 7.05 (m, 2H), 6.84 – 6.75 (m, 2H), 6.08 (s, 1H), 5.12 (q, *J* = 1.3 Hz, 1H), 4.93 (d, *J* = 1.3 Hz, 1H), 4.23 (t, *J* = 6.9 Hz, 2H), 3.83 (s, 3H), 3.66 (q, *J* = 6.8 Hz, 2H), 2.85 (t, *J* = 6.8 Hz, 2H), 2.74 (td, *J* = 7.0, 1.1 Hz, 2H), 1.54 (s, 6H).
^{13}C NMR (126 MHz, $CDCl_3$) δ 174.1, 167.8, 166.3, 154.1, 146.5, 143.6, 137.6, 132.9, 132.3, 131.7, 130.1, 130.0, 129.4, 129.2, 128.8, 128.2, 127.3, 119.5, 115.1, 79.1, 63.8, 52.0, 41.2, 36.5, 34.7, 29.7, 25.3.
HRMS-ESI(m/z): $[M+Na]^+$: Calcd for $C_{31}H_{32}ClNNaO_6$, 572.1810; Found, 572.1801.

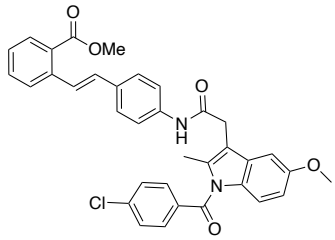

methyl (*E*)-2-(4-(2-(1-(4-chlorobenzoyl)-5-methoxy-2-methyl-1*H*-indol-3-yl)acetamido)styryl)benzoate (9ab) The reaction was carried out in a 0.05 mmol scale. The title compound was obtained by column chromatography (Hexane: EtOAc = 2:1) as a white solid (27.2 mg) in 92% yield.

^{1}H NMR (400 MHz, DMSO) δ 10.35 (s, 1H), 7.88 – 7.80 (m, 2H), 7.75 (d, *J* = 16.3 Hz, 1H), 7.72 – 7.68 (m, 2H), 7.68 – 7.63 (m, 4H), 7.59 (td, *J* = 7.7, 1.5 Hz, 1H), 7.55 – 7.50 (m, 2H), 7.38 (td, *J* = 7.6, 1.2 Hz, 1H), 7.21 (d, *J* = 2.6 Hz, 1H), 7.15 (d, *J* = 16.2 Hz, 1H), 6.94 (d, *J* = 9.0 Hz, 1H), 6.72 (dd, *J* = 9.0, 2.6 Hz, 1H), 3.87 (s, 3H), 3.78 (s, 2H), 3.76 (s, 3H), 2.30 (s, 3H).
^{13}C NMR (101 MHz, DMSO) δ 168.4, 167.8, 167.3, 155.5, 138.9, 137.9, 137.5, 135.3, 134.1, 132.1, 132.0, 131.1, 130.8, 130.7, 130.2, 130.1, 129.0, 128.4, 127.2, 126.4, 124.9, 119.3, 114.5, 114.0, 111.1, 101.9, 55.4, 52.1, 32.0, 13.3.

HRMS-ESI(m/z): $[M+Na]^+$: Calcd for $C_{36}H_{25}ClN_6NaO$, 615.1671; Found, 615.1681.

IR (neat): 3320, 1688, 1603, 1537, 1327, 1277, 1088.

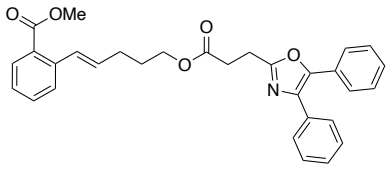

methyl (*E*)-2-(5-((3-(4,5-diphenyloxazol-2-yl)propanoyl)oxy)pent-1-en-1-yl)benzoate (9ac) After the reaction, the crude mixture was purified by column chromatography (Hexane: EtOAc = 5:1) to afford inseparable products **9ac** and **9ac-1** as a colorless oil (58.9 mg) in 79% yield with a ratio of 4:1. The title compound was further purified by preparative HPLC.

^{1}H NMR (400 MHz, $CDCl_3$) δ 7.84 (dd, *J* = 8.0, 1.3 Hz, 1H), 7.65 – 7.60 (m, 2H), 7.59 – 7.53 (m, 2H), 7.51 – 7.47 (m, 1H), 7.46 – 7.40 (m, 1H), 7.33 (m, 6H), 7.28 – 7.23 (m, 1H), 6.07 (dt, *J* = 15.7, 6.9 Hz, 1H), 4.20 (t, *J* = 6.6 Hz, 2H), 3.88 (s, 3H), 3.21 (t, *J* = 7.5 Hz, 2H), 2.93 (t, *J* = 7.5 Hz, 1H), 2.38 – 2.26 (m, 2H), 1.91 – 1.80 (m, 2H).
^{13}C NMR (101 MHz, $CDCl_3$) δ 172.1, 168.1, 162.0, 145.6, 139.5, 135.2, 132.4, 132.2, 132.1, 130.4, 129.6, 129.0, 128.7, 128.7, 128.6, 128.2, 128.2, 128.1, 127.4, 126.8, 126.6, 64.4, 52.1, 31.3, 29.5, 28.3, 23.7.
HRMS-ESI(m/z): $[M+Na]^+$: Calcd for $C_{31}H_{29}NNaO_5$, 518.1938; Found, 518.1935.

IR (neat): 2950, 1719, 1569, 1433, 1250, 1164.

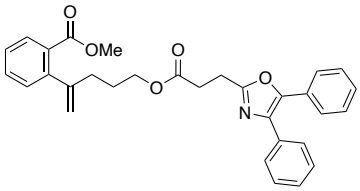

methyl 2-(5-((3-(4,5-diphenyloxazol-2-yl)propanoyl)oxy)pent-1-en-2-yl)benzoate (9ac-1)

^{1}H NMR (500 MHz, $CDCl_3$) δ 7.80 (dd, *J* = 7.8, 1.4 Hz, 1H), 7.62 (dd, *J* = 8.3, 1.7 Hz, 2H), 7.56 (dd, *J* = 8.3, 1.8 Hz, 2H), 7.43 (td, *J* = 7.6, 1.4 Hz, 1H), 7.38 – 7.28 (m, 7H), 7.19 (dd, *J* = 7.6, 1.3 Hz, 1H), 5.10 (q, *J* = 1.5 Hz, 1H), 4.90 (d, *J* = 1.7 Hz, 1H), 4.15 (t, *J* = 6.6 Hz, 2H), 3.83 (s, 3H), 3.18 (t, *J* = 7.6 Hz, 2H), 2.9 (t, *J* = 7.6 Hz, 2H), 2.45 (t, *J* = 7.7 Hz, 2H), 1.84 – 1.73 (m, 2H).

^{13}C NMR (126 MHz, $CDCl_3$) δ 172.0, 168.2, 161.9, 149.4, 145.4, 144.0, 135.0, 132.3, 131.5, 129.9, 129.7, 129.6, 128.9, 128.6, 128.5, 128.4, 128.1, 127.9, 127.1, 126.4, 113.3, 64.3, 52.0, 33.7, 31.1, 27.0, 23.5.

HRMS-ESI(m/z): $[M+H]^+$: Calcd for $C_{31}H_{30}NO_5$, 496.2118; Found, 496.2122.

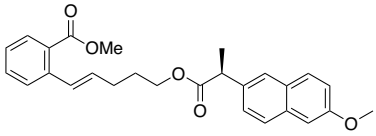

methyl (*S*,*E*)-2-(5-((2-(6-methoxynaphthalen-2-yl)propanoyl)oxy)pent-1-en-1-yl)benzoate (9ad) After the reaction, the crude mixture was purified by column chromatography (Hexane: EtOAc = 5:1) to afford inseparable products **9ad** and **9ad-1** as a colorless oil (57.0 mg) in 88% yield. The title compound was further purified by preparative HPLC.

^{1}H NMR (500 MHz, $CDCl_3$) δ 7.84 (dd, *J* = 7.9, 1.4 Hz, 1H), 7.69 (t, *J* = 8.4 Hz, 1H), 7.49 – 7.39 (m, 3H), 7.28 – 7.24 (m, 2H), 7.17 – 7.04 (m, 3H), 6.02 (dt, *J* = 15.6, 6.9 Hz, 1H), 4.15 (td, *J* = 6.6, 2.7 Hz, 2H), 3.91 (s, 3H), 3.87 (s, 4H), 2.23 (q, *J* = 6.9 Hz, 2H), 1.78 (p, *J* = 6.9 Hz, 2H), 1.58 (d, *J* = 7.2 Hz, 3H).

^{13}C NMR (126 MHz, $CDCl_3$) δ 174.7, 167.9, 157.6, 139.4, 135.8, 133.6, 132.1, 131.9, 130.3, 129.4, 129.2, 128.9, 128.1, 127.2, 127.1, 126.6, 126.2, 125.9, 118.9, 105.6, 64.1, 55.3, 52.0, 45.5, 29.3, 28.1, 18.5.

HRMS-ESI(m/z): $[M+Na]^+$: Calcd for $C_{27}H_{28}NaO_5$, 455.1829; Found, 455.1816.

IR (neat): 2952, 1716, 1606, 1253, 1176, 1076

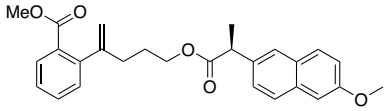

methyl (*S*)-2-(5-((2-(6-methoxynaphthalen-2-yl)propanoyl)oxy)pent-1-en-2-yl)benzoate (9ad-1)

^{1}H NMR (500 MHz, $CDCl_3$) δ 7.78 (dd, *J* = 7.7, 1.5 Hz, 1H), 7.70 – 7.63 (m, 3H), 7.41 – 7.35 (m, 2H), 7.30 (td, *J* = 7.6, 1.3 Hz, 1H), 7.13 (dd, *J* = 8.9, 2.6 Hz, 1H), 7.11 – 7.07 (m, 2H), 5.00 (q, *J* = 1.5 Hz, 1H), 4.84 (d, *J* = 1.4 Hz, 1H), 4.09 (t, *J* = 6.5 Hz, 2H), 3.92 (s, 3H), 3.88 – 3.81 (m, 1H), 3.78 (s, 3H), 2.34 (t, *J* = 7.7 Hz, 2H), 1.72 – 1.68 (m, 3H), 1.56 (d, *J* = 7.1 Hz, 3H).

^{13}C NMR (126 MHz, $CDCl_3$) δ 174.6, 168.2, 157.6, 149.3, 144.0, 135.7, 133.6, 131.4, 129.9, 129.6, 129.2, 128.9, 128.7, 127.1, 127.0, 126.2, 125.9, 118.9, 113.2, 105.6, 64.2, 55.3, 51.9, 45.5, 33.6, 26.9, 18.4.

HRMS-ESI(m/z): $[M+Na]^+$: Calcd for $C_{27}H_{28}NaO_5$, 455.1829; Found, 455.1826.

3.4.7. Mechanistic studies of Heck coupling reactions

Synthesis of 8_{ket}-Cl

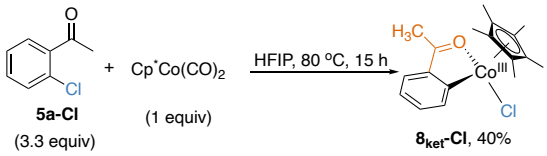

In an argon-filled the glovebox, Cp*Co(CO)$_2$ (3.8 mg, 0.015 mmol, 1 equiv) was charged into a 5 mL crimped vial and then 0.5 mL HFIP and 2-chloroacetophenone **5a-Cl** (6.7 μL, 0.05 mmol, 3.3 equiv) were added. The vial was crimped, taken out of the glovebox and the mixture was stirred for 15 hours at 80 ºC. The **8_{ket}-Cl** was obtained by preparative TLC (Hexane: EtOAc = 2:1) as a brown solid (2.09 mg) in 40% yield.

^{1}H NMR (500 MHz, CD_2Cl_2) δ 8.31 (dd, *J* = 7.7, 1.1 Hz, 1H), 7.58 (dd, *J* = 7.7, 1.4 Hz, 1H), 7.47 (td, *J* = 7.6, 1.4 Hz, 1H), 7.12 (td, *J* = 7.5, 1.1 Hz, 1H), 2.58 (s, 3H), 1.36 (s, 15H).

^{13}C NMR (126 MHz, CD_2Cl_2) δ 214.7, 195.6, 149.0, 140.1, 133.3, 130.7, 122.9, 92.9, 24.9, 9.4.

HRMS-ESI(m/z): $[M-Cl]^+$: Calcd for $C_{18}H_{22}CoO$, 313.0997; Found, 313.0990.

Catalytic activity of 8_{ket}-X complexes

Base, additive and **8_{ket}-X** were weighted in a vial equipped with a stir bar inside a glovebox, and then HFIP (0.5 mL), 2-iodoacetophenone **5a** (7 μL,0.05 mmol, 1.0 equiv) and methyl acrylate **6a** (9 μL, 0.1 mmol, 2.0 equiv) were then added and the vial was sealed. Outside the glovebox, the reaction mixture was stirred at 80 °C in a sand bath for 15 hours. After cooling down to room temperature, the reaction mixture was filtrated through a small silica plug, and the solvent was removed under vacuum. Then, CH_2Br_2 was added as internal standard, and the mixture was analyzed by ^{1}H NMR.

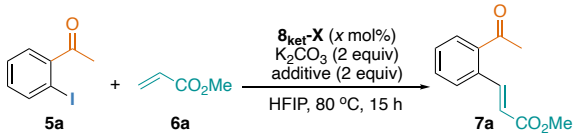

Entry	8_{ket}-X (mol%)	Additive (2 equiv)	Yield of **7a** (%)
1	**8_{ket}-I** (10)	$NaBF_4$	traces
2	**8_{ket}-I** (10)	$AgBF_4$	traces
3	**8_{ket}-I** (10)	$AgSbF_6$	traces
4	**8_{ket}-I** (10)	-	10
5	**8_{ket}-I** (30)	$NaBF_4$	15
6	**8_{ket}-Cl** (10)	$NaBF_4$	traces

[a]Reaction conditions: **5a** (0.05 mmol, 1.0 equiv), **6a** (0.1 mmol, 2.0 equiv), **8_{ket}-X** (*x* mol%), additive (0.1 mmol, 2.0 equiv), K_2CO_3 (0.1 mmol, 2.0 equiv), HFIP (0.5 mL) at 80 °C for 15 h. The yields were determined by analysis of the crude mixture by ^{1}H NMR spectroscopy by using CH_2Br_2 as an internal standard.

Synthesis of 8_{ket}-CO

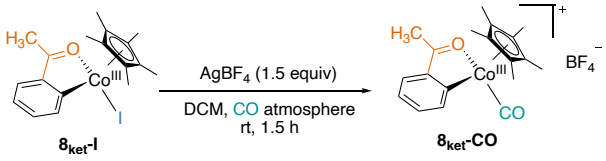

In an argon-filled glovebox, **8_{Ket}-I** (225.0 mg, 0.51 mmol, 1 equiv) and $AgBF_4$ (149.2 mg, 0.76 mmol, 1.5 equiv) were weighed into a Schlenk flask with a stir bar. The flask, sealed with a rubber septum, was taken outside the glovebox. The flask's atmosphere was evacuated under reduced pressure, and a CO-filled balloon was prepared and attached to the septum. After addition of 25 mL of DCM, the mixture was stirred and CO gas was bubbled through the solvent, as the solvent evaporated, 5 mL of DCM was added. After 10 minutes, stop bubbling and continue stirring. After 1.5 hours, stirring was stopped to allow settling of solids to the bottom of the flask. The supernatant was filtered into another Schlenk flask using a syringe filter under an argon atmosphere. DCM was removed under reduced pressure, and the residue was washed with Et_2O (4 times ca. 10 mL). The washed residue was dried under reduced pressure, then transferred to the glovebox. The brown solid target compound (128.5 mg) was obtained in a 58% yield.

^{1}H NMR (400 MHz, CD_2Cl_2) δ 7.90 (dd, *J* = 7.7, 1.5 Hz, 1H), 7.78 – 7.65 (m, 2H), 7.44 (td, *J* = 7.5, 1.2 Hz, 1H), 2.77 (s, 3H), 1.66 (s, 17H).

^{13}C NMR (101 MHz, CD_2Cl_2) δ 219.8, 198.1, 179.4, 147.8, 139.3, 137.4, 134.2, 127.2, 105.1, 25.8, 9.6.

HRMS-ESI(m/z): [M^+]: Calcd for $C_{19}H_{22}CoO_2$, 341.0946; Found, 341.0956.

IR (neat): 3550, 2926, 2064, 1571, 1325, 1046, 774.

Heck reaction using 8_{ket}-CO as pre-catalyst

Table 3.6. Heck reaction using 8_{ket}-CO as pre-catalyst

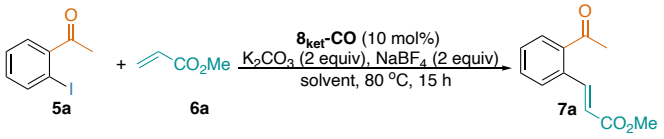

Entry	Solvent	Yield of **7a** (%)
1	HFIP	100
2	TFE	0
3	^{i}PrOH	traces

K_2CO_3 (13.8 mg, 0.1 mmol, 2 equiv), $NaBF_4$ (10.9 mg, 0.1 mmol, 2 equiv), and **8$_{ket}$-CO** (2.1 mg, 10 mol%) were weighted in a vial equipped with a stir bar inside an argon-filled glovebox, and then after solvent (0.5 mL), 2-iodoacetophenone **5a** (7 μL, 0.05 mmol, 1.0 equiv) and methyl acrylate **6a** (9 μL, 0.1 mmol, 2.0 equiv) were added, the vial was sealed. Outside the glovebox, the reaction mixture was stirred at 80 °C for 15h. After cooling down to room temperature, the reaction mixture was filtrated through a small silica plug, and the solvent was removed under vacuum. CH_2Br_2 was added as internal standard, and the mixture was analyzed by ^{1}H NMR.

HRMS studies for the Heck reaction

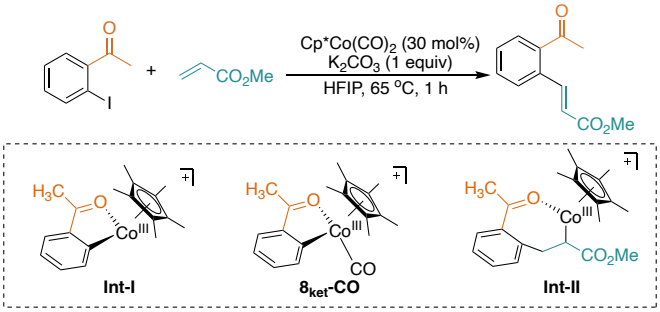

K_2CO_3 (6.9 mg, 0.05 mmol, 1 equiv), $Cp^*Co(CO)_2$ (3.8 mg, 0.0015 mmol, 30 mol%) were weighted in a vial equipped with a stir bar inside a glovebox, and then after HFIP (0.5 mL), aryl 2-iodoacetophenone **5a** (7μL, 0.05 mmol, 1.0 equiv) and methyl acrylate **6a** (9 μL, 0.1 mmol, 2 equiv) were added, the vial was sealed. Outside the glovebox, the reaction mixture was stirred at 65 °C in the sand bath for 1 h. After cooling down to room temperature, the crude residue was submitted for HRMS. (Note: due to the solubility issues of K_2CO_3 and $NaBF_4$, the reaction performed without NaBF4 and with 1 equivalent of K_2CO_3)

Int-I HRMS-ESI(m/z): [M^+]: Calcd for: $C_{18}H_{22}CoO$: 313.0997, found: 313.0985.

8$_{ket}$-CO HRMS-ESI(m/z): [M^+]: Calcd for: $C_{19}H_{22}CoO2$: 341.0946, found: 341.0946.

Int-II HRMS-ESI(m/z): [M^+]: Calcd for: $C_{22}H_{28}CoO_3$: 399.1365, found: 399.1364.

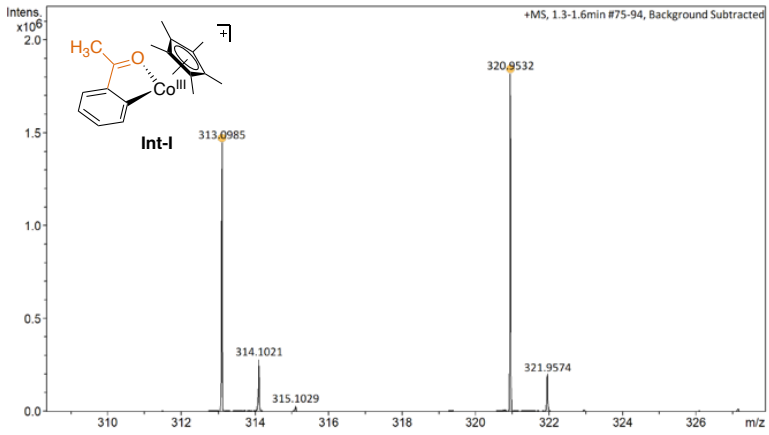
Intens.
x10^6
+MS, 1.3-1.6min #75-94, Background Subtracted
Int-I
313.0985
320.9532
314.1021
321.9574
315.1029
m/z

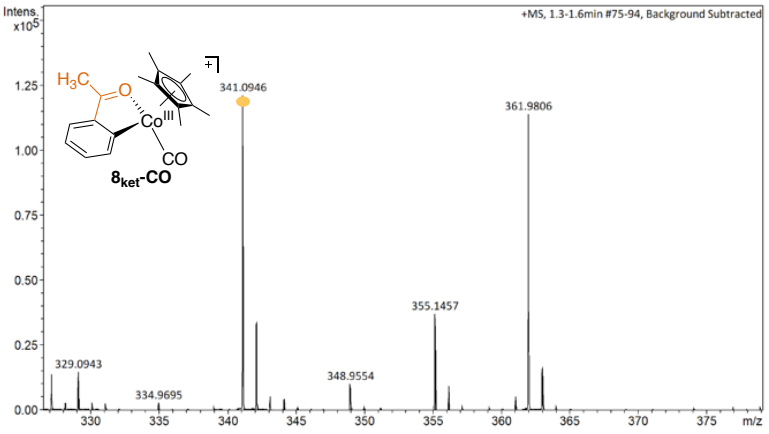
Intens.
x10^5
+MS, 1.3-1.6min #75-94, Background Subtracted
8ket-CO
341.0946
361.9806
355.1457
329.0943
348.9554
334.9695
m/z

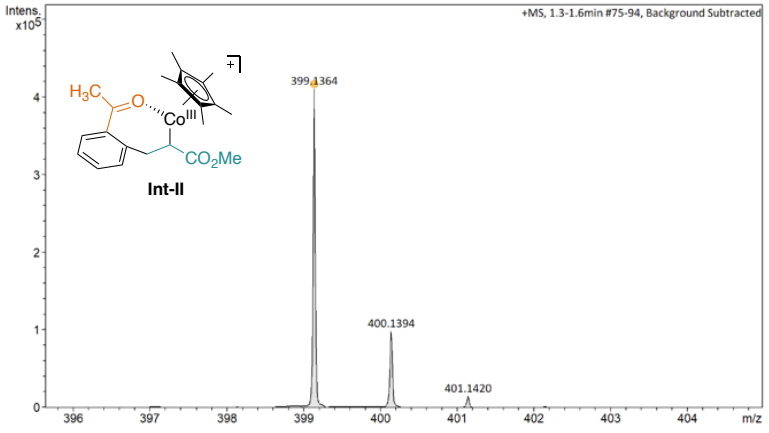
Intens.
x10^5
+MS, 1.3-1.6min #75-94, Background Subtracted
Int-II
399.1364
400.1394
401.1420
m/z

Effect of radical scavengers in the Heck reaction

In order to test if the reaction goes through radical mechanism, we tested the reaction of 2-iodoacetophenone and methyl acrylate in the presence of commonly used radical scavengers (TEMPO, BHT).

Table 3.7. Effect of radical scavengers in the Heck reaction

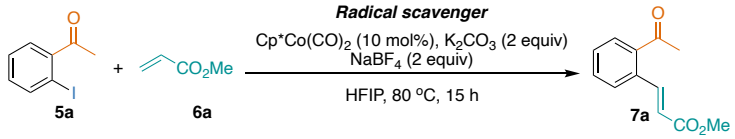

Entry	Radical scavenger	Yield of **7a** (%)
1	BHT (2 equiv)	100
2	TEMPO (2 equiv)	0
3	TEMPO (10 mol%)	8

K_2CO_3 (13.8 mg, 0.1 mmol, 2 equiv), $NaBF_4$ (10.9 mg, 0.1 mmol, 2 equiv), $Cp^*Co(CO)_2$ (1.3 mg, 10 mol%) and radical scavenger (2 equiv) were weighted in a vial equipped with a stir bar inside an argon-filled glovebox, and then after HFIP (0.5 mL), 2-iodoacetophenone **5a** (7 μL, 0.05 mmol, 1.0 equiv) and methyl acrylate **6a** (9 μL, 0.1 mmol, 2 equiv) were added, the vial was sealed. Outside the glovebox, the reaction mixture was stirred at 80 °C in the sand bath for 15h. After cooling down to room temperature, the solvent was removed under vacuum. Then, CH_2Br_2 was added as internal standard, and the mixture was analyzed by ^1H NMR.

The presence of BHT does not have an impact in the outcome of the reaction (Table 3.7, entry 1), which indicates that there´s no radical within the catalytic cycle. However, no product was observed in the presence of 2 equivalents of TEMPO (Table 3.7, entry 2), and a decreased yield was obtained when using 10 mol% TEMPO (Table 3.7, entry 3), but no TEMPO-adduct was observed. This result could be associated to TEMPO poisoned the cobalt catalyst.[39]

Radical clock experiments

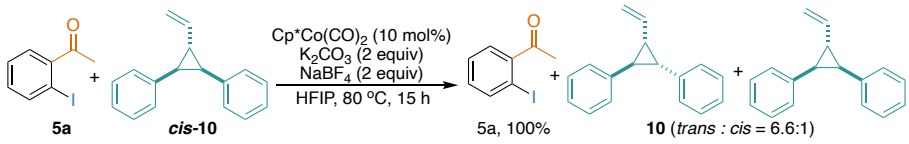

K_2CO_3 (41.5 mg, 0.3 mmol, 2 equiv), $NaBF_4$ (32.9 mg, 0.3 mmol, 2 equiv), and $Cp^*Co(CO)_2$ (3.8 mg, 10 mol%) were weighted in a vial equipped with a stir bar inside a glovebox, and then after HFIP (1.5 mL), 2-iodoacetophenone **5a** (21 μL, 0.15 mmol, 1.0 equiv) and ***cis*-10** (66 mg, 0.3 mmol, 2.0 equiv) were added, the vial was sealed. Outside the glovebox, the reaction mixture was stirred at 80 °C in the sand bath for 15h. After cooling down to room temperature, the solvent was removed under vacuum. Then, CH_2Br_2 (33.9 mg, 0.19 mmol) was added as internal standard, and the mixture was analyzed by ^1H NMR. It shows that 2-iodoacetophenone **5a** remains 100%, while the isomers of ***trans*-10: *cis*-10** were obtained with a rario of 6.6:1.

Control experiments of radical clock experiments

K_2CO_3 (13.8 mg, 0.1 mmol, 1 equiv), $NaBF_4$ (10.9 mg, 0.1 mmol, 1 equiv), and $Cp^*Co(CO)_2$ (1.3 mg, 5 mol%) or $CpCo(CO)_2$ (0.9 mg, 5 mol%)) were weighted in a vial equipped with a stir bar inside a glovebox, and then after solvent (0.5 mL), ***cis*-10** (22 mg, 0.1 mmol, 1.0 equiv) were added, the vial was sealed. Outside the glovebox, the reaction mixture was stirred at 80 °C or room temperature for 15h. After cooling down to room temperature, the solvent was removed under vacuum. Then, CH_2Br_2 (33.9 mg, 0.19 mmol) was added as internal standard, and the mixture was analyzed by ^1H NMR.

Table 3.8. Control experiments of radical clock experiments

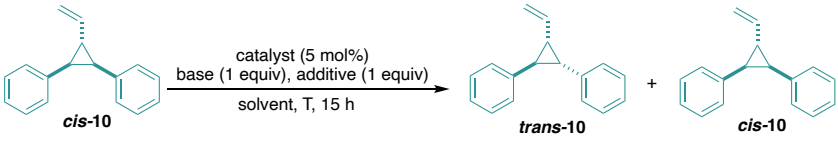

Entry	Catalyst	Additive	Base	Solvent	Temperature (°C)	Ratio of **trans-10:cis-10**
1	$Cp^*Co(CO)_2$	$NaBF_4$	K_2CO_3	HFIP	80	6.6:1
2	$Cp^*Co(CO)_2$	$NaBF_4$	K_2CO_3	^{i}PrOH	80	0:1
3	$Cp^*Co(CO)_2$	$NaBF_4$	K_2CO_3	TFE	80	1.6:1
4	-	$NaBF_4$	K_2CO_3	HFIP	80	0:1
5	$Cp^*Co(CO)_2$	-	-	HFIP	80	6.3:1
6	$Cp^*Co(CO)_2$	-	-	HFIP	rt	6.6:1
7	$CpCo(CO)_2$	-	-	HFIP	rt	5:1
8	$Cp^*Co(CO)_2$	-	-	PFTB	rt	6:1

3.4.8. X-Ray crystallography

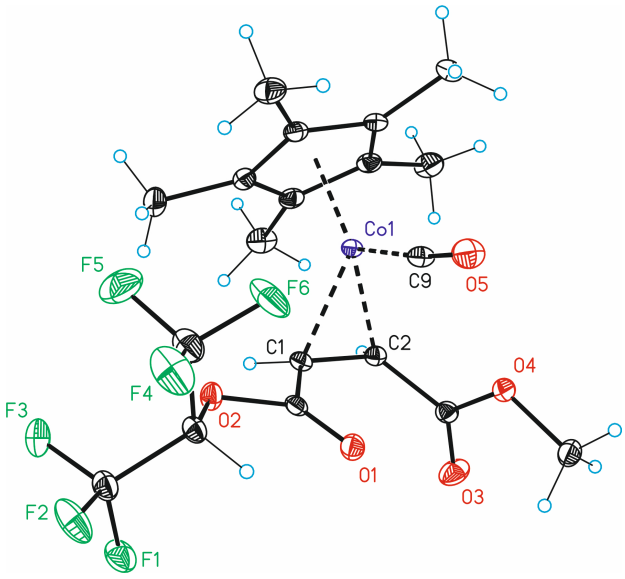

Figure 3.23. Crystal data and structure refinement for compound **7as-1**

Table 3.9. Crystal data and structure refinement for compound **7as-1**

Identification code	mo_Z911_0m
Empirical formula	$C_{38}H_{42}Co_2F_{12}O_{10}$
Formula weight	1004.57
Temperature/K	100(2)
Crystal system	monoclinic
Space group	$P2_1/n$
a/Å	13.0396(9)
b/Å	8.6089(6)
c/Å	19.0573(13)
α/°	90
β/°	105.5041(18)
γ/°	90
Volume/Å^3	2061.5(2)
Z	2
ρ_{calc}g/cm^3	1.618
μ/mm^{-1}	0.915
F(000)	1024.0
Crystal size/mm^3	0.4 × 0.05 × 0.02
Radiation	MoKα (λ = 0.71073)
2Θ range for data collection/°	3.404 to 63.342
Index ranges	$-19 \leq h \leq 19$, $-12 \leq k \leq 11$, $-20 \leq l \leq 28$
Reflections collected	38625
Independent reflections	6916 [R_{int} = 0.0317, R_{sigma} = 0.0235]

Data/restraints/parameters	6916/0/286
Goodness-of-fit on F^2	1.056
Final R indexes [I>=2σ (I)]	R_1 = 0.0306, wR_2 = 0.0772
Final R indexes [all data]	R_1 = 0.0398, wR_2 = 0.0821
Largest diff. peak/hole / e $Å^{-3}$	0.68/-0.43

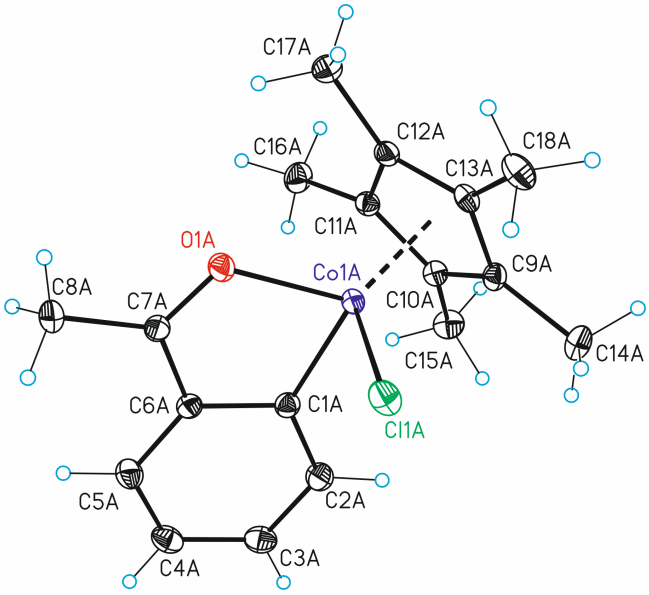

Figure 3.24. Crystal data and structure refinement for compound **8_{ket}-Cl**

Table 3.10. Crystal data and structure refinement for compound **8_{ket}-Cl**

Identification code	Z1242_JB
Empirical formula	C36 H44 Cl2 Co2 O2
Formula weight	697.47
Temperature	100(2)K
Wavelength	0.71073 Å
Crystal system	triclinic

Space group	P -1
Unit cell dimensions	a=8.2321(3)Å a= 86.423(3)°. b=14.0952(6)Å b=78.633(4)°. c=14.4492(6)Å g= 83.863(3)°.
Volume	1632.81(12) $Å^3$
Z	2
Density (calculated)	1.419 Mg/m^3
Absorption coefficient	1.210 mm^{-1}
F(000)	728
Crystal size	0.500 x 0.400 x 0.100 mm^3
Theta range for data collection	2.002 to 32.229°.
Index ranges 21<=l<=21	-12<=h<=12,-20<=k<=20,-
Reflections collected	24649
Independent reflections	10378[R(int) = 0.0713]
Completeness to theta =32.229°	89.7%
Absorption correction	Multi-scan
Max. and min. transmission	1.00 and 0.69
Refinement method	Full-matrix least-squares on F^2
Data / restraints / parameters	10378/ 0/ 391
Goodness-of-fit on F^2	1.041
Final R indices [I>2sigma(I)]	R1 = 0.0485, wR2 = 0.1307
R indices (all data)	R1 = 0.0551, wR2 = 0.1381
Largest diff. peak and hole	1.347 and -1.119 e.$Å^{-3}$

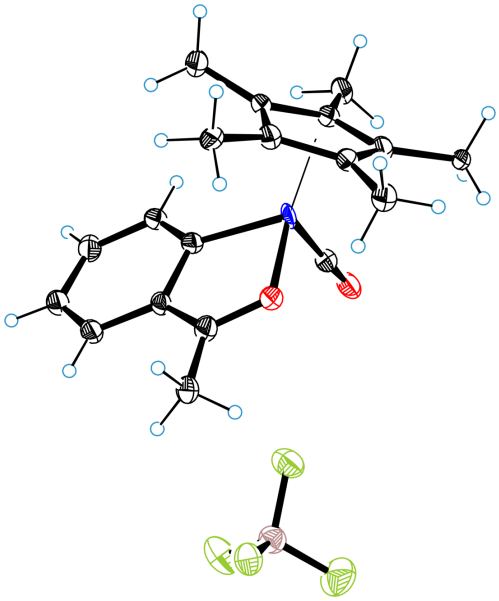

Figure 3.25. Crystal data and structure refinement for compound **8_{ket}-CO**

3.4.9. NMR spectra

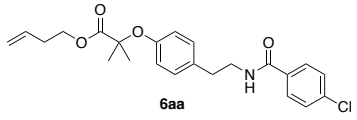

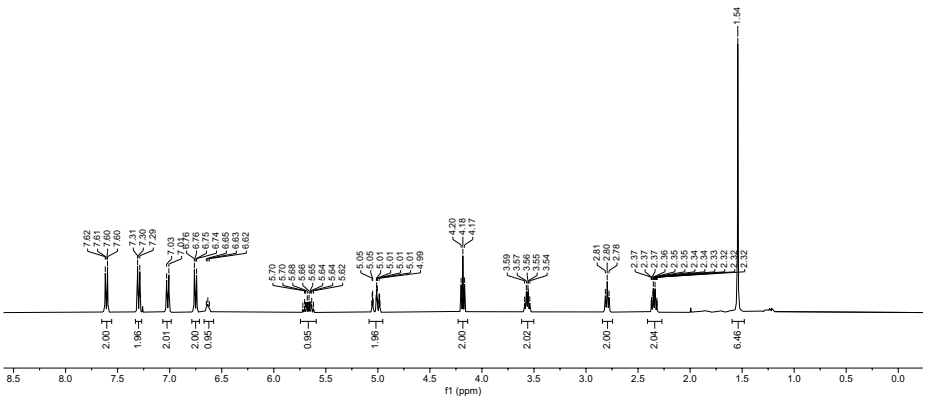

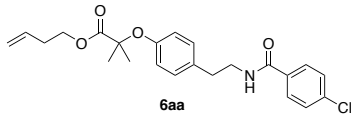

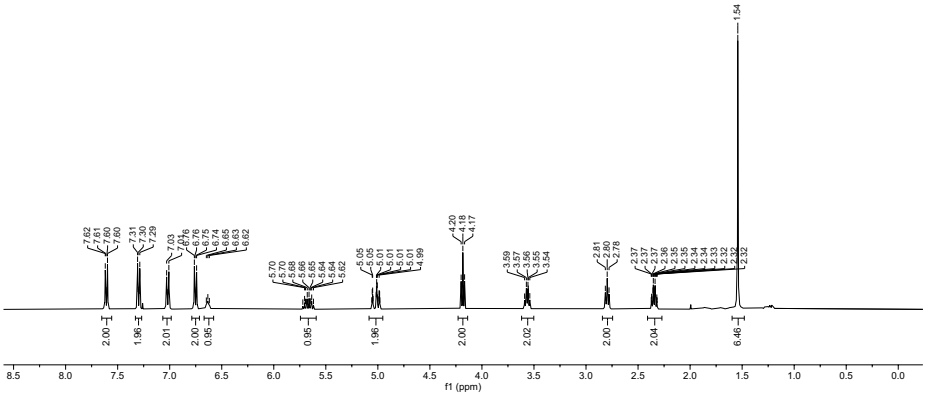

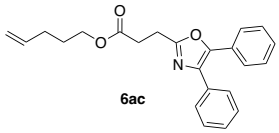
6ac

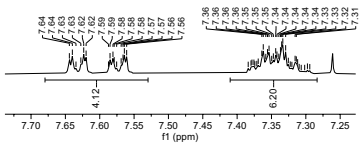
4.12
6.20
f1 (ppm)

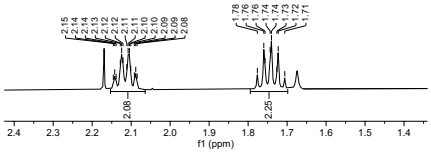
2.08
2.25
f1 (ppm)

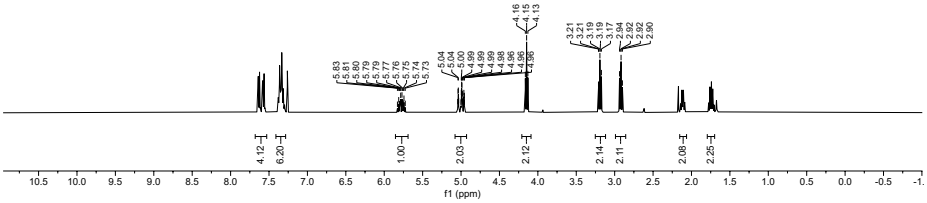
4.12
6.20
1.00
2.03
2.12
2.14
2.11
2.08
2.25
f1 (ppm)

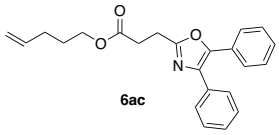
6ac

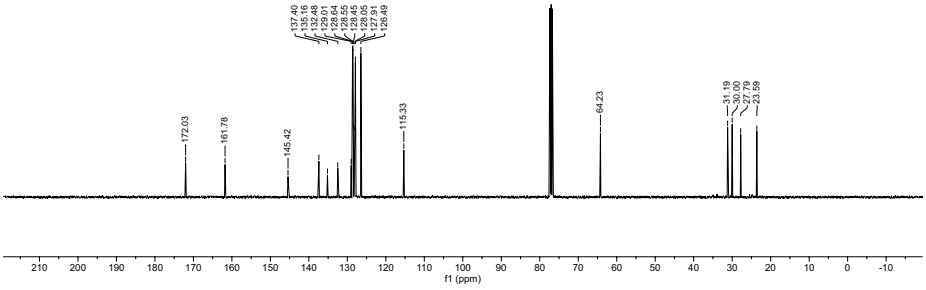
172.03
161.78
145.42
115.33
64.23
31.19
30.00
27.79
23.69
f1 (ppm)

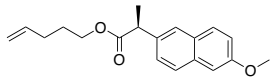

6ad

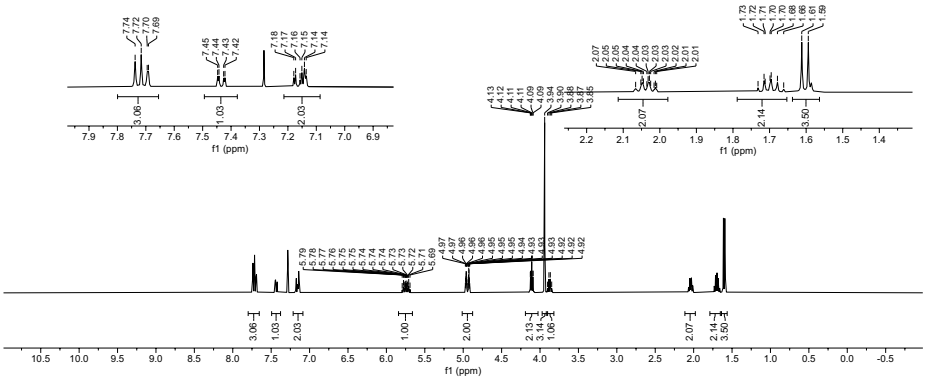

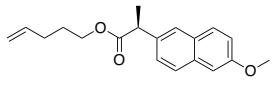

6ad

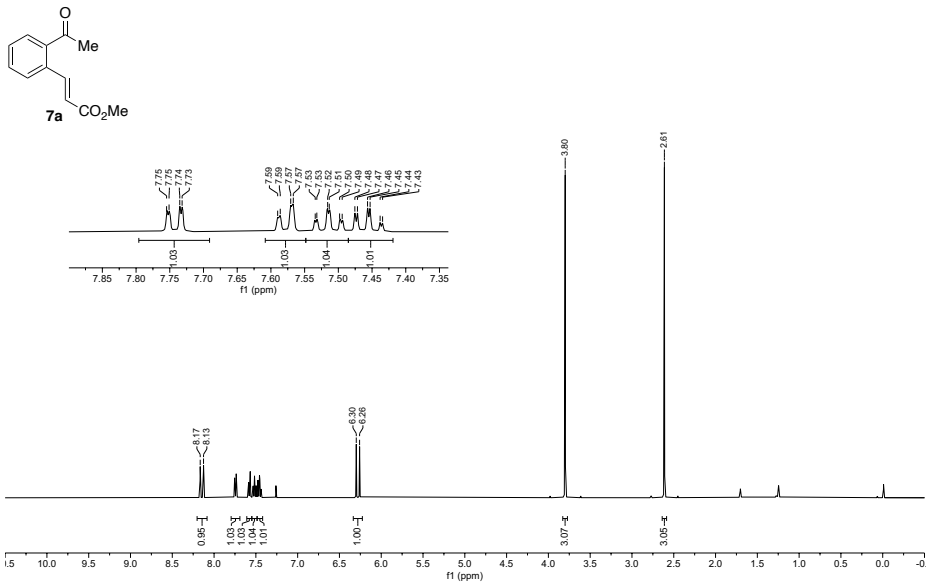
O
Me
CO2Me
7a
7.75
7.75
7.74
7.73
7.59
7.59
7.57
7.57
7.53
7.53
7.52
7.51
7.50
7.49
7.48
7.47
7.46
7.45
7.44
7.43
3.80
2.61
8.17
8.13
6.30
6.28
1.03
1.03
1.04
1.01
1.00
3.07
3.05
f1 (ppm)

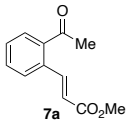
O
Me
CO2Me

7a

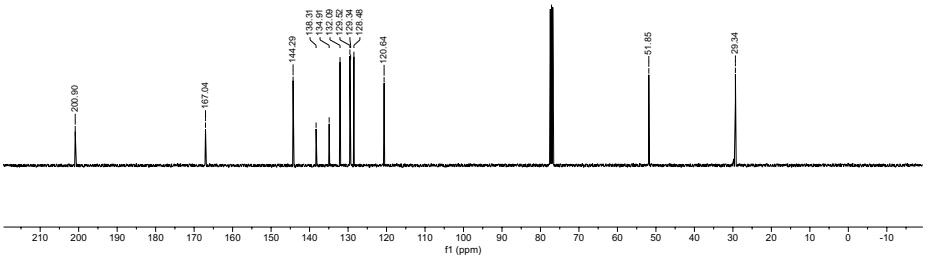
200.90
167.04
144.29
138.31
134.91
132.09
129.53
129.34
128.48
120.64
51.85
29.34
f1 (ppm)

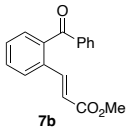
O
Ph
CO2Me

7b

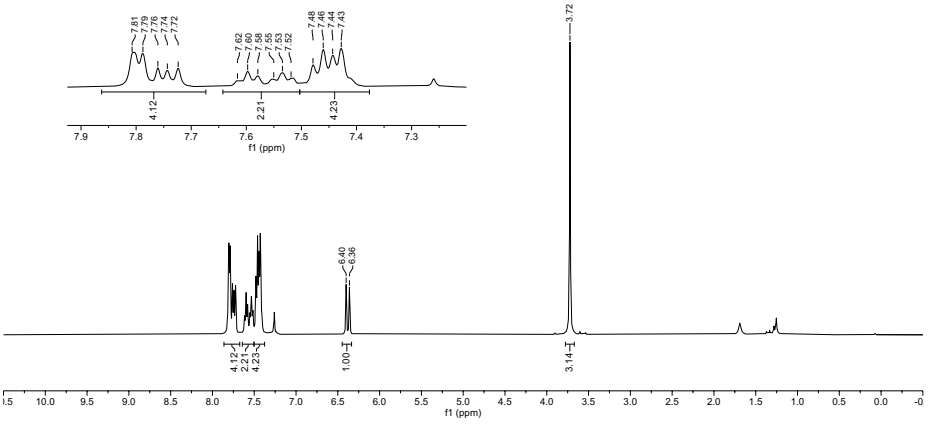
7.81
7.79
7.78
7.76
7.74
7.72
7.62
7.60
7.58
7.55
7.53
7.52
7.48
7.46
7.44
7.43
3.72
6.40
6.38
4.12
2.21
4.23
1.00
3.14
f1 (ppm)

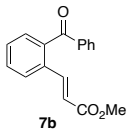
O
Ph
CO2Me

7b

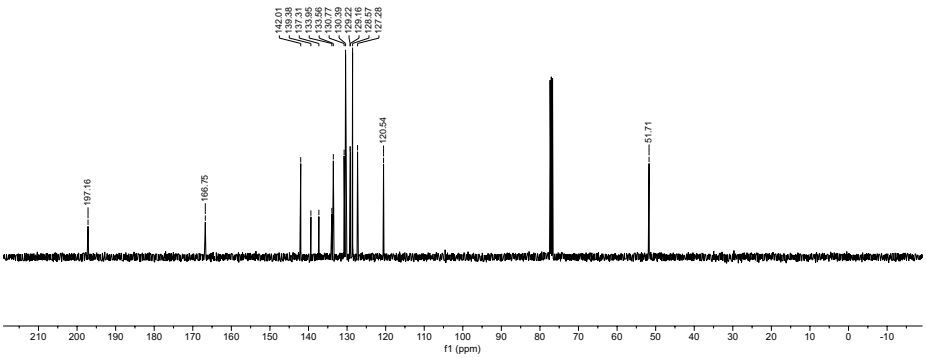
142.01
139.38
137.31
133.95
133.66
130.77
130.39
129.22
129.16
128.57
127.26
120.54
51.71
197.16
166.75
f1 (ppm)

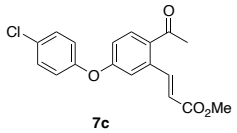
Cl
O
O
CO2Me

7c

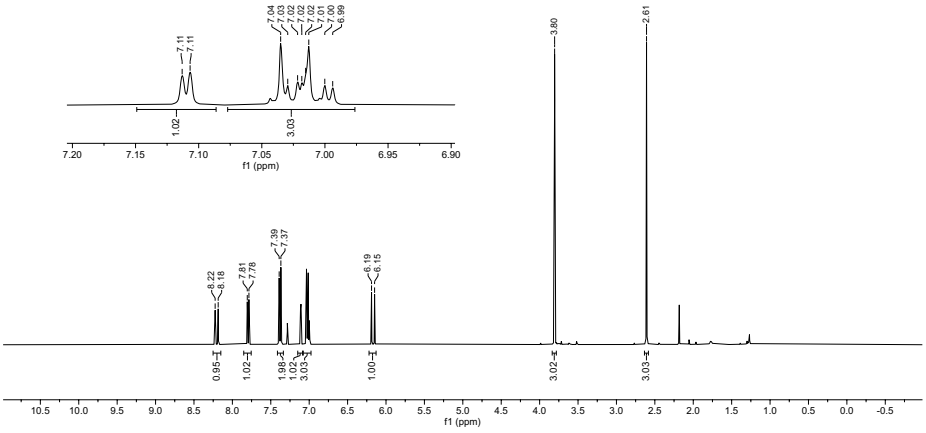
7.04
7.03
7.02
7.02
7.02
7.02
7.01
7.00
6.99
7.11
7.11
1.02
3.03
f1 (ppm)
3.80
2.61
8.22
8.18
7.81
7.78
7.39
7.37
6.19
6.15
0.95
1.02
1.98
1.02
3.05
1.00
3.02
3.03
f1 (ppm)

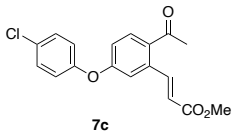
Cl
O
O
CO2Me

7c

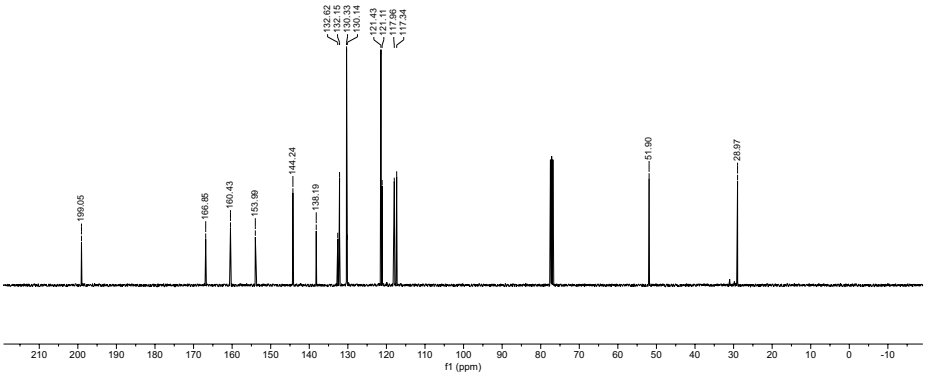
199.05
166.85
160.43
153.99
144.24
138.19
132.62
132.15
130.33
130.14
121.43
117.96
117.34
51.90
28.97
f1 (ppm)

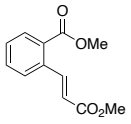
O
OMe
CO2Me

7d

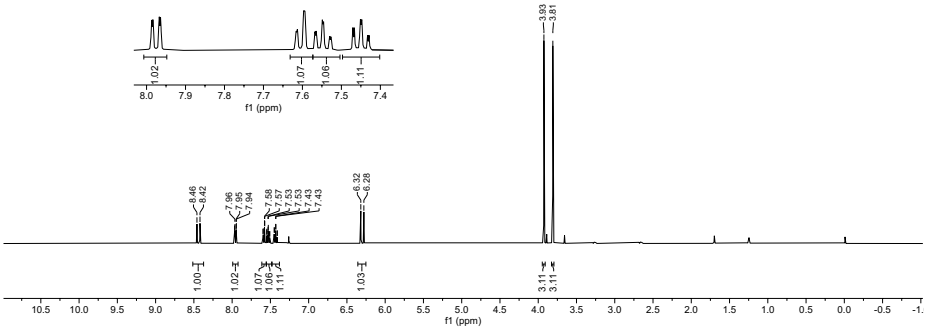
8.46
8.42
7.96
7.95
7.94
7.58
7.57
7.53
7.53
7.43
7.43
6.32
6.28
3.93
3.81
1.00
1.02
1.07
1.08
1.11
1.03
3.11
3.11
f1 (ppm)

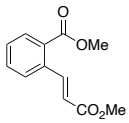
O
OMe
CO2Me

7d

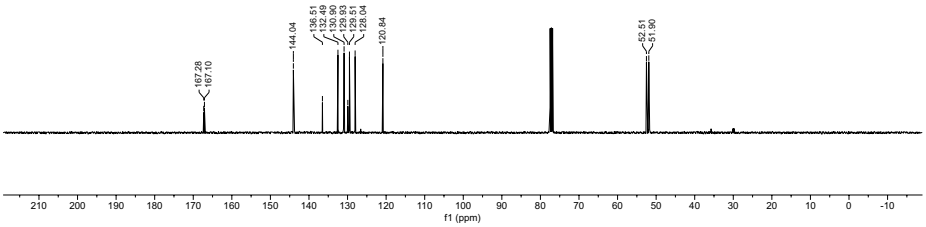
167.28
167.10
144.04
136.51
132.49
130.69
129.93
129.51
128.04
120.84
52.51
51.90
210 200 190 180 170 160 150 140 130 120 110 100 90 80 70 60 50 40 30 20 10 0 -10
f1 (ppm)

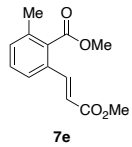
Me
O
OMe
CO2Me

7e

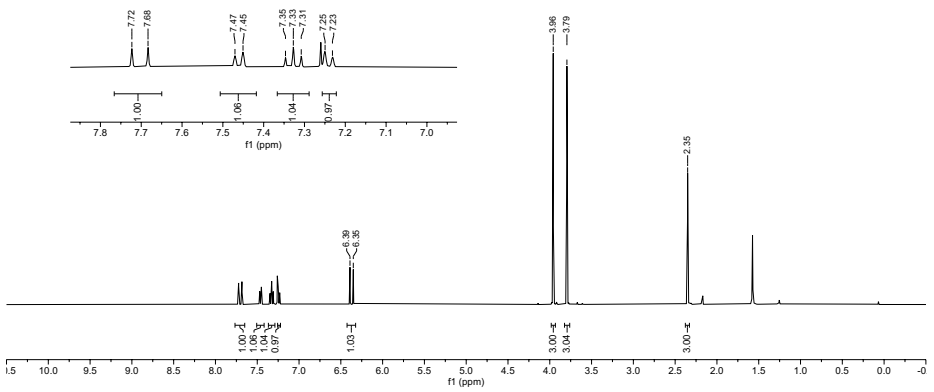
7.72
7.68
7.47
7.45
7.35
7.33
7.31
7.25
7.23
3.96
3.79
2.35
8.39
8.35
1.00
1.06
1.04
0.97
1.03
3.00
3.04
3.00
f1 (ppm)

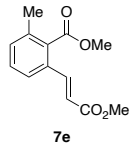
Me
O
OMe
CO2Me

7e

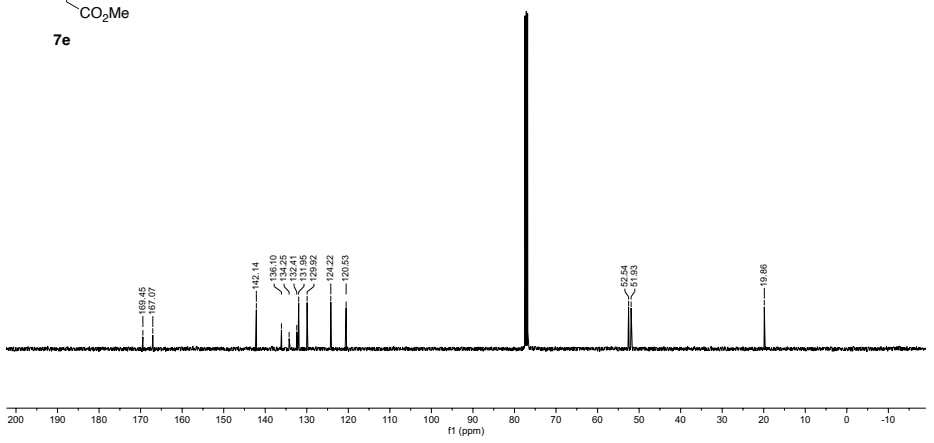
169.45
167.07
142.14
136.10
134.25
132.41
131.95
129.92
124.22
120.53
52.54
51.93
19.86
f1 (ppm)

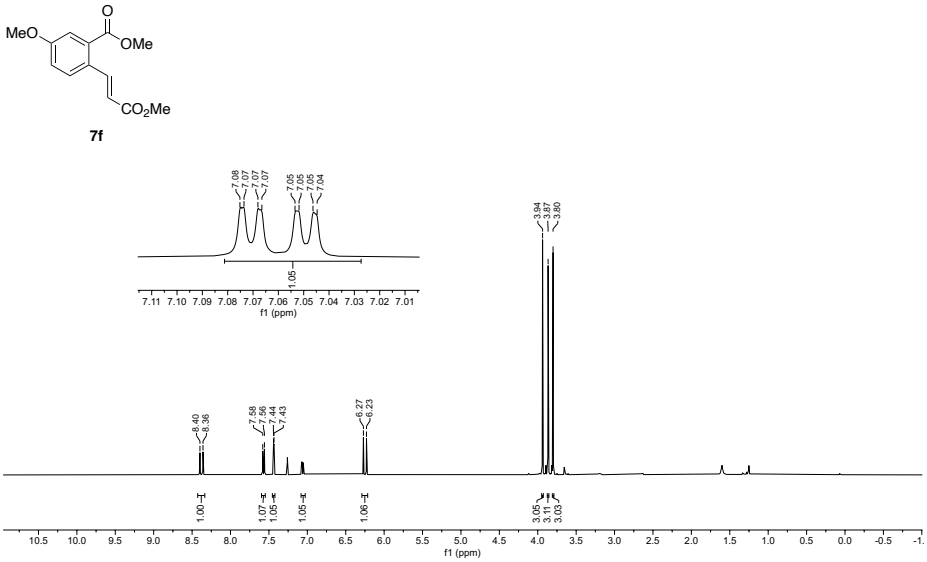
MeO
O
OMe
CO2Me
7f
7.08
7.07
7.07
7.07
7.05
7.05
7.05
7.04
1.05
7.11 7.10 7.09 7.08 7.07 7.06 7.05 7.04 7.03 7.02 7.01
f1 (ppm)
3.94
3.87
3.80
8.40
8.38
7.58
7.56
7.44
7.43
6.27
6.23
1.00
1.07
1.05
1.05
1.06
3.05
3.11
3.03
10.5 10.0 9.5 9.0 8.5 8.0 7.5 7.0 6.5 6.0 5.5 5.0 4.5 4.0 3.5 3.0 2.5 2.0 1.5 1.0 0.5 0.0 -0.5
f1 (ppm)

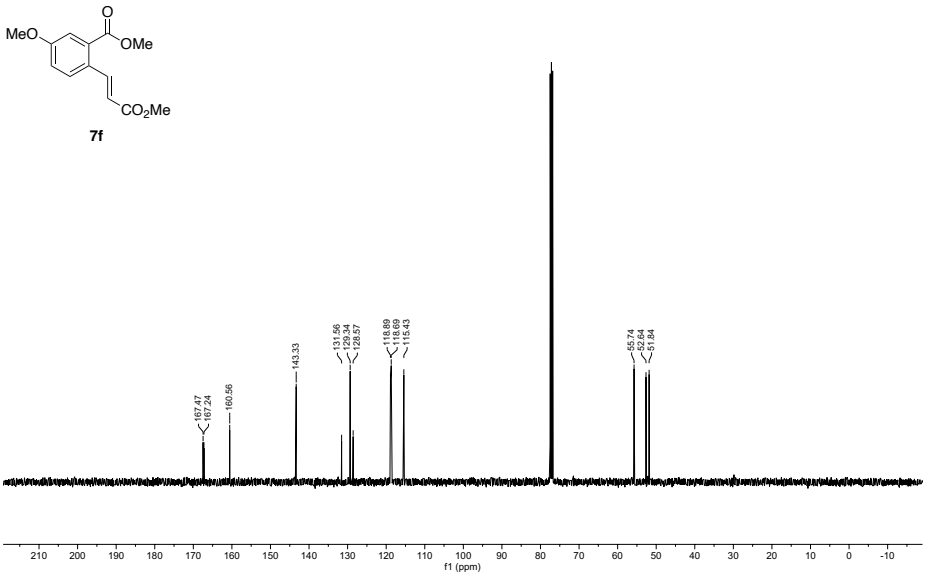
MeO
O
OMe
CO2Me
7f
167.47
167.24
160.56
143.33
131.56
129.34
128.57
118.89
118.69
115.43
55.74
52.24
51.84
210 200 190 180 170 160 150 140 130 120 110 100 90 80 70 60 50 40 30 20 10 0 -10
f1 (ppm)

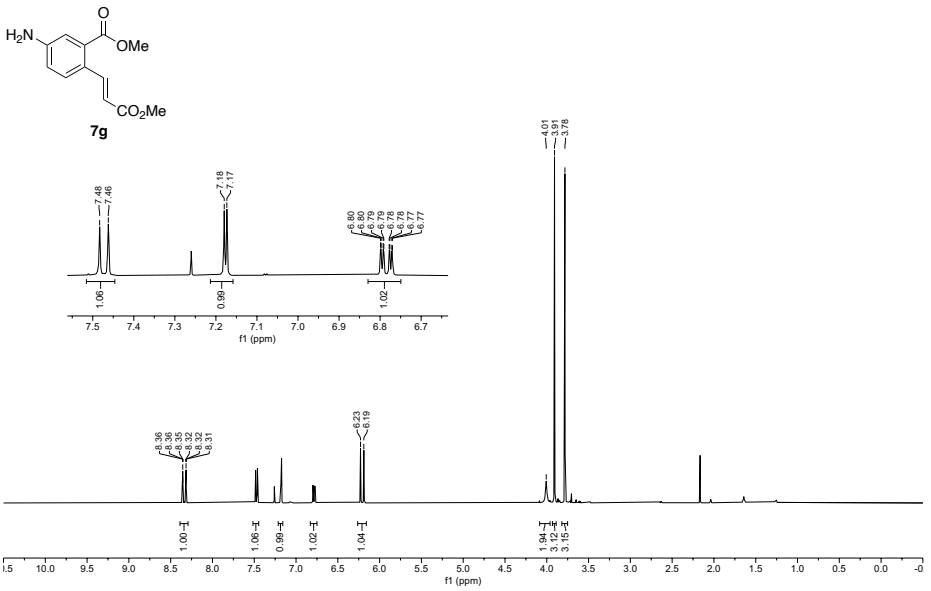
H2N
O
OMe
CO2Me
7g
8.36
8.35
8.32
8.32
8.31
7.48
7.46
7.18
7.17
6.80
6.80
6.79
6.79
6.78
6.78
6.77
6.77
6.23
6.19
4.01
3.91
3.78
1.00
1.06
0.99
1.02
1.04
1.94
3.12
3.15
f1 (ppm)

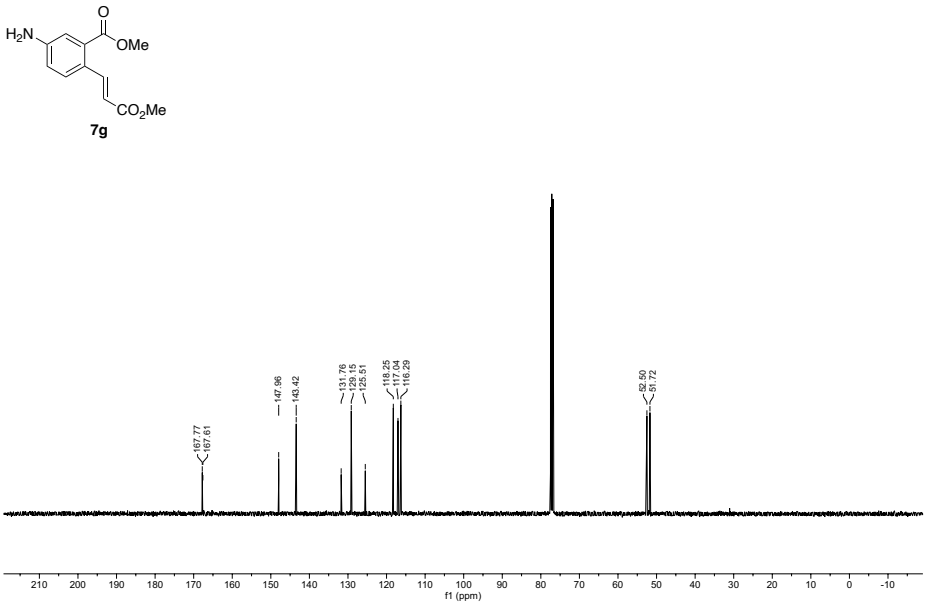
H2N
O
OMe
CO2Me
7g
167.77
167.61
147.96
143.42
131.76
129.15
125.51
118.25
117.64
116.29
82.50
51.72
f1 (ppm)

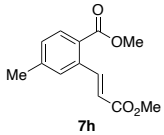
O
OMe
Me
CO2Me

7h

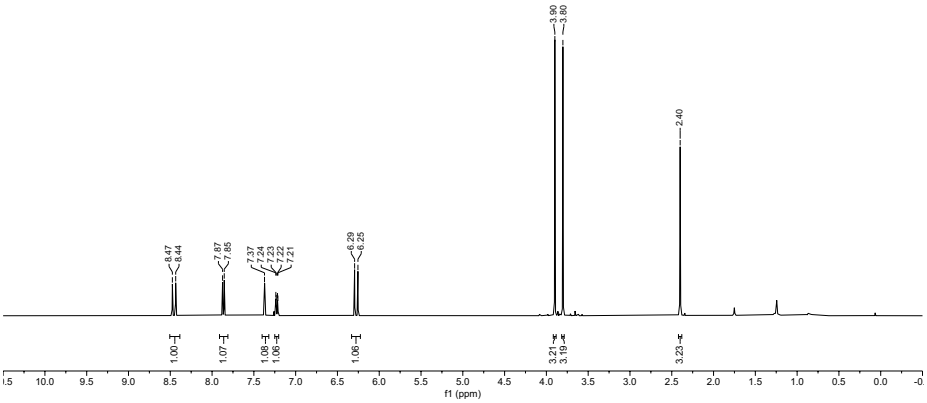
8.47
8.44
7.87
7.85
7.37
7.24
7.23
7.22
7.21
6.29
6.25
3.90
3.80
2.40
1.00
1.07
1.08
1.06
1.06
3.21
3.19
3.23
f1 (ppm)

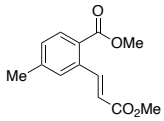
O
OMe
Me
CO2Me

7h

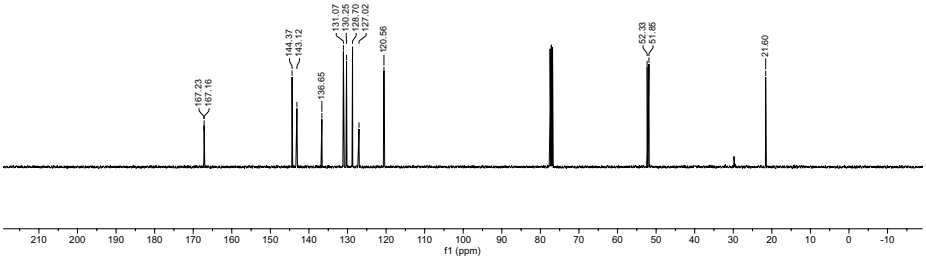
167.23
167.16
144.37
143.12
136.65
131.07
130.25
128.70
127.02
120.56
52.33
51.85
21.60
f1 (ppm)

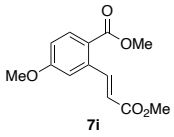
O
OMe
MeO
CO2Me

7i

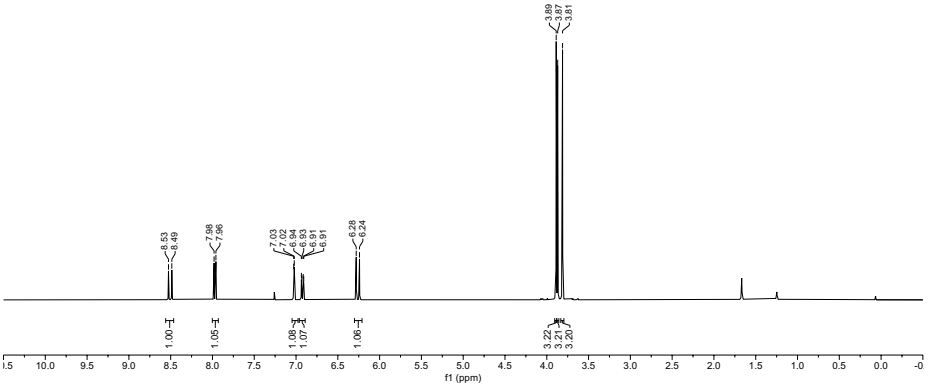
8.53
8.49
7.98
7.96
7.03
7.02
6.94
6.93
6.91
6.91
6.28
6.24
3.89
3.87
3.81
1.00
1.05
1.08
1.07
1.05
3.22
3.21
3.20
f1 (ppm)

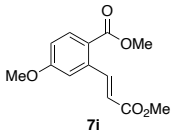
O
OMe
MeO
CO2Me

7i

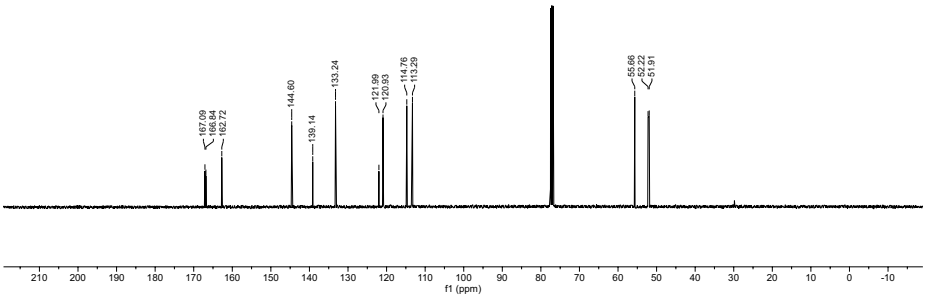
167.09
166.84
162.72
144.60
139.14
133.24
121.99
120.93
114.76
113.29
55.66
52.22
51.91
f1 (ppm)

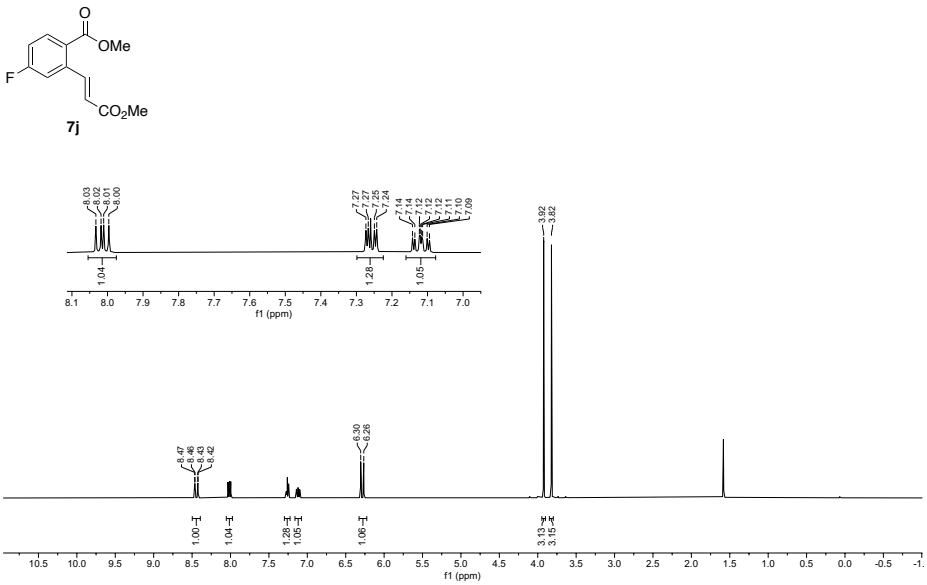
O
OMe
F
CO2Me
7j
8.03
8.02
8.01
8.00
7.27
7.27
7.26
7.25
7.24
7.14
7.14
7.13
7.12
7.12
7.12
7.11
7.10
7.09
3.92
3.82
1.04
1.28
1.05
f1 (ppm)
8.47
8.46
8.43
8.42
6.30
6.26
1.00
1.04
1.28
1.05
1.06
3.13
3.15
f1 (ppm)

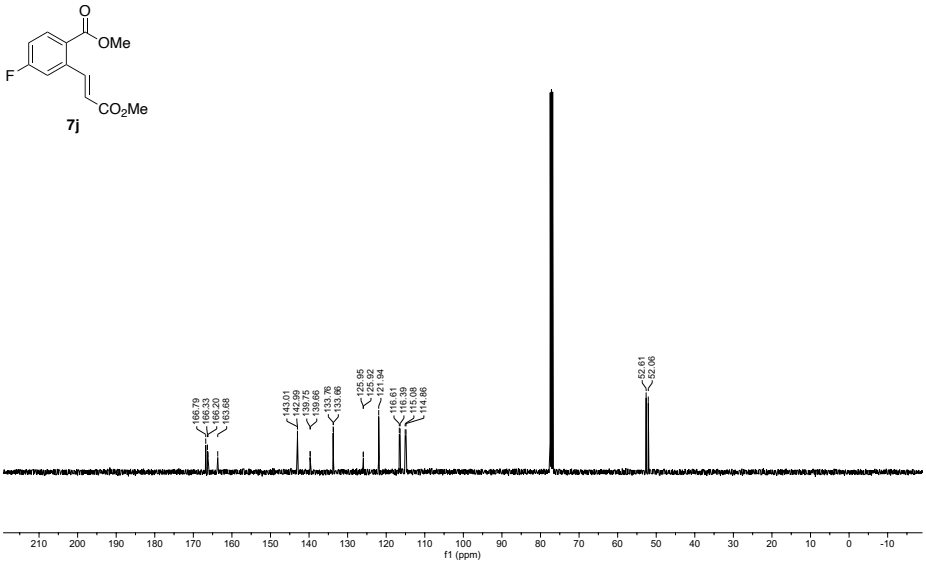
O
OMe
F
CO2Me
7j
166.79
166.53
166.20
163.68
143.01
142.99
139.95
139.86
133.76
133.66
125.95
125.92
121.94
116.61
116.39
115.08
114.86
52.61
52.06
f1 (ppm)

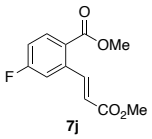
O
OMe
F
CO2Me

7j

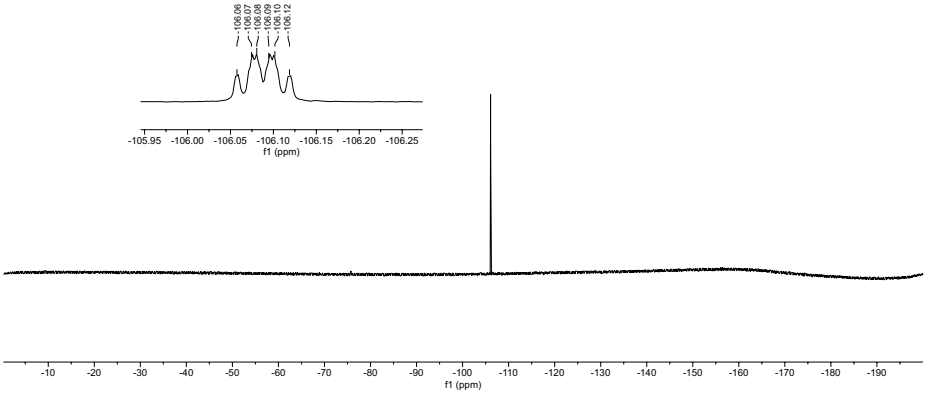
-106.06
-106.07
-106.08
-106.09
-106.10
-106.12
-105.95 -106.00 -106.05 -106.10 -106.15 -106.20 -106.25
f1 (ppm)
-10 -20 -30 -40 -50 -60 -70 -80 -90 -100 -110 -120 -130 -140 -150 -160 -170 -180 -190
f1 (ppm)

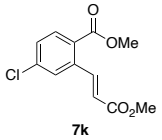
O
OMe
Cl
CO2Me

7k

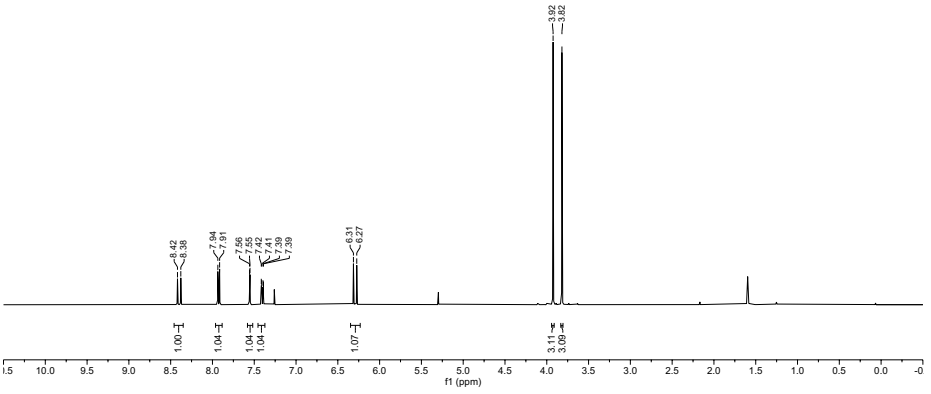
8.42
8.38
7.94
7.91
7.56
7.55
7.42
7.41
7.39
7.39
6.31
6.27
3.92
3.92
1.00
1.04
1.04
1.04
1.07
3.11
3.08
10.0 9.5 9.0 8.5 8.0 7.5 7.0 6.5 6.0 5.5 5.0 4.5 4.0 3.5 3.0 2.5 2.0 1.5 1.0 0.5 0.0
f1 (ppm)

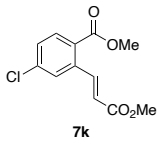
O
OMe
Cl
CO2Me

7k

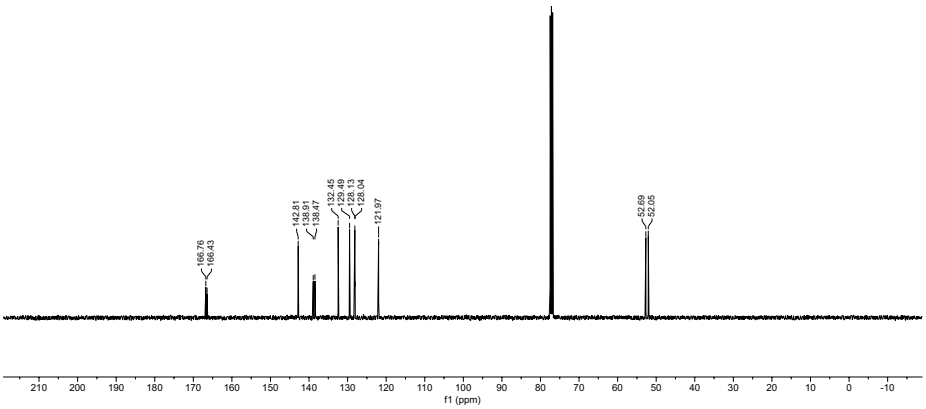
166.76
166.43
142.81
139.61
138.47
132.45
129.49
128.13
126.64
121.97
52.69
52.05
f1 (ppm)

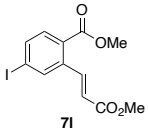
O
OMe
I
CO2Me

7l

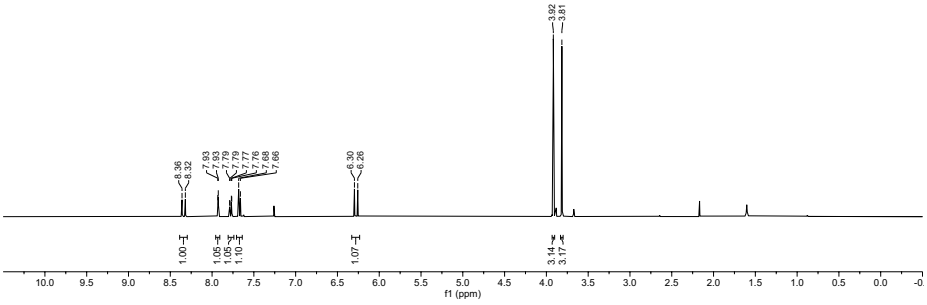
8.36
8.32
7.93
7.93
7.79
7.79
7.77
7.76
7.68
7.68
6.30
6.28
3.92
3.81
1.00
1.05
1.05
1.10
1.07
3.14
3.17
f1 (ppm)

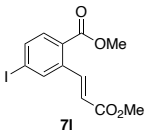
O
OMe
I
CO2Me

7l

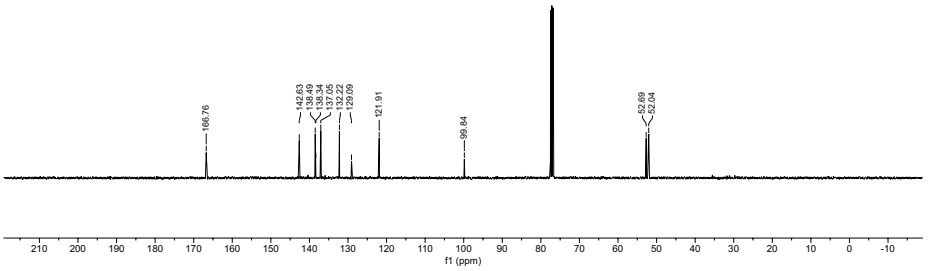
166.76
142.63
142.49
138.34
137.05
132.22
129.09
121.91
99.84
52.69
52.04
f1 (ppm)

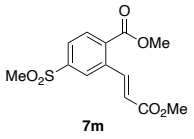
O
OMe
MeO2S
CO2Me

7m

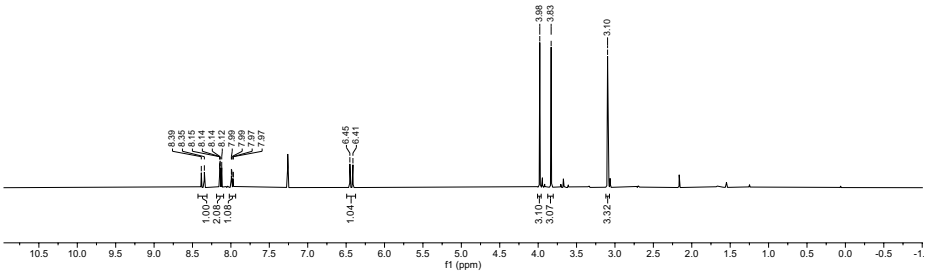
8.39
8.35
8.15
8.14
8.14
8.12
7.99
7.99
7.97
7.97
6.45
6.41
3.98
3.83
3.10
1.00
2.08
1.08
1.04
3.10
3.07
3.32
f1 (ppm)

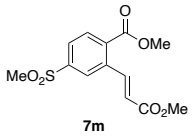
O
OMe
MeO2S
CO2Me

7m

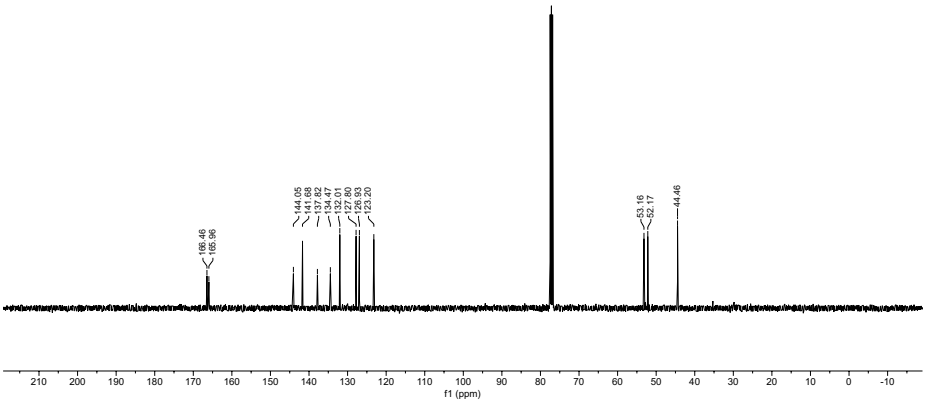
166.46
165.96
144.05
141.88
137.82
134.47
132.01
127.80
126.93
123.20
53.16
52.17
44.46
f1 (ppm)

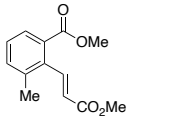
O
OMe
Me
CO2Me

7n

3.85
3.81
2.36
2.36
5.94
5.90
8.06
8.04
7.72
7.71
7.71
7.70
7.39
7.37
7.31
7.29
7.27
1.00
1.01
1.09
1.07
1.10
3.04
3.05
3.17
f1 (ppm)

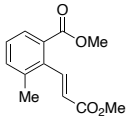
O
OMe
Me
CO2Me

7n

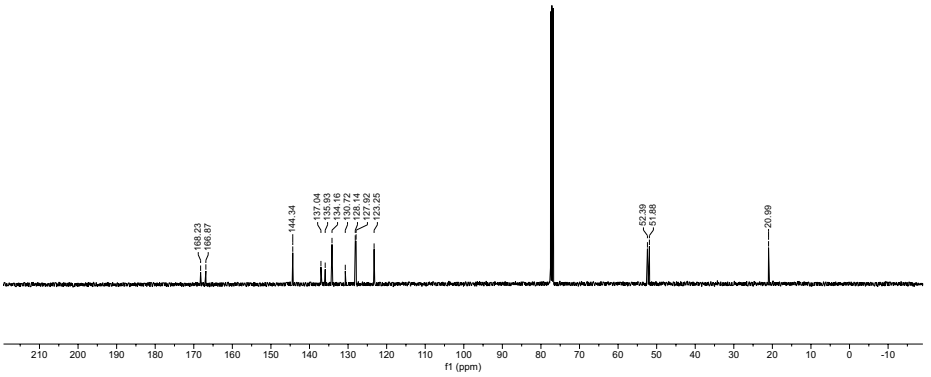
168.23
166.87
144.34
137.04
135.13
134.15
130.72
128.14
127.02
123.25
52.39
51.88
20.99
f1 (ppm)

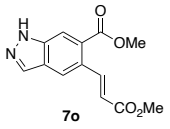
H
N
N
O
OMe
CO2Me

7o

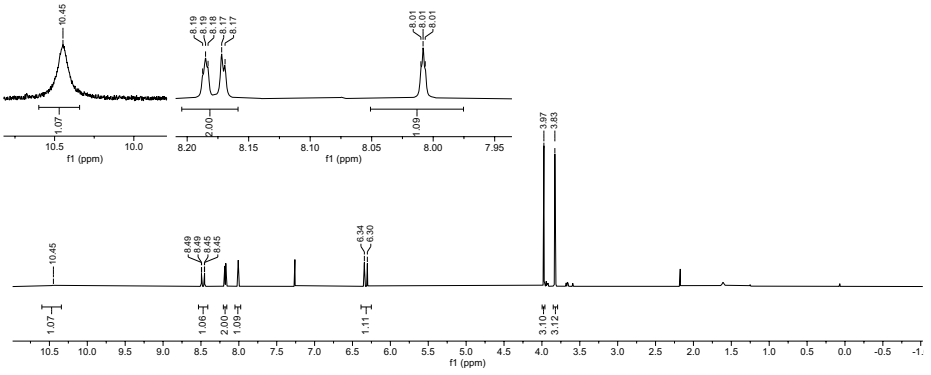
10.45
8.19
8.19
8.18
8.17
8.17
8.01
8.01
8.01
3.97
3.83
8.49
8.49
8.45
8.45
6.34
6.30
1.07
1.06
2.00
1.09
1.11
3.10
3.12
f1 (ppm)

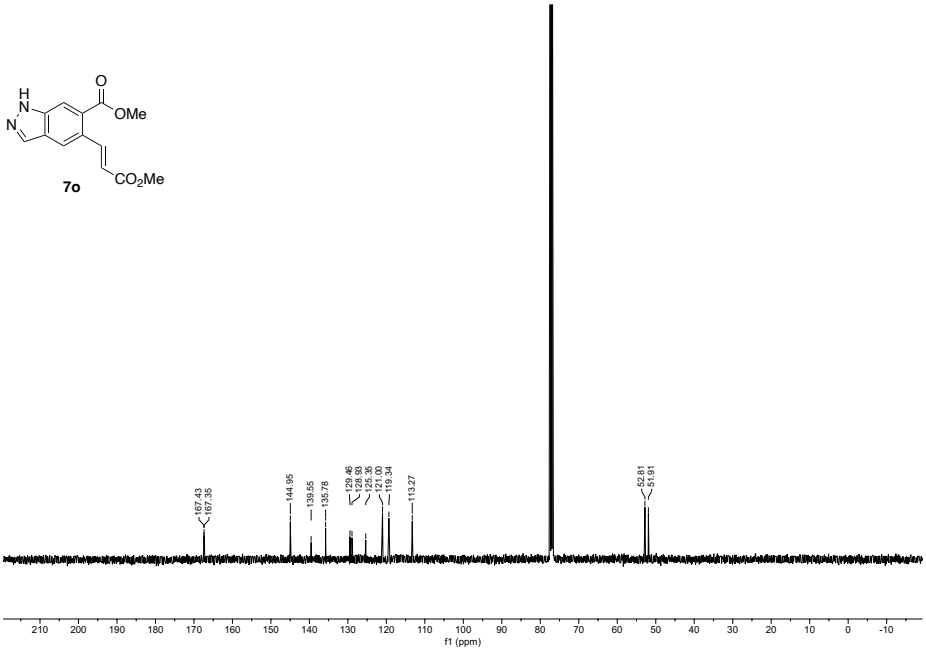
7o
167.43
167.35
144.95
139.55
135.78
129.46
129.09
125.35
121.00
119.54
113.27
52.81
51.91
f1 (ppm)

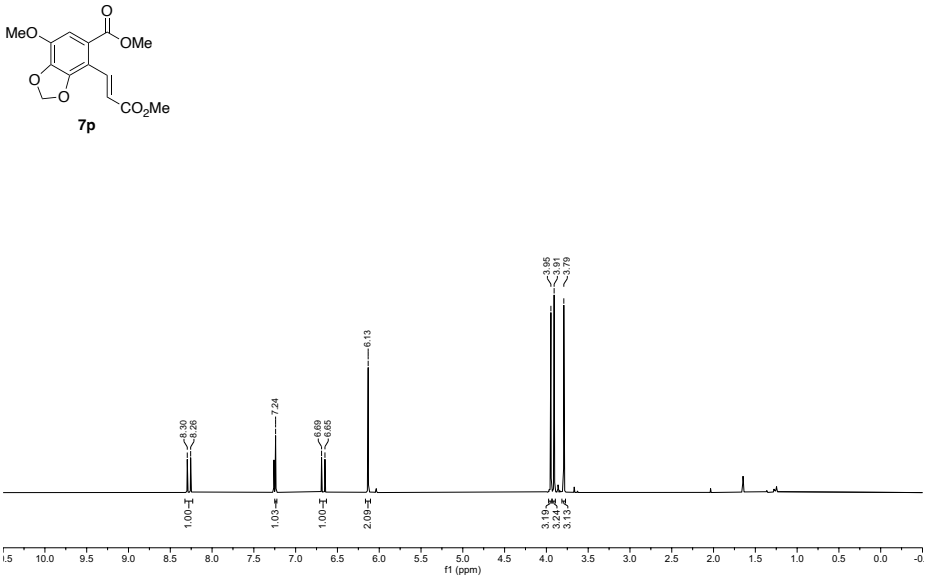
7p
8.30
8.26
7.24
6.69
6.65
6.13
3.95
3.91
3.79
1.00
1.03
1.00
2.09
3.19
3.24
3.13
f1 (ppm)

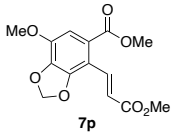
MeO
O
OMe
O
O
CO2Me

7p

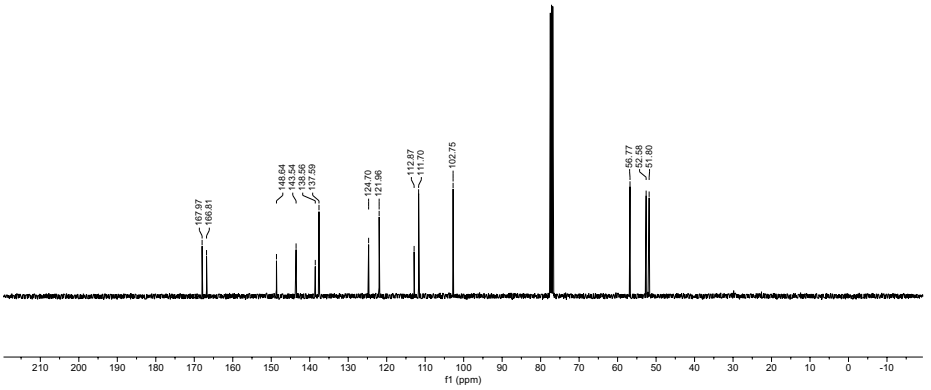
167.97
166.81
148.64
143.54
138.56
137.59
124.70
121.96
112.97
111.70
102.75
56.77
52.58
51.80
f1 (ppm)

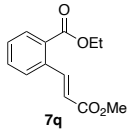
O
OEt
CO2Me

7q

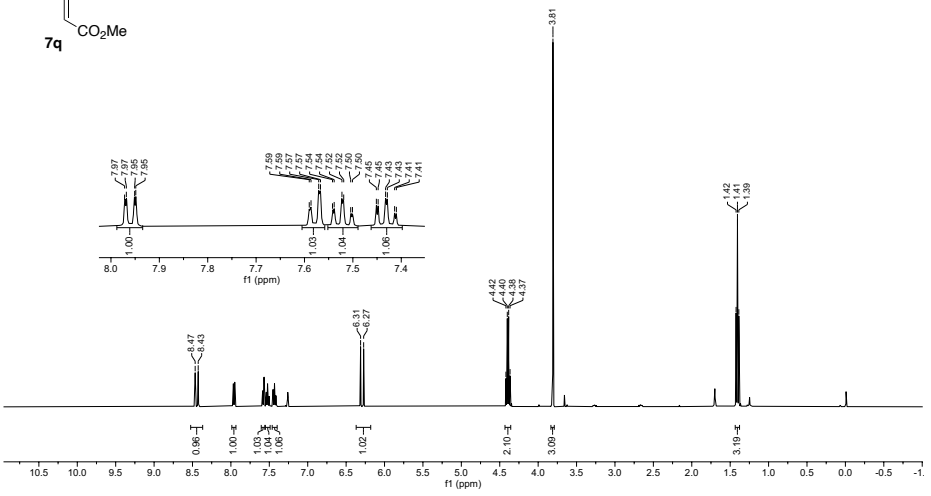
7.97
7.97
7.95
7.95
7.59
7.59
7.57
7.57
7.54
7.54
7.52
7.52
7.50
7.50
7.46
7.46
7.43
7.43
7.41
7.41
1.00
1.03
1.04
1.06
f1 (ppm)
3.81
8.47
8.43
6.31
6.27
4.42
4.40
4.38
4.37
1.42
1.41
1.39
0.96
1.00
1.03
1.04
1.06
1.02
2.10
3.09
3.19
f1 (ppm)

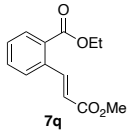
O
OEt
CO2Me

7q

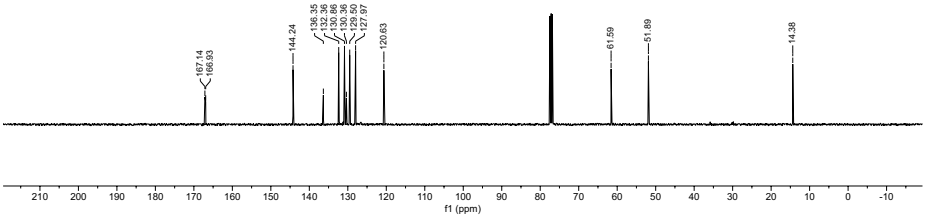
167.14
166.93
144.24
138.35
132.36
130.86
130.36
129.50
127.97
120.63
61.59
51.89
14.38
f1 (ppm)

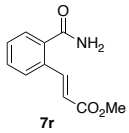
O
NH2
CO2Me

7r

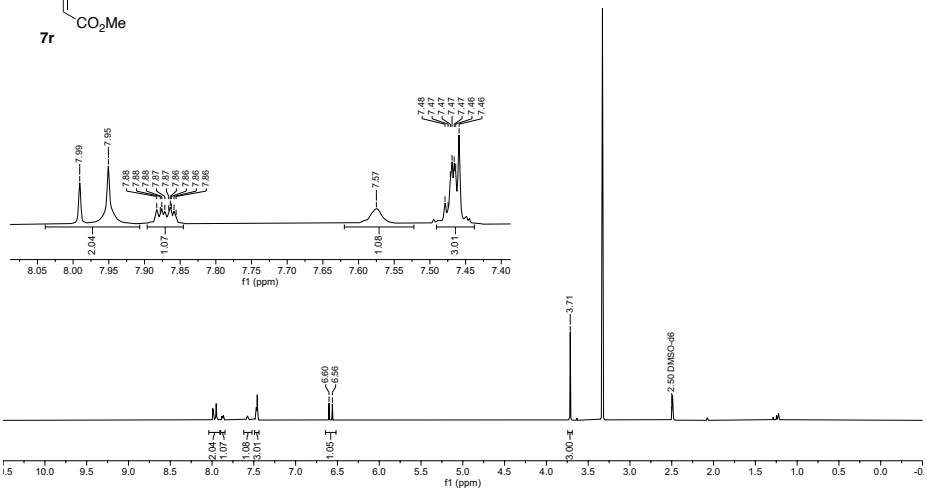
7.99
7.95
7.88
7.88
7.88
7.87
7.87
7.86
7.86
7.86
7.86
7.57
7.48
7.47
7.47
7.47
7.47
7.46
7.46
2.04
1.07
1.08
3.01
f1 (ppm)
6.60
6.56
3.71
2.50 DMSO-d6
2.04
1.07
1.08
3.01
1.05
3.00
f1 (ppm)

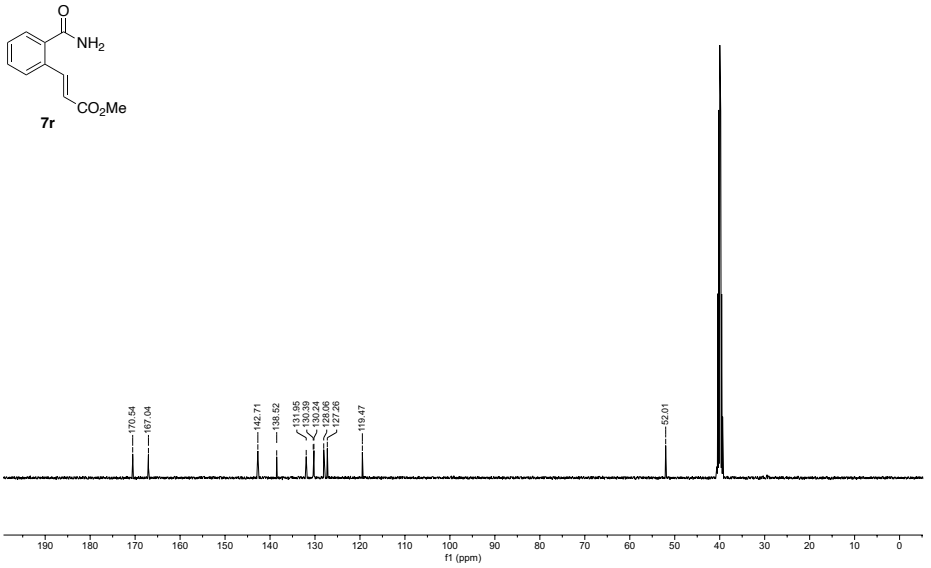
O
NH2
CO2Me
7r
170.54
167.04
142.71
138.52
131.95
130.39
130.24
129.66
127.26
119.47
52.01
f1 (ppm)

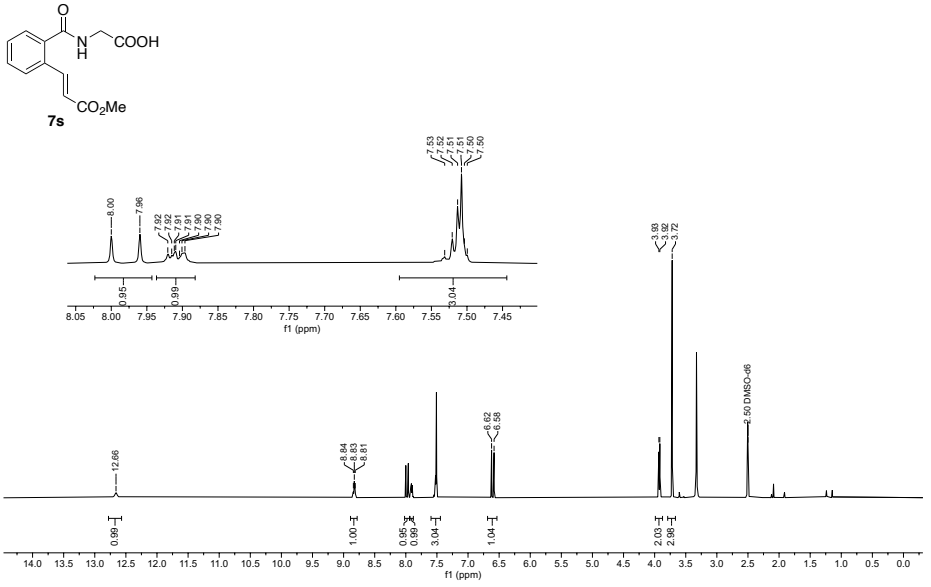
O
N
H
COOH
CO2Me
7s
8.00
7.96
7.92
7.91
7.91
7.90
7.90
7.53
7.52
7.51
7.51
7.50
7.50
0.95
0.99
3.04
f1 (ppm)
3.93
3.92
3.72
2.50 DMSO-d6
12.66
8.84
8.83
8.81
6.62
6.58
0.99
1.00
0.95
0.99
3.04
1.04
2.03
2.98
f1 (ppm)

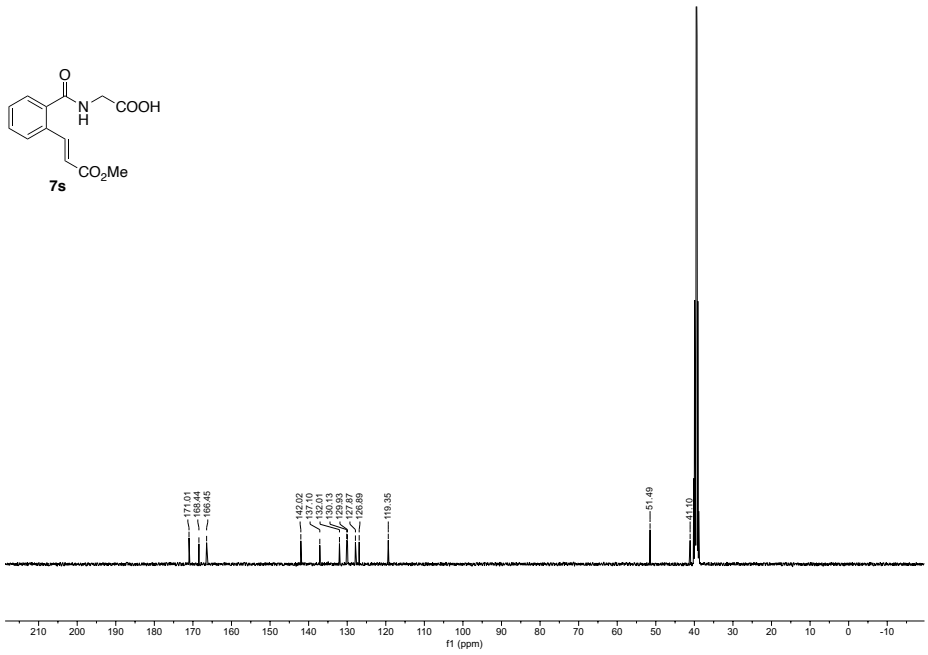
7s
171.01
168.44
168.45
142.02
137.10
132.01
130.13
129.93
127.87
126.89
119.35
51.49
41.10
f1 (ppm)

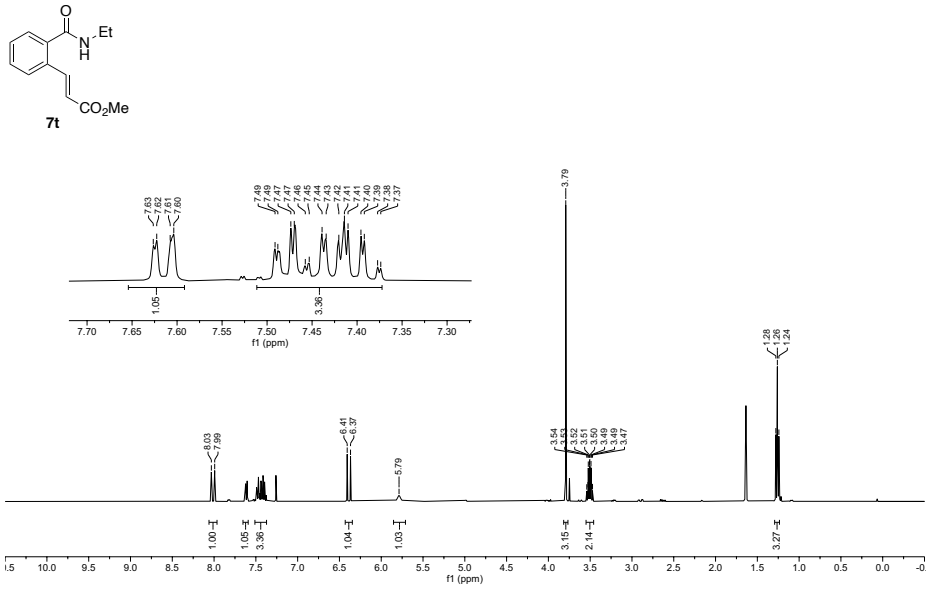
7t
7.63
7.62
7.61
7.60
7.49
7.49
7.47
7.47
7.46
7.45
7.44
7.43
7.42
7.41
7.41
7.40
7.39
7.38
7.37
1.05
3.36
f1 (ppm)
3.79
1.28
1.26
1.24
8.03
7.99
6.41
6.37
5.79
3.54
3.53
3.52
3.51
3.50
3.49
3.48
3.47
1.00
1.05
3.36
1.04
1.03
3.15
2.14
3.27
f1 (ppm)

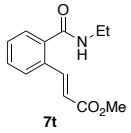
O
N
H
Et
CO2Me

7t

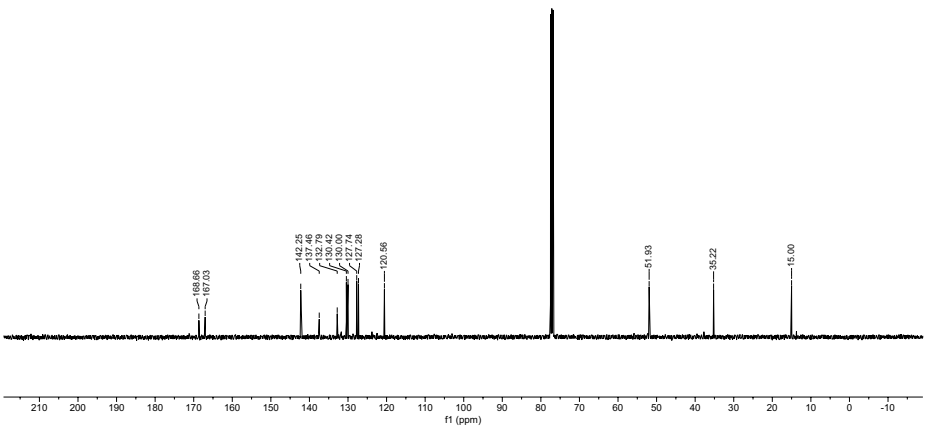
168.66
167.03
143.25
137.46
132.79
130.42
130.00
127.74
127.28
120.56
51.93
35.22
15.00
f1 (ppm)

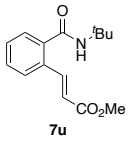
O
N
H
tBu
CO2Me

7u

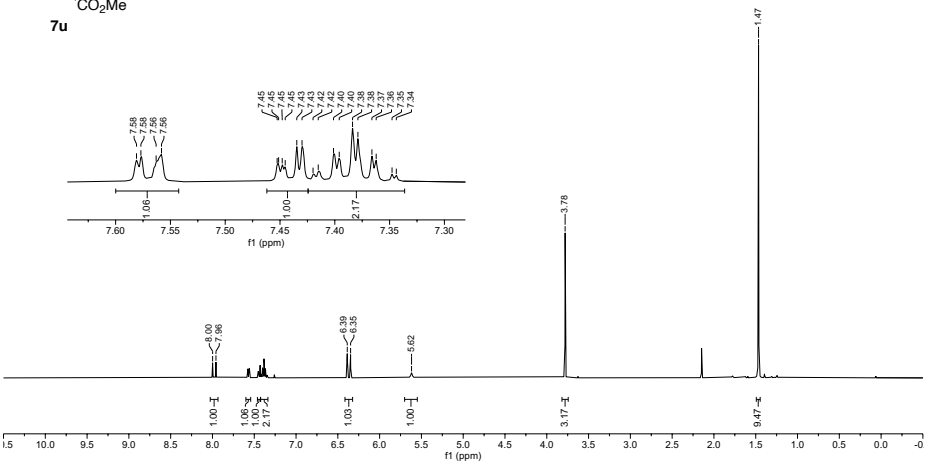
1.47
3.78
8.00
7.96
8.39
8.35
5.62
f1 (ppm)

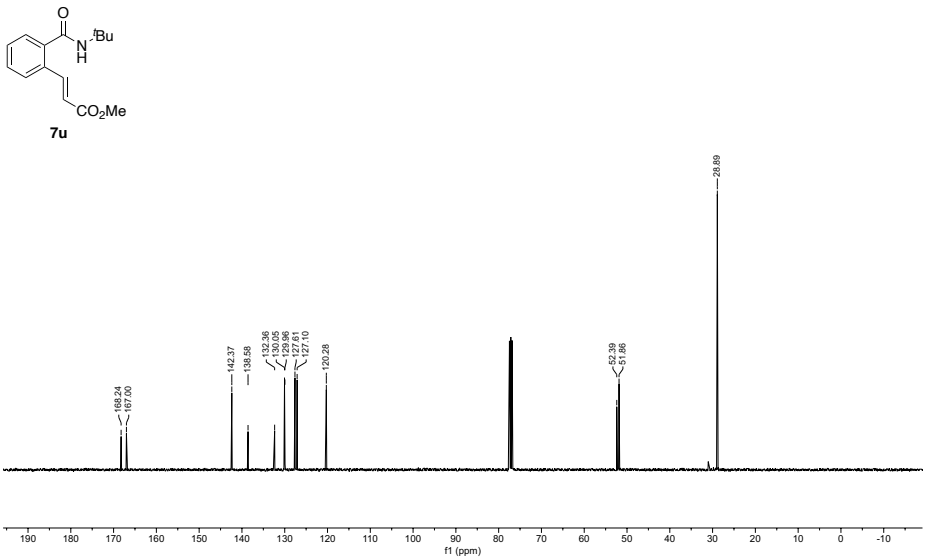
O
N
H
tBu
CO2Me
7u
168.24
167.00
142.37
138.58
132.36
130.05
129.96
127.61
127.10
120.28
52.39
51.86
28.89
f1 (ppm)

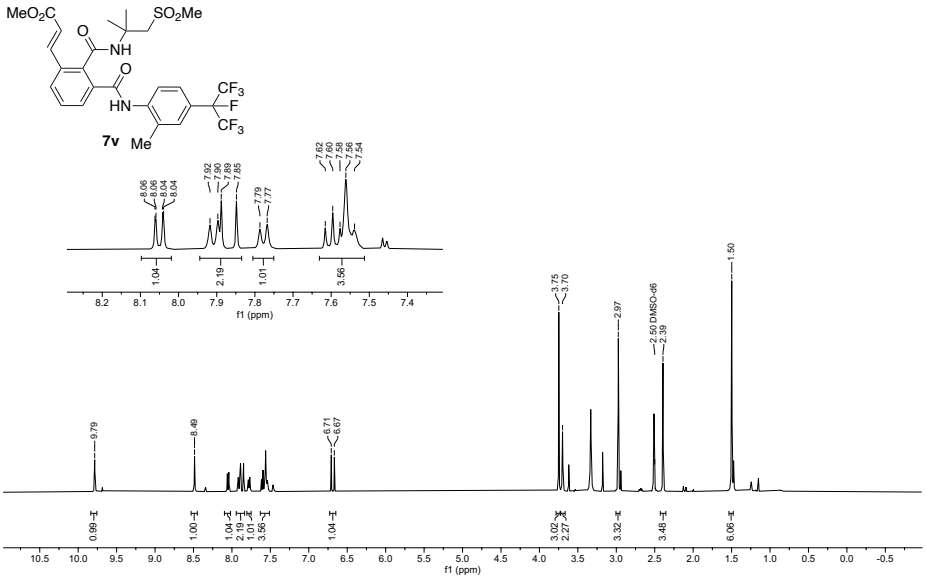
MeO2C
SO2Me
O
NH
O
HN
CF3
F
CF3
Me
7v
8.06
8.06
8.04
8.04
7.92
7.90
7.89
7.85
7.79
7.77
7.62
7.60
7.58
7.56
7.54
1.04
2.19
1.01
3.56
f1 (ppm)
9.79
8.49
6.71
6.67
3.75
3.70
2.97
2.50 DMSO-d6
2.39
1.50
0.99
1.00
1.04
2.19
1.01
3.56
1.04
3.02
2.27
3.32
3.48
6.06
f1 (ppm)

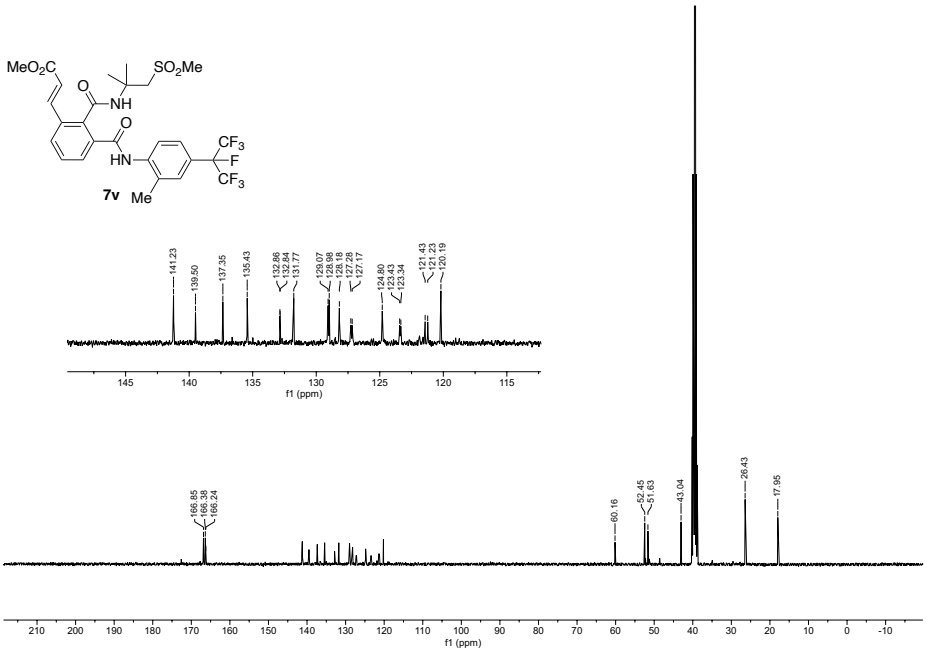
MeO2C
SO2Me
NH
O
HN
CF3
F
CF3
7v
Me
141.23
139.50
137.35
135.43
132.86
132.84
131.77
129.07
128.98
128.18
127.28
127.17
124.80
123.43
123.34
121.43
121.23
120.19
166.85
166.38
166.24
60.16
52.45
51.63
43.04
26.43
17.95
f1 (ppm)

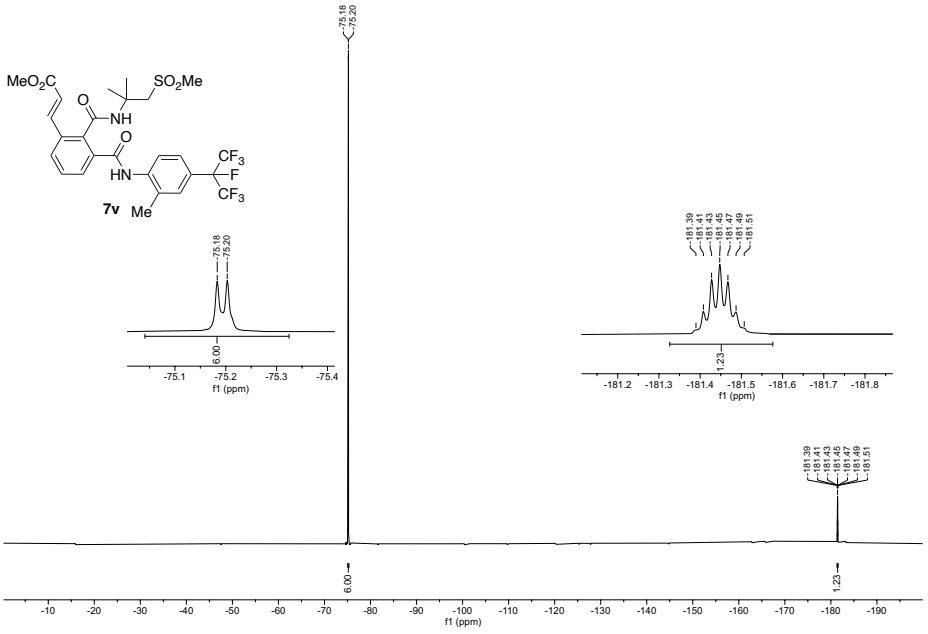
MeO2C
SO2Me
NH
O
HN
CF3
F
CF3
7v
Me
75.18
75.20
6.00
f1 (ppm)
181.39
181.41
181.43
181.45
181.47
181.49
181.51
1.23
f1 (ppm)
6.00
1.23
f1 (ppm)

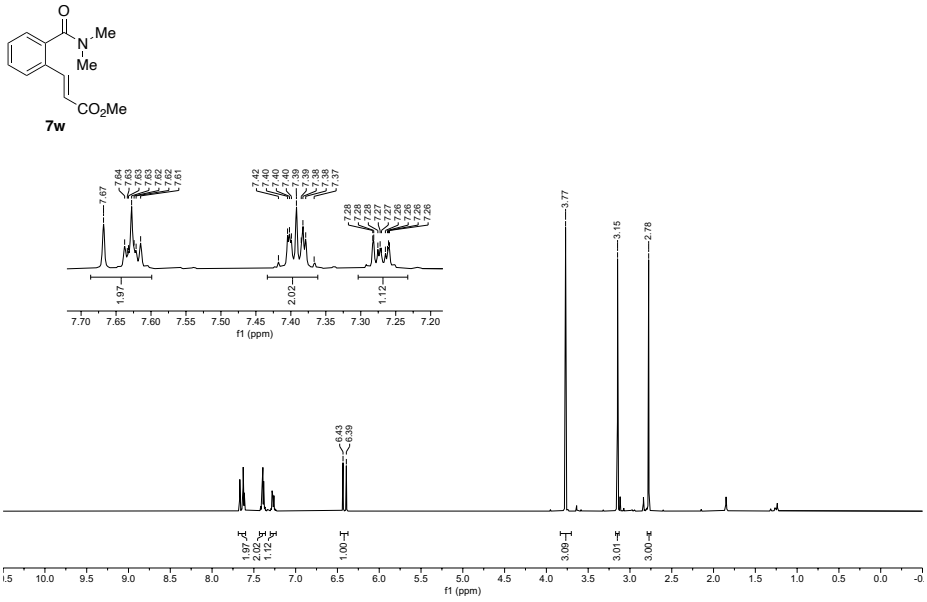
O
N
Me
Me
CO2Me
7w
7.67
7.64
7.63
7.63
7.63
7.62
7.62
7.61
7.42
7.40
7.40
7.40
7.39
7.38
7.38
7.37
7.28
7.28
7.28
7.27
7.27
7.26
7.26
7.26
7.26
3.77
3.15
2.78
6.43
6.39
1.97
2.02
1.12
1.00
3.09
3.01
3.00
f1 (ppm)

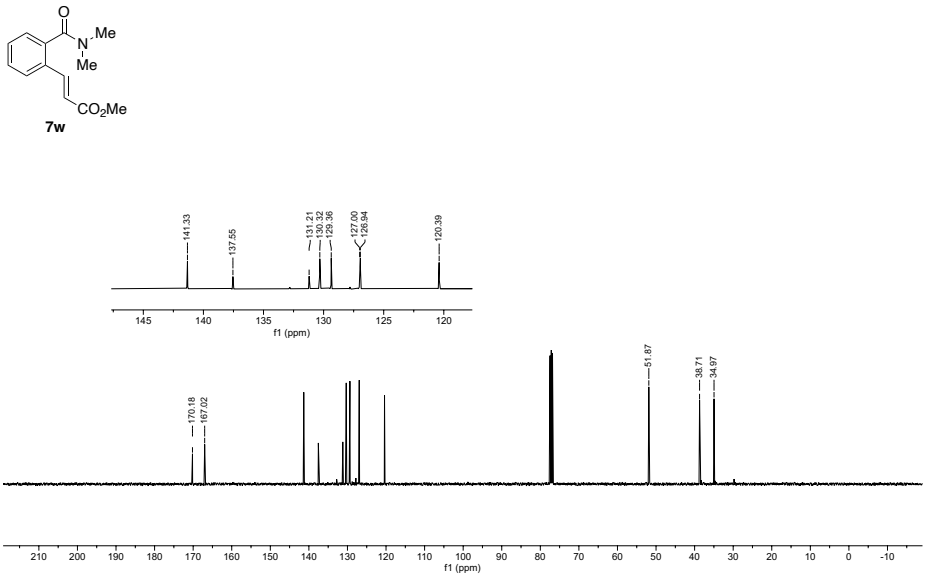
O
N
Me
Me
CO2Me
7w
141.33
137.55
131.21
130.32
129.36
127.00
126.84
120.39
51.87
38.71
34.97
170.18
167.02
f1 (ppm)

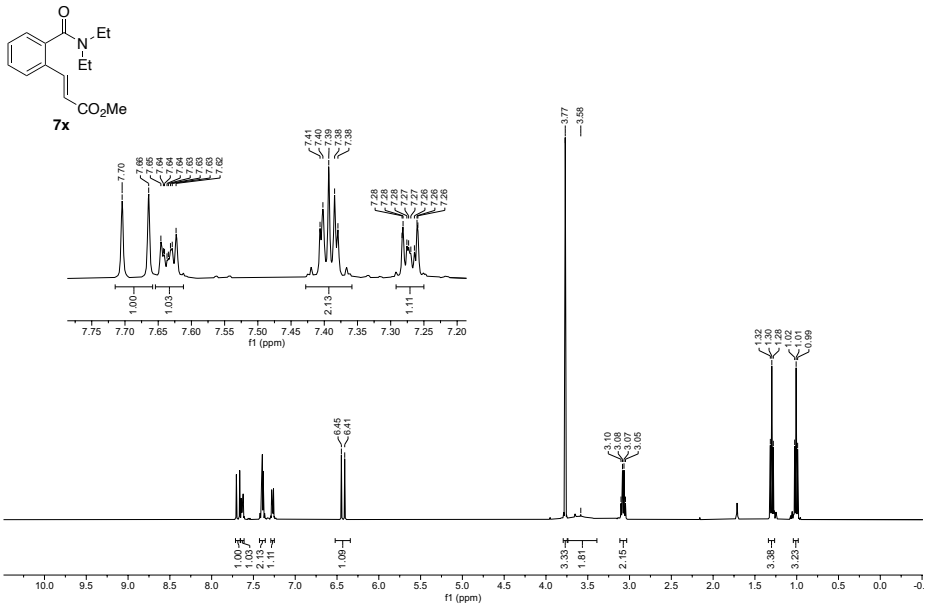
O
N
Et
Et
CO2Me
7x
7.70
7.66
7.65
7.64
7.64
7.64
7.63
7.63
7.63
7.62
7.41
7.40
7.39
7.38
7.38
7.38
7.28
7.28
7.28
7.28
7.27
7.27
7.26
7.26
7.26
3.77
3.58
6.45
6.41
3.10
3.09
3.07
3.05
1.32
1.30
1.28
1.02
1.01
0.99
1.00
1.03
2.13
1.11
1.09
3.33
1.81
2.15
3.38
3.23
f1 (ppm)

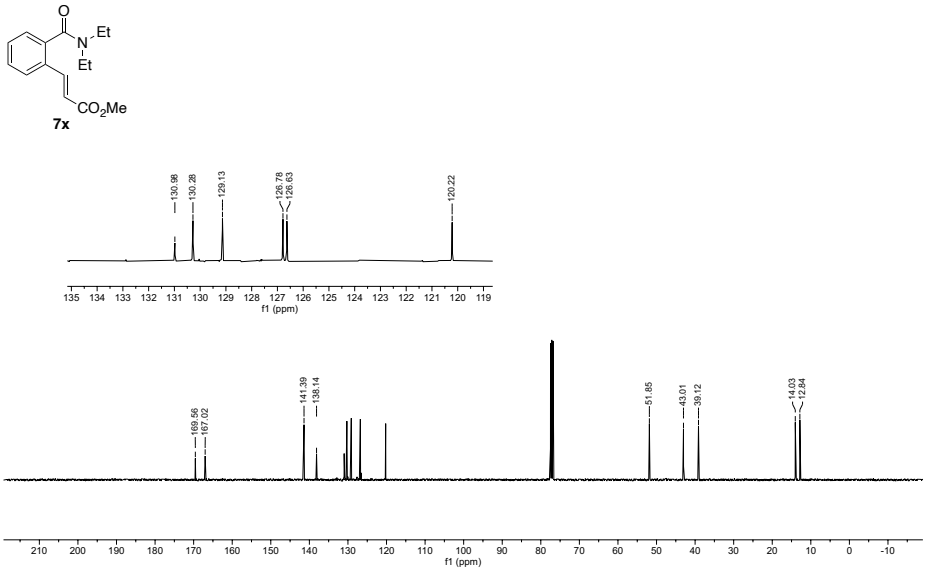
O
N
Et
Et
CO2Me
7x
130.98
130.28
129.13
126.78
126.63
120.22
169.56
167.02
141.39
138.14
51.85
43.01
39.12
14.03
12.84
f1 (ppm)

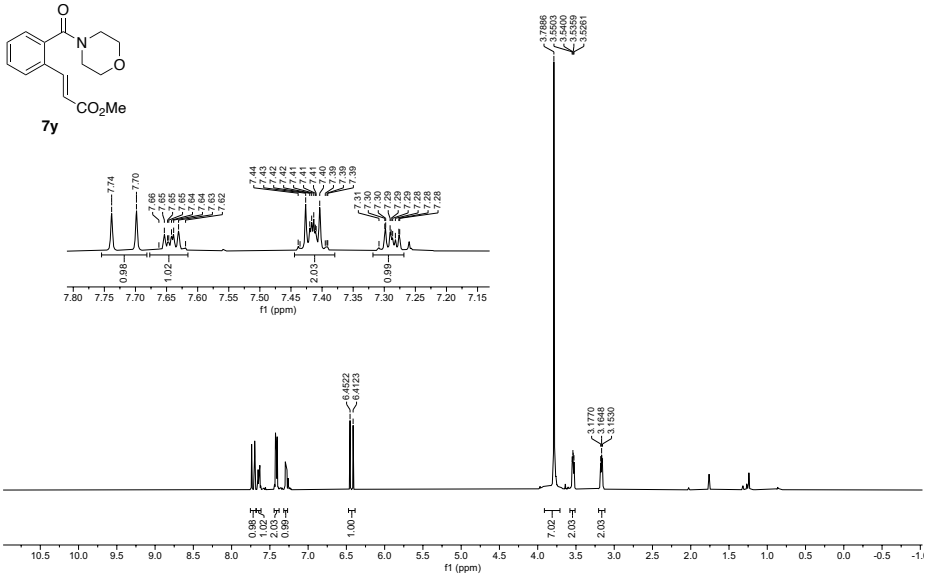
7y
f1 (ppm)

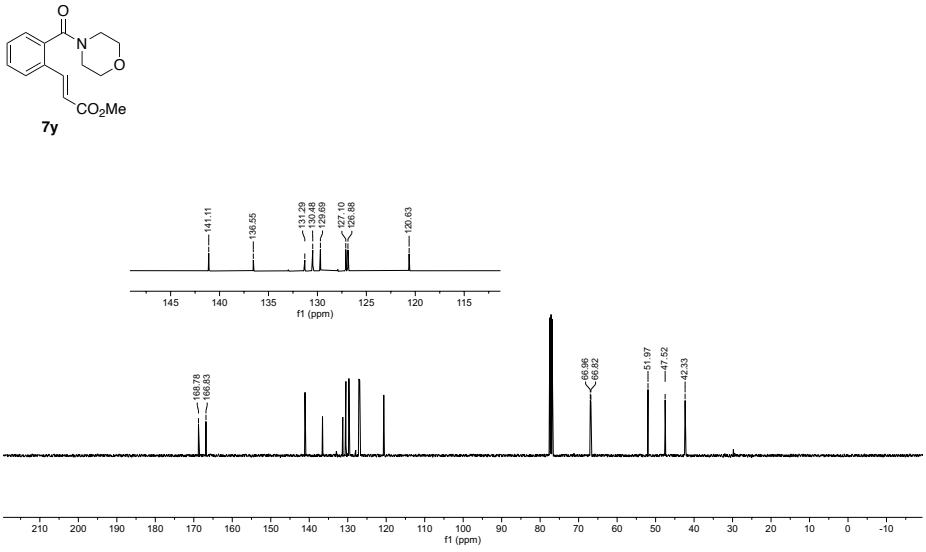
7y
f1 (ppm)

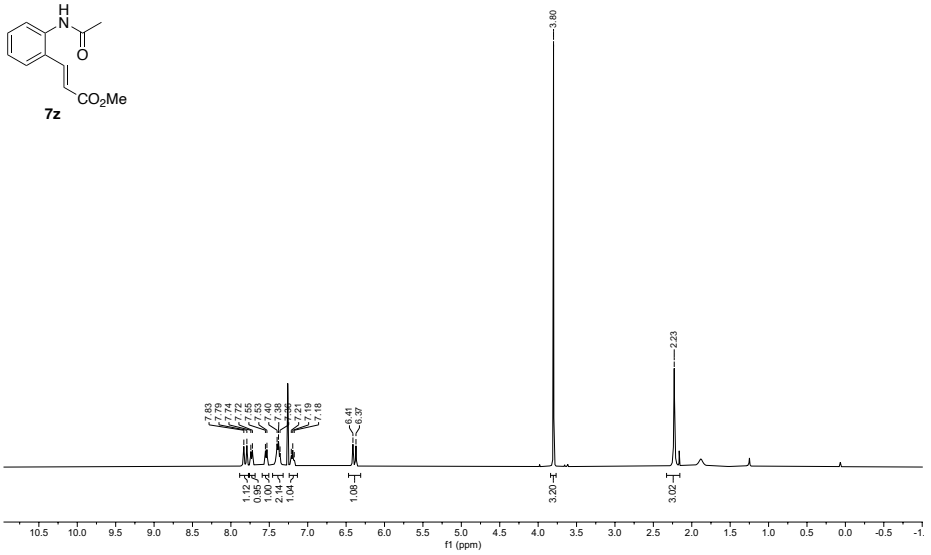
7z
7.83
7.79
7.74
7.72
7.72
7.55
7.53
7.40
7.38
7.36
7.21
7.19
7.18
6.41
6.37
3.80
2.23
1.12
0.86
1.00
2.14
1.04
1.08
3.20
3.02
f1 (ppm)

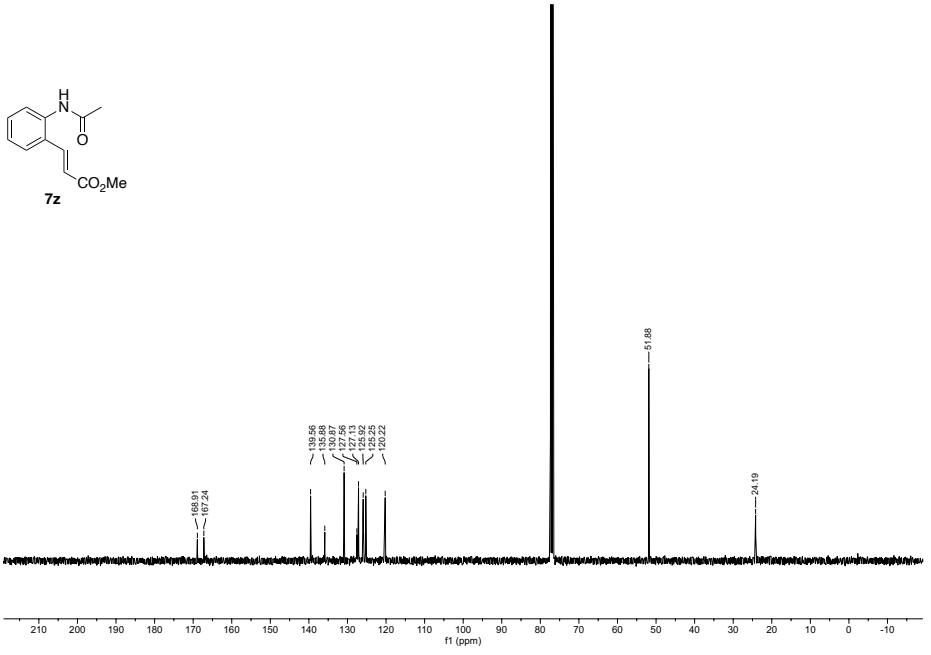
7z
168.91
167.24
139.56
135.88
130.87
127.56
127.13
125.92
125.25
120.22
51.88
24.19
f1 (ppm)

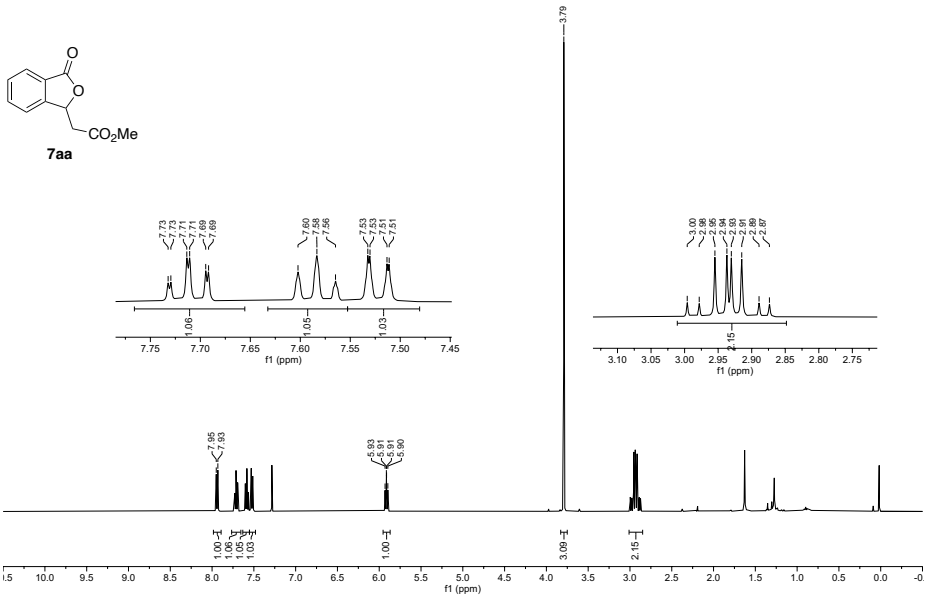
O
O
CO2Me
7aa
7.73
7.73
7.71
7.71
7.69
7.69
7.60
7.58
7.56
7.53
7.53
7.51
7.51
1.06
1.05
1.03
7.75
7.70
7.65
7.60
7.55
7.50
7.45
f1 (ppm)
3.00
2.98
2.95
2.94
2.93
2.91
2.89
2.87
2.15
3.10
3.05
3.00
2.95
2.90
2.85
2.80
2.75
f1 (ppm)
3.79
7.95
7.93
5.93
5.91
5.91
5.90
1.00
1.06
1.05
1.03
1.00
3.09
2.15
f1 (ppm)

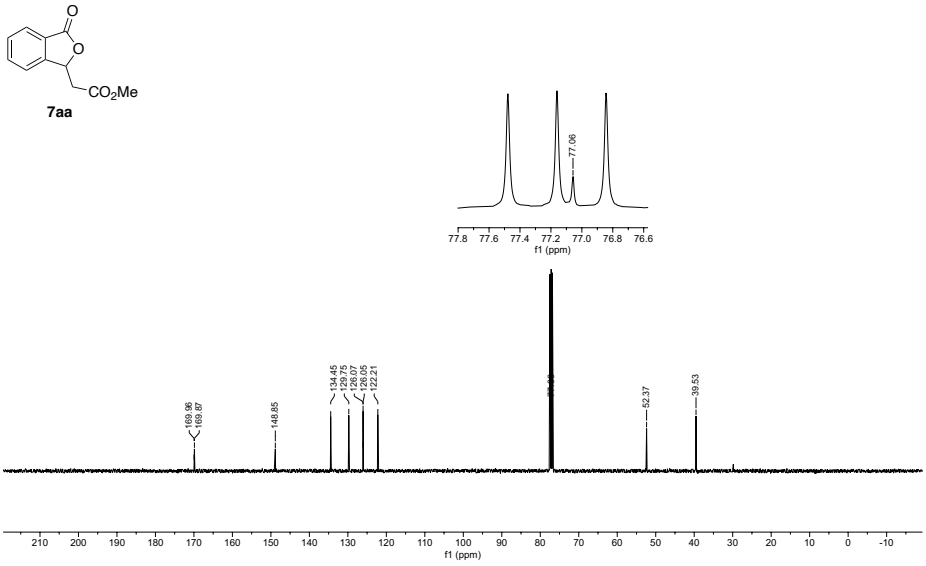
O
O
CO2Me
7aa
77.06
77.8
77.6
77.4
77.2
77.0
76.8
76.6
f1 (ppm)
169.96
169.87
148.85
134.45
129.75
126.07
125.05
122.27
52.37
39.53
f1 (ppm)

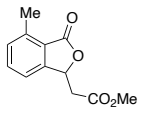
Me
O
O
CO2Me

7ab

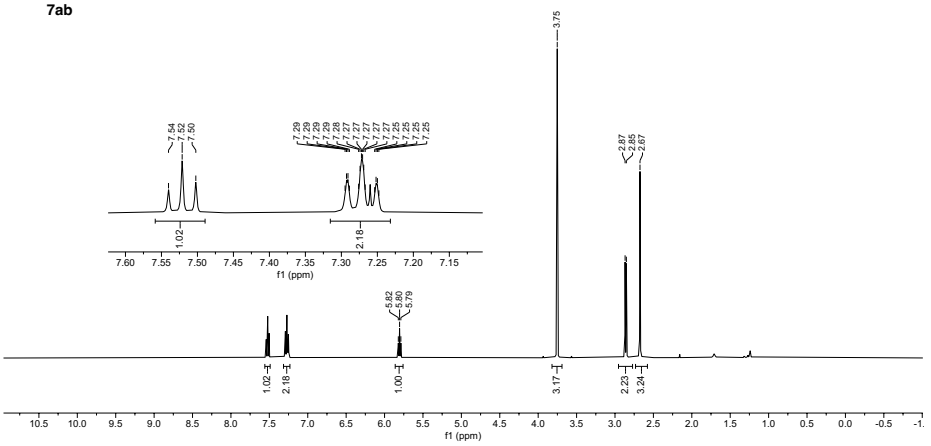
7.54
7.52
7.50
7.29
7.29
7.29
7.28
7.28
7.27
7.27
7.27
7.27
7.27
7.27
7.27
7.26
7.25
7.25
7.25
3.75
2.87
2.85
2.67
5.82
5.80
5.79
1.02
2.18
1.00
3.17
2.23
3.24
1.02
2.18
7.60 7.55 7.50 7.45 7.40 7.35 7.30 7.25 7.20 7.15
f1 (ppm)
10.5 10.0 9.5 9.0 8.5 8.0 7.5 7.0 6.5 6.0 5.5 5.0 4.5 4.0 3.5 3.0 2.5 2.0 1.5 1.0 0.5 0.0 -0.5
f1 (ppm)

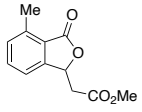
Me
O
O
CO2Me

7ab

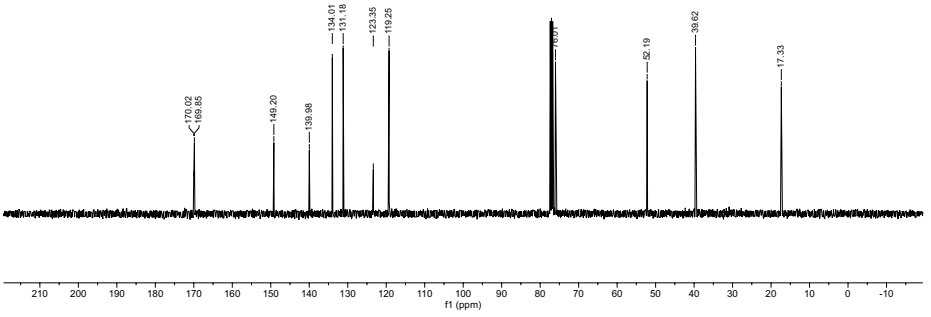
170.02
169.85
149.20
139.98
134.01
131.18
123.35
119.25
77.01
52.19
39.62
17.33
210 200 190 180 170 160 150 140 130 120 110 100 90 80 70 60 50 40 30 20 10 0 -10
f1 (ppm)

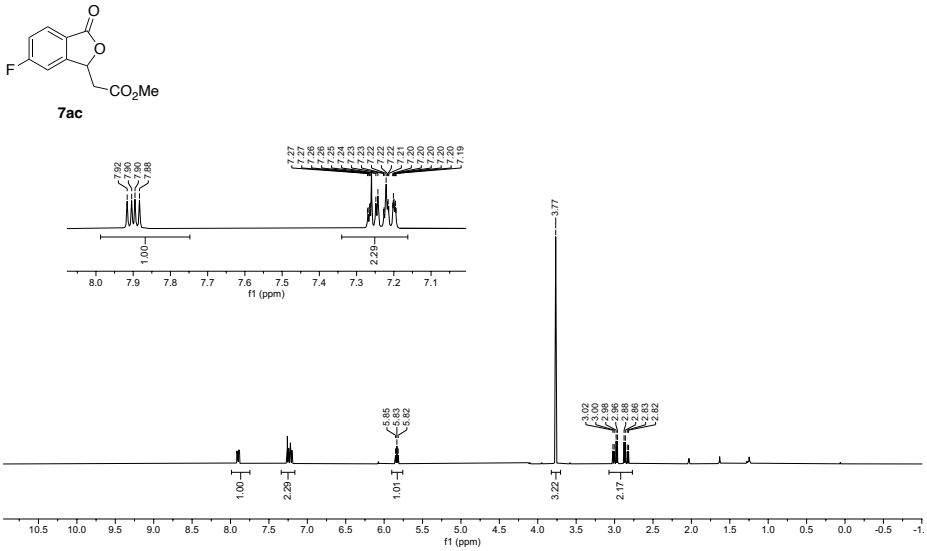
O
O
F
CO2Me
7ac
7.92
7.90
7.89
7.88
7.27
7.26
7.25
7.24
7.23
7.22
7.21
7.20
7.19
1.00
2.29
3.77
5.85
5.83
5.82
3.02
3.00
2.98
2.96
2.88
2.86
2.83
2.82
1.00
2.29
1.01
3.22
2.17
f1 (ppm)

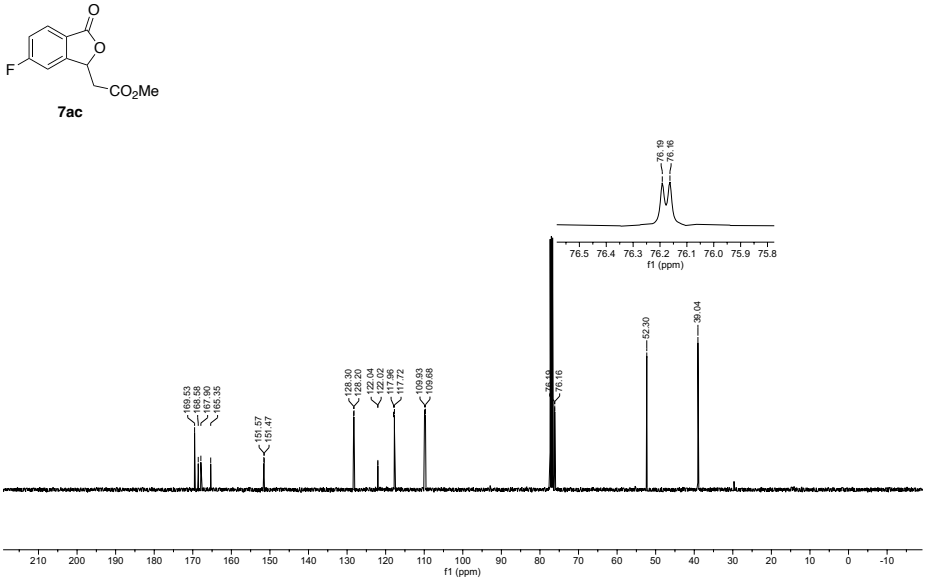
O
O
F
CO2Me
7ac
76.19
76.16
76.5 76.4 76.3 76.2 76.1 76.0 75.9 75.8
f1 (ppm)
169.53
168.58
167.80
165.35
151.57
151.47
128.30
128.20
122.02
117.86
117.72
109.93
109.88
77.48
77.16
52.30
39.04
f1 (ppm)

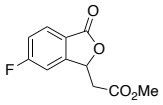
O
O
F
CO2Me

7ac

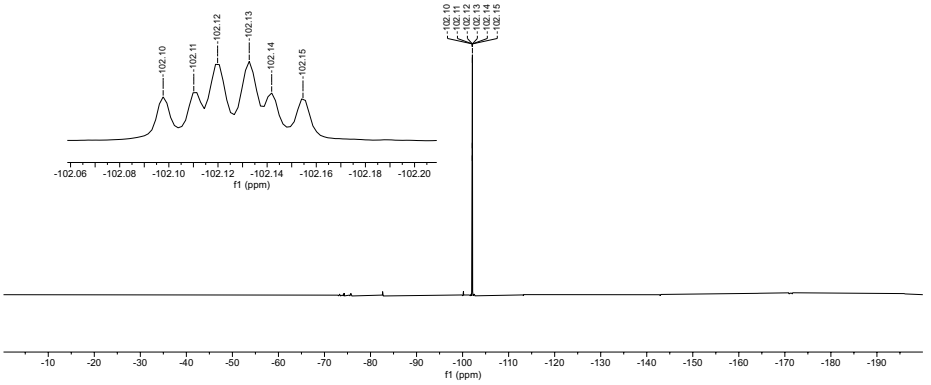
-102.10
-102.11
-102.12
-102.13
-102.14
-102.15
-102.06 -102.08 -102.10 -102.12 -102.14 -102.16 -102.18 -102.20
f1 (ppm)
-10 -20 -30 -40 -50 -60 -70 -80 -90 -100 -110 -120 -130 -140 -150 -160 -170 -180 -190
f1 (ppm)

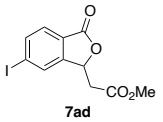
O
O
I
CO2Me

7ad

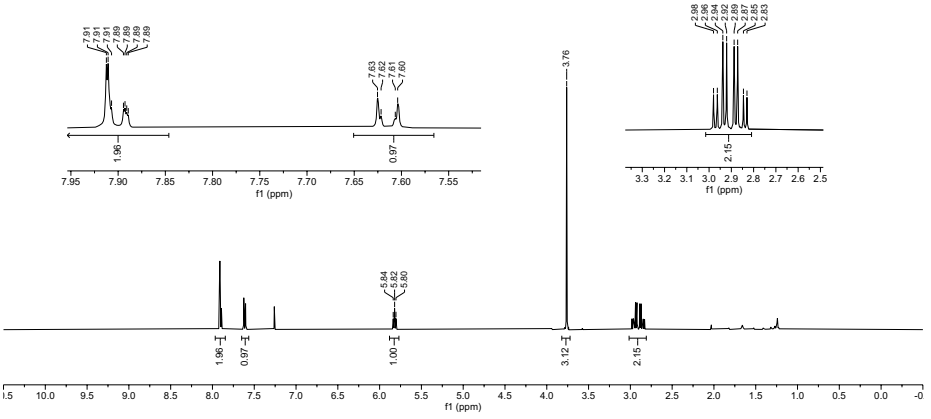
7.91
7.89
7.63
7.61
7.60
1.96
0.97
7.95 7.90 7.85 7.80 7.75 7.70 7.65 7.60 7.55
f1 (ppm)
3.76
2.98
2.94
2.92
2.89
2.87
2.85
2.83
2.15
3.3 3.2 3.1 3.0 2.9 2.8 2.7 2.6 2.5
f1 (ppm)
5.84
5.82
5.80
1.96
0.97
1.00
3.12
2.15
10.5 10.0 9.5 9.0 8.5 8.0 7.5 7.0 6.5 6.0 5.5 5.0 4.5 4.0 3.5 3.0 2.5 2.0 1.5 1.0 0.5 0.0
f1 (ppm)

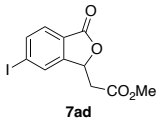
O
O
I
CO2Me

7ad

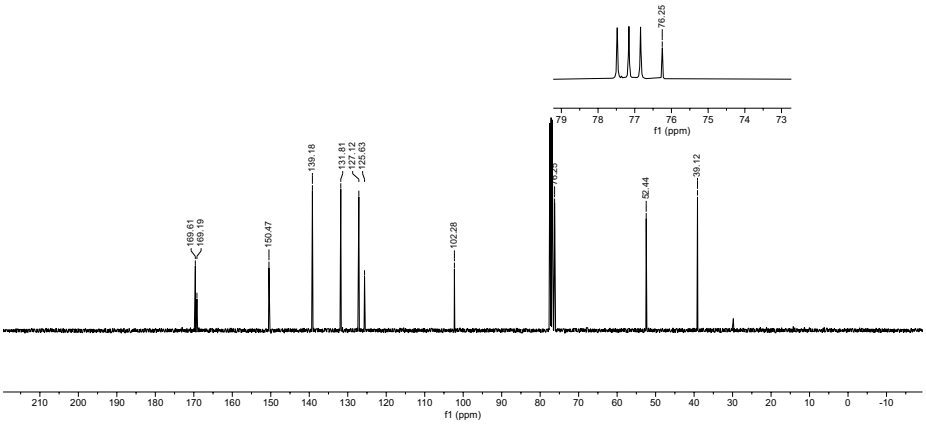
76.25
169.61
169.19
150.47
139.18
131.81
127.12
125.63
102.28
52.44
39.12
f1 (ppm)

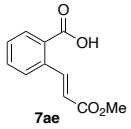
O
OH
CO2Me

7ae

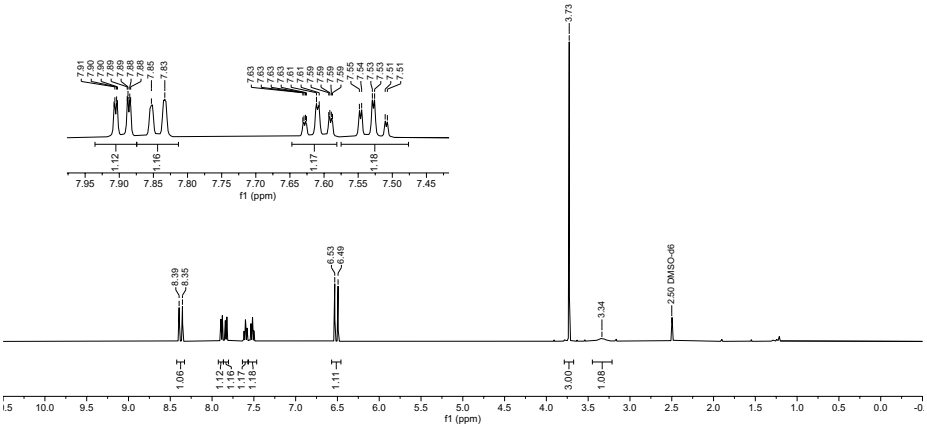
3.73
8.39
8.35
6.53
6.49
3.34
2.50 DMSO-d6
f1 (ppm)

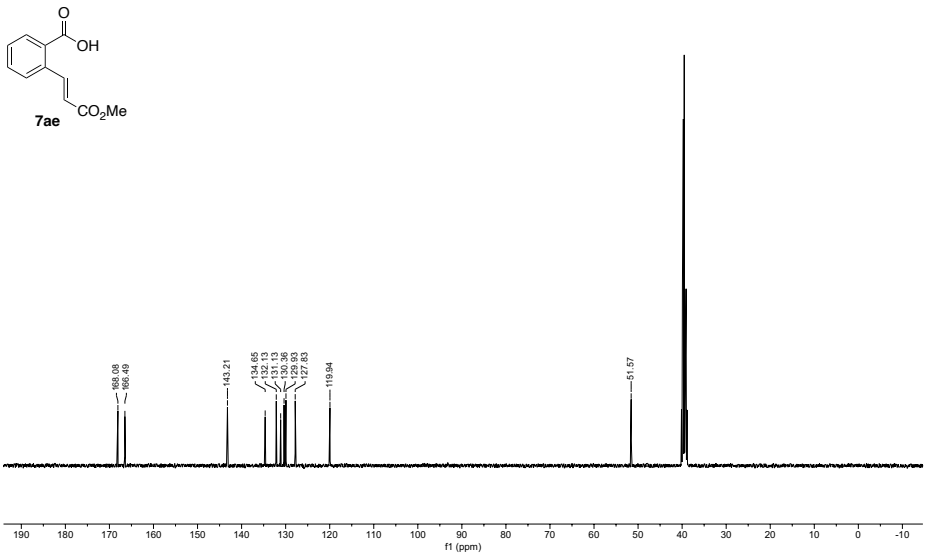
O
OH
CO2Me
7ae
168.08
166.49
143.21
134.65
132.13
131.13
130.95
129.93
127.83
119.94
51.57
f1 (ppm)

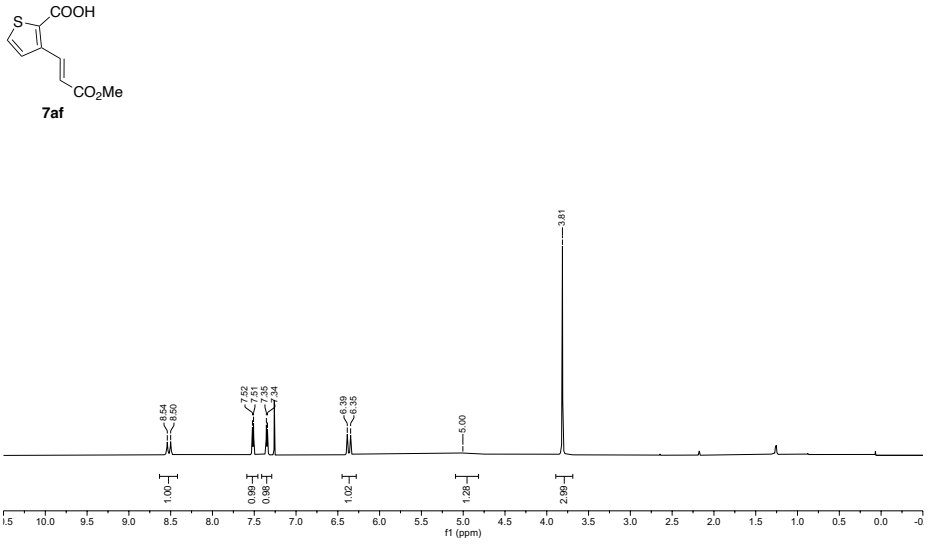
S
COOH
CO2Me
7af
8.54
8.50
7.52
7.51
7.35
7.34
6.39
6.35
5.00
3.81
1.00
0.99
0.98
1.02
1.28
2.99
f1 (ppm)

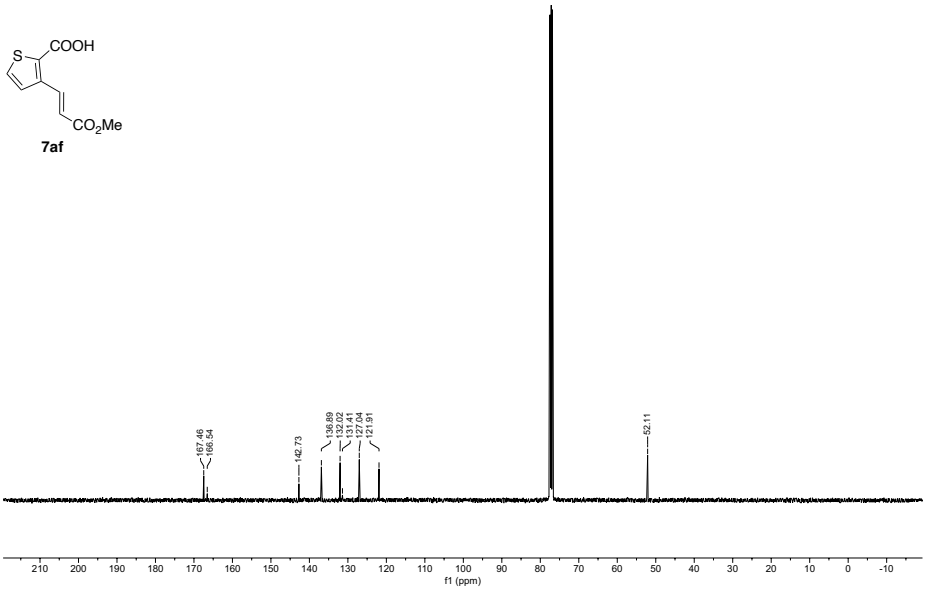
COOH
S
CO2Me
167.46
166.54
142.73
136.89
132.02
131.41
127.74
121.91
52.11
f1 (ppm)

7af

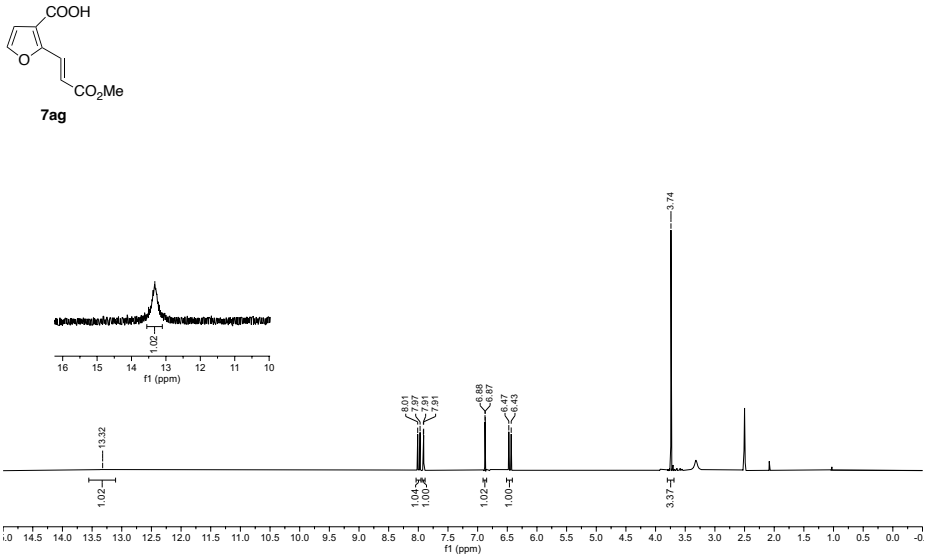
COOH
O
CO2Me
1.02
f1 (ppm)
13.32
8.01
7.97
7.91
7.91
6.88
6.87
6.47
6.45
3.74
1.02
1.04
1.00
1.02
1.00
3.37
f1 (ppm)

7ag

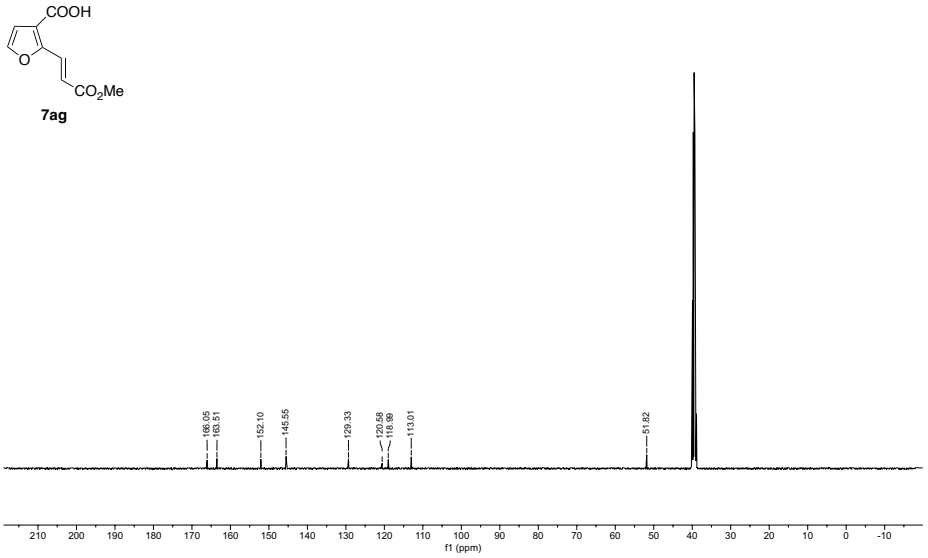
COOH
O
CO2Me
7ag
166.05
163.51
152.10
145.55
129.33
120.58
118.99
113.01
51.82
f1 (ppm)

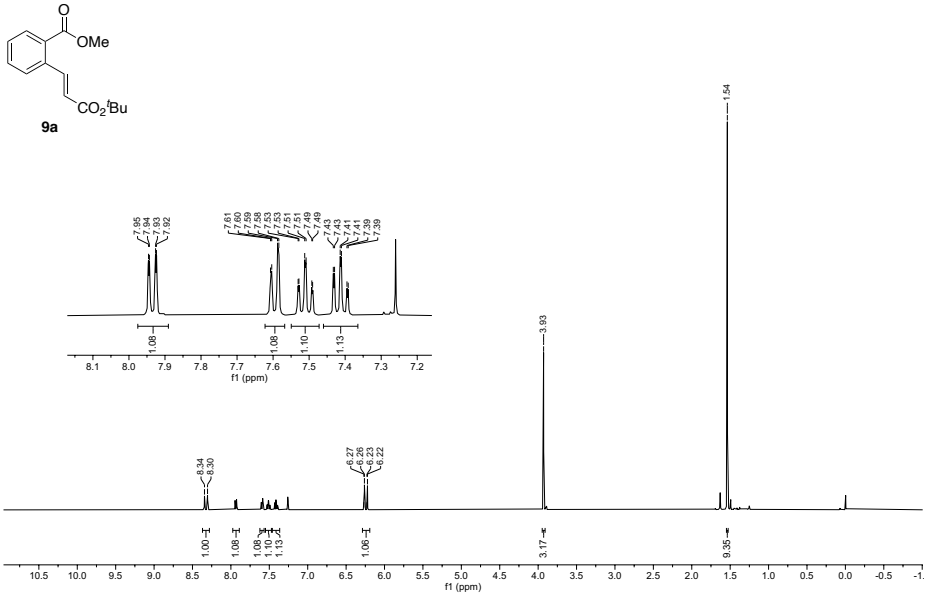
O
OMe
CO2tBu
9a
7.95
7.94
7.93
7.92
7.61
7.60
7.59
7.58
7.53
7.51
7.50
7.49
7.43
7.42
7.41
7.40
7.39
1.08
1.08
1.10
1.13
f1 (ppm)
8.34
8.30
6.27
6.26
6.23
6.22
3.93
1.54
1.00
1.08
1.08
1.10
1.13
1.06
3.17
9.35
f1 (ppm)

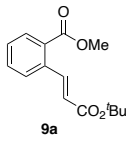
O
OMe
CO2tBu

9a

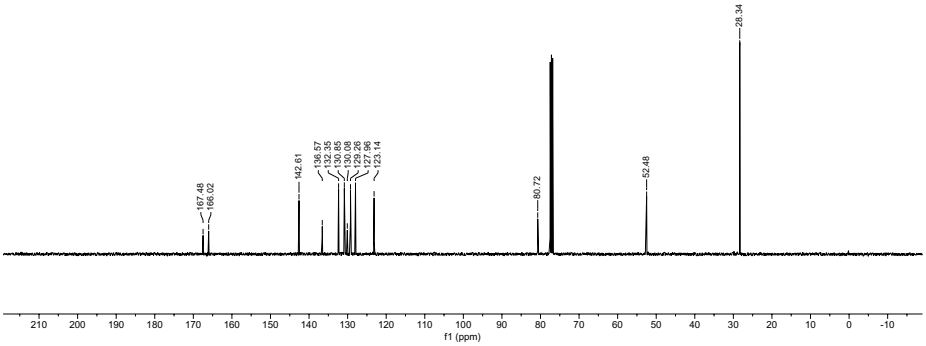
167.48
166.02
142.61
136.57
132.35
130.85
130.69
129.26
127.96
123.14
80.72
52.48
28.34
f1 (ppm)

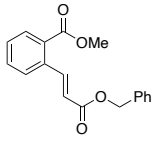
O
OMe
O
Ph
O

9b

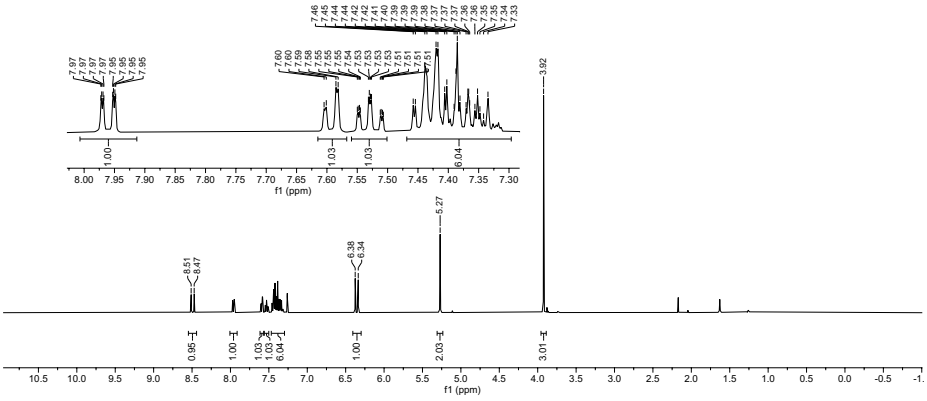
7.97
7.97
7.97
7.97
7.96
7.96
7.95
7.95
7.60
7.59
7.58
7.56
7.55
7.54
7.53
7.53
7.53
7.51
7.51
7.51
7.46
7.45
7.44
7.44
7.42
7.42
7.41
7.40
7.39
7.39
7.39
7.38
7.37
7.37
7.37
7.36
7.36
7.35
7.34
7.33
3.92
1.00
1.03
1.03
6.04
f1 (ppm)
8.51
8.47
8.38
8.34
5.27
0.95
1.00
1.03
1.03
6.04
1.00
2.03
3.01
f1 (ppm)

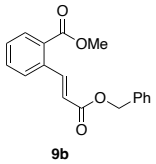
O
OMe
O
Ph
O

9b

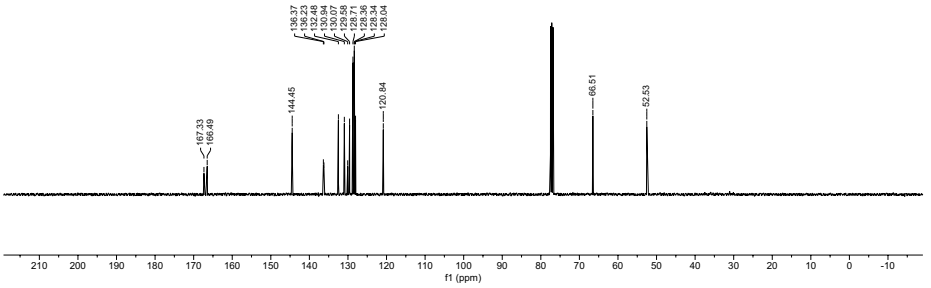
136.37
136.23
132.48
130.84
130.07
129.58
128.71
128.36
128.34
128.04
167.33
166.49
144.45
120.84
66.51
52.53
f1 (ppm)

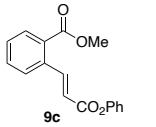
O
OMe
CO2Ph

9c

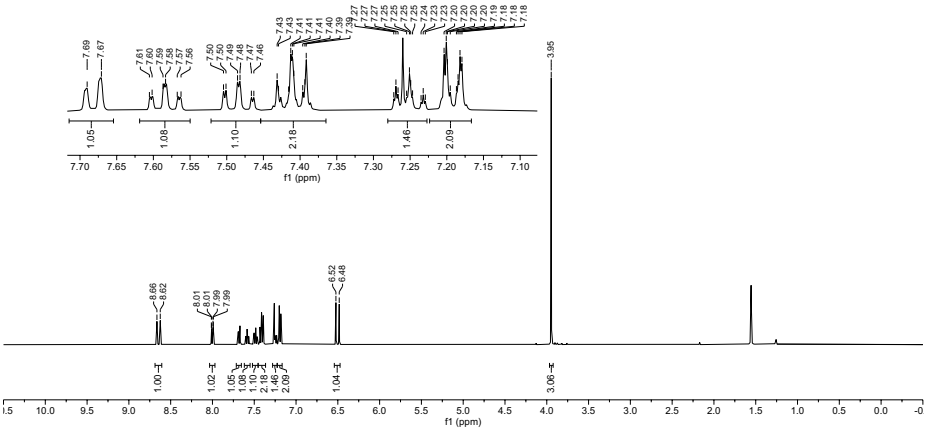
7.69
7.67
7.61
7.60
7.59
7.58
7.57
7.56
7.50
7.50
7.49
7.48
7.47
7.46
7.43
7.43
7.41
7.41
7.41
7.40
7.40
7.39
7.27
7.27
7.25
7.25
7.25
7.25
7.24
7.23
7.23
7.20
7.20
7.20
7.20
7.19
7.18
7.18
7.18
3.95
1.05
1.08
1.10
2.18
1.46
2.09
f1 (ppm)
8.66
8.62
8.01
8.01
7.99
7.99
7.99
6.52
6.48
1.00
1.02
1.05
1.08
1.10
2.18
1.46
2.09
1.04
3.06
f1 (ppm)

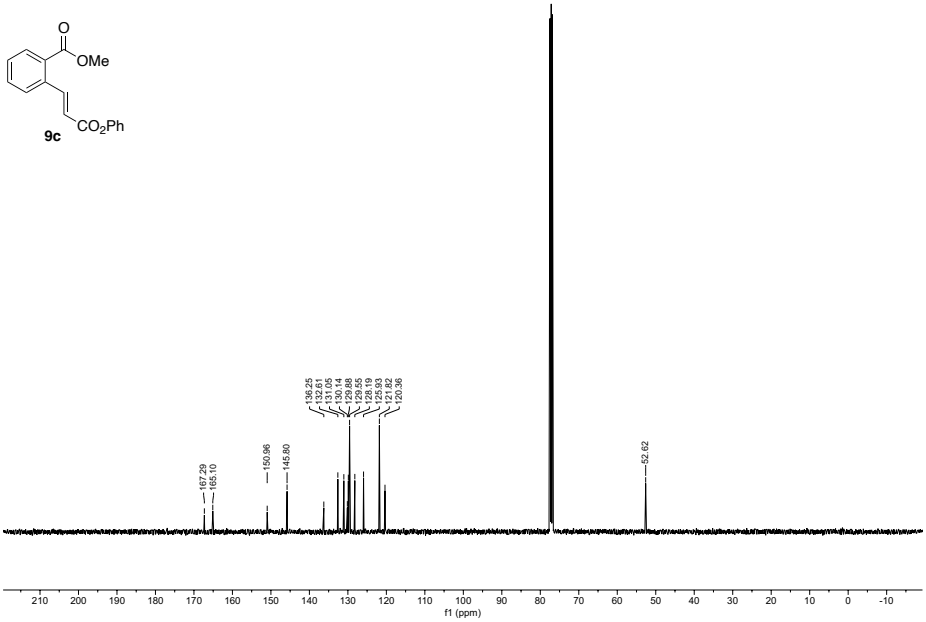
O
OMe
CO2Ph
9c
167.29
165.10
150.96
145.80
135.25
132.51
131.05
130.14
129.88
129.55
128.19
125.93
122.82
120.36
52.62
f1 (ppm)

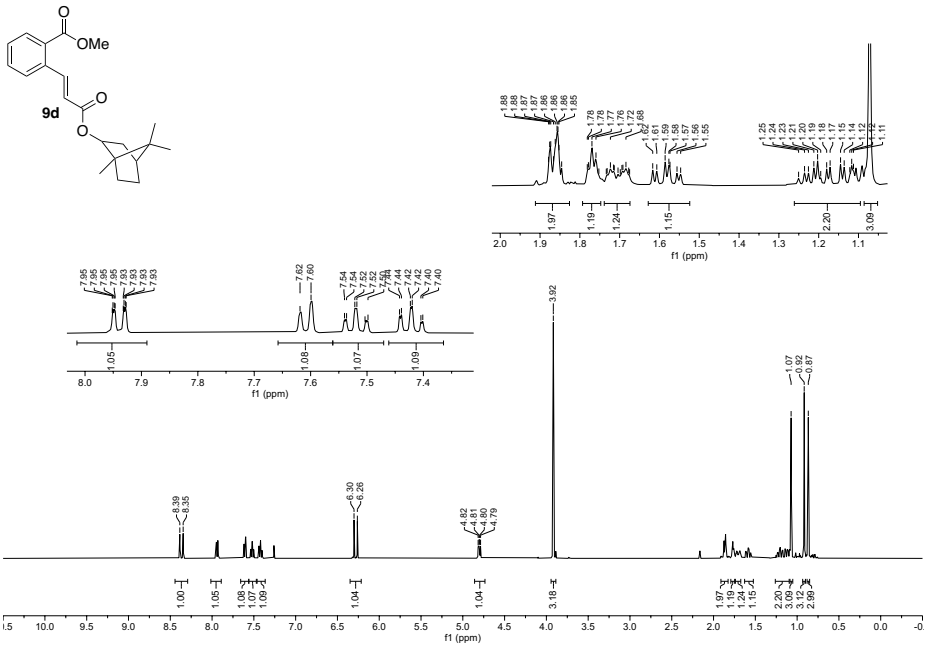
O
OMe
O
O
9d
1.97
1.19
1.24
1.15
2.20
3.09
f1 (ppm)
1.05
1.08
1.07
1.09
f1 (ppm)
3.92
1.07
0.82
0.87
8.39
8.35
6.30
6.26
4.82
4.81
4.80
4.79
1.00
1.05
1.08
1.07
1.09
1.04
1.04
3.18
1.97
1.19
1.24
1.15
2.20
3.09
3.12
2.99
f1 (ppm)

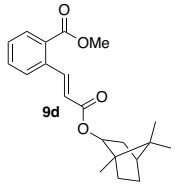
O
OMe
O
O
9d

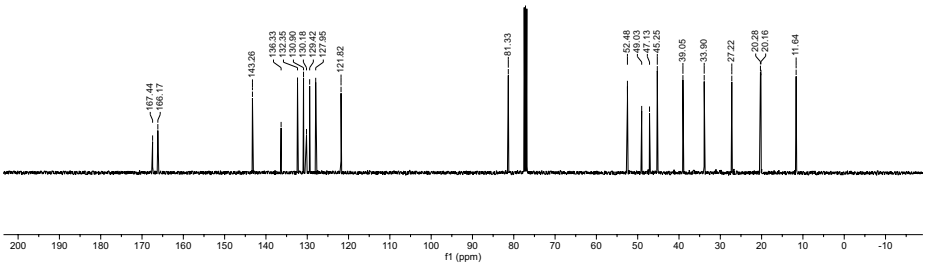
167.44
166.17
143.26
136.33
132.35
130.90
130.18
129.03
127.64
121.82
81.33
52.48
49.03
47.13
45.25
39.05
33.90
27.22
20.28
20.16
11.64
f1 (ppm)

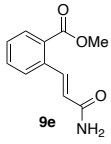
O
OMe
O
9e
NH2

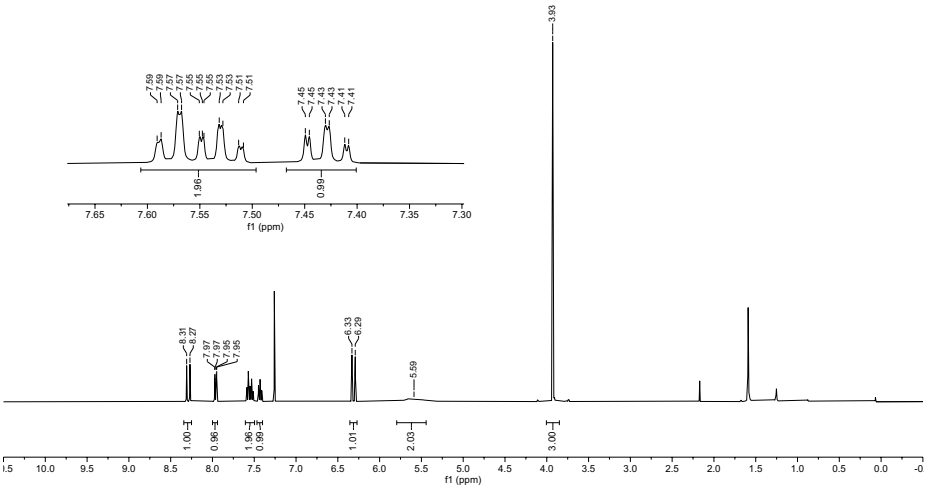
3.93
7.59
7.59
7.57
7.57
7.55
7.55
7.55
7.53
7.53
7.51
7.51
7.45
7.45
7.43
7.43
7.41
7.41
1.96
0.99
f1 (ppm)
8.31
8.27
7.97
7.97
7.95
7.95
6.33
6.29
5.59
1.00
0.96
1.96
0.99
1.01
2.03
3.00
f1 (ppm)

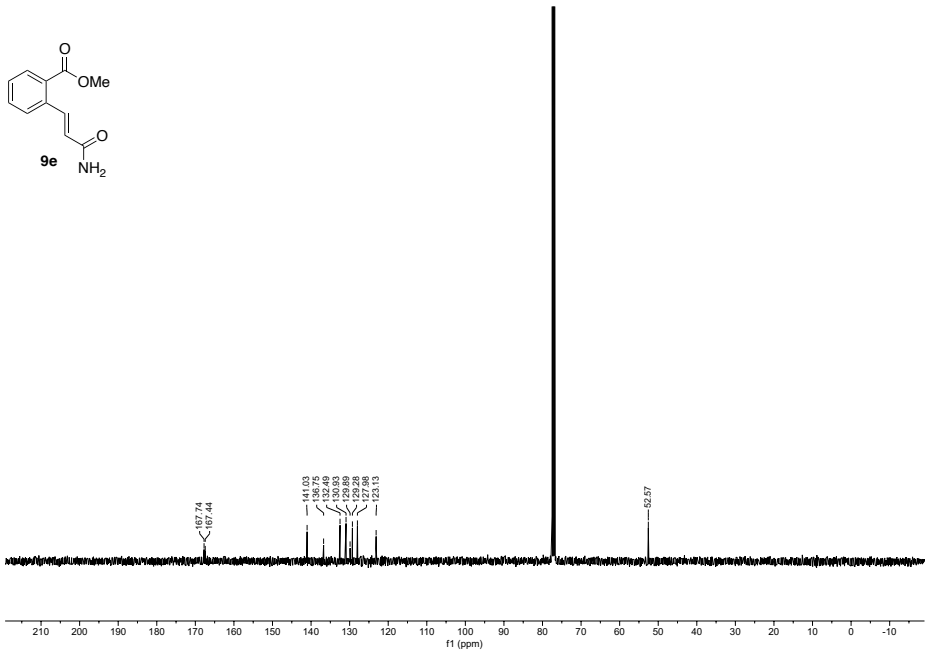
O
OMe
O
NH2
9e
167.74
167.44
141.03
136.75
132.49
130.63
129.89
129.28
127.98
123.15
52.57
f1 (ppm)

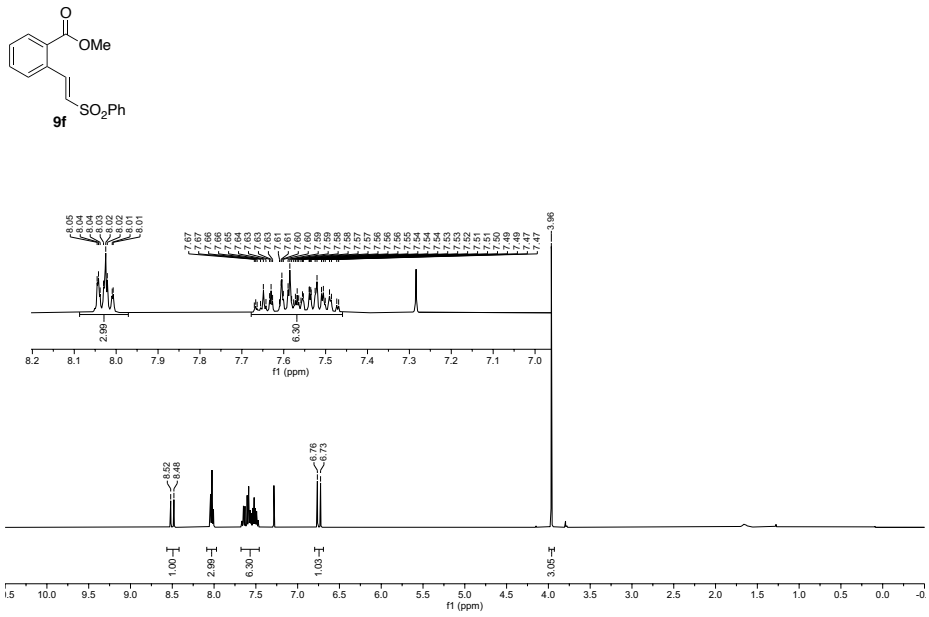
O
OMe
SO2Ph
9f
8.05
8.04
8.04
8.03
8.02
8.02
8.02
8.01
8.01
7.67
7.67
7.67
7.66
7.66
7.65
7.64
7.64
7.63
7.63
7.61
7.61
7.60
7.60
7.59
7.59
7.58
7.58
7.57
7.57
7.56
7.56
7.55
7.55
7.54
7.54
7.54
7.53
7.53
7.52
7.51
7.51
7.50
7.49
7.49
7.47
7.47
3.96
2.99
6.30
f1 (ppm)
8.52
8.48
6.76
6.73
1.00
2.99
6.30
1.03
3.05
f1 (ppm)

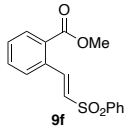
O
OMe
SO2Ph

9f

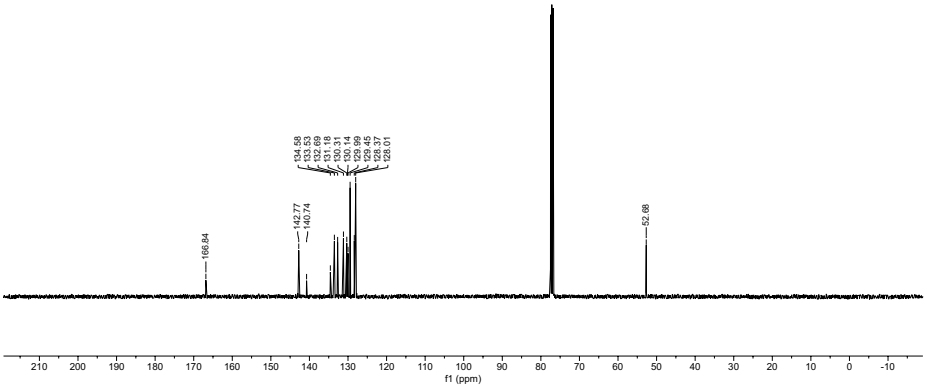
166.84
142.77
140.74
134.58
133.53
132.69
131.16
130.31
130.14
129.99
129.45
128.37
128.01
52.68
f1 (ppm)

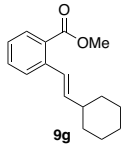
O
OMe

9g

7.87
7.87
7.85
7.85
7.57
7.55
7.47
7.47
7.45
7.45
7.28
7.27
7.26
7.25
7.24
7.16
7.12
3.92
2.23
2.22
2.22
2.21
2.21
2.20
2.20
2.19
2.19
2.19
1.89
1.88
1.86
1.85
1.85
1.85
1.81
1.78
1.37
1.35
1.34
1.33
1.31
1.28
1.28
1.27
1.27
1.25
1.24
1.24
1.23
1.22
1.21
6.14
6.12
6.10
6.08
1.00
0.98
1.10
1.18
0.97
0.97
3.02
1.14
5.42
5.29
f1 (ppm)

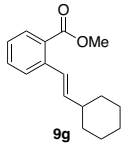
O
OMe

9g

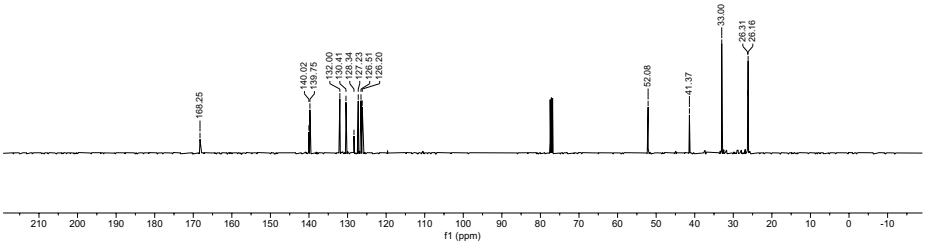
168.25
140.02
139.75
132.00
130.41
129.24
127.43
126.51
126.20
52.08
41.37
33.00
26.31
26.16
f1 (ppm)

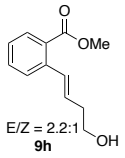
O
OMe
OH

E/Z = 2.2:1

9h

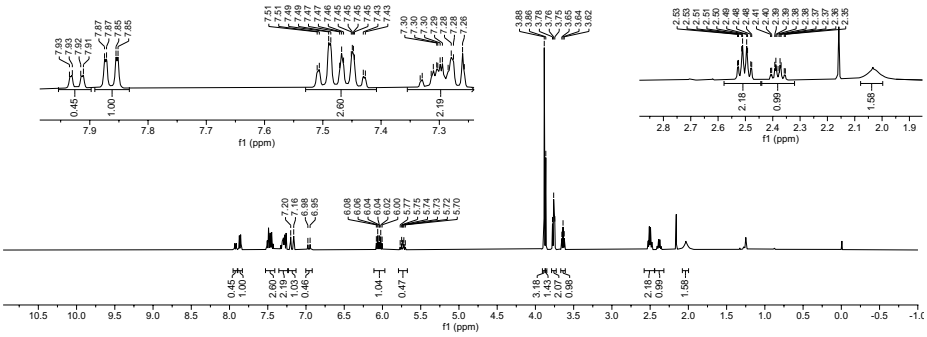
f1 (ppm)

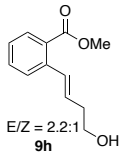
O
OMe
E/Z = 2.2:1
OH

9h

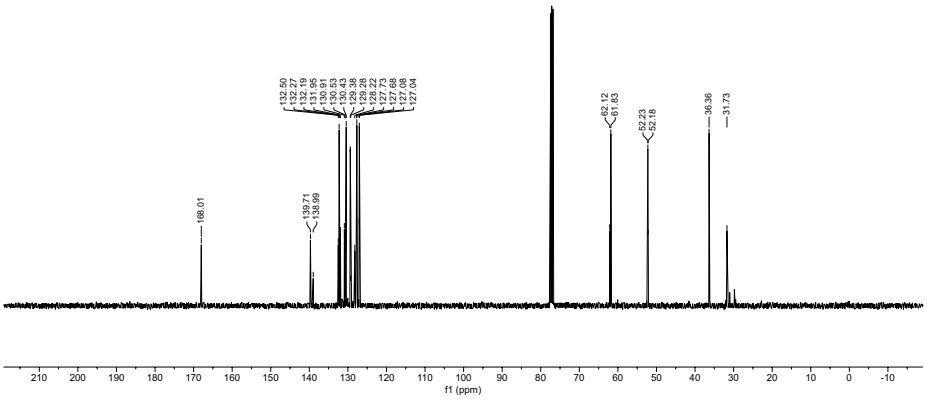
168.01
139.71
138.99
132.50
132.27
132.19
131.95
130.91
130.53
130.43
129.38
129.28
128.22
127.73
127.68
127.08
127.04
62.12
61.83
52.23
52.16
36.36
31.73
f1 (ppm)

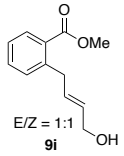
O
OMe
E/Z = 1:1
OH

9i

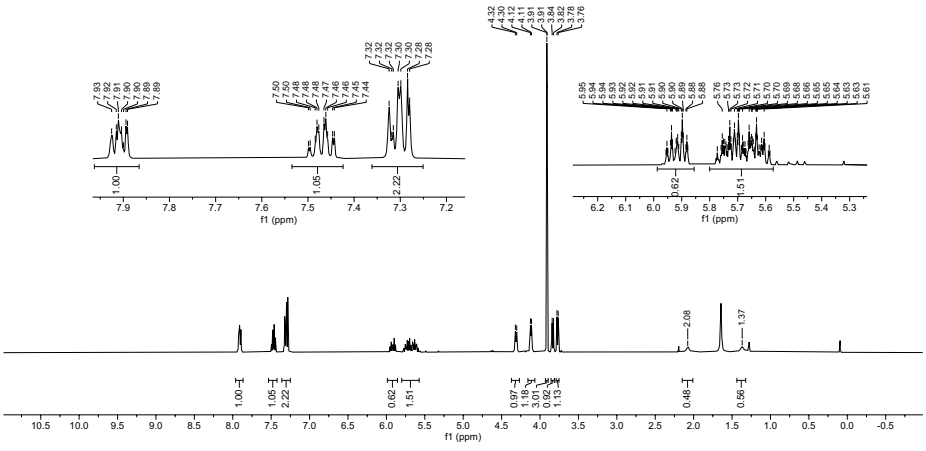
7.93
7.92
7.91
7.90
7.89
7.89
7.50
7.50
7.48
7.48
7.47
7.46
7.46
7.45
7.44
7.32
7.32
7.32
7.30
7.30
7.28
7.28
4.32
4.30
4.12
4.11
3.91
3.84
3.82
3.78
3.76
5.95
5.94
5.94
5.93
5.92
5.92
5.91
5.91
5.90
5.90
5.89
5.88
5.88
5.76
5.73
5.73
5.72
5.71
5.71
5.70
5.70
5.69
5.68
5.66
5.65
5.64
5.63
5.63
5.61
2.08
1.37
f1 (ppm)

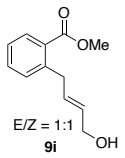
O
OMe
E/Z = 1:1
OH

9i

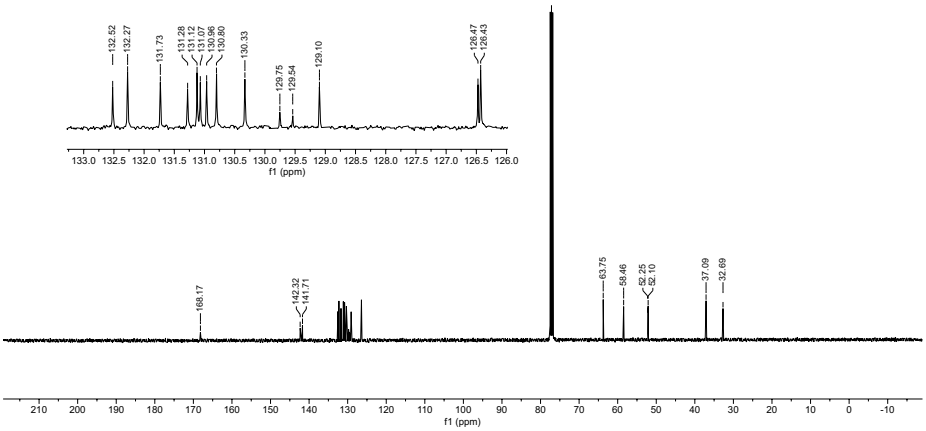
132.52
132.27
131.73
131.28
131.12
131.07
130.96
130.80
130.33
129.75
129.54
129.10
126.47
126.43
168.17
142.32
141.71
63.75
58.46
52.25
52.10
37.09
32.69
f1 (ppm)

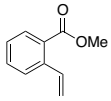
O
OMe

9j

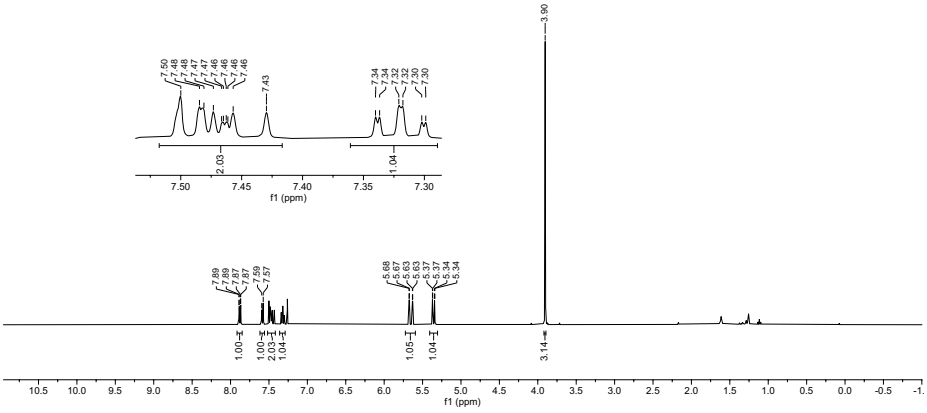
7.50
7.48
7.48
7.47
7.47
7.46
7.46
7.46
7.46
7.43
7.34
7.34
7.32
7.32
7.30
7.30
2.03
1.04
f1 (ppm)
7.89
7.89
7.87
7.87
7.59
7.57
5.68
5.67
5.63
5.63
5.37
5.37
5.34
5.34
3.90
1.00
1.00
2.03
1.04
1.05
1.04
3.14
f1 (ppm)

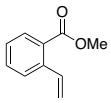
O
OMe

9j

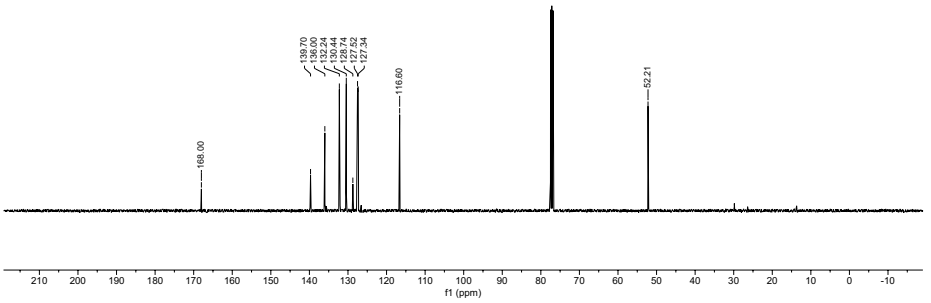
139.70
138.00
132.44
130.44
128.74
127.93
127.34
116.60
52.21
168.00
f1 (ppm)

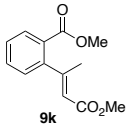
O
OMe
CO2Me

9k

7.92
7.92
7.90
7.90
7.52
7.51
7.50
7.50
7.48
7.48
7.41
7.41
7.39
7.39
7.37
7.37
7.20
7.20
7.18
7.18
3.86
3.74
2.46
2.45
5.75
5.74
1.06
1.17
1.12
1.02
1.08
3.00
3.03
3.01
f1 (ppm)

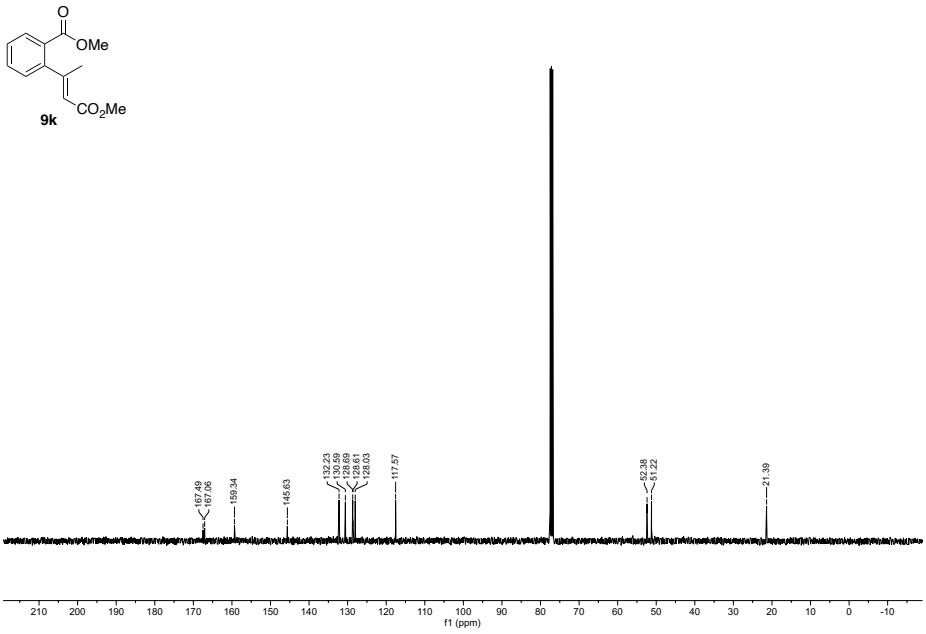
O
OMe
CO2Me
9k
167.49
167.06
159.34
145.63
132.23
130.59
130.09
128.61
128.03
117.57
55.28
51.22
21.39
f1 (ppm)

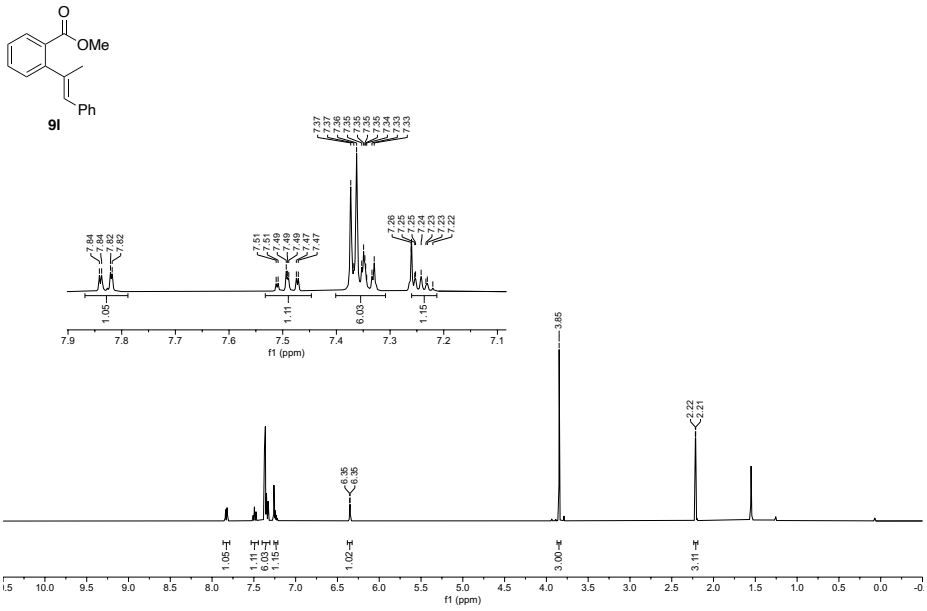
O
OMe
Ph
9l
7.84
7.82
7.51
7.49
7.47
7.37
7.36
7.35
7.34
7.33
7.26
7.25
7.24
7.23
7.22
1.05
1.11
6.03
1.15
3.85
2.22
2.21
6.35
6.35
1.05
1.11
6.03
1.15
1.02
3.00
3.11
f1 (ppm)

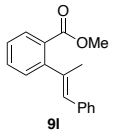
O
OMe
Ph

9l

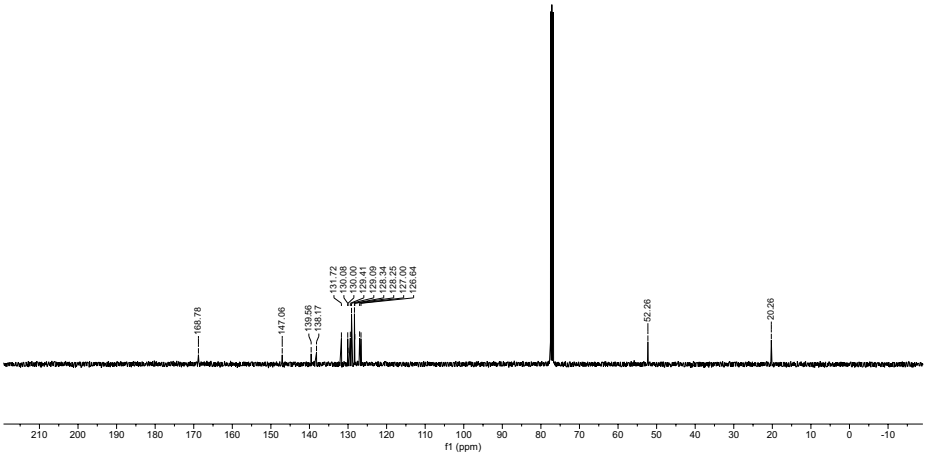
160.76
147.06
139.56
138.17
131.72
130.08
130.00
129.41
129.09
128.34
128.25
127.00
126.64
52.26
20.26
f1 (ppm)

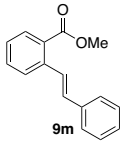
O
OMe

9m

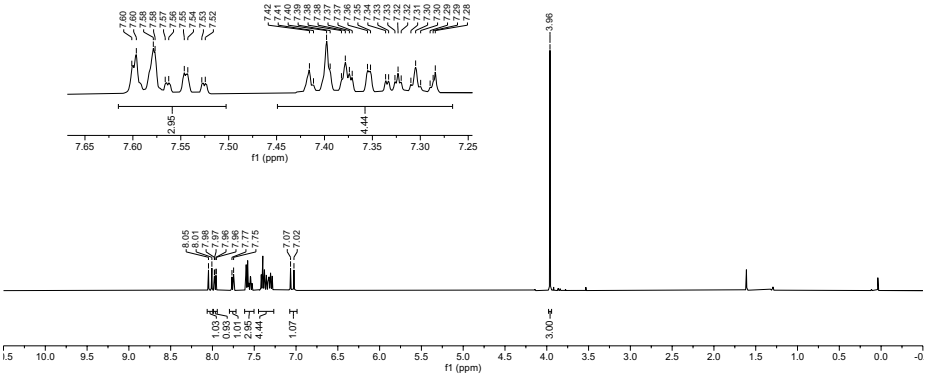
7.60
7.60
7.58
7.58
7.58
7.57
7.56
7.55
7.54
7.53
7.52
7.42
7.41
7.40
7.39
7.38
7.38
7.37
7.37
7.36
7.35
7.34
7.33
7.33
7.32
7.32
7.31
7.30
7.30
7.29
7.29
7.28
3.96
2.95
4.44
f1 (ppm)
8.05
8.01
7.98
7.97
7.96
7.96
7.77
7.75
7.07
7.02
1.03
1.03
1.01
2.95
4.44
1.07
3.00
f1 (ppm)

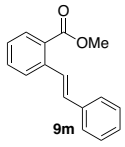
O
OMe

9m

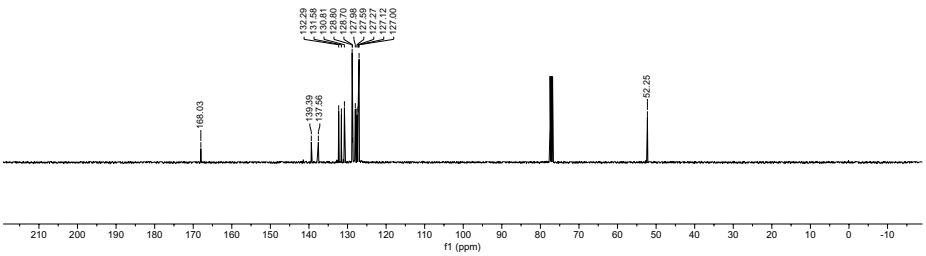
132.29
131.58
130.81
129.60
128.70
127.98
127.79
127.27
127.12
127.00
168.03
139.39
137.56
52.25
f1 (ppm)

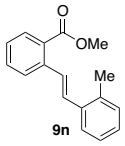
O
OMe
Me

9n

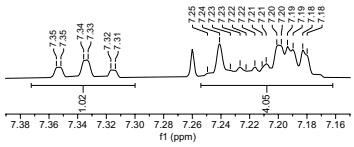
7.35
7.35
7.34
7.33
7.32
7.31
7.25
7.24
7.24
7.23
7.23
7.22
7.22
7.21
7.21
7.20
7.20
7.19
7.19
7.18
7.18
1.02
4.05
f1 (ppm)

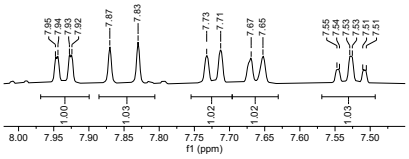
7.95
7.94
7.93
7.92
7.87
7.83
7.73
7.71
7.67
7.65
7.55
7.54
7.53
7.53
7.51
7.51
1.00
1.03
1.02
1.02
1.03
f1 (ppm)

3.93
3.93
2.44
1.00
1.03
1.02
1.02
1.03
1.02
4.05
3.12
3.01
f1 (ppm)

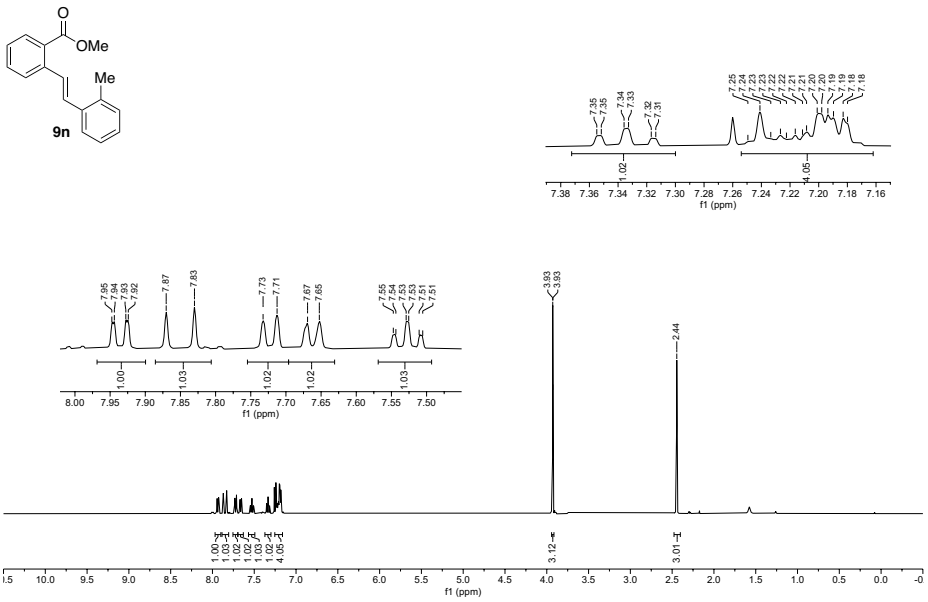
O
OMe
Me
9n
f1 (ppm)

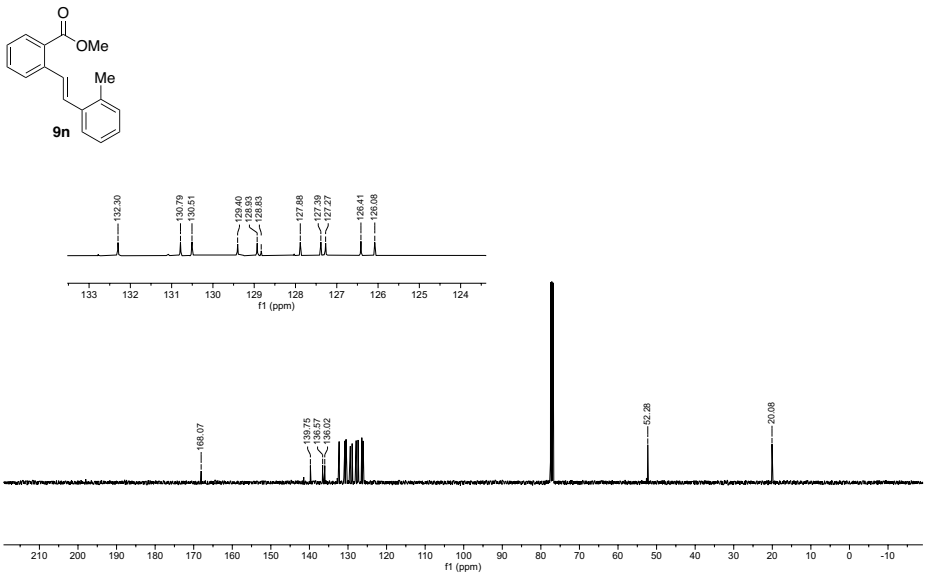
O
OMe
Me
9n
f1 (ppm)

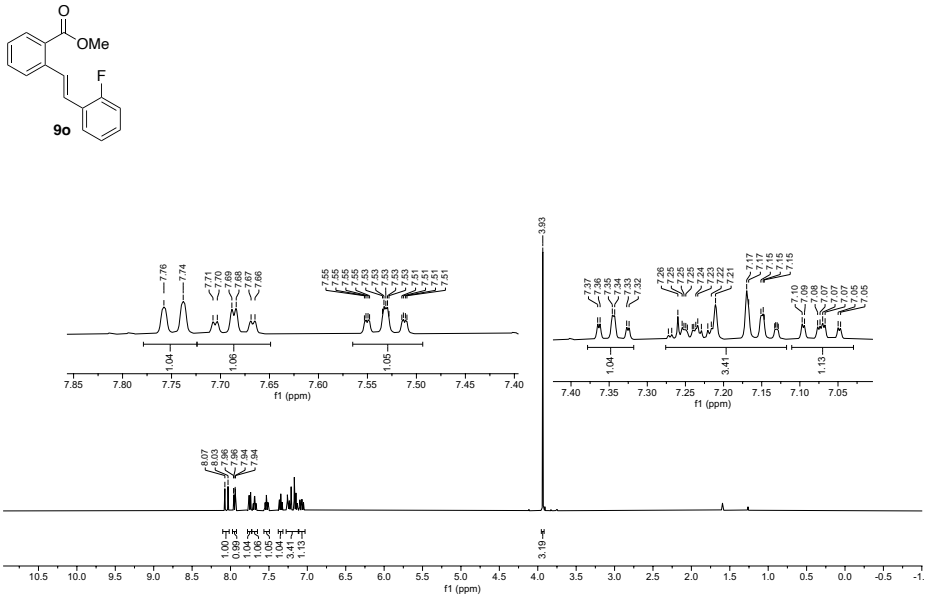
O
OMe
F
9o
f1 (ppm)

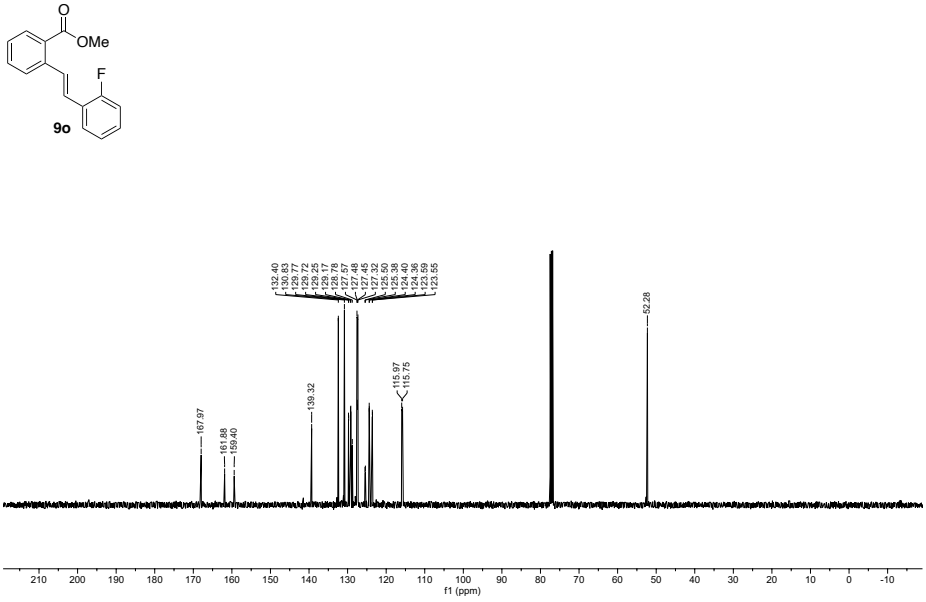
O
OMe
F
9o
f1 (ppm)

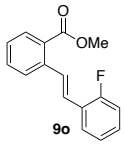
O
OMe
F

9o

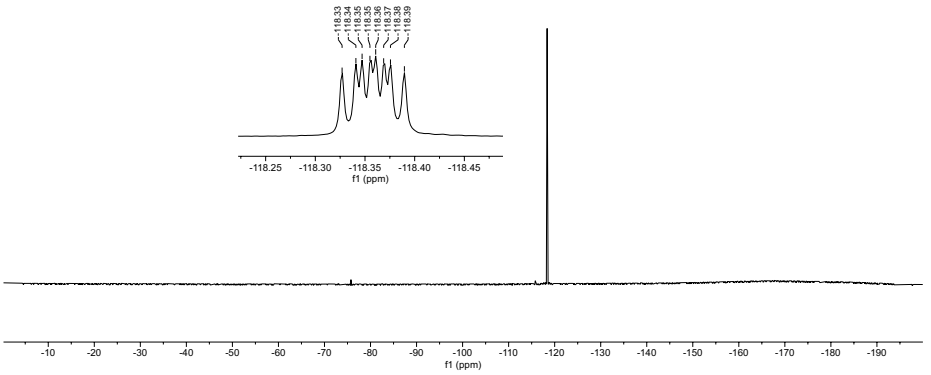
-118.33
-118.34
-118.35
-118.35
-118.36
-118.37
-118.38
-118.39
-118.25
-118.30
-118.35
-118.40
-118.45
f1 (ppm)
-10
-20
-30
-40
-50
-60
-70
-80
-90
-100
-110
-120
-130
-140
-150
-160
-170
-180
-190
f1 (ppm)

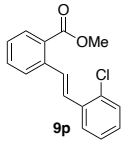
O
OMe
Cl

9p

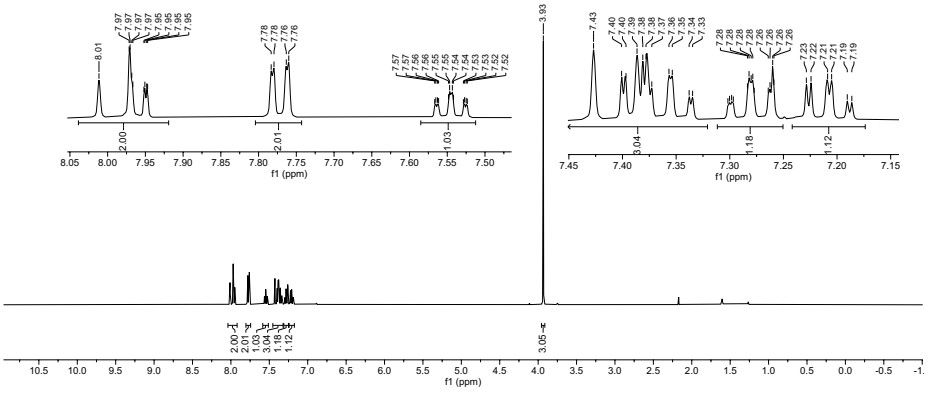
8.01
7.97
7.97
7.97
7.97
7.96
7.95
7.95
7.95
7.78
7.78
7.78
7.76
7.76
7.57
7.57
7.56
7.56
7.55
7.55
7.54
7.54
7.53
7.53
7.52
7.52
2.00
2.01
1.03
8.05
8.00
7.95
7.90
7.85
7.80
7.75
7.70
7.65
7.60
7.55
7.50
f1 (ppm)
3.93
7.43
7.40
7.40
7.39
7.38
7.38
7.37
7.36
7.35
7.34
7.33
7.28
7.28
7.28
7.28
7.26
7.26
7.26
7.26
7.23
7.22
7.21
7.21
7.19
7.19
3.04
1.18
1.12
7.45
7.40
7.35
7.30
7.25
7.20
7.15
f1 (ppm)
2.00
2.01
1.03
3.04
1.18
1.12
3.05
10.5
10.0
9.5
9.0
8.5
8.0
7.5
7.0
6.5
6.0
5.5
5.0
4.5
4.0
3.5
3.0
2.5
2.0
1.5
1.0
0.5
0.0
-0.5
f1 (ppm)

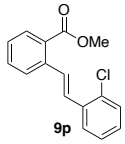
O
OMe
Cl

9p

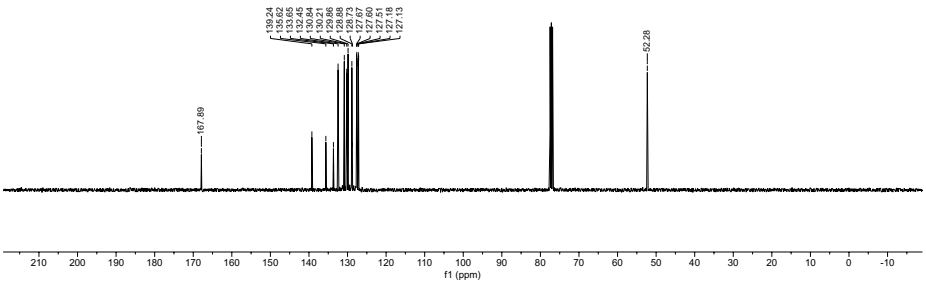
139.24
135.62
133.66
132.45
130.84
130.21
129.86
128.88
128.73
127.67
127.60
127.51
127.18
127.13
167.89
52.28
f1 (ppm)

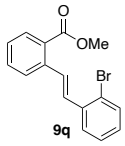
O
OMe
Br

9q

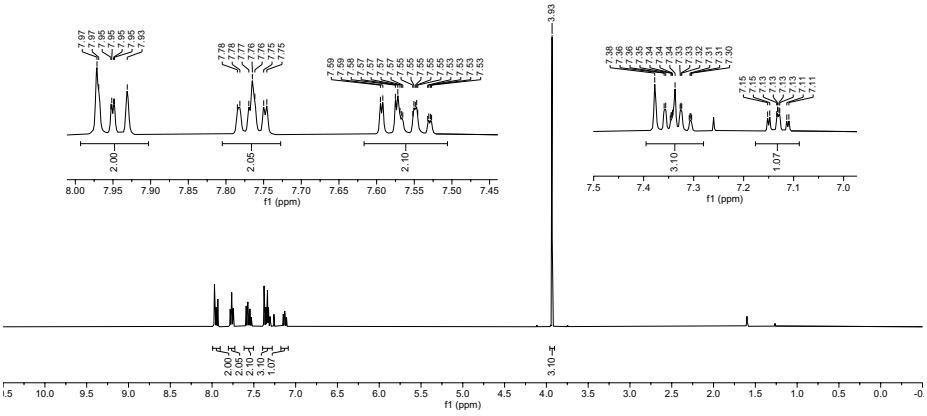
7.97
7.97
7.95
7.95
7.95
7.95
7.93
7.78
7.78
7.77
7.77
7.76
7.76
7.75
7.75
7.59
7.59
7.58
7.58
7.57
7.57
7.57
7.55
7.55
7.55
7.55
7.53
7.53
7.53
7.53
3.93
7.38
7.36
7.36
7.35
7.34
7.34
7.34
7.33
7.32
7.31
7.31
7.30
7.15
7.15
7.13
7.13
7.13
7.13
7.11
7.11
2.00
2.05
2.10
3.10
1.07
f1 (ppm)

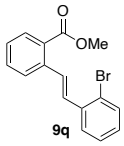
O
OMe
Br

9q

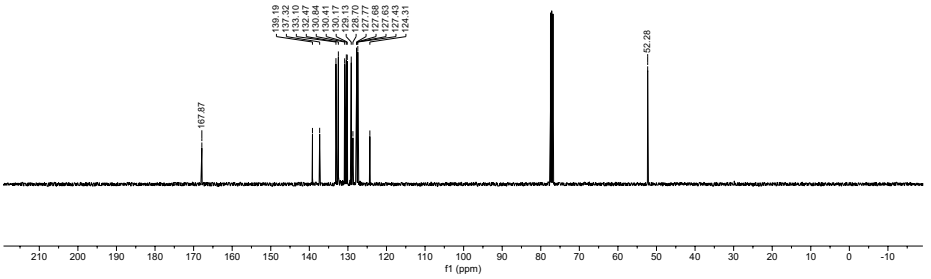
167.87
139.19
137.32
133.10
132.47
130.84
130.41
130.17
129.13
128.70
127.77
127.68
127.63
127.43
124.31
52.28
f1 (ppm)

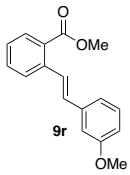
O
OMe
OMe

9r

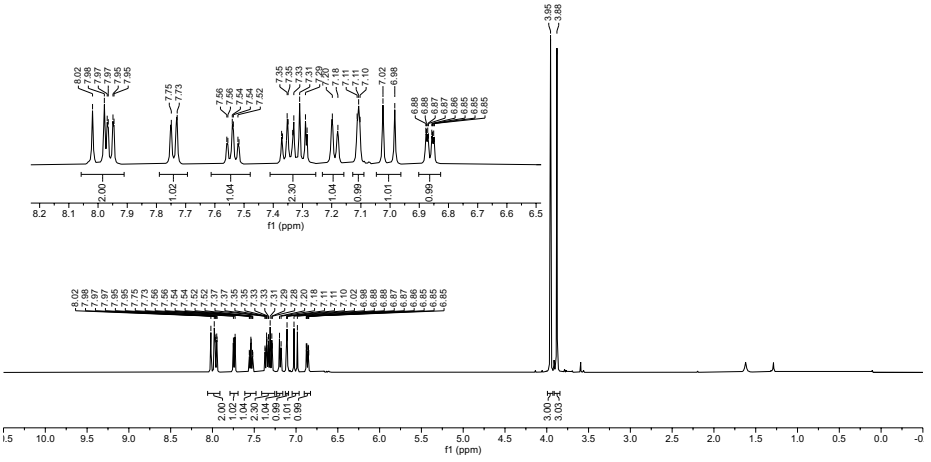
3.95
3.88
f1 (ppm)

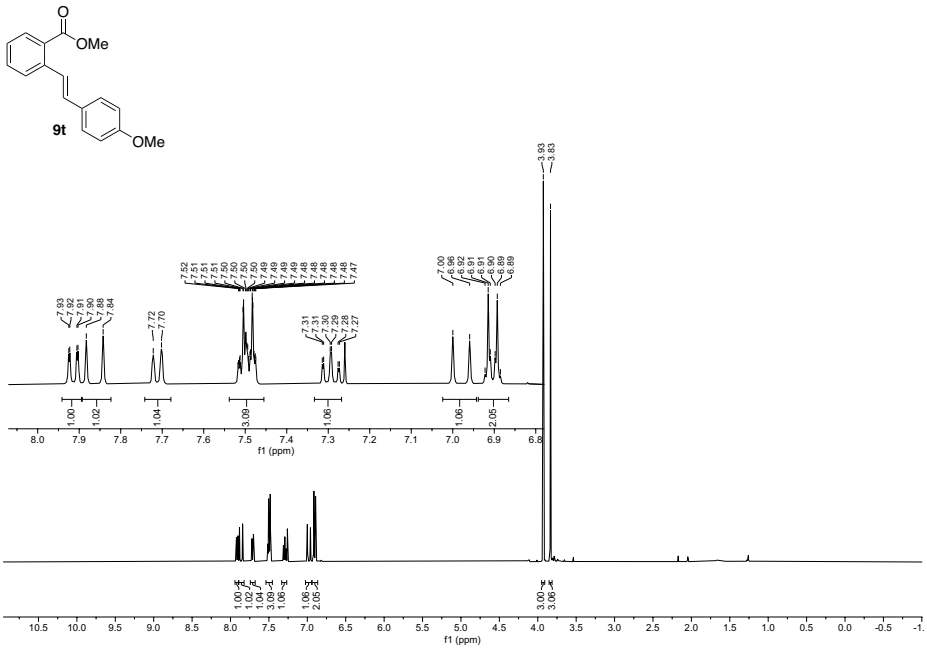
O
OMe
9t
OMe
f1 (ppm)

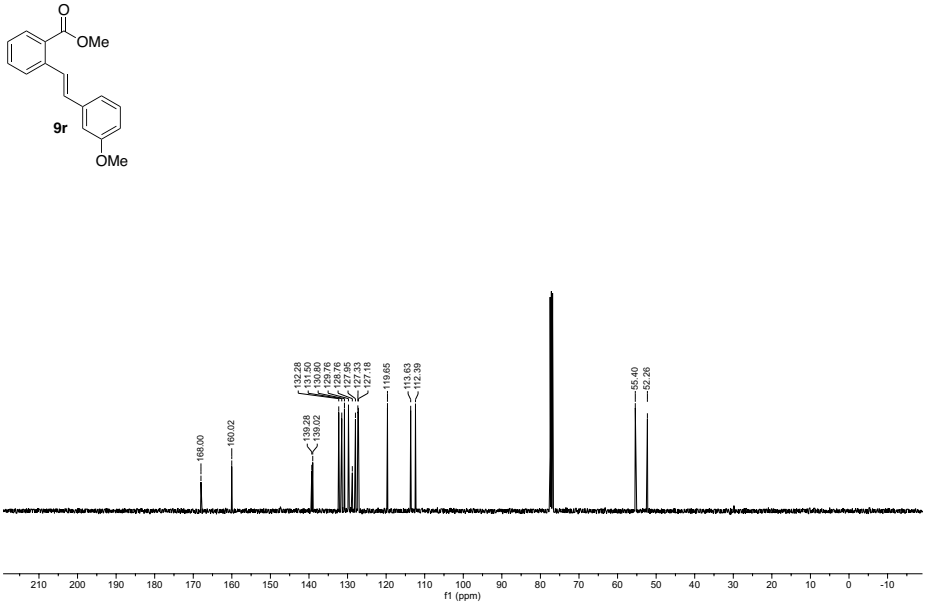
O
OMe
9r
OMe
f1 (ppm)

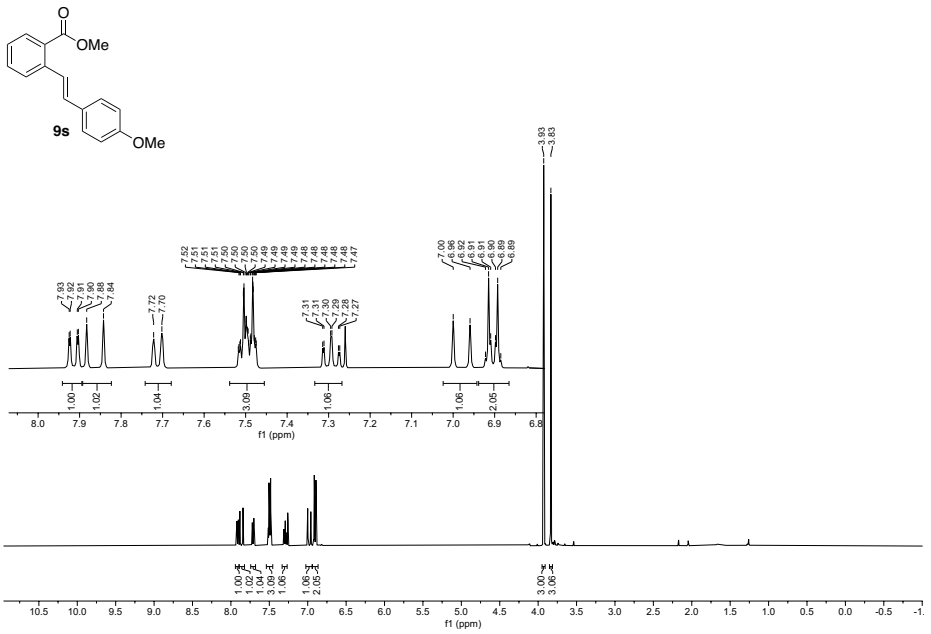
O
OMe
9s
OMe
3.93
3.83
7.52
7.51
7.51
7.51
7.50
7.50
7.50
7.50
7.49
7.49
7.49
7.49
7.48
7.48
7.48
7.48
7.47
7.00
6.95
6.92
6.91
6.91
6.90
6.89
6.89
7.93
7.92
7.91
7.90
7.88
7.84
7.72
7.70
7.31
7.31
7.30
7.29
7.28
7.27
1.00
1.02
1.04
3.09
1.06
1.06
2.05
f1 (ppm)
3.00
3.06

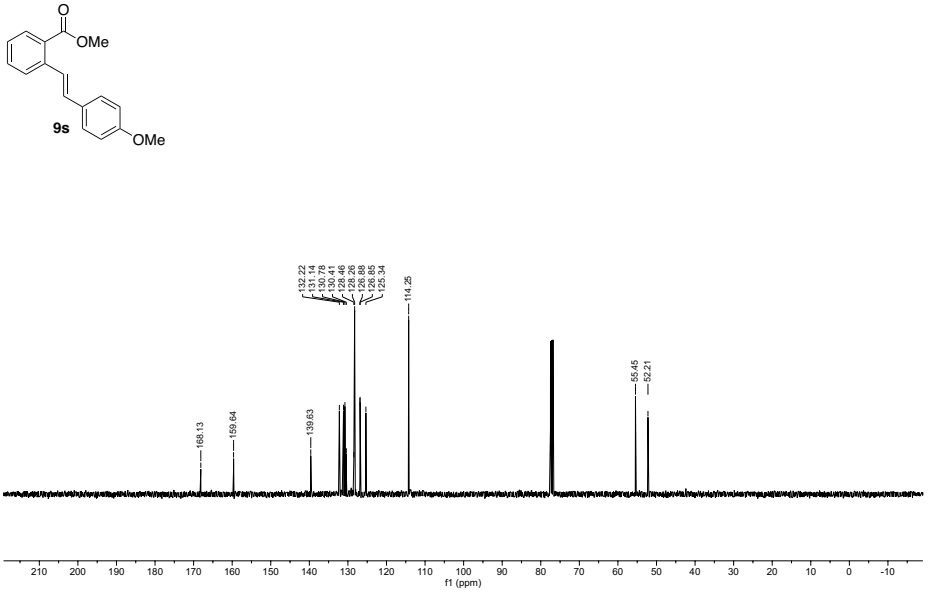
O
OMe
9s
OMe
132.22
131.14
130.78
130.41
128.46
128.25
126.88
126.85
125.34
114.25
168.13
159.64
139.63
55.45
52.21
f1 (ppm)

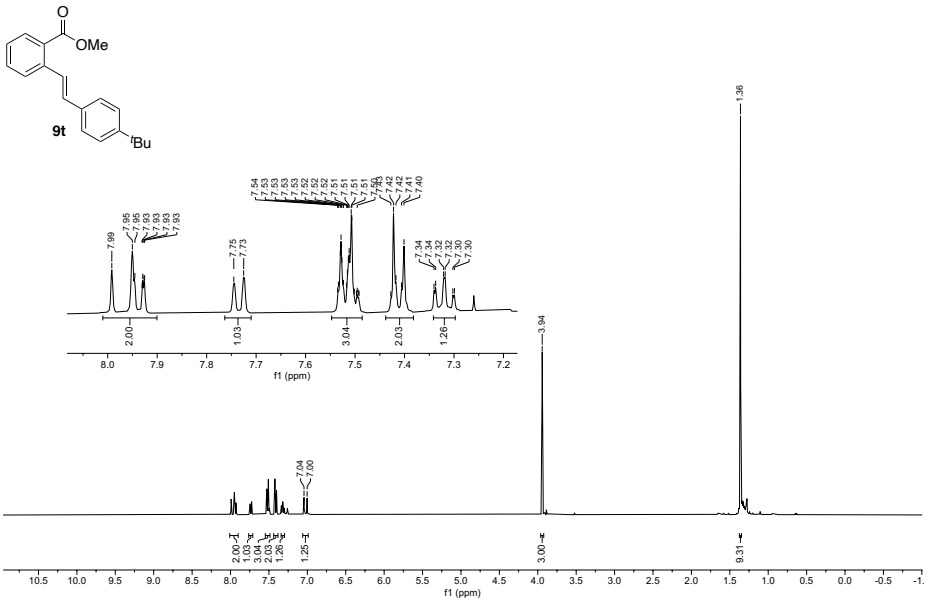
O
OMe
9t
tBu
7.99
7.96
7.95
7.93
7.93
7.93
7.93
7.75
7.73
7.54
7.53
7.53
7.53
7.53
7.52
7.52
7.52
7.51
7.51
7.51
7.51
7.50
7.43
7.43
7.42
7.41
7.40
7.34
7.34
7.32
7.32
7.30
7.30
1.36
3.94
7.04
7.00
2.00
1.03
3.04
2.03
1.26
1.25
3.00
9.31
f1 (ppm)

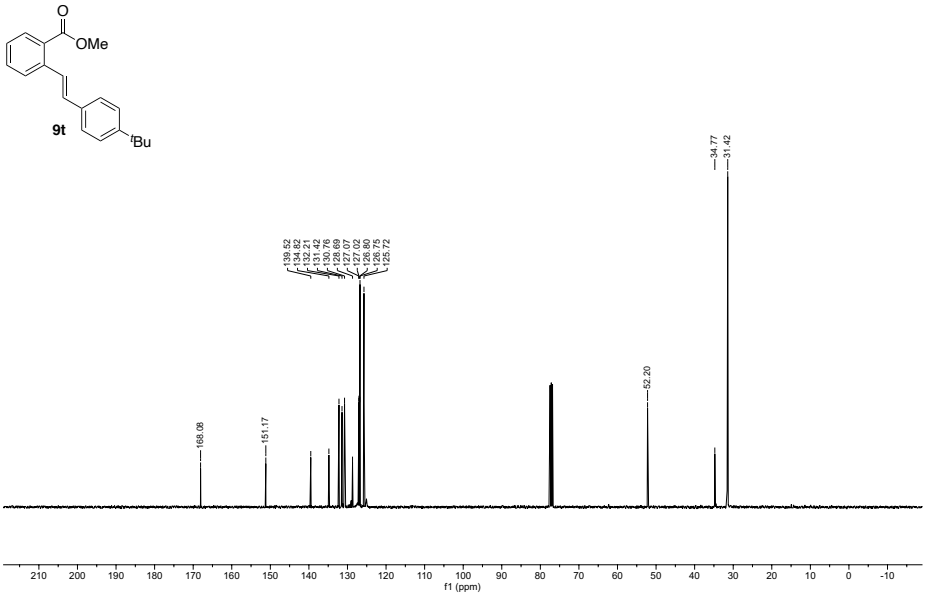
O
OMe
9t
tBu
34.77
31.42
139.52
134.82
134.21
131.42
130.76
129.69
127.07
127.02
126.80
125.75
125.72
52.20
168.08
151.17
f1 (ppm)

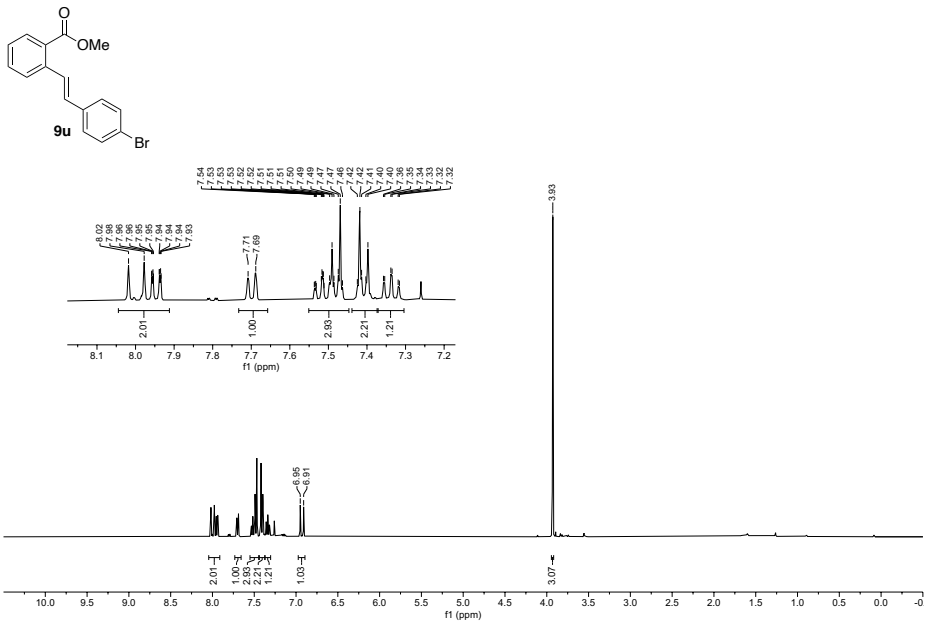
O
OMe
9u
Br
f1 (ppm)

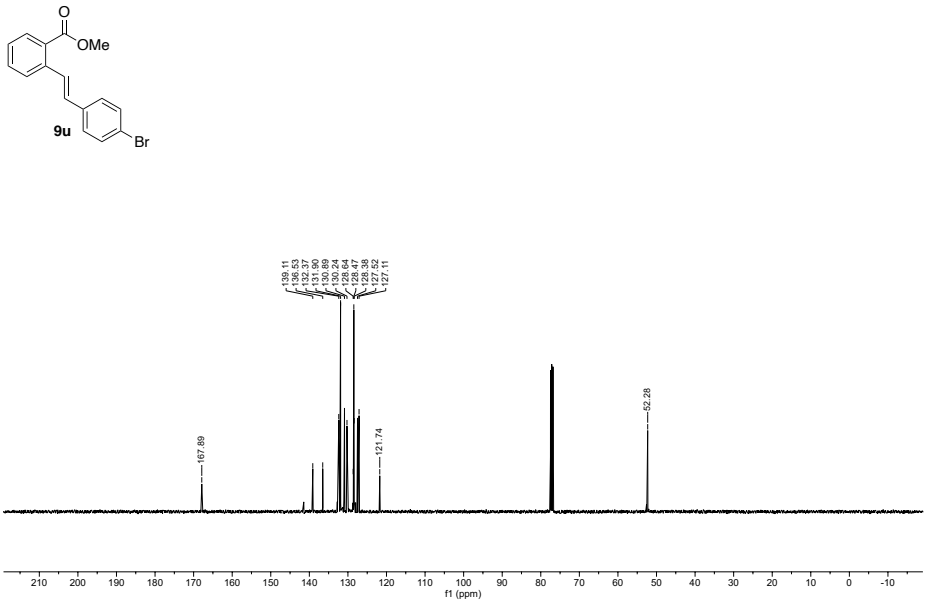
O
OMe
9u
Br
f1 (ppm)

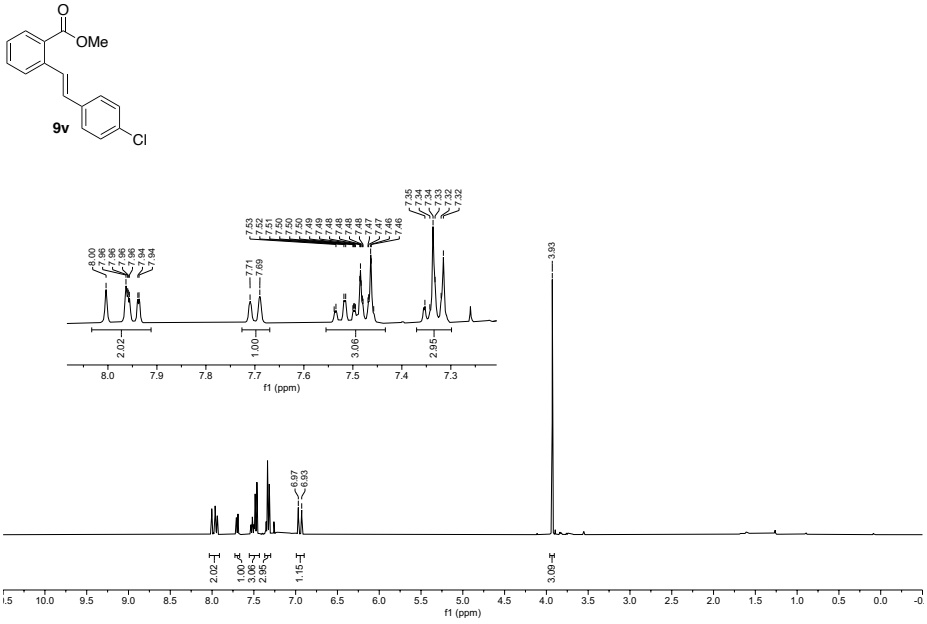
O
OMe
9v
Cl
8.00
7.96
7.96
7.96
7.96
7.94
7.94
7.71
7.69
7.53
7.52
7.51
7.50
7.50
7.50
7.49
7.49
7.48
7.48
7.48
7.48
7.47
7.47
7.46
7.46
7.35
7.34
7.34
7.33
7.32
7.32
3.93
6.97
6.95
2.02
1.00
3.06
2.95
1.15
3.09
f1 (ppm)

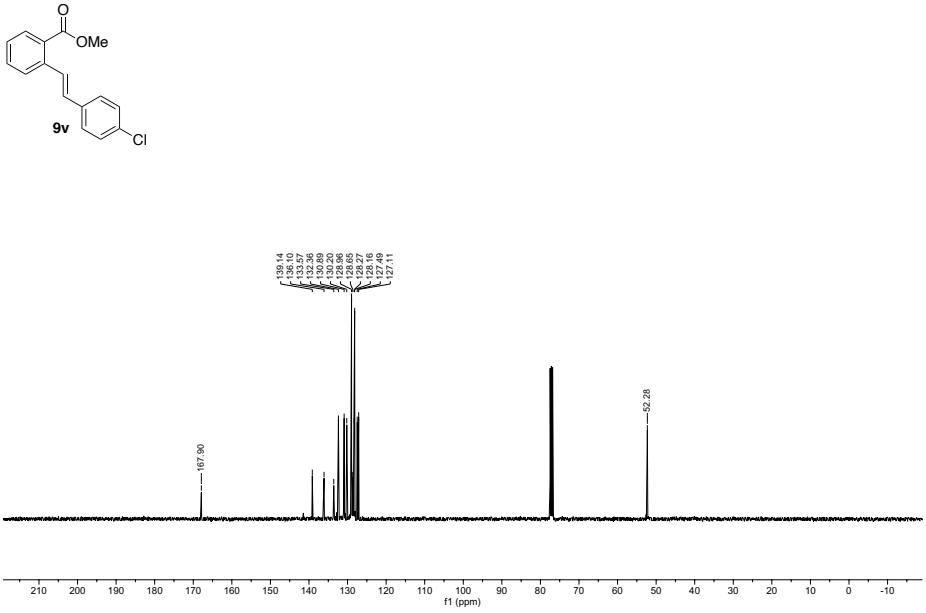
O
OMe
9v
Cl
139.14
136.10
133.57
132.36
130.89
130.20
128.96
128.85
128.77
128.27
128.16
127.49
127.11
167.90
52.28
f1 (ppm)

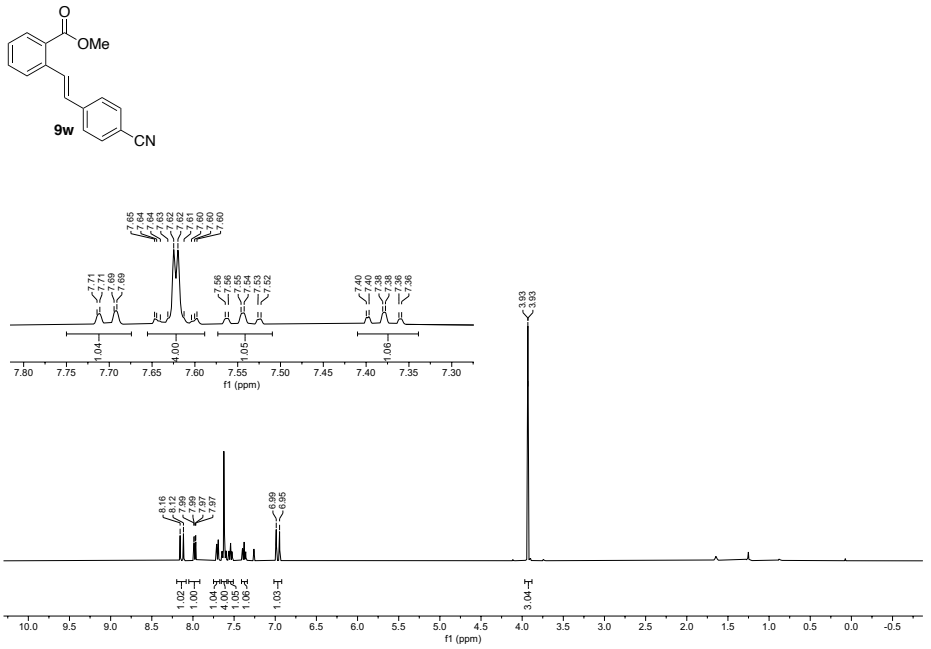
O
OMe
9w
CN
7.65
7.64
7.64
7.63
7.62
7.62
7.61
7.60
7.60
7.60
7.71
7.71
7.69
7.69
7.56
7.55
7.55
7.54
7.53
7.52
7.40
7.40
7.39
7.38
7.36
7.36
3.93
3.93
1.04
4.00
1.05
1.06
7.80
7.75
7.70
7.65
7.60
7.55
7.50
7.45
7.40
7.35
7.30
f1 (ppm)
8.16
8.13
7.99
7.98
7.99
7.97
7.97
6.99
6.95
1.02
1.00
4.00
1.04
1.05
1.06
1.03
3.04
10.0
9.5
9.0
8.5
8.0
7.5
7.0
6.5
6.0
5.5
5.0
4.5
4.0
3.5
3.0
2.5
2.0
1.5
1.0
0.5
0.0
-0.5
f1 (ppm)

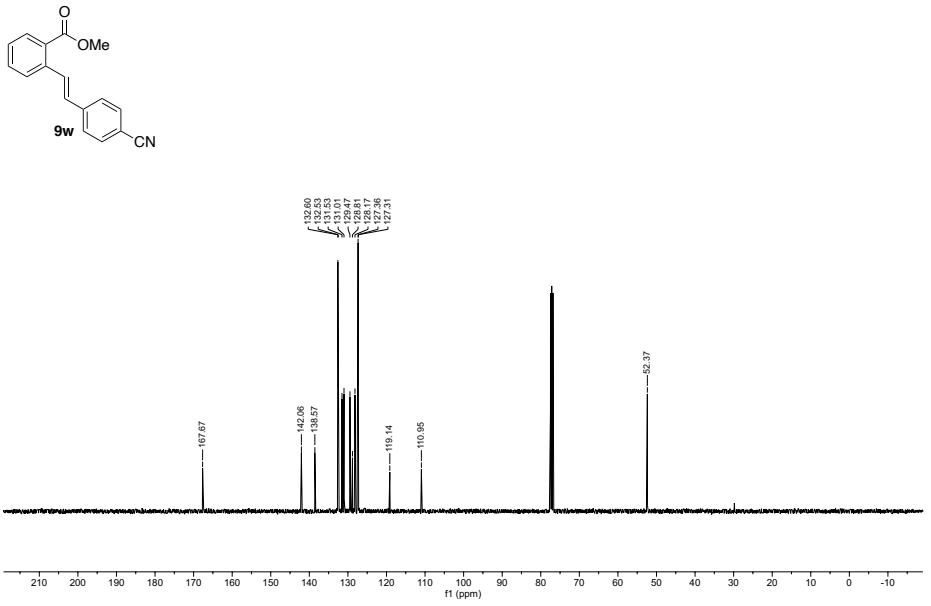
O
OMe
9w
CN
132.60
132.53
131.53
131.01
129.47
128.81
128.77
127.36
127.31
167.67
142.06
138.57
119.14
110.95
52.37
210
200
190
180
170
160
150
140
130
120
110
100
90
80
70
60
50
40
30
20
10
0
-10
f1 (ppm)

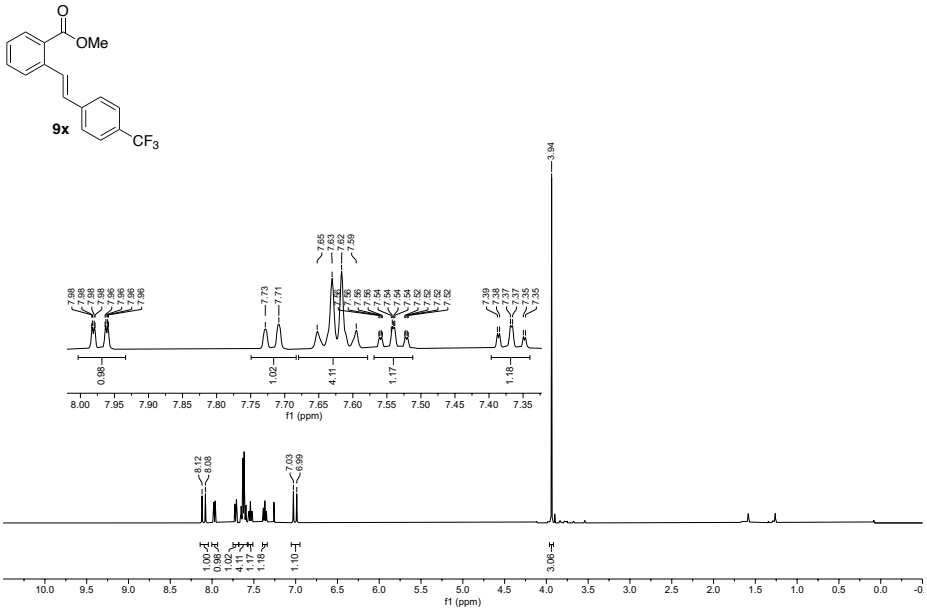
O
OMe
9x
CF3
3.94
7.65
7.63
7.62
7.59
7.98
7.96
7.73
7.71
7.39
7.38
7.37
7.35
0.98
1.02
4.11
1.17
1.18
f1 (ppm)
8.12
8.08
7.03
6.99
1.00
0.98
1.02
4.11
1.17
1.18
1.10
3.06
f1 (ppm)

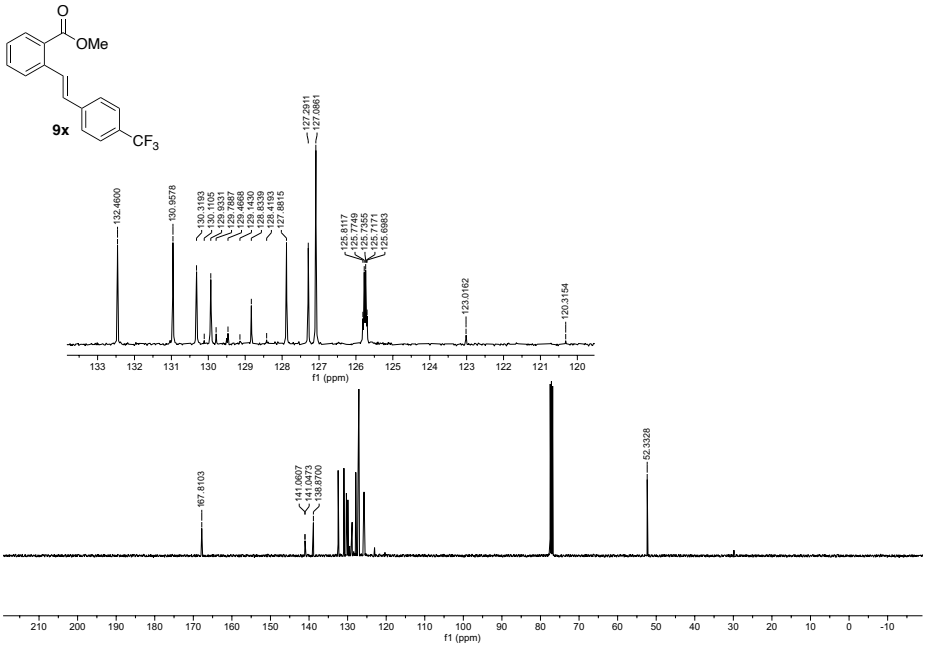
O
OMe
9x
CF3
127.2911
127.0861
132.4600
130.9578
130.3193
130.1105
129.9051
129.7887
129.4668
129.4140
128.8339
128.4193
127.8815
125.8117
125.7749
125.7355
125.7171
125.6983
123.0162
120.3154
f1 (ppm)
167.8103
141.0607
141.0473
138.8700
52.3328
f1 (ppm)

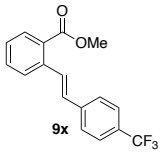
O
OMe
9x
CF3

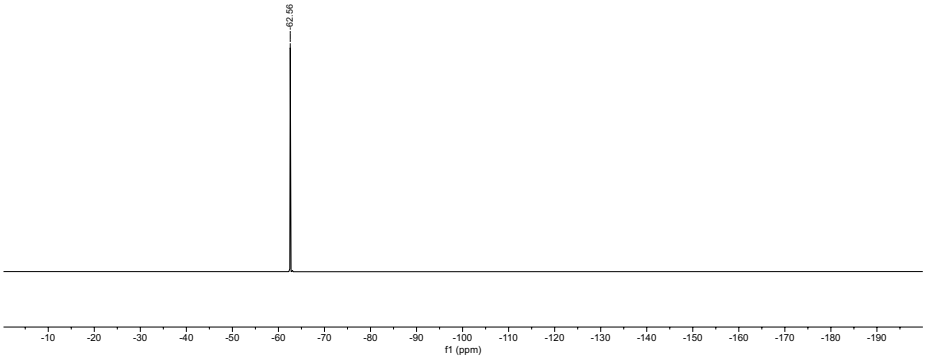
-62.56
f1 (ppm)

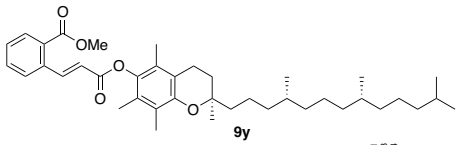
O
OMe
O
O
O
9y

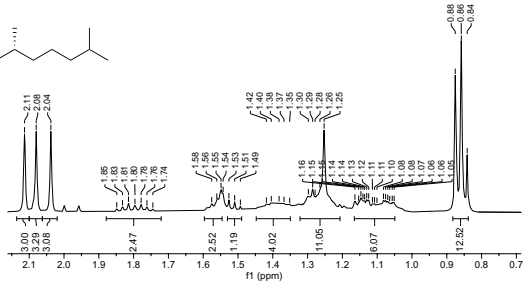
f1 (ppm)

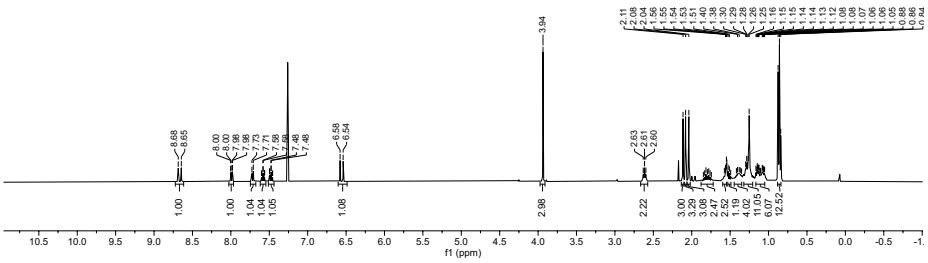
f1 (ppm)

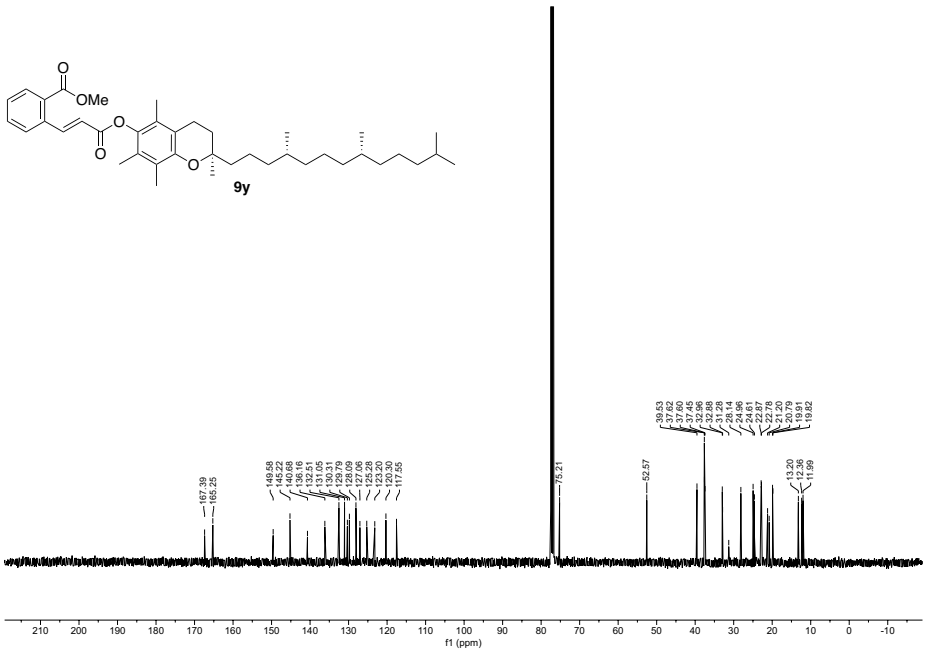
9y
167.39
165.25
149.58
145.23
140.68
136.16
132.51
131.15
130.31
129.79
129.08
127.06
125.28
123.20
120.30
117.55
77.21
52.57
39.53
37.82
37.60
37.45
32.88
32.66
31.28
28.14
24.86
24.61
22.87
22.78
21.26
20.79
19.91
19.82
13.20
12.36
11.99
f1 (ppm)

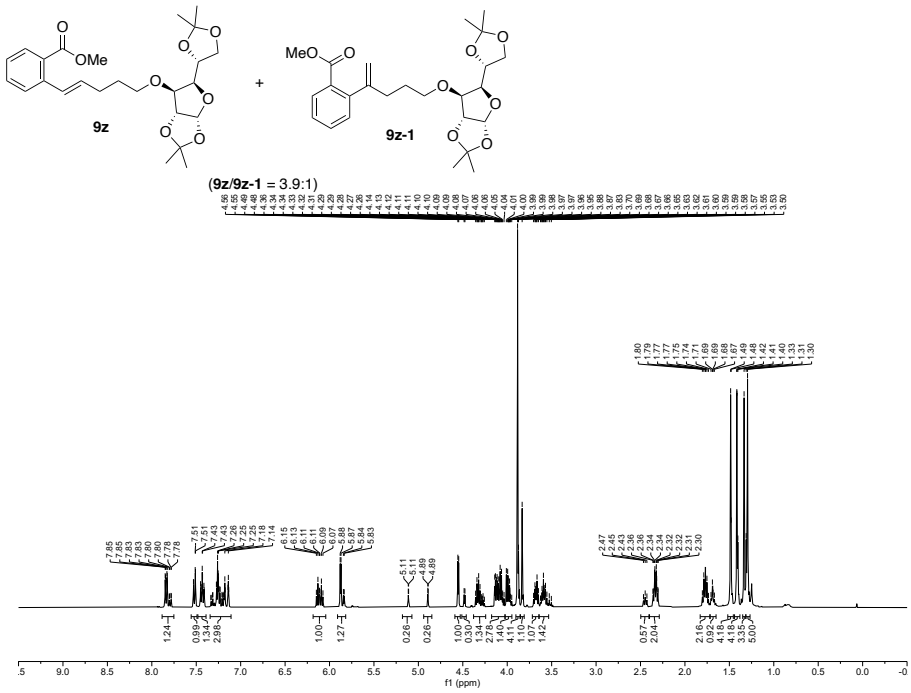
9z
9z-1
(9z/9z-1 = 3.9:1)
f1 (ppm)

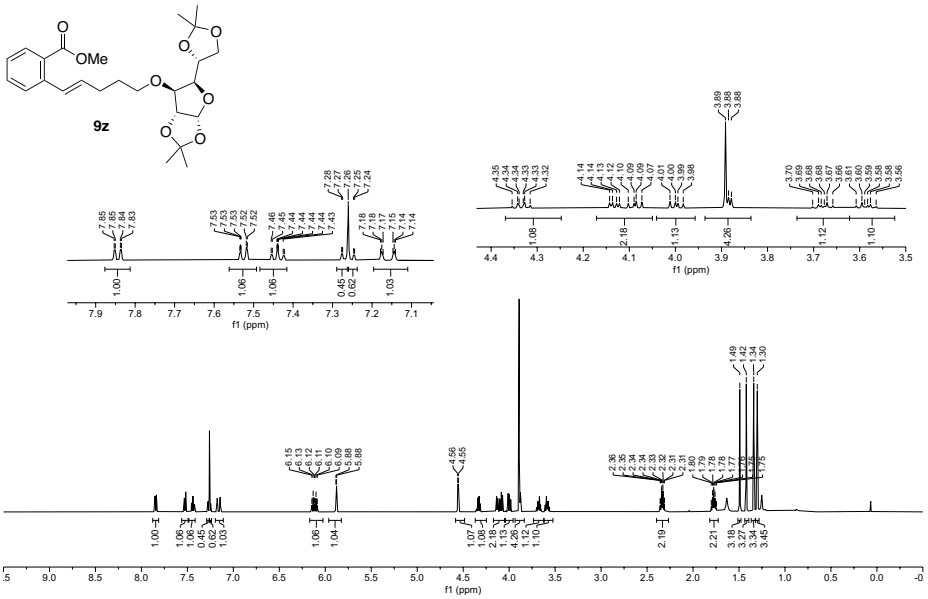
OMe
9z
f1 (ppm)

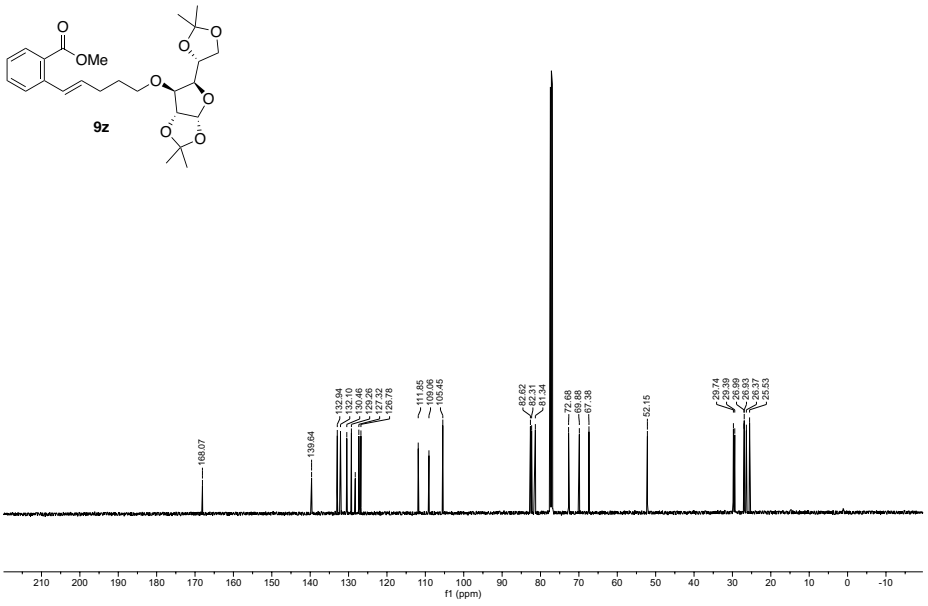
OMe
9z
168.07
139.64
132.94
132.10
130.46
129.26
127.32
126.78
111.85
109.06
105.45
82.62
82.31
81.34
72.68
69.88
67.38
52.15
29.74
29.39
26.99
26.83
26.37
25.53
f1 (ppm)

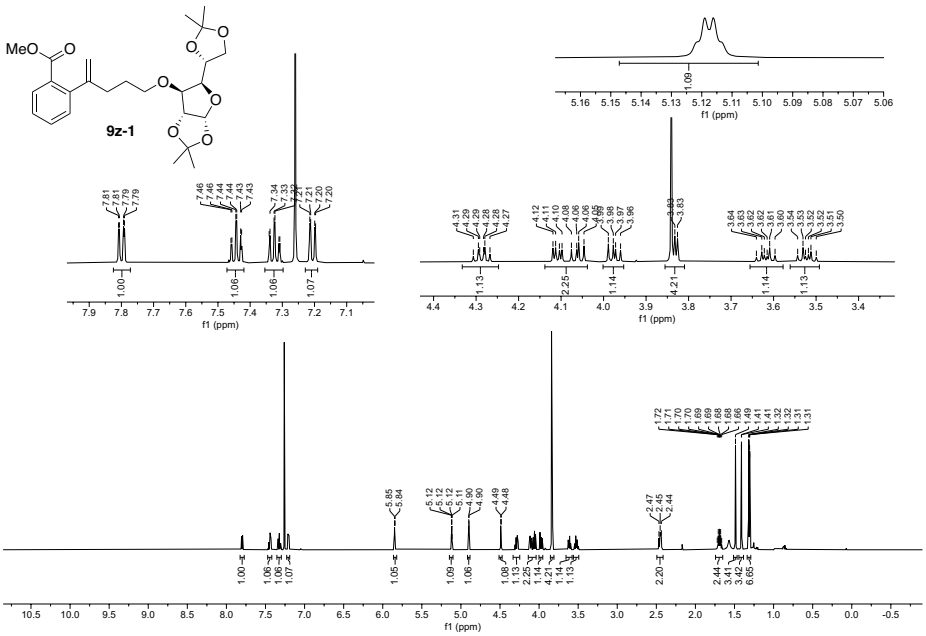
MeO
O
O
O
O
O
O
O
9z-1
f1 (ppm)

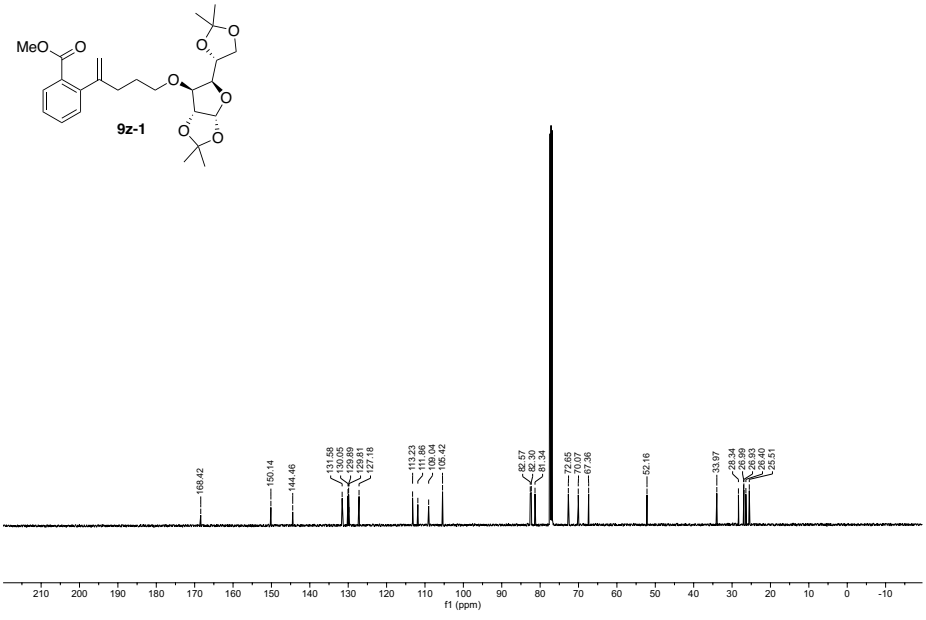
MeO
O
O
O
O
O
O
O
9z-1
f1 (ppm)

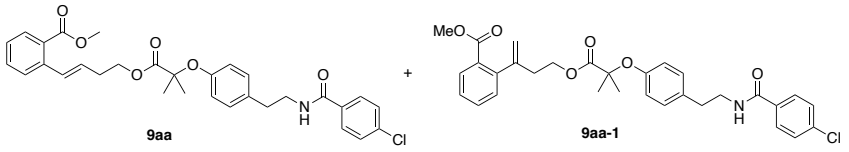
9aa
9aa-1
(9aa/9aa-1 = 5.9:1)

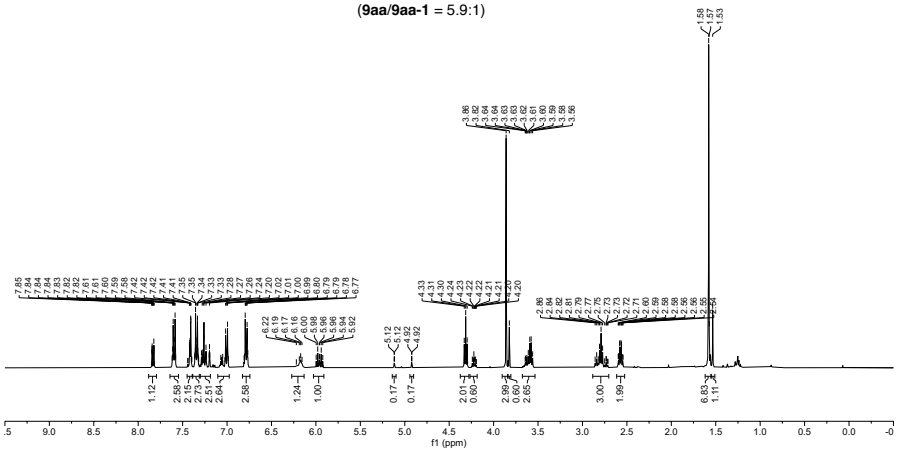
f1 (ppm)

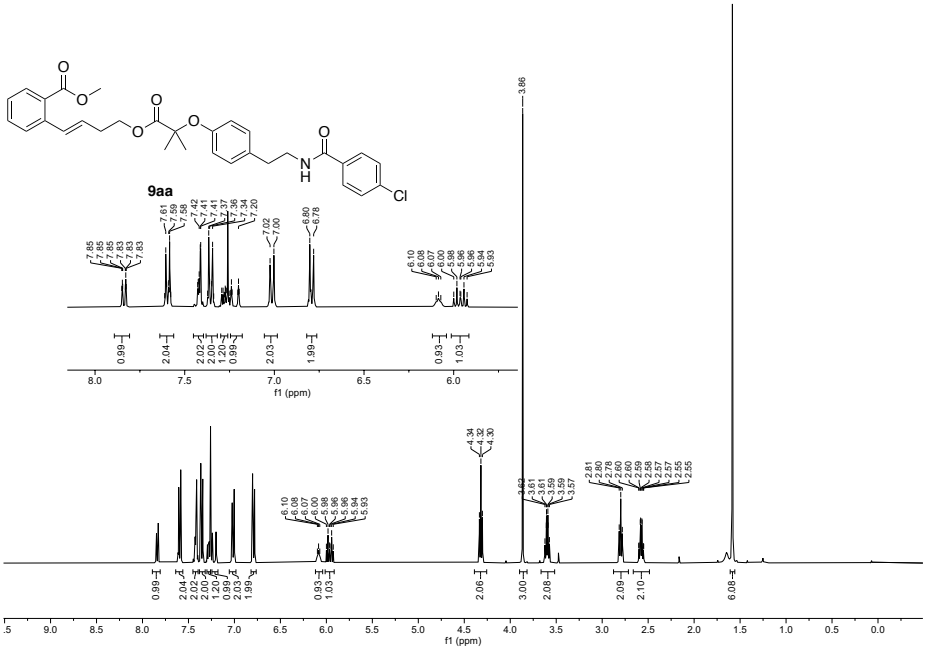
9aa
f1 (ppm)

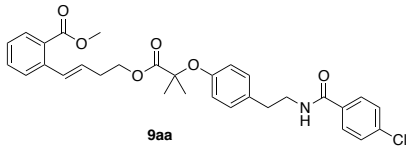

9aa

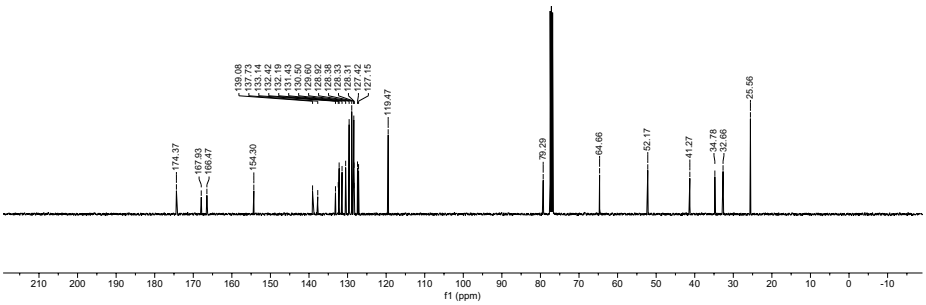

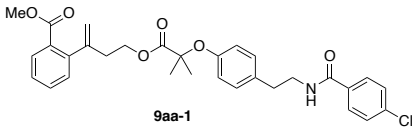

9aa-1

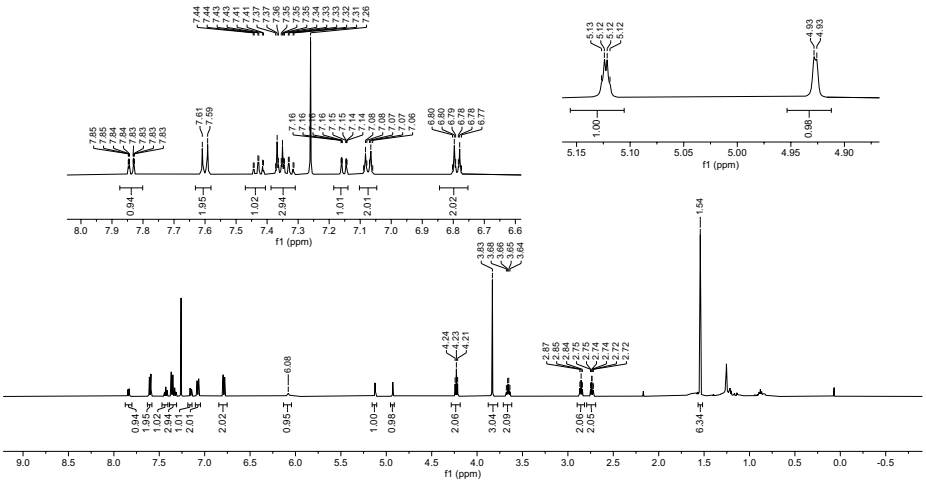

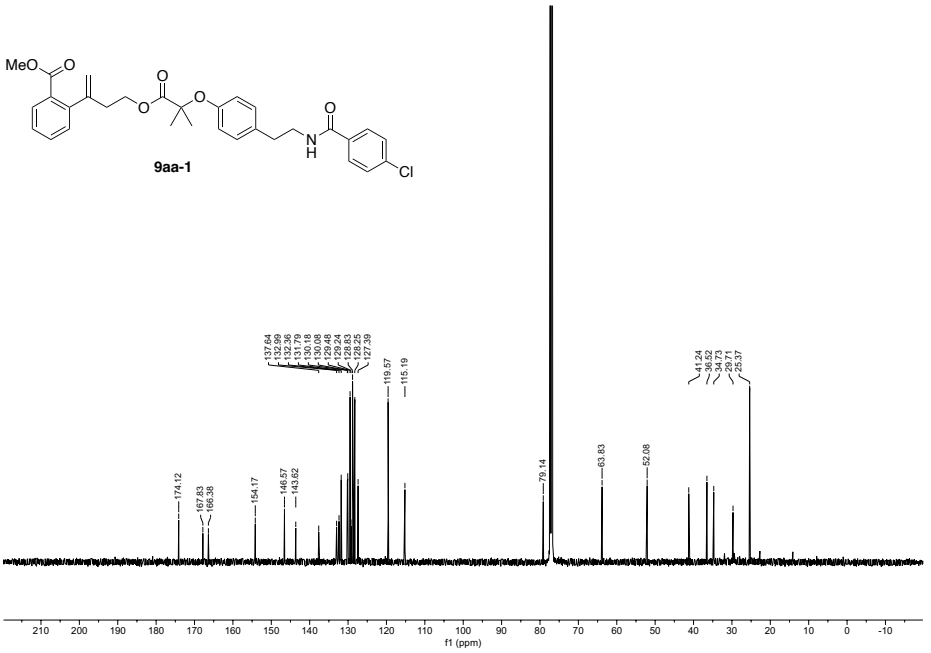
MeO
O
O
O
O
O
N
H
Cl
9aa-1
137.64
132.99
132.36
131.79
130.18
130.08
129.48
129.44
128.83
128.25
127.39
119.57
115.19
174.12
167.83
166.38
154.17
146.57
143.62
79.14
63.83
52.08
41.24
36.52
34.73
29.71
25.37
f1 (ppm)

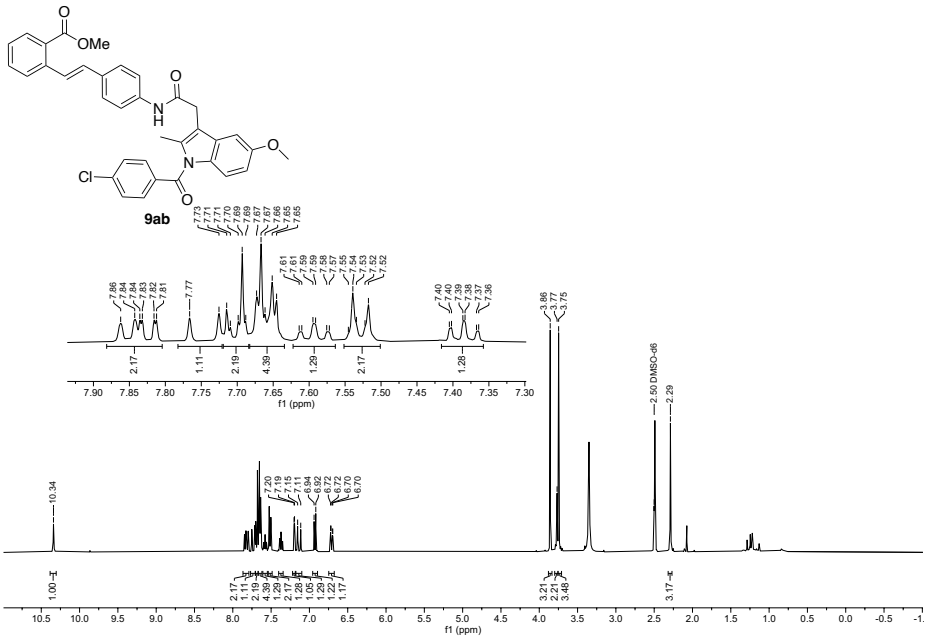
O
OMe
O
N
H
O
N
Cl
O
9ab
7.73
7.71
7.71
7.70
7.69
7.69
7.67
7.67
7.66
7.65
7.65
7.61
7.61
7.59
7.59
7.58
7.57
7.55
7.54
7.53
7.52
7.40
7.40
7.39
7.38
7.37
7.36
7.86
7.84
7.84
7.83
7.82
7.81
7.77
3.86
3.77
3.75
2.50 DMSO-d6
2.29
10.34
7.20
7.19
7.15
7.11
6.94
6.92
6.72
6.72
6.70
6.70
f1 (ppm)

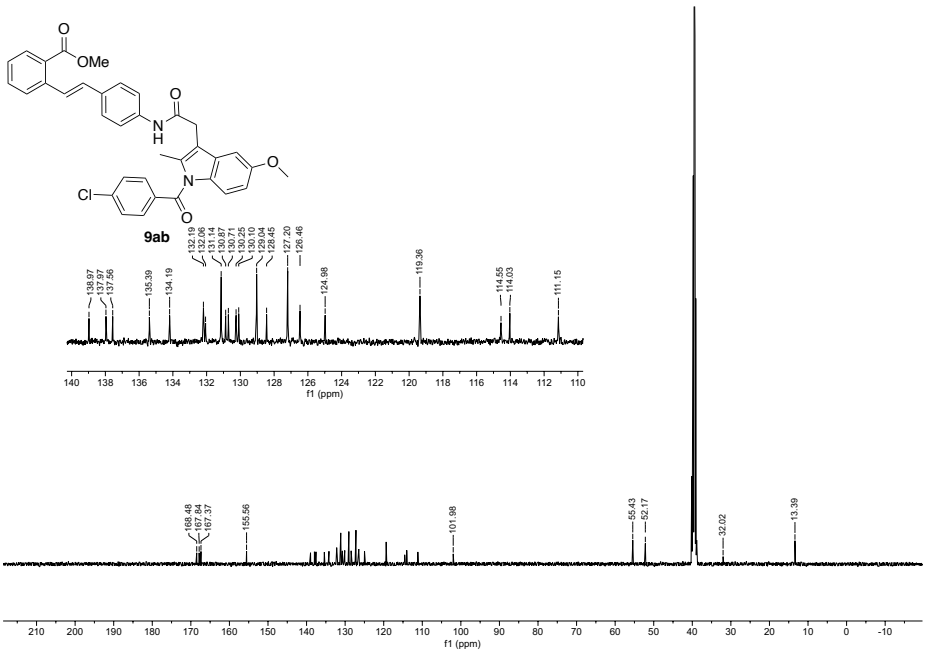
9ab
f1 (ppm)

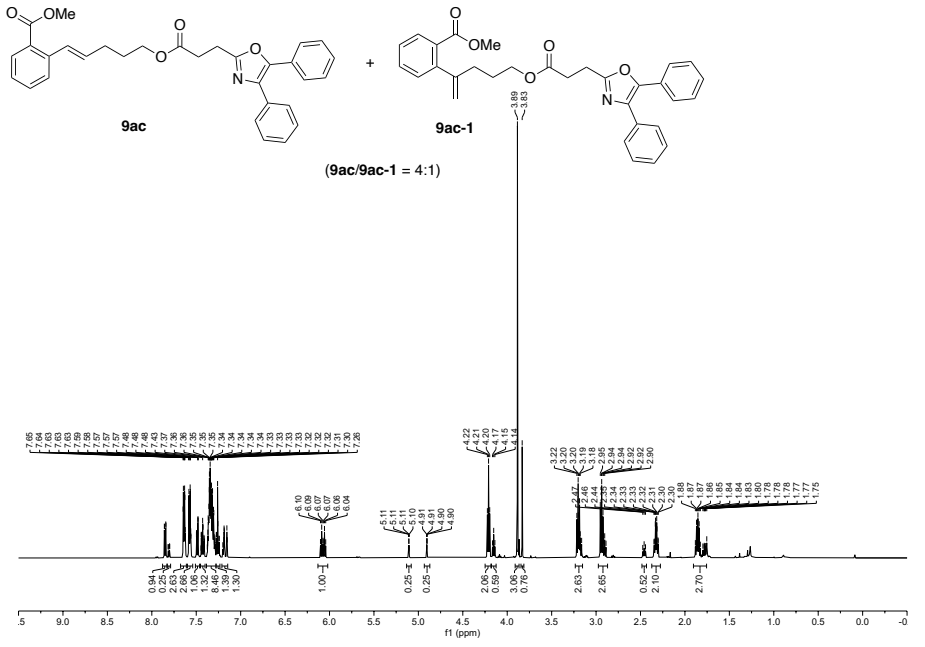
9ac
9ac-1
(9ac/9ac-1 = 4:1)
f1 (ppm)

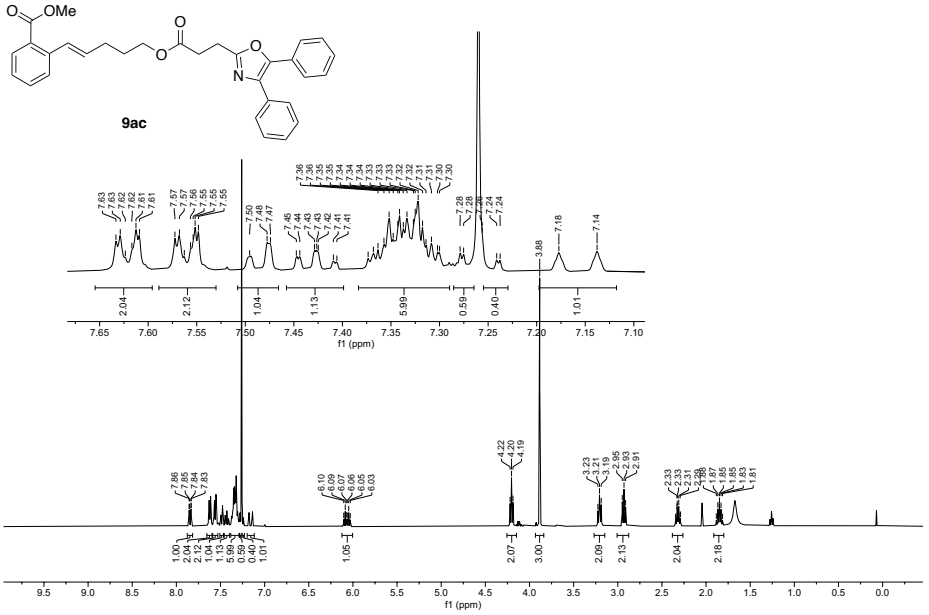
O
OMe
O
O
O
N
9ac
f1 (ppm)

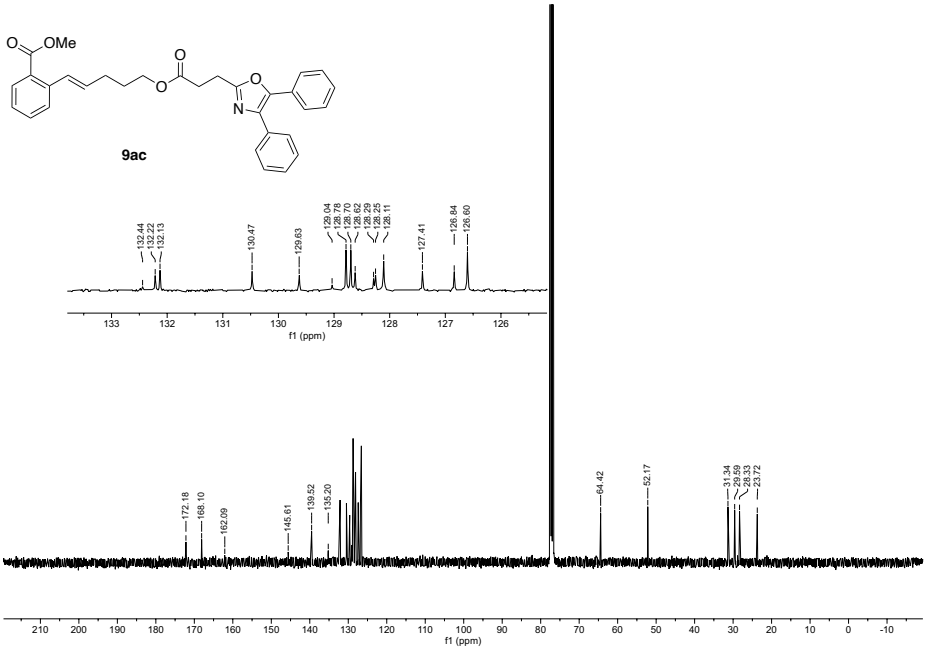
O
OMe
O
O
O
N
9ac
f1 (ppm)

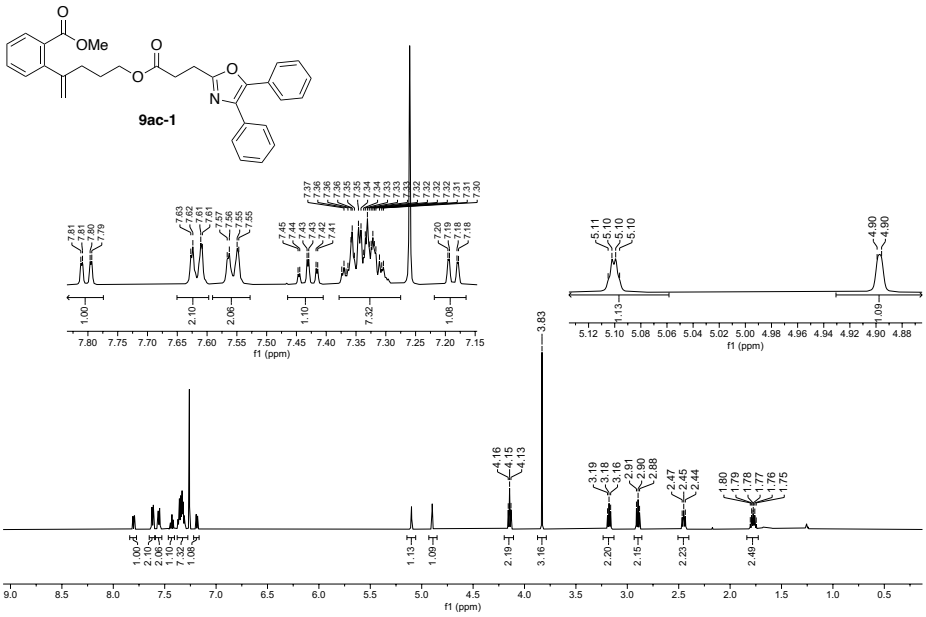
9ac-1
f1 (ppm)

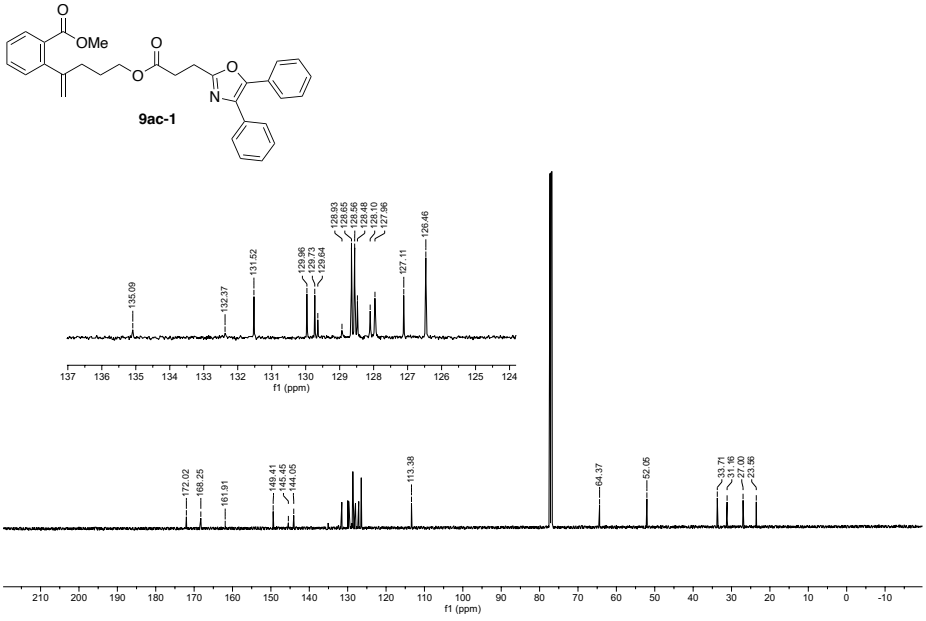
9ac-1
f1 (ppm)

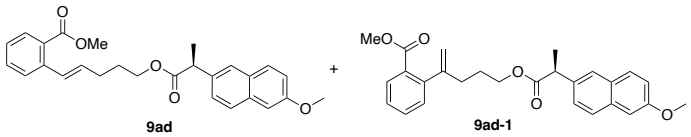

(**9ad/9ad-1** = 4.5:1)

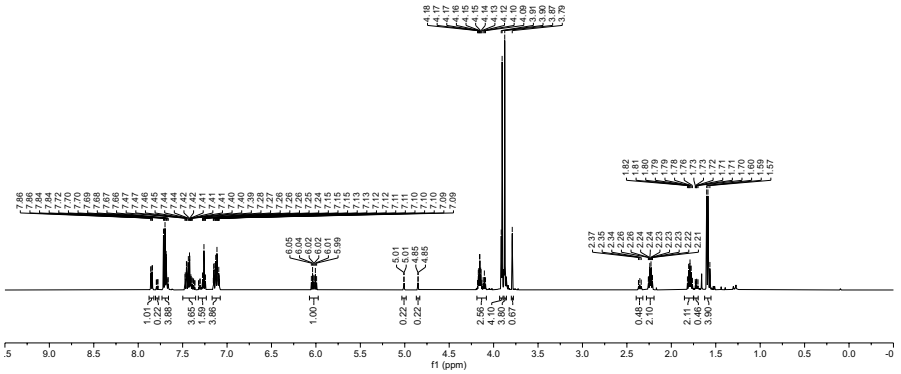

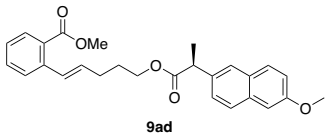

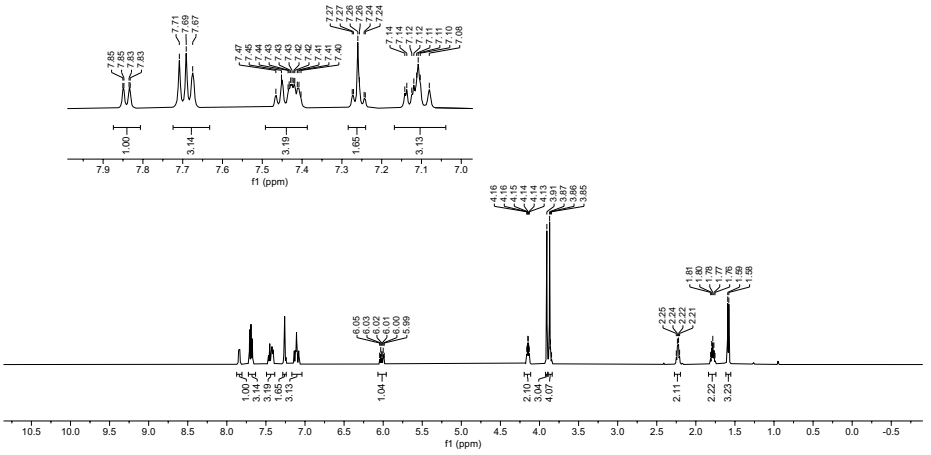

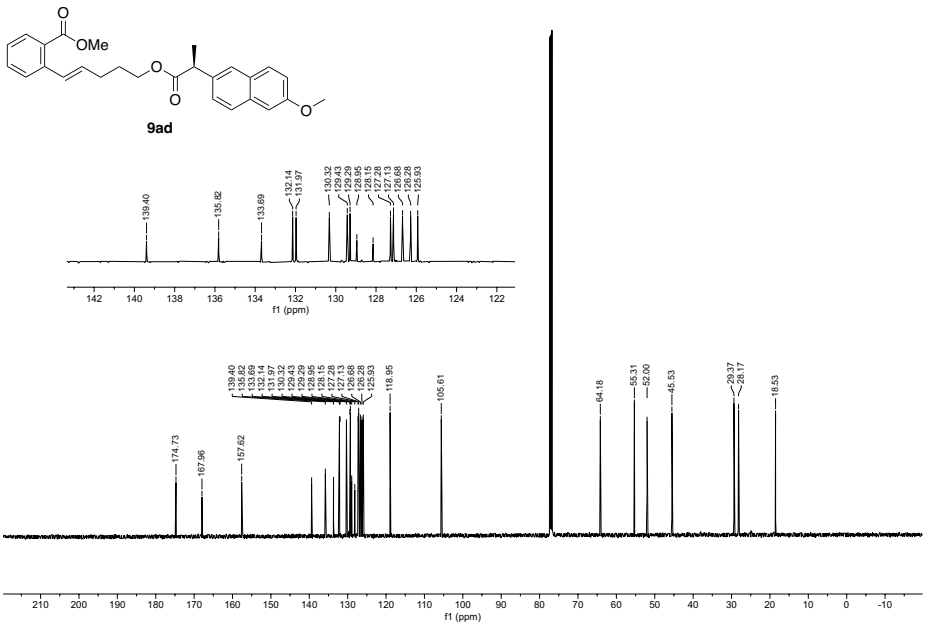
OMe
O
O
O
O
9ad
139.40
135.82
133.69
132.14
131.97
130.32
129.43
129.29
128.95
128.15
127.28
127.13
126.68
126.28
125.93
174.73
167.96
157.62
118.95
105.61
64.18
55.31
52.00
45.53
29.37
28.17
18.53
f1 (ppm)

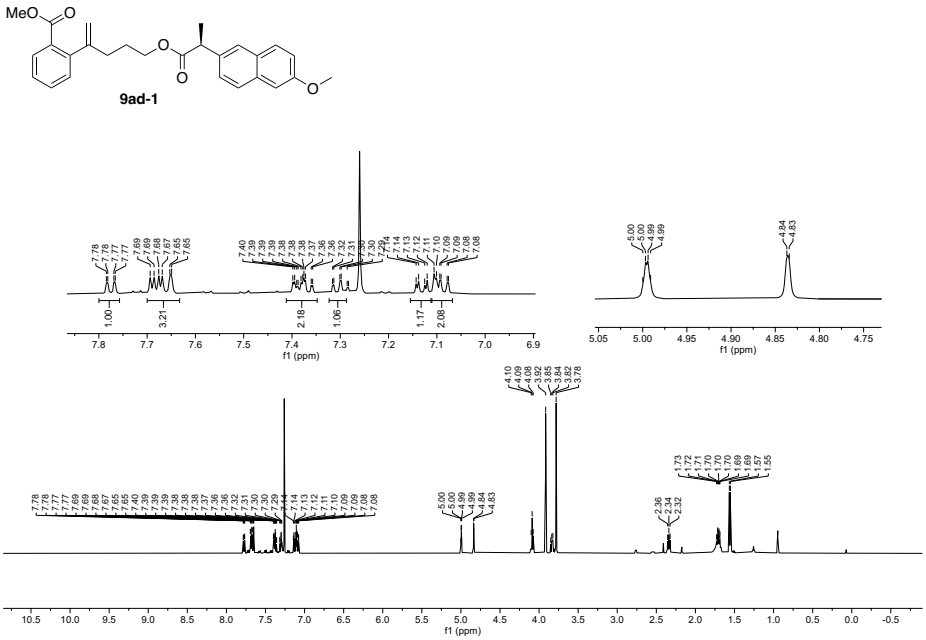
MeO
O
O
O
O
9ad-1
7.78
7.77
7.69
7.68
7.67
7.65
7.40
7.39
7.38
7.37
7.36
7.32
7.31
7.30
7.29
7.14
7.13
7.12
7.11
7.10
7.09
7.08
5.00
4.99
4.84
4.83
4.10
4.09
4.08
3.92
3.85
3.84
3.42
3.78
1.73
1.72
1.71
1.70
1.69
1.57
1.55
2.36
2.34
2.32
1.00
3.21
2.18
1.05
1.17
2.08
f1 (ppm)

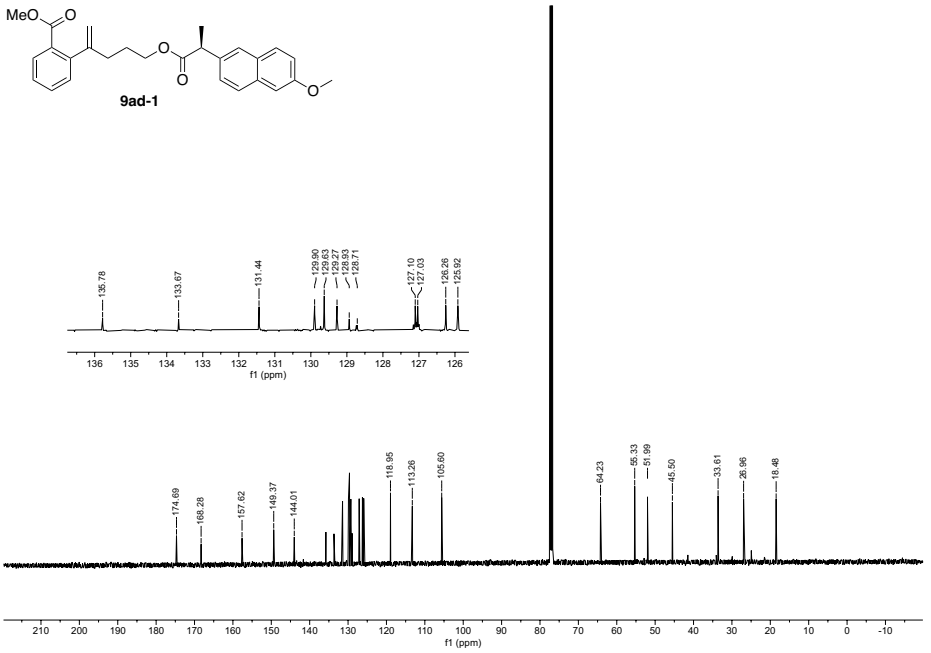
MeO
O
O
O
O
9ad-1
135.78
133.67
131.44
129.90
129.63
129.27
128.93
128.71
127.10
127.03
126.26
125.92
f1 (ppm)
174.69
168.28
157.62
149.37
144.01
118.95
113.26
105.60
64.23
55.33
51.99
45.50
33.61
26.96
18.46
f1 (ppm)

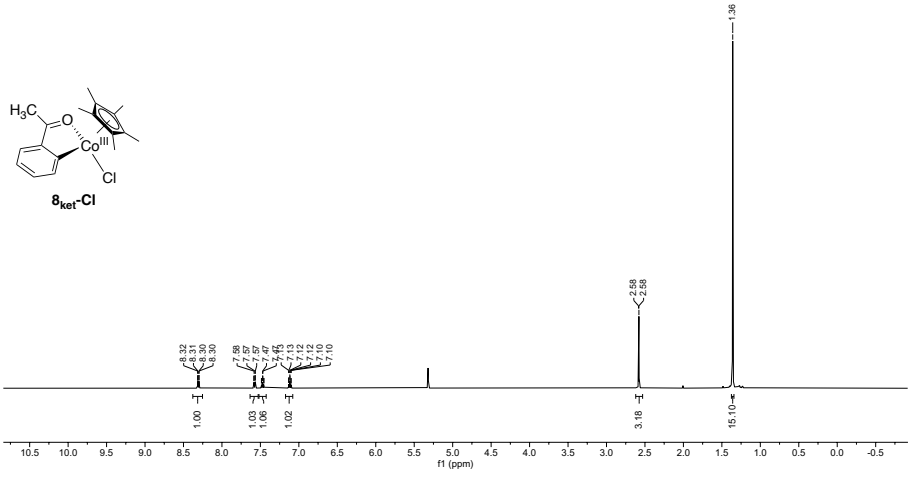
H3C
O
Co III
Cl
8ket-Cl
1.36
2.59
2.58
8.32
8.31
8.30
8.30
7.58
7.57
7.57
7.47
7.46
7.13
7.12
7.12
7.10
7.10
1.00
1.03
1.06
1.02
3.18
15.10
f1 (ppm)

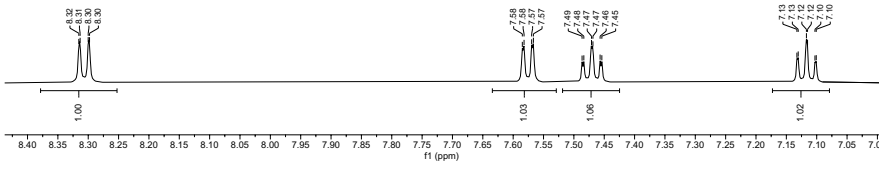
8.32
8.31
8.30
8.30
7.58
7.58
7.57
7.57
7.49
7.48
7.47
7.47
7.46
7.45
7.13
7.13
7.12
7.12
7.10
7.10
1.00
1.03
1.06
1.02
f1 (ppm)

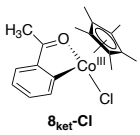

8$_{ket}$-Cl

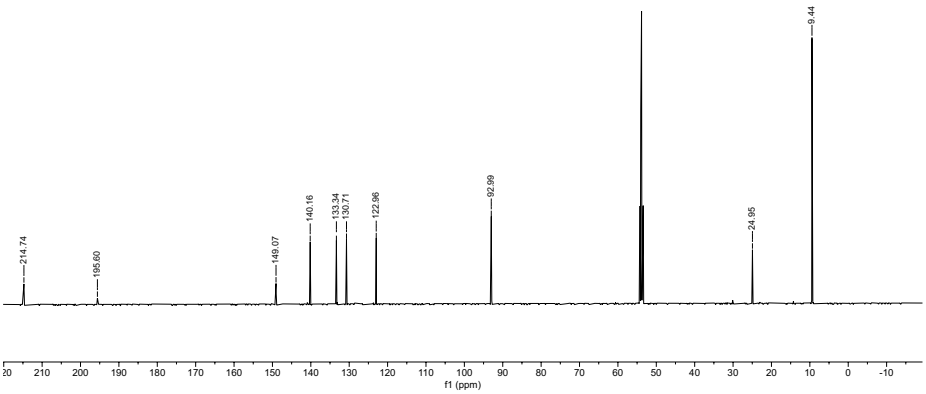

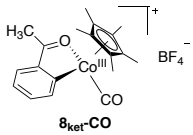

8$_{ket}$-CO

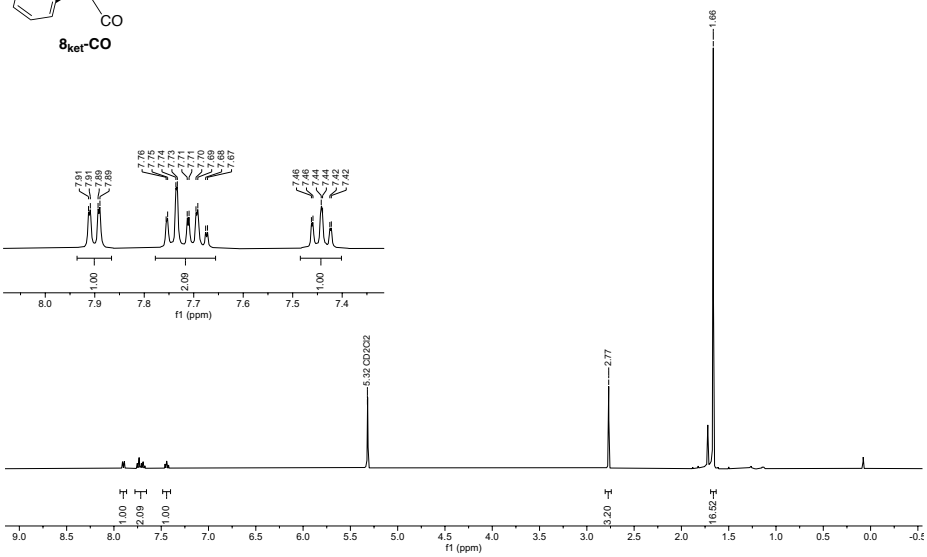

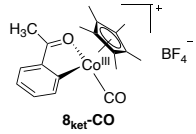
H3C
O
Co III
CO
BF4 −
+

8_{ket}-CO

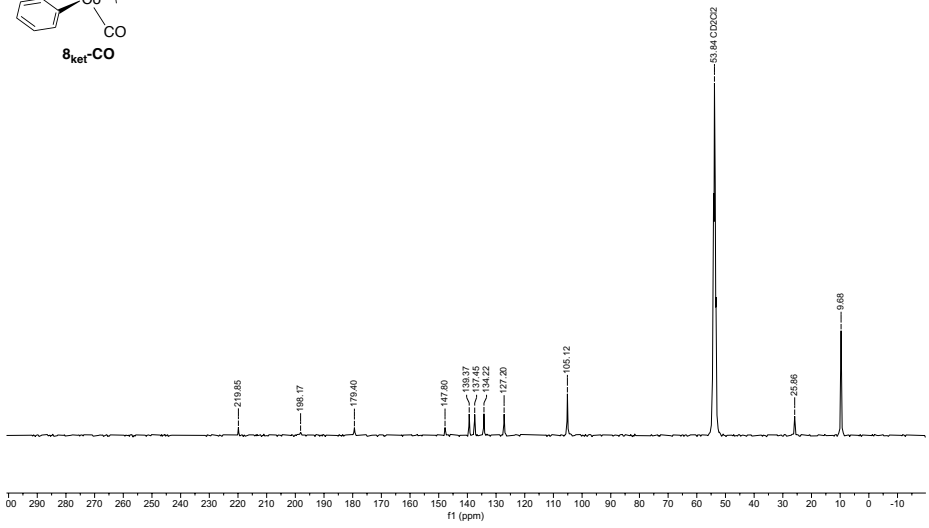
53.84 CD2Cl2
219.85
198.17
179.40
147.80
139.37
137.45
134.22
127.20
105.12
25.86
9.68
f1 (ppm)

Chapter IV. General Conclusions

This dissertation has expanded the repertoire of roles that 1,1,1,3,3,3-hexafluoroisopropanol (HFIP) can play in organic synthesis, untapping unprecedented reaction modes in metal-free transformations and TM catalysis.

In *Chapter II*, we have engineered a general and mild PIFA-mediated intramolecular C(sp^3)–H functionalization protocol facilitated by HFIP that enables the preparation of valuable pyrrolidines, piperidines and O-heterocycles. Our strategy complements the traditional Hofmann-Löffler-Freytag reactions by circumventing existing synthetic shortcomings related to the preparation saturated heterocycles via hydrogen atom transfer (HAT). The success of this reaction relies on a SET event between PIFA and the substrate that leads to a key aromatic radical cation intermediate. Experimental and computational studies support two different pathways for the generation of the corresponding radical cation depending on the electron density of the starting material. For electron-rich substrates, the intracomplex SET process takes place via a charge transfer (CT) complex formed between PIFA and the substrate. On the other hand, for the substrates without electron-donating substituents, it occurs under the assistance of the blue light. As it was shown along the chapter, HFIP is crucial for the accomplishment of the intramolecular process, playing a multifunctional role along the reaction pathway.

In *Chapter III*, we have disclosed a "non-excited" singlet-triplet intersystem crossing (ISC) via secondary-coordination sphere interactions with HFIP. We uncovered the light-free access to a long-lived reactive triplet Cp*Co(CO) species, after CO dissociation, by simply dissolving $Cp^*Co(CO)_2$ in this perfluorinated alcohol. This behavior has no precedents in the literature and provides proof-of-principle for new concepts and prospects in the intriguing behavior of ISC in organometallics. Indeed, we have capitalized on this unusual phenomenon to develop a versatile site-selective cobalt-catalyzed Mizoroki-Heck protocol, which features (i) a wide range of starting materials, including readily available aryl chlorides; (ii) a great functional group tolerance and (iii) enables the employment of targeted drug derivatives. For the first time, we provide experimental and computational evidence that the solvent-induced SCO is responsible for the C–X bond-cleavage. This opens the door to explore the effect of HFIP in additional cross-coupling reactions and the application of ISC events in first-row transition metal catalysis.

UNIVERSITAT ROVIRA I VIRGILI
DISCOVERY OF NEW REACTION MODES IN ORGANIC SYNTHESIS TRIGGERED BY HFIP
Jiayu Zhang

UNIVERSITAT
ROVIRA i VIRGILI

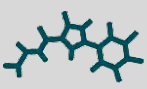

ICIQ

Institut
Català
d'Investigació
Química